Development of a Harvesting Robot for Heavy-weight Crop

(重量作物のための収穫ロボットの開発)

2018

北海道大学大学院農学院

環境資源学専攻　博士後期課程

Ali ROSHANIANFARD

Development of a Harvesting Robot for Heavy-weight Crop

HOKKAIDO
UNIVERSITY

By

Ali ROSHANIANFARD

Dissertation

Submitted to Department of Environment Resources in the Graduate school of Agriculture

Hokkaido University, Sapporo, Japan, 060-8589 in particular fulfillment of the requirements for the degree of

Doctor of Philosophy

March 2018

Table of contents

Acknowledgment

Firstly, I would like to express my deepest gratitude to my supervisor **Dr. Noboru Noguchi**, Professor of the Laboratory of Vehicle Robotics (VeBots), for his relentless aids, motivation, enthusiasm, immense knowledge, and the continuous support of my Ph.D. that made the topic truly pellucid. I thank him for the systematic guidance and heroic effort he put into training me in the field of agricultural robotic, harvesting system, and positive belief to success my idea in term of first heavy-weight robotic crops harvester in the world. He has trust in my capability to complete the work even at times when I myself had none. His guidance helped me in all the time of research and writing of this thesis. I could not have imagined having a better advisor and mentor for my Ph.D. study.

Besides my advisor, heartfelt thanks go to thesis committee: **Dr. Kazunobu Ishii**, and **Dr. Hiroshi Okamoto** for their insightful comments, encouragement, and offered the professional systems and other components for my designs, but also for the hard question which incented me to widen my research from various perspectives.

My deepest appreciation to **Mr. Wada**, who have access to the laboratory and research facilities. Without his precious support, it would not be possible to conduct this research. Special thanks to **Mr. Sato** and his colleagues in the experimental farms of Hokkaido University for giving me the technical aids in components manufacturing and field experimentation.

My warmest appreciation goes to the professors of NARO center, **Dr. Sugiyama** and **Dr. Kami** to their faithful support; and to the professors of Division of Materials Science and Engineering, **Dr. Miura** and **Dr. Ikeda** for their aids to do the compression tests.

I am deeply indebted to the secretaries of the laboratory **Mrs. Aoki** and **Mrs. Namikawa**, who have helped me a lot on the preparing of this thesis, ordering needed components and guiding me in scientific travels to conferences. I warmly thank my gratitude to the **graduate school of agriculture of Hokkaido University** for the support of the thesis. My sincere gratitude goes to all my **colleagues in the Laboratory of Vehicle Robotics** for support and helps to investigate the experimental field and manufacturing period, and their advice and kind friendship especially **Mr. Kamata**. They helped me to understand the Japanese culture and specially dealt with Japanese documents. My life and research in Sapporo would have never been the same without them.

My gratitude overflows to **the deputy of scholarship and student's affair in abroad of I.R. IRAN** for letting me have this fantastic opportunity to come to Japan and improve my knowledge in the field of "Robotic in Agriculture" and to all their supports in during of my Ph.D.; to the **Mitsubishi company**, **Konoshuji company**, **Aihara company**, **Tsubaki company**, and **Bendo company** for their excellent productions, constant helps, faithful support, and laboratory assistance.

Last but not the least, my warmest appreciation goes to my wife **Dr. Behnaz Pahlousay**, for her humor and cheery encouragement, patience, love, and constant wise guidance that she has given me, for standing with me despite many difficult times in during of Sapporo's harsh winter and for supporting me spiritually throughout writing this thesis and helping me to succeed in all aspects of life; to **my father**, **my mother**, **my siblings**, who have supported me throughout my life and motivate me to finish my Ph.D.

I would also like to thank all those who have contributed to the completion of the thesis and are not included here.

List of figures

List of tables

Acronyms and Abbreviations

2D	Two-dimensions
3D	Three-Dimensions
AC	Alternating Current
AL	Aluminum
APF	Application Functions
APT	Administrate Power Transmission system
ASME	American Society of Mechanical Engineers
AV	Absolute Velocity
AVC	Agriculture Value Chain
AXF	Auxiliary Functions
CAD/CAM	Computer-aided design / Computer-aided manufacturing
CAN bus	Controller Area Network
COM	Center of Mass
CP	Central Position
CT	Cycle Time
DGPS	Differential GPS
D-H	Denevit - Hartenberg method
DOF	Degree(s) of Freedom
DR	Diameter Ratio
DR	Damage Rate
ECM	engine control module
ECU	Engine control unit
EE	End-Effector
EMG	Electromyography
FA	front access
FCT	Full Cycle Time
FK	Forward Kinematics
FOS	Factor of safety
FR	Force Ratio
GAP report	Global Agricultural Productivity Report
GCLT method	grasping/picking the crop, cutting the stem, lifting and transportation method
GDP	Gross Domestic Product
GDS	Global distribution system
GM	General Motors
GPS	Global Positioning System
GV	Grasping Velocity
HA	height access
HBH	Human-Based Harvesting
HRHC system	harvesting robot for heavy-weight crops

HLH	Human-Lead Harvesting
HSR	Harvest Success Rate
IK	Inverse Kinematics
IMU	Inertial measurement unit
IP	Image Processing
ISO	International Organization for Standardization
JARA	Japanese Robot Association
JIS	Japanese Industrial Standards
JOG	Jogging Operation
JPY	Japanese Yen
LDMSM	Language Directed Mater-Slave Manipulation
LiDAR	Light Detection and Ranging
LM	Linear Motion
LVC	Learning Vibration Control
MAFF	Ministry of Agriculture, Forestry, and Fishery
MR	Magnetic Resonance
OPF	Operational Functions
PC	Personal Computer
PCI Express	Peripheral Component Interconnect Express
PLC	Programmable logic controller
PPW	Payload Per Weight
PTO	Power take-off
PTP	Point to Point motion
PUMA	Programmable Universal Machine for Assembly
RA	Robotic Arm
RAVeBots-1	Robotic Arm for Vehicle Robotics-first generation
RFID	Radio-frequency identification
RMS	Robot Management System
RT	Robot tractor
RTK-GPS	Real Time Kinematic - Global Positioning System
SAE	Simultaneous Algebraic Equations
SAE	Society of Automotive Engineers
Sc	land surface cover
SCM	Speed Control Mode
SM	Sinusoidal Motion
SO	Stem Orientation
SOM	Second Order Motion
SP	Stem Position
SR	System resolution
SU	switch unit
TCM	Torque Control Mode
TECU	Tractor Engine control unit

Chapter 1. Introduction

1.1. Agriculture in the world

Agriculture as one of the key aspects to develop human civilization plays significant rule to food surpluses. The history of agriculture dates back to thousands of years, and its development has been driven by greatly different climates, cultures, and technologies. The combination of agricultural science and new technologies like robotic can open a new horizon to produce more food for future generation. As mentioned in the Global Agricultural Productivity Report (GAP report) published by Global Harvest Initiative (Washington, USA), a global surge in food prices pushed millions of people into hunger and researchers galvanized attention to this issue in 2008-2009. Today, by contrast, lower global commodity prices and sufficient stockpiles have created a new and different set of challenges for producers, the wider agricultural industry, and policymakers. Conflict within fragile states has created significant threats to peace and food security, and geopolitical forces threaten the coherence of political institutions and economic alliances, giving rise to investment uncertainty. Indebtedness places pressure on government budgets, resulting in stagnating investments in agricultural research and development and extension. And globally, nearly 800 million people continue to go hungry, with two billion people suffering from malnutrition and poor health.

Figure 1 illustrates a long-term global trend point to a growing demand for food and agriculture products due to an increasing population and other parameters. The turbulent of the global economy, along with the boom and bust cycles that have long affected the agriculture sector, will continue to impact farmers and other agriculture value chain (AVC) participants such as seed, fertilizer, crop protection and machinery suppliers, agricultural financial services, buyers, processors, and retailers. The different world incidents such as the great depression, the world war II, the post-war boom, oil crisis, farm crisis, and food price crisis have an effect on agriculture price index gain. In response to these cycles, farmers can manage their risk, reduce waste and loss, cut costs and identify new market opportunities. Government and private industry can provide additional risk management tools and safety nets. Understanding the drivers of these cycles and helping agricultural value chain participants prepare for volatility while building stronger, more competitive operations is a strategy to manage the inevitable storms and ensure longer-term business success. It also involves getting the right public policies in place, along with a dedicated commitment to increasing productivity throughout the agricultural value chain, with the goal of fostering resilient, sustainable and successful operations that provide needed food and agriculture products for a growing world (Global Harvest Initiative, 2013, 2014, 2015, 2016).

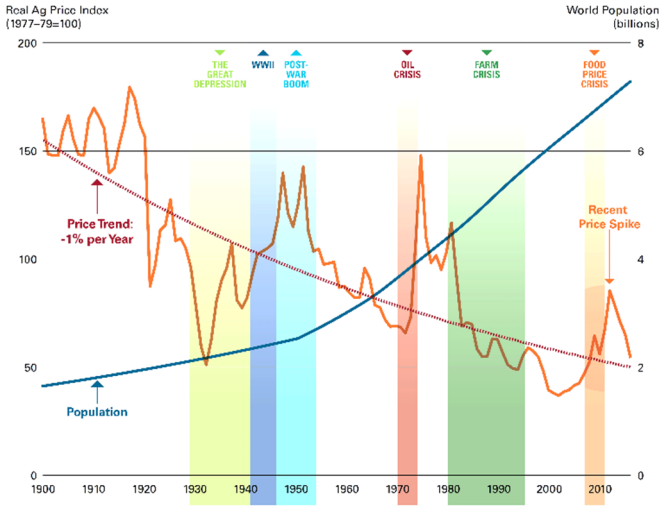

Figure 1. The Grilli-Yang agricultural price index adjusted for inflation.

Today’s food and agriculture system must rise to the challenge of improving productivity to meet growing demand while becoming increasingly focused on sustainability. The challenge is how can we manage the current storms and foster more sustainable inclusive growth during the agricultural business cycle, both now and in the years ahead.

Farmers must manage through the current agricultural business cycle by staying competitive and by participating in new markets. They must also reduce their costs. To do this, farmers and ranchers are adopting precision agriculture systems to make their crop, livestock, aquaculture, dairy and orchard operations more profitable. Precise agriculture is the use of data and technology to increase the productivity and profitability of agricultural systems by applying inputs. Agriculture is increasingly becoming a high-tech business, not only for farmers in high-income countries but across the globe. Accelerating the access to new technologies, data and precision systems will help farmers in low-income countries close their productivity gaps and manage their natural resource base to conserve soil and water. Precision systems enable each farmer to manage and track, year after year, progress towards maximizing the productivity of each field while placing less productive areas. Using their own data, precision systems also help farmers raise healthier animals and manage grazing lands for sustainability.

Using equipment such as in-field monitors and sensors, farmers and service providers can record data on temperature, rainfall, soil conditions and plant growth, capturing the information for analysis and to generate models that help them make good decisions about operations and investments. New livestock systems can check animals for breeding cycles and disease, notifying farmers of potential problems before they spread to the entire herd. Monitors also track food and water consumed. Machinery equipped with precision systems of parallel steering, GPS and data history enables farmers to cover every inch of the field and avoid even the slightest overlap, saving time, costs of seeds, inputs and fuel, and reducing wear on the equipment. Remote sensing is widely used with satellite imagery to collect data. Unmanned aerial vehicles (commonly called drones) are used to fly over fields and generate maps and assess crop health. Precision systems can monitor irrigation, farm vehicles, livestock, greenhouses and stables, aquaculture, forests and storage of crop and livestock products and can reduce the amounts of water and fuel that are used.

1.2. Agriculture in Japan and recent concerns

As reported from statistics bureau ministry of internal affairs and communications of Japan in the statistical handbook of Japan (2016), over the course of Japan's economic growth, it's agricultural, forestry and fishing industries employ fewer and fewer workers every year, and their GDP share has also dropped. The number of workers decreased from 13.40 million in 1960 (30.2 percent of the total workforce) to 2.30 million in 2014 (3.6 percent), and the GDP share of the industries fell from 12.8 percent in 1960 to 1.2 percent in 2014. Japan's total agricultural output in 2014 was 8.36 trillion yen, down 1.2 percent from the previous year. Crops yielded 5.37 trillion yen, down 6.0 percent from the previous year. This was due to the rice and vegetable output decreasing despite outputs of fruits and nuts increasing as shown in Table 1 and Table 2.

As shown in Table 3, the number of farm households engaged in commercial farming (which refers to households with cultivated land under the management of 0.3 hectares and over, or with annual sales of agricultural products amounting to 500,000 yen or more) was 1.33 million in 2015. Of these commercial farm households, 33.3 percent were full-time farm households, 12.4 percent were part-time farm households with farming income exceeding non-farming income, and 54.3 percent were part-time farm households with non-farming income exceeding farming income. Of the commercial farm household members, 2.10 million people were engaged in farming as their principal occupation (commercial farmers) in 2015, of whom 63.5 percent were aged 65 years and over. In 2014, the total income per commercial farm household was 4.56 million yen, down 3.5 percent from the previous year. Of that amount, 1.19 million yen was from farming income, 1.46 million yen from non-farming income, and 1.91 million yen from pension benefits and other sources. Japan's cultivated acreage shrank year after year from 6.09 million hectares in 1961 to 4.50 million hectares in 2015. In the one-year period of 2015, there were 4,380 hectares of new cultivation

but also a 25,900-hectare decrease. The most common cause of the decrease was degraded farmland, accounting for approximately 50 percent of all cases, followed by land-use conversion for residential and other land uses, making up approximately 30 percent. (SBJ, 2016).

Table 1. Agricultural, forestry and fisheries output in Japan

(Billion yen)

Item	2010	2011	2012	2013	2014
Total	10,026	10,082	10,335	10,331	10,321
Agriculture	8,121	8,246	8,525	8,467	8,364
Crops	5,513	5,639	5,879	5,703	5,363
Rice	1,552	1,850	2,029	1,781	1,434
Vegetables	2,249	2,134	2,190	2,253	2,242
Fruits and nuts	750	743	747	759	763
Livestock and its products	2,553	2,551	2,588	2,709	2,945
Beef cattle	464	463	503	519	594
Dairy cattle	773	751	775	778	805
Pigs	529	536	537	575	633
Chickens	735	753	724	784	853
Forestry	422	417	392	425	451
Fisheries	1,483	1,419	1,418	1,440	1,506

Table 2. Agricultural production in Japan

(Thousand tons)

Products	2000	2005	2010	2013	2014
Cereal grains					
Rice	9,490	9,074	8,483	8,607	8,439
Wheat	688	875	571	812	852
Vegetables, potatoes and legumes					
Potatoes	2,898	2,752	2,290	2,408	2,456
Sweet potatoes	1,073	1,053	864	a) 942	887
Soybeans, dried	235	225	223	200	232
Cucumbers	767	675	588	574	549
Tomatoes	806	759	691	748	740
Cabbages	1,449	1,364	1,360	1,440	1,480
Chinese cabbages	1,036	924	889	906	914
Onions	1,247	1,087	1,042	1,068	1,169
Lettuces	537	552	538	579	578
Japanese radishes	1,876	1,627	1,496	1,457	1,452
Carrots	682	615	596	604	633
Fruits					
Mandarin oranges	1,143	1,132	786	896	875
Apples	800	819	787	742	816
Grapes	238	220	185	190	189
Japanese pears	393	362	259	267	271
Industrial crops					
Crude tea	a) 85	100	85	a) 85	84
Sugar beets [1)]	3,673	4,201	3,090	3,435	3,567

1), a) Figures are total of major producing prefectures.
Source: Ministry of Agriculture, Forestry and Fisheries.

Table 3. Commercial farm household and commercial farmers in Japan.

Year	Commercial farm households (1,000)				Commercial farmers	
	Total	Full-time	Part-time		(1,000)	Aged 65 years and over (%)
			Mainly farming	Mainly other job		
1995	2,651	428	498	1,725	4,140	43.5
2000	2,337	426	350	1,561	3,891	52.9
2005	1,963	443	308	1,212	3,353	58.2
2010	1,631	451	225	955	2,606	61.6
2015	1,330	443	165	722	2,097	63.5

Japan's present food self-sufficiency rate is the lowest among major industrialized countries, and Japan is thus the world's leading net importer of agricultural products as shown in Figure 2.

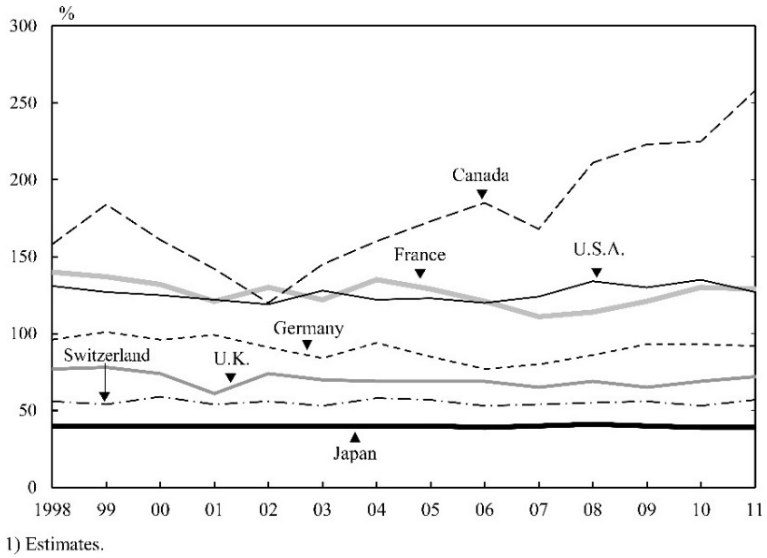

Figure 2. Food self-sufficiency rates of major countries.

1.2.1.Robotic in agriculture

Figure 3 and Figure 4 illustrate the estimated number of research which was done in the field of agricultural robotic in the world. The researcher has interested to assess the agricultural industry by developing robotic systems which can increase the efficiency of systems, quality and quantity of agricultural production, and farmer's life in different countries such as Japan and USA.

In the US, automation of machine guidance functions has been an interest for agricultural researchers in North America since the early days of the tractor. The patent was presented in the early 1920s, diagram systems that can follow furrows to guide a machine across a field (Willrodt, 1924). In the late 1930s, Sisson developed a circle farming based system upon a large diameter spool positioned centrally in a field (Sissons, 1939). In the 1970s, a low-current and low-frequency signal were used to identify pathways machinery in the field (R.L. Schafer & Young, 1979). In the 1980s, a combination of computers and image sensors have provided for machine vision-based guidance systems. During the mid-1980s, researchers at Michigan State University and at Texas A&M were exploring machine vision guidance. The harvesting of oranges was performed at the University of Florida (R.C. Harrell, Adsit, Pool, & Hoffman, 1990). Precision agriculture has helped advance vehicle guidance: (1) in terms of providing position information that is required for vehicle guidance, (2) precision agriculture has placed the notion of vehicle automation within the conceptual boundary of equipment manufacturers and agricultural producers. Between the 1980s to 1990s, changes in the funding structure of research in defense exposed new research teams to the opportunities in the agriculture sector and have resulted in traditionally non-agricultural research teams attacking the challenges of agricultural vehicle guidance. Researchers at Carnegie-Mellon University and Stanford University are representative groups. The University of Illinois also formed a research team to address the needs of vehicle automatic guidance to precision farming in the North Central USA.

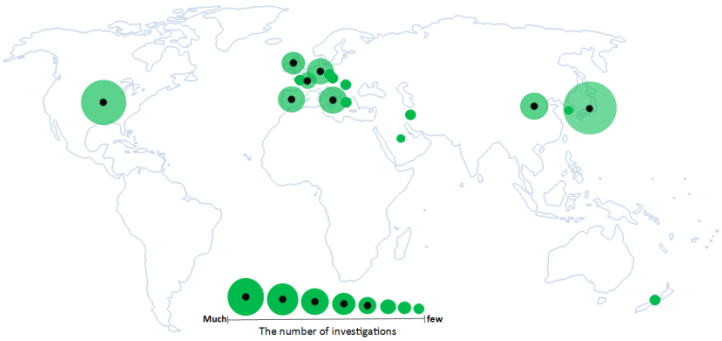

Figure 3: The number of investigation in agricultural robot around the world

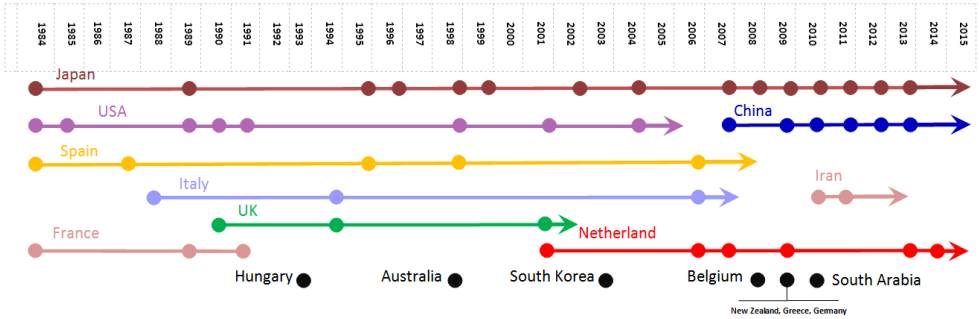

Figure 4: Timeline for research work in agricultural robot around the world

In Japan, the Ministry of Agriculture, Forestry, and Fishery (MAFF) promoted a policy to improve production and strengthen the agricultural infrastructure in 1993. The policy was set out in the document basic direction of new policies for food, agriculture and rural area published. Under these guidelines, the Agricultural Machine Development Project and the Practical Promotion Project were initiated in 1995. These were included the development of agricultural robots and techniques for autonomous navigation in the field. After that, the national and public research institutes have been pooling their expertise in the new technology of autonomous navigation. Much research on automation in agriculture has also been performed in universities. In the universities, due to funding limitations, most research has involved methodologies, such as navigation, sensing, and application of control theory. At research institutes and manufacturers more practical systems were tested (Torii, 2000). Between 1996 and 1999, the scope of research and development activities was expanded. Investigations into the integration of the location and navigation techniques for vehicles using GPS were performed. The efforts focused on theoretical and experimental studies on the coupling of the available automatic precision guidance system and modified differential GPS techniques for the development of a safeguard system for mobile farm machinery. Knowing the actual position in the field, orientation either along existing guidelines or along freely adjustable virtual rows should be possible and the required reliability of course correction and/or stop signals when critical positions are encountered (field margins, obstacles, no-go areas) must be guaranteed.

In the different countries, the scientists were focused on the search for strategies of automatic guidance. An autonomous speed sprayer for orchards has been developed using machine vision and fuzzy control (Cho, Ki, Lee, & Choi, 1996; Cho & N.H. Ki, 1996). Image analysis of the orchard, which was used for the direction of motion, and signal processing of ultrasonic sensors, used to measure the distance from obstacles, were performed in real time. An autonomous speed sprayer using DGPS and fuzzy control was also implemented, with RMS errors not exceeding 0.3 m (J. H. Lee, Cho, & Lee, 1998). Guidance using an ultrasonic sensor has been performed in the field (Sheng, Chen, & Hwang, 1997).

Some agricultural robots studies were focused on a general aspects of intelligent agricultural technology as: a new automatic tractor guidance system (Widden & Blair, 1972), mobile robot with wireless patent (Zweig, 2007), development of a teleoperation system for agricultural vehicles (Murakami et al., 2008), automation on fruit and vegetable grading system and food traceability (Kondo, 2010), 3D path planning for a biomass processing robot via motion simulation (Starcevic, Thullner, Bux, & Müller, 2010), autonomous navigation using a robot platform in a sugar (Bakker, van Asselt, Bontsema, Müller, & van Straten, 2011), farm machinery management information system (Fountas, Sorensen, et al., 2015), farm machinery management information system, current situation and future (Fountas, Carli, et al., 2015), and highlights and preliminary results for autonomous crop protection (Pérez-Ruiz et al., 2015). Some research was focused on sensors like: automatic guidance sensors for agricultural (Tillett, 1991), automatic guidance for agricultural vehicles (Keicher & Seufert, 2000), agricultural automatic guidance research in North America (Reid, Zhang, Noguchi, & Dickson, 2000), and automatic velocity control of a self-propelled windrow (Foster, Strosser, Peters, & Sun, 2005). Some others were interested in Laser optical navigation system or real-time position determination like automatic guidance sensors for agricultural (Tillett, 1991), automatic guidance of agricultural vehicles using a laser sensor (Chateau, Debain, Collange, Trassoudaine, & Alizon, 2000), automatic guidance for agricultural vehicles in Europe (Keicher & Seufert, 2000), development of an autonomous navigation system using a two-dimensional laser scanner in an orchard application (Barawid, Oscar, Mizushima, Ishii, & Noguchi, 2007), autopilot for a combine harvester (Coen, Vanrenterghem, Saeys, & De Baerdemaeker, 2008), an agent of behavior architecture for unmanned control of a farming vehicle (García-Pérez, García-Alegre, Ribeiro, & Guinea, 2008), comparison of two 2D laser scanners for sensing object distances, shapes, and surface patterns (K.-H. Lee & Ehsani, 2008), potential of a terrestrial LiDAR-based system to characterize weed vegetation in maize crops (Andújar, Escolà, Rosell-Polo, Fernández-Quintanilla, & Dorado, 2013), and development of a Human-driven tractor following a Robot System (C. Zhang, Yang, & Noguchi, 2015).

Recently, using GPS and machine vision technology for precision farming was most interested. Automatic tractor guidance using carrier-phase differential GPS (Bell, 2000), automatic guidance for agricultural vehicles in Europe (Keicher & Seufert, 2000), agricultural automatic guidance research in North America GPS and GDS (Reid et al., 2000), guidance of agricultural vehicles (Wilson, 2000), autonomous guidance for rice transplanting using global positioning and gyroscopes (Nagasaka, Umeda, Kanetai, Taniwaki, & Sasaki, 2004), a six-legged robot-based system for humanitarian demining missions (Gonzalez de Santos, Cobano, Garcia, Estremera, & Armada, 2007), an agent of behavior architecture for unmanned control of a farming vehicle (García-Pérez et al., 2008), and highlights and preliminary results for autonomous crop protection (Pérez-Ruiz et al., 2015), were the examples of auto-guidance projects based on GPS.

In the case of machine vision aspect some researched as a computer-vision algorithm for automatic guidance of micro-plant harvesting (McFarlane, 1991), application accuracy of a machine vision-controlled robotic micro-dosing system (Feng, Xiao, Willette, McGee, & Kamat, 2015), inspection and grading of agricultural and food products by computer vision systems(Brosnan & Sun, 2002), Machine vision technology for agricultural application (Chen, Chao, & Kim, 2002), Machine Vision-based Guidance System for Agricultural Grain Harvesters (Benson, Reid, & Zhang, 2003), Stereo vision with texture learning for fault-tolerant automatic baling (Blas & Blanke, 2011), A vision based row-following system for agricultural field machinery, Autonomous robotic weed control systems (Åstrand & Baerveldt, 2005), robotic harvesting of gerbera Jamesonii based on detection and Analysis of natural images processing for the extraction of agricultural elements (Rath & Kawollek, 2009), design and control of an apple harvesting robot (De-An, Jidong, Wei, Ying, & Yu, 2011), automatic segmentation of relevant textures in agricultural images (Guijarro et al., 2011), a computer vision approach for weeds identification through Support Vector Machines (Tellaeche, Pajares, Burgos-Artizzu, & Ribeiro, 2011), automatic expert system based on images for accuracy crop row detection in maize field (Montalvo et al., 2012), and applications of image processing in agriculture (Vibhute & Bodhe, 2012), was done.

In the case of navigation application, autopilot for a combine harvester (Coen et al., 2008), path planning for in-field navigation-aiding of service units (Bochtis, Sørensen, & Vougioukas, 2010), automated generation of guidance lines for operational field planning (Hameed, Bochtis, Sørensen, & Nøremark, 2010), and autonomous navigation using a robot platform in a sugar beet field (Bakker et al., 2011) was investigated some navigation planner.

Some researchers were done the researched in the case of autonomous agricultural vehicles as the global key to precision agriculture and sustainability (Cox, 2002), a Windows-based design environment for combine automation via CAN bus (Craessaerts, Maertens, & De Baerdemaeker, 2005), robot design and testing for greenhouse applications (Belforte, Deboli, Gay, Piccarolo, & Ricauda Aimonino, 2006), direct application end effector for a precise weed control robot (Jeon & Tian, 2009), automatic X-ray quarantine scanner and pest infestation detector for agricultural products (Chuang et al., 2011), assessment of forage mass from grassland swards by height measurement using an ultrasonic sensor (Fricke, Richter, & Wachendorf, 2011), and robotics software frameworks for multi-agent robotic systems development (Iñigo-Blasco, Diaz-del-Rio, Romero-Ternero, Cagigas-Muñiz, & Vicente-Diaz, 2012).

1.3. Progress of robotic research

1.3.1. Robotic research in Japan

Japan as one of the pioneers in the robotic technology could successfully occupy this technology in daily life. Most of the current robotic technology in our daily life is owing Japanese and American researchers. Many of the Japanese robots have used in the distinct aspects of today's life as humanoid entertainment robots, social robots, guard robots, industrial robots, and agricultural robots. The Robotics industry plays a significant role in Japan as well as other countries. Japan employs over a quarter of a million industrial robot workers. In the next 15 years, Japan estimates that number industrial robot can jump to over one million and they expect revenue for robotics to be near $70 billion by 2025. According to the last report of The Robotics Society of Japan, classification all Japanese robotic research include 5 groups (RSJ, 2015): Integration and Intelligence, Manipulation, Locomotion, Sensing, Business. Figure 5 is the illustration the percentage of robotic studies in Japan. Obviously shown that percentage of each aspect has no significant difference (integration and intelligence by 22.01%, manipulation development by 22.01%, locomotion and localization by 22.1%, sensing and sensor fusion by 12.92%, and robotic research aimed for business by 22.97%). This result was the output of more than 340 Japanese papers evaluation in the case of journal and conference papers, websites, books. In the coming section, each aspect will discuss in detail.

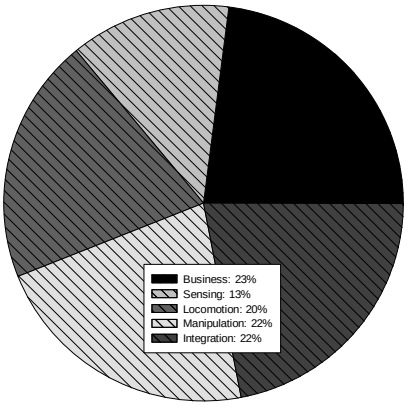

Figure 5: Robotics research percentage in Japan.

1.3.1.1. Integration and intelligent

The integration and intelligence are an inseparable unit of robotic technology. A robotic system without decisions unit is unimaginable. In 1970, Professor Masahiro Mori starts first steps to access intelligence by

a study on the Uncanny Valley in Tokyo Institute of Technology. The first contribution appeared in an obscure Japanese journal called “energy” in 1970. However, the concept of the uncanny valley has rapidly attracted interest in robotics and other scientific circles as well as in popular culture in 2005 (M. Mori, 1970, 2012). Ejiri, Uno, Yoda, Goto, and Takeyasu (1972) developed first intelligent robot in the central research laboratory in Hitachi company (Ejiri et al., 1972). This was the first intelligent robot in Japan that was demonstrated to the public at Hitachi’s Technology Fair in 1970. After two years, the development process of that robot finished. Aiming at the revolutionary advances in production technology for the future industry, a vision-based prototype intelligent robot was developed in 1970. This robot executed a variety of assembly tasks by responding to the assembly drawings shown to its eye (T. Goto, T., & Takeyasu, 1974; Uno, Ejiri, & Tokunaga, 1976). Masayoshi, Taketoshi, and Tadashi (1973) did a study on a memory structure and its application to a route-finding. In this study, an effective memory structure for an intelligent robot and a flexible route-finding algorithm based on the memory structure was discussed (Masayoshi et al., 1973). In 1973, Yoshiaki and Hirochika were succeeded to guide a robot by visual feedback in assembling tasks. This study has described the realization of assembly tasks with a hand-eye system by integrating a computer vision and a computer controlled manipulator. A vision system of ETL robot which was developed in 1970, analyzes a scene with a block and a box to make the line drawing and then computes their relative error of the position and that of the posture (Yoshiaki & Hirochika, 1973; Yoshiaki Shirai, 1971). In the same year, Kato et al. developed an information-power machine with senses and limbs (Ichiro Kato, Ohteru, Kobayashi, Shirai, & Uchiyama, 1973; S. O. Kato, H, K, & A, 1973; K. Shirai & Fujisawa, 1974).

Uno et al. (1976) developed an automatic bolting robot with visual and tactile sensors, which an automatic bolting robot for the concrete industry was developed before in 1973. This robot was used for automating the molding process of concrete piles and poles, and fastened bolts arranged side by side on the mold flange before pouring liquid concrete or loosened them after the concrete solidified (Takeshi, Masakazu, & Takeshi, 1976; Uno et al., 1976). In 1981, Tsutomu and Hasegawa developed an interactive system for modeling and monitoring a manipulation environment (Tsutomu Hasegawa & kameyama, 1989; Tsutomu Hasegawa & Terasaki, 1987; T. Hasegawa & Terasaki, 1988; Tsutomu & Hasegawa, 1981; h. Tsutomu, 1986). After 3 years, Ogasawara and Inoue (1984) design a total programming system for the integrated intelligent robot (Inoue, Ogasawara, Shiroshita, & Naito, 1981; Ogasawara & Inoue, 1984). At the same time, Shigeoki and Tomomasa (1984) published a paper in the title of "language directed master-slave manipulation method". This system incorporates a high-level robot language with a master-slave manipulator system. A new teaching-operating method named LARTS/T using Language Directed Mater-Slave Manipulation (LDMSM) was presented. The LARTS/T allows the operator to use language instruction and the master-slave operation cooperatively while preserving the merits of each (Hirai & Sato, 1984; Sato & Hirai, 1987; Shigeoki & Tomomasa, 1984).

Masayuki and Hirochika (1985) developed hand-eye coordination in rope handling (Masayuki & Hirochika, 1983, 1985, 1987) and M. Hideo, Shinji, Hiroshi, Satoshi, and Yukiko (1987) developed Self-contained mobile robot in campus road. A stereotyped motion by sign pattern was drawn from a study of lower animal which was applied to mobile robot “Harunobu” (M. Hideo et al., 1987; Jansson, 1990; kotani, Mori, & Charkari, 1996; H. Mori, Charkari, & Matsushita, 1994; Seiichi, 1995; Tinbergen, 1951). Ohteru, Shirai, and Narita (1985) developed the robot musician (Fujisawa, Seki, & Narita, 1985; I. Kato et al., 1987; Matsushima, Kanamori, & Ohteru, 1985; Ohteru et al., 1985; K. Shirai, Kobayashi, Iwata, & Fukasawa, 1985; Sugano, Tanaka, Ohoka, & Kato, 1985) and S. Fukuda and Arimoto (1989) developed fast interference check method using octree representation (S. Fukuda & Arimoto, 1989; H Noborio & Arimoto, 1989; H. Noborio, S. Fukuda, & S. Arimoto, 1987a, 1987b; H Noborio, S Fukuda, & S Arimoto, 1987; H. Noborio, Fukuda, & Arimoto, 1988a, 1988b). In 1988, Kawamura et al. (1986) presented the realization of high-speed and high-precision robot motion using iterative learning control (Sadao Kawamura, Fumio Miyazaki, & Suguru Arimoto, 1986; Sadao Kawamura, Fumio Miyazaki, & Suguru Arimoto, 1986).

Michitaka Kameyama, Egami, and Higuchi (1988) developed a high-speed coordinate transformation LSI for manipulators. An LSI for high-speed inverse kinematics computation was developed for robot manipulators. The computation time of a special purpose processor which was composed of the chip and a few memory chips was approximately 50μsec for a typical six degree-or-freedom manipulators (Michitaka Kameyama et al., 1988; Michitaka Kameyama, Matsumoto, Egami, & Higuchi, 1989, 1991). Tomomasa, Toshihiro, and Shigeoki (1991) designed a telerobot system featuring man-robot cooperative task execution. This study was a new teleoperation system where man and robot cooperatively execute tasks (Sato & Hirai, 1987; Shigeoki Hirai, 1984; Shigeyuki Hirai, 1990; Tomomasa et al., 1991; S. H. Tomomasa Sato, 1986, 1987; S. H. Tomomasa Sato, Toshihiro Matsui,, 1991). Several researchers developed the various system in this period, for instant: T. Hasegawa developed an integrated robot system with a geometric environment model and manipulation skills (Tsutomu Hasegawa & kameyama, 1989; T Hasegawa et al., 1990; T Hasegawa, Suehiro, & Takase, 1991; Suehiro & Takase, 1988, 1990); Hirohisa et al. developed a general algorithm for deriving constraint of contact between polyhedra from geometric model (Hirohisa, Toshihiro, & Kunikatsu, 1991a, 1991b; Hirukawa, Matsui, & Takase, 1994); and Kuniyoshi et al. developed generating robot command sequences based on real-time visual recognition of human pick and place actions.

“Teaching by Showing” was a straightforward teaching method in which a human instructor shows an assembly task to a robot by simply performing it with his own hand, and the robot automatically generates a program by watching the example task. For such a method to be realized, visual recognition of human action sequences becomes a crucial issue (Kuniyoshi, H, & M, 1991; Y. Kuniyoshi, 1995; H. I. Y. Kuniyoshi, 1993; M. I. Y. Kuniyoshi, H. Inoue,, 1994). Yun-Hui and Suguru (1990) designed a motion planning based on local sensor information for two mobile robots amidst unknown environments on the basis of local information from their sensors (S. A. Y. H. Liu, 1990; S. K. Y. H. Liu, T. Naniwa, H. Noborio, S. Arimoto,, 1989; Yun-Hui & Suguru, 1990). Katsushi and Takashi (1993) found a task model for assembly plan from observation system. They have been developing a system which observes a human executing an assembly task, recognizes the task, and generates a robot program to achieve the same task (Jun & Katsushi, 1996; Katsushi & Takashi, 1993; K. I. Takashi SUEHIRO, 1993). Kazuo, Yoshitsugu, Toshiaki, Shoichi, and Tadashi (1994) developed a 3-DOF parallel mechanism and application to space-borne smart end-effector to develop a smart end effector which added the dexterous capability to a long space manipulator arm (Kazuo et al., 1994; Machida, Toda, Iwata, & Komatsu, 1992). H. Kobayashi, Hara, Uchida, and Ohno (1994) studied on the face robot for the active human interface. They developed the face robot which has a human-like face that was able to express human-like facial expressions. Tomomasa, Yoshifumi, Junri, Yotaro, and Hiroshi (1995) studied on an active understanding of human intention by a robot through monitoring of human behavior. This study proposes a new function of active understanding of human intentions by a robot through monitoring of human behavior and proposed a robot architecture to realize the function.

Jun and Katsushi (1996) developed a vision-guided robotic operation titled “task-oriented generation of visual sensing strategies”. In the proposed method, using the task analysis based on face contact relations between objects, necessary information for the current operation was first extracted (Jun & Katsushi, 1996, 1998; Katsushi & Takashi, 1993; Miura & Ikeuchi, 1999). Satoshi, Masayuki, and Hirochika (1997) developed construction and implementation of a software platform in remote-brained robot approach; and Mitsushige (1997) developed a coordinated control of the satellite's attitude and its manipulator - stability of the satellite attitude against the robot arm motion (M. Oda, 2000; Mitsushige, 1997). In 1999, Takushi et al. was presented a mobile robot navigation by a distributed vision system which a general infrastructure for robot navigation in an outdoor environment which called a distributed vision system, consists of vision agents connected with a computer network, monitors the environment, maintains the environment models, and provides various information for robots by organizing communication between the vision agents (G, H, & T, 1997; Ishiguro, 1997; Ishiguro, Tanaka, & Ishida, 1996; Sogo, Ishiguro, & Ishida, 1999; Takushi, Katsumi, Hiroshi, & Toru, 1999). Ikuta et al. designed a general evaluation method of safety strategies for

welfare robot (Ikuta, M, & H, 2000; K. Ikuta & Nokata, 2001; K. Ikuta, Nokata , & Ishii, 2001; K. Ikuta, Nokata, & Ishii, 2001; M. N. Koji Ikuta, 1998, 1999a, 1999b; M. N. Koji Ikuta, Hideki Ishii,, 2001).

Kazuo, Yoshitsugu, Tatsuo, and Satoru (2000) published a paper titled "precise task execution and tele-sensing in space by sensor-fused telerobotics". Namiki Akio and Masatoshi (2000) studied on optimal grasping method by using visual and tactile feedback (Namiki Akio & Masatoshi, 2000; Namiki Akio, Nakabo Yoshihiro, Ishii Idaku, & Ishikawa Masatoshi, 1999; Namiki Akio, Nakabo Yoshihiro, Ishii Idaku, & Ishikawa Masatoshi, 1999; Namiki Akio, Yoshihiro, Idaku, & Masatoshi, 2000; Nakabo, Ishii, & Ishikawa, 1997; Ishikawa Watanabe, 2015). Masahiko et al. developed RSNP (robot service network protocol), targeting a robot service platform in diffusion period (Masahiko et al., 2009; Masahiko NARITA, 2010; Masahiko NARITA, Yoshihiko MURAKAWA, 2011; Yuka KATO). In the next year, Japanese scientific present more research. Arimoto, Sekimoto, Hashiguchi, and Ozawa (2005) presented a natural resolution of ill-posedness of inverse kinematics for redundant robots which was a robot designed to mimic a human becomes kinematical redundant; Shinichiro et al. reproduced human dance motions by a biped humanoid robot which they achieved the way of the motion generation for the whole-body motions of a biped humanoid robot (Shin'ichiro Nakaoka, 2007; Shinichiro et al., 2005; Shinichiro Nakaoka, 2006); and Susumu studied on mutual tell existence communication system transmitting both presence and existence (Susumu, Naoki, Hideaki, Kouichi, & Kouta, 2008; Susumu Tachi, 2006).

In 2006, Tomomasa et al. studied on modeling, recognition and supporting trajectory generation of daily object-handling based on acquired motion models. The system was composed of such algorithms as object handling motion clustering, human motion recognition, assisting task prediction and trajectory generation, which was learned from human motion (Tomomasa, Hideyuki, Tatsuya, & Taketoshi, 2007). Emmanuel, Vander, and Yasuyoshi (2007) developed a rigid virtual world through an impulsive haptic display. Ryo et al. (2008) studied on CPS slam - 3D laser measurement system for large-scale architectures to aim of design robot town project. They had proposed a new approach to an intelligent robot working within an everyday environment to support human life. The also developed an informationally structured environment "Robot Town", where vision, other sensors, and RFID tags are distributed and are connected to the network (Kouji Murakami, 2008; Ryo, Yukihiro, Kouji, & Tsutomu, 2007; Tsutomu Hasegawa, 2008).

In 2009, a motion-copying system was developed by Seiichiro et al. and published a paper in the title by stability analysis and experimental validation of a motion-copying system. Haptic technology makes it possible to preserve and reproduce human motion using a paired master and slave system (Noboru Tsunashima, 2009; Seiichiro, Yuki, & Kiyoshi, 2009). The "Throwing & Batting Robot" project was developed by Masatoshi et al. They developed a high-speed vision system with the sampling rate of 1 kHz, which leads to direct and stable sensory feedback control of actuators. In addition, they have developed new high-torque mini actuators and the high-speed multi-fingered hand with these incorporated (Senoo, Namiki, & Ishikaw, 2008; Senoo, Namiki, & Ishikawa, 2004, 2006; Taku Senoo, 2006).

In 2011, Joo-Ho Lee developed a human-centered information transfer robot. The main goal of this research was realizing an active information display system which could afford a human-centered information transfer method (J.-E. Lee et al., 2012). Tarou et al. developed a principle for continual autonomous learning in open-ended environments called "self-regulation mechanism". That study considered learning progress only when the learner is exposed to an appropriate level of uncertainty (Tarou, Ichirou, & Jirou, 2011). Also, Atsushi, Ryo, Daisuke, and Ryohei (2010) realized fully autonomous brain-machine hybrid system using an insect brain. They have created a brain-machine hybrid system which could solve the chemical plume tracing problem using a micro brain of a male silkworm moth. The purpose of the system was to investigate adaptability which was derived from interactions between the micro-brain, body, and environment (Atsushi et al., 2010; Minegishi, Takashima, Kurabayashi, & Kanzaki, 2012).

Finally, in 2012, Takaya et al. developed online object categorization using multimodal information autonomously acquired by a mobile robot. They had proposed a framework for object concept formation based on multimodal categorization by robots using statistical models (Takaya et al., 2012; Takaya Araki, 2012). Kahori et al. developed EMG-to-motion classification for prosthetic applications which was a self-organizing approach with the level of proficiency which was aimed to enhance the control of prosthetics by discriminating between different types of motions from their EMG signal (Kita Kahori, Kato Ryu, & Yokoi Hiroshi, 2010; Kita Kahori, Kato Ryu, & Yokoi Hiroshi, 2010).

1.3.1.2. Manipulation

The first Japanese practical research on Manipulators was started by Mori and Yamashita at the University of Tokyo in 1964. They have researched on finger function and presented a paper was titled by "mechanical fingers as control organ and its fundamental analyses" (M. M & T, 1964; Tadashi Yanmashita, 1964). In 1970, Hirochika developed a computer-controlled bilateral manipulator (Hirochika, 1971). In 1974, Nakano et al developed a co-operational control of the anthropomorphous manipulator which aimed to achieve manipulation of objects, without human intervention and automatically (Nakano, Ozaki, Ishida, & Kato, 1974). In 1975, Shigeru developed a cooperation control of pair artificial hands (S.Fujii & S.Kurono, 1975). Hideo et al. studied on gripping mechanics form by artificial fingers (H. Hideo & Haruhiko, 1976). Takase presented a paper in the title of "generalized decomposition and control of a motion of a manipulator" (K.Takase, 1977; Kunikatsu Takase, 1976). After 3 years, Okada developed an object-handling system for manual industry. The system had three fingers and structures similar to human fingers (Tokuji Okada, 1979). Masaru studied on computer control of a mechanical arm motion in Tokyo University. An articulated robotic arm with 6 DOF was designed by Sumiji Fujii and made by Tokico company (Masaru Uchiyama, 1979a, 1979b, 1979c).

In 1981, Makino et al. were developed SCARA robot (Makino, Murata, & Furuya, 1982). In 1983, Hanafusa et al. were studied on redundancy analysis of articulated robot arms (H. Hideo, Tsuneo, & Yoshihiko, 1983). Between 1984 to 1985, Yoshikawa was researched on manipulability and dynamic hybrid control of robot manipulators (Tsuneo. Yoshikawa, 1984). In 1986, many research was performed on a flexible arm, master salve system, and manipulators application. Sakawa was modeled a controlling algorithm for flexible arms; Tatsuo and Nakano studied on teleoperation with configuration differing bilateral master-slave system; Haruhisa and Kunitoshi estimated parameter of robotic manipulators; and Nakamura had a research on mechanics of coordinative manipulation by multiple robotic mechanisms (T. Arai & Nakano, 1956; Haruhisa & Kunitoshi, 1986; Y. Sakawa, 1986). Tsusaka has developed a parallel manipulator (Yuji Tsusaka, 1987). In 1988, Kazuhiro has developed a virtual internal model following control (Kazuhiro Kosuge, 1988); Shinichi et al. were studied on the kinematics of manipulation using the theory of polyhedral convex cones and its applications to grasping and assembly operations (Shinichi Hirai, 1988). Zaho and Masaru were designed a flexible robot arm. They analyzed the mapping relation between the position and orientation of a flexible-robot-arm end-effector, the joint displacements, and link elastic deformations that affect the end-effector position and orientation, directly. The analysis was exploited to clarify the arm characteristics in the task.

In 1989, Koichi and Hirohisa designed and manufactured a pneumatic flexible micro-actuator with an internal air chambers which were developed for small flexible robots (Koichi Suzumori, 1989; S. I. Koichi Suzumori, Hirohisa Tanaka,, 1986-7); Arai and Tachi developed a position control for a manipulator composed of active and passive joints (H. Arai & Tachi, 1991; Hirohiko & Susumu, 1989). In 1990, Suehiro and Takase developed a skill-based manipulation system (Takashi Suehiro & Kunikatsu Takase, 1990). In 1991, Yushida was controlled multiple-manipulators in space robots (Kazuya Yoshida, 1991). In 1992, Mitsubishi company was manufactured a user-friendly manufacturing system for hyper-environments (M. Mitsuishi, 1992); and Kotoku et al. were studied on bilateral master-slave teleoperation using virtual environments (Tetsuo Kotoku, 1992). Kawamaru et al. developed an ultrahigh speed robot falcon using parallel wire drive systems in 1994 (Kawamura, Choe, Tanaka, & Kino, 1997; Tetsuya Morizono, 1997). At the same year, development of a 6-DOF high-speed parallel robot and his group and bilateral control of

master-slave manipulators for ideal kinesthetic coupling -formulation and experiment by were presented by Uchiyama and Yokokohji, respectively (Y.Yokokohji & T.Yoshikawa, 1994). One year after, Uchiyama et al. presented a prototype was a very fast 6-DOF parallel robot (Masaru Uchiyama and Ken-ichi Iimura, 1992; T. S. Masaru Uchiyama, Kazuyuki Masukawa,, 1996).

In 1995, Omato and Nagata studied on statics of power grasps with a multifigured hand (Toru Omata, 1995); and Maekawa et al developed a manipulation of an unknown object by multi-fingered hand with the rolling contact using tactile feedback. The proposed control algorithm was capable of determining the motion of each finger so that the object was manipulated along the desired trajectory according to the tactile feedback at the fingertip of the hand. (Hitoshi, Kazuo, & Kiyoshi, 1995). In 1995, Nakmura had a theoretical design a non-holonomic manipulator (Yoshihiko Nakmura, 1995). In 1997, Tatsuo and Tamio developed a dexterous two-fingered micro hand as a total micromanipulation system. They would like to handle and manipulate a micro-object within the size of 1 to 100 μm (Tamio Yanikawa, 2002; Tanikawa & Arai, 1999); and Saku et al. developed a pulse-driven induction-type electrostatic film actuator (Saku Egawa, 1997). In 1997, Kitagaki et al. developed a sensor based parallel processing manipulation system (Kosei Kitagaki, 1997).

In 1999, Nakamura et al. were researched on a dynamics computation of structure-varying kinematic chains and its application to human figures (Yoshihiko Nakamura, 1998). In 2000, Hirata et al. handled a single object by the distribution of robot helpers (Yasuhisa Hirata, 2003). In 2002, Fumihito et al. developed a non-contact micromanipulation by bilateral control. And also they proposed a transportation of a microbe with micro tools trapped by the laser for safe (F. Arai, Ogawa, & Fukuda, 1999; Fumihito, Masanobu, & Toshio, 2002). In 2003, Hirohiko developed a human interface for maneuvering non-holonomic systems which utilized for human ability (Hirohiko, 2003). In 2005, Takeshi and Toru proposed a load-sensitive variable transmission for robot hands (Takeshi Takaki, 2005, 2006). In 2008, Keisuke evaluated the mobility of robotic mechanisms using computer algebra within three steps: (1) express the geometrical constraints in a mechanism based on the dual quaternion expression and form simultaneous algebraic equations (SAE) that comprise constraint equations, (2) calculate Groebner basis of the SAE, wherein the variable order is specified such that the joint variables are greater than the hand variables and the term order is specified as lexicographic, and (3) determine mobility by determining the variables that can be freely specified (Keisuke Arikawa, 2009).

At the same time, Kenta et al. developed a robotic hand that folds an origami form “Tadpole”. They published a paper in the title of "desired trajectory and sensory feedback control law synthesis for an origami-folding robot based on the statistical feature of direct teaching by a human"(Kenta Tanaka, 2009). In 2009, Kosuke et al. developed a magnetic resonance (MR)-compatible compact surgical robotic system (Kosuke Kishi, Hidekazu Nakamoto, 2007; Kosuke Kishi, Masakatsu G Fujie, Makoto Hashizume, Ichiro Sakuma, Takeyoshi Dohi, 2009). Kota et al. developed a robot hand with low backlash and a prototype mechanisms of a light-weight robot hand and evaluation of the mechanisms (Anzawa, Sasaki, Jeong, & Takahashi, 2010). Namiki developed another unique high-speed robot in 2011, which exceeds human capabilities (A. N. Yuji Yamakawa, Masatoshi Ishikawa, Makoto Shimojo,, 2009). In 2012, Jumpei et al. development an outer shell type 2 DOF bending manipulator using a spring-link mechanism that included spring elements in its kinematic structure (Jumpei Arata, 2011).

1.3.1.3. Locomotion

In 1975, Masahiro Mori developed Triops Congregations Masahiro (Three-eyed Beatles) which consists of seven small robots with same electronic circuits and mechanical parts. The author supposed that they were the first autonomous distributed system in the world (Sueo Matsubara, 1975). A control theoretic study on dynamical biped locomotion had done 5 years later by Miyazaki and Arimoto (1980). In this study, the case divided into two modes with respect to time scale, fast and slow modes. these modes dynamical control of biped locomotion was developed. In 1977, Kiyotoshi Matsuoka had some studies on hopping and

running mathematical model of human and animals, however, a lot of studies had been accomplished for walking models, but there were not any running and hopping models for human and animal bodies till that time (Matsuoka, 1977). Shigeo et al. bring up an active cord mechanism with oblique swivel joints and its control system. At the same time, Toshihiro et al. developed a vessel automatic guidance control based on route course commanding on the map in 1981 (S. Hirose, 1981; Shigeo Hirose, 1981). Hirofumi and Isao (1984) implemented a dynamic model of biped structure on their small handmade robot. In 1984, another study had done on robot locomotion dynamic while it was a low order model with hierarchical control system strategy (Junji Furusho, 1983).

Tachi, Tanie, Komoriya, Hosoda, and Abe (1981) started a 6 years' study based on their proposal that was provided in 1975 which was a guide dog robot called MELDOG. This research had done based on conceptualization, invention, and feasibility for guide robot to help and guide people who had visually impaired. One year later Hirose, Fukuda, and Kikuchi (1985) developed a control system for a quadruped walking vehicle in Tokyo Institute of technology. Ohmichi and Ibe (1984) conducted a project to build up a hybrid walking system with wheels and legs at Mitsubishi heavy industries. Kimura, Shimoyama, and Miura (1988) did another study on quadruped robot walking dynamics at Tokyo University in 1988. In the next year, Juniji Furusho, Sano, and Goto (1989) had accomplished a study of dynamic control of quadruped robots with a different mechanism which was based on the free movement on gravity field. A study of the brachiation type of mobile robot was done by T. Fukuda, Hosokai, and Kondo (1990). A nonholonomic path planning space robots with Bi-directional approach was performed in 1991. Hirose, Morishima, Tsukagoshi, Tsumaki, and Monobe (1991) designed a snake like a vessel with an articulated body that the mobile robot called KR II. Yamafuji, Kobayashi, Kawanura, and Kondo (1992) released first reports of their research which were done for Brachiation type of mobile robot dynamics and simulations. A leg-wheel robot was developed by Hiroshi Kimura et al (1991) and their main target was the cooperation of legs and wheels to obtain more flexibility and efficiency in mobile robot locomotion. Asama, Ozaki, Matsumoto, Ishida, and Endo (1992) had done a study in the field of task assignment by multiple autonomous robots. In 1993, Masakatsu Fujie et al had been built a quadrupedal walking robot for the hazardous environment (Fujie, 1993; Sakakibara, Kan, Hosoda, Hattori, & Fujie, 1990).

Shigeru Fujiwara et al. manufactured an articulated multi-vehicle robot for monitoring and testing in the pipe (Fujiwara, Kanehara, Okada, & Sanemori, 1994; T. Okada & Sanemori, 1987). A dynamic biped walking control system for uneven terrain was proposed by S. Kajita and Tani (1995). This control system was based on the linear inverted pendulum and an ideal biped robot with massless legs was assumed. Yamaguchi, Kinoshita, Takanishi, and Kato (1996) expanded a walking control system for robots by developing a biped walking robot which was adapted to the unknown uneven surface and had a special foot mechanism for controlling method. Miyagawa, Suzumori, Kimura, and Hasegawa (1999) built a micro inspection robot for small piping. In 2000, Gen and Shigeo presented Leg-Wheel hybrid vehicle roller-walker however many studies were done on and were on the progress in mentioned time but in most of the cases, the waking mechanisms were developed by walking and rolling for taking advantage of moving on the irregular ground and smooth terrain. (Gen & Shigeo, 1998, 2000, 2012). HONDA began the research of the consumer robot as the next commodity to automobiles in 1986 (Yoshino, 2000). They started with stabilization research by walking on the uneven floor. Kimura, Fukuoka , and Konaga (2001) built a quadruped robot, to walk dynamically on the irregular terrain by using a nervous system model. In 2004, Takayama and Hirose (2004) proposed a new kind of propulsion principle for the underwater active cord mechanism, in which each articulated body segment creates distortion motion while keeping the whole body in a helical shape. Mae, Takahashi, Arai, Inoue, and Koyachi (2004) developed a new Limb mechanism robot named "ASTERISK" in 2004. ASTERISK had 6 limbs which each had 4 DOF. Shuuji Kajita et al. (2004) introduced a method to generate whole body motion of a humanoid robot in 2004 (Hyon, 2009; Hyon & Cheng, 2006; yon, Hale, & Cheng, 2007).

In 2006, Hyon et al. (2011) proposed a practical contact force control framework for force-controllable legged robots with redundant joints, which was applicable to automatic/semi-automatic control of mobile

robots, construction robots, bipedal humanoid robots, and assistive devices. Thereafter in 2009, the researcher applied the method to hydraulic biped humanoid robots, quadruped robots and exoskeleton robots (Tokuji Okada, Tanaka, Botelho, & Shimizu, 2011). Tokuji Okada et al. (2011) designed a concept for renovating a legged robot to a hybrid mobile robot of minimal 4 DOF and its motion analyzes for switching locomotion from leg-type to wheel-type and vice versa. Hyon et al. (2011) proposed novel exoskeleton robot prototypes aimed to brain-machine-interface-based rehabilitation for biped locomotion and postural control for elderly people, people with spinal cord injury, stroke patients, and others with similar needs.

Nishiwaki and Kagami (2011) developed a method for autonomous navigation of a humanoid over unknown rough terrain by the integration of online perception, footstep planning, and walking control. Hidetoshi et al. (2010) proposed a cooperative step climbing and descending technic with using a wheelchair and a partner robot. The robot used in this research was the wheeled "Tateyama" which was developed in the Ikeda laboratory. A new dynamic rolling-walk motion for a multi-legged robot with sensory compensation was proposed by Chayooth, Takubo, Ohara, Mae, and Arai (2011). Toru Takenaka et al. proposed a method to generate running gait patterns for biped robots by using dynamics model that includes mass on feet, an inverted pendulum, and a flywheel. (Takenaka, Matsumoto, Yoshiike, & Shirokura, 2011). T. Okada, Tezuka, and Sasaki (2011) proposed a mechanism and control of a wheeled skid-steering mobile robot equipped with six feet for each wheel. Luciano et al. (2013) presented a decentralized controller to guide a group of aerial robots to converge to and to move along a simple closed curve specified in a three-dimensional environment. Hiroaki, Taiki, Keita, and Fumio (2012) made a discovery that links with influential hypotheses that the CNS may produce movements by combining units of motor output.

1.3.1.4. Sensing

Based on the available references and according to the report of RSJ, the first robotic project in sensing aspect was done in 1971 in the title of "Pattern Recognition by the Artificial-Tactile Sense". Kinoshita et al. were presented a paper to proposes an artificial-tactile pattern recognition which was composed of the recognition by touching the object surface with the artificial-tactile sense and the recognition by grasping the object with the artificial-hand (Gen-ichiro, Kunikatsu, & Masahiro, 1971). In 1974, Ishii and Nadata were researched on feature determination of 3D objects with a laser tracker (Masaru Ishii, 1974). In 1976, Yoshiaki Shirai has presented a method which could recognize different kinds of objects in a gray image of a complex scene and named in "research on desk scene analysis" (Y. Shirai, 1976). In 1981, Ryosuke Masuda has developed a simple optical proximity sensor which was worked based on measuring the phase shift of modulated reflex light (Ryosuke Masuda, 1981). In 1982, Masatoshi Ishikawa has presented a method to measure the center position of a two-dimensional distributed load using pressure-conductive rubber (Masatoshi Ishikawa, 1981). In 1983, Masaki Oshima was a pioneer to develop a methodology for object recognition in a 3D environment (MasakiOshima, 1982). In 1984, Toshio Matsushita was the first researcher who was presented a robot vision language for detection and measurement of 3D objects (Toshio. Matsushita, 1984). In 1985, Katsushi Ikeuchi developed a gripper configuration in bin-picking tasks using the photometric stereo system and prism stereo system (Ikeuchi, Nagata, Horn, & Nishihar, 1985). In 1987, Hirochika et al. were developed a window control LSI chip for multi-window robot vision system (Hirochika, Hiroshi, Masayuki, Shigeki, & Fumihiko, 1989).

In 1988, Masaru Uchiyama has evaluated a robot force sensor structure by using singular value decomposition (Masaru. Uchiyama, 1987, 1991). At the same time, Kousuke et al. were developed a high-speed driven structured light projector which realized to apply a liquid crystal shutter to the projection system by using the below techniques (Kousuke. Sato, 1988). In 1991, Hiroshi et al. were presented a method which reconstructs a global map of the indoor environment from omnidirectional view obtained at several robot locations (Horoshi, Masashi, & Saburo, 1991). In 1993, Makoto Kaneko was studied on a 6-axis force sensor design based on combination theory (K. Makoto & Toshiharu, 1993). In 1995, Ivan Godler developed an angular acceleration sensor (I. Godler, A. Akahane, T. Maruyama, & T. Yamashita, 1995).

In 1995, Nobuyuki has developed a real-time binocular tracking system based on virtual horopter (Kita, Rougeaux, Kuniyoshi, & Sakane, 1995); and Yasushi Yagi developed a real-time omnidirectional image sensor (Yagi, 1995). In 1997, Takeo Kanade has developed a video-rate stereo machine (Kanade et al., 1997). In 1997, Natsuki Terada developed a tensor cell tactile sensor utilizing multimode acoustic resonance (Terada, Shinoda, & Ando, 1997); and Yoshihiro Nakabo has presented a target tracking system by using parallel processing vision (Nakabo et al., 1997).

In 1999, Masayuki Inaba has developed a full-body tactile sensor suit which electrically conductive fabric (Masayuki Inaba, 1998). In 2001, Takashi Maeno has developed a curved elastic finger for grasp force control. This method was suited to control the grasping force when objects were grasped by artificial elastic fingers (Maeno, Hiromitsu, & Kawa, 2001). In 2005, Tokuji Okada was present a method to measure the acceleration of motion and gravity in 3D space (K. K. Tokuji Okada, 2005). In 2006, Tomohiro et al. were proposed a non-contact stiffness imager which should enhance the definition of a stiff point by imparting a fluid force to the environment (Makoto Kaneko, 2003; M. K. Tomohiro Kawahara, 2005; S. M. Tomohiro Kawahara, Shinji Tanaka, Makoto Kaneko,, 2006). In 2007, Yoshihiro has developed a time-sequential high-frame-rate 3D sensing system for moving and deforming objects (Yoshihiro Watanabe, 2007). In 2008, Hiromasa et al. developed high-speed optical components for robot vision (Hiromasa, Takahiko, & Masatoshi, 2009; Kohei Okumura, 2011). In 2012, Shanhai Jin has proposed a sliding mode filter for removing various noise (Shanhai Jin, 2012, 2014); and Yuji et al. were presented a 3D shape recognition and measurement (Yuji Ichimaru, 2011). In 2013, Jeong Yongjin et al. was developed a method for global localization for a mobile robot using a large-scale 3D environmental map and RGB-D camera (Jeong Yongjin, 2012, 2013).

1.3.1.5. Business

Unimation by J. F. Engelberger was the world first industrial robot in practice which was developed in 1969. In 1968 Kawasaki heavy industries Ltd. had a technical association with Unimation after evaluating the robot as a creative and promising machine and in 1969. The first industrial robot in Japan was born with the first Kawasaki Unimate. The Kawasaki heavy industries introduced the first industrial robots in 1990 (Akashi, 1990). After 2 years, the Kawasaki heavy industries started to introduce a large scale of spot welding robots in car assembly. As in the 70s, Kawasaki heavy industries manufactured a robot undertook a task of replacing the earlier manual spot welding with robot spot welding in cooperation with car body production engineers. In 1972 they delivered the first robotized spot welding line in Japan (Akashi, 1990).

In 1973, Yaskawa electric corporation shipped their first fully electrically-driven, vertically-articulated MOTOMAN robot to an automobile parts manufacturing company. After some improvements, the first Japanese fully electrically-driven robot was developed in 1973. In the 1970s, Yaskawa focused on arc welding applications and developed the first MOTOMAN robot for arc welding with high-accuracy and smooth movement. Within twenty-four years since the first shipment of the MOTOMAN robot, Yaskawa Electric has continued to improve the performance of its MOTOMAN robots and developed a wide range of robot models to meet the needs of ever-expanding robot applications, so that the total number of shipped robots was reached to 70,000 units in 2001 (Itsuro Matsumoto, 1978). After that, the industrial robots had rapidly been spread into the market from the 1970s, when the typical application was spot welding for the automotive industry. Automation of arc welding, which needs continuous path control, had been delayed due to the complexity of path teaching and the difficulty of individual error correction of workpieces.

In 1973, Hitachi Ltd. was succeeded to develop first transistor assembly system. This system was able to automatically detect electrode positions on tiny transistor chips (Kashioka, Ejiri, & Sakamoto, 1976). In 1975, Akira et al. developed an intelligent arc welding robot named “AROS-san” (Yutaka Yakano, 1975). In 1976, Goto et al. designed a control algorithm for precision insert operation robots (T Goto, Takeyasu, & Inoyama, 1980). In 1978, Toshiba Corporation and Fujitsu established SCARA robot which was at the SCARA study group which means “selective compliance assembly robot arm”. In 1982, Yoshitaka developed a personal micro robot named “move master”. it has been launched in 1982, as a table-top

personal robot for education, research, and hobby. Its first series “RM-101” was a novel original robot that could be controlled by a personal computer through a Centronics printer cable. The “move master” was widely exported to the world because it was affordable and was easy to use (Sawada & Kanohara, 1982). In 1984, Iwamoto et al. developed an intelligent mobile robot with transformable crawler (Iwamoto, Yamamoto, Fujie, & Nakano, 1984) and in 1985, Ohtsu et al. developed biped walking robot WHL-11 (I Kato, Fujie, Yoshida, Ichiryu, & Nakano, 1986). In 1989, Watanabe et al. developed a teleoperation system for space experiments (Ichiro Watanabe & Uchiyama, 1989).

In 1990, Ken and Takeo from Mitsubishi Heavy Industries developed a multifigured multisensory bilateral master-slave controlled manipulator system. After 4 years, in 1994 Yaskawa electric corporation presented a small actuator that contained a motor, encoder, and gear in a 30-mm square space named “Compliant Motion Control of Arm-Hand System” (Mayumi, 1994); Takashi et al. developed motion tracking processing system, named “tracking vision” (Morita, 1999). Onishi designed an open controller of the MHI PA-10 robot. MHI general purpose robot PA-10 had the layer structure and makes the I/F between layers simple and open to make the controller open (ONISH, 1998). In 1995, Yaskawa electric corporation and Kyushu electric corporation have been working together to develop a semi-automatic hot-line work robot system named "Phase II" (Yakabe et al., 1995). In 1996, Tomokazu et al. developed a method of initializing angle of the robot arm which has a reduction gear using an incremental encoder. They developed a new method of initializing angle of the robot arm which has a reduction gear using an incremental encoder (Tomokazu, Hiroshi, & Noriaki, 1998); and Masayuki designed new automated assembly cell for small volume production (T. M, 2001)

In 1996, various companies and institutions were developed several robots. Manabu et al. from Mitsubishi Co. studied on robot vision using stereo vision with random-dot pattern projection (Manabu, Kazuhiko, Tetsuji, Shin'ichi, & Shotaro, 1999); Shinsuke et al. from FANUC have innovative an automatic assembly system where a two-armed intelligent robot builds mini robots (S.Sakakibara, A.Terada, & K.Ban, 1996); Makoto et al. from Toshiba Machine Co. developed a force controlled finishing robot named “Valibo” (J. Makoto et al., 199); and Masakatsu et al. developed a walk training system and walk supporting system (Tomoyuki, Atsushi, Akihiko, & Shizuko, 1996). In 1997, Sony company announced the development of a prototype of a small autonomous quadruped robot, and in 1999, they started selling AIBO ERS-110 as a consumer product. It was costed 250,000 JPY, which was expensive as a consumer product. However, 3000 of AIBO were sold out in only 20 minutes through the internet in Japan.

In 1998, Tatsuno et al. from Toshiba company introduced a beach ball volley playing a robot with a human (Kyoichi, 2000). In 2000, Matsuyama et al. under the support of Mitsubishi electric corporation developed a small-size and high-precision robot with a closed-loop mechanism with an accuracy of 1mm (Matsuyama, 2001). Nakayama et al. developed motion-media contents sharing via audio which could vividly read the mail text with the neck motion inspired by the emotional words inside the text (Nakayama, Machino, Kitagishi, Iwaki, & Okudaira, 2005). Nakasha under supporting of Mitsubishi heavy industries developed of steam generator tube sheet walking robot “MR-III” and the present state of the automatic eddy current test system (Shusaku, 2000). In 2001, Takashi et al. from Fujitsu laboratories introduced to the public the “HOAP”. The HOAP series robots were an advanced humanoid robot platform (Jiang & Fumio, 2001). In the same year, Panasonic corporation presented omnidirectional power-assisted cart which could carry a heavy load of 600 kgf. It could not make it conscious of the existence of a motor but can be operated as easily as a shopping cart in a supermarket (Maeda, Fujiwara, Kitano, & Yamashita, 2002). After that, Kawasaki Heavy Industries, Ltd. developed a marking/cutting and welding robot systems for thick steel pipes which were used stadiums, steel tower and so on (M. Kobayashi et al., 2000).

In 2002, Naoyuki et al. from Fujitsu Ltd. developed an internet-based robot MARON-1 which was a robot specifically for home use which was a robot that can link with mobile phones via the Internet (Ueki et al., 2004). Masahiro et al. from Sony company proposed “entertainment robot AIBO” as a new robotics application aiming at a new entertainment in which a robot interacts with users in the real world. In 2003,

Kawasaki et al. developed “Anthropomorphic Robot Hand - Gifu Hand III” which was the world’s first anthropomorphic robot hand until that time. This had an almost same number of joints and degrees-of-freedom (DOF) as the human hand and was equipped with all servomotors within the hand frame. This robot hand had a thumb and four fingers with 20 joint and 16 DOF like a human hand, and the ratios of the link length of thumb to each finger were near to that of the human hand. (Kawasaki, Uchiyama, & komatu, 2000).

In 2004, Fujitsu developed another service robot called “Enon”. They developed Enon as a production-type service robot to provide services for people in offices or public places (Shinji et al., 2005; Y et al., 2005). Kawasaki heavy industries developed friction spot joining robot system. Friction Spot Joining robot system was developed by applying frictional heat to solve several problems (Yoshitaka, Mitsuo, Yasunori, & Kazumi, 2007). In 2005, Fujitsu laboratories from Kyushu network technologies and Manabu et al. developed an image recognition module for a common basis for next-generation robots (N. M & N, 2009). And Hitachi construction machinery by Ishii et al. developed double-arm working machine named “ASTACO”. In 2008, a 7-t-test machine began trials with a fire brigade for rescue use in disaster situations (Akinori, 2006). In 2006, Hisashi et al. developed a home-use robot “Miuro” which focused its application to “music”, and owner can enjoy on a daily basis (Hisashi et al., 2008). In 2007, Ichiro et al. designed a people-friendly interactive device named socially interactive teddy bear robot prototype that provided gentle support to bring people and ICT together in a wide range of situations (Ichiro, Takahiro, & Yoshihiko, 2007). Hideyuki et al. developed a human cooperation robot for assembly operation assist. Two assist robots for front/rear windows had worked at Takaoka Plant of TOYOTA since 2007 (Hideyuki, Naoyuki, Kuniyasu, Hitoshi, & Hideo, 2010).

In 2009, Aria et al. developed a force-controlled metal spinning machine for forming non-axisymmetric shapes (Hirohiko, 2010); and Ryosuke et al. designed a blood sample courier system with autonomous mobile robots (R et al., 2010). In 2010, Katsumi et al. developed an automated cell culture system (Nakashima, Hasunuma, Habata, & Kanazawa, 2012); Mitsubishi heavy industries by Noriaki et al. designed an advanced inlay system for inlet/outlet nozzles of reactor vessel of nuclear power plant (Shimonabe, Onishi, Ohira, Hinami, & Sugiura, 2012); and Panasonic corporation developed a head-care robot to make users more comfortable (Ando et al., 2013). In 2011, Panasonic corporation presented another production named “Telecommunication assist robot” or “HOSPI-Rimo” which was pseudo-nurse providing support, improving operation efficiency, and hence, allowing nurses to concentrate on core nursing duties (Panasonic, 2011). Finally, in 2012, Hitachi developed a single-passenger robot named “ROPITS (robot for Personal Intelligent Transportation System)” which could autonomously navigate pedestrian space within communities to support the short-distance transportation of the elderly or those with walking difficulties (Yuji, Masashi, & Kenjiro, 2010).

1.3.2.Robotic and industrial robotic arm progress in the world

Today, more than 1.1 million industrial robots are operating in the factories all over the world to reach the several goals as improving quality of work for employees, increasing production output rates, improving product quality and consistency, increasing flexibility in product manufacturing, and reducing operating costs. But, the first experience to think about a robotic system come back to 270 BC that an ancient Greek engineer named Ctesibus made organs and water clocks with movable figures. In 1961, the first industrial robot was online in a General Motors automobile factory in New Jersey that was called UNIMATE. In 1962, the first cylindrical robot was installed called Versatran. The first artificial robotic arm to be controlled by a computer was designed in 1963. In 1959, the first industrial robot in Europe was developed. In 1961, Unimation installed the first industrial robot at GM. The world’s first industrial robot was used on a production line at the GM Ternstedt plant in Trenton, NJ, which made door and window handle, gearshift knobs, light fixtures and other hardware for automotive interiors. In 1969, The GM installed the first spot-welding robots at its Lordstown assembly plant.

In 1971 Hirochika developed computer-controlled bilateral manipulator (Hirochika, 1971). Also, the Japanese Robot Association was established which was the first national robot association ever. The JARA was formed in 1971 as the Industrial Robot Conversazione, a voluntary organization. In this year, the first robot which has six electromechanically driven axes KUKA moved from using Unimate robots to developing their own robots. In 1973, Ichiro Kato from Waseda University developed the world's first full-scale humanoid robot called Wabot-1. The robot consisted of a limb-control system, a vision system, and a conversation system. The robot walked with its lower limbs and was able to grip and transport objects with hands that used tactile-sensors. This research led to various humanoid research in Japan and other countries, including Kato's own "robot musician". In 1974, Björn Weichbrodt developed the first fully electric, microprocessor-controlled industrial robot for ASEA, Sweden. The first minicomputer-controlled industrial robot comes to market in this year. The first commercially available minicomputer-controlled industrial robot was developed by Richard Hohn for Cincinnati Milacron Corporation. The robot was called the T3 that means the tomorrow tool. Also, in this year, the first arc welding robots go to work in Kawasaki developed a version of the Unimate to be used for spot-welding, fabricating Kawasaki motorcycle frames.

In 1974, Nakano et al got an acceptable result to cooperation control of the anthropomorphous manipulator (Nakano et al., 1974). In 1975, the Olivetti "SIGMA" a cartesian-coordinate robot, was one of the first used in assembly applications. The Olivetti SIGMA robot was used in Italy for assembly operations with two hands. In 1975, Shigeru developed cooperation control of pair artificial hands (S.Fujii & S.Kurono, 1975). After one year, In Hideo et al. studied on mechanics of gripping form by artificial fingers (H. Hideo & Haruhiko, 1976). At the same time, Takase presented "Generalized decomposition and control of a motion of a manipulator" (Kunikatsu Takase, 1976; Takase, 1977). In 1978, Programmable Universal Machine for Assembly (PUMA) was developed by Unimation / Vicarm, in the USA. Hiroshi was developed the SCARA-Robot (Selective Compliance Assembly Robot Arm) By virtue of the SCARA's parallel axis joint layout.

In Tokyo University, Masaru has finalized a study on computer control of motion for a mechanical arm (Masaru Uchiyama, 1979a, 1979b, 1979c). In1981, the world's first direct drive arm was developed by PaR Systems, USA (PaR 50th Anniversary, 2010). In 1981, Makino et al. developed SCARA robot, and in 1983 Hanafusa et al. studied on redundancy analysis of articulated robot arms and its utilization for tasks with priority (H. Hideo et al., 1983). In 1984, Adept co. was introduced the AdeptOne as first direct-drive SCARA robot Electric-drive motors connected directly to the arms eliminating the need for intermediate gear or chain system. In 1984 and 1985, research was conducted on manipulability and dynamic hybrid control of robot manipulators by Yoshikawa (Tsuneo. Yoshikawa, 1984). In1985, KUKA has introduced a new Z-shaped robot arm whose design ignores the traditional parallelogram. In 1986, several types of research were performed flexible arm, master-slave system, and manipulators application. Sakawa modeled control of a flexible arm; Tatsuo and Nakano studied on teleoperation with configuration differing bilateral master-slave system; Haruhisa and Kunitoshi estimated parameter of robotic manipulators and Nakamura had a research on mechanics of coordinative manipulation by multiple robotic mechanisms (T. Arai & Nakano, 1956; Haruhisa & Kunitoshi, 1986; Y. Sakawa, 1986). In 1987, Tsusaka developed a parallel manipulator (Yuji Tsusaka, 1987). In 1988, IFR/UNECE published the first global statistics on industrial robots. In 1988, Kazuhiro developed a virtual internal model following control system application to mechanical impedance control (Kosuge, Furuta, & Yokoyama, 1988). Shinichi et al. studied on the kinematics of manipulation using the theory of polyhedral convex cones and its applications to grasping and assembly operations (Shinichi Hirai, 1988).

At the same time, Zaho and Masaru designed flexible robot arms. They analyzed the mapping relation between the position and orientation of a flexible-robot-arm end-effector, joint displacements and link elastic deformations that directly affect the end-effector position and orientation. In 1989, Takeo Kanade was designed a direct drive arm. He also founded the world's first doctoral program in robotics, which he chaired from 1989-1993 at Carnegie Mellon. In 1989, Koichi and Hirohisa designed and manufactured a pneumatic flexible micro-actuator (FMA) which had internal air chambers was developed for small flexible

robots (Suzumori, 1989; Suzumori, Iikura, & Tanaka, 1986-7). Arai and Tachi developed a method of position control of a manipulator which was composed of active and passive joints (H. Arai & Tachi, 1991; Hirohiko & Susumu, 1989). In 1997, the first National Symposium on Industrial Robots was held in 1970 in Chicago, USA.

Yanikawa and Arai (1997) have been developed dexterous Two-fingered micro hand which was a total micromanipulation system. Egawa, Niino, and Higuchi (1997) developed a pulse-driven induction-type electrostatic film actuator. Kitagaki, Suehiro, Ogasawara, and Liu (1997) also developed a sensor based parallel processing manipulation system. In 1999, Nakamura, Yamane, and Nagashima (1998) were studied on dynamics computation of structure-varying kinematic chains and its application to human figures. In 1998, ABB company (Sweden) was developed the FlexPicker. It was the world's fastest picking robot based on the delta which could pick 120 objects a minute or pick and release at a speed of 10 meters per second, using image technology. In 1999, The Reis (Germany) introduced an integrated laser beam guiding within the robot arm Reis Robotics receives a patent on the integrated laser beam guiding through the robot arm and launches the RV6L-CO2 laser robot model. This technology replaces the need for an external beam guiding device thus allowing to use the laser in combination with a robot at high dynamics and no collision contours. In 2000, Hirata, Kosuge, Asama, Kaetsu, and Kawabata (2003) were handled by a single object by distributed robot helpers in cooperation with a human. They believed that a single mobile robot is not suitable for handling a large and heavy object because there is a limitation with respect to the size and the weight of an object handled by the single robot. To overcome this problem, they consider a human-robot cooperation using multiple mobile robots. Fumihito et al. (2002) were developed a non-contact micromanipulation by bilateral control. For safe and secure transportation of the microbe, they proposed to transport a microbe with micro tools trapped by the laser. Hirohiko (2002) was developed a human interface for maneuvering non-holonomic systems, which utilizes the human ability to maneuver easy systems. In 2004, the Motoman (Japan) was introduced the improved robot control system (NX100) which provided the synchronized control of four robots, up to 38 axes The NX100 programming pendant has a touchscreen display and is based on WindowsCE operative system.

In 2006, the Comau company (Italy) was introduced the first Wireless Teach Pendant (WiTP). All the traditional data communication/robot programming activities can be carried out without the restrictions caused by the cable connected to the CU. The KUKA (Germany) presented the first "Light Weight Robot" developed in cooperation with DLR, Institute of Robotics and Mechatronics. After 3 years, Keisuke evaluated the mobility of robotic mechanisms using a computer in 2008 (Arikawa, 2009). Tanaka, Kihara, and Yokokohji (2009) were developed a robotic hand that folds an origami form "Tadpole". They published a paper titled by "desired trajectory and sensory feedback control law synthesis for an origami-folding robot based on the statistical feature of direct teaching by a human". In 2009, Kosuke et al. developed a magnetic resonance (MR)-compatible compact surgical robotic system. This system used MR-guided navigation and can augment the surgeon's eye-hand skills that are limited by endoscopic surgery (Kishi, Fujie, Hashizume, Sakuma, & Dohi, 2009; Kishi et al., 2007). In 2010, the Fanuc company was launched the first "Learning Control Robot" FANUC's Learning Vibration Control (LVC) allows the robot to learn its vibration characteristics for higher accelerations and speeds.

In recent years, almost all robot systems have been designed with a primary goal of the emulation of human capabilities, and with less attention to pushing the envelope in terms of speed as mechanical systems. Some designed a high-speed multi-fingered robot hand system, which exceeds human capabilities (A. N. Yuji Yamakawa, Masatoshi Ishikawa,, 2012), some was developed various high-speed manipulations for catching of a raw egg, dribbling of a ball, pen spinning, dynamic regrouping of a cell phone, knotting of a rope, catching of a minute object, folding of a cloth, and rock-paper-scissors (Namiki Akio, Imai, Ishikawa, & Kaneko, 2003; Furukawa, Namiki, Senoo, & Ishikawa, 2006; Yamakawa, Namiki, Ishikawa, & Shimojo, 2009). Namiki et al. were developed another unique high-speed robot between 2003 to 2010 (Namiki Akio et al., 2003; Yamakawa et al., 2009). In 2012, Arata, Saito, and Fujimoto (2011) development an outer shell

type 2 DOF bending manipulator using a spring-link mechanism that included spring elements in its kinematic structure.

1.3.3.manipulator and end-effectors in farm use

In the Japan, Tanigaki, Fujiura, Akase, and Imagawa (2008) developed a cherry-harvesting robot (Figure 6). This system includes a 4-DOD manipulator, a 3-D vision sensor, an end effector, a computer, and a mobile device. The 3-D vision sensor was equipped with red and infrared laser diodes. Both laser beams scan the object simultaneously. By processing the images from the 3-D vision sensor, the locations of the fruits and obstacles were recognized, and the trajectory of the end effector was determined. Fruits were picked by the end effector while avoiding collisions with obstacles.

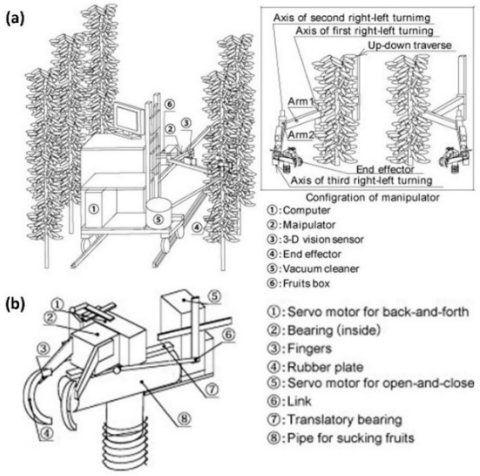

Figure 6: (a) Cherry-harvesting robot; (b) End Effector. It consisted of a fruit sucking device, an open-close mechanism, a back-and-forth mechanism, and a pair of fingers.

In Greece, Tanner, Kyriakopoulos, and Krikelis (2001) studied on an advanced agricultural robot specifically on kinematics and dynamics of multiple mobile manipulators handling non-rigid material (Figure 7). The equations of motion for a system of multiple mobile manipulators that handle a deformable object during an agricultural task was developed. The model is based on Kane's approach. The imposed kinematic constraints were included and incorporated into the dynamics. Sufficient conditions for avoiding tipping over of the mechanisms were also provided. The deformable nature of the object can easily accommodate a variety of agricultural products and the analysis allowed for the inclusion of specific handling limitations for the objects not to be damaged during manipulation.

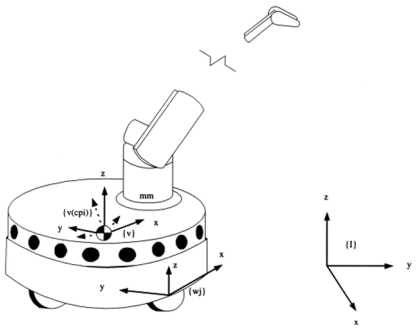

Figure 7: Frame assignment on mobile manipulator k.

In the Netherlands, E. J. Van Henten, Van't Slot, Hol, and Van Willigenburg (2009) designed an Optimal manipulator for a cucumber harvesting robot (Figure 8). The design objective was included the

time needed to perform a collision-free motion from an initial position to the target position as well as a dexterity measure to allow for motion corrections about the fruits. A four-link PPRR type manipulator was found to be most suitable. For cucumber harvesting four degrees-of-freedom, i.e. three translations and one rotation around the vertical axis, were sufficient. Although computationally expensive, the methodology used in this research was found to be powerful and offered an objective way to evaluate and optimize the kinematic structure of a robot to be used for cucumber harvesting.

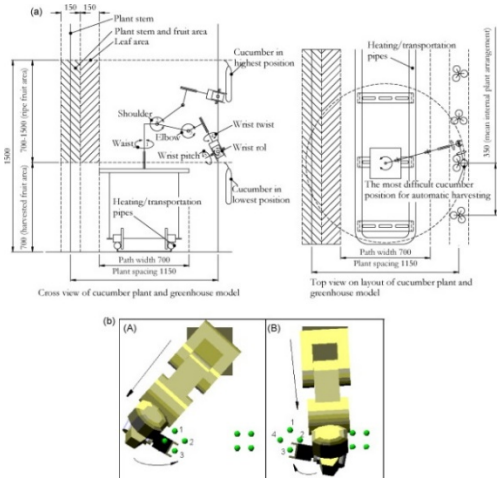

Figure 8: Manipulator choice based on two-dimensional (a) and quasi-three-dimensional (b) models of the working environment of the harvesting robot.

Zion et al. (2014) developed a harvest-order planning for a multi-arm robotic harvester. A multi-arm robotic harvester was developed for two-dimensional crops such as melons. The robotic arms reach down to pick melons and place them on adjacent lateral conveyors. The coordinates of the fruits to be harvested were assumed to be known prior to harvest so that the robot gets a bank of targets in local coordinates.

In Iran, Korayem, Shafei, and Seidi (2014) studied on the symbolic derivation of governing equations for dual-arm mobile manipulators used in fruit-picking and the pruning of tall trees (Figure 9). Mobile manipulators with only a single robotic arm have been successfully exploited in many agricultural tasks. The performance of these kinds of robotic systems has been improved by adding another robotic arm. However, for some agricultural applications such as pruning and fruit picking from tall trees, the number of links of each robotic arm should increase so that the arm can reach the target.

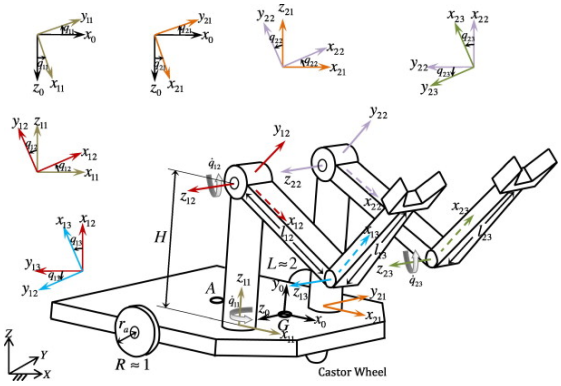

Figure 9: Dual-arm mobile robotic manipulator with symmetrical configuration.

Hu et al. (2014) simulated a dimensional synthesis and kinematics of a high-speed plug seedling transplanting robot (Figure 10). To improve the automation and efficiency of plug seedlings transplanting

in the greenhouse, a high-speed plug seedling transplanting robot was designed by using a 2-DOF parallel translation mechanism with a pneumatic manipulator. Based on the inverse kinematics of parallel mechanism, a global comprehensive performance index was proposed to synthesize a set of optimized dimension parameters for a good dynamic performance throughout the entire workspace.

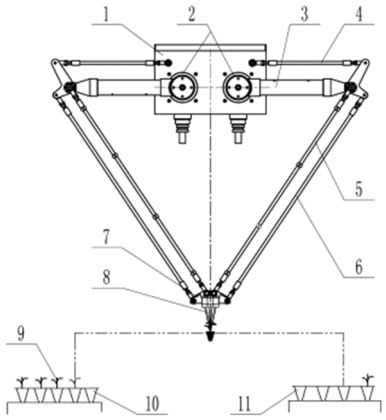

Figure 10: Sketch of plug seedling transplanting robot, (1) Frame, (2) Servomotor, (3) Inner active arm, (4) Outer active arm, (5) Inner followed arm, (6) Outer followed arm, (7) Moving platform, (8) Manipulator, (9) Plug seedling, (10) Supplying tray and (11) Planting tray.

In Spain, Blanes, Ortiz, Mellado, and Beltrán (2015) assessed of eggplant firmness with accelerometers on a pneumatic robot gripper (Figure 11). A pneumatic robot gripper capable of sorting eggplants according to their firmness has been developed and tested. The gripper has three fingers and one suction cup. Each finger had an inertial sensor attached to it. One of the fingers adapts to and copies the shapes of eggplants when the jamming of its internal granular material changes from soft to hard. The other fingers adapt to the shape of the eggplant with the use of extra degrees of freedom.

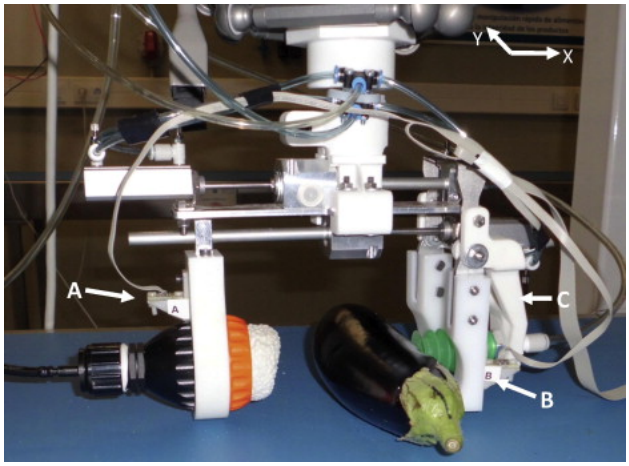

Figure 11: Robot gripper with inertial sensors.

1.4. Current situation of heavy-weight crops harvesting

Over the past few decades, the agriculture industry has faced new challenges. Previously, self-sufficiency in food and rural migration to cities were the significant concerns. With the advancement of science, however, more challenges now threaten the industry. One problem involves age distribution of farmers. According to global agriculture statistics, the average age of farmers is 65.9 years (SBJ, 2015), compared to 55.9 years old in USA (USDA, 2015), and 52 years old in Iran (Asadollahpour, Omidinajafabadi, & Jamalhosseini, 2014). With a declining farming population, the majority of farmers are

considered “too old” to handle the rigorous demands of the industry. Another issue is utilizing new agricultural technology; learning how to operate new technology requires time and physical effort, not to mention that the work itself is susceptible to unpredictable weather conditions. According to the last report from the Statistics Bureau of Japan, the number of laborers continues to decrease, from 20.33 million (30.2% of total workers) to 13.40 million (3.7% of total workers) over the period from 1960 to 2013. This problem and others have had a negative effect on agricultural output, which was 8.47 trillion yen in 2013, down 0.7% from 2012 (SBJ, 2015). Furthermore, based on the Global Agricultural Productivity report, agricultural production needs to increase by 100% over the next 40 years. Giver consumers’ changing attitudes toward organic products, the total income per commercial farm household has decreased (Global Harvest Initiative, 2013).

These problems represented only some of the challenges that agriculture currently faces. Smart technology is a potential answer aimed at solving such issues. In terms of technology, agricultural robotics can help address and solve the issues that farming communities encounter on a regular basis (Cassinis & Tampalini, 2007). Examples include a multi-arm robotic harvester (Zion et al., 2014), robots designed to harvest strawberries (Hayashi et al., 2010), apples (De-An et al., 2011), white asparagus (Barawid Jr, Mizushima, Ishii, & Noguchi, 2007), cherries (Tanigaki et al., 2008), tomatoes, petty-tomatoes, cucumbers and grapes (Kondo, Monta, & Fujiura, 1996). Stationary robots are used for sheep shearing (Tanner et al., 2001), wearable robots are available for agricultural work (Toyama & Yamamoto, 2009a), and robot tractors have been designed(Noguchi & Barawid Jr, 2011; C. Zhang et al., 2015). Most robotic laboratories have shown interest in studying a new generation of agricultural robots to solve the problems described above. Yet another concern is that most current agricultural robots were designed for light crops and fruits. For these machines, harvesting heavy products, such as pumpkin, watermelon, and melon, still, represents really hard work. Harvesting of these heavy crops is generally selective harvesting. This means it is not possible to harvest the entire product at the same time and has accepted to the market. In Japan, farmers are challenged to find workers to pick pumpkin and watermelon. Wearable robots (Toyama & Yamamoto, 2009a) are not helpful in this case because of the low number of workers. Another view is that it is better to modify farmer attitudes from “human-based harvesting (HBH)” to “human-lead harvesting (HLH)”. It is thought that HLH can help increase farming efficiency by altering harvest methodology towards human decision makers and robot controllers, instead of human workers.

As mentioned, heavy-weight crops are counted as time-consuming and hard-work harvesting plants, because of the rheology and physical behavior. Pumpkin, watermelon, melon, cabbage, and squash are considered in the list of heavy-weight agricultural productivity. The harvesting of this crops not only needed a powerful farmer but also current equipment is not appropriate for the precision harvesting of such crops. In the case of pumpkin harvesting, all harvesters are semi-automatic. These devices increase the damage possibility, financial loss, labor cost, chance of injury, and decrease the harvesting efficiency.

1.5. Research motivation

As mentioned, most of the current studies were focused on the small sized and light weighted crops. Although, the heavyweight crops like pumpkin, watermelon, cabbage, melon are playing a significant role in the marketing basket of most country’s people like Japan, USA, and Iran. This is even though the mentioned crops are expensively priced in Japanese markets. Based on this reason, development of a heavy-weight crops robotic harvesting system can be valuable. In this regard, this study was presented the development procedure and performance evaluation of a specially designed robotic system for heavy-weight crops harvesting.

1.6. Objectives

The objectives and originalities of this study are as follows:

- Development of an applicable low-cost robotic arm for farm use with optimized DOF.
- Development of an optimized controlling algorithm for a proper harvesting.

- Come up with economic evaluation and optimization of design robotic arm.
- Come up with DOF optimization methodology to select optimized DOF and joint structure.
- Development of a controlling system by using PLC system.
- Come up with accuracy, resolution and reputability evaluation of the system.
- Come up with unique rapid harvesting technique to improve harvesting cycle-time and efficiency of the system.
- Parametrization of physical and mechanical properties of pumpkin.
- Come up with a methodology for characterization of heavy-weight crops such as pumpkin.
- Development of a specifically designed end effector (EE) based on the properties of target crop (Pumpkin).
- Development of rapid harvesting methodology.
- Development of communication system: EE vs Robotic arm, and Robotic arm vs Robot tractor.
- Development of vision system for target crop recognition

The remainder of this thesis is organized as follows: Chapter 2 introduce the heavy crops robotic harvesting system including robot tractor, robotic arm, end-effector and controlling unit and their components. Chapter 3 explains the designed robotic arm development and related parameters. The designing procedure, used standards, torque and inertia calculation, computer simulation, manufacturing methodology, and calibration, are some of the mentioned sections in this chapter. In Chapter 4, popular Japanese pumpkins have taken under different evaluation. Pumpkin anatomy investigation, physical properties evaluation, bending-shear test, compression test, and different field experimentation have mentioned in this chapter. In Chapter 5, the end-effector development was explained. In this chapter, harvesting methodology, design procedure, structure design, component simulations, different calculation, modification stages, and manufacturing, was explained. Chapter 6 introduces the controlling system including robot tractor TECU, PLC system, amplifiers, servo system, wires, power source, algorithm, and data communication. Chapter 7 explains the field experimentation and the article finishes with the conclusion in Chapter 8.

Chapter 2. Material and methods of a harvesting robot for heavy-weight crops (HRHC system)

2.1. Introduction

The harvesting robot for heavy-weight crops (abbreviated as HRHC) designed for a real-world robotic harvesting in the daily use, unlike to the most of the researchers which mostly evaluated in an isolated laboratory condition. This system is a prototype design to evaluate the dream harvester and optimize the possible issues. In this chapter, the explanation of the whole system presented. The platform of HRHC (see section 2.2), robot tractor (see section 2.2.1), developed robotic arm (see section 2.2.2), developed end - effector (see section 2.2.3), and controlling system (see section 2.2.4) was presented.

2.2. HRHC system configuration

Agricultural robots usually consist of three units: a mobile platform, actuating system, and recognizing system. As shown in Figure 12, the HRHC system has different units including a robot tractor as a mobile platform, a controlling system, a robotic arm and its end-effector as actuators, vision system as recognition system, and RTK-GPS. The vision system and image processing algorithm was not mentioned in this thesis because it is a separate study. In this section, each unit was introduced including robot tractor, robotic arm, end-effector and controlling unit, respectively. Each unit was explained in detail in the separate chapter as well. As a general view, an auto-guidance system will guide the robot tractor in the field by using GPS and IMU; the vision system will recognize the targets and send commands (location, orientation, variety, shape, and size) to the main PC; the PC will calculate the location of target and convert it by using developed algorithm; after receiving the location command, the manipulator will move to the location by using a controlling algorithm of robotic arm; the robotic arm will move the target location; the end-effector will grasp the target crop and the manipulator will lift it; finally, the whole system will harvest the crop by using designed harvesting methodology. This loop will complete by carrying the crop to a mobile truck and repeat the determined procedure.

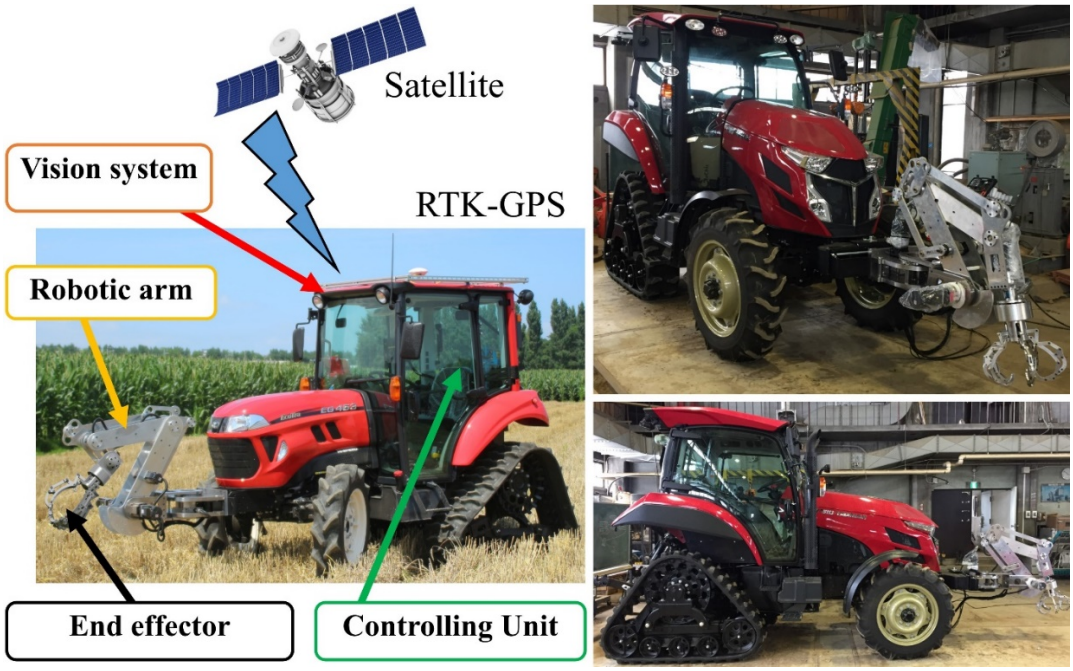

Figure 12. Different units of the designed system

2.2.1.Robot tractor

In 2010, Takai, Barawid Jr, Ishii, and Noguchi (2010) were developed the first crawler-type robot tractor based on GPS and IMU in the laboratory of vehicle robotics of Hokkaido University in Japan. They

did this research by equipping a controller, algorithm, RTK-GPS, and IMU on the YANMAR CT801 crawler-type robot tractor. This laboratory was continued their research by introducing robot farming system using multiple robot tractors as the first time in Japan (Noguchi & Barawid Jr, 2011). They also did some other researchers in this target including: development of robot tractor associating with human-driven tractor (C. Zhang, Yang, Zhang, & Noguchi, 2013), a robot combine harvester for wheat and paddy harvesting (Z. Zhang, Noguchi, Ishii, Yang, & Zhang, 2013), a robot tractor and its utilization (Yang & Noguchi, 2014), a human-driven tractor following a robot system (C. Zhang, Yang, & Noguchi, 2014), a robot tractor controlled by a human-driven tractor system (C. Zhang et al., 2015), and a 5DOF robotic arm (RAVebots-1) applied to heavy products harvesting (Roshanianfard & Noguchi, 2016).

C. Zhang et al. (2015) were developed a robot tractor controlled by a human-driven tractor system in the laboratory of vehicle robotics in the Hokkaido University. They published a paper in the title of "Leader-follower System using Two Robot Tractors to Improve Work Efficiency". In this study, the developed robot tractor was used as a mobile platform which was a Yanmar EG453 (YANMAR Co., Ltd., Japan) as shown in Figure 13. Table 4 shows the specifications of this tractor including steering control ($[40^{\circ}L, 40^{\circ}L]$), a switch for forward and backward movements, easy-change power transmission, a switch for power take-off, hitch function, engine speed set ($[9300rpm, 2330\ rpm]$), engine stop, and brake. The Tractors' Electronic Control Unit (abbreviated as TECU) uses a CANBUS to control the tractor, and it uses another CANBUS to communicate with the control PC.

The CANBUS (or computer area network bus) is a vehicle bus standard designed to allow microcontrollers and devices to communicate with each other in applications without a host controller (Wikipedia, 2017a). In 2001, agriculture machinery manufacturers agreed to implement the common standards, ISO 11783, for communication interfaces on tractor, implements, and farm management system. ISOBUS (or ISO 11783) is a communication protocol for the agriculture industry based on the SAE (Society of Automotive Engineers), J1939 protocol (which includes CANBUS). The ISOBUS standard specifies a serial data network for control and communications on forestry or agricultural tractor and implements. It consists of several parts: general standard for mobile data communication, physical layer, data link layer, network layer, network manages, tractor ECU, task controller and management information system data interchange, mobile data element dictionary, diagnostic, file server. The robot tractor has a GPS, and IMU, a control PC, a laser scanner and a remote switch. The GPS and IMU were used for navigation. The control PC was used for data processing and communication with tractor's ECU. The remote switch was used to control the tractor engine for a human operator, who can stop the tractor under certain situation. The robot tractor was modified from a commercial tractor, and global navigation satellite system is used as a navigation system.

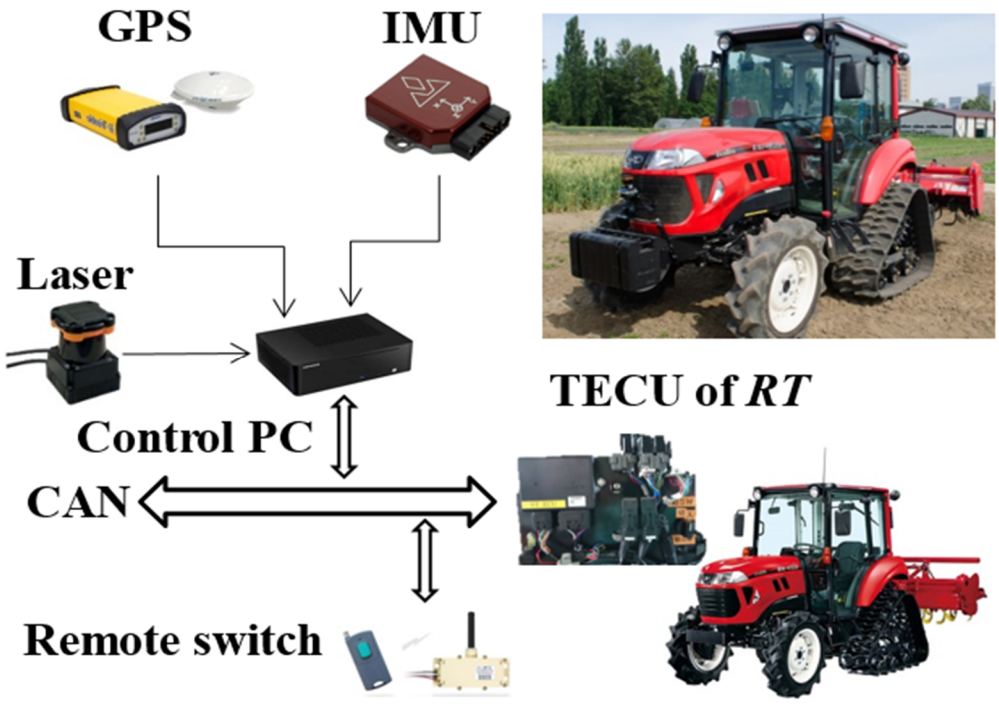

Figure 13. Platform of robot tractor (C. Zhang, 2017)

Table 4. Specification of EG453.

Model	Yanmar EG453	
Drive	4-wheel drive	
Size	Length (mm)	3410
	Width (mm)	1540
	Height (mm)	2265
Weight (kg)		1895
Engine	Power (kw)/ Engine speed (rpm)	53.0/ 2300
Steering		Hydraulic power steering
Brake		Wet disc
Gear Box		1-HMT
Speed	Forward (km/h)	0.15~32
	Backward	0.15~24
PTO	Forward rotation (rpm)	534/758/964/1254
	Backward (rpm)	675
Hitch		3-point link (JISI)

2.2.2.Robotic Arm

Because of several concerns in using the current industrial robotic arm (see sections 3.1 and 3.2), a new robotic arm named RAVeBots-1 (robotic arm for vehicle robotics-first generation) was developed. The RAVeBots-1 which shown in Figure 14 is a newly designed articulated robotic arm for outdoor applications, specifically agricultural applications, in terms of material, flexibility, actuator type, power source, rapid reparability, and cost-effectiveness. Quickly changeable components, a controlling methodology that is adaptable to complex conditions, and PPW ($\frac{payload}{robot\ weight}$) were among the key parameters considered in the design of robotic arm for agricultural application in this study. The chosen

robotic arm is composed of serial links, connected to each other with revolute joints to the end-effector (4R joint structure). Revolute joints were selected as linkage connectors from among collinear, orthogonal, rotational, and twist joints for optimal control of unpredictable forces, vibration, and to control the moment of inertia effect.

Figure 14. Designed robotic arm (RAVeBots-1)

As the RAVebots-1 was intended specifically for a heavyweight harvesting application, the material likely had a significant effect on robot performance. Therefore, aluminum (AL5052) and steel (ASTM A36) were chosen for structure manufacturing. Figure 2-b contains a detailed illustration of the RAVeBots-1 components, including; the developed robotic arm; a PC for programming and controlling with a position board; amplifiers to increase position-board output signals; and a brake unit designed for emergency stops (Roshanianfard & Noguchi, 2018). Due to the special methodology used in pumpkin and watermelon harvesting and its required parameters, 4-DOF was necessary to design of RAVeBots-1 and economic indexes must be minimum. The payload of this robotic arm is designed for almost 25 Kg by FOS of 2 (factor of safety). The required values of the robotic arm parameters, including workspace volume, land surface covered (Sc), front access (FA), and height access (HA) must be maximum. The maximum torque value of each joint must be less than mentioned maximum torque of servo motor in the datasheet.

2.2.3.End-effector

As shown in Figure 15, the designed end-effector (EE) consist of two main unit including (1) frame structure, and (2) fingers and some sub-units as the main connector, linear screw, and joint-4 structure. The frame structure connects the finger mechanism to the robotic arm and the structure designed for doing multifunction applications. The brake mechanism, linear motion actuator, and motion switch mechanism were some units of the equipped components in the frame unit. The mentioned EE contains 5 fingers which designed and optimized to grasp and harvest heavy-weight crops like pumpkin, watermelon, and cabbage. The fingers are especial designed mechanism including 7 links, 8 joints which have the mobility of 1 ($M = 1$). It was designed based on the extracted physical properties of pumpkin (see Chapter 4), statically simulated by using Solidworks software (see section 5.6), and optimized in SAM software (ARTAS Engineering Software, Netherlands) in kinematic and dynamic aspect (see section 5.6.2).

One of the initiated technique to design this system was inventing the Administrate Power Transmission system (abbreviated as APT) to manage the input power path which can support 2-degree of freedom (DOF)

by (see section 5.6.2) only using one servo motor which supplies only 1-DOF. This technique was increased the harvesting speed and efficiency and decreased the size, cost, and weight of EE. The fingers have combined mechanism to support various size between 170 to 500 mm in diameter. This requirement is necessary because of the pumpkin's shape and size diversity in the natural farms. As the EE has 5 fingers, it can support most of the ripe pumpkins in during of harvesting period. For damage possibility reduction, it was necessary to use some rubber cover on fingers, micro-switch to control the motion and capacitive sensors to sense the crops grasping.

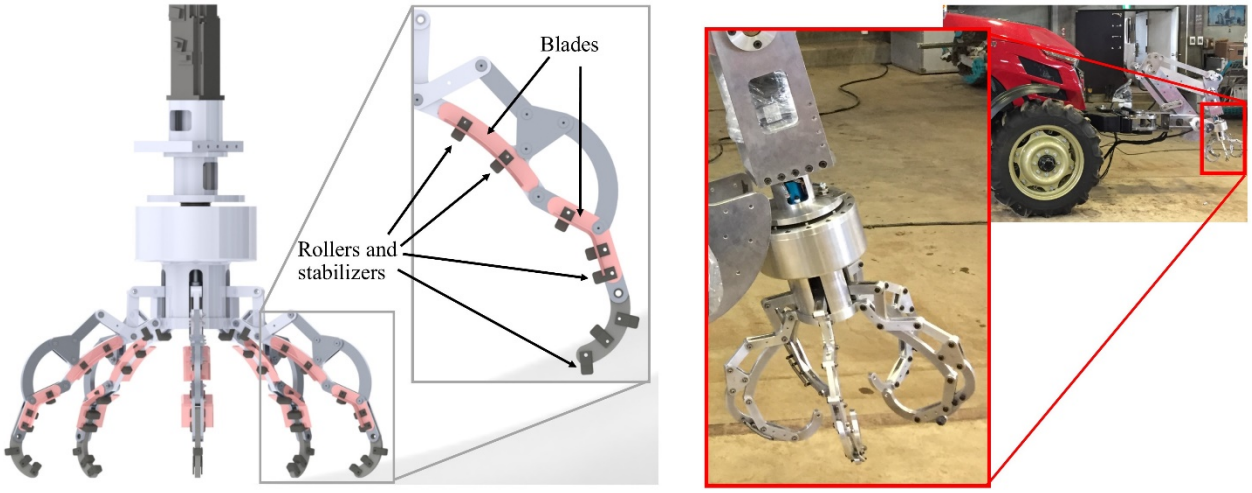

Figure 15. CAD design EE to heavy-crops harvesting (left), developed EE installed on HRHC system.

2.2.4. Controlling unit

The controlling unit of RAVeBots-1 was based on a programmable logic controller (PLC) system. This unit consists of a position board installed on a PC, a controlling program, servo motors, servo amplifiers, and optical cables for data transfer as compact circuits (Figure 16). The PLC systems usually drive a servo motor or a pneumatic/hydraulic cylinder. In this study, the PLC controlled five AC servo motors using 200ACV. All other components were selected or developed based on servo motor properties and the expected effects of lifted-object weight on joint torque and moment of inertia. A specific management-control program was developed based on parameters of the servo motor functions. To investigate a controller program, it is necessary to set some control functions. These were divided into three groups: operational functions (abbreviated as OPF); application functions (abbreviated as APF); and auxiliary functions (abbreviated as AXF). OPF included jogging operation (JOG), incremental feeds, linear interpolation, and home-position return. APF was based on servo speed, acceleration, deceleration, force, torque, limit switch alarm, interlock and other related parameters. The AXF controlled parameters for data reading/writing/changing, monitor functions, sampling, and interruptions.

After utilizing the functions, all servo-motor commands are transferred to the position board installed on PC's PCI Express protocol. To speed up data transfer, servo motor control signals were sent to the position board via an optical cable. The control-management program was developed using C++. The program included three control modes: torque control mode (TCM), speed control mode (SCM), and position control mode (PCM). The priority of each mode was servo-motor feedback torque, servo-motor feedback speed, and the position of the end effector, respectively. Figure 17 shows functions switched by the "control mode command". Switching to/from PCM to/from SCM/TCM must be done while the motor is off, while it is possible to switch between SCM and TCM any time.

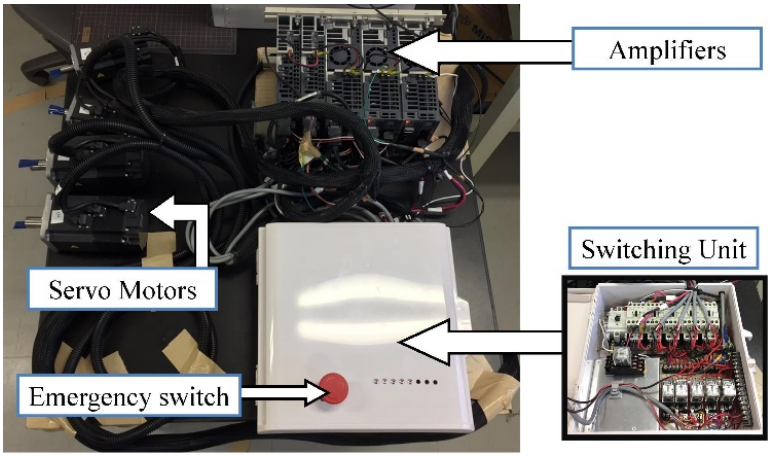

Figure 16. Controlling unit

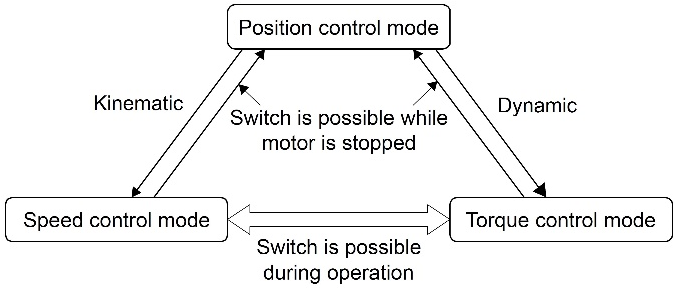

Figure 17. Controlling modes.

The controlling algorithm was developed next. Robotic arms are the most complex robots from a mathematical point of view, involving numerous parameters. Once an optimized algorithm is determined using kinematic and dynamic modeling, the PLC system parameters can be adopted by algorithm parameters. In robotic arm design, different methods were used to identify optimized controlling algorithms based on robot structure, linkage length, joint angles, and motion limitations. The optimized algorithm was needed because of the harvesting cycle time reduction. Kinematic simulation and dynamic analysis are essential for functional evaluation as well. In the design of the controlling algorithm for the RAVeBots-1, the Denevit-Hartenberg method (abbreviated as D-H) was used to find the optimized algorithm (Roshanianfard & Noguchi, 2018). The D-H method was chosen because it has a minimum delay and highest accuracy in experiments, and more versatility properties in terms of real-world conditions. The D-H is the accepted method for drawing a free body diagram of a robotic arm, which is based on joint motion, including rotation and translation. Subsequently, the controlling program was developed based on OPF, APF, AXF functions using the D-H algorithm.

2.3. Conclusion

This chapter introduces a general information about the designed HRHC system's units and their specifications. A robot tractor was chosen as a mobile platform and the equipped PC play the controlling platform. The robot tractor was found the harvesting path by using RTK-GPS signal and well-designed controlling algorithm. A 5-DOF (4-DOF robotic arm + 1-DOF end effector) was developed as a harvesting manipulator which was controllable by using a PLC system and brake unit. The PLC system was supported by a motion control board which connected to the main PC by using PIC-Express port. The C++ programming was used to control the system. A specifically designed end-effector was developed to grasp, lift and harvest the pumpkins. Also in this chapter, the controlling algorithm and controlling parameters

were briefly introduced. However, a vision system was predicted in this development, but the details and specification were not the aims of this study. The vision system will be presented in the future research.

As a general view, an auto-guidance system will guide the robot tractor in the field by using GPS and IMU; the vision system will recognize the targets and send commands to the main PC; the PC will calculate the location of target and convert it by using developed algorithm; after receiving the location command, the manipulator will move to the location by using a kinematic algorithm; the end-effector will grasp the target crop and the manipulator will lift that; finally, the whole system will harvest the crop by using designed harvesting methodology. This loop will complete by carrying the crop to a mobile truck. As this chapter is presenting a general view of the system, the experimentation and their results were not presented in the next chapters.

Chapter 3. Design and manufacture of robotic arm

3.1. Introduction

Among the various kinds of robots, robotic arms tend to be speedier, accurate and efficient. Their capacity leads processes by higher protection rate than human labor. Based on the mentioned reasons in section 1.5, the harvest of heavy crops requires a special robotic arm to ensure a big payload and acceptable price. Current industrial robotic arms, however, are not designed for complex agricultural conditions such as vibration, oscillation, and light reflection in a dusty environment. Moreover, a robot arm system installation on a fixed base limits the workspace. The typical industrial robotic arm is not suited and should not be used in agricultural task because mostof them were designed for a specifically isolated environment that could not be translated to farm use; each has a specially patterned workspace that cannot support a required harvesting surface when the arm attached to robot tractor; all designed for general use with complex algorithm that increases the harvesting cycle time (an average of 33 s (Bac, van Henten, Hemming, & Edan, 2014)); optimized for different performance hence they are pricey and heavy; and the pneumatic or hydraulic power sources that drive powerful industrial robotic arms are not suitable for a mobile agricultural robot with limited power source, that is why it would not be appropriate to use an available industrial robot which wasn't designed for agricultural conditions.

A unique approach to solving this issue involves installing a specially designed robotic arm on a mobile agriculture platform, like a robot tractor. A robotic arm designed for farm use must be able to maneuver toward a final point along an ideal path at a specified velocity (Angeles, 1997). Furthermore, it is necessary that the system is modeled and analyzed dynamically (Wang et al., 2003) ; it is essential to use forward / inverse kinematics and dynamics (Karlik & Aydin, 2000). This research presents the development process and performance characteristics of a specifically designed 4-degrees-of-freedom (abbreviated as 4-DOF) robotic arm mounted on a robot tractor for heavyweight crop harvestings like pumpkin and watermelon.

3.2. The limitation of current robotic system for farm use

In the past three decades, harvesting robot projects (including 50 projects) mostly focused on apple harvesting (Baeten, Donné, Boedrij, Beckers, & Claesen, 2008; Peter & Michael, 1988; Sarig, 1993), orange harvesting (B. S. & U. A., 2006; Plá, Juste, & Ferri, 1993; Roy, 1987; Sarig, 1993), strawberry harvesting (Hayashi et al., 2011), and tomato harvesting (Kondo, Nishitsuji, Ling, & Ting, 1996),which cultivate in four production environment such as orchard (32%), greenhouse (41%), indoor (4%), and open field (22%) (Bac et al., 2014). The number of developed harvesting robots for open filed was only 11 projects, which mostly aimed asparagus (Arndt, Rudziejewski, & Stewart, 1997; Carter et al., 2007), melon (Edan, 1995; Yael, Dima, Tamar, & Gaines, 2000), Radicchio (Giulio, 2006), saffron(Raparelli, 2011) , and watermelon (Sakai, Iida, Osuka, & Umeda, 2008) harvesting. From 1992 to 2014, Japan was the pioneer in the development of harvesting robots by 15 projects. Other countries such as USA (7 projects), Italy (5 projects), China (4 projects), France (4 projects), and New Zealand (3 projects) have considered on different robotic harvesting system as well (Bac et al., 2014; Libin et al., 2008; Shamshiri, Ismail, & Ishak, 2012).

Various factors such as uncontrollable wind, rain, and lighting can influence the harvesting procedure in the open field environment. Yet another concern is that most current agricultural robots were designed for light crops and fruits. For these machines, harvesting heavy products, such as pumpkin, watermelon, and melon, still represents hard work, and only four projects have considered on heavy-weight crops harvesting (watermelon and melon). However, These crops have high market demand in Japan, none of the mentioned projects didn't commercialize yet (SBJ, 2015, 2016). Harvesting of these heavy crops as a fruit (not for seed harvesting) is generally selective harvesting. This means it is not possible to harvest the entire product at the same time and have it been acceptable to the market. In Japan, farmers are challenged to find workers to pick pumpkin and watermelon. Wearable robots (Toyama & Yamamoto, 2009a) are not helpful in this case because of the low number of workers.

As shown in Figure 18 and Table 5, most of the available industrial robotic arms could not meet the requirements of the described application including specified workspace, front access, and harvesting height. As mentioned, the typical industrial robotic arm is not suited in the agricultural task because most of them were designed for a specially isolated environment that could not be translated to farm use. As shown in Figure 18, there was limited number of industrial robots which could meet some of the requirements. However, most of them were too heavy for this task; some of them had complex algorithm; some other had no open source programming, and some couldn't lift the maximum required payload. Between the different industrial robot producers, the companies of FANUC, Motoman, ABB, Omron, and Comanu had some products which could have enough payloads. In the case of the agricultural task, the height of installation stage (front stage of robot tractor) was needed to install the robotic arm somewhere higher than ground. In this case, the robotic arm should have launched higher than usual. In such described condition, most of the industrial robotic arms couldn't access the ground because of workspace limitation (As shown in Figure 18). As another perspective, most of them have small PPW which described in section 3.6.4 in detail.

As shown in Table 5, the specifications of mentioned industrial robots were mentioned including maximum payload and robot weight. The required payload for describes application was 25Kg that only FANUC M-20iB/25, Motoman DX1350D, ABB IR260, and Comanu NJ40-25 could handle it. In the between, the maximum loadable weigh for determined robot tractor was 180 Kg which is less than the weight of all mentioned industrial robots. As a conclusion, there wasn't any suitable industrial robotic arm which could select for the specified application, that's why a specifically designed robotic arm vas developed.

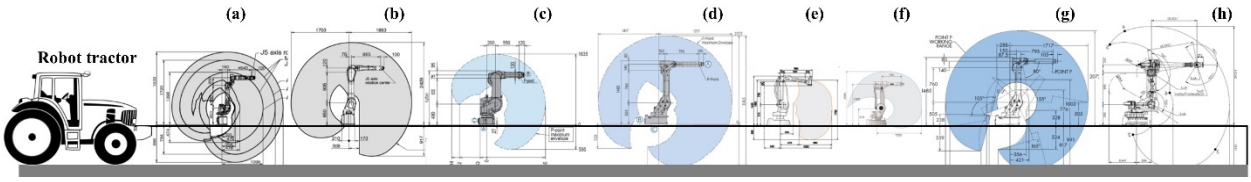

Figure 18. Available industrial robotic arm with a payload of 10~40kg, specifications in Table 5.

Table 5. Specification of industrial robotic arm mentioned in Figure 18

Model	Payload (kg)	Weight (kg)
FANUC 100iC	10	130/135/250
FANUC M-20iB/25	25	210
Motoman DX1350D	35	250
Motoman HP20	20	250
ABB IR260	30	340
ABB IR2400-16	20	380
Omron S1700D	20	268
Comanu NJ40-25	40	655

3.3. Objectives

The objectives of this chapter are as follow:

- Development of an applicable low-cost robotic arm for farm use by optimized DOF.
- Come up with economic evaluation and optimization of design robotic arm.
- Come up with DOF optimization methodology to select optimized DOF and joint structure.
- Come up with accuracy, resolution and reputability evaluation of the system.

3.4. Design procedure

3.4.1. Required parameters

The robotic arm payload capacity is an important parameter that must be fully addressed in the design. In agriculture, the loaded object weight is not predictable. Therefore, parameters such as torque and force, which depend on the loaded object weight, may vary at every moment during harvesting. Although payload estimation plays a significant role in robotic arm control. This estimation is not a quick access parameter during harvesting. To sustain requirement impacts, other factors such as speed, size, and platform weight must be considered. Subsequently, power source, propulsion system, clearance, maneuverability, and control algorithm must be factored in.

3.4.2. CAD/CAM design

Structure design is the most important stage to develop a new system. In this phase of the study, one must consider analysis methodology, material selection, boundary conditions, meshing method, and FOS. The standard design process for robotic structures consists of nine main stages: (1) defining the problem; (2) synthesis; (3) creating a prototype model; (4) simulation/calculation/modification; (5) manufacture of the robot; (6) programming; (7) testing/calibration; (8) final evaluation; and (9) definition of optimal conditions. In this study, the design of a robotic arm with appropriate degrees of freedom for agricultural usage was chosen as the design purpose. From the available options, we selected a 4-DOF robotic arm due to its simple structure and cost efficiency. The components and their assembly models were designed using Solidworks software (Dassault Systèmes SolidWorks Corporation, Canada), as shown in Figure 19-a. The chosen robotic arm is composed of serial links, connected to each other with revolute joints to the end-effector. Revolute joints were selected as linkage connectors from among collinear, orthogonal, rotational, and twist joints for optimal control of unpredictable forces, vibration, and to control the moment of inertia effect. All dynamic simulations, motion studies, and other essential parameters were analyzed by using Solidworks software. After several modifications, all components were manufactured and assembled based on the final characterization.

As the RAVebots-1 was intended specifically for a heavyweight harvesting application, the material likely had a significant effect on robot performance. Therefore, aluminum (AL5052) and steel (ASTM A36) were chosen for structure manufacturing. AL5052 is one of the light alloys of aluminum, with good weldability by gas, arc, and resistance. Figure 19-b contains a detailed illustration of the RAVeBots-1 components, including; the robotic arm with the designed end effector and crop picking function; a PC for programming and controlling with a position board; amplifiers to increase position-board output signals; and a brake unit designed for emergency stops.

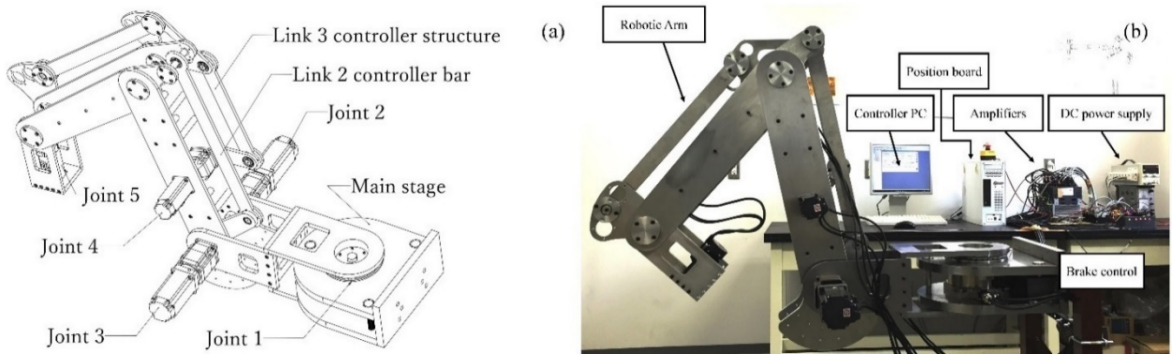

Figure 19. RAVeBots-1 (a) assembled the model, (b) developed system and its controlling units.

3.5. Standards (Drawing and Manufacturing)

Following the goal of unambiguous communication, engineering drawings are often made professionally and expected to follow certain national and international standards, such as ISO standards.

Standardization also aids with internationalization, because people from different countries who speak different languages can share the common language of engineering drawing, and can thus communicate with each other quite well, at least as concerns the geometry of an object. The usual standards areas: ISO Standards, ASME Standards, BS Standards, DIN Standards, and JIS Standards (Bales & Vlamakis, 2010; Drake, 1999; NASA, 1994). The following ISO and JIS standards were applied in designing components and preparation of drawing files for manufacturing.

3.5.1.ISO standards

Standardization is a dynamic and continuous procedure. The standards follow the development in engineering. ISO 128 is an international standard organization (ISO), about the general principles of presentation in technical drawings, specifically the graphical representation of objects on technical drawings. ISO 1101 represents the initial basis and describes the required fundamentals for geometrical tolerancing. Nevertheless, it is advisable to consult the separate standards referenced (Ghorani, 2017). The used ISO standards in this study are as follow:

- **ISO 128** Technical drawings - General principles of presentation
- **ISO 129** Technical drawings - Indication of dimensions and tolerances
- **ISO 1101** Geometrical tolerancing
- **ISO 1302** Indication of surface texture in technical product documentation
- **ISO 1660** Geometrical tolerancing - Profile tolerancing
- **ISO 2203** Technical drawings - Conventional representation of gears
- **ISO 2553** Symbolic representation on drawings - Welded joints
- **ISO 2692** Geometrical tolerancing - Maximum material requirement (MMR), least material requirement (LMR) and reciprocity requirement (RPR)
- **ISO 3040** Dimensioning and tolerancing - Cones
- **ISO 5261** Technical drawings - Simplified representation of bars and profile sections
- **ISO 5845** Technical drawings - Simplified representation of the assembly of parts with fasteners - Part 1: General principles
- **ISO 6410** Technical drawings - Screw threads and threaded parts
- **ISO 6411** Technical drawings - Simplified representation of center holes
- **ISO 7083** Technical drawings - Symbols for geometrical tolerancing - Proportions and dimensions
- **ISO 10579** Dimensioning and tolerancing - Non-rigid parts
- **ISO 13715** Technical drawings - Edges of undefined shape - Vocabulary and indications
- **ISO 14660-2** Geometrical features - Extracted median line of a cylinder and a cone, extracted median surface, local size of an extracted feature
- **ISO 15785** Technical drawings - Symbolic presentation and indication of adhesive, fold and pressed joints
- **ISO 15786** Technical drawings - Simplified representation and dimensioning of holes
- **ISO 16249** Springs - Symbols
- **ISO 216** paper sizes, e.g. the A4 paper size
- **ISO 406:1987** Technical drawings - Tolerancing of linear and angular dimensions
- **ISO 1660:1987** Technical drawings - Dimensioning and tolerancing of profiles
- **ISO 2203:1973** Technical drawings - Conventional representation of gears
- **ISO 3040:1990** Technical drawings - Dimensioning and tolerancing - Cones
- **ISO 5261:1995** Technical drawings - Simplified representation of bars and profile sections
- **ISO 5455:1979** Technical drawings - Scales
- **ISO 5456** Technical drawings - Projection methods
- **ISO 5457:1999** Technical product documentation - Sizes and layout of drawing sheets

- **ISO 5845-1:1995** Technical drawings - Simplified representation of the assembly of parts with fasteners-Part 1: General principles
- **ISO 6410-1:1993** Technical drawings - Screw threads and threaded parts, Part 1: General conventions
- **ISO 6411:1982** Technical drawings - Simplified representation of center holes
- **ISO 6412-1:1989** Technical drawings - Simplified representation of pipelines - Part 1: General rules and orthogonal representation
- **ISO 7200:2004** Technical drawings - Title blocks
- **ISO 8560:1986** Technical drawings - Construction drawings - Representation of modular sizes, lines, and grids
- **ISO 13567** International Computer-aided design (CAD) layer standard.
- **ISO 9283 (1998)** Manipulating industrial robots -- Performance criteria and related test methods.
- **ANSI/RIA R15.05** Industrial robots and robot systems - path-related and dynamic performance characteristics – evaluation standard.

3.5.2. JIS standards

The present Japanese Standards Association was established after Japan's defeat in World War II in 1949. The industrial standardization law was revised in 2004 and the "JIS mark" (product certification system) was changed. Japan has been further promoting consistency with international standards to respond to demands in and outside the country. Standards are named like "JIS X 0208:1997", where X denotes area division, followed by four digits (or five digits for some of the standards corresponding ISO standards), and the revision release year. Divisions of JIS and significant standards are:

A – Civil Engineering and Architecture
B – Mechanical Engineering
C – Electronic and Electrical Engineering
D – Automotive Engineering
E – Railway Engineering
F – Shipbuilding
G – Ferrous Materials and Metallurgy
H – Nonferrous materials and metallurgy
K – Chemical Engineering
L – Textile Engineering
M – Mining
P – Pulp and Paper
Q – Management System
S – Domestic Wares
T – Medical Equipment and Safety Appliances
W – Aircraft and Aviation
X – Information Processing
Z – Miscellaneous

In designing procedure of this study, the following JIS standards were used:

- **JIS B 0001-2010** Technical drawing for mechanical engineering
- **JIS B 7512-1993** Steel tape measures
- **JIS B 7516-1987** Metal Rules
- **JIS H 3100** Copper and copper alloy sheets, plates, and strips
- **JIS H 4040** Aluminum and aluminum alloy rods, bars and wires

3.6. Calculation and prerequisite parameters for design

Before the designing RAVeBots-1, many calculation and simulation including DOF optimization, joint required torque and moment of inertia calculation, PPW, and repeatability optimization was needed. The details of each mentioned parameters described in coming sections.

3.6.1.DOF optimization

In the selection of an appropriated DOF for a robotic arm, it was needed to evaluate an invariant structure (with constant main parameters) in different conditions to design an optimized structure. The DOF optimization in this study shown in Figure 20.In this section, a harvesting access length (HL), and the height of the installation position (h) were considered constant. The HL and h was the maximum front access and height of robotic arm from ground. By considering the constant parameters, the other parameters such as the number of joints, type of joints and DOF were changed and the results were compared. As shown in Figure 21, the structure of a robotic arm with a constant length with different DOF (1 DOF ~ 5 DOF) was compared in this section. In the all determined structures, the HA and h were considered constant as 7a and 1.5a, respectively. In all conditions, the distance between installation location to J1 (Link-1), and h was considered a and $1.5\ a$, respectively. The $a = 20cm$ was a constant length and all parameters were simplified based on this unit. The a was chosen randomly and the ratios was set based on designed robotic arm parameters. The length of the main link was chosen $6a$ which divided equally to reach the desired *n-DOF*. As shown in Figure 21, the workspace of *1-DOF* and *2-DOF* was zero because this *DOF* could move only in a constant length in 2D and 3D space, respectively. The 3-DOF, 4-DOF, and 5-DOF have covered a certain workspace (green volume (V)) and harvesting surface (brown area (S_c)). Finally, the related parameters including V, S_c, and HL of each *DOF* were simulated and compared.

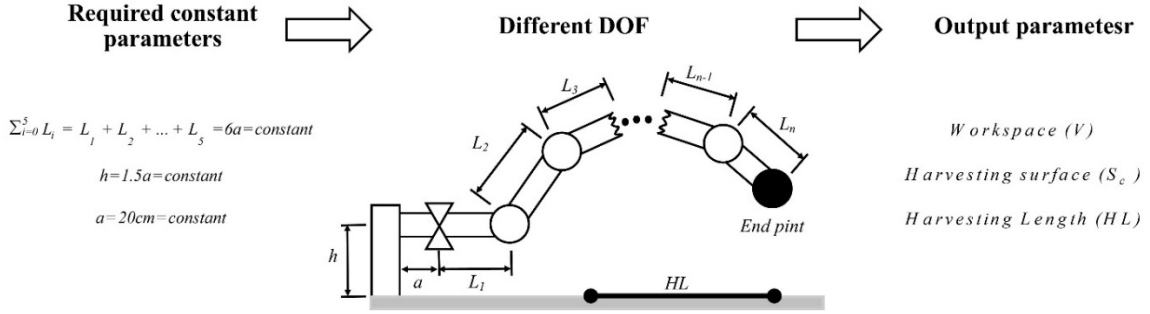

Figure 20. DOF optimization illustration.

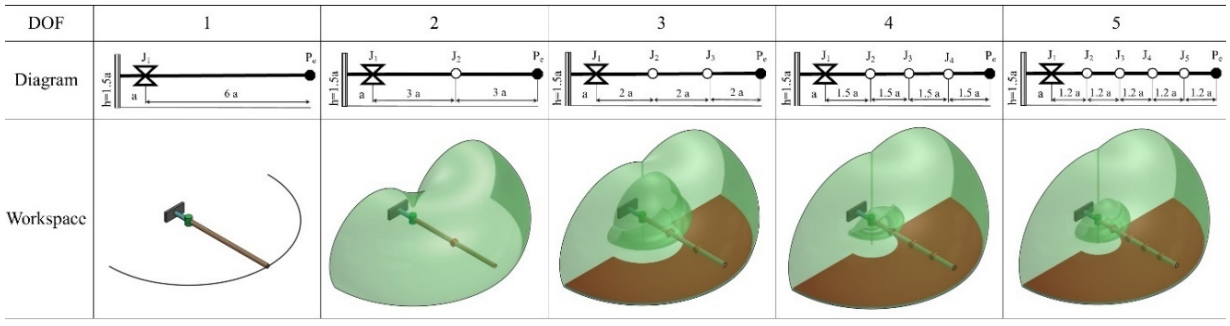

Figure 21. Comparison of different DOF on the workspace.

3.6.2.Joint torque calculation

Selection of a proper motor and a motor driver to meet a specific application needs motor torque calculation. At first, the user must calculate the inertia, friction, and load torque of joints. After that,

determine the required motor torque for the specific application. Finally, select the proper motor and driver based on their speed-torque characteristics. The torque of the servo motor was calculated as follow:

$$T_t = \left((I.\omega) + (N.K_i + T_{FM} + T_{FD}) + (T_g + T_s)\right) \times \frac{FOS}{\eta} \quad (1)$$

The symbols are defined as:

Symbol	Meaning	Unit	Symbol	Meaning	Unit
I	Total moment of inertia in conversion into the motor's shaft	Nms2	T_{FD}	Friction torque of the transmission system	N.m
ω	Motor shaft angular acceleration	Rads-2	η	Efficiency of Servomotor	-
N	Motor usage rpm	rpm	FOS	Factor of Safety	-
K_i	Braking constant	Nm/rpm	T_g	Gravity holding torque	N.m
T_{FM}	Motor static friction torque	N.m	T_s	Interference torque	N.m

3.6.3. Moment of inertia

Designing a robotic arm for accurate operations requires actual values for kinematic parameters. Since precise measurement is an expensive and error-prone task, calibration and optimization make the assignment of kinematic parameters easier (Barati, Khoogar, & Nasirian, 2011). In this study, both joint and link parameters were needed for the analysis. Link parameters consisted of link mass, the center of mass, and moment of inertia in different directions; joint parameters included joint angle, angular velocity, and acceleration. Table 6 presents the RAVeBots-1 link parameters obtained from a simulation of the designed model in Solidworks software. The manufactured model had approximately 2% tolerance.

Table 6. Link parameters

Link	Center of mass (m)	Mass (Kg)	Moment of inertia					
			Ixx	*Iyy*	*Izz*	*Ixy*	*Iyz*	*Izx*
1	0.21	23.1	0	0	0	0	0	0
2	0.29	7.9	0.684	0.126	0.74	0.21	0.043	0.013
3	0.24	7.34	0.242	0.281	0.474	-0.23	0.063	-0.01
4	0.77	3.8	0.055	0.015	0.051	0.008	0.004	0.002
5	0.13	20	0.05	0.01	0.05	0.007	0.003	0.001

3.6.4.PPW and repeatability

In the case of a new robotic arm development, PPW (Payload Per Weight), accuracy and repeatability are important parameters. These parameters have to measure and optimize after development which is usually provided by the manufacturers, calibration issues, and environmental conditions. Repeatability is a measure of the ability of a robot to consistently reach a specified point, and accuracy is a measure of the distance error associated with the desired point and achieved point (Shimon, 1999; Şirinterlikçi, Tiryakioğlu, Bird, Harris, & Kweder, 2009). In this study, two standards were used to determine the accuracy and repeatability including ISO 9283 (1998) and ANSI/RIA R15.05 using maximum speed of operation and maximum payload (25 Kg). These parameters have calculated by using following equations:

$$A_{p_x} = \frac{1}{n_1}\sum_{i=1}^{n_1}\sqrt{(\bar{x} - x_c)^2}\,;\; A_{p_y} = \frac{1}{n_1}\sum_{i=1}^{n_1}\sqrt{(\bar{y} - y_c)^2}\,;\; A_{p_z} = \frac{1}{n_1}\sum_{i=1}^{n_1}\sqrt{(\bar{z} - z_c)^2} \quad (2)$$

$$L_i = \sqrt{(x_r - \bar{x})^2 + (y_r - \bar{y})^2 + (z_r - \bar{z})^2} \quad (3)$$

$$\bar{L} = \frac{1}{n_2}\sum_{i=1}^{n_2} L_i \tag{4}$$

$$R_p = 3\sqrt{\frac{\sum_{i=1}^{n_2}(L_i - \bar{L})^2}{n-1}} + \bar{L} \tag{5}$$

Which A_{p_i}, n_1, n_2, $\bar{x}$, x_c, and x_r are positional accuracy (mm), number of attained points in each mission, number of repetition, average value of attained position (in y and z direction as well), commanded position (in y and z direction as well), and attained position (in y and z direction as well), respectively, according to ANSI/RIA R15.05. The experimentations were done in 35 repetitions, and 4 missions (different motion methodology: (a) circular, (b) rectangular, (c) square, (d) triangular), 140 repetitions in total. The results were calculated and compared. The final evaluations of accuracy and repeatability was mentioned in section 7.6 as well.

3.7. Designing of RAVeBots-1

A robotic arm mounted on a driverless robot tractor and intended for use in outdoor conditions such as agricultural fields raises different concerns than one intended for indoor use (Figure 22-a). It is important to consider the environmental conditions under which the robotic arm will operate. Such factors will determine the base platform of the robot and affect other aspects and components such as the power source, actuators, and controlling system. Determining the agricultural conditions for the robotic arm will foster selection of the best materials and components. Outdoor conditions are not controllable, so the robot must be designed to withstand climate conditions (rain, wind, and sun), wet or muddy terrain, vibration, hot or cold temperature, and light reflection. In the agricultural environment, the mentioned parameters can change at any moment. That is why it would not be appropriate to use an available industrial robot not designed for agricultural conditions.

The robotic arm payload capacity is an important parameter that must be fully addressed in the design. In agriculture, the loaded object weight is not predictable. Therefore, parameters like torque and force, which depend on loaded object weight, may vary at every moment during harvesting. Although payload estimation plays a significant role in robotic arm control. This estimation is not a quick access parameter during harvesting. To sustain impacts, other factors such as speed, size, and platform weight must be considered. Subsequently, power source, propulsion system, clearance, maneuverability, and controlling algorithm must be factored in. Most of the available industrial robotic arms could not meet the requirements of the described application. For example, most were designed for a specially isolated environment that could not be translated to farm use; each has a specially patterned workspace that does not cover a wide horizontal area, and the pneumatic or hydraulic power sources that drive powerful industrial robotic arms are not suitable for a mobile agricultural robot. Quickly changeable components, a controlling methodology that is adaptable to complex conditions, and PPW ($\frac{payload}{robot\ weight}$) were among the key parameters considered in the design of robotic arm for agricultural application in this study.

The RAVeBots-1 (robotic arm for vehicle robotics-first generation) shown in Figure 22 is a newly designed articulated robotic arm for outdoor applications, especially agricultural applications, in terms of material, flexibility, actuator type, power source, rapid reparability, and cost-effectiveness. Agricultural robots usually consist of three parts: a moving system, actuating system, and recognizing system. Figure 22-b shows the system developed for this study, consisting of a robot tractor as the mobile platform (developed at the laboratory of Vehicle Robotics of Hokkaido University); the RAVeBots-1 as an actuating system; a especially designed end-effector for grasping, lifting, cutting, and crop transferring; and a control unit. The RAVeBots-1 is a 5-DOF robotic arm (4-DOF for robotic arm + 1-DOF for end-effector). Due to the special methodology used in pumpkin and watermelon harvesting, this DOF number is necessary. The payload of this robotic arm is designed for almost 200N by FOS (factor of safety) = 2. The required values

of the end effector's parameters, including workspace volume (V), land surface covered (S_c), front access (FA), harvesting length (HL), and height access (HA) must be proper enough to do the harvesting process. In addition, the maximum torque value of joint 1(J1), Joint 2 (J2), Joint 3 (J3), and Joint 4 (J4) must be less than 92, 270, 126 and 35 N.m, respectively, because of the capacity of each servo motor mentioned in datasheet. The important stages and parameters for designing a new system, including structure design, development of controlling unit, and development of controlling algorithm, will described in the following sections.

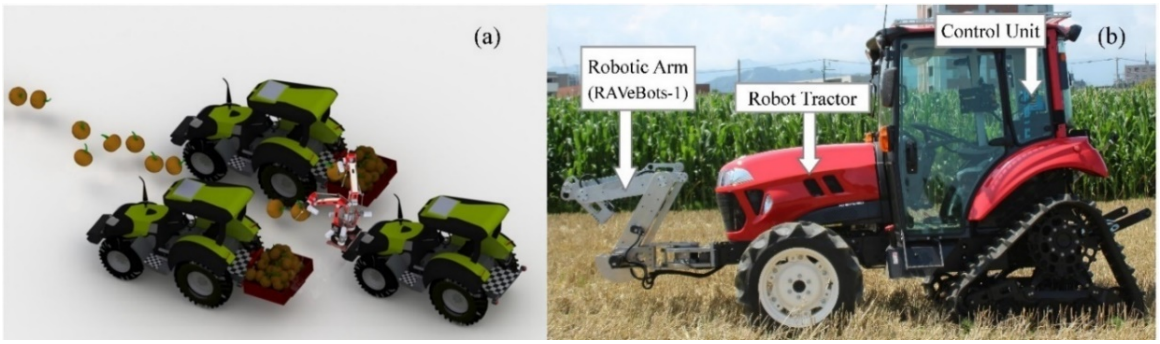

Figure 22. (a) Designed RAVeBots-1 and application illustration, (b) Developed robotic arm mounted on a robot tractor

3.8. Material improvement

In during of designing procedure, The ASTM A36 steel was chosen for the material of the component. The material was changed based on the simulations and also because of the high density of material which causes heaviness. After several modifications, it was decided to change the location of joint-3 and Joint-2 to reduce the required torque of Joint-1 and Joint-2. Figure 23 shows a comparison between 3 design models of RAVebots-1 (A, B, and C) in terms of different material and structure. The A-design was the reference design (first design) which was designed by ASTM A36 steel material and all the servomotors were located on the related joints location. The B-design was same design but the material was changed to AL5202. The C-designed had AL5202 as used material and the install location of servo motors 3 and 4 was changed to a location nearby the Joint-2. Overall, the main differences between A and B designs are related mainly to the linkage material; A used STM A36 steel and B used AL5202. The difference between A and B designs with design C relies not only on the material used but also in the servo motor position. A special alloy of Aluminum AL5202 was used in design C, and the positions of the servo motors from joint 3 and 4 are closer to the position of joint 2.

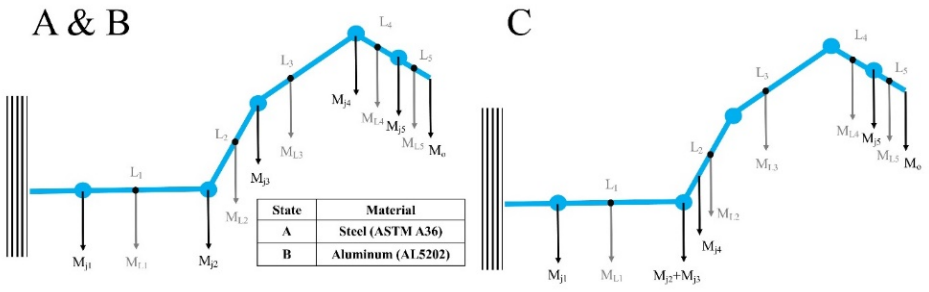

Figure 23- Components weight diagram in A, B, and C design

3.9. Computer simulation

The dynamic components were analyzed by using standard mechanical formulas. Table 7 shows the simulation categories including 4 main aspects (displacement/velocity/acceleration, forces,

momentum/energy/power, and other quantities), 17 sub-categories which each can have several components. In total, 73 different simulations were done on the designed robotic arm. The designed robotic arm has 259 different components which have a different application in the designed structure. Generally, the number of simulation in all aspects could be 18907 different simulations. This number individually indicates that how big engineering work was done in the designing of a RAVeBots-1. To simplify the simulation, some of them combined and some other was omitted. In the coming sections, the results of simulation briefly presented in two categories as Stress, Strain, and FOS of main components, and motion analysis results in two upward and downward motion.

Table 7. Simulation categories

Simulation aspects	Sub-category	components
Displacement/ Velocity/ Acceleration	Trace path	
	Center of mass position	x, y, z
	Linear displacement/ velocity/ acceleration	x, y, z, magnitude, radial component, tangential component, normal component
	Angular displacement/ velocity/ acceleration	x, y, z, magnitude
Forces	Motor force/ torque	x, y, z, magnitude
	Reaction force/ moment	x, y, z, magnitude
	Friction force/ moment	x, y, z, magnitude
	Contact force	x, y, z, magnitude
Momentum/energy/ power	Translational/ angular momentum	x, y, z, magnitude
	Translational/ angular/ total kinetic energy	
	Potential energy delta	
	Power consumption	
Other quantities	Euler angles	Psi, Theta, Phi
	Pitch/ Yaw/ Roll	
	Rodrigues parameter	Parameters
	Bryant angles	Angles
	Reflection load mass/ inertia	

In the coming section the stress, strain, torque and FOS simulation will be presented.

3.9.1.Stress, strain, and FOS of main components

Due to the sensitivity of the main components of the system such as the main stage, link-1, Link-2, Link-3 and Link-4, a static simulation was conducted on them by using the Solidworks Simulation. The safety factor range for linkage and structure design was selected from 1.96 to 3; the FOS range for joints and servo motor designs was selected from 1.1 to 2. The main stage and Link-1 were manufactured by steel (ductile ASTM A36 steel), and Link2, 3 and 4 were made of aluminum (specifically, AL5205). The simulation type of Solidworks simulator was linear elastic isotropic. Based on the calculation result, the applied direct force on the main stage, link-1, Link-2, Link-3 and Link-4 were 799.5 N, 558.3 N, 425 N, 270.7 N and 245.15 N, respectively. Stress analysis results were shown in Figure 24. Table 8 shows the simulation results on main components. The standard yield strength of ASTM A36 and AL5205 were 6.024×10^{8}, and 9×10^{7}, respectively. As the results show the maximum stress of the Mainstage, Link-1, Link-2, Link-3, and Link-4 was 5.29×10^{6} , 2.22×10^{7} , 3.06×10^{7} , 7.21×10^{6} , and 3.06×10^{6} , respectively, which all are less than the yield strength of used materials. The maximum FOS which used of all the components is 3 which is more than usual FOS for agricultural application. The static simulation results show that the used material and the designed structure was developed with equivalent strength and the structure can support the system in the static situation.

Table 8. The range of stress, strain, and values o FOS in the main components.

	Stress ($^{N}/_{m^3}$)		Strain		FOS	Material	Yield strength
	Max	Min	Max	Min			
Mainstage	5.29×10^{6}	2.85×10^{2}	1.59×10^{-5}	1.24×10^{-9}	3	ASTM A36	6.024×10^{8}
L-1	2.22×10^{7}	4.99×10^{3}	7.58×10^{-5}	3.66×10^{-8}	3	ASTM A36	6.024×10^{8}
L-2	3.06×10^{7}	0	2.77×10^{-4}	5.6×10^{-9}	3	AL5205	9×10^{7}
L-3	7.21×10^{6}	55.22	8.2×10^{-5}	5.05×10^{-10}	3	AL5205	9×10^{7}
L-4	3.06×10^{6}	39.78	2.8×10^{-5}	1.08×10^{-9}	3	AL5205	9×10^{7}

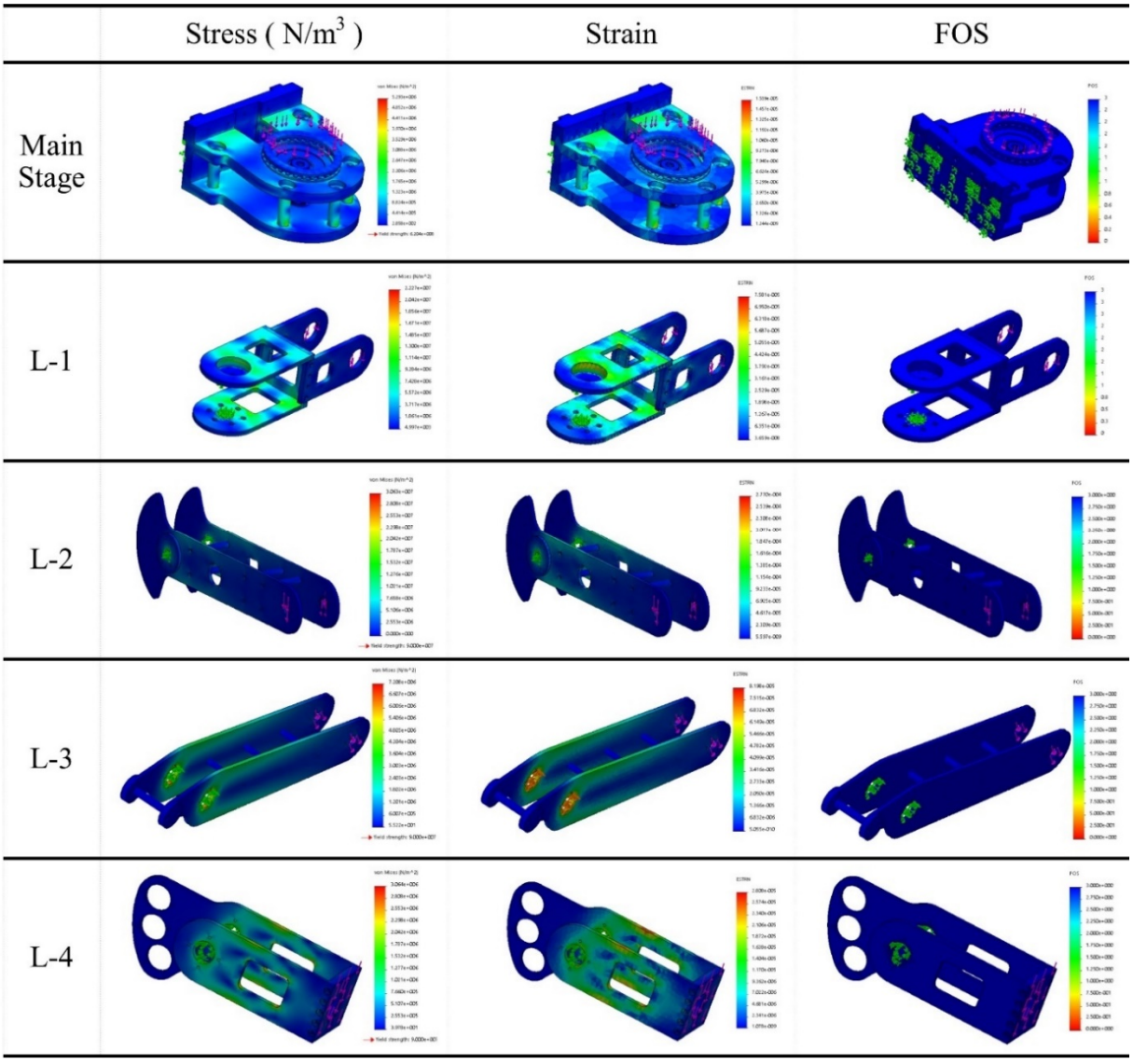

Figure 24. Static simulation results illustration.

3.9.2. motion analysis

The motion analysis or the dynamic simulation of the designed system could be done in infinite different situations because of infinite possible dynamical motions in 3D space. But as an example, two different motions including upward motion which can simulate the lifting situation, and downward motion

which can simulate the grasping and picking situation, was analyzed. Table 9 shows the different dynamical simulation which was done on the RAVeBots-1 structure. The dynamic simulation was down in two motion types (upward, and downward), four joints (Joint-1 to Joint-4), four motion simulation (Angular displacement, Angular velocity, Angular acceleration, and Torque), four links and four dynamic parameters. In total 64 different simulations were done on the structure (2-types × ((4-joints + 4-simulations) + (4-links + 4-simulations))). In the coming sections, the simulation results of each motion types will explain in detail.

Table 9. Dynamic motion result categories.

Type			Motion study	Dynamic simulation		
Upward	J_1	×	Angular displacement	L_1	×	Stress
	J_2		Angular velocity	L_2		Strain
	J_3		Angular acceleration	L_3		Displacement
	J_4		Torque	L_4		FOS
Downward	J_1	×	Angular displacement	L_1	×	Stress
	J_2		Angular velocity	L_2		Strain
	J_3		Angular acceleration	L_3		Displacement
	J_4		Torque	L_4		FOS

A general illustration of simulation methodology in the upward situation was shown in

Figure 25. The aim of this analysis was an object lifting and carrying simulation when the robotic arm wants to lift and carry a heavy-weight crop to a trunk. In this simulation, a box as a trunk was set at a certain height and a robotic arm control the endpoint to access the box with minimum torque and maximum speed. At the same time, the 3D motion in X, Y and Z direction was studied. A general illustration of simulation methodology in the upward situation was shown Figure 26. The aim of this analysis was a simulation of the real grasping situation when the robotic arm wants to grasp, harvest and lift a heavy-weight crop. In this simulation, the robotic arm has to move with minimum distance by ground (in average 5 mm). The motion was done based on the developed equations and the distances were measured by using a virtual sensor on the endpoint.

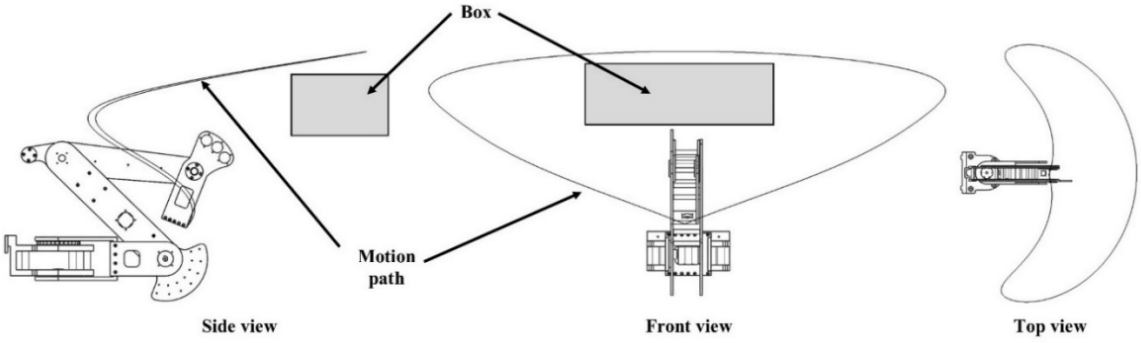

Figure 25. Upward motion test illustration

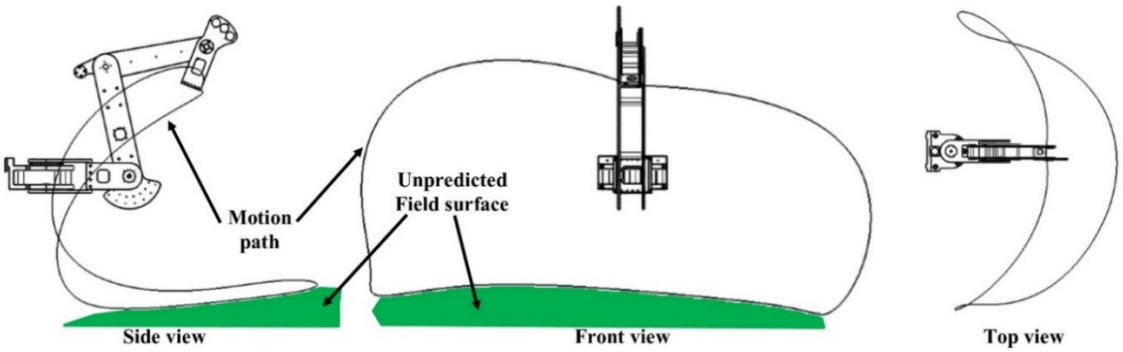

Figure 26. Downward motion test illustration.

3.10. Structure manufacturing

The structure of RAVeBots-1 was designed by using Solidworks software. Each component was designed one by one. The total number of components was 259-components in the robotic arm including links, stages, servo motors, bolts, nuts, spacers and so on. Figure 27 illustrates the RAVeBots-1 drawing which is the manipulator of the HRHC system. The drawings of each component were drawn by using JIS and ISO standards and the drawings were sent to a manufacturing company to develop each component. After manufacturing, the components were assembled in the laboratory of vehicle robotics – Hokkaido University. After finishing the assembly, the RAVeBots-1 was mounted on the robot tractor as shown in Figure 28. The detailed drawings of each component were indicated as Appendix-1 and 2 of this thesis.

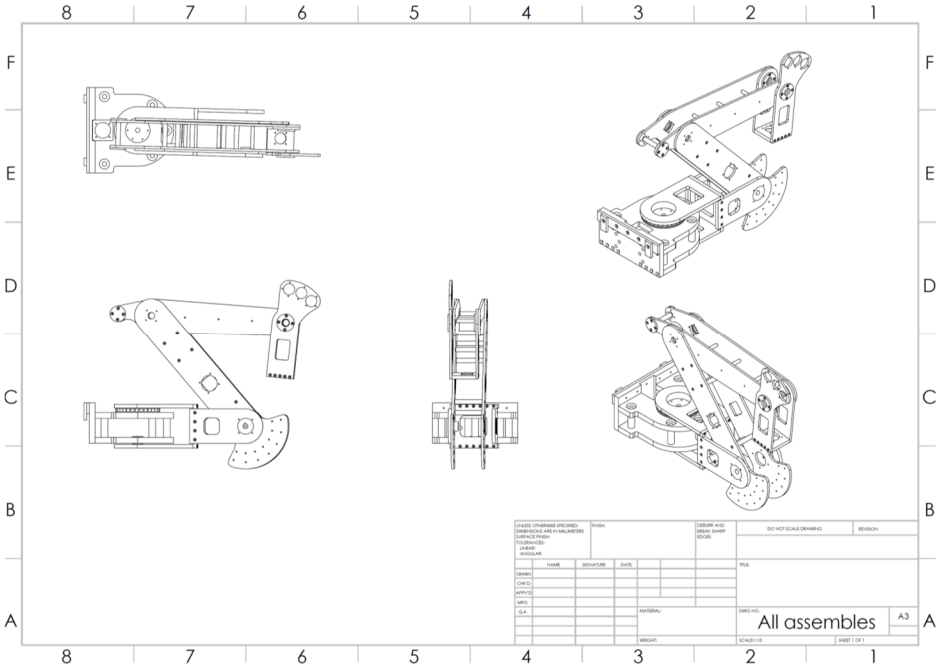

Figure 27. RAVeBots-1

Figure 28. RAVeBots-1 on different mobile platforms and field conditions.

3.11. Controlling methodology

The robotic arm can maneuver between an infinite number of positions inside the workspace. Sometimes, there are infinite trajectories to reach a particular point. Deciding between them by solving the inverse kinematics takes time. Such time delay is not acceptable for fast applications. The robot algorithm must select the best answer in the shortest possible time. In this regard, for grasping an object with a robotic arm, it is better to investigate an efficient methodology. In this study, the arm was needed to harvest a heavy crop; reviewing optimized harvesting methods could, therefore, help to increase reaction speed. After reviewing the various methods, the GCLT method as an efficient way to harvest heavy crops was designed. The GCLT method includes the following four steps: (1) grasping/picking the crop; (2) cutting the stem; (3) lifting; and (4) transportation (see Figure 29). Before beginning these steps, however, the robotic arm must change from the transportation to the working position. The transportation position is a particular position in which all servo motors are set at the minimum angle, and the robot is ready to start. Based on the structure of robot, $\theta_i(0, 119.3, -105, -119.8)$ were chosen as the rest angles. During harvesting, the grasping position is chosen based on recognition-system (manually in this study) commands regarding a crop's location. According to the physical properties of a crop like pumpkin, the stem-cutting stage must be next. In this stage, the robot has the opportunity to cut the crop's stem. The lifting and transportation stages are the essential steps that follow to carry the crops to the truck. As mentioned above, switching from the transportation to the working position must occur before the GCLT process can begin again. The working position was set as an initial point in the controlling system, and the recognition system assesses it as a start point. After harvesting, the program returns the robot to the transportation position when the operator decides to finish. This position is important because it protects the joints and structure against tractor vibration and oscillation during work in the field.

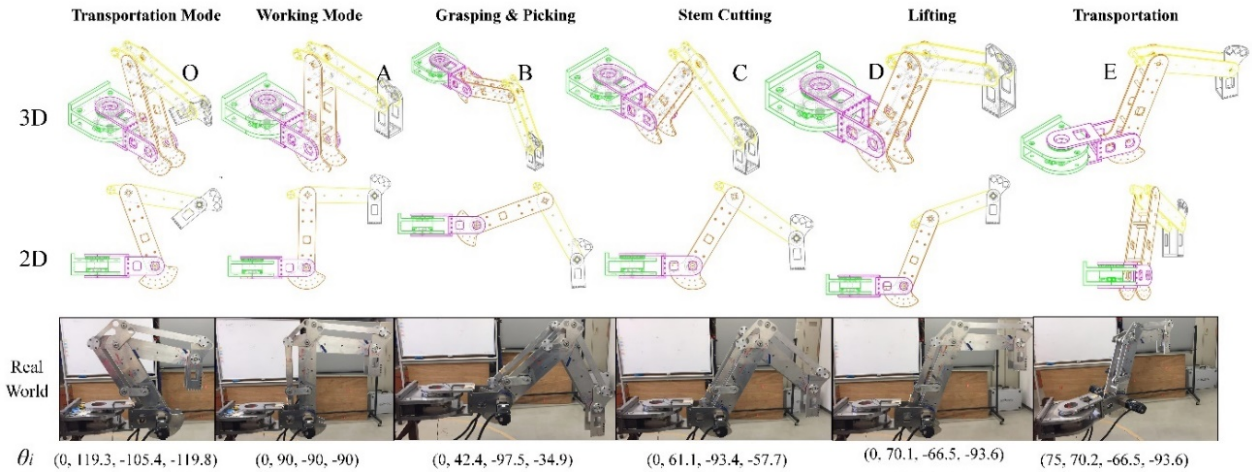

Figure 29. Harvesting stage and related parameters based on a developed algorithm.

3.12. Results

In robotic arm development, experiments and optimizations must focus on three areas. First, on the workspace to ensure the system meets all requirements; second, on the system's accuracy based on the intended function and component parameters; and third, on system reaction speed to ensure sufficient accuracy to pass the determined trajectories in minimum time.

3.12.1. DOF and economic optimization

As shown in Figure 30, the I_v, HA_{max}, $|HA_{min}|$ and HL was increased between 3-DOF to 5-DOF, but I_s, FA_{max}, FA_{min} almost remained constant. The I_v, I_s , FA, HA, HL, V_n, and S_n were workspace index (V/a^3), harvesting surface index (S_n/a^2), front access, height access and harvesting length, workspace volume, and covered land surface for harvesting, respectively. Based on the calculations, the minimum acceptable harvesting length has to be more than $4\ a$. In the cases of 3-DOF, 4-DOF, and 5-DOF, the S_n was calculated $41.36\ a^2$, $48.26\ a^2$, and $49.65\ a^2$, and the HA was $3.2\ a$, $4.24\ a$ and $4.5\ a$, respectively. The HA of 3-DOF was less, than requirement, while these values have no significantly different in the case of 4-DOF and 5-DOF.

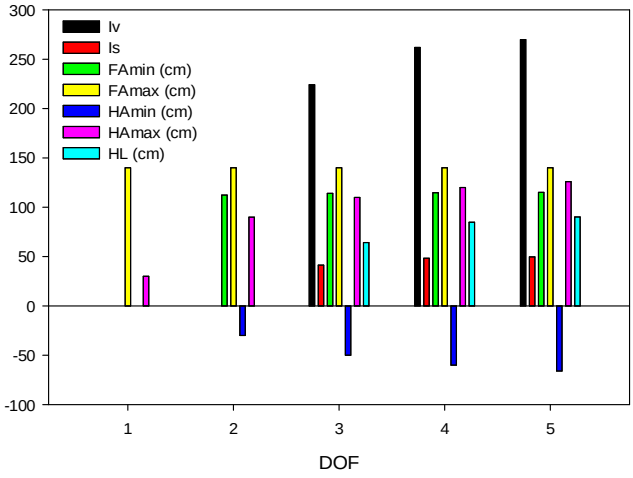

Figure 30. required parameters in different DOF.

Figure 31 indicates the economic and energy evaluation different n-DOF. In this evaluation, different expense sources such as actuating cost, material cost, manufacturing expenses, mechanical parts, electronic component prices, and energy consumption was considered. Each parameter was calculated based on Japanese market rate and indexes were describes. Each economic and energy index was increased by the DOF growth. When the DOF increase, the number of the needed actuator (servo motor), amplifier, connection cables, joint components, controlling components; manufacturing time, increase subsequently; and more servo motor needs more energy to supply and more connection cable, and the controlling algorithm gets more complex. But, increasing the DOF from 4 to 5, was not increase the I_s and HL significantly, then 5-DOF robotic cannot be an optimized structure to described application and required parameters. As a conclusion, by consideration a constant length and different DOF, a 4-DOF could be an adequate structure which can support a maximum V_n and S_n, at a minimum cost. Based on these evaluations, a 4-DOF structure was selected to develop a harvesting robotic system.

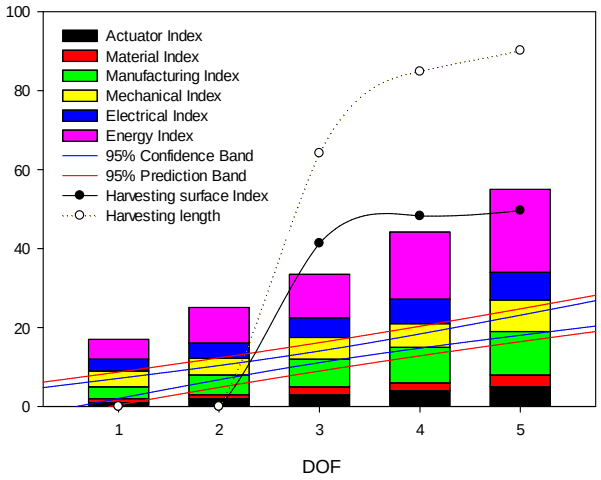

Figure 31. economic optimization indexes.

3.12.2. PPW

To design of a mobile robot, the weight of the robotic arm and its payload are important parameters. As a combination of a robotic arm with a robot tractor was aimed in this study, a minimum weight of robotic arm with maximum payload ration (PPW) was required. Figure 32 indicates the PPW of different industrial robots which has a payload within the desired range. Several industrial robots from different companies which has a payload in the required range such as: FANUC (FANUC CO., Japan), Motoman (Yaskawa Inc., America), ABB (ABB, Swedish-Swiss), Denso (DENSO Co., Japan), Comau (FCA Group, Italy), Kawasaki (Kawasaki Heavy Industries Ltd., USA), and OTC Daihen (OTC Daihen Inc., Japan) was studied. The average PPW was almost 0.085 that means a robotic arm with 8.5 kg payload and 100kg weight. The weight of a pumpkin could reach to 10kg and by consideration of FOS=2, the minimum PPW must be more than 0.2, when the weight of the robotic arm is 100kg. As shown in Figure 32, the PPW of all the evaluated robotic arm was less than 0.2, except of FANUC, LR Mate 200iD (PPW=0.28), and Denso, VS-6577 (PPW≅0.2) models which are heavy weight and small workspace, respectively, which cannot provide the required parameters (mentioned in section 3.12.1). The maximum front balance weight of the developed robot tractor was 150kg which is smaller than the weight of mentioned industrial robotic arm. Based on the final experimentation of designed robotic arm (RAVeBots-1), its maximum PPW is 0.21 which not only is more than average PPW of all robotic arms but also is more than the required range to harvest heavy-weight crops. Based on the mentioned reasons, the RAVeBots-1 with high PPW, and payload (25 kg) meet the needed required parameters to harvest heavyweight crops.

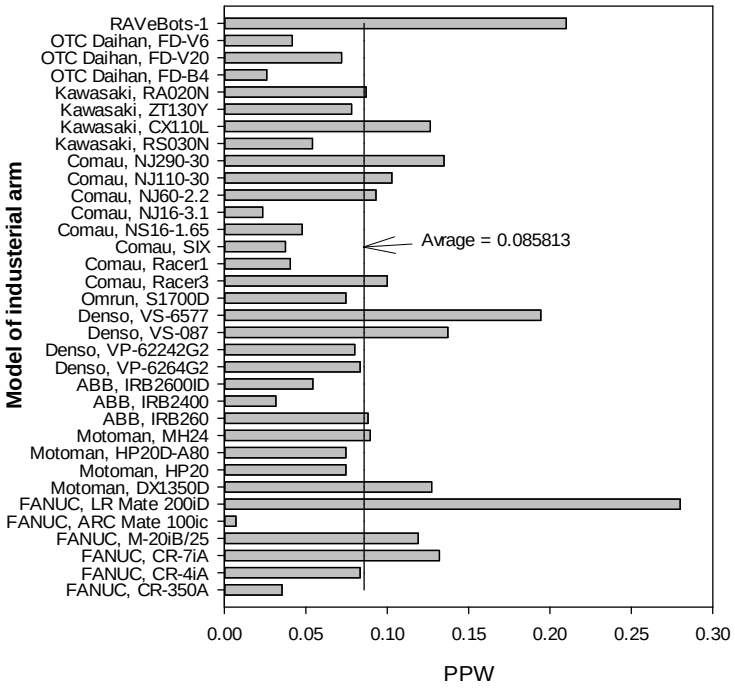

Figure 32. The PPW comparison.

3.12.3. Joint torque

Table 10 presents the results of torque calculation explained in section 3.6.2. In agricultural robots, the speed has secondary priority. The servo motor's speeds of RAVebots-1 is set to 15 rpm in J_1 and 60 rpm in J_5. Above this speed values, $T_{Dynamic}$ and the inertia increase dramatically. A bigger $T_{Dynamic}$ requires a more powerful power supply in order to control the servo motors. T_{Static} in J_1 and J_5 is zero, because in the designing process the angle between the total force vector and the perpendicular length from pivot to force is 90°. In other words, the direction of the total force vector is not in the rotation direction. In general, because of the rotation speed, $T_{Dynamic}$ in each joint is not zero. Also, in J_2, J_3 and J_4, T_{Static} is bigger than $T_{Dynamic}$. It is shown, that the effect of T_{Static} is greater than $T_{Dynamic}$. As a conclusion, J_2 needs the most powerful servo motor for the highest torque, and J_5 needs the weakest one.

Table 10- Maximum joints specification in C design.

Joint	Speed (rpm)	T_{Static} $(N.m)$	$T_{Dynamic}$ $(N.m)$	T_{Total} $(N.m)$	T_{Total} (include FOS) $(N.m)$
J_1	15	0	5.15	6.15	18.5 (FOS=3)
J_2	30	253	4.35	257.35	287.3 (FOS=1.1)
J_3	30	101.9	1.5	103.4	173.5 (FOS=1.7)
J_4	30	20.1	0.1	20.2	32.9 (FOS=1.6)
J_5	60	0	0.1	0.1	0.2 (FOS=2)

3.12.4. Simulation results

3.12.4.1. Upward motion

The upward motion parameters including angular displacements, velocities, and accelerations were shown in Figure 33, Figure 34 and Figure 35, respectively. The maximum angular displacement of J_1, J_2, J_3, and J_4 are 88.1, 88.4, 75.52, and 84.3 degree, respectively. Each joint has two-way motion from start

point to target point and reverse. That's why the angular velocities and accelerations are almost zero in 1.5 s and 5.5 s; and 3.5 s, respectively. The motion direction was changing in the 1.5 s and 5.5 s, and the robotic arm was in the half of the way at the 3.5ed second. The J_2 has two torque peaks including 31.91 and 27.89 N.m, while, the maximum torque value was significantly lower in the J_1, J_3, and J_4 including 16.22, 8.3, and 1.63 N.m, respectively (Figure 36). The peak torque values are depending on the shaped of motion path at the direction changing moments. If the direction changing paths was sharp, the peak torque values were increase because the servo motors need more power to control the speed and inertia of structure. If the path was curvier, the peak torque values were decreased significantly and this changing effect on power consumption as shown in Figure 37. This figure shows that the power consumption was ascending respect to time. The power consumption of J_1 was significantly higher than other joints, because this joint was the only joint that support the horizontal motion.

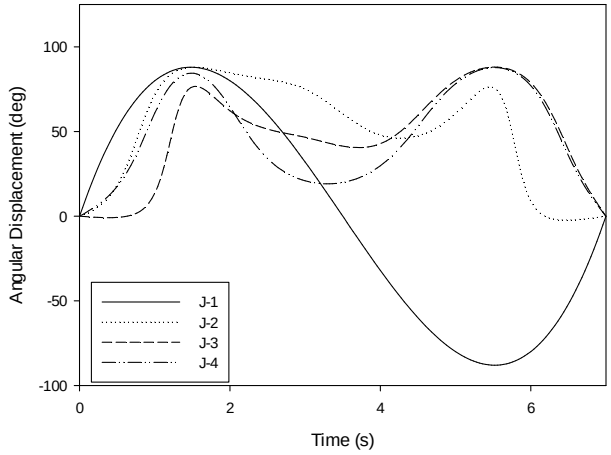

Figure 33. The angular displacement of joints in upward motion.

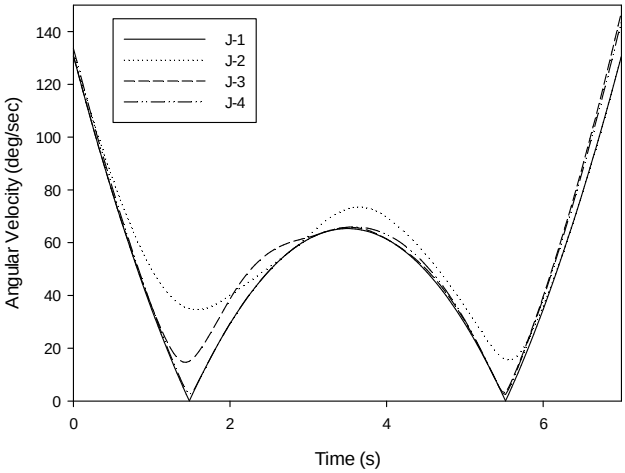

Figure 34. The angular velocity of joints in upward motion.

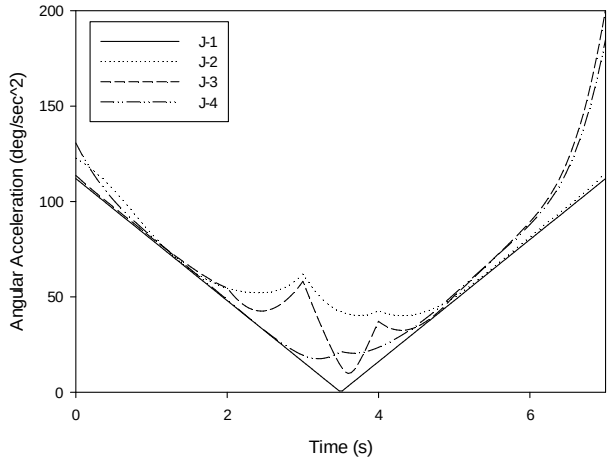

Figure 35. Angular acceleration of joints in upward motion.

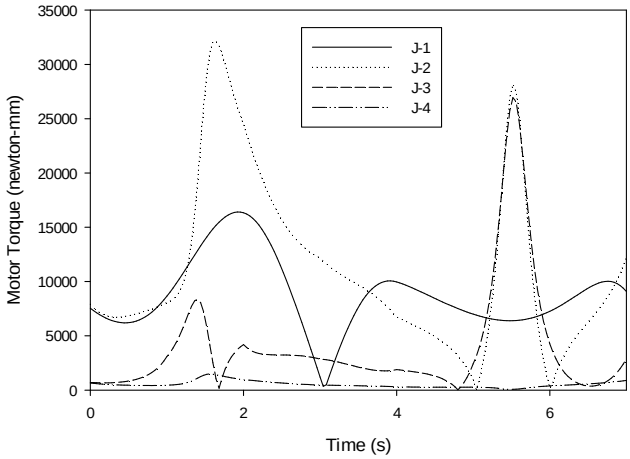

Figure 36. The torque of joints in upward motion.

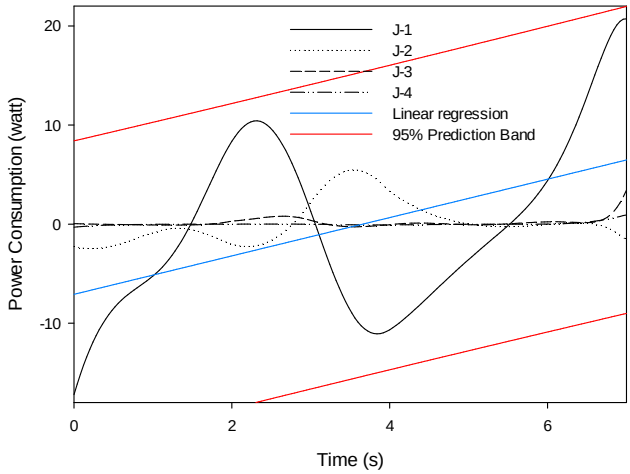

Figure 37. The power consumption of joints in upward motion.

3.12.4.2. Downward motion

The downward motion parameters including angular displacements, velocities, and accelerations were shown in Figure 38, Figure 39, and Figure 40, respectively. The maximum angular displacement of J_1, J_2, J_3, and J_4 are 88, 120, 90, and 88 degrees, respectively. The J_2 has two torque peaks including 152.68 and 92.08 N.m which is significantly larger than upward motion. The maximum torque value was significantly lower in the J_1, J_3, and J_4 including 25.08, 45.47, and 19 N.m, respectively as shown in Figure 41. The peak torque values are depending on the sharpness of motion path at the direction changing moments. If the direction changing paths was sharp, the peak torque values was increase because the servo motors needs more power to control the speed and inertia of structure. If the path was curvier, the peak torque values was decrease significantly; and this changing could affect on power consumption as shown in Figure 42. This figure shows that the power consumption was ascending respect to time and the ascending of downward motion was bigger than upward motion. The summarizing the motion results was shown in Table 11.

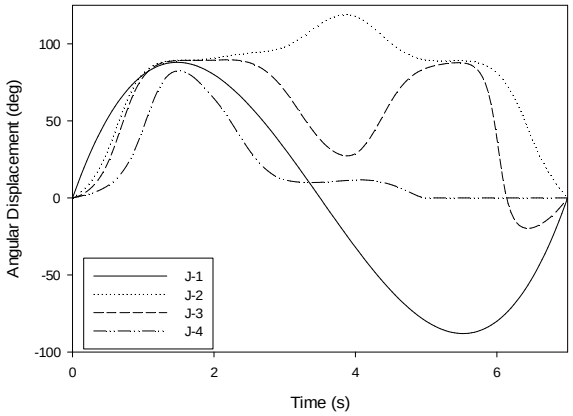

Figure 38. The angular displacement of joint in downward motion.

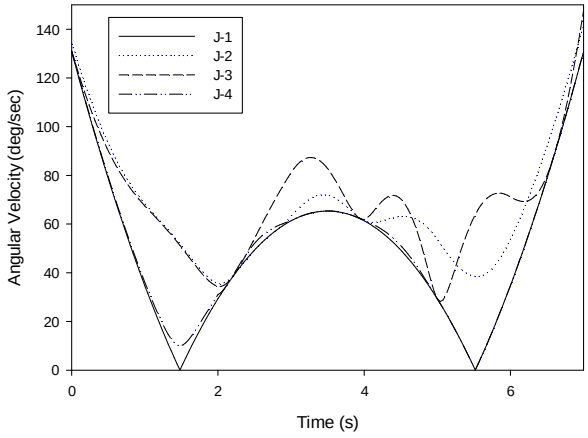

Figure 39. The angular velocity of joint in downward motion.

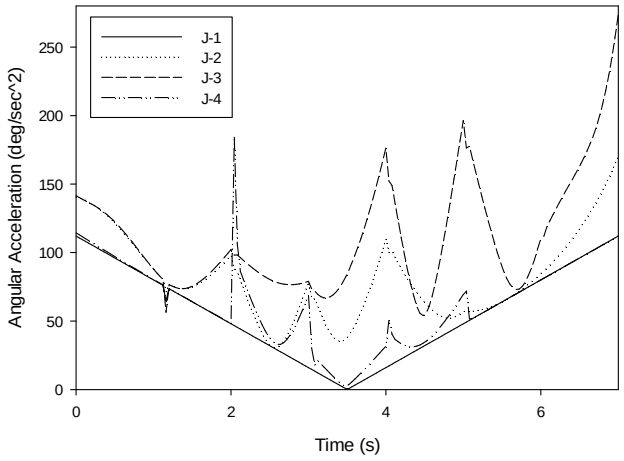

Figure 40. Angular acceleration of joint in downward motion.

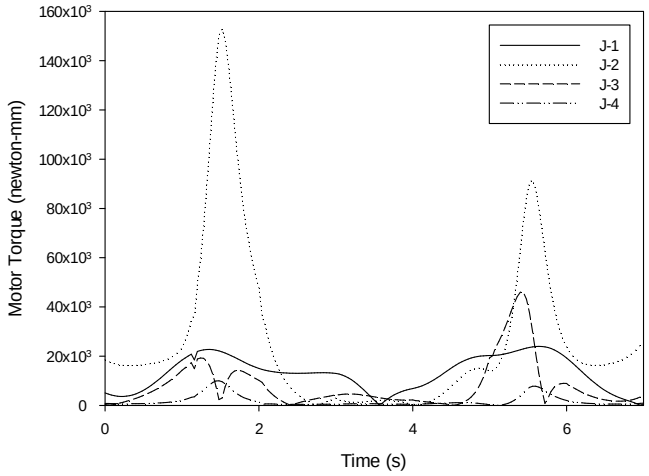

Figure 41. Joint's torque in a downward motion.

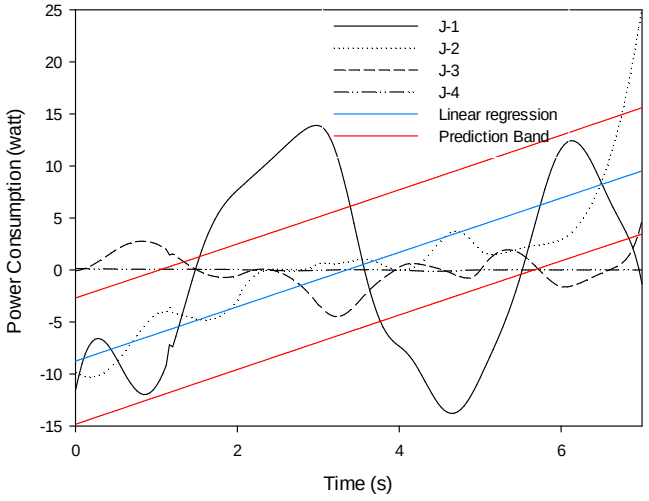

Figure 42. The power consumption of torque in a downward motion.

Table 11. Summarizing the motion results.

	Upward	Downward
Displacement	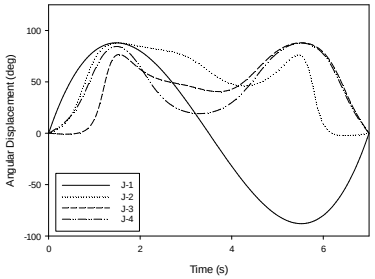	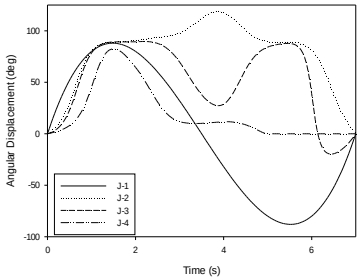
Velocity	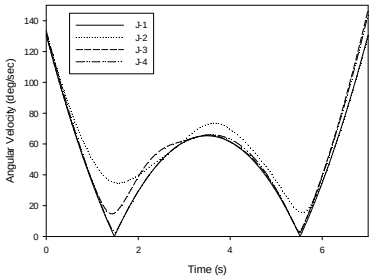	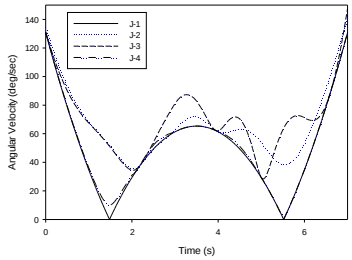
Acceleration	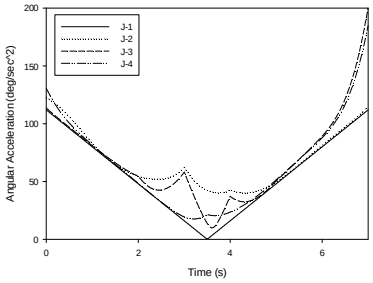	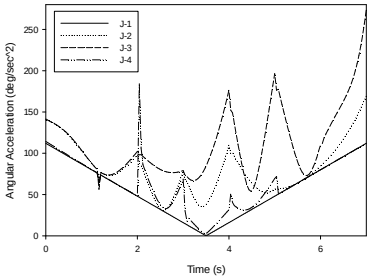
Torque	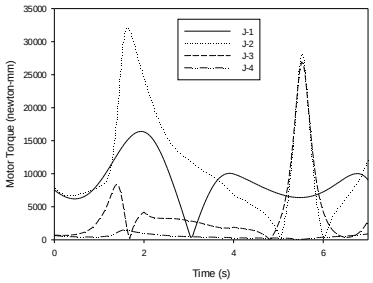	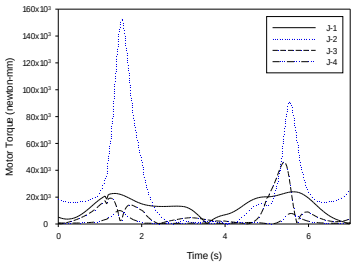
Power	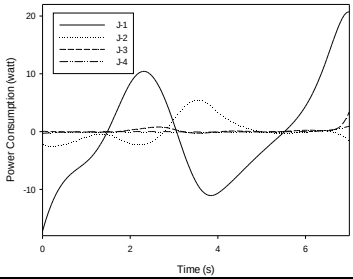	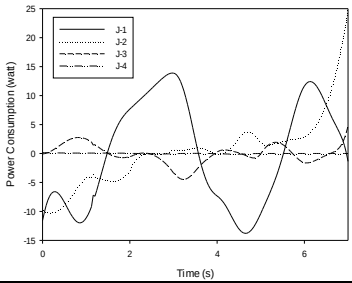

3.12.5. Accuracy and repeatability of robotic arm in different type of motion

Before using the developed robotic arm, it is necessary to calibrate the motion. Such calibration must involve combining experimental values for end-effector position in space with algorithm standard expected values. Calibration of the system was conducted for four missions, including circular, rectangular, square, and triangular (Figure 43). It was assumed that the motions had to follow a point-to-point (PTP) motion with variable velocity in most of the cases. A linear trajectory is not a priority in the agricultural application. Calibration results showed that the average error of the system in different motions was 2.2 mm in X-direction, 2.11 mm in Y-direction and 1.24 mm in Z-direction. The average resultant positional accuracy of the designed robotic arm was 1.85 mm. The maximum and minimum accuracy in X and Y-direction ($error_x, error_y$) were found with the rectangular motion (2.42 mm, 2.55mm) and circular motion (1.66 mm, 1.24 mm), respectively (see Table 12). But in the Z-direction, the maximum and minimum accuracy was found with square motion (2.74 mm) and triangular motion (0.49 mm), respectively. In the rectangular motion, the algorithm adhered to linear motion, but torque optimization caused non-linear motion. In contrast, a special step was developed in the algorithm to drive the system in a circular motion. This means that circular motions did not follow PTP motion.

The results show the accuracy of different missions has no significantly different, while PTP motion (which used in rectangular, square, and triangular motions) has less accuracy than linear motion (which used in a circular motion). It should be noted that the PTP motion spends a short time to finish a mission than a linear motion. It means for high accuracy and high-speed applications, it is recommended to use linear motion and PTP motion, respectively. The calculation results indicate that the repeatability of each mission (circular (±0.62 mm), rectangular (±0.59 mm), square (±0.62 mm), and triangular (±0.21 mm)) are not significantly different. The average reparability of the system was calculated ±0.51 mm. Also, the results demonstrated that the average system error was suitable for the defined application, and the robotic arm had sufficient accuracy to harvest a heavyweight crop. Over short distances, the error could be reduced to 1 mm due to algorithm behavior. This indicates the robotic arm also has the capacity to maneuver in situations that require accuracy. After final development including EE development and installation of robot tractor, these parameters were evaluated again by using various objects (pumpkins).

Table 12. PTP motion error.

		Circular	**Rectangular**	**Square**	**Triangular**	**Average**
Accuracy A_p (mm)	X-direction	1.66	2.42	2.31	2.4	2.2
	Y-direction	1.24	2.55	2.37	2.28	2.11
	Z-direction	0.25	1.51	2.72	0.49	1.24
	Resultant	1.05	2.16	2.47	1.72	**1.85**
Repeatability, R_p (mm)		±0.62	±0.59	±0.62	±0.21	±**0.51**

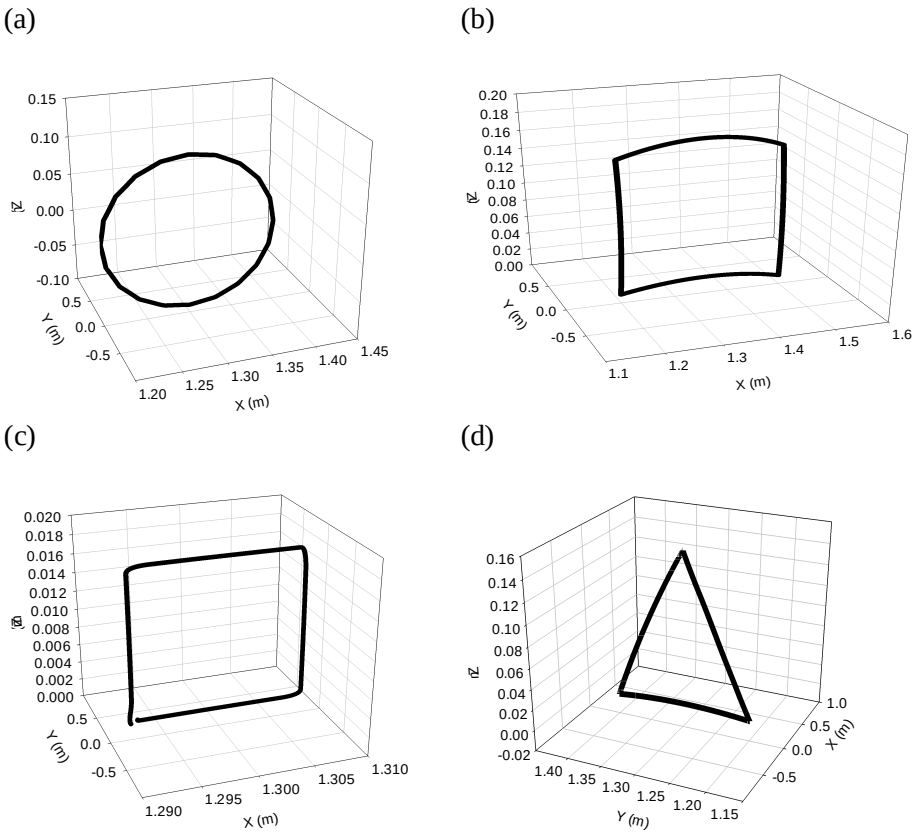

Figure 43. PTP motions calibration results, (a) circular, (b) rectangular, (c) square, (d) triangular.

3.12.6. The effect of material changes in the required torque

Table 13 illustrates the values of required torque in three different A, B, and C designs (in the cases of material and servo motor location). It is obvious that the static, dynamic and total torque declines during of each modification from A to B, and from B to C, whereas the robot fundamental structure, remained unchanged. In A-design which was the reference design, the material of the components was ASTM A36 steel and all servo motors were set their respective joint position (it means that the servo motor number 2 is set in the joint 2, the servo motor number 3 is set in the joint 3, and so on). In condition B, the material of components was changed to AL5202. In condition C, not only the component materials changed to AL5202 but also the positions of servo motors were changed to the locations nearby the joint-2. As shown in Figure 44, all torque values were reduced dramatically from condition A to C. The total torque in J_1, J_2, J_3 and J_4 was reduced from condition A to B due to the change in the material. There is no a balance weight for decreasing static torque because of the complex structure of the body. Also, the material changing was done only on the main body components, not on joints, bolts, and nuts. The position of the servo motors changed for the conditions C; giving as a result reductions of total torque in J_1, J_2 and J_3 joints. Because of the RAVebots-1 special structure, the static torque in J_1 and J_5 is equal to zero for all conditions. As a conclusion, adjusting the material of the body and the servo motor location directly affects the torque values.

Table 13- Effect of linkage material changing and servo motor position improving joints torque.

condition	Torque $(N.m)$	J_1	J_2	J_3	J_4	J_5
A	Static	0	634	233.5	33.1	0
	Dynamic	14.48	14	3.1	0.17	0
	Total	15.48	648	236.6	33.27	0
B	Static	0	360.5	134.25	20.1	0
	Dynamic	7.57	8.5	1.95	0.1	0.1
	Total	8.57	369	136.20	20.2	0.1
C	Static	0	253	101.9	20.1	0
	Dynamic	5.15	4.35	1.5	0.1	0.1
	Total	6.15	257.35	103.4	20.2	0.1

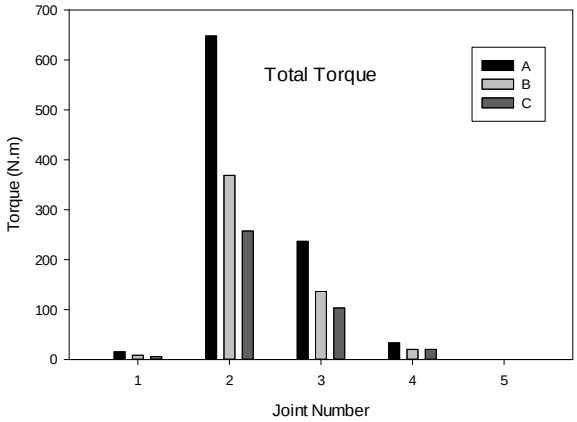

Figure 44- The impact of changing the type of material and the joint position in the total torque

3.12.7. Joint velocity

In designing of a robotic arm, it is necessary to compare the analytical output of joint speed and torque with the experimental output. The speed of all servo motors must follow the specified equation, $V = V_0 + a^{0.5\,(^{T-T_0}/_b)^2}$ (mentioned as the optimized standard motion in the datasheet). The V, V_0, T and T_0 are servo normal velocity (speed), servo velocity at the starting point, time, and time at the starting point, respectively. In the equation, a and b are the constant values of the designed algorithm determined at each time-step. Figure 45 compares experimental output to analysis results. The behavior of this change was steady for all joints at each functional step. As shown in Table 14 and Table 15, there was no significant difference between scores for real-world experimental results (M = 3.03, SD = 1.73) and analysis results (M = 3.04, SD = 1.7); t (-7.42) =8099, p = 0.064. This indicates that output of controlling and determined equation in the algorithm has no significant difference. And also, we could, therefore, conclude that torque change in the real-world experiments was not significantly different from the analytical results.

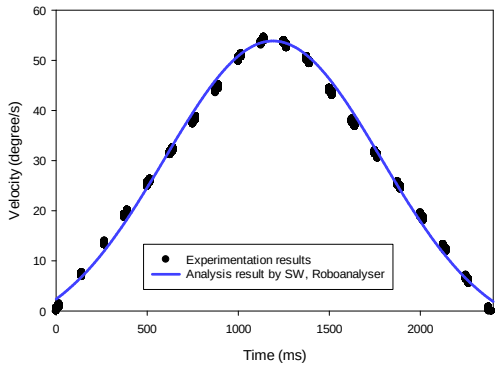

Figure 45. Joints velocity behavior based on analysis and real-world experimentation.

Table 14. Paired samples statistics.

		Mean	N	Std. Deviation	Std. Error Mean
Pair 1	Experiments	3.03	8100	1.73	0.019
	Analysis	3.04	8100	1.69	0.018

Table 15. Completion of experimentation result of paired samples T-Test.

	Mean	Std. Deviation	Std. Error Mean	95% Confidence Interval of the Difference		t	df	Sig. (2-tailed)
				Lower	Upper			
Experiments - Analysis	-0.015	0.185	0.00207	-0.019	-0.011	-7.418	8099	0.064

3.12.8. Harvesting methodology

For heavy-crop harvesting, a special methodology is needed. As mentioned in section 2.3, such a methodology can increase harvesting speed by eliminating unnecessary motions. A sample controlling methodology was determined (Figure 29). In Figure 46, robot motion begins in the transportation position. It moves through the working position, grasping position, stem-cutting position, and then begins to carry the object (crop) to the truck. This methodology was accomplished in the analysis environment using Solidworks software, and in real-world experiments, as shown in Figure 47. The statistical analysis did not find a significant difference between the scores for real-world experimental results and analysis results in the X, Y and Z directions, as shown in Table 16. Average standard deviation in the X, Y and Z directions was 3.78, 3.81 and 3.91 mm, respectively. Thus, accuracy and authenticity of the controlling program were shown to be quite high.

As result, it was necessary to assess velocity and torque behavior in the course of the methodology from point O to E. As shown in Figure 48, velocity ranged between -96.14 and 110.55 $degrees/s$. Although the velocity was changeable based on the described programming parameters, the experimental and analytic results were in good accord, as shown in Figure 48. The torque behavior was not predictable due to the different parameters indicated in a nonspecific pattern, shown in Figure 49. Assuming FOS=2 in those results, the maximum torque of J1, J2, J3 and J4 was 143.75, 530.78, 242.81 and 24.68 N.m, respectively. This means the torque value J1 to J4 in a regular real-world situation was 71.87, 265.4, 121.4 and 12.34 N.m, respectively, without FOS consideration. These values are in a safe range as mentioned in section 2.

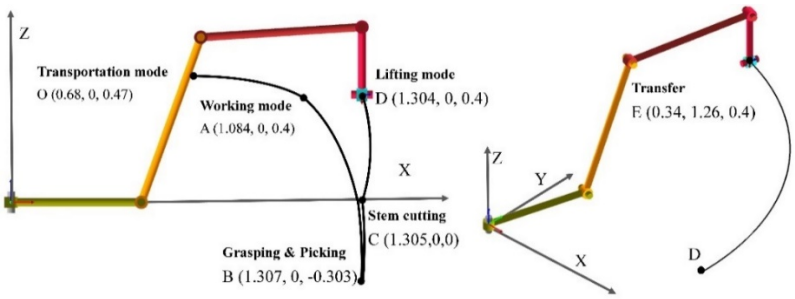

Figure 46. Endpoint position movement methodology.

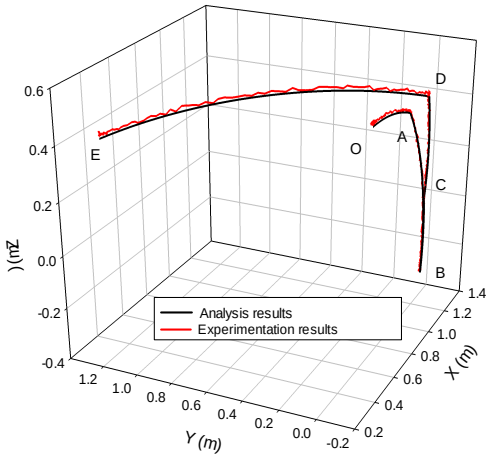

Figure 47. Endpoint position in 3D space

Table 16. statistical result of path compression.

	Mean (mm)	Std. Deviation (mm)	Std. Error Mean	95% Confidence Interval of the Difference		t	df	Sig. (2-tailed)
				Lower	Upper			
Pair 1 $X_{analysis}$ - X_{exp}	-5.82	3.78	0.169	-6.16	-5.49	-34.46	500	0.076
Pair 2 $Y_{analysis}$ - Y_{exp}	-6.15	3.81	0.170	-6.49	-5.82	-36.10	500	0.055
Pair 3 $Z_{analysis}$ - Z_{exp}	-6.09	3.91	0.174	-6.44	-5.75	-34.86	500	0.092

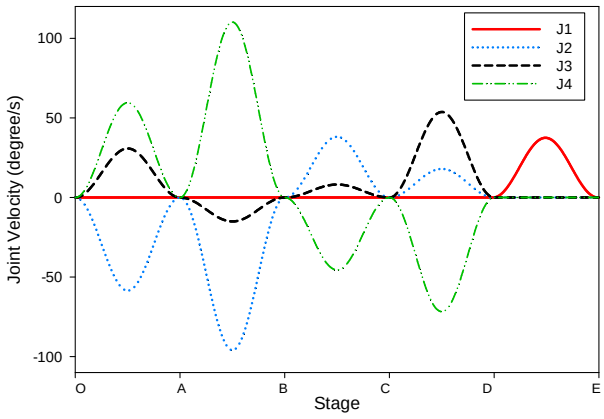

Figure 48. Joints velocity in during of harvesting, based on software analysis.

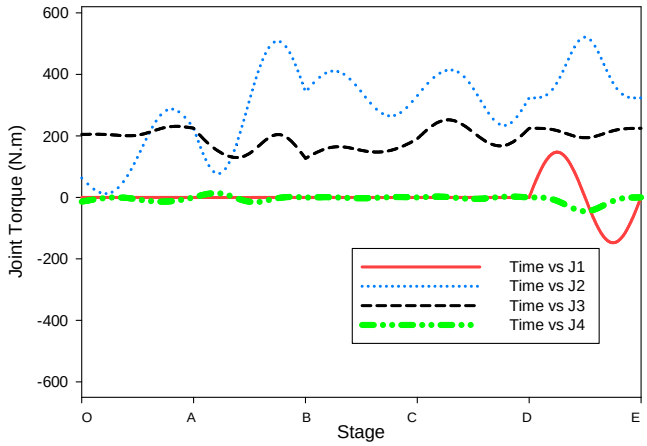

Figure 49. Joints torque in during of harvesting, based on software analysis.

3.13. Conclusion

This chapter has presented a development process of a robotic arm (robotic arm) for a mobile platform (robot tractor). The reviewing of previous agricultural robotic projects in last 30 decades was presented and tried to improve the Japanese farmer life by developing a heavy-crop harvesting system. The limitations and concern of current agriculture were described. The objective of this chapter was mentioned. The designing procedure of RAVeBots-1 described and all the details were explained in detail. The required parameter including desired workspace, front access, and height access was mentioned. All used standards in different stages of designing including parts designing, assemblies, drawing, testing, calibration, and optimization were mentioned. The different calculation including joint torque, a moment of inertia, DOF optimization, economic indexes, PPW, and repeatability was mentioned.

The economic and DOF calculations indicate that a 4R structure can cover a proper harvesting surface; and has optimized workspace index, front access, height access, and workspace. However, a 5-DOF structure can support more value of indexes and parameter, but it has no significant difference with 4-DOF. This even though the 5-DOF uses 23% more electrical power than 4-DOF, it can only increase 6% of harvesting area, and 3% of harvesting surface index. The manufactured RAVeBots-1 workspace volume was 8.27 m^3, allowing it to cover 3.52 $m^2$of field surface. After being equipped with a specially designed end effector, these values could increase to 12.06 m^3 and 6.37 m^2. That means the workspace can cover the desired volume for the determined application. The PPW compression illustrated that the PPW of RAVeBots-1 is 144% more than the average PPW of the current industrial robotic arm within payload range of 10 ~ 40kg and minimum weight. This result also indicates that the optimized structure for specific application not only can reduce the cost but also significantly increase the application parameters. It is clear, the industrial robotic arm is developing for multi-function and they can have some parameter which will never use is agriculture application. This reason makes them pricey, complex, heavy and sensitive.

Different components, all related elements, and their designing procedure was mentioned. In during of designing some modification in material and servo motor location was applied which mentioned in detail. The presented strategy for material improvement and heavy components modification has positive results on maximum payload, mass center position, and total components weight. Also, it improved the servo motor's required torque more effectively. The Solidworks simulation results and the detailed mass effect on required torque for situation A, B, and C confirm this conclusion.

As the number of CAD simulation was so much, the important simulations were illustrated. The stress, strain, and FOS of the designing process were explained and reported. Because of infinite possibility in motion analysis, two upward and downward simulations were discussed only. The component

manufacturing and final assembled system were illustrated. Regarding the methodology selected exclusively for heavy-crop harvesting, the results for the end-point position, servo motor speed, and torque showed no significant difference between the experimental and analytical results. The control system, synchronized using an algorithm developed based on kinematic and dynamic calculations and coordinated parameters of the PLC system, established a smooth trajectory.

The calibration experimentations show that the designed robotic arm has an average accuracy and repeatability of 1.85 mm and ±0.51 mm in, 3D space. However, these values were increase after final developments because of some reasons like EE's weight. The circular mission with linear motion has shown the highest accuracy of 1.05 mm and the square mission with PTP motion have indicated the minimum accuracy of 2.47 mm. However, the linear motion was more accurate than PTP motion but it takes long cycle time to finish a mission. It is shown that the motion type directly depends on the accuracy or speed priorities which can change based on the harvesting methodology.

In the future study, the performance evaluations of the designed robotic system with end-effector will be defined by different missions, loads, positions, speed, and type of motion in a field environment. Hopefully, the RAVebots-1 design will be produced and utilized in everyday agricultural practices, especially in the harvest of heavy-weight crops. This agricultural robot will be capable of harvesting due to the attached camera and specially designed end-effector. The robot can collect physical data on crops (weight, volume, density, etc.), harvesting crops, and then deposit them at a designated location.

Chapter 4. Characterization of physical properties of pumpkin

4.1. Pumpkin

The pumpkin is a cultivar of a squash plant, most commonly that is round, with smooth, slightly ribbed skin, and deep yellow to orange coloration. The thick shell contains the seeds and pulp. Some exceptionally large cultivars of squash with similar appearance have also been derived from Cucurbita maxima. Specific cultivars of winter squash derived from other species, including C. Argyros Perma, and C. Moschella, are also sometimes called "pumpkin". Kabocha (a Japanese variety of the species Cucurbita maxima) is a type of winter squash. It is also called kabocha squash in North America. In Japan, "kabocha" may refer to either this squash or to the Western pumpkin (Wikipedia, 2016, 2017b). The aim of this chapter is parametrization and characterization of physical and mechanical properties of pumpkin and determine a methodology for characterization of heavy-weight crops such as pumpkin.

4.1.1.Pumpkin anatomy

As shown in Figure 50, the pumpkin is made up of many different parts which matured including stem, tendril, leaves, lid, shell, skin, pulp, ribs, blossom end, fibrous strands, cavity, seed, seed coat, and nut. The stem is located at the very top of the pumpkin. Brown to brownish green in color and slightly curved, the stem is attached to the vine and provides nutrients to grow the fruit, just like an umbilical cord. The Tendrils are green, thin and hair-like. While the plant is growing, the tendrils twist around objects on the ground to help anchor the vine and protect it from the elements, like the wind. The leaves of the pumpkin absorb energy from the sun to allow the plant and fruit to grow. After cutting a pumpkin (for carving) around the stem to open it, is known as the lid. The pumpkin shells refer to both the skin and the pulp of the fruit. The external layer of the pumpkin is called the skin, or rind. This is a protective layer that keeps insects and disease out of the fruit. The is also known as the meat of the fruit which is used to cook with. The ribs are the external shape of the pumpkin is made up of indented ridges running from top to bottom. When the fruit is young a flower blossom is at the end of the fruit. This is known as the blossom end, which becomes the bottom of the fruit. As the female flowers become pollinated a fruit develops and the flower dies off; Fibrous Strands consists of its fibrous strings and seeds. Once the fibrous strings and seeds are removed, you are left with the empty cavity of the fruit. Seeds are located in the center of the pumpkin and attached to the fibrous strings. The seeds can be separated, dried and eaten, or used for the next harvest. Seed Coat is the outer layer of the seed which helps to protect the nut inside that will eventually grow into a pumpkin plant. This is also known as the seed jacket, and Nut is located inside of the seed. When a seed is planted the moisture and warmth triggers the nut to begin to grow into a new plant (WordPress, 2017).

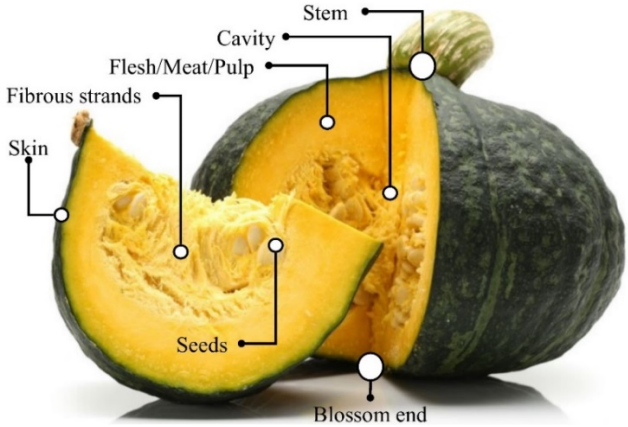

Figure 50. Anatomy of pumpkin.

4.1.2.Popular varieties in Japan

Pumpkin is widely grown all over the world. It is a warm-weather crop, selective-harvesting, and its bush grows nearby the ground. Most of the pumpkin (kabocha) grown in Japan today is related to a western variety originally from the western part of South America that was first brought to Japan in the 19th century. Japan kabocha pumpkin and mocha kabocha pumpkin are also related to varieties brought from Portugal in the 16th century that originally were from Central America and the northern part of South America. There is also pepo kabocha pumpkin, which is used primarily for decorative purposes. In addition to the main variety called Ebisu, which when cooked offers a perfect hearty warmth and stickiness, there is also Kuriyutaka, which is hot and flaky when cooked, and Ajihei DX, which has a high sugar content. Each variety features a different taste, but each has become a staple in Japanese cuisine. Japan has a custom of eating kabocha pumpkin in the winter and the event food called Itokoni, which is rice porridge with soybeans and kabocha pumpkin, is well known.

Hokkaido has the largest yield of kabocha pumpkin than any other part of Japan, accounting for almost half the market. For many years, the annual schedule was for Kanto-grown kabocha pumpkin to hit stores from spring to summer, while that grown in Hokkaido appears in stores from September to October, with imported pumpkins sold thereafter until the next spring. As shown in Figure 51, the Kabocha pumpkin is mainly grown in the Kamikawa area, with most cultivated in the northern municipalities of Wassamu Town, Nayoro City, Bifuka Town, Mukawa City, Shibetsu City, Memuro Town, Furano City, Kamifurano Town, Mori Town, Kenbuchi Town. However, Wassamu Town, known as the town of pumpkins, began growing multiple varieties of pumpkins with different growing periods, which extended the harvest and, through extended storage, made it possible for people in Japan to eat domestically grown kabocha pumpkin until December. This is the successful outcome of producers using trial and error to make it possible to obtain Hokkaido-grown kabocha pumpkin during the winter, which is a customary time to eat it. Seeds are planted from the middle of May to end of June and raised in a greenhouse until they become seedlings. These seedlings are then planted and harvested between the beginning of September and middle of October. Later, the kabocha pumpkins are shipped after drying and storage. They can be stored for a period of up to around 2 months (Hokkaido Food library, 2017). In this study, three popular pumpkins as main specimens including JEJEJ, TC2A, and Hokutokou, and three more varieties including Sukuna, Kikusui, and Ebisu were studied as shown in Figure 52.

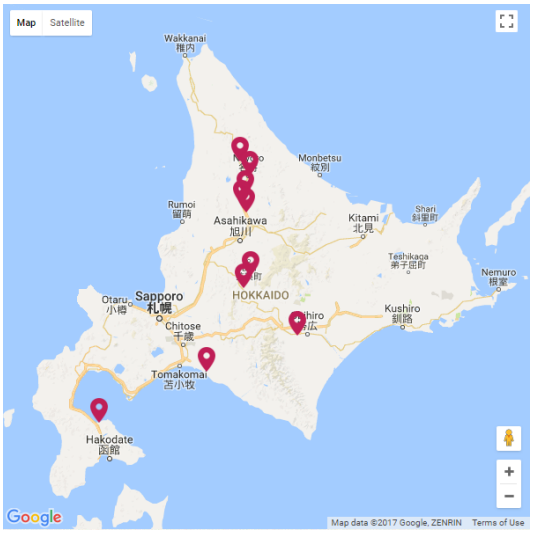

Figure 51. Main producing municipalities

Figure 52. Experimented varieties.

4.2. Pumpkin parameterization

As the complexity and non-uniformity of agricultural products, parametrization, and physical properties evaluation of target crop are necessary. As the pumpkin is round shaped and it has smooth and slightly ribbed skin, the harvesting parameterization could be different in comparing to other robotic harvestable crops as tomato, strawberry, and cucumber. In this regard, some field experimentation, physical properties tests, and compression strength test was done on JEJEJ, TC2A, and Hokutokou, Sukuna, Kikusui, and Ebisu as most popular pumpkin verities in Japan.

4.3. Experimentations

In this study, four different experimentations were done on pumpkins including (1) stem orientation in the field, (2) physical proprieties, (3) compression strength test, and (4) bending-shear test.

4.3.1. Pumpkin orientation in field and physical properties

The location and orientation of each pumpkin are unique and unpredictable, that why robotic harvesting of this crop has unique challenges. In a usual field, the pumpkins grow in different orientation based on the soil density and sun irradiation. The orientation of pumpkins can change in during of life by weight increasing. Because of that, it is important to design a special end effector that can harvest pumpkins with an unpredictable orientation. In this regard, several experimentations were done in the Hokkaido agricultural research center (NARO). The aims of these experimentations were an investigation of pumpkin orientation, pure weight, lift weight, and possible harvesting methodologies consideration. The pumpkin's pure and lifts weight was measured by using a digital scale with 0.001g sensitivity. The pure weight was the pumpkin weight itself, and the lift weight was the weight of pumpkin when its stem is connected to the bush yet; the applied to lift the pure weight is less than lift weight because of stem connection. The approximate orientation angle was measured by standard methods. After measuring field parameters, the pumpkins were cleaned of soil and brought to the laboratory to extract the physical properties.

For pumpkin harvesting, the stem cutting and harvested pumpkin transferring are two main actions. Most of the pumpkin has a hard stem, and the location of the stem is not predictable, the cutting unit of end effector must specially design to cover all possible locations. As shown in Figure 53, the stem orientation (SO) is a vector from center coordinates or central position (CP) has passed from stem position (SP). The SO is the main parameter of pumpkin anatomy was indicated the pumpkin orientation. This orientation was

specified the reference direction of pumpkin. In the pure situation (without applying any forces), the SO has an angle named pure situation orientation (θ_{PSO}). The pumpkins are connected to the ground via its stem before harvesting. This connection can apply a force when the pumpkin lifting and the pumpkin rotate relative to the CP which the angle changes to angle of lift situation orientation (θ_{LSO}). That's why the θ_{PSO} can change to θ_{LSO}, that always $\theta_{PSO} \geq \theta_{PSO}$. This behavior of pumpkin was made the principles of harvesting methodology in this chapter. As in the designing of a special robotic end effector for agricultural products, having knowledge about physical properties of the crop is essential (Ludger O. Figura & Teixeira, 2007), in the coming sections, some of the physical properties of pumpkin like mass and volume was measured.

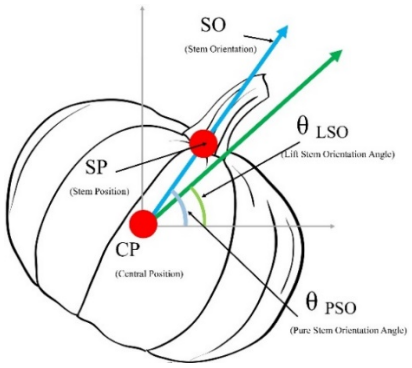

Figure 53. Pumpkin parametrization.

4.3.2. Compression strength test

Each robotic end effector directly connects to the intended crop in during of harvesting. This connection applies force and the force cause deformation and sometimes damages, that called contact deformation or strain (Blahovec, 1994). The strain can be described using elastic theories like Hook's theory and Hertz theory (Khodabakhshian & Emadi, 2011). A force contact on pumpkin structure can cause the product damage when the applied force be more than rupture stress (Ludger O. Figura & Teixeira, 2007). That is why the compression strength test is understood as an important test to keep crop's quality high in during of harvesting and storage procedure.

The designed EE have 5 fingers which located symmetrically with 72° angles in between which providing a force distribution as shown in Figure 54-a. Each pumpkin located among five fingers which each connected in two points as shown in Figure 54-a and b. As the forces (like F_1 and F_2 in finger-1) applied with (almost) same certain values of symmetric angle relative to x axis, the action of both forces neutralized in y-direction ($F_{y,1} = F_{y,2}$). The small difference is ignorable. As the direction of the mentioned forces are both in same direction (+/-), the action of them in x-direction multiply ($F_{t,1} = F_{x,1} + F_{x,2}$) as shown in Figure 54-b. If we apply this logic in applied forces of each finger, the sum of applied forces summarized as shown in Figure 54-c and the pumpkin will be under five forces which are orthogonal by SO and 72° angle in between. In this case, the sum of applied forces in x and y-directions will be zero ($\sum_{i=1}^{5} F_{t,i-x} = 0, and \sum_{i=1}^{5} F_{t,i-x} = 0$). Then, it is not important how big is the $F_{t,i}$, because from scientific of view the structure of any spaceman will not damage under the forces which has the resultant of zero in x and y-directions. However, the damage is highly passible to happen in z-direction but the value of yield force will be highly big. The possible break points are shown in Figure 54-c (yellow lines). It is obvious that the possible rupture lines all are towards the CP.

In the critical condition of force apply via EE's fingers, if we suppose that only one finger connected the pumpkin and only one force applied to the pumpkin's structure, the condition can be similar to the compassion test as shown in Figure 54-d, e, and f. In the compression test, the force applies until the yield point and the maximum force and related parameters will be the output of the test. If we want to compare

the yield force in compression test and EE's finger; the yield force of EE's finger highly possible to be bigger than the yield force of compression test on the same kind of specimen (pumpkin). This is because the EE's apples five forces which neutralize each other ($\sum_{i=1}^{5} F_{t,i-x} = 0, and \sum_{i=1}^{5} F_{t,i-x} = 0$) and the rupture will happen in high value of force which is always smaller than the rupture point force (yield force) of compression test as shown in Figure 55. It means, the yield force of a pumpkin which evaluated under the compression test condition can cover or predict the yield force of EE's fingers. The condition is slightly same when an fragile egg squeeze as hard as possible without any breaking. Also, it is important to say that a small value of force is needed for grasping and carrying the pumpkin which can be less than 40% if the yield force of compression test (Figure 55). Based on these reasons and in the author's opinion, the compression test can evaluate the pumpkin parameter's sufficiently. That's why the compression test was chosen to evaluate the yield compression force of pumpkins in different varieties.

In this study, the compression test was done by using compression testing device (INSTRON 5584) as shown in Figure 56 (a and b). The specimens were intact pumpkins that collected randomly from the field. The pumpkins were fixed on a plate and the compression force was applied to a parallel plate when the SO was approximately orthogonal with plates as shown in Figure 56 (c). The force applied with speed of 30 mm/s in room temperature until the pumpkin structure collapsed. The strain of each specimen was calculated by using Hertz theory (Jan Gliński, Józef Horabik, & Lipiec, 2011; L. R. Wilhelm, Suter, & Brusewitz, 2005). For parallel plates method, the elastic/deformability module of pumpkins as a convex body was determined by the following equations.

$$\varepsilon = {}^{\delta}/_{2R_0} \tag{6}$$

$$E_p = \frac{E}{(1-\mu^2)} = \frac{0.5 \,.\, F}{\delta^{1.5}} \left(\frac{1}{R_0} + \frac{1}{R_1}\right)^{0.5} \tag{7}$$

Where E_p, E, δ, R_0, P, μ and R_1 are proportional deformability module (Pa), deformability module (Pa), deformation (mm), major radius of curvature (mm), applied compression load (N), Poisson's modulus and minor radius of curvature, respectively.

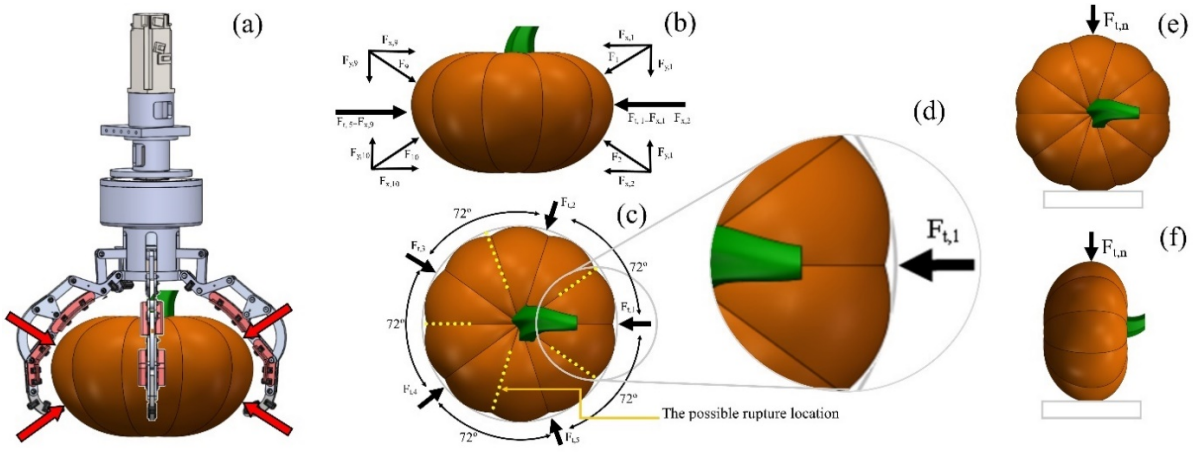

Figure 54. The forces distribution, (a) in during of harvesting, (b) side view, (c) top view; (d) the applied force when the only one finger contacted; compression test illustration (e) front view, (f) side view.

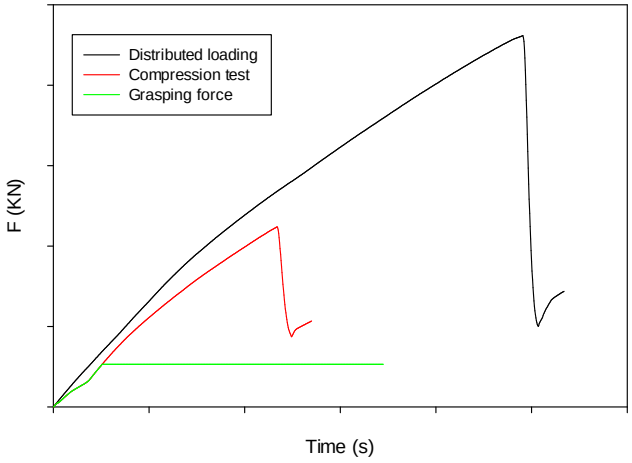

Figure 55. The difference of yield force by EE and under compression test.

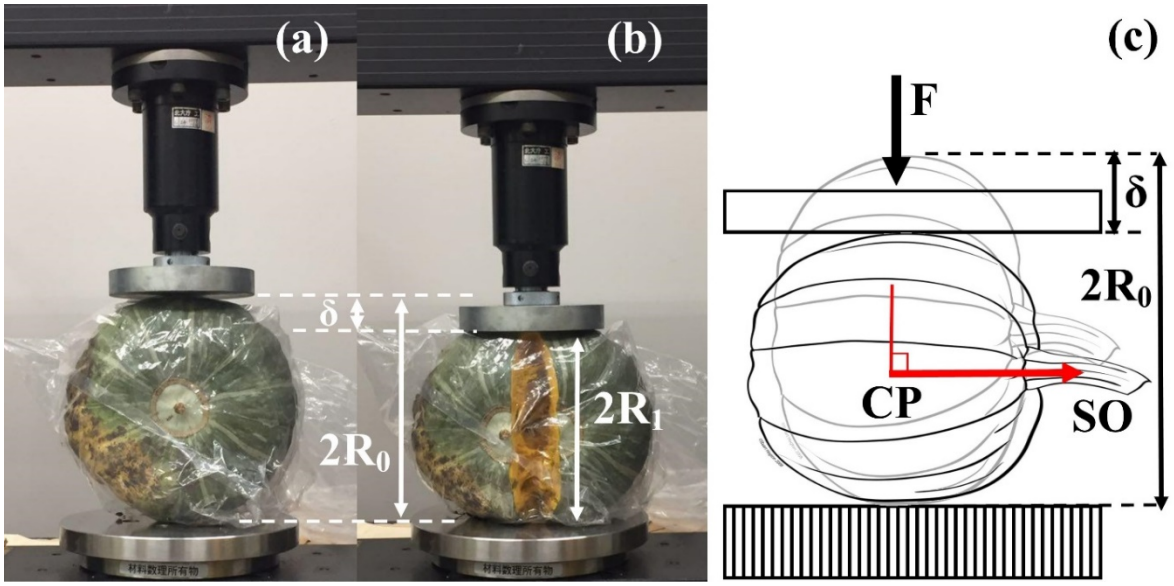

Figure 56. Compression strength test (a) before loading, (b) rupture, (c) parallel plates contact of the whole specimen (Hertz theory).

4.3.3.Bending-shear test

Bending tests are often used when it is desirable to measure the stiffness of individual specimens or the resistance to breakage (Wilhelm, Luther, Dwayne, & and Gerald, 2004). Before designing the blades of EE in this study, it was essential to do some bending tests on pumpkin's stem. The applied blades on each finger for harvesting procedure (Figure 57) must be designed based on the real physical properties of the stem. The objective of this experimentation was a characterization of pumpkin stem under the bending-shear test to modify an optimized cutting system by using specially designed loading bars. As Figure 57- a, b, c, and d, four different loading tools (blades) was designed for this experimentation including flat, single angles (with $30^{\circ}, 45^{\circ}$, and 60°), and double angles ($with\ 30^{\circ}, 45^{\circ}$, and 60°), respectively. These blades were started to cut the stems and the rupture stress were measured. These parameters were used as input parameters for final blade designing. In this test, the specimens were the pumpkins stems by certain length

(L). The experimentation was done in the pumpkin field because the structure of the stems starts to deform immediately after harvesting (cutting the stems) and laboratory experimentation would not be appropriate The stems were getting stiffer in a short term after harvesting. The force was applied at the middle of the specimens as shown Figure 57- e. To doing this experimentation, a portable loading device was designed as shown in Figure 57-d, g, & h. The aim is measuring the elasticity modulus in bending (E_{bend}), flexural stress (σ_f) and strain (ε_f). For a standard procedure of the bending test on a circular cross-section beam shaped specimen, following equations was used.

$$E_{bend} = \frac{F.L^3}{12\delta\pi R^4} \tag{8}$$

$$\sigma_f = \frac{F.L}{\pi R^3} \tag{9}$$

$$\varepsilon_f = \frac{6\,R\delta_{max}}{L^2} \tag{10}$$

Where F, L, δ, and R are applied load at the middle of the beam (N), support span (mm), deflection due to the load F (mm), and radius of the beam (mm), respectively. The experimentations were done by using 7 different blades and different number of reputations for each variety. To reduce the blades depreciation effect on experimentations, the blades was changed in each test and a new blade was used. Finally, the elasticity modulus in bending, flexural stress, and strain of each specimens was calculated and the results was compared.

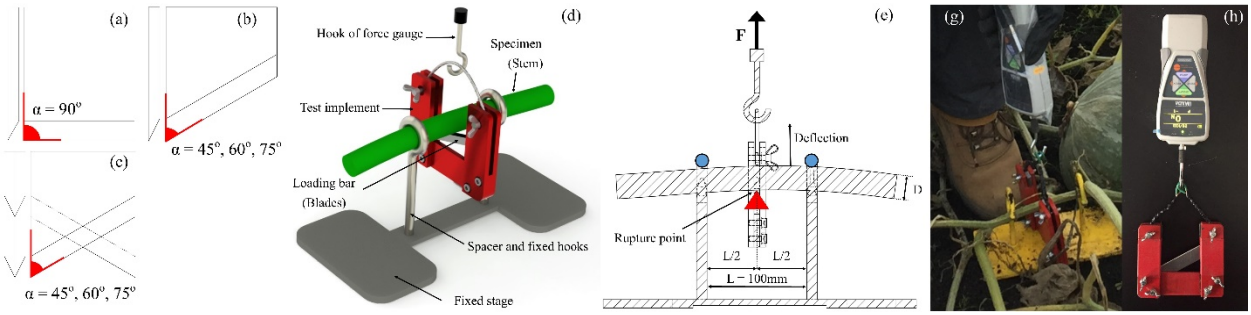

Figure 57. (a) Flat blade, (b) Circular blade, (c) single angled blade, (d) double angled blade, (e) Designed portable bending test device, (f) Bending test illustration, (g) Experimentation, (h) testing tools.

4.4. Results

4.4.1. Physical properties

The field experimentations were indicated that the average pumpkin's lift weight (the required applied force to lift when the stem is connected) was 26% more than pumpkin's pure weight (the required applied force to lift when the stem is not connected). This means in during of harvesting, the pumpkin's lift weight has a significant difference in pure weight. Unlikely to most of the other crops, the stem connection of pumpkin has an effective impact on the pumpkin harvesting. Also, the applied force on EE due to the pumpkin pure weight in the beginning of grasping stage was increased until the end of this stage because of stem connection. This force changing can effect on the EE's structure and considered in the EE's dynamic simulation. From another perspective, the stem connection in during of lifting stage not only applies a force for pumpkin rotation but also keeps the pumpkin fixed until the end of cutting stage. It was considered that the rotatory speed in the cutting stage (ω_c) must be rapid enough to cut the stem. Because, if the total reaction forces from surface friction and stem connection will be more than applied force from blades in during of rotation; the pumpkin will start to rotate; and the cutting stage will be incomplete.

The field experimentations also show that the SO of each pumpkin changes due to the stem applied force. In the pure situation, the θ_{PSO} could be in four different situations as shown in Table 17. The θ_{PSO} was predicted to be sometimes $+90^{\circ}$, mostly between -90° and $+90^{\circ}$, and rarely -90°. The experiments show that the SO could not be -90° because of grows procedure and anatomy of pumpkin. Most of the pumpkins has θ_{PSO} between -90° and $+90^{\circ}$, and less than 1% could have SO of $+90^{\circ}$ which was ignorable. After lifting, the θ_{LSO} of all of specimens was changed to the range of $-90^{\circ} < \theta_{LSO} < +90^{\circ}$ due to the applied force from stem connections. The lifting technique combination with pumpkin parametrization were simplified the harvesting algorithm in during of robotic harvesting, specifically in the stem cutting stage. Ans also, the physical properties experimentations show that the average weight of JEJEJ, TC2A, Hokutokou, Sukuna, Kikusui, and Ebisu were 3.13, 2.58, 3.12, 2.8, 1.16, and 2.37 Kg, respectively as shown in Figure 58.

Table 17. Orientation angles changing due to lifting

	θ_{PSO}	θ_{LSO}
1	$\cong +90^{\circ}$	$\theta_{PSO} > \theta_{LSO};\ -90^{\circ} < \theta_{LSO} < +90^{\circ}$
2	$-90^{\circ} < \theta_{PSO} < +90^{\circ}$	$\theta_{PSO} > \theta_{LSO};\ -90^{\circ} < \theta_{LSO} < +90^{\circ}$
3	$+90^{\circ} < \theta_{PSO} < -90^{\circ}$	$\theta_{PSO} > \theta_{LSO}; -90^{\circ} < \theta_{LSO} < +90^{\circ}$
4	$\theta_{PSO} \cong -90^{\circ}$	×

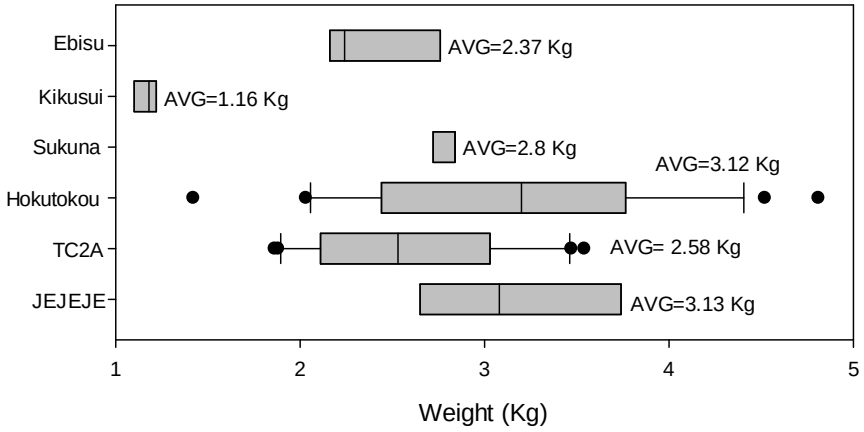

Figure 58. The range of weight for each variety of pumpkin.

One of the important parameters to feed the harvesting algorithm was the diameter ratio (DR). This parameter was important because it can indicate the relationship between the diameter of pumpkin (D_p) and diameter of stem (D_s). The DR is one of the parameters to simplify the cutting procedure and make it more precise. The D_p was the output of image processing (IP) and the D_s will predict by using the DR equations. The average, maximum and minimum value of DR and its physical parameters can present representative parameters of pumpkin. The results show that the average value of diameter ratio (DR_{AVG}) and variance for JEJEJ, TC2A and Hokutokou varieties were 15.56, 14.11, 16.25 mm, and 1.24, 1.77, 4.23 mm respectively (Figure 59). These results show that the Hokutokou variety is more variable in size and diameter ratio than JEJEJ and TC2A. Based on the results, a $DR_{max} = 20$ was selected as a maximum limitation which can cover all values of the DRs. Then if the FOS_{DR} was $\frac{DR_{max}}{DR_{AVG}}$, it is possible to calculate the FOS_{DR} of JEJEJ, TC2A, and Hokutokou as 1.28, 1.41, and 1.21, respectively. Then in the case of algorithm optimization to predict the applied force the DR_{max} was used to convert D_p to D_s with mentioned FOS_{DR} for each variety. One of the application of DR could be in the prediction of D_s and angular velocity of EE in during of harvesting to reduce the cycle time and increase the harvesting accuracy and speed. The application of DR

was discussed in the section 4.4.3 with more details. This evaluation of ideology is recommended for future studies.

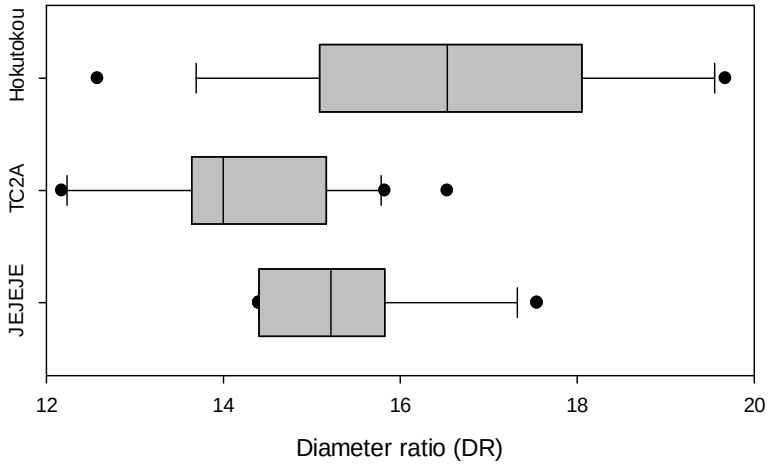

Figure 59. The diameter ratio of specimens.

4.4.2. Compression strength test results

The results of compression test were discussed in four aspects including maximum compression force (F_{ct}), strain (ε), deformability module (E_p), and a relationship between F_{ct} and diameter of pumpkin (D_p). The F_{ct} values were indicated the maximum capacity of pumpkin under direct force and it was necessary to control the applied force on pumpkin via EE's fingers and frame. Applying a force more than F_{ct} will damage the inner structure of pumpkin and reduce the marketing indexes. Each variety of pumpkin has an average yield compression force and it has a relationship with the maximum diameter of pumpkin. This relationship could follow an equation (regression equation) and the image processing system (detection system) could predict the force limitation based on the diameter of pumpkin. The strain and E_p was indicated the maximum strain and deformability of each pumpkin, respectively.

Figure 60 shows the results of compression test for 6 varieties of pumpkin including JEJEJ, TC2A, Hokutokou, Sukuna, Kisusui, and Ebisu. The main experimentation was done on JEJEJ, TC2A, and Hokutokou in 7, 21, and 21 repetitions, respectively. Because of the limited numbers of specimens, only three repetitions were done on Sukuna, Kisusui, and Ebisu varieties. Each graph shows the procedure of loading on each specimen. The compression testing machine increasing the force until the rupture. The rupture point was called maximum compression force (F_{ct}), yield force, or yield compact force in different references. Figure 61 illustrates the range of F_{ct} in 6 varieties. The maximum ($F_{ct,max}$), minimum ($F_{ct,min}$) and average ($F_{ct,avg}$) of F_{ct} in JEJEJ, TC2A, Hokutokou, Sukuna, Kikusui, and Ebisu was 4.66, 4.58, 4.61, 1.94, 2.21, and 2.5 KN; 2.81, 2.06, 2.24, 1.83, 1.53, 1.74 KN; and 3.37, 3.1, 3.23, 1.88, 1.92, 2.22 KN, respectively. Based on the results, the JEJEJ and Sukuna have shown the maximum and minimum response under the loading. As input of the algorithm, the $F_{ct,min}/2$ was considered as a final applicable force for apply the structure of pumpkin in during of grasping and harvesting. However, the experimentation shows that the grasping force are always less than the 40% of yield force. The number 2 considered as a safety factor to predict critical conditions.

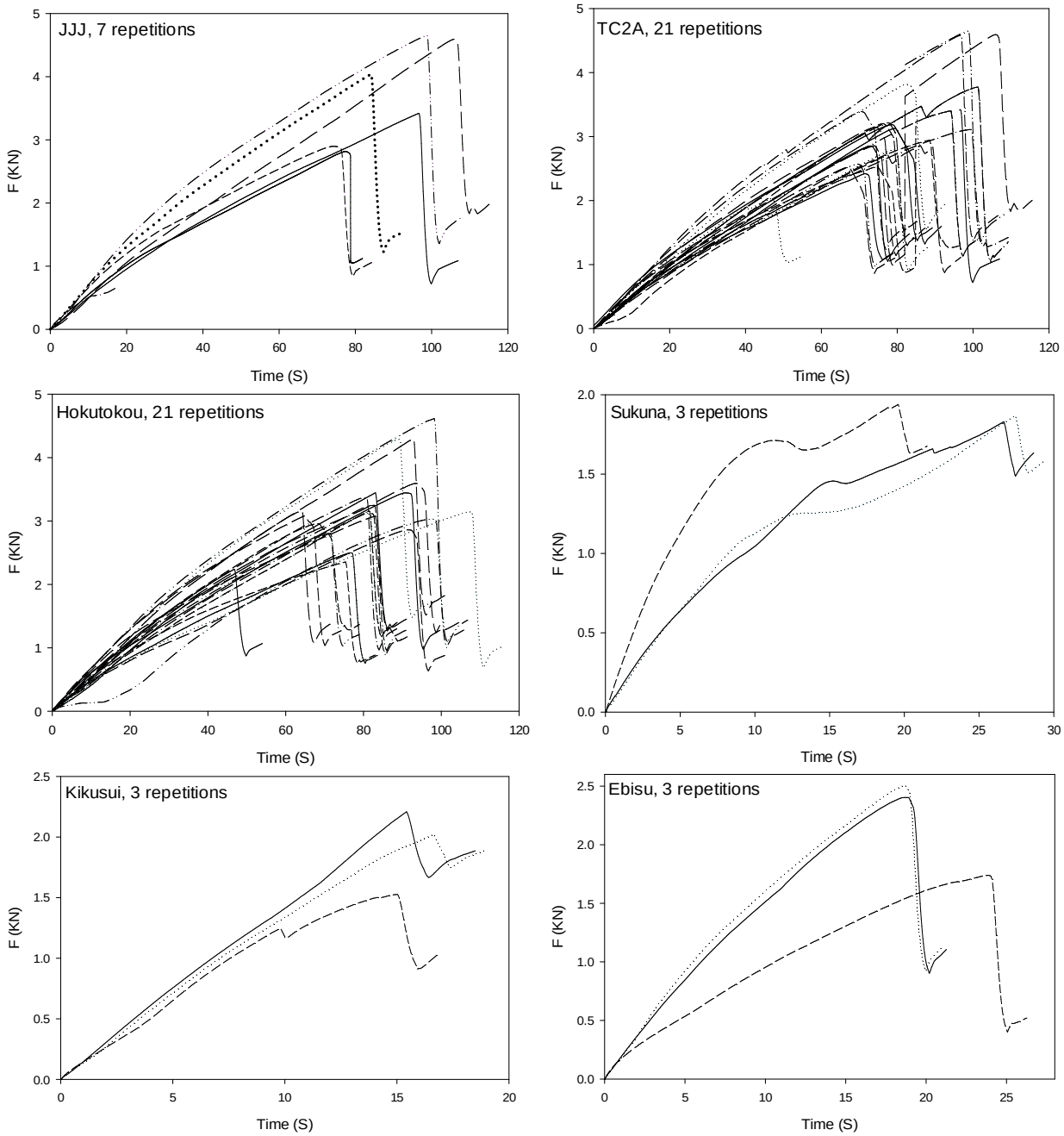

Figure 60. The results of compression test on 6 varieties.

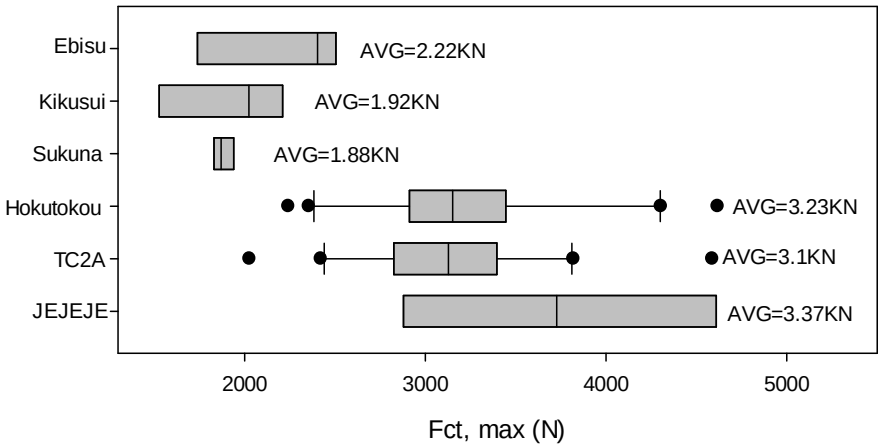

Figure 61. The maximum compression force of different varieties.

The strain and deformability module of each variety resulted as shown in Figure 62 and Figure 63. However, these parameters were not used directly to controlling the harvesting procedure, the results were presented for other researcher's studies. As shown in Figure 62, the maximum, minimum, and average strain of JEJEJ, TC2A, Hokutokou, Sukuna, Kikusui, and Ebisu were 0.2519, 0.2915, 0.2601, 0.3183, 0.14, and 0.18 $^{mm}/_{mm}$; 0.177, 0.108, 0.098, 0.307, 0.122, and 0.136 $^{mm}/_{mm}$; and 0.208, 0.204, 0.19, 0.313, 0.131, 0.154 $^{mm}/_{mm}$, respectively. The Sukuna and Kikusui show the maximum and minimum strain. As Figure 63 shows, the maximum, minimum, and average deformability module of JEJEJ, TC2A, Hokutokou, Sukuna, Kisusui, and Ebisu were 1.012, 1.269, 1.3155, 1.4062, 1.555, and 1.274 MPa; 0.733, 0.674, 0.6008, 0.677, 1.0849, and 0.615 MPa; and 0.903, 0.95, 0.904, 0.931, 1.3, and 1.01 MPa, respectively. The Kikusui and Sukuna show the maximum and minimum deformability module.

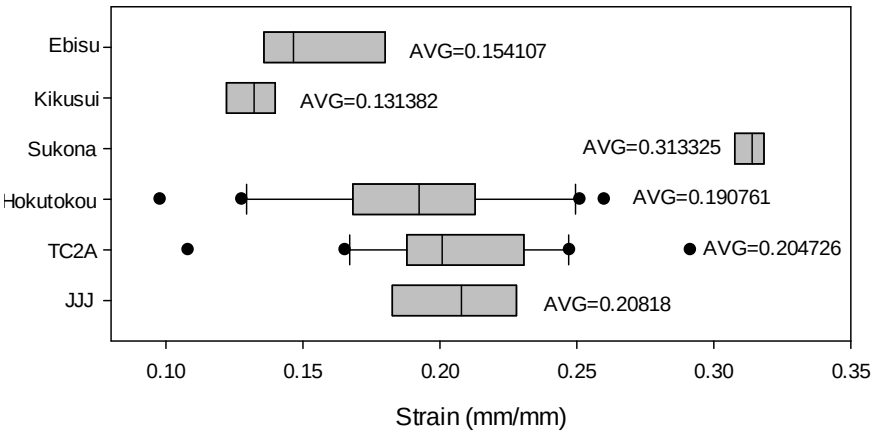

Figure 62. The maximum strain of different varieties.

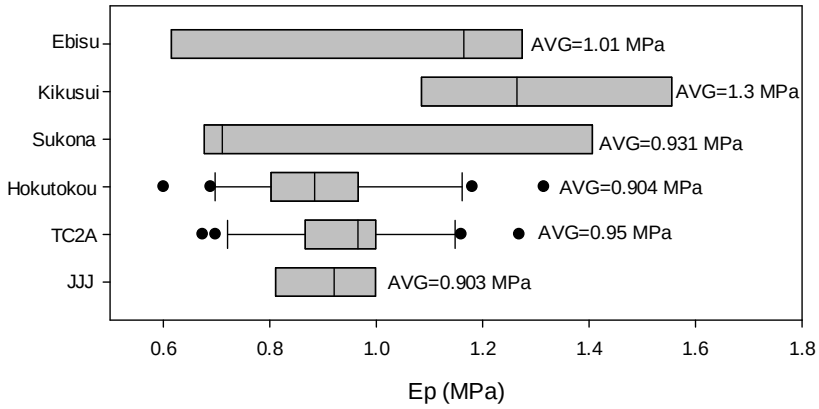

Figure 63. The deformability module of different varieties.

One of the outputs of compression test in this study can be the finding of function, relationship, or equation between F_{ct} and D_p like $f(F_{ct}, D_p)$. As, each variety has specifically physical behavior, each shows different reaction under compression test. Then, each could have a different $f(F_{ct}, D_p)$. Figure 64 shows the results of compression test and relationships between the maximum applied force and diameter of pumpkin. The experimentations were done in 7, 21, 21, 3, 3, and 3 repetitions for JEJEJ, TC2A, Hokutokou, Sukuna, Kikusui, and Ebisu, respectively. In each graph, the linear regression was outlined and confidence band and prediction band was calculated by using SigmaPlot 12.0 software. Based on the lower prediction band, a constant factor of compression test (Cf_n) was calculated. The linear regression was outlined on each graph and an unmodified equation $f(F_{ct}, D_p)$ was extracted. The Cf_n was subtracted to $f(F_{ct}, D_p)$ and the maximum compressive force to apply to pumpkin body ($F_{c,max}$) was calculated. The $F_{c,max}$ for each variety was calculated by adding a $-Cf_n$ in $f(F_{ct}, D_p)$ equation as follow:

$$JJJ: \quad F_{c,max} = 26.18\, D_p - 1905.038 - Cf_{JJJ} \tag{11}$$

$$TC2A: \quad F_{c,max} = 6.175\, D_p + 1892.37 - Cf_{TC2A} \tag{12}$$

$$Hokutokou: \quad F_{c,max} = 12.55\, D_p + 492.45 - Cf_{Hokutokou} \tag{13}$$

$$Sukona: \quad F_{c,max} = -2.175\, D_p + 2136.26 - Cf_{Sukona} \approx 2136.26 - Cf_{Sukona} \tag{14}$$

$$Kikusui: \quad F_{c,max} = -72.435\, D_p + 14915.5 - Cf_{Kikusui} \tag{15}$$

$$Ebisu: \quad F_{c,max} = -0.377\, D_p + 2290.5 - Cf_{Ebisu} \approx 2290.5 - Cf_{Ebisu} \tag{16}$$

However, in this study the image processing system was not discussed, but the algorithm, flowcharts and its parameters were predicted and investigated for future studies as an infrastructure. The $f(F_{ct}, D_p)$ could use as an input parameter in during of pumpkin grasping when the image processing system detected the pumpkin's image, its variety, and calculated the D_p.

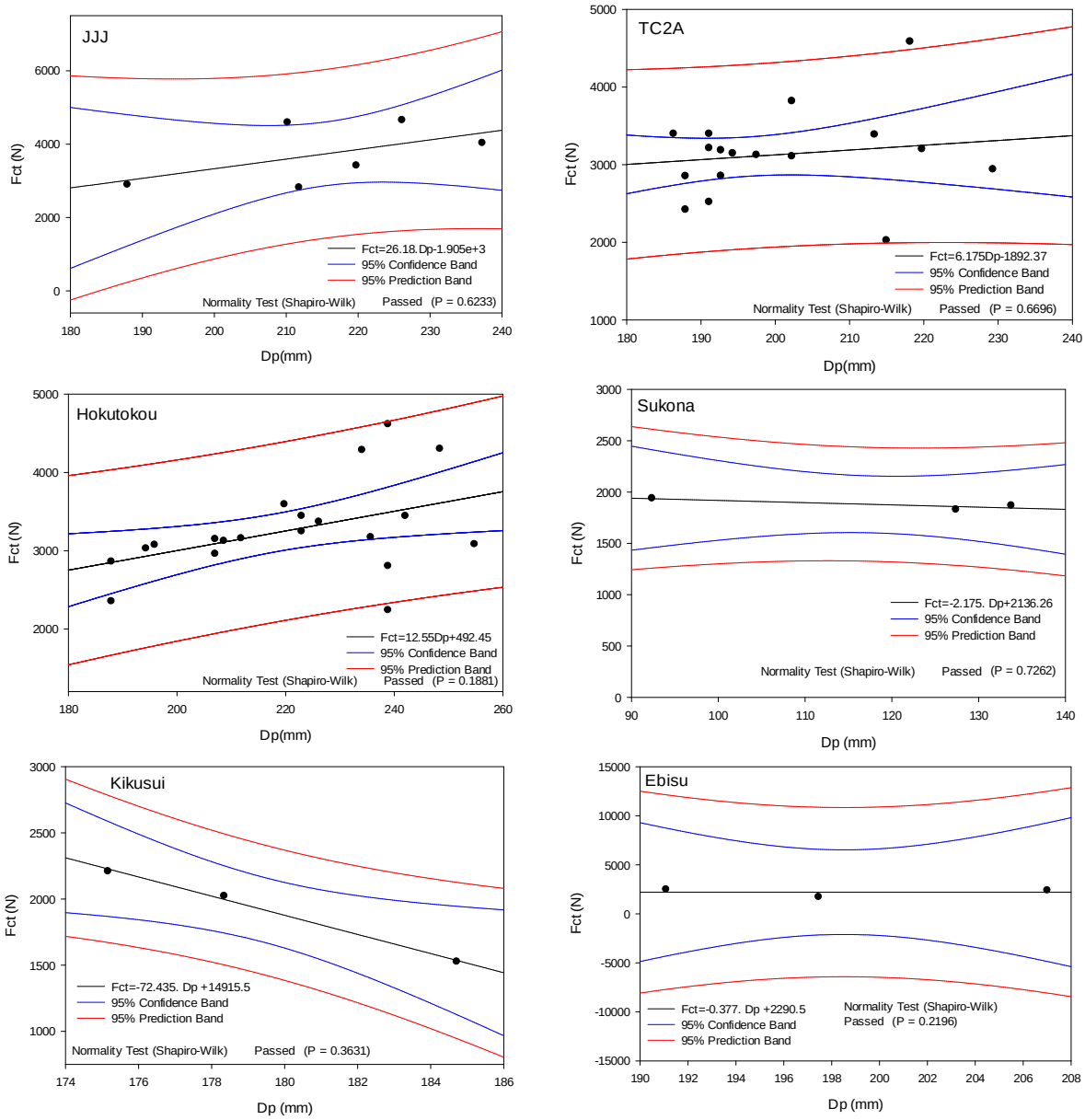

Figure 64. Compression index graph (The relationship between F_{ct} and D_p in different varieties).

4.4.3. Bending-shear test result

The results of the bending-shear test were shown in Figure 65 and Figure 66. Figure 65 (left) shows the cutting period of specimens by using seven different blades including flat (F), single angled with 45 (S-45), 60 (S-60), and 75 (S-75) degree, and double angled with 45 (D-45), 60 (D-60), and 75 (D-75) degree. It is obviously shown that the cutting period of TC2A (2.03 s) and Hokutokou (1.39 s) was minimum value when the single angles blade with 60° (S-60) was used. But, in the case of JEJEJ, the minimum cutting period (2.4 s) resulted when a double angled blade with 45° (D-45) used. However, the cutting period result was varying in different varieties, the minimum stress happened when the S-60 was used (Figure 65 (right)). The stress results show that the minimum stress value to cut the stems was 2.84, 3.3, and 2.01 $^{N}/_{mm^2}$ for JEJEJ, TC2A, and Hokutokou, respectively. These results indicate that the single angles blade with 60° angle is the appropriated blade to harvest the mentioned varieties of pumpkin with minimum time-consumption, and stress. Using S-60 could decrease the cycle time of harvesting and energy consumptions,

and also it can increase the energy efficiency because of the short cutting period, and smallest needed force to cut a stem.

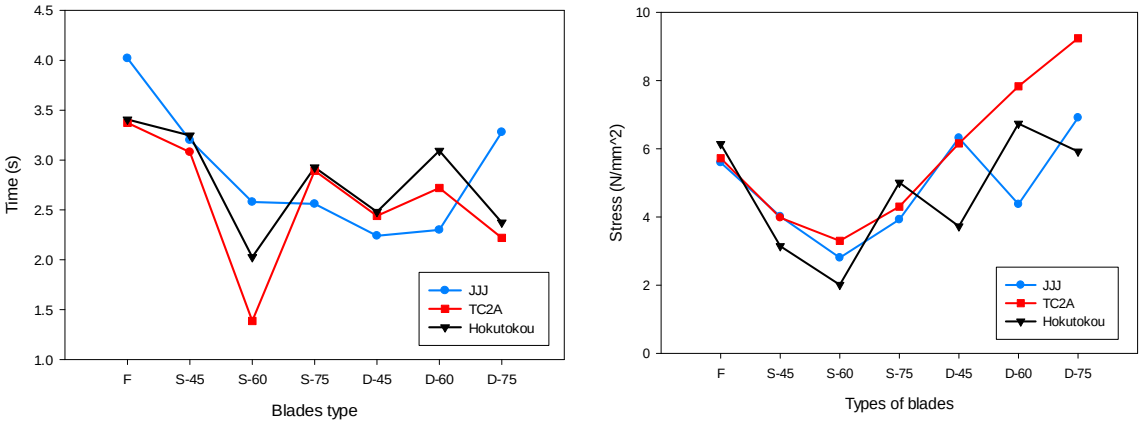

Figure 65. Cutting period (left), Yield shear stress (right).

The force ratio (FR) as one of the outputs of bending-shear test, indicates the relationship between flexural force (F_m) and diameter of stem (D_s). Each variety of pumpkin must have an individual range of FR which is depends on the physical properties of different varieties. However, a predicted constant parameter like FR, could have a dispersed tolerance because of nonlinearity and variegation of agricultural products, the results could be acceptable if the diffusion indexes have a small tolerance in comparing by average value. In other word, if the regression line includes the average value, and the prediction bands covers all experimented results, the average value with a FOS can be acceptable as a constant FR. Figure 66 shows the result of FR for the tested varieties. Obviously, all regression plots were interrupted by the average line which is shows the average FR of specimens. Also, the prediction bands with a factor of safety, were covered all values of FR. Then the average values of force ratio (FR_{AVG}) was applied as a constant value of FR to predict the D_s. The FR_{AVG} was resulted 4.4, 4.28, and 4.83 $^{N}/_{mm}$ for JEJEJ, TC2A, and Hokutokou, respectively. The predicted applied force before harvesting was figured out based on the D_p, DR and FR. In during of harvesting, the image processing was simulating the pumpkin images, then the position and size of pumpkin and the surface of pumpkin (S_p) results as the output parameter. By using S_p and related parameters like roundness constant factor (N), average diameter ratio (DR_{AVG}), force ratio (FR), variance of DR (VAR), and constant factor of bending test (C_{DR}), the angular velocity of end-effector was predicted. Each ω_{ee} can apply an individual amount of force to cut a stem, then based on the output parameter of IP, the applied force could predicted before harvesting. In this study, the force prediction based on the image processing evaluations was called Pre-evaluation procedure. The pre-evaluation was reduced the cycle time and energy consumptions in during of harvesting. As the image processing system was not designed in this study, using the extracted parameters for future studies on image processing of HRHC system is recommended.

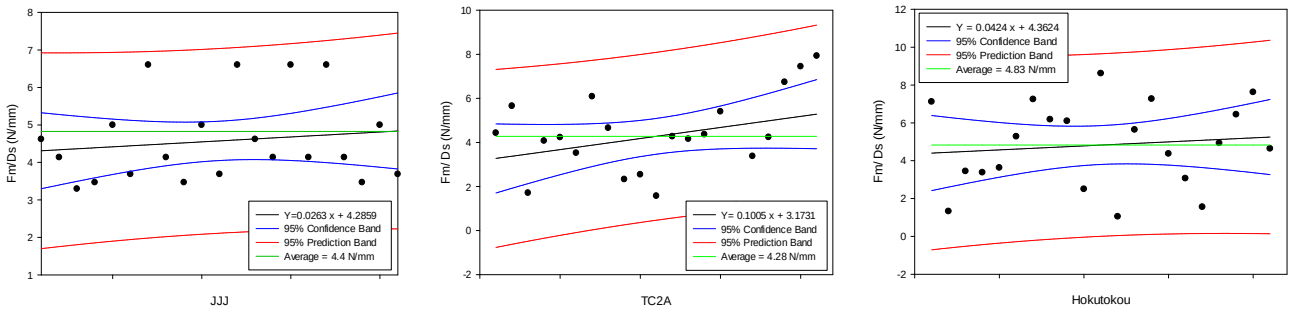

Figure 66. Force per stem diameter ($f(F_m, D_p)$) in JEJEJ, TC2A, and Hokutokou.

4.5. Conclusion

In this chapter, the physical behavior of common pumpkins in Hokkaido-Japan was evaluated. The experimented varieties of pumpkins were included: JEJEJ, TC2A, Hokutokou, Sukuna, Kikusui, and Ebisu which were some specialized combination of standard varieties of Cucurbita maxima and Cucurbita pepo L. (C. pepo L.) The aim of this chapter was a parametrization of each variety and estimate physical behaviors and extract the related physical equations. In this regard, firstly, the anatomy of pumpkin and main physical behaviors of each variety including average weight, shape, pure stem orientation (θ_{PSO}), lift stem orientation (θ_{LSO}), volume, section area was measured. The results show; however, each pumpkin can have different θ_{PSO}, but if the pumpkin lift with the designed EE, all pumpkins was unified as $\theta_{PSO} > \theta_{LSO}; -90^{\circ} < \theta_{LSO} < +90^{\circ}$.

Secondly, to measure the maximum compression force of each variety of pumpkin (F_{ct}), the compression test was done on six varieties of pumpkin (JEJEJ, TC2A, Hokutokou, Sukuna, Kisusui, and Ebisu) in different repetitions (7, 21, 21, 3, 3, and 3 repetitions, respectively) by using a compression testing device (INSTRON 5584). The numbers of repetitions was because of limited numbers of pumpkins. The results show that the maximum ($F_{ct,max}$), minimum ($F_{ct,min}$) and average ($F_{ct,avg}$) of F_{ct} in JEJEJ, TC2A, Hokutokou, Sukuna, Kisusui, and Ebisu was 4.66, 4.58, 4.61, 1.94, 2.21, and 2.5 KN; 2.81, 2.06, 2.24, 1.83, 1.53, 1.74 KN; and 3.37, 3.1, 3.23, 1.88, 1.92, 2.22 KN, respectively. The JEJEJ and Sukuna have shown the maximum and minimum response under the loading.

Thirdly, a bending-shear testing system was designed to measure the maximum force to cut the stem of the pumpkin. As the cutting blades can have different angles, the different blades with different angles were designed. The bending-shear test was done on three varieties (JEJEJ, TC2A, and Hokotokou), with 7 different blades (flat, single angles ($30^{\circ}, 45^{\circ}$, and 60°), and double angles ($30^{\circ}, 45^{\circ}$, and 60°)), in 3 repetitions. The results show that the single angles blade with 60° angle can cut the stem of different varieties with minimum force and time. So, this blade was chosen as an appropriated blade to harvest the pumpkins with minimum time-consumption and stress. Using S-60 could decrease the cycle time of harvesting and power consumptions, and also increase the energy efficiency because of the shortest cutting period, and smallest needed force to cut a stem. Finally, the relationship between F_m and D_p as $f(F_m, D_p)$, and also between F_{ct} and D_p as $f(F_{ct}, D_p)$ were calculated. As conclusion, the parametrization of each pumpkin was necessarily needed to predict an applied force on pumpkin's body in during of grasping and an applied force to cut a stem in during of stem cutting. It was not only needed to predict the forces, but also was essential to know about the behavior of each variety; make a library of parametrization; reduce the harvesting damage and cost, and; and increase the efficiency.

Chapter 5. Design and manufacture of end-effector

5.1. Introduction

As mentioned before, the agricultural robots were made a new horizon for future farming. This technology was developed because of the current concerns in agriculture industry like farmers aging, depopulation and land limitation in some countries. The agricultural robots not only have to improve labor issue, but also have to merge the potential capability of robotic science and farming experiences. Some of the mentioned concern is related to the natural resources changing; while some others appeared because of human resources. In this regard, laboratories were inclined to lead their researchers in agricultural robotics. Qiao, Sasao, Shibusawa, Kondo, and Morimoto (2005) were studied on a database that was created for sweet pepper by using the mobile fruit grading robot. Belforte et al. (2006) were developed an agricultural robot, especially for the greenhouse to improve the quality of products, cost, and safety. Kondo et al. (2009) were presented a machine vision system for automatic tomato harvesting. Toyama and Yamamoto (2009b) were developed a wearable-agri-robot mechanism for farmers. Rajendra et al. (2009) were used a methodology to develop an image processing algorithm for a strawberry harvester robot. Keita Kurashiki et al. (2010) were studied on laser-based vehicle control in the orchard because of the challenges and difficulties of daily working in an orchard on slope lands. They also proposed a self-localization algorithm of a 2D laser fingers for mobile robots (Kurashiki, Fukao, Ishiyama, Kamiya, & Murakami, 2010). Weiss and Biber (2011) were presented a paper to discuss the advantage of 3D LIDAR in comparing by traditional sensor fusion. Kurita, Iida, Suguri, and Masuda (2012) were introduced technology for unloading automation of robotic head-feeding combine harvester using image processing. Faizollahzadeh Ardabili, Mahmoudi, Mesri Gundoshmian, and Roshanianfard (2016) was modeled a fuzzy controller in a mushroom growing hall. As another agricultural robot is worth mentioning to a cucumber harvesting robot (E. J. Van Henten et al., 2009), robot platform in a sugar beet field (Bakker et al., 2011), asparagus harvesting robot (Dong, Heinemann, & Kasper, 2011), a mobile grading machine for citrus fruit (Kohno et al., 2011), a robot combine harvester for beans (Saito, Tamaki, Nishiwaki, Nagasaka, & Motobayashi, 2013), a robotic system for paddy field farming (Tamaki et al., 2013), and sweet pepper harvester (Eizicovits, van Tuijl, Berman, & Edan, 2016).

Some of the agricultural products are harvestable at a specific time like wheat (whole-harvesting-system), corn and potato; while some others are selective harvestings like tomato, pumpkin, and watermelon. There is various kind of combine harvesting for whole-harvesting products made by Yanmar, John deer, and other companies. But current selective harvesting is highly dependent on human labors. As another perspective, development of a selective harvesting robotic system is needed a specially designed end-effector. This end effector must be developed based on the physiology of crop because, the structure of this fruits and vegetables which are fragile, variable in shape and vulnerable due to pressure and high stress. Although, many studies have not been done yet. Some researchers have designed end effectors for some small crops like apples and tomato. Choi and Koç (2006) were developed a flexible gripper based on inflatable rubber pockets which are suitable to grasp an egg without damaging. Pettersson, Davis, Gray, Dodd, and Ohlsson (2010) were designed a magnetorheological robot gripper for handling of food products with varying shapes like carrot, strawberry, tomato, and grape. Pettersson, Ohlsson, Davis, Gray, and Dodd (2011) were designed end effector by the same target to handle variable small sized crops. Blanes, Mellado, and Beltrán (2016) were developed a pneumatic gripper equipped with a pressure sensor to grasp eggplant and apple. Also, Kim, Hwang, and Cho (2008) were designed and manufactured a hybrid robotic system for heavy crops like melon, by combining a parallel mechanism and using an end effector.

As mentioned, most of the current studies were focused on the small sized and light weighted crops. Although, the heavyweight crops like pumpkin, watermelon, cabbage, melon are playing a significant role in the marketing basket of most countries people like Japan, USA, and Iran. This is even though the mentioned crops are expensively priced in Japanese markets. Based on this reason, development of a heavy-weight crops robotic harvesting system can be valuable. In this regards, this chapter was presented the

development procedure of a specially designed robotic end effector for pumpkin. Development of this end effector is a continuation of Roshanianfard and Noguchi (2016) studies to complete a heavyweight crop robotic harvesting system (Roshanianfard & Noguchi, 2017).

5.2. Objectives

The objectives and originalities of this study are as follow:

- Development of a specifically designed end effector (EE) based on the properties of target crop (Pumpkin).
- Development of rapid harvesting methodology to improve harvesting cycle-time and efficiency of the system.

5.3. Novelty

The novelties of the developed end-effector are as follow:

- Designing a unique harvesting methodology based on the physical properties of the crop.
- Parameterization of real field condition to develop an end-effector suitable for real harvesting situation.
- Specifically designed fingers based on the pumpkin morphology.
- Using one servo motor to feed 2-DOF motions in EE.
- Development of the first specialized end-effector for robotic harvesting of pumpkin

5.4. Harvesting methodology

As the pumpkin is unique as physical properties and harvesting procedure aspects, designing a new harvesting methodology was essential. After physical behavior evaluation of pumpkin, designing the special EE, kinematic calculation, and computer simulations, the pumpkin robotic harvesting methodology was designed as shown in Figure 67. This methodology consists of six steps as crop reorganization by vision system, adjustment of EE's orientation (O_{ee}) along pumpkin location, lifting the pumpkin for using the physical behavior, cutting stem in during of EE's rotation, and transportation to the trunk position. After finding the location of pumpkin, the RA was adjusted the orientation of EE so that be along the position of pumpkin. The CP was considered as the location of pumpkin. The orientation of EE along CP point (O_{cp}) would be better to be perpendicular to the ground. After adjustment, the RA moves EE to the point of CP and grasp the pumpkin. As the SP was not predictable, the grasping could have a tolerance that called grasping angle (θ_g). After the grasping, the EE was lift the pumpkin until a predefined height that called lift height (H_L). The H_L was depended on the pumpkin weigh, size and shape that directly affected on θ_{LSO}. Unlikely to the previous robotic harvesting systems which mostly used a robotic cutter or a separate pneumatic scissor to cut the stems, in this study some sharp blades that was connected to the both sides of each fingers was embedded for stem cutting procedure. When the lifting stage was completed, the EE start to rotate rapidly and the nearest blades was cut the stem. This system not only reduce the complexity of the controlling algorithm, but also simplified the harvesting procedure and reduce the total harvesting cycle time. By using a special technique, both power applied for finger motion and EE rotation that need 2-DOF, was embedded from one servo motor (1-DOF). Finally, after finishing the harvesting stages, the pumpkin was unloaded to a trunk that was connected to another robot tractor (RT) which moving parallel with harvesting RT.

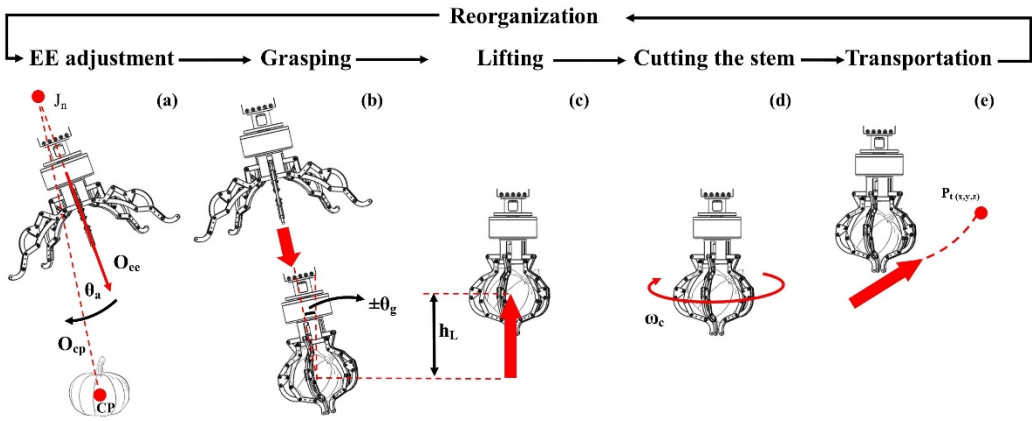

Figure 67. Robotic harvesting methodology.

5.5. Design

After several calculations and simulations, an end-effector was designed for the specified application. The components were designed in Solidworks (with a similar development process as mentioned in section 3.4.2) and after several modifications, the final structure as illustrated as shown in Figure 68. In this figure, the designed robotic arm with end-effector was mounted in a robot tractor and the combination of them make the heavy-weight crop harvesting system.

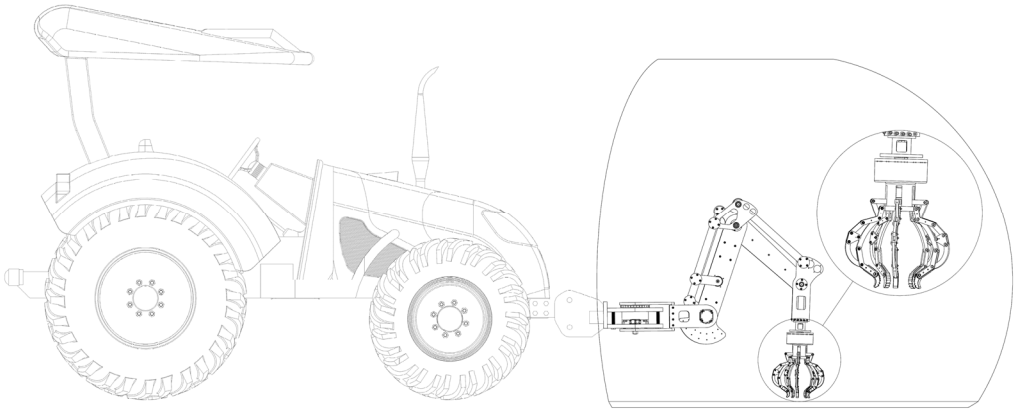

Figure 68. Designed end-effector for heavy-weight crops harvesting.

5.5.1.Design procedure

As shown in Figure 69-a and Figure 70, the designed end-effector (EE) consist of two main unit including (1) frame structure, and (2) fingers and some sub-units as the Main connector, linear screw, and joint-4 structure. The frame structure to the connects the finger mechanism of the robotic arm (RA). The brake mechanism, linear motion actuator, and motion switch mechanism were some of the equipped components in the frame unit. The mentioned EE contains 5 fingers which designed and optimized to grasp and harvest heavy-weight crops like pumpkin, watermelon, and cabbage (Figure 69-c). The fingers are specially designed mechanism including 7 links, 8 joints which have the mobility of 1 ($M = 1$). It was designed based on the extracted physical properties of pumpkin, statically simulated by using Solidworks software, and optimized in SAM software in kinematic and dynamic aspect. One of the initiated technique to design this system was inventing the Administrate Power Transmission system (APT) to managed the input power path which can support 2-degree of freedom (DOF) by only using one servo motor that can supply 1-DOF. This technique was increased the harvesting speed and efficiency, and decreased the size and weight of EE.

The fingers have combined mechanism to support various size between 152 to 530 mm in diameter. This requirement is necessary because of the pumpkin's shape and size diversity in the natural farms. As shown in Figure 69-d, e & f. The designed figure consists of a combination of three A, B, and C mechanisms. The A-mechanism was a slider-crank mechanism with an active crank that connected to the servo motor to supply the motion power of whole finger mechanism. The B-mechanism and C-mechanism are four-bar-linkage were connected and supported by the previous mechanism, respectively. The combination of all mechanism was made the finger mechanism. As the EE has 5 fingers, it can support most of the ripe pumpkins in during of harvesting period. For damage possibility reduction, it was necessary to use some rubber cover on fingers, micro-switch to control the motion and capacitive sensors to sense the crops grasping.

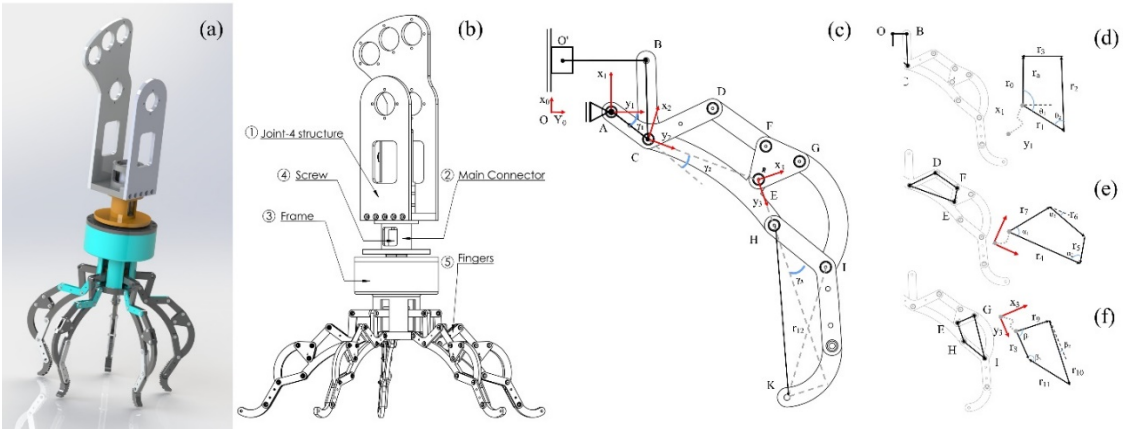

Figure 69. (a) CAD designed end-effector, (b) EE's units (c) finger linkage, (d) A- mechanism, (e) B- mechanism, (f) C-mechanism

Figure 70. Developed EE.

5.5.2. CAD/CAM design and components

After checking several mentioned parameters, the structure was designed in Solidworks software. The EE has included 92 components which were 21-components in the frame and 71-components in the fingers as shown in Table 18 and Table 19. The drawing of each component was presented as Appendix-3. The EE has two main components including frame and fingers; and several sub-components including brake

system, rotary connector, servo motor, and APT system. The components were explained in following sections in Figure 71.

Table 18. The component list of end-effector (Frame).

Item no.	Part number	Description	Quantity	Material
1	15-2	Manufacturing	1	AL5052P-H112-JISH4000
2	13-2	Manufacturing	1	AL5052P-H112-JISH4000
3	7-2	Manufacturing	1	AL5052P-H112-JISH4000
4	14	Ball bearing	2	
5	10-2	Main screw	1	Steel
6	12-3-brass	Main nut	1	
7	6	Manufacturing	1	AL5052P-H112-JISH4000
8	3	NSK 51106	2	
9	4	Manufacturing	1	AL5052P-H112-JISH4000
10	2	Connector	1	
11	5	Rotary connector	1	
12	Finger with bearings	Table 19	5	
13	a21	Manufacturing	1	ASTM A36
14	a23	Manufacturing	1	ASTM A36
15	1-2	Manufacturing	1	AL5052P-H112-JISH4000
16	1-1	Manufacturing	1	AL5052P-H112-JISH4000

Table 19. The component list of end-effector (fingers).

ITEM NO.	PART NUMBER	DESCRIPTION	Quantity	Material
1	F-2 - Improved	Manufacturing	5	AL5052P-H112-JISH4000
2	F-3-Left - Improved	Manufacturing	5	AL5052P-H112-JISH4000
3	F-3-Right - Improved	Manufacturing	5	AL5052P-H112-JISH4000
4	F-5-Right	Manufacturing	5	AL5052P-H112-JISH4000
5	F-5-Left	Manufacturing	5	AL5052P-H112-JISH4000
6	F-4	Manufacturing	5	AL5052P-H112-JISH4000
7	F-6	Manufacturing	5	AL5052P-H112-JISH4000
8	F-7-Right	Manufacturing	5	AL5052P-H112-JISH4000
9	F-7-Left- Copy	Manufacturing	5	AL5052P-H112-JISH4000
10	FL675ZZ_2_03	Ball bearing	16	
11	DBTB3-16-5_2_03	Bolts	8	ASTM A36
12	JIS B 1181 Hexagon	Nuts	8	
13	17	Manufacturing	5	AL5052P-H112-JISH4000

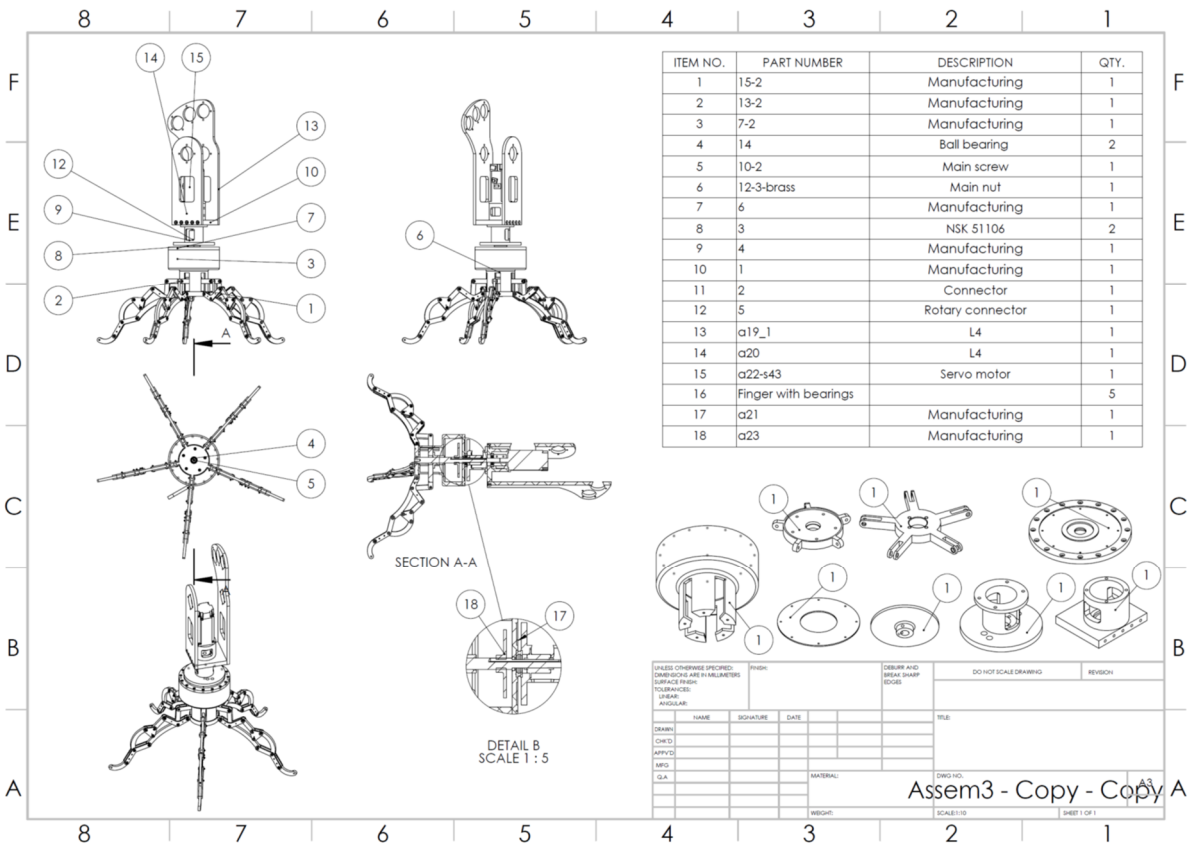

ITEM NO.	PART NUMBER	DESCRIPTION	QTY.
1	15-2	Manufacturing	1
2	13-2	Manufacturing	1
3	7-2	Manufacturing	1
4	14	Ball bearing	2
5	10-2	Main screw	1
6	12-3-brass	Main nut	1
7	6	Manufacturing	1
8	3	NSK 51106	2
9	4	Manufacturing	1
10	1	Manufacturing	1
11	2	Connector	1
12	5	Rotary connector	1
13	a19_1	L4	1
14	a20	L4	1
15	a22-s43	Servo motor	1
16	Finger with bearings		5
17	a21	Manufacturing	1
18	a23	Manufacturing	1

Figure 71. Drawing of designed end-effector.

5.5.2.1. Frame

The frame of EE was a combination of different structures and components which have a protective rule to transfer the power from the servo motor or fingers. The inner structure of frame includes a main screw, power transportation, rotary connector, ball bearings and so on. Figure 72 illustrates the frame schematic. The main linear actuator transfers the power from an AC servo motor to the fingers by using a high-power screw. The brake systems we located in and on the frame to control the motion type. The material of structure was mainly AL5052, however, some components were made of stainless steel.

Figure 72. The frame of EE.

5.5.2.2. Fingers structure

The most important unit in the designing of an end-effector is fingers. The fingers not only are directly connected to the crop, but also the structure is under different forces in different directions. An appropriate design could be successful if the mechanism can support all required necessities. In the designing of an end-effector for heavy-weight crop harvesting, supporting a flexible volume and wide grasping surface was needed. The flexible volume is being necessary because of the diversity of pumpkin in shape and size aspects. The big grasping surface could improve the manipulator tolerances when the vision system recognizes a target crop (pumpkin), while the determined position has some tolerances. In this case, a wide grasping surface can correct the system. This technique could reduce the controlling algorithm complexity and increase the cycle time and harvesting speed.

As the first step of designing, a linkage mechanism was designed for this application as shown in Figure 73. First, the mechanism was selected, optimized and adapted based on the physical properties of pumpkins. Second, the mechanism parameter including link length, joint type, mobility, the shape of linkage, and type of linkages, was designed in the laboratory of vehicle Robotic-Hokkaido university. Third, the mechanism was optimized in SAM software by using determined mechanism and required motion path as shown in Figure 73-c. After optimizations and different simulations including dynamic simulation, the components were designed and assembled by Solidworks. Then, the finger structure was simulated as static and dynamic aspects. Several modifications were applied at this stage. Finally, the fingers were applied to the frame and final evaluations were done on completed structure. The drawings of each component were done and sent to the company for manufacturing. After manufacturing, the components were assembled in the laboratory and evaluated in different aspects.

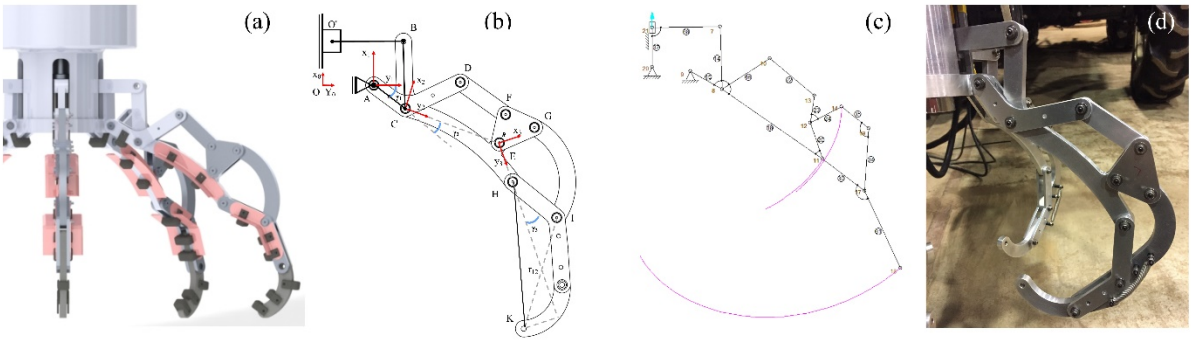

Figure 73. Finger structure illustration, (a) CAD designed, (b) linkage structure, (c) open diagram, (d) developed EE's finger.

5.5.2.3. Brake system

A magnetic brake system was applied to the servo motor to stop system at the necessary time as shown in Figure 74. The dynamic brake was designed to decelerate the servo motor immediately at an alarm occurrence, power failure, or forced stop. The electromagnetic brake was provided to prevent a drop in a power failure or servo alarm occurrence during the vertical drive or to hold a shaft at a stop. The electromagnetic brake has a time lag. servo motor control starts after the electromagnetic brake has completely opened.

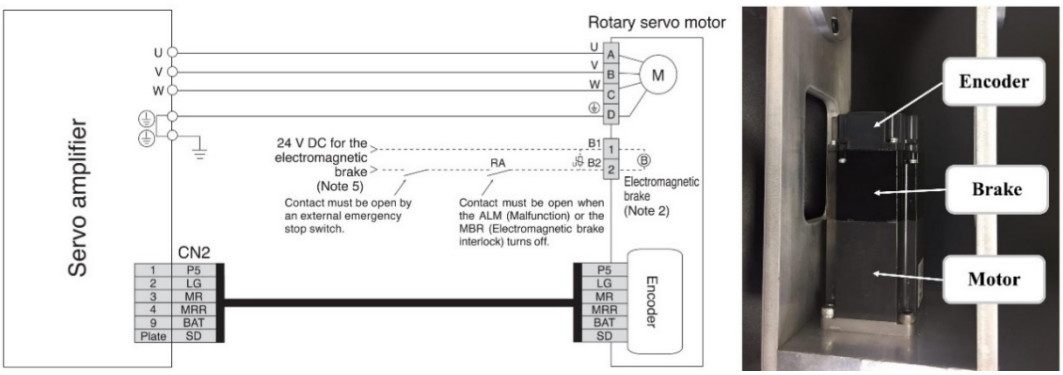

Figure 74. The connection of brake system to the servo motor.

5.5.2.4. Rotary connector

To keep the electronic connection in during of EE rotation, a rotary electrical connector was used named SNH015A which shown in Figure 75. Rotary electrical Connectors operate on a superior principle. They offer an extremely low resistance electrical connection because the electrical conduction path is a liquid metal which is molecularly bonded to the contacts. The specification of ANH015A was shown in Table 20.

Figure 75. Rotary connector SNH015A.

Table 20. The technical specifications of SNH015A.

circuits	2~24	current	standard 2A (paralleling wires use as 5A/10A)
voltage	250 VDC/VAC	Max speed	250RPM
Hole size	15mm	OD	32.8mm
Housing material	aluminum alloy	Torque	0.1N.m; +0.03N.m/6 circuits
Working life	>50 million revolutions (depend on working speed, environment)	Contact material	precious metal: gold-gold
Electrical noise	<10mΩ at 6VDC,50mA,5RPM	Contact resistance	<20mΩ(AWG16#,300mm)
Dielectric strength	800VDC at 50Hz,10s	Wires spec.	UL Teflon at Awg28
Dielectric strength	1000MΩ at 600VDC,10s	Wire length	300mm
Working temperature	-40°C ~ 85°C	IP grade	IP51
Mechanical vibration	MIL-STD-810E	Working humidity	10% ~ 85% RH
material	RoHS certification	CE certification	yes

5.5.2.5. Cutting unit

One of the creativity and originality of the designed system was its low-cost rapid cutting system. The aim to design this system was developing a unique mechanism to cut the stem of pumpkin in the shortest

time. The previous harvesting robots mostly developed based on a combination of sensors which make the system complex, slow and sensitive. In this end-effector, the cutting system was developed based on the target crop's (pumpkin) parameterization so that the number of sensors decreases. In the first stage of the study, no sensors were used in this end effector which could be one of the advantages of the designed system. As shown in Figure 76, the designed end effector has 5 fingers. Each finger is a unique mechanism including seven elements, which can grasp the pumpkin in during of harvesting system. The inner surfaces of each element which have connected to the pumpkin in during of harvesting were equipped with several rollers and stabilizer. The roller and stabilizers were rubber volumes to control the connections, prevent the damage of crop, and make a distance between blades and pumpkin surface. Some unique designed blades were determined in design on the lateral surface of each finger. This sharp blade could cut the stems in during of harvesting. As for the evaluation of the cutting system, some safety requirements were needed, the evaluation of the dreamed cutting system was postponed to a separated study. The cutting sequence is illustrated in Figure 77. The mention sequence begins after detection the object and RAVeBots-1 movement to the location of pumpkin. First, the end-effector located on the pumpkin with an opened mode to approach the target. In this stage, end-effector has no connection with pumpkin. Second, the end-effector rotate 72° clockwise or clockwise. This action is for contacting one of the blades to the stem with low speed. The aim of this action is controlling the stem angle, move the stem to a suitable location, and prepare for next stage. This technique has been solved the need for a contact sensor. Third, the EE's actuator moves and the fingers grasp the pumpkin. In this stage, one of the bales was connected to the stem and fingers were grasped the pumpkin. Finally, the EE rapidly rotates and the stem of pumpkin was cut off from the stem.

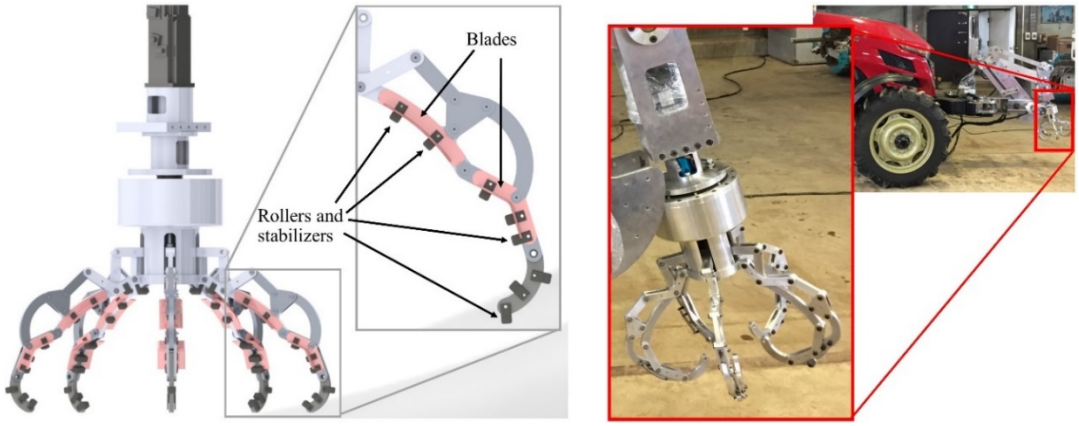

Figure 76. Cutting system.

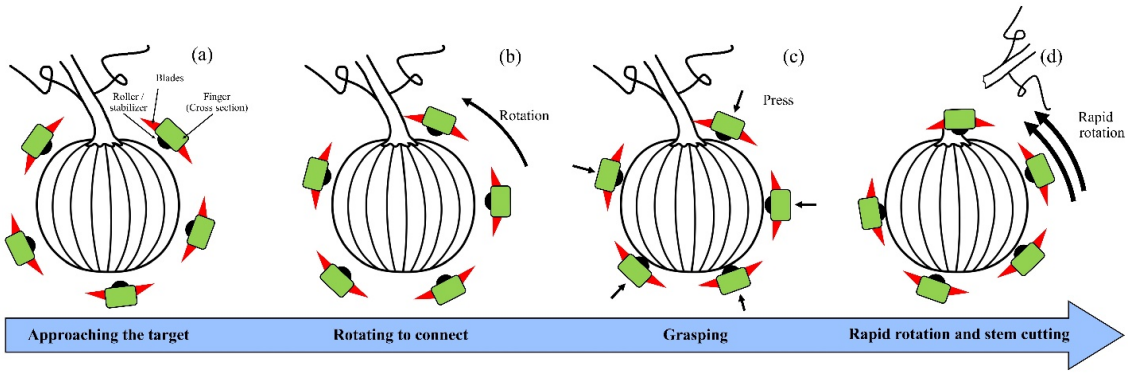

Figure 77. Cutting procedure sequence.

5.5.3.Mobility

The mobility of a mechanism is its number of degrees of freedom. This translates into a number of independent input motions leading to a single follower motion. A single unconstrained link has three DOF in planar motion: two translational and one rotational. Thus, two disconnected links will have six DOF. If the two links are welded together, they form a single link having three DOF. A revolute joint in place of welding allows a motion of one link relative to another, which means that this joint introduces an additional (in the case of welded links) DOF. Thus, the two-links connected by a revolute joint have four DOF. One can say that by connecting the two previously disconnected links by a revolute joint, two DOF are eliminated. Similar considerations are valid for a prismatic joint. Since the revolute and prismatic joints make up all low-pair joints in planar mechanisms, the above results can be expressed as a rule: a low-pair joint reduces the mobility of a mechanism by two DOF. For a high-pair joint, the situation is different. A roller and a cam are shown in various configurations. If the two are not in contact, the system has six DOF. If the two are welded, the system has three DOF. If the roller is not welded, then two relative motions between the cam and the roller are possible: rolling and sliding. Thus, in addition to the three DOF for a welded system, another two are added if a relative motion becomes possible. In other words, if disconnected, the system will have six DOF; if connected by a high-pair joint, it will have five DOF. This can be stated as a rule: a high-pair joint reduces the mobility of a mechanism by one DOF (Vinogradov, 2000). These results are generalized in the following formula, which is called Kutzbach's criterion of mobility:

$$m = 3(n-1) - 2j_1 - j_2 \tag{17}$$

where n is the number of links, j_1 is the number of low-paid joints, and j_2 is the number of high-pair joints. As shown in Figure 73, the designed finger structure for end-effector includes 7 links, 8 low-pair joints, and one high-pair joint, then each finger has one mobility of one ($m = 3(7-1) - 2(8) - 1 = 1$), which means only one link can be used as input links (driver) in this mechanism. The end-effector has 5 fingers which are connected to a linear actuator and all fingers move together, then the whole system mobility is also one.

5.5.4.Kinematic

As EE's geometrical parameters shown in Figure 69-c, this mechanism consists of three different mechanisms that called A-mechanism (Figure 69-d), B-mechanism (Figure 69-e), and D-mechanism (Figure 69-f). For the kinematic calculation of the whole mechanism, firstly, it was needed to calculate the kinematic parameters and joint location of each mechanism separately, and then, finding the final point's location equation with related equations of each mechanism. In the finger structure, the A-mechanism is a slider-crank mechanism by $\begin{bmatrix} x_0 \\ y_0 \end{bmatrix}$ coordination axis. This coordination axis has offset from main coordination of finger $\begin{bmatrix} x_0 \\ y_0 \end{bmatrix}$. The coordination transformation of this mechanism was calculated by Denavit-Hartenberg (D-H) method (Denavit & Hartenberg, 1955a) that is as follow:

$$\begin{bmatrix} x_1 \\ y_1 \end{bmatrix} = Trans(x_0, |OA|).\begin{bmatrix} x_0 \\ y_0 \end{bmatrix} = CT_{01}.\begin{bmatrix} x_0 \\ y_0 \end{bmatrix} = \begin{bmatrix} x_1 + |OA| \\ y_1 \end{bmatrix} \tag{18}$$

That the $Trans(x_0, |OA|)$ is the transformation of $\begin{bmatrix} x_0 \\ y_0 \end{bmatrix}$ coordination axis to $\begin{bmatrix} x_1 \\ y_1 \end{bmatrix}$ by $|OA|$ in the x_0 direction that called coordination transformation from 0 to 1 (CT_{01}). This technique was used because of calculation complexity reduction. After finding the coordination, the loop-closure equation of A-mechanism is as follow:

$$r_1(cos\theta_1, sin\theta_1)^T + r_2(cos\theta_2, sin\theta_2)^T + r_3(-1,0)^T - r_0(0,1)^T = 0 \tag{19}$$

That the parameters of this equation were shown in Figure 69-d including vectors and angles. After simplifying this equation, the relationship of r_0 with $\theta_1$can be like:

$$r_0 = [(r_1.cos\theta_1 - (r_2^2 - r_1^2\,sin^2\theta_1)^{0.5})^2 - r_3^2]^{0.5} \quad (20)$$

That r_0 is the motion vector length in y_1 direction which can control the θ_1 directly. The r_0 is active / motion input vector that can control the mechanism motion. The motion of this mechanism coms from a servo motor of by using linear screw as power transportation. This screw was connected to the joint-4 of designed robotic arm ((Roshanianfard & Noguchi, 2016, 2017, 2018)) specially for this application. By using this equation, it was easy to find the θ_1 angle based on the r_0 length that has directly effect on the coordination of B-mechanism. The B-mechanism's coordination axis is as follow:

$$\begin{aligned}\begin{bmatrix}x_2\\y_2\end{bmatrix} &= Rot(Z_1, 90^\circ - \theta_1).Trans(x_1, |AC|).Rot(Z, \gamma_1).\begin{bmatrix}x_1\\y_1\end{bmatrix} = CT_{12}.\begin{bmatrix}x_1\\y_1\end{bmatrix}\\ &= CT_{01}.CT_{12}.\begin{bmatrix}x_0\\y_0\end{bmatrix}\\ &= \begin{bmatrix}(x_1.\cos\gamma_1 - y_1.\sin\gamma_1).\sin\theta_1 + (x_1.\sin\gamma_1 - y_1.\cos\gamma_1).\cos\theta_1 + AC\\ -(x_1.\cos\gamma_1 - y_1.\sin\gamma_1).\cos\theta_1 + (x_1.\sin\gamma_1 - y_1.\cos\gamma_1).\sin\theta_1\end{bmatrix}\end{aligned} \quad (21)$$

That not only has transformation in x_1 axis as $Trans(x_1, |AC|)$, but also it has rotation a of $Rot(Z_1, 90^\circ - \theta_1)$, that means a rotation along Z_1 axis by $90^\circ - \theta_1$ degree. The $\begin{bmatrix}x_2\\y_2\end{bmatrix}$ is coordination axis of B-mechanism that supports the loop-closure equations of this mechanism as follow:

$$r_7(cos\alpha_1, sin\alpha_1)^T + r_6(cos\alpha_3, -sin\alpha_3)^T + r_5(cos\alpha_2, -sin\alpha_2)^T - r_4(1,0)^T = 0 \quad (22)$$

This mechanism is a Four-bar-mechanism which α_1 and α_2 are input and output angles respectively. To finding the relation of these two angles, first it was needed to find the location of points D and F by geometrical methods, and after simplification by using Pythagoras theorem, the equation 7 become like:

$$A.sin\alpha_2 + B.cos\alpha_2 = C \quad (23)$$

Where A, B, and C are as follow:

$$A = -\sin\alpha_1\ ; B = \cos\alpha_1 - \frac{r_4}{r_7}; C = \frac{r_4}{r_5}.\cos\alpha_1 + \frac{r_6^2 - r_4^2 - r_5^2 - r_7^2}{2.r_7.r_5} \quad (24)$$

After simplification of the Equations 8 and 9, the α_2 was resulted.

$$\alpha_2 = 2.\arctan\left(\frac{A \pm \sqrt{A^2 + B^2 + C^2}}{B + C}\right) \quad (25)$$

The C-mechanism is also a Four-bar-mechanism like B-mechanism but with different values in parameters. A reference coordination axis of $\begin{bmatrix}x_3\\y_3\end{bmatrix}$ support this mechanism.

$$\begin{aligned}\begin{bmatrix}x_3\\y_3\end{bmatrix} &= Trans(x_2, |CE|).Rot(Z, \gamma_2).\begin{bmatrix}x_2\\y_2\end{bmatrix} = CT_{23}.\begin{bmatrix}x_2\\y_2\end{bmatrix} = \begin{bmatrix}x_2.cos\gamma_2 - y_2.sin\gamma_2 + |CE|\\ x_2.sin\gamma_2 + y_2.cos\gamma_2\end{bmatrix}\\ &= CT_{01}.CT_{12}.CT_{23}.\begin{bmatrix}x_0\\y_0\end{bmatrix}\end{aligned} \quad (26)$$

This coordination axis was the final axis before finding the location of final point which was resulted by a transformation $Trans(x_2, |CE|)$ and a rotation $Rot(Z, \gamma_2)$ of $\begin{bmatrix}x_2\\y_2\end{bmatrix}$. The rotation angle was $\gamma_2 = \beta_1 + \alpha_2 - 126^\circ$. The loop-closure equation of C-mechanism can be written in the form of

$$r_9(cos\beta_1, sin\beta_1)^T + r_{10}(cos\beta_2, -sin\beta_2)^T + r_{11}(cos\beta_3, -sin\beta_3)^T - r_8(1,0)^T = 0 \quad (27)$$

That the parameters of this equation were shown in Figure 69-f, as well. After simplifying this equation, the relationship of β_3 with β_1 can be

$$D.sin\beta_3 + E.cos\beta_3 = F \tag{28}$$

Where

$$D = \sin\beta_1 \; ; E = \frac{r_8}{r_9} + \cos\beta_1 \; ; F = \frac{r_8}{r_{11}}.\cos\beta_1 + \frac{r_9^2 + r_8^2 + r_{11}^2 - r_{10}^2}{2.r_9.r_{11}} \tag{29}$$

After simplification, it resulted as

$$\beta_3 = 2.\arctan\left(\frac{D \pm \sqrt{D^2 + E^2 + F^2}}{E + F}\right) \tag{30}$$

Finally, as shown in Figure 69-c, the location of point K point as the final point of finger mechanism is

$$\begin{bmatrix} x_k \\ y_k \end{bmatrix} = CT_{01}.CT_{12}.CT_{23}.\begin{bmatrix} r_8 + r_{12}.cos\gamma_3 \\ r_{12}.sin\gamma_3 \end{bmatrix} \tag{31}$$

That CT_{01}, CT_{12}, and CT_{23} are coordination transformation of axis $\begin{bmatrix} x_1 \\ y_1 \end{bmatrix}$, $\begin{bmatrix} x_2 \\ y_2 \end{bmatrix}$, and $\begin{bmatrix} x_3 \\ y_3 \end{bmatrix}$ from the previous axis respectively.

5.5.5.Inertia

The inertia calculation was done on the joint-4 because the servo motor-5 will be under affected by inertia in during the harvesting. The calculations were done for a target object of 10 kg, while the structure weight was 11.5 kg. To calculate joint-4 inertia, following equation was used.

$$I_t = \left(I_{j_4} + I_{m_1}\right) \times FOS = \left(\frac{1}{2}m_{j_4}.d_a^2 + \frac{1}{2}m_o.d_o^2\right) \times FOS \tag{32}$$

$$I_t = \left(\frac{1}{2} \times 11.5 \times 0.3^2 + \frac{1}{2} \times 10 \times 0.63^2\right) \times 2 = (0.5175 + 1.9845) \times 2 = 5.004\ kg.m^2 \tag{33}$$

Where the I_t, I_{j_4}, I_{m_1}, and FOS were total inertia, inertia of structure, inertia of target object and factor of safty, respectively. The other parameters were illustrated in the Figure 78. The total calculated inertia was $5.004\ kg.m^2$. To controls sudden damages, the potential energy equation was calculated as:

$$PE_t = \frac{1}{2}I_t.\omega^2 = 2.502\ \omega^2 \tag{34}$$

It was considered in controlling algorithm for speed limitation and motion optimizations.

Error! Reference source not found.. End-effector

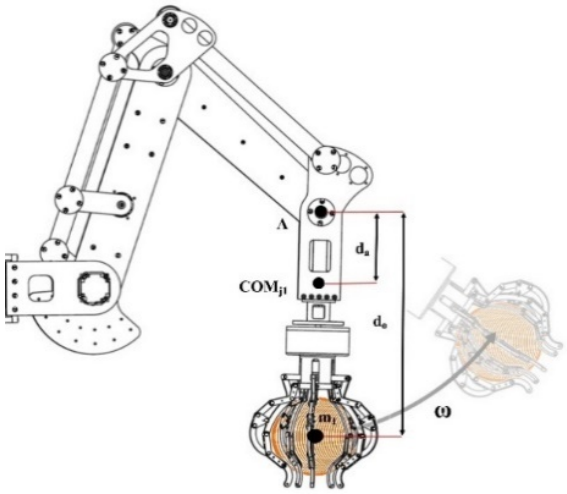

Figure 78. The inertia calculation parameters.

5.6. Computer simulation

5.6.1. CAD simulation

CAD simulation by different software like Solidworks allows engineers to regulate and resolve the impact of required forces on the designed mechanism efficiently to ensure quality, safety, and performance. Each dynamic mechanism must simulate under specific force, torque or other needed tensions. This simulation proves the designed parameters and material selection. This EE contains different parts that designed for different dynamic/static condition. Some of the static components should simulate under direct force in the different direction, and some others that have a dynamic application, have to simulate under desired torque as well. If the simulation results show low resistance nodes; the component needs to redesign and re-simulate until meeting the requirements. In this study, the designed EE includes five types of components: fingers which are needed to simulate in opened and closed situation, Joint-4 structure, main connector, frame, and main screw.

The CAD-integrated simulation was used to efficiently optimize and validate each design step and to ensure quality, performance, and safety of the EE. The Solidworks simulation uses the displacement formulation of the finite element method to calculate component displacements, strains, and stresses under internal and external loads (Roshanianfard & Shahgholi, 2017). Due to the sensitivity of some parts of EE such as the main finger, Joint-1 structure, main connector, frame and main screw, stress analysis was conducted on them (Figure 79 and Figure 80). Analysis of stress and strain of mentioned parts was accomplished using Solidworks simulation 2012. Safety factors range of 1.5-3 was considered for all parts during the design process. The components made of ASTM A36 steel (Tensile strength $4\times10^8\ {}^{N}/_{m^2}$, Yield strength $2.5\times10^8\ {}^{N}/_{m^2}$, Elastic modulus $2\times10^5\ {}^{N}/_{m^2}$, Shear modulus $7.93\times10^4\ {}^{N}/_{m^2}$, Density $7850\ kg.m^3$) and AL5052 (Tensile strength $3\times10^8\ {}^{N}/_{m^2}$, Yield strength $2.75\times10^8\ {}^{N}/_{m^2}$, Elastic modulus $7\times10^4\ {}^{N}/_{m^2}$, Shear modulus $2.59\times10^4\ {}^{N}/_{m^2}$, Density $2680\ kg.m^3$). The simulation type was linear elastic isotropic and meshing type was standard solid mesh by the four-point-nodded tetrahedron.

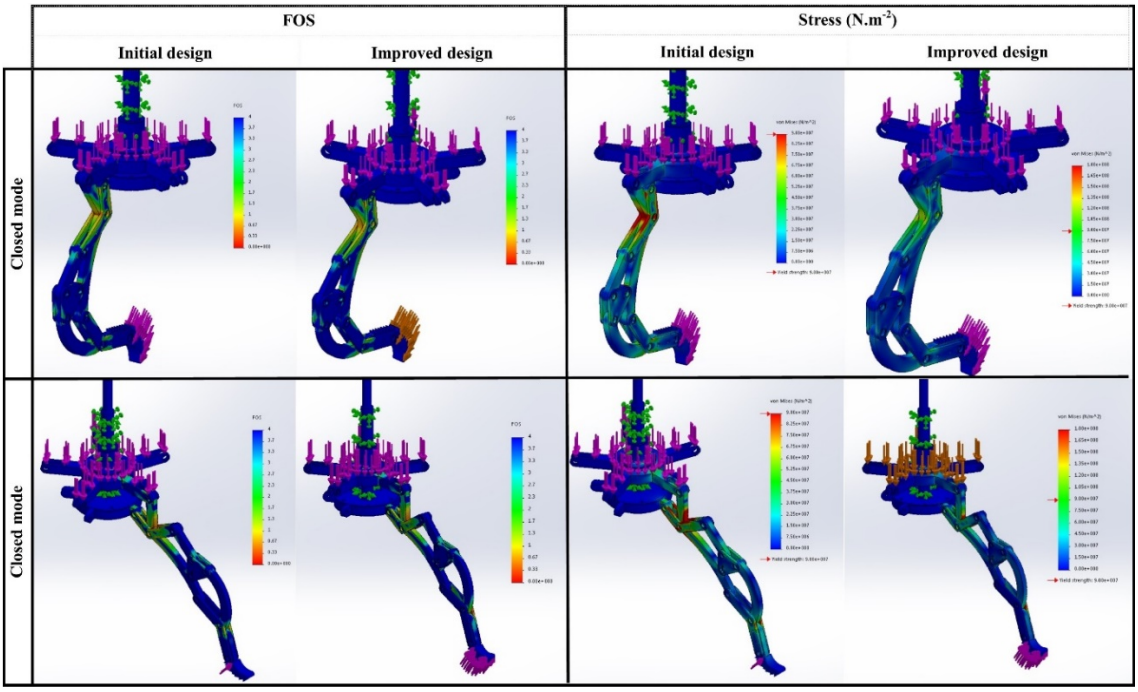

Figure 79. The Effect of finger design improvement on FOS and stress (opened and closed mode).

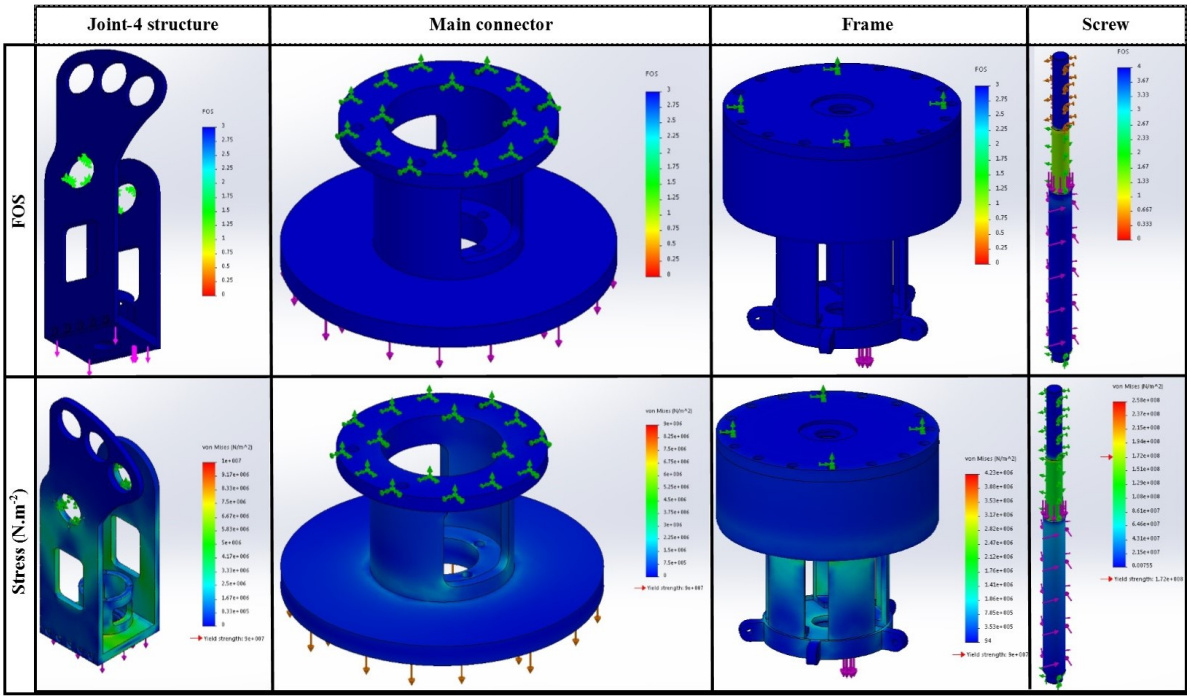

Figure 80. Static simulation of main components.

5.6.2.Kinematic simulation

After several simulations, three different input motions for Joint-5 were selected for final evaluation and compression. Figure 81 shows the linear motion (LM), sinusoidal motion (SM), and second order motions (SOM) plots. The LM has constant acceleration; the SM has semi-sinusoidal velocity, and the SOM controlled the motion by accelerations and decelerations at the start and stop points, respectively. The LM,

SM, and SOM were focused on displacement, velocity, and acceleration respectively to compare the difference. As shown in Figure 83-b, the displacement range of all motions was limited between 0 to 33 mm because of linkages angle range. But the moving patterns are different because of the velocity and acceleration variation.

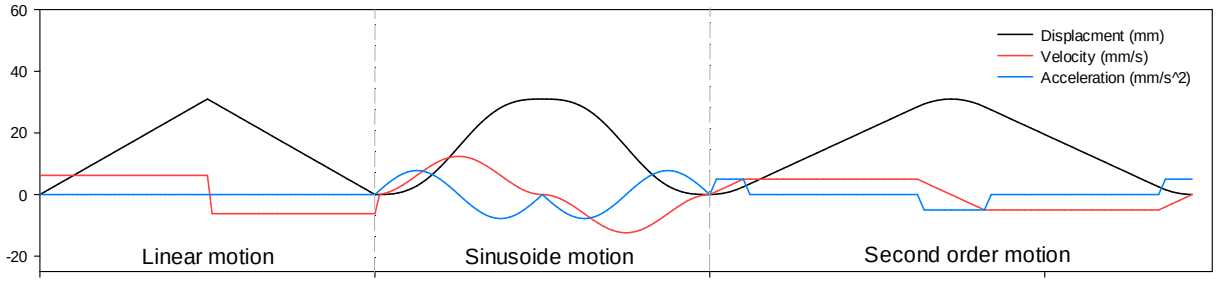

Figure 81. Motion types in the kinematic simulation of EE.

5.7. Results

5.7.1.Structure Simulation

In this study, the maximum allowable stress was chosen as final stress. Table 21 shows the results of finite element simulation under 200 N forces in required directions on each finger as maximum possible loading. The simulation results of initial design show that the maximum stress of finger in the main linkage is 9.8×10^7 and 1.2×10^8 $N.m^2$ in the opened and closed mode respectively. However, these stresses value are not bigger than yield strength of AL5202, but the finger can damage under impact force because of unpredictable farm environment that can increase the rupture possibility. The improved design was modified by adding some filets on the edges. These filets reduced the stress concentration, then the stress values were decreased to 6.2×10^7 and 7.8×10^7 $N.m^2$ in the opened and closed mode, respectively. These are not only less than tensile strength of used material but also are smaller than yield strength by considering FOS and other parameters. The data proved that the fingers components have enough capability under the maximum capacity of the system.

Table 21. Stress simulation result of a finger.

	Stress ($N.m^2$)	
	Initial design	Improved design
Opened-mode	9.8×10^7	6.2×10^7
Closed-mode	1.2×10^8	7.8×10^7

Table 22. Simulation results of main components.

Part name	Vertical force (N)	FOS_{Max}	Max stress ($N.m^2$)	Material
J1-structure	300	3	7.2×10^7	AL5052
Connector	300	3	8.7×10^7	ASTM A36
Frame	600	3	4.23×10^6	AL5052
Screw	450	3	2.58×10^8	ASTM A36

5.7.2.Supported volume, diameter and payload

Table 23 shows the specification of designed EE and it compared by the average physical parameters of tested varieties of pumpkin. The EE can grasp and harvest a hard skin crop (such as pumpkin) within a radius of 76.2 to 265 mm. The physical experimentation results on JEJEJ, TC2A, Hokutokou, Sukuna, Kikusui, and Ebisu show that the average radius of them are 109.53, 98.2, 109.12, 58.92, 89.7, and 99.26mm,

respectively, which are in the radius support range of EE. The volume and mass support range of EE are $1.5\times10^6 mm^3$ to $31.2\times10^6 mm^3$, and 1 to 20 kg, respectively. The average volume of the mentioned varieties were $5.5\times10^6 mm^3$, $3.96\times10^6 mm^3$, $5.4\times10^6 mm^3$, $0.85\times10^6 mm^3$, $3.02\times10^6 mm^3$, and $4.09\times10^6 mm^3$ and average the mass of them were 3.13, 2.58, 3.12, 2.8, 1.16, and 2.38 kg, respectively. These results show that the designed EE can harvest the mentioned varieties of pumpkin because the supportive range of radius, volume and mass can cover the extracted physical parameter of pumpkins. An illustration of support range and the physical parameter of pumpkins was shown in Figure 82. It should be noted that, the diameter of pumpkin $(A'B')$ has to be smaller than mazimum puss length of EE $(A'B')$ in the opened mode of EE. That's because, in the grasping stage the EE should be able to cover more than 55% of pumpkin's surface. Otherwise, it is possible that the pumpkin jumps out and damage.

Table 23. Compression of designed EE specification with tested pumpkins parameters.

Parameters	Max	Min	JEJEJ	TC2A	Hokutokou	Sukuna	Kikusui	Ebisu
Radius of pumpkin (mm)	265	76.2	109.53	98.2	109.12	58.92	89.7	99.26
Volume ($\times10^6$ mm^3)	31.2	1.5	5.5	3.96	5.4	0.85	3.02	4.09
Mass (kg)	20	1	3.13	2.58	3.12	2.8	1.16	2.38

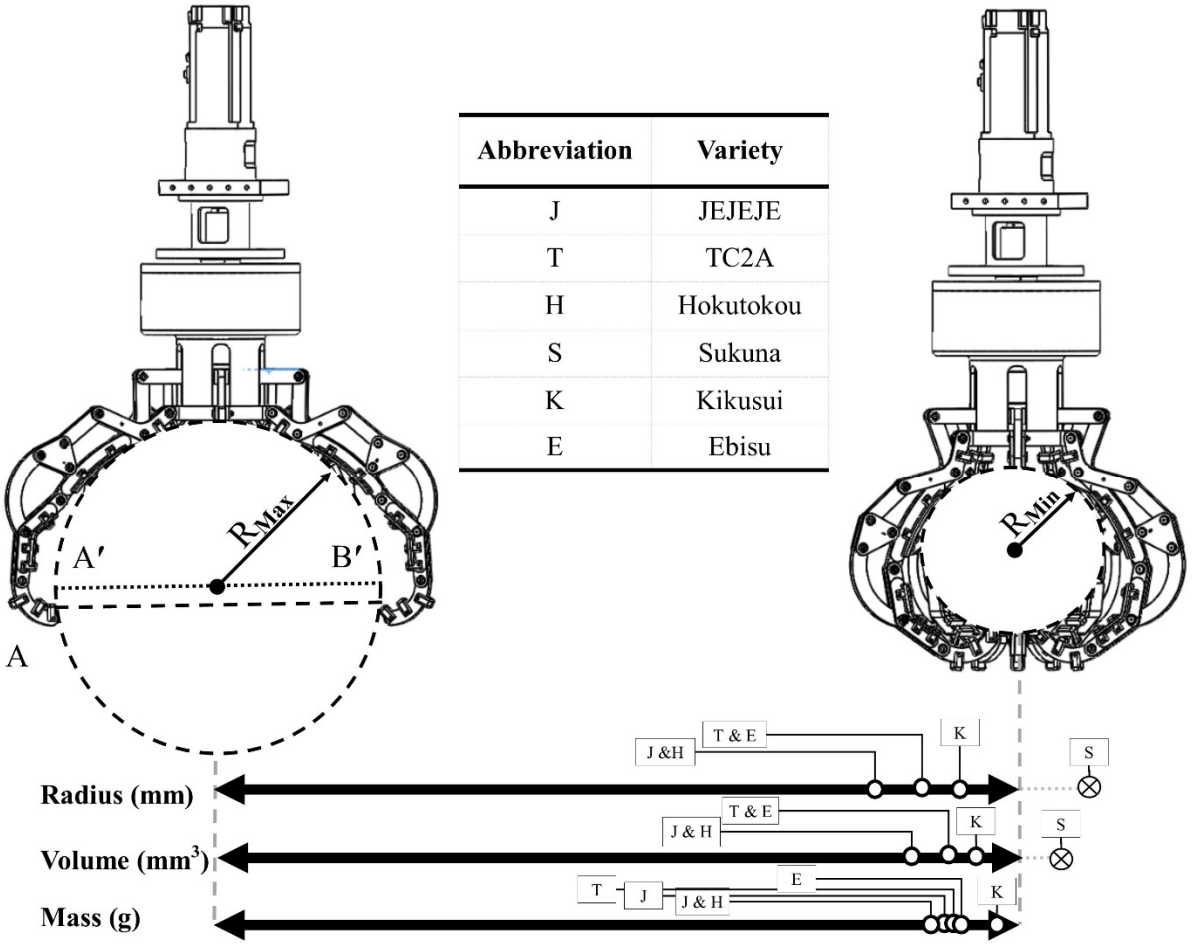

Figure 82. Designed EE's specification.

5.7.3.Motion comparison

After kinematic calculation, the finger mechanism was simulated by using SAM software. In these simulations, some kinematic parameter like position, displacement, velocity, acceleration, and angles was considered. As shown in Figure 83, the kinematic simulation was done by compression of different input's effects on the output motions. A linear motion in the range of 0 to 32mm was chosen as fundamental motion type (Figure 83-a-linear), and the effects of this motion on the other links and joints was investigated. The most important point was K-point (Figure 69-c) which the parameter of this point could directly effect on the harvesting methodology and crops damage possibility. The input motion is a special parameter. If the velocity/acceleration of this point is more than requirements, the input motion must be in controlled to avoid the crop damages. In the other perspective, if the velocity and acceleration plots were changed dramatically, it was highly possible to damage the EE's structure.

As shown in Figure 83-c, the maximum value of absolute velocity (AV) of K-pint in the LM, SM, and SOM was 123.1, 153.8 and 70.5 $^{mm}/_{S}$ respectively. The velocity range of K-point in the X-direction was effected on grasping possibility that called grasping velocity (GV). The GV's range in the three mentioned motions was -82.5 to 84.5, -150 to 150, and -67.7 to 67.8 $^{mm}/_{S}$ respectively. The velocity of K-point in the Y-direction called sweep velocity (SV) which in necessary when the EE's center of mass (COM) is not exactly among the same line as pumpkin COM. In other word, if the vision system has some small tolerance, the EE can compensate it by using controlled SV and large covered space that was included in the finger design. The SV's range in the three mentioned motions was -86.7 to112.7, -80 to 79.5, and -56 to 54.9 $^{mm}/_{S}$, respectively. The results show that the SOM could be most efficient motion to control the fingers as it has minimum AV, GV, and SV. The Figure 83-d proves this ratiocination so that acceleration of K-point in the LM has sharply changing. In the SM, the acceleration has a range of -87 to 106.9 $^{mm}/_{S^2}$, whereas in the SOM it has minimum range as -42 to 73 $^{mm}/_{S^2}$. The SOM could be the best motion to heavy-weight crop harvesting by using EE.

The hodograph of K-point in the three input motions was proved the simulation results. A hodograph or velocity diagram is a diagram that gives a vectorially visual representation of the movement of a body. It is the locus of one end of a variable vector, with the other end fixed (Hamilton, 2000). The Figure 84-a shows the hodograph of K-point by the different input motions. The hodograph of the LM was indicated that the K-point velocity sharply increased at each direction changing points (Figure 84-b, balloon A and B). In the balloon A, the sharp hodograph expresses that the large velocity increases the rapture possibility and decrease the safety of the operator. In the case of SM, the sharp velocity was modified, but the velocity in during of motion is obviously high (Figure 84-c, balloon C). As shown in the Figure 84-d, the SOM's hodograph has no high velocity in the motion range. Actually, the definition of SOM by acceleration and decelerations in the motion changing moments resulted in an intersection of LM's and SM's hodographs. This means the motion modification has a positive impact on the k-pint motion. As a conclusion, The SOM with included acceleration and deceleration, can reduce backlash of the used servo motor, control the motion velocity, provide minimum hodograph, decrease the crop damage possibility, and protect the finger structure from impact forces.

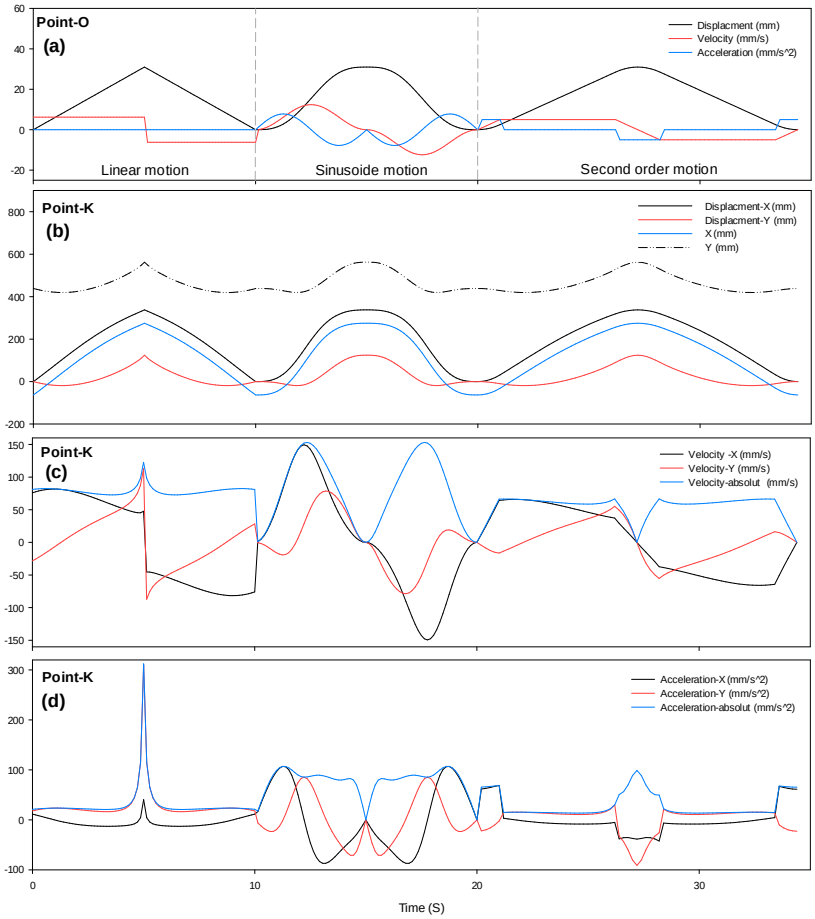

Figure 83. The compression of (a) different input motions: linear, sinusoidal, and second-order effects on (b) position and displacement, (c) velocity, and (d) acceleration of point-k.

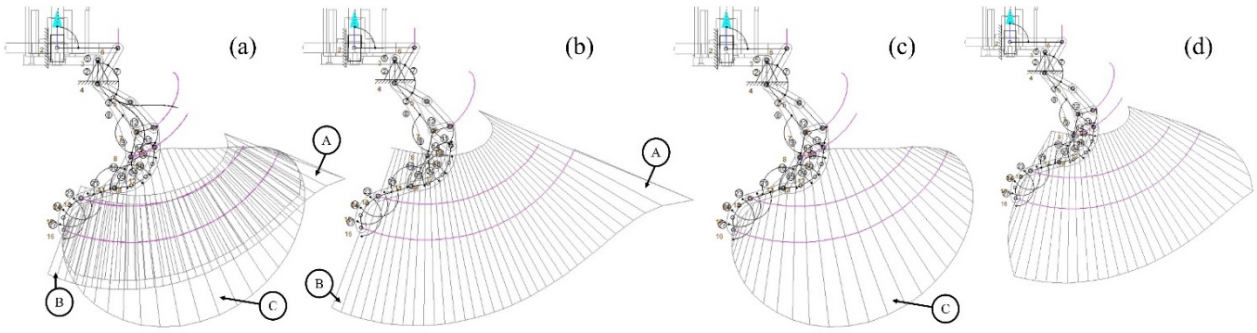

Figure 84. Hodograph of K-point in (a) overall illustration, (b) LM, (C) SM, and (d) SOM.

5.8. Conclusion

In this chapter, the designing and manufacturing procedure of a specifical design end-effector was discussed. The aim of this design was the development of a specifically designed end effector (EE) based on the properties of target crop (Pumpkin); designing a rapid harvesting technique to improve harvesting cycle-time and efficiency of the system; and development of rapid harvesting methodology. A harvesting methodology was designed for pumpkins based on the parametrization which was done in Chapter 4. This

methodology consists of six steps including crop reorganization by vision system or other methodologies, adjustment of EE's orientation (O_{ee}) along pumpkin location, lifting, cutting the stem in during of EE's rotation, and transportation to the trunk position.

The designing procedure was discussed. The EE and its components were designed in Solidworks software. The components illustrated and each unit which included several components were presents and application were explained. The EE consist of two main unit including (1) frame structure, and (2) fingers and some sub-units as the Main connector, linear screw, and joint-4 structure. The frame of EE was a combination of different structures and components which have a protective role to transfer the power from the servo motor or fingers. The EE has 5 fingers which consist of several linkages which designed, optimized, simulated, and modified based on the physical behaviors of pumpkin.

The mobility of each finger, kinematic behaviors, and inertia of Joint-4 was calculated. The static CAD simulation and kinematic simulation were done on each component of EE by using Solidworks simulation software, and SAM software, respectively, which discussed in section 5.6. The supported volume, diameter, and payload of EE were measured. The EE can grasp and harvest a hard skin crop (such as pumpkin) within a radius of 116.2 to 265 mm. The volume and mass support range of EE are $1.5\times10^{6}mm^{3}$ to $31.2\times10^{6}mm^{3}$, and 1 to 20 kg, respectively.

Chapter 6. Controlling unit

6.1. Introduction

The Control Unit (CU) is digital circuitry contained within the processor that coordinates the sequence of data movements into, out of, and between a processor's many sub-units. The result of these routed data movements through various digital circuits (sub-units) within the processor produces the manipulated data expected by a software instruction. It controls (conducts) data flow inside the processor and additionally provides several external control signals to the rest of the computer to further direct data and instructions to/from processor external destination's (Patterson & Hennessy, 2012). An engine control unit (ECU), also commonly called an engine control module (ECM), is a type of electronic control unit that controls a series of actuators on an internal combustion engine to ensure optimal engine performance. It does this by reading values from a multitude of sensors within the engine bay, interpreting the data using multidimensional performance maps (called lookup tables), and adjusting the engine actuators accordingly (Gunston, 1989).

The robot tractor has a TECU (Tractor Engine Control Unit) which was connected to a PC. The position data received from RTK-GPS and camera. The positioning system which installed on PCI express port of PC, transfer the signals to the PC. The switch unit (SU) control the servo motor rotation by using different components such as amplifiers, and magnetic switches. As another perspective, the position signals which come from RTK-GPS and camera, the analysis in the PC and the PC sends the commands to servo motor via position board and SU, and TECU directly. This circulation repeats for several times until finishing a mission (Figure 85).

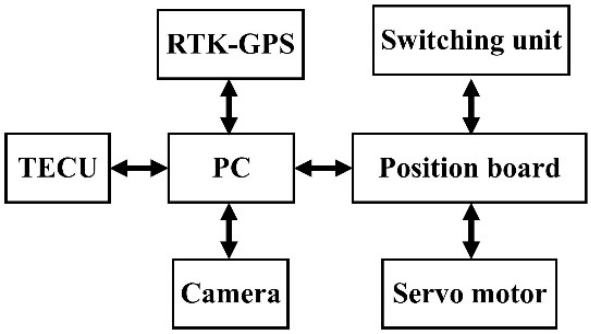

Figure 85. Controlling system of HRHC system.

6.2. Controlling system

The controlling unit of RAVeBots-1 was based on a programmable logic controller (PLC) system. This unit consists of a position board installed on a PC, a controlling program, servo motors, servo amplifiers, and optical cables for data transfer as compact circuits (see in Figure 86). The PLC systems usually drive a servo motor or a pneumatic/hydraulic cylinder. In this study, the PLC controlled five AC servo motors using 200ACV. All other components were selected or developed based on servo motor properties and the expected effects of lifted-object weight on joint torque and moment of inertia. A specific management-control program was developed based on parameters of the servo motor functions. To investigate a controller program, it is first necessary to set some control functions. These were divided into three groups: operational functions (OPF); application functions (APF); and auxiliary functions (AXF). OPF included jogging operation (JOG), incremental feeds, linear interpolation, and home-position return. The APF was adjust based on servo speed, acceleration, deceleration, force, torque, limit switch alarm, interlock and other related parameters. The AXF controlled parameters for data reading/writing/changing, monitor functions, sampling, and interruptions.

After utilizing the functions, all servo-motor commands were transferred to the position board installed on PC's PCI Express protocol. To speed up data transfer, servo motor control signals were sent to the position board via an optical cable. The control-management program was developed using C++. The program included three control modes: torque control mode (TCM), speed control mode (SCM), and position control

mode (PCM). The priority of each mode was servo-motor feedback torque, servo-motor feedback speed, and the position of the end effector, respectively. Figure 87 shows functions switched by the "control mode command". Switching to/from PCM to/from SCM/TCM must be done while the motor is off, while it is possible to switch between SCM and TCM any time.

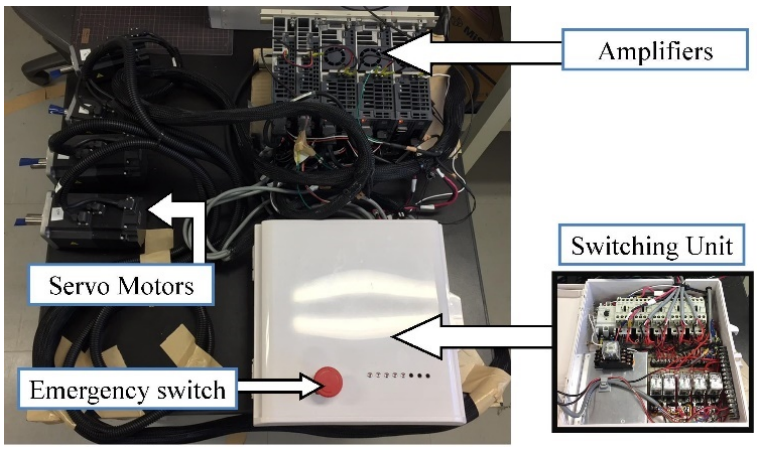

Figure 86. Controlling unit of RAVeBots-1

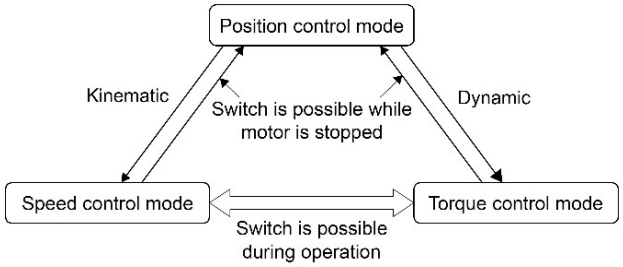

Figure 87. Controlling modes.

The controlling algorithm was developed next. Robotic arms are the most complex robots from a mathematical point of view, involving many parameters. Once an optimized algorithm is determined using kinematic and dynamic modeling, the PLC system parameters can be adopted by algorithm parameters. In robotic arm design, different methods were used to identify optimized controlling algorithms based on robot structure, linkage length, joint angles, and motion limitations. Kinematic simulation and dynamic analysis were essential for functional evaluation as well. In the design of the controlling algorithm for the RAVeBots-1, the Denevit-Hartenberg method (D-H) was used to find the optimized algorithm. The D-H method was chosen because it has the fastest response in experiments and more versatility properties in terms of real-world conditions. The D-H is the accepted method for drawing a free body diagram of a robotic arm, which is based on joint motion, including rotation and translation. Subsequently, the controlling program was developed based on OPF, APF, AXF functions using the D-H algorithm.

6.2.1. General configuration of controlling unit

The controlling unit of HRHC system consists of: a PC, a position board (Mitsubishi Model: MR-MC240), Amplifiers (MR-J4-100, MR-J4-73B, and MR-J4-73B), servo motors (HG-JR-103B, HG-MR73B, and HG-MR43B), switching unit, emergency switches, GPS, TECU and IMU as shown in Figure 88 and Figure 89. Each of above-mentioned components will explain in coming sections detailly.

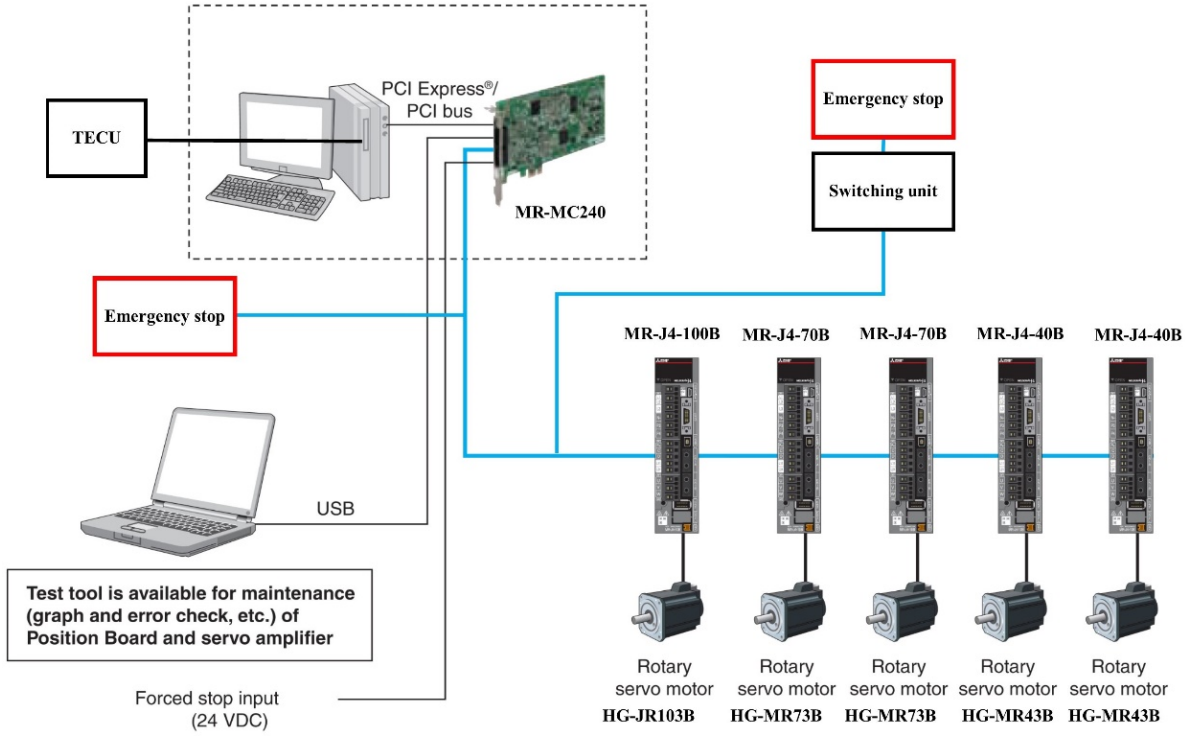

Figure 88. PLC system configuration.

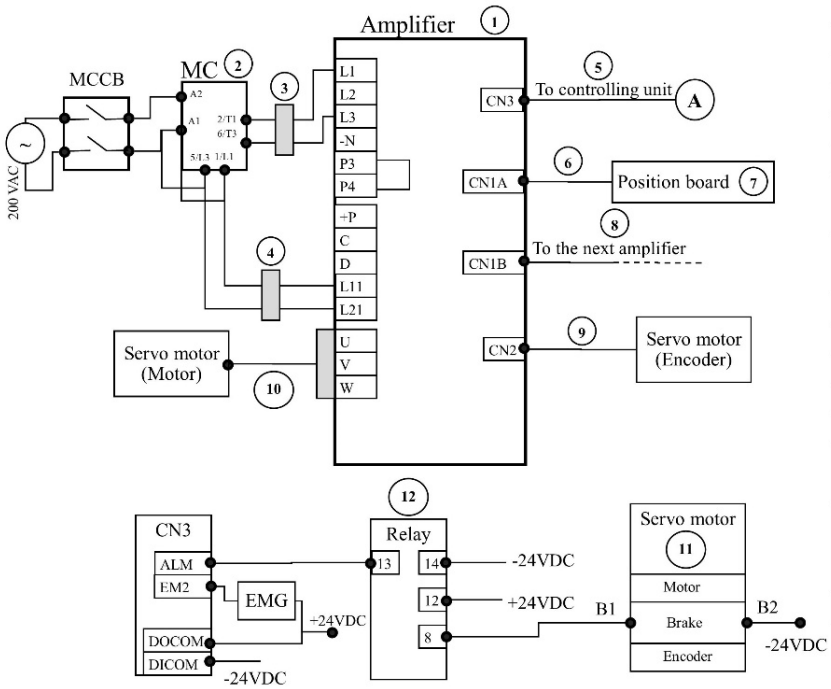

No.	details	Component ID
1	S-1	MR-J4-100B
	S2 and 3	MR-J4-70B
	S4 and 5	MR-J4-40B
2	S-T10	
3	S-1	Mitsubishi 2PNCT 3.5mm^2
	S2 ~5	VCTF JCT JC0607004 0.75mm^2
4	S-1	Mitsubishi 2PNCT 3.5mm^2
	S2 ~5	VCTF JCT JC0607004 0.75mm^2
5	VCTF JCT JC0607004 0.75mm^2	
6	MR-J3BUS3M	
7	MR-MC240	
8	MR-J3BUS015M	
9	MR-J3ENSCBL5M H Lot. 167SB	
10	S-1	SC-PWC4CBL5M-A3-SBH
	S2 ~5	MR-J3ENCBL5M-AI-Lot. 15*5B
11	S-1	HG-JR103B
	S2 and 3	HG-MR-73B
	S4 and 5	HG-MR-43B
12	OMRON MY2ZND2 24VDC	

Figure 89. Wiring and details of the amplifier, servo motor, magnetic switch, and relay.

6.2.2.Position board

In this study, a Position Board (Model MR-MC240- Mitsubishi company) was used (Figure 90). This board type controller is used for controlling MELSERVO-J4 SSCNET III/H compatible servo amplifiers, through a user program. The PCI Express compatible Position Board is one of the advantages of this board

(Mitsubishi Electronic, 2015). This position board newly created in Mitsubishi company as a series including of C Controller-embedded type and also PC-embedded type servo system controllers, which are compatible with C language programming and PC control which realize high-speed and fast-response positioning control. Table 24 and Table 25 show the control specifications and position board specifications, respectively.

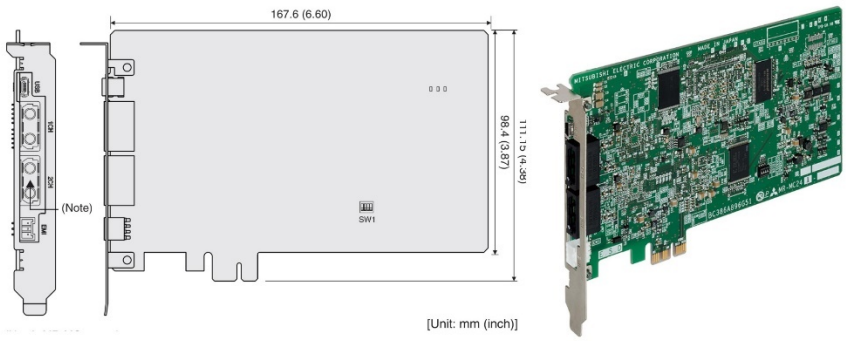

Figure 90. Position board (MR-MC240).

Table 24. Control specification of position board (MR-MC240).

Function		**MR-MC240**
System function	Number of control axes	Up to 20 axes
	Control cycle	0.22ms/0.44ms/0.88ms (Select using parameters.)
	Control mode	Position control, Tightening & press-fit control
Operation functions	JOG operation	Provided
	Incremental feed	Provided
	Automatic operation	Point table method, 1-axis control, Tightening & press-fit control
	Linear interpolation	Point table method, Up to 4 axes interpolation
	Home position return	Dog method, Dog cradle method, Dog front end method, Dataset method, Stopper method, Z-phase detection method, Limit switch combined method, Limit switch front-end method, Scale home position signal detection method, Scale home position signal detection method 2
		Home position reset (dataset)
Application functions 1	Electronic gear	Electronic gear numerator: 1 to 5242879 Electronic gear denominator: 1 to 589823
	Speed units	Command unit/min, command unit/s, and r/min
	Acceleration/deceleration	Command speed limits: 1 to speed limit value, Start speed limits: 1 to speed limit value, Time constant limits: 0 to 20000 ms, Separate setting of constants for deceleration and acceleration: Provided, Separate setting of constants for each point: Provided, Acceleration/deceleration method: Linear acceleration/deceleration, smoothing filter, startup speed, S-curve acceleration/deceleration (sine acceleration/deceleration)
	Stop function	Forced stop, Operation stop, Rapid stop
	Command change	Position, Speed, Time constant

Application functions 2	Rough match output, Torque limit, Backlash compensation, Position switch, Interference check (Note-3), Home position search limit, Gain switching, PI-PID switching, Absolute position detection system, Home position return request, Other axes start, Digital input/output, Servo amplifier general input/output, Pass position interrupt, Tandem operation, Mark detection	
Auxiliary function	Monitor	Current command position, Current feedback position, Speed command, Position droop, Electrical current command, Servo alarm number, External signal status, etc.
	High-speed monitor	Current command position, Current feedback position, Moving speed, Feedback moving speed, External signal, Electrical current feedback
	Interrupt	During start operation, Operation stoppage (During operation, in-position, during smoothing stop, rough match, etc.) When an alarm occurs (servo alarm/operation alarm), etc.
	Host PC watchdog	Provided (Check for the watchdog of the CPU of the host computer)
	Parameter backup	Parameters can be saved to the flash ROM.
	Test mode	By connecting MR Configurator2 via the controllers, the servo amplifier can be easily tested.
	Connect/disconnect	Provided
	Sampling	The maximum sampling point: 65536 (Ring buffer of 8192 points)
	Log	History of operation start, alarms, etc., can be recorded.
	Alarm history	Provided
	Externally forced stop disabled	Provided
Board ID		0 to 3

Table 25. Position board specifications.

Item		Specification
Servo amplifier connection system		SSCNET III/H (1 line)
Maximum overall cable distance [m(ft.)]		SSCNET III/H: 2000 (6561.68)
Maximum distance between stations [m(ft.)]		SSCNET III/H: 100 (328.08)
Peripheral I/F		USB
Forced stop input signal (EMI)	Number of input points	1 point
	Input method	Positive Common/ Negative Common Shared Type (Photocoupler isolation)
	Rated input voltage/current	24 VDC/approx. 2.4 mA
	Operating voltage range	20.4 to 26.4 VDC (24 VDC +10%/−15%, ripple ratio 5% or less)
	ON voltage/current	17.5 VDC or more/2.0 mA or more
	OFF voltage/current	1.8 VDC or less/0.18 mA or less
	Input resistance	Approx. 10kΩ
	Response time	1ms or less (OFF to ON, ON to OFF)
	Recommended wire size	AWG22 to 28 (0.08 to 0.32 mm2)
Number of Position Boards for one computer		PCI Express®1.1 × 1
	Size [mm(inch)]	Short sized version (111.2(4.38) × 167.6(6.60))
Power supply voltage		3.3 VDC
Current consumption [A]		1.1
Mass [kg]		0.11

6.2.3. Amplifiers

Servo amplifiers are components of a so-called motion control system. This concept is a different type of motion control such as single axis positioning in micro-installations but also for the solution of sophisticated tasks like multiple-axis positioning in a large-scale installation. With a motion control system, it is possible to solve different positioning applications from positioning with one axis in small production lines up to multi-axis positioning in a large-scale system. Figure 91 illustrates the components of a motion control system with CPUs, modules, servo amplifiers and motors (Mitsubishi Electronic, 2014). In this study, three different amplifiers produced by Mitsubishi company was used. The MR-J4-100B amplifier was used for joint-1 operation; the MR-J4-70B amplifier was used for joint-2 and joint-3, and the MR-J4-40B was used for Joint-4 and end-effector as shown in Figure 92 and Figure 93.

.

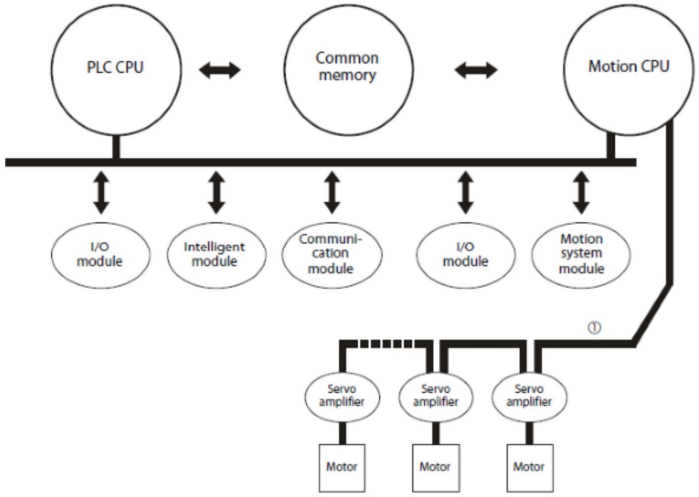

Figure 91. The components of motion control system (Mitsubishi Electronic, 2014).

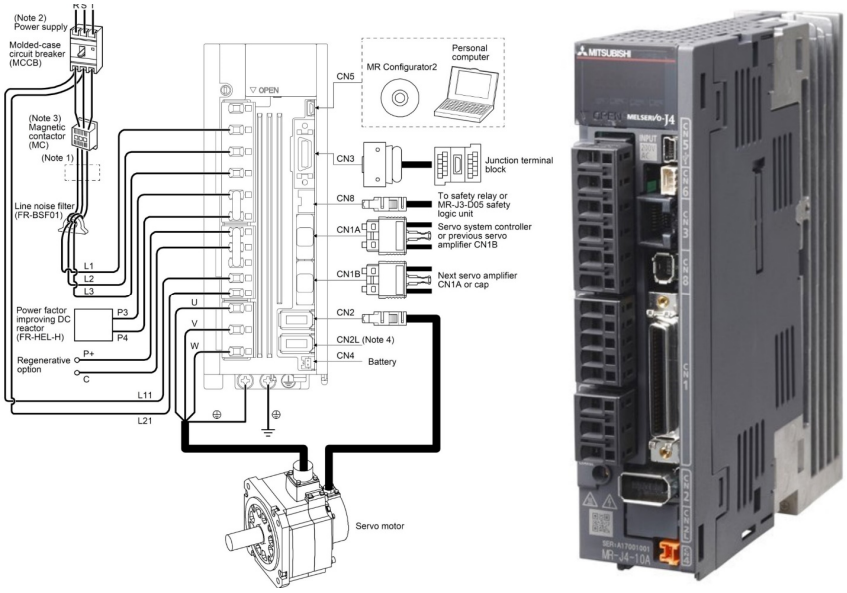

Figure 92. Amplifier MR-J4-100B configurations (Mitsubishi Electronic, 2014).

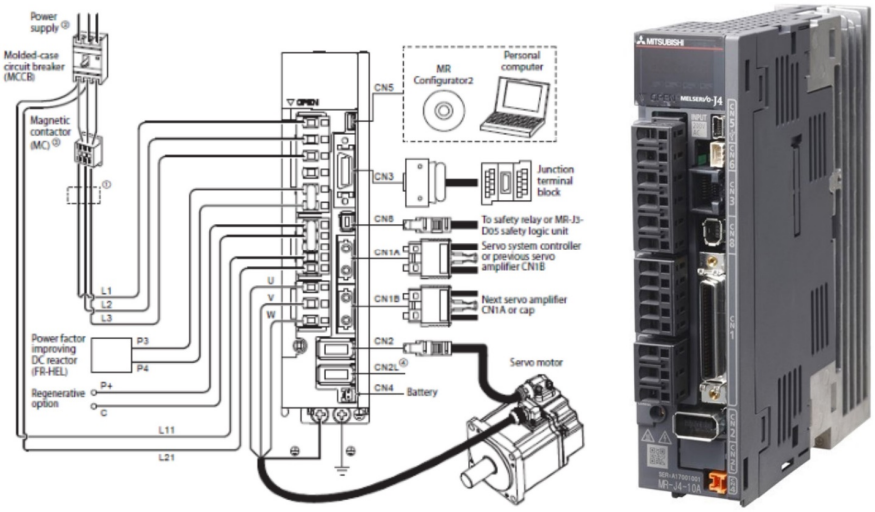

Figure 93. Amplifier MR-J4-70B and MR-J4-40B configurations (Mitsubishi Electronic, 2014).

6.2.4. Servo motors

As shown in Figure 94, three different servo motors of Mitsubishi company was used as actuators. An HG-JR103B for Joint-1, HG-MR73B for Joint-2 and Joint-3, and HG-MR43B for Joint-4 and end-effector (Figure 94).

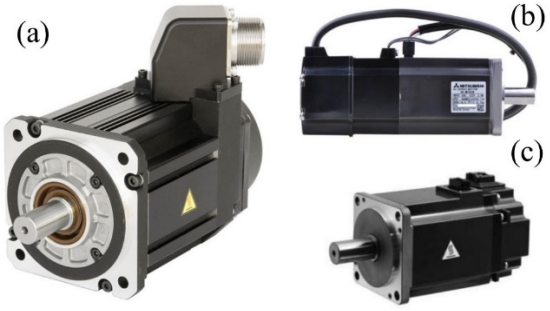

Figure 94. Servo motors, (a) HG-JR103B, (b) HG-MR73B, and (c) HG-MR43B.

6.2.5. Connector Wires

There was used several connection wires as shown in

Table 26. Connecting wires list.

From	Wire type	To
Position board	SSCNETIII	MR-J4-100B
MR-J4-100B	SC-PWC4CBL5M-A3-SBH A602071 (motor) MR-J3ENSCBL5M-H lot. 167 SB (encoder)	HG-JR103B
Switching unit	SC-BKC1CBL5M-A2-H A602071 (brake)	HG-JR103B
MR-J4-70B	MR-PWS1CBL5M-A1 lot. 15YTK (motor) MR-J3ENCBL5M-A1 lot. 15XSB (encoder)	HG-MR73B

Switching unit	MR-J3ENCBL5M-A1 lot. 15XTK (brake)	HG-MR73B
MR-J4-40B	MR-PWS1CBL5M-A1 lot. 15YTK (motor) MR-J3ENCBL5M-A1 lot. 15XSB (encoder)	HG-MR43B
Switching unit	MR-J3ENCBL5M-A1 lot. 15XTK (brake)	HG-MR43B
Amplifier (n)	Optical cable	Amplifier (n+1)
Other connection	Various wires	

6.2.6. Other components

In this study, the main power source was 200VAC which was supplied from a PTO-mobile generator. The PTO-mobile generator was installed on PTO of robot tractor. For safety an emergency situation, two fast-punch emergency switches were used as shown in Figure 95-a and b. Used magnetic switches for PLC system was a Mitsubishi S-T10 model as shown in Figure 95-c. And for switching system and relays power, an AD 24VDC converter was used as shown in Figure 95-d.

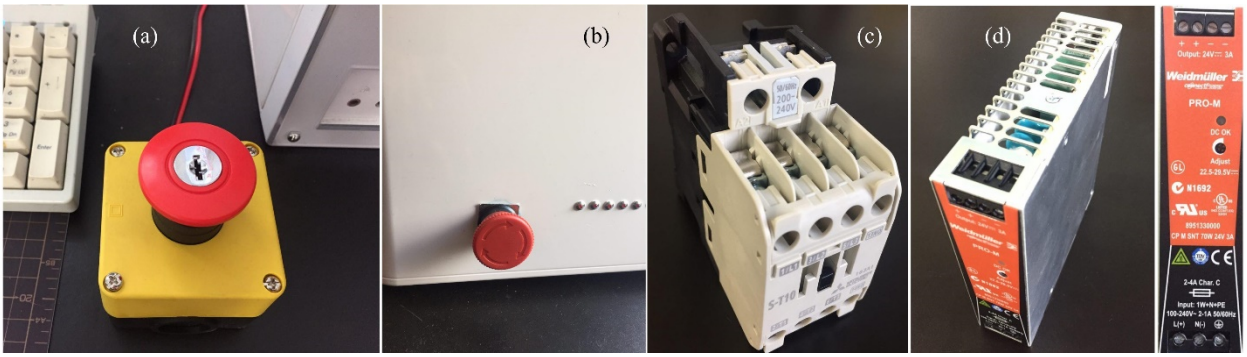

Figure 95. (a, b) emergency switches, (c) magnet switch, (d) 24VDC AD converter.

6.3. Controlling functions

More than 100 functions used for creating user application, such as operating functions, monitor functions, other axes start functions, pass position interrupt functions, sampling functions, and log functions as shown in Table 27.

Table 27. Programming functions.

Function Type	Function (some functions are omitted)	Function Content
Support Functions	sscGetLastError	Gets the detailed error codes.
Device Functions	sscOpen	Opens memory access port.
	sscClose	Closes memory access port.
Parameter Functions	sscResetAllParameter	Writes the initial values in all parameters before system startup.
	sscChangeParameter	Writes the parameter.
	sscCheckParameter	Reads the parameter set value.
	sscLoadAllParameterFromFlashROM	Loads all the parameters from a flash ROM before system startup.
	sscSaveAllParameterToFlashROM	Saves all the parameters into a flash ROM before system startup.
System Functions	sscReboot	Reboots the system.
	sscSystemStart	Starts the system.
	sscGetSystemStatusCode	Gets the system status code.
	sscReconnectSSCNET	Reconnects the SSCNET communication.
	sscDisconnectSSCNET	Disconnects the SSCNET communication.
	sscSetCommandBitSignalEx	Arbitrarily sets the command bit.

Command/ Status Functions	sscGetStatusBitSignalEx	Arbitrarily gets the status bit.
	sscWaitStatusBitSignalEx	Waits until the specified bit turns on/off.
Point Table Functions	sscSetPointDataEx	Sets the point data.
	sscCheckPointDataEx	Gets the point data.
	sscSetPointOffset	Sets the point number offset.
	sscGetDrivingPointNumber	Gets the operation point number.
Operating Functions	sscJogStart	Starts JOG operation.
	sscJogStop	Stops JOG operation.
	sscIncStart	Starts incremental feed.
	sscAutoStart	Starts automatic operation.
	sscHomeReturnStart	Starts home position return.
	sscLinearStart	Starts linear interpolation.
	sscDataSetStart	Starts the home position reset (dataset).
	sscDriveStop	Stops operation.
	sscGetDriveFinStatus	Gets the operation completion status.
Change Functions	sscChangeAutoPosition	Changes position during automatic operation.
	sscChangeLinearPosition	Changes position during linear interpolation.
Alarm Functions	sscGetAlarm	Gets the alarming number.
	sscResetAlarm	Resets the alarm.
General Monitor Functions	sscSetMonitor	Starts monitoring.
	sscStopMonitor	Stops monitoring.
	sscGetMonitor	Gets monitoring data.
High Speed Monitor Functions	sscGetCurrentCmdPositionFast	Gets the current command position.
	sscGetCurrentFbPositionFast	Gets the current feedback position.
	sscGetIoStatusFast	Gets the external signal status.
	sscGetCmdSpeedFast	Gets the moving speed.
	sscGetFbSpeedFast	Gets the feedback moving speed.
	sscGetCurrentFbFast	Gets the current feedback.
User Watchdog Functions	sscWdEnable	Enables the user watchdog function.
	sscWdDisable	Disables the user watchdog function.
	sscChangeWdCounter	Updates the watchdog counter.
Other Axes Start Functions	sscSetOtherAxisStartData	Sets the data for starting other axes.
	sscGetOtherAxisStartData	Gets the data for starting other axes.
	sscOtherAxisStartAbortOn	Turns the other axes start to cancel signal ON.
	sscOtherAxisStartAbortOff	Turns the other axes start to cancel signal OFF.
	sscGetOtherAxisStartStatus	Gets the other axes start status.
Pass Position Interrupt Functions	sscSetIntPassPositionData	Sets the pass position interrupt condition data.
	sscSetStartingPassNumber	Sets the pass position condition start and end numbers.
	sscGetExecutingPassNumber	Gets the running pass position condition number.
Sampling Functions	sscStartSampling	Starts sampling.
	sscStopSampling	Stops sampling.
	sscGetSamplingStatus	Gets the sampling execution information.
	sscGetSamplingData	Gets the sampling data.
Log Functions	sscStartLog	Starts the log.
	sscStopLog	Stops the log.
	sscCheckLogStatus	Gets the running status of the log.
	sscReadLogData	Reads the log data.
	sscClearLogData	Clears (initializes) the log data.
	sscGetAlarmHistoryData	Gets alarm history data.
	sscClearAlarmHistoryData	Clears (initializes) the alarm history data.
Digital Input/Output Functions	sscGetDigitalInputDataBit	Gets the DI data of the designated digital input on the 1-point basis.
	sscSetDigitalOutputDataBit	Sets the DO data of the designated digital output on the 1-point basis.
Interrupt Functions	sscIntStart	Starts up the interrupt driver.
	sscIntEnd	Closes the interrupt driver.
	sscIntEnable	Enables interrupt output.
	sscIntDisable	Disables interrupt output.
	sscRegisterIntCallback	Registers the interrupt callback function.

	sscUnregisterIntCallback	Unregisters the interrupt callback function.
	sscResetIntEvent	Sets the interrupt event signal status to nonsignaled.
	sscSetIntEvent	Sets the interrupt event signal status to signaled.
	sscWaitIntEvent	Waits until the interrupt event status becomes signaled.
	sscResetIntOasEvent	Sets the status of the other axes start interrupt event to nonsignaled.
	sscSetIntOasEvent	Sets the status of the other axes start interrupt event to signaled.
	sscWaitIntOasEvent	Waits until the status of the other axes start interrupt event becomes signaled.
	sscResetIntPassPosition	Sets the status of the pass position interrupt event to nonsignaled.
	sscSetIntPassPosition	Sets the status of the pass position interrupt event to signaled.
	sscWaitIntPassPosition	Waits until the status of the pass position interrupt event becomes signaled.
	sscResetIntDriveFin	Sets the status of the operation completion interrupt event to nonsignaled.
	sscSetIntDriveFin	Sets the status of the operation completion interrupt event to signaled.
	sscWaitIntDriveFin	Waits until the status of the operation completion interrupt event becomes signaled.

6.4. Limit switch circuit

The limit switches were set for an emergency which the servo motor passed the limitation of movement. In this case, one of the limit switches which was located at start point or endpoint, sending a positive command to the amplifier and the command sending to position board. The signal came from position board to stop the servo motor. Figure 96 illustrates the details of limit switch connections. Based on the motion type, the limit switches could have connected to DI1, DI2, or DI3.

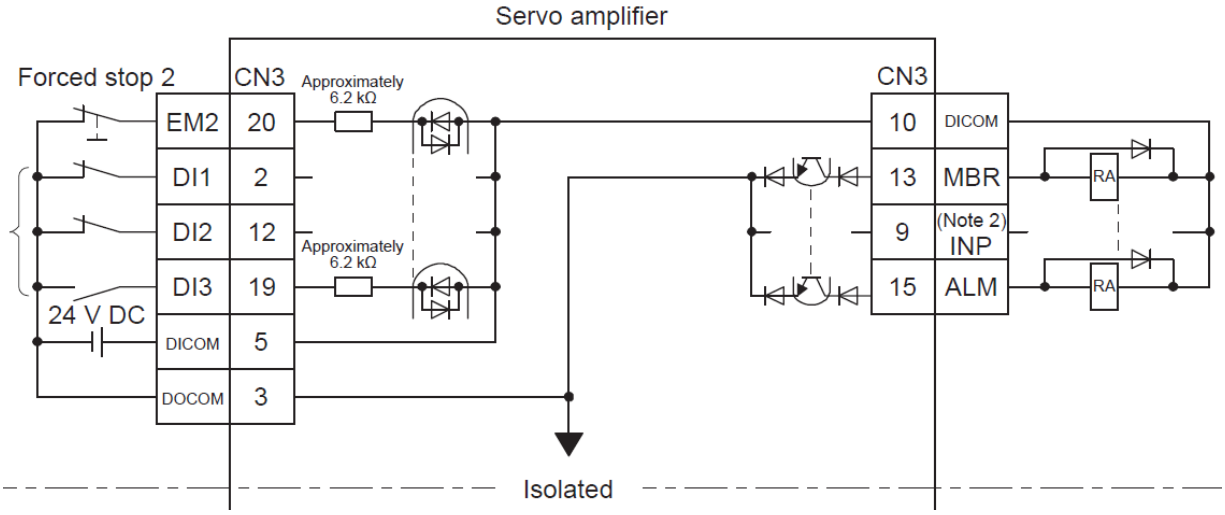

Figure 96. limit switch diagram.

6.5. Algorithm

To design a robotic arm for agricultural applications, it is necessary to move the final point of a manipulator along some desired path at a prescribed speed (Angeles, 1997). Furthermore, it is necessary for the system to be dynamically analyzed and modeled (Wang et al., 2003). To reach this goal, it is essential to use forward and inverse kinematics (Karlik & Aydin, 2000). The motion takes place in the Cartesian space; but most of the industrial robots, especially the articulated robotic arm, are controlled in rotary joint spaces. Therefore, a kinematic transformation between the Cartesian space and joint space is needed (Balkan, Özgören, Sahir Arıkan, & Baykurt, 2000). The most widely proposed methods for solving the inverse

kinematic problem for redundant manipulators involve the use of the Jacobian pseudoinverse manipulator (Yahya, Moghavvemi, & Mohamed, 2011). Thanks to this method, many excellent types of research in the kinematics community had been done by the end of the 1980s and the beginning of 1990s. At the same time, resolving of inverse kinematics was considered to be the most difficult task in the field of kinematics. In 1988 H.-Y. Lee and Liang (1988) came up with a solution which was not very transparent, so most of the time the Raghavan and Roth (1990) solution is cited in the literature. There were many attempts to improve the controlling algorithm (Ghazvini, 1993). As a result, there are many thousands of robots in the industry (Satoru, 2011) but only a few are designed for agriculture application.

The promising results of laboratory investigations can be considered as a cornerstone for the development of models for farming robots. Currently, the agricultural robotic technology is in the development stage, and it is expected that the agricultural robots can cover all the needs of agriculture. However, researchers had not investigated the topic of heavy harvesting crops like cabbage, pumpkin, and watermelon as much as light crops. Since users intend to take advantage of fully automated processes in different aspects of agriculture through the use of robotic technology, further research; especially on harvesting agricultural heavy products is required. This research presents a new type of 5 DOF robotic arm mounted on a tractor for heavy crop harvestings like pumpkin and cabbage.

6.5.1.Robotic arm controlling algorithm

In this study, a 5 DOF robotic arm for the harvesting the heavy agricultural products (RAVebots-1) was developed, which is shown schematically in Figure 97. The presented robotic arm is composed of serial links which are affixed to each other with revolute joints from the base frame to the end-effector. The RAVebots-1's structure was chosen to be manufactured for heavy product harvesting application. All components were designed, assembled and analyzed using Solidworks 2014. Dynamic components of the system were analyzed using standard mechanical formula. After finishing all component development, The RAVebots-1 was attached to a robot tractor.

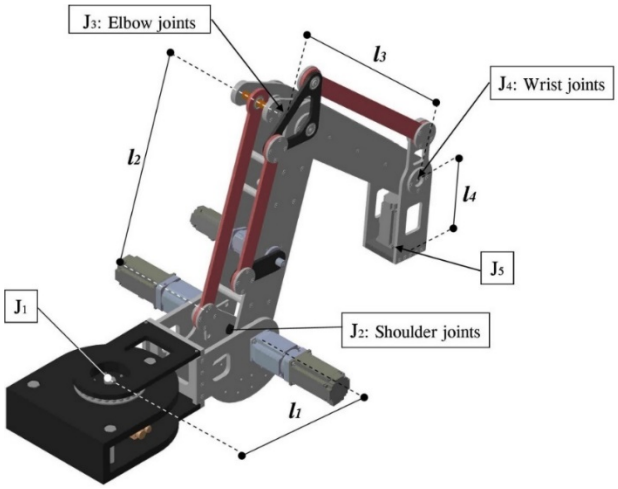

Figure 97- An assembled model of RAVebots-1.

6.5.2.Kinematics calculation

Robot kinematics refers to the analytical study of the motion of a robot manipulator. Denavit and Hartenberg (1955b) showed that a general transformation between two joints requires four parameters. These parameters, known as the Denavit-Hartenberg (D-H) parameters have become the standard for describing robot kinematics (Funda, Taylor, & Paul, 1990). The robot kinematics can be divided into forward and inverse kinematics. Forward kinematics problems are straightforward, with little to no complexity in driving their respective equations. Inverse kinematics is more difficult to solve than forward kinematics (Satoru, 2011; Serdar & Zafer, 2006). In this section, the analytical solution for the manipulator is presented using

the D-H parameter into forward kinematics and inverse kinematics. Robotic arm kinematics deal with time-dependent/geometry arm motion without consideration of other parameters like force and moment (Balafoutis & Patel, 1991). For the analytical study of robotic arm motion, it is best to use robot kinematics. The essential aspect in analyzing the behavior of industrial manipulators is the optimized kinematics model formulation. The kinematics analysis of a robotic arm has two aspects: forward kinematics (FK) and inverse kinematics (IK). Kinematics simulation was conducted using the D-H method, as shown in Figure 98. In this case, suppose P_E (p_x, p_y, p_z) is the desired target position for the end effector, and θ_i in which i=1,..,5 is the joint angle. Then we have a relationship like $P_E = k(\theta_i)$, that k is a unique geometric calculation. The k depends on robotic arm morphology, which includes link length, joint angle ranges, and joint position. Next is the inverse kinematics (IK), which is the geometrical and mathematical calculations needed to find a proportional relationship between joint angle and position as $\theta_i = k^{-1}(P_E)$. It corresponds to finding the appropriate joint angles of each link from a known position in space. For redundant robotic arms like that in Figure 99, however, there can be infinite solutions (Mitrovic, 2006).

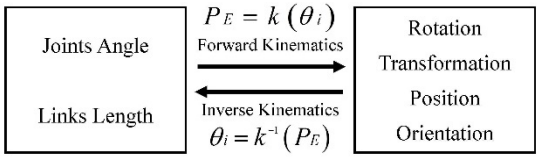

Figure 98. Kinematic simulation parameters.

As shown in Figure 99-a, IK solutions based on the goal-point position can vary in number. In other words, depending on whether the object is located on/in the workspace or outside of it, the IK will have a different number of answers. For the RAVeBot-1 application, it was necessary to provide some limitations and to omit unnecessary workspace volume to reach the optimized logical number of answers. Thus, after the structure was developed and mounted on the robot tractor, joint rotations were limited to a particular range for safety and output of body interferences extracted from experiments. In addition, the height access was limited due to robot tractor height. Once these limitations were applied, IK solutions were optimized, as shown in Figure 99-b. In the figure, volume V, located under link-1 and the tractor chassis, was negligible in terms of workspace volume. Looking at it a different way, when the robot tractor was moving, the V volume scanned and harvested available pumpkins in the previous step, so there was no need to rescan it again. From this and limitations applied to the recognition system, the RAVeBots-1 workspace was optimized, as shown in Figure 99-b. The system has two kinds of output. In the first, the robotic arm can grasp, pick, and lift crop produce located at A or B. In the second, when the object is located out of the workspace at C, the robot tractor begins to move forward as quickly as coded length allows for each step in the controlling program.

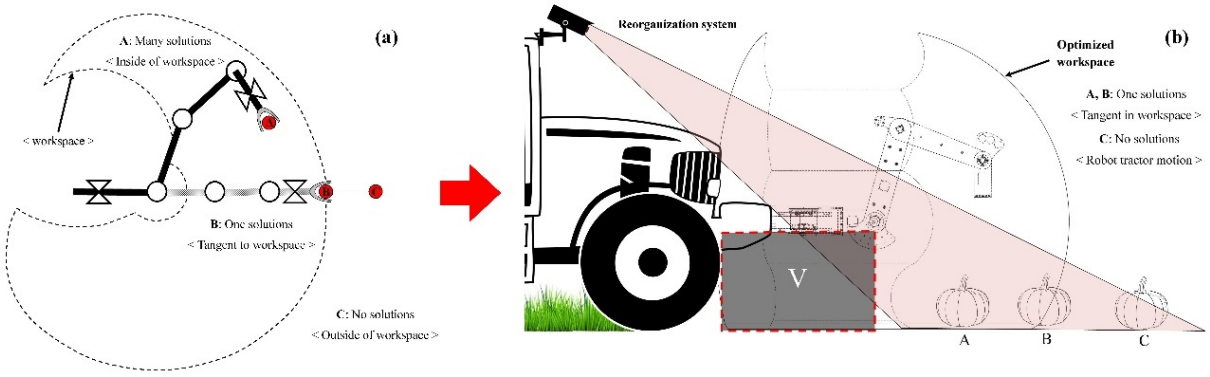

Figure 99. Kinematic scenarios illustrations, (a) Pure developed an algorithm, (b) improved algorithm adapted to crops harvesting.

6.5.2.1. Forward Kinematics

Forward kinematics problem involves finding the position and orientation of a robot end-effector as a function of its joint angles. Denavit-Hartenberg (D-H) method uses the four parameters a_{i-1}, α_{i-1}, d_i and θ_i; which are the link length, link twist, link offset and joint angle, respectively. Figure 100 presents the coordinate frame assignment for a general manipulator (Serdar & Zafer, 2006).

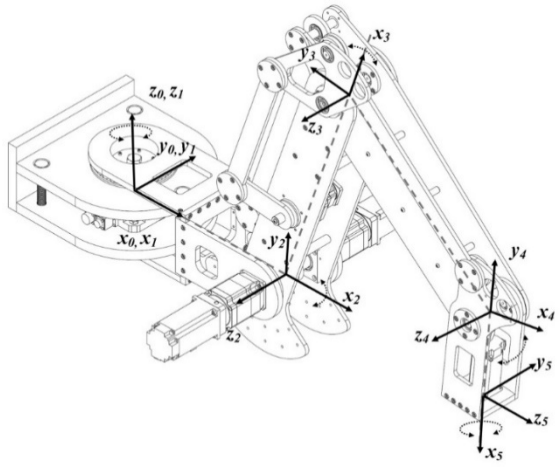

Figure 100. Axis's direction and angle parameters.

The matrix T_i^{i-1} is known as a D-H convention matrix given as follow:

$$T_i^{i-1} = \begin{bmatrix} \cos\theta_i & -\cos\alpha_{i-1}\sin\theta_i & \sin\alpha_{i-1}\sin\theta_i & a_{i-1}\cos\theta_i \\ \sin\theta_i & \cos\alpha_{i-1}\cos\theta_i & -\sin\alpha_{i-1}\cos\theta_i. & a_{i-1}\sin\theta_i \\ 0 & \sin\alpha_{i-1} & \cos\alpha_{i-1} & d_i \\ 0 & 0 & 0 & 1 \end{bmatrix} \quad (35)$$

In the matrix T_i^{i-1}, the quantities $\alpha_{i-1}, a_{i-1}, d_i$ are constant for a given link while the parameter θ_i for a revolute joint is variable. The next step was determining the D-H parameters by first determining α_i. The completed D-H parameters for RAVebots-1 are listed in Table 28.

Table 28- D-H Parameters of the RAVebots-1.

Axis Number	Twist Angle (α_{i-1})	Link Length (a_{i-1})	Link Offset (d_i)	Joint Angle (θ_i)
1	90°	l_1	0	$-105^\circ < \theta_1 < 105^\circ$
2	0	l_2	0	$0^\circ < \theta_2 < 125^\circ$
3	0	l_3	0	$-130^\circ < \theta_3 < -10^\circ$
4	−90°	l_4	0	$-115^\circ < \theta_4 < 0^\circ$
5	0	l_5	0	$0^\circ < \theta_5 < 360^\circ$

Using the expressions, the A-matrices of each joint can be built as follow:

$$T_1^0 = \begin{bmatrix} \cos\theta_1 & 0 & \sin\theta_1 & l_1\cos\theta_1 \\ \sin\theta_1 & 0 & -\cos\theta_1 & l_1\sin\theta_1 \\ 0 & 1 & 0 & 0 \\ 0 & 0 & 0 & 1 \end{bmatrix}, T_2^1 = \begin{bmatrix} \cos\theta_2 & -\sin\theta_2 & 0 & l_2\cos\theta_2 \\ \sin\theta_2 & \cos\theta_2 & 0 & l_2\sin\theta_2 \\ 0 & 0 & 1 & 0 \\ 0 & 0 & 0 & 1 \end{bmatrix}$$

$$T_3^2 = \begin{bmatrix} \cos\theta_3 & -\sin\theta_3 & 0 & l_3\cos\theta_3 \\ \sin\theta_3 & \cos\theta_3 & 0 & l_3\sin\theta_3 \\ 0 & 0 & 1 & 0 \\ 0 & 0 & 0 & 1 \end{bmatrix}, T_4^3 = \begin{bmatrix} \cos\theta_4 & 0 & -\sin\theta_4 & l_4\cos\theta_4 \\ \sin\theta_4 & 0 & \cos\theta_4 & l_4\sin\theta_4 \\ 0 & 1 & 0 & 0 \\ 0 & 0 & 0 & 1 \end{bmatrix} \quad (36)$$

$$T_5^4 = \begin{bmatrix} \cos\theta_5 & -\sin\theta_5 & 0 & l_5\cos\theta_5 \\ \sin\theta_5 & \cos\theta_5 & 0 & l_5\sin\theta_5 \\ 0 & 0 & 1 & 0 \\ 0 & 0 & 0 & 1 \end{bmatrix}$$

The T-matrix is created by multiplying each T_5^0 matrix. The result is as:

$$T_5^0 = \prod_{i=1}^{5} T_i^{i-1} = T_1^0\, T_2^1\, T_3^2\, T_4^3\, T_5^4 = \begin{bmatrix} r_{11} & r_{12} & r_{13} & r_{14} \\ r_{21} & r_{22} & r_{23} & r_{24} \\ r_{31} & r_{32} & r_{33} & r_{34} \\ r_{41} & r_{42} & r_{43} & r_{44} \end{bmatrix} \quad (37)$$

Where the matrix elements are defined as:

$$\begin{aligned} &\mathbf{r_{11}} = c_1c_{(2+3+4)}c_5 + s_1s_5, \mathbf{r_{12}} = s_5\left(s_1 - c_1c_{(2+3+4)}\right), \mathbf{r_{13}} = -c_1s_{(2+3+4)} \\ &\mathbf{r_{14}} = c_1\left(l_1 + l_2c_2 + l_3c_{(2+3)} + l_4\,c_{(2+3+4)} + l_5c_5c_{(2+3+4)}\right) + l_5s_1s_5 \\ &\mathbf{r_{21}} = s_1c_{(2+3+4)}c_5 - c_1s_5, \mathbf{r_{22}} = -s_1c_{(2+3+4)}s_5 - c_1c_5, \mathbf{r_{23}} = -s_1s_{(2+3+4)} \\ &\mathbf{r_{24}} = s_1\left(l_1 + l_2c_2 + l_3c_{(2+3)} + l_4\,c_{(2+3+4)} + l_5c_5c_{(2+3+4)}\right) - l_5c_1c_5 \\ &\mathbf{r_{31}} = s_{(2+3+4)}c_5, \mathbf{r_{32}} = -s_{(2+3+4)}s_5, \mathbf{r_{33}} = c_{(2+3+4)}, \mathbf{r_{34}} = l_5s_{(2+3+4)}c_5 \\ &\mathbf{r_{14}} = \mathbf{r_{24}} = \mathbf{r_{34}} = 0, \mathbf{r_{44}} = 1 \end{aligned} \quad (38)$$

In the expressions of Equation 5, the variables are defined as:

$$\mathbf{c_i} = \cos\theta_i,\ \mathbf{s_i} = \sin\theta_i,\ \mathbf{c_{ij}} = \cos(\theta_i + \theta_j),\ \mathbf{s_{ij}} = \sin(\theta_i + \theta_j) \quad (39)$$

By using the T-matrix, it is possible to calculate the values of (P_x, P_y, P_z) with respect to the fixed coordinate system. Then the P_x, P_y, P_z obtained with direct kinematics are expressed as shown as follow:

$$\begin{aligned} P_x = {} & \cos\theta_1\,[l_1 + l_2\cos\theta_2 + l_3\cos(\theta_2 + \theta_3) + l_4\cos(\theta_2 + \theta_3 + \theta_4) + \\ & l_5\cos\theta_5\cos(\theta_2 + \theta_3 + \theta_4)] + l_5\sin\theta_1\sin\theta_5] \\ P_y = {} & \sin\theta_1\,[l_1 + l_2\cos\theta_2 + l_3\cos(\theta_2 + \theta_3) + l_4\cos(\theta_2 + \theta_3 + \theta_4) + \\ & l_5\cos\theta_5\cos(\theta_2 + \theta_3 + \theta_4)] - l_5\cos\theta_1\sin\theta_5] \\ P_z = {} & l_2\sin\theta_2 + l_3\sin(\theta_2 + \theta_3) + l_4\sin(\theta_2 + \theta_3 + \theta_4) + l_5\cos\theta_5\sin(\theta_2 + \theta_3 + \theta_4) \end{aligned} \quad (40)$$

The orientation of RAVebots-1's end-effector in space can be described by attaching a coordinate system to it and then describing the vector of its coordinate axes on the reference frame. Figure 101 shows the normal vector ($\vec{n}$), orientation vector ($\vec{o}$), approach vector ($\vec{a}$) and the resultant of all vectors ($\vec{D}$) of the end-effector described in more detail in Equation 8:

$$\begin{aligned} &\vec{n} = \begin{bmatrix} c_1c_{(2+3+4)}c_5 + s_1s_5 \\ s_1c_{(2+3+4)}c_5 - c_1s_5 \\ s_{(2+3+4)}c_5 \end{bmatrix}, \vec{o} = \begin{bmatrix} s_5\left(s_1 - c_1c_{(2+3+4)}\right) \\ -s_1c_{(2+3+4)}s_5 - c_1c_5 \\ -s_{(2+3+4)}s_5 \end{bmatrix}, \vec{a} = \begin{bmatrix} -c_1s_{(2+3+4)} \\ -s_1s_{(2+3+4)} \\ c_{(2+3+4)} \end{bmatrix}, \\ &\vec{D} = (\vec{n} + \vec{o}) + \vec{a} = \begin{bmatrix} c_1\left(c_{(2+3+4)}(c_5 - s_5) - s_{(2+3+4)}\right) + 2s_1s_5 \\ s_1\left(c_{(2+3+4)}(c_5 - s_5) - s_{(2+3+4)}\right) + c_1c_4 \\ s_{(2+3+4)}(c_5 - s_5) + c_{(2+3+4)} \end{bmatrix} \end{aligned} \quad (41)$$

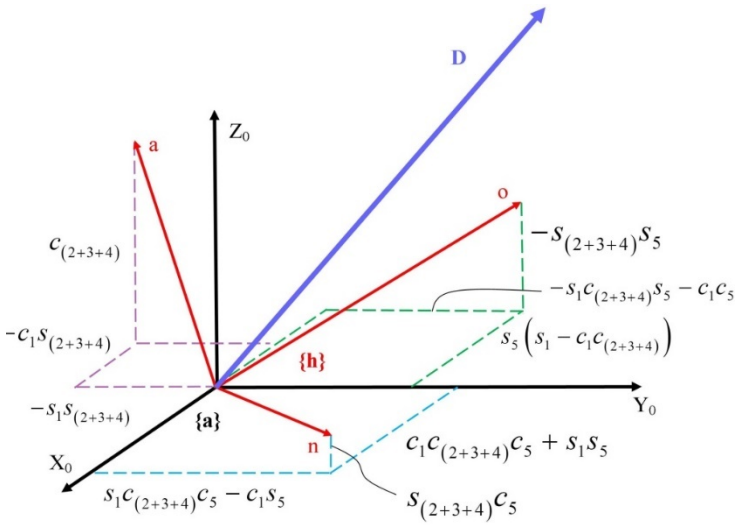

Figure 101- Rotation matrix elements

6.5.2.2. Inverse kinematics

The conversion of the position and orientation of the manipulator's end-effector from Cartesian space to joint space is known as inverse kinematics problem. The inverse kinematics solution uses the position and orientation (px, py, pz) of the robot's end-effector, which has been known to solve the joint angles $(\theta_1, \theta_2, \theta_3, \theta_4, \theta_5)$. In this study, the geometrical method was used. The axes of the last two joints intersect at one point, which is referred to as point A. The position of point A is independent of the last two joints θ_4, and θ_5. Therefore, only the three previous joints should be considered when solving the position of point A. The position of A is denoted as $P_a = [P_{ax}, P_{ay}, P_{az}]$. The position of point A can be described by:

$$P_{ax} = P_x - P_{x_5}^3, \qquad P_{ay} = P_y - P_{y_5}^3, \qquad P_{az} = P_z - P_{z_5}^3 \tag{42}$$

Solutions of the arm joint angles ($\theta_1, \theta_2, and\ \theta_3$)

The position of point A can be determined from the homogeneous transformation matrix, which is derived from T_1^0, T_2^1, T_3^2 as follow:

$$T_3^0 = \prod_{i=1}^{3} T_i^{i-1} = T_1^0 T_2^1 T_3^2 = \begin{bmatrix} c_1c_{23} & -c_1s_{23} & s_1 & c_1(l_3c_{23} + l_2c_2 + l_1) \\ s_1c_{23} & -s_1s_{23} & -c_1 & s_1(l_3c_{23} + l_2c_2 + l_1) \\ s_{23} & c_{23} & 0 & l_3s_{23} + l_2s_2 \\ 0 & 0 & 0 & 1 \end{bmatrix} \tag{43}$$

Where

$$P_{ax} = c_1(l_3c_{23} + l_2c_2 + l_1), P_{ay} = s_1(l_3c_{23} + l_2c_2 + l_1), P_{az} = l_3s_{23} + l_2s_2 \tag{44}$$

And

$$\frac{P_{ay}}{P_{ax}} = \frac{s_1}{c_1} \rightarrow \theta_1 = \text{Atan } 2(P_{ay}, P_{ax}) \tag{45}$$

Then

$$P_{ax}.c_1 + P_{ay}.s_1 = (c_1^2 + s_1^2)(l_3c_{23} + l_2c_2 + l_1) = l_3c_{23} + l_2c_2 + l_1 = \mathbf{A} \tag{46}$$

In the RAVebots-1, c_{23} can be obtained from as follows:

$$c_{23} = \frac{(P_{ax}.c_1 + P_{ay}.s_1) - l_2c_2 - l_1}{l_3} \tag{47}$$

It is possible to obtain s_{23} as follows:

$$s_{23} = \frac{P_{az} + l_2s_2}{l_3} \tag{48}$$

By the equation ${c_{23}}^2 + {s_{23}}^2 = 1$ yields:

$$\begin{gathered}\left((P_{ax}.c_1 + P_{ay}.s_1 - l_1) - l_2c_2\right)^2 + (P_{az} + l_2s_2)^2 = {l_3}^2 \\ P_{az}s_2 + (P_{ax}.c_1 + P_{ay}.s_1 - l_1)c_2 = \frac{(P_{ax}.c_1 + P_{ay}.s_1 - l_1)^2 + {l_2}^2 + {P_{az}}^2 - {l_3}^2}{2l_2} = A\end{gathered} \tag{49}$$

Consider the variables d, f, and g as defined:

$$d = P_{az};\ f = P_{ax}.c_1 + P_{ay}.s_1 - l_1;\ \ g = \frac{(P_{ax}.c_1+P_{ay}.s_1-l_1)^2+{l_2}^2+{P_{az}}^2-{l_3}^2}{2l_2} \tag{50}$$

Then:

$$d\sin\theta_2 + f\cos\theta_2 = g \tag{51}$$

Considering the approximations shown as:

$$\begin{gathered}f + g \neq 0, \quad d\sqrt{d^2 + f^2 - g^2} - d^2 - f^2 - fg \neq 0 \rightarrow \theta_2 \\ \approx 2.\left(3.14159\,n + \tan^{-1}\left(\frac{d - \sqrt{d^2 + f^2 - g^2}}{f + g}\right)\right), n \in z \\ f + g \neq 0, \quad d\sqrt{d^2 + f^2 - g^2} + d^2 + f^2 + fg \neq 0 \rightarrow \theta_2 \\ \approx 2.\left(3.14159\,n + \tan^{-1}\left(\frac{d + \sqrt{d^2 + f^2 - g^2}}{f + g}\right)\right), n \in z \\ d \neq 0,\ d^2 + f^2 \neq 0\,, g \approx -f \rightarrow \theta_2 \approx 2.\left(3.14159\,n + \tan^{-1}\left(\frac{f}{d}\right)\right), n \in z \\ g = -f \rightarrow \theta_2 = 2\pi n + \pi, n \in z\end{gathered} \tag{52}$$

And if $g = -f, x = 2n\pi + \pi$ it is possible to obtain:

$$\begin{gathered}\theta_2 = \text{Atan}\,2\left(\frac{fg - \sqrt{d^4 + d^2f^2 - d^2g^2}}{d^2 + f^2}, \frac{1}{d}\left(\frac{f\sqrt{-d^2(-d^2 - f^2 + g^2)} - f^2g}{d^2 + f^2} + g\right)\right) \\ \theta_2 = \text{Atan}\,2\left(\frac{fg + \sqrt{d^4 + d^2f^2 - d^2g^2}}{d^2 + f^2}, \frac{1}{d}\left(\frac{-f\sqrt{-d^2(-d^2 - f^2 + g^2)} - f^2g}{d^2 + f^2} + g\right)\right)\end{gathered} \tag{53}$$

The result of using Equation 14 and 15 yields:

$$\tan(\theta_2 + \theta_3) = \frac{P_{az} + l_2s_2}{(P_{ax}.c_1 + P_{ay}.s_1) - l_2c_2 - l_1} \tag{54}$$

Then

$$\theta_3 = \text{Atan}\,2\left(P_{az} + l_2s_2,\ (P_{ax}.c_1 + P_{ay}.s_1) - l_2c_2 - l_1\right) - \theta_2 \tag{55}$$

Solutions of the wrist joint angles (θ_4 and θ_4).

The orientation of the robot is controlled by the rotation matrix, and the orientation of A is described by T_3^0. The orientation of the end-effector is described by T_5^0. The relationship between T_3^0 and T_5^0 is $T_5^0 = T_3^0\,T_5^3$. Matrix T_5^3 can be described as follow:

$$T_5^3 = \prod_{i=3}^{5} T_i^{i-1} = T_4^3 T_5^4 = \begin{bmatrix} c_4c_5 & -c_4s_5 & -s_4 & (l_5c_5 + l_4)c_4 \\ s_4c_5 & -s_4s_5 & c_4 & (l_5c_5 + l_4)s_4 \\ s_5 & c_5 & 0 & l_5s_5 \\ 0 & 0 & 0 & 1 \end{bmatrix} \quad (56)$$

The elements of $P_{A_5}^3$ come from the fourth column of the 4*4 matrix, which can be described as:

$$P_{x_5}^3 = (l_5c_5 + l_4)c_4,\ P_{y_5}^3 = (l_5c_5 + l_4)s_4,\ P_{z_5}^3 = l_5s_5 \quad (57)$$

And

$$\frac{P_{y_5}^3}{P_{x_5}^3} = \frac{s_4}{c_4} \rightarrow \theta_4 = \text{Atan 2}\left(P_{y_5}^3, P_{x_5}^3\right) \quad (58)$$

Also,

$$\sin\theta_5 = \frac{P_{z_5}^3}{l_5} \quad (59)$$

$$\cos\theta_5 = \frac{P_{x_5}^3 - l_4c_4}{l_5c_4} \quad (60)$$

Then

$$\theta_5 = \text{Atan 2}\left(\frac{P_{z_5}^3}{l_5}, \frac{P_{x_5}^3 - l_4c_4}{l_5c_4}\right) \quad (61)$$

The length of the body links is l_1 = 484 mm; l_2 = 650 mm; l_3 = 600 mm; l_4 = 250 mm and l_5 = 250 mm. The direct kinematics can be used to find the end-effector coordinate of the robot movement by substituting the constant parameters values. The final equation of the end-effector's envelopment for the D-H convention of forward kinematics is listed as follow:

$$\begin{aligned} P_x &= \cos\theta_1 [0.484 + 0.65\cos\theta_2 + 0.6\cos(\theta_2 + \theta_3) + 0.25\cos(\theta_2 + \theta_3 + \theta_4) + \\ &0.25\cos\theta_5\cos(\theta_2 + \theta_3 + \theta_4)] + 0.25\sin\theta_1\sin\theta_5] \\ P_y &= \sin\theta_1 [0.484 + 0.65\cos\theta_2 + 0.6\cos(\theta_2 + \theta_3) + 0.25\cos(\theta_2 + \theta_3 + \theta_4) + \\ &0.25\cos\theta_5\cos(\theta_2 + \theta_3 + \theta_4)] - 0.25\cos\theta_1\sin\theta_5] \\ P_z &= 0.65\sin\theta_2 + 0.6\sin(\theta_2 + \theta_3) + 0.25\sin(\theta_2 + \theta_3 + \theta_4) + \\ &0.25\cos\theta_5\sin(\theta_2 + \theta_3 + \theta_4) \end{aligned} \quad (62)$$

In the zero position, the orientation vectors are defined as follows in Equation 30:

$$\text{Zero position} \xrightarrow{\forall\theta_i,\ 1\le i\le 5,\ \theta_i=0} \vec{n} = \begin{bmatrix}1\\0\\0\end{bmatrix}, \vec{o} = \begin{bmatrix}0\\-1\\0\end{bmatrix}, \vec{a} = \begin{bmatrix}0\\0\\1\end{bmatrix}, \vec{D} = \begin{bmatrix}0\\0\\1\end{bmatrix} \quad (63)$$

Generally, the direction of the orientation vectors in the zero position proves the algorithm validity. It means, in the zero position, the normal vector ($\vec{n}$), the orientation vector ($\vec{o}$) and the approach vector ($\vec{a}$) should be in the same direction of the axes X, -Y and Z respectively. Therefore, all the coordinate frames in Figure 100 were removed except the base, which is the reference coordinate frame for determining the link parameters in zero position. The zero position is necessary to choose a home position. The home position is the initial position of the arm and can be any arbitrary position within the workspace. However, it is better to have a defined home position as a reference point to start the algorithm run.

The dynamics of a robotic arm must address the actuator torque or force relation by arm motion. In this analysis, it was necessary to consider mass and moment of inertia (Balafoutis & Patel, 1991). The dynamic parameters (payload, a moment of inertia, etc.) were varied, together with boundary conditions during all phases of system work manipulation. The boundary conditions were a manipulating mechanism movement in the free workspace, and the appearance of dynamical reactions under constrained robot gripper movement in the mechanical assembly and metal machining (Miomir, 1989).

Forward dynamic analysis gave the velocity and acceleration of each joint using the calculated torque (Roshanianfard & Noguchi, 2018) and physical properties of RAVeBots-1 elements (e.g. link length, mass, the center of mass, and moment of inertia). The aim of this analysis was to determine the maximum velocity and acceleration values. This was necessary to assess and determine how to limit velocity and acceleration for optimized operation of each joint. Figure 102 indicates the dynamic analysis process of the RAVeBots-1.

Unlike kinematics simulation, joint torque and gravity affect the physical behavior of a robotic arm in dynamic simulations. In this calculation, S is the supposed function of the two parameters θ_i (joint angle) and $\dot{\theta}_i$ (joint angular velocity). Moreover, joint angular acceleration ($\ddot{\theta}_i$) represented the dynamic behavior of the system. Based on $S = (\theta, \dot{\theta})$, the $\ddot{\theta}_i$, and τ (torque) as $\ddot{\theta}_i = d(s, \tau)$ foundation d was the forward dynamics of the robotic arm.

The inverse dynamic analyzed the joints torque using kinematic parameters, a moment of inertia parameters, and the specially designed algorithms. Results were used to determine torque range and a suitable controlling signal. The d^{-1} (inverse dynamics function), which must be adapted to the system to reach $\tilde{\ddot{\theta}}_i$ (desired acceleration), calculates the joint torques. The inverse dynamic was formulized as $\tau = d^{-1}(s, \tilde{\ddot{\theta}}_i)$.

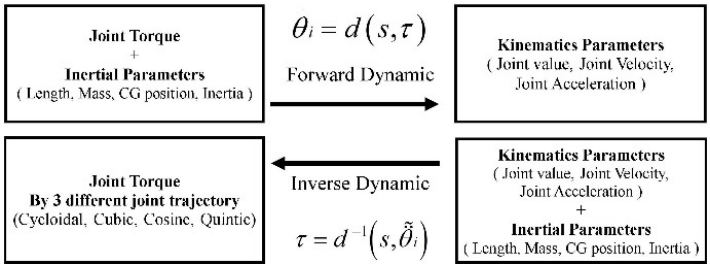

Figure 102. Dynamic analysis process.

6.6. Conclusion

In this chapter, the controlling system of HRHC system was explained. The controlling system is one of the three main aspects of a robotic system. Firstly, the general introduction of PLC system and controlling unit was explained. The general illustration and detailed wiring were presented. The controlling system of HRHC system consisted of a position board installed on a PC, a controlling program, servo motors, servo amplifiers, and optical cables for data transfer as compact circuits. The controlling functions of programming were explained. The controlling algorithm was developed by using Denavit-Hartenberg methods. Finally, the data communications between the robotic arm and end-effector / Robot tractor were explained. The performance of controlling system in detail and HRHC system, in general, as explained in Chapter 7.

Chapter 7. Performance evaluation of harvesting robot for heavy-weight crops

7.1. Introduction

The performance evaluation of a new designed robotic system is the most important stage in the study of agricultural harvesting system. To evaluate the performance, performance indicators must be evaluated. The performance indicators can be varying based on the system's application, target crop, environment, and study goals. Two performance indicators can be measured categorically: whether robots were autonomous (true/false), and whether robots were tested in the lab or the field. In this study, the performance of HRHC system was evaluated in the field/lab environment based on a designed algorithm. The difference between lab and field tests was considered important because a lab environment is usually much more structured than a field environment. It means that a higher performance can be achieved in a lab environment than in the field. In this chapter, the performance evaluation of HRHC system was analyzed in six performance indicators as follow:

1. **Harvest success rate:** The number of successfully harvested fruit per total number of ripe fruit in the canopy. This indicator measures the overall performance of a harvest cycle.
2. **Harvesting speed (cycle time):** Time of an average full harvest operation, including all steps of harvesting, and transportation to the next fruit. This time includes time loss caused by failed attempts. This indicator is relevant to determine the economic feasibility of the robot.
3. **Damage rate:** the number of damaged fruit or peduncles per total number of harvested fruit, caused by the robot. A peduncle is a connecting stem between the fruit and the main stem or branch. Peduncle pull of apples was considered peduncle damage. Damage to fruit or peduncle reduces the market value of fruit and is therefore relevant for the economic feasibility of the robot.
4. **Working space ratio:** The volume of real workspace per volume of the designed workspace. As the workspace of the designed system was modified in several stages, the working space can compare by each modification separately.
5. **Accuracy:** The ability of the robot to reach a specific programmed position with a minimum of error.
6. **Repeatability:** The ability of the robot to achieve repetition of a task (position).
7. **Control resolution:** The minimum possible distance between two steps of motion which the robotic arm can move. This indicator shows the resolution of movement which directly effects on accuracy, repeatability, and manipulator ability to grasp the crop.

In the coming section, each a bow mentioned performance indicators was discussed in detail.

7.2. Harvest success rate

The harvest success rate (HSR) in this study is the number of successfully harvested pumpkin per total number of harvested pumpkins. In the evaluation of this indicator, the harvesting procedure has been tested from recognition of pumpkin location (In this study: insert the location of pumpkin to controlling system manually) to place it in the trunk and also a movement to the next crop position. This indicator measures the overall performance of a harvest cycle. The pumpkin should not fall or damage in during of harvest cycle. If the pumpkin falls in any part of harvesting cycle, the measurement counts as a fail experiment and the harvesting ratio decrease due to the failure. The equation to calculate the harvest success rate (HSR) is as follow:

$$Harvesting\ success\ rate\ (\%) = \frac{Successful\ harvests}{Total\ number\ of\ harvests} \times 100 \quad (64)$$

In the sections 7.2, 7.3, and 0, five positions selected to evaluate the performance of the system as shown in Table 29. In this regard, the experimentation was done in 5 points and 5 repetitions. The pumpkins were put inside each point and the location of them was inputted to the controlling unit manually. The robot should move automatically to the location, grasp the pumpkin, harvest it and carry it into the predicted place as a truck. The results of experimentations are shown in Table 30. As the results show, the HSR of HRHC system was almost 100% except for point-1 which is 60%. The average HSR of the system was measured 92% which seems good enough for the first experiment. The fails in point-1 were related to the distance of position and the delays of the controlling system which was improved in the future harvesting algorithm. For the future study, this indicator has to evaluated for more than 50 points and 100 repetitions.

Table 29. The coordination of 5 points for performance evaluation.

Point	X (mm)	Y (mm)	Z (mm)
Point-1	200	-1500	-100
Point-2	600	1000	-110
Point-3	800	1300	-110
Point-4	1500	-300	-90
Point-5	1000	-800	-100

Table 30. Harvesting success results.

Point	Harvesting success repetitions					HSR
	1	2	3	4	5	(%)
Point-1	F	S	S	F	S	60
Point-2	S	S	S	S	S	100
Point-3	S	S	S	S	S	100
Point-4	S	S	S	S	S	100
Point-5	S	S	S	S	S	100
Average HSR (%)						92

* S: Success; F: fail

7.3. Harvesting speed (cycle time)

As mentioned, the harvesting speed or cycle time of a robotic manipulator is an average time for full harvesting operation, including localization, fruit grasp, harvest, transport of pumpkin, and robot transport to the next fruit. This time includes time loss caused by failed attempts (Bac et al., 2014). Some authors reported it as full harvest cycle, and some were unclear to mention whether the harvest operation also includes platform transport to the next fruit. In this study, two cycle time including cycle time (CT) and full cycle time (FCT) was measured. The CT was the time of harvesting including localization, fruit grasping, lifting, cutting the stem, and transformation, whether in the FCT the transportation of robot to the next pumpkin was included as well. It is essential to mention, the cutting stage was not tested at this stage of study because of some safety reasons and the cutting stage counted a constant 5 seconds as a delay time of cycle time. After finishing the development of safety system for cutting unit, the tests will repeat by new conditions. The experimentation was done on 5 points (5 pumpkins) and 5 repetitions. The results of harvesting speed are shown in Table 31. As the results show, the average CT and FCT were almost 42.4, and 53 seconds, respectively. However, the CT and FCT look quite long for harvesting a pumpkin, but those time can reduce based on the determined rotation speed of servo motor. If the rotatory speed increased to reach high-speed harvesting (short CT and FCT), the HSR can be reduced. In this stage, the rotary motion of the servo motor was set in a low range to evaluate the real performant of the system. In the next studies, it is recommended to evaluate the performance of the system under different condition and different rotary speeds.

Table 31. Harvesting speed results.

Point	Harvesting speed repetitions					CT (ms)
	1	2	3	4	5	
Point-1	65950	58291	61347	60753	71003	63468.8
Point-2	56259	63749	61150	60718	68703	62115.8
Point-3	56400	57291	56919	63203	65306	59823.8
Point-4	52316	59125	53640	53625	57265	55194.2
Point-5	52117	51187	56578	51421	53611	52982.8
	Average values (ms)					58717.1

Table 32. Efficient cycle time based on scenario-2 (ECT-1) is HP to HP without delays.

Point	Harvesting speed repetitions					ECT-1 (ms)
	1	2	3	4	5	
Point-1	47154	41678	43863	43438	50767	45380
Point-2	40225	45581	43722	43413	49123	44413
Point-3	40326	40963	40697	45190	46694	42774
Point-4	37406	42274	38353	38342	40944	39464
Point-5	37264	36599	40453	36766	38332	37883
	Average values (ms)					41983

Table 33. Efficient cycle time based on scenario-2 (ECT-2) is HP to Unloading without delays.

Point	Harvesting speed repetitions					ECT-2 (ms)
	1	2	3	4	5	
Point-1	39372	34800	36624	36270	42389	37891
Point-2	33587	38058	36507	36249	41016	37083
Point-3	33671	34203	33981	37732	38988	35715
Point-4	31233	35298	32023	32014	34187	32951
Point-5	31114	30559	33777	30698	32006	31631
	Average values (ms)					35054

7.4. Damage rate

One of the main reason to develop an agricultural robotic system is its advantages in compare by farmers as a human operator. The robotic system designing for simplifying the harvesting procedure; increase the speed of harvesting; improve the efficiency of harvesting, and reduce the damage rate of crops. In human harvesting, the crops could damage based on human mistakes buts its possibility is low because of the specification of the human body and its adaptability to the different conditions. A human arm and hand can control itself to adopt by the shape of crop and it is one of the big advantages. Also, a farmer can control the applied force on the crop structure to reduce the damage rate but it needs some tests and depends on their experiences in harvesting. However, farmer manually harvesting can damage the structure of some fruits like apple and peach, which reduce the market value. The human power and efficiency are low because of farmer tiredness and after a particular time, they need to rest which reduce the efficiency. In the case, a robotic system can control the applied force by using force gauges or other sensors. However, the applied position and end-effector's contact points are strongly depending on the End-effector's design specifications. If an End-effector doesn't design efficiently, it can damage the crop and subsequently, the efficiency of a designed robotic system can reduce dramatically. Then, an optimized designed robotic system (End-effector specifically) can reduce the damage rate of the harvesting, and if the harvesting speed and period time will be more than a human operation, the designed system known as an efficient and an applicable robotic system.

In this study, the damage rate of HRHC system was evaluated. The damage rate is the number of intact harvested pumpkins per total harvested pumpkins. The pumpkins have to be completely intact and in the case of small damages due to physical contact, high force apply sudden fall, and cracks were counted as a damaged crop. The damage can be because of harvesting procedure by using end-effector in during of grasp, lift, or stem cut, or it can be because of the wrong methodology in during of placement in the trunk. In this case, the stem cutting was not included because of some safety reasons. In all mentioned condition, the experimentation known as a fail or damaged crop. The damage rate of experimentation in this section was done on 5 points and 5 repetitions. The results of experiments are as for Table 34. As shown in Table 34, there was no damaged recognized in during of harvesting and the damage rate resulted as 0%. It is recommended to increase the number of specimens to evaluate the system performance more precisely.

Table 34. Damage rate results.

Point	Harvesting success repetitions					DR
	1	2	3	4	5	(%)
Point-1	S	S	S	S	S	0
Point-2	S	S	S	S	S	0
Point-3	S	S	S	S	S	0
Point-4	S	S	S	S	S	0
Point-5	S	S	S	S	S	0
Average DR (%)						0

* S: Success; F: fail

7.5. Working space compression

In this section, the workspace parameters in different stages of development were discussed. The workspace is one of the important parameters in designing of a new robotic arm and it is important to evaluate it in during of development stages. In this study, the designing of robotic arm completed and after development, the workspace was measured and then compared by required designed workspace. After development, some limitations found for controlling because of the connection of some links and components; some components were modified which limited the workspace, and some parameters applied to controlling algorithm which effect on the workspace of the system after manufacturing. This limitation reduced the workspace in a real situation. After evaluation of the limitation, improvements were applied on the robotic arm to increase the workspace and harvesting surface. The results were measured and compared as shown in Figure 103.

The results show that the workspace volume (V), harvesting surface (S_c), and harvesting length (HL)of the designed system were $8.024\times10^9\ mm^3$, $3.518\times10^6\ mm^2$, and $808\ mm$, respectively. But after development, the workspace volume, harvesting surface, and harvesting length were reduced to 48.48, 52.2, and 50.5% designed parameters, respectively, which reached to $4.134\times10^9\ mm^3$, $1.681\times10^6\ mm^2$, and $400\ mm$, respectively. These values was not meet the requirements, so that some modification in structure, and algorithm including spacer remove, pulley and belt power transmission, link modification, and recodification of controlling algorithm was applied. After that the workspace volume, harvesting surface, and harvesting length of the modified system were reached to $5.662\times10^9\ mm^3$, $2.86\times10^6\ mm^2$, and $800\ mm$, respectively. In the improved system the workspace, harvesting surface, and harvesting length was increase by 37, 70.1, and 100% in comparing by developed system, the respectively, which was 70.6, 81.3, and 99%, of required parameters in designed system, respectively. As a conclusion, the final system (modified system) was meet the required parameters of designed workspace, then the system could be applicable to harvest the crops like pumpkin efficiently. The designed HRHC system and final development are as shown in Figure 104.

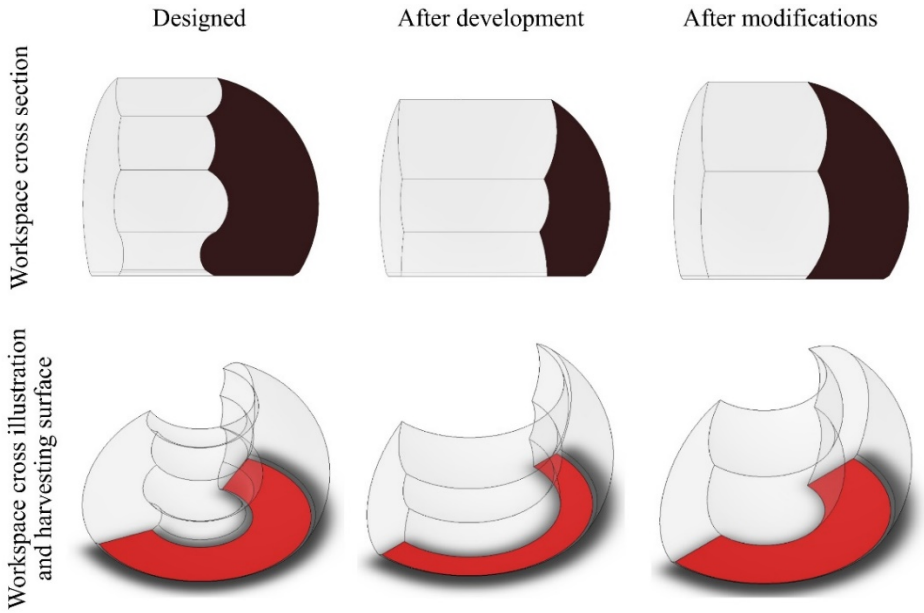

Figure 103. The comparison of workspaces in three different steps (designed system, the system after development, and the system after improving the workspace).

Table 35. The workspace parameters in the different system.

	Volume of workspace (mm^3)	Harvesting surface (mm^2)	Harvesting length (mm)
Designed system	8.024×10^9	3.518×10^6	808
Developed system	4.134×10^9	1.681×10^6	400
Modified system	5.662×10^9	2.86×10^6	800

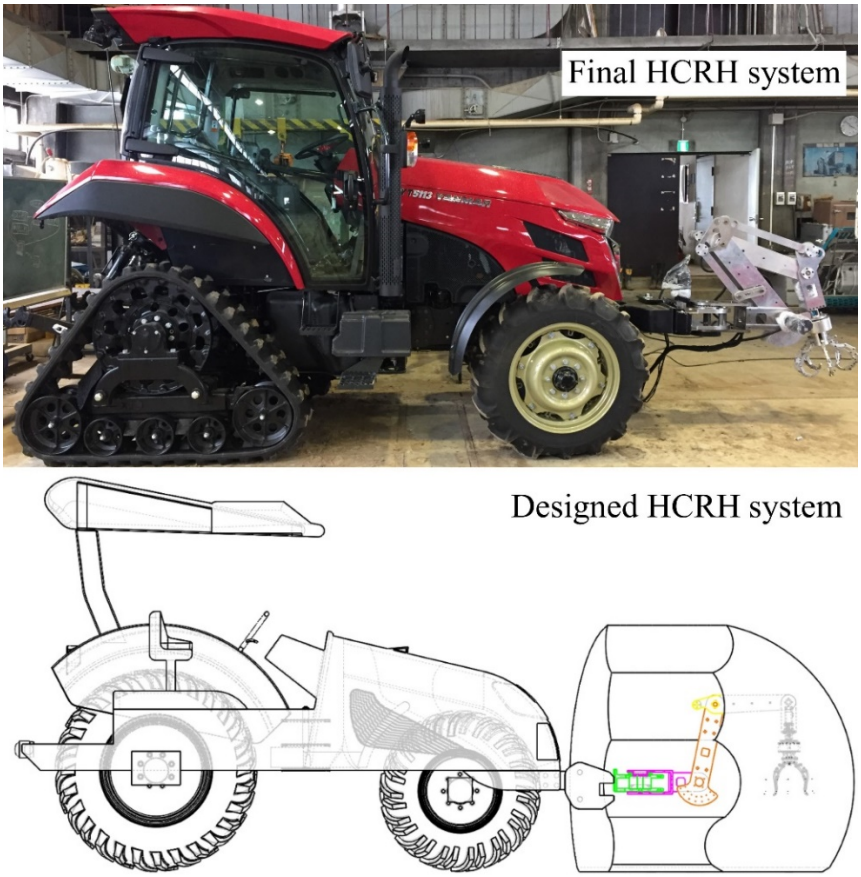

Figure 104. The illustration of a designed system and developed system.

7.6. Accuracy and Repeatability

An agricultural robot has many measurable characteristics, which have a direct impact on the effectiveness of the robot during harvesting. The main measurable characteristics are repeatability and accuracy. The repeatability of a robot was defined as its ability to achieve repetition of a task. Accuracy is the difference (i.e. the error) between the requested task and the obtained task. In robotics, when talking about repeatability and accuracy, their meanings are often confused. So, repeatability is doing the same task repeatedly, while accuracy is hitting one target each time. Repeatability and accuracy are likely to be important to evaluate: path, position, and orientation. The combination of position and orientation with the robot's end-effector is called a pose. Furthermore, the pose accuracy generally will have some effect on the path accuracy, which because of its inherent movement is a dynamic characteristic. The static characteristics without considering motion effects were considered in this study. Therefore, only the pose accuracy and repeatability will be discussed. The pose accuracy and repeatability of the robot are divided into the two previously mentioned components: position and orientation.

The absolute position accuracy is the ability of the robot to reach a specific programmed position with a minimum of error. The word absolute was used to refer to the fact that the position accuracy is evaluated with respect to a unique reference frame, mainly the work reference frame (or the world reference frame). Often these are arbitrary frames of reference used specifically to measure the variations in position accuracy. To assess the static accuracy of the robot movement, the position measurements are carried out after a complete stop of the end-effector's movement (regardless of the path taken to reach the desired position) from the previous pose of the end-effector (Figure 105).

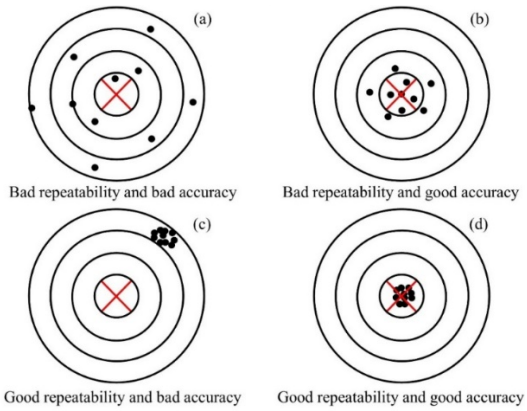

Figure 105. Repeatability and accuracy illustration.

Geometrically, the position accuracy of the robot for a given position can be defined as being the distance between the desired position and the centroid position (centroid is the mean position of all the points in all of the coordinate directions) which is actually achieved after repetitive movements of the end-effector toward the original desired position (Figure 106). Mathematically, absolute accuracy is the compilation of the composed errors for each of the x, y, z cartesian positional errors. Finally, the robot position accuracy for a specific workspace can be described as the maximum composed error available for several positions uniformly distributed inside the predetermined workspace or reference frame. Repeatability can be defined as the closeness of agreement between several positions reached by the robot's end-effector for the same controlled position, repeated several times under the same conditions. Geometrically, the position repeatability can be defined as the radius of the smallest sphere that encompasses all the positions reached for the same requested position (ISO: International Organization for Standardization, 1998).

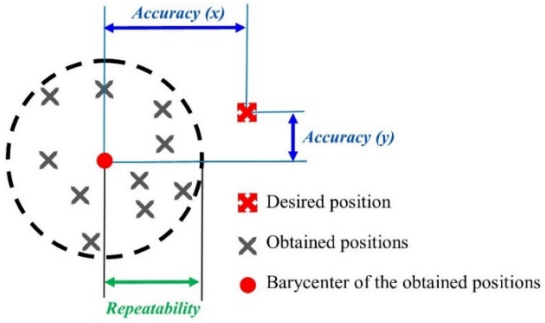

Figure 106. 2D Illustration of the Geometric Meaning of Accuracy and Repeatability.

Related equations were mentioned in section 3.6.4 as follow:

$$A_{p_x} = \frac{1}{n_1}\sum_{i=1}^{n_1}\sqrt{(\bar{x} - x_c)^2}\,;\; A_{p_y} = \frac{1}{n_1}\sum_{i=1}^{n_1}\sqrt{(\bar{y} - y_c)^2}\,;\; A_{p_z} = \frac{1}{n_1}\sum_{i=1}^{n_1}\sqrt{(\bar{z} - z_c)^2} \tag{65}$$

$$L_i = \sqrt{(x_r - \bar{x})^2 + (y_r - \bar{y})^2 + (z_r - \bar{z})^2} \tag{66}$$

$$\bar{L} = \frac{1}{n_2}\sum_{i=1}^{n_2} L_i \tag{67}$$

$$R_p = 3\sqrt{\frac{\sum_{i=1}^{n_2}(L_i - \bar{L})^2}{n-1}} + \bar{L} \tag{68}$$

Which A_{p_i}, n_1, n_2, $\bar{x}$, x_c, and x_r are positional accuracy (mm), number of attained points in each mission, number of repetition, average value of attained position (in y and z direction as well), commanded position (in y and z direction as well), and attained position (in y and z direction as well), respectively, according to ANSI/RIA R15.05. In this section, the harvesting area of the workspace was divided into 10 segments (A~J) as shown in Figure 107.This segmentation is because of performance evaluation and its results compression in different zones. In the case, if the performance indicators of each segment have a significant difference, the application of robotic arm can vary in some specific areas and reachability of robot should be discussed. Otherwise, if the indicators will be almost same in all segments, the performance indicators of the robotic system will be the average number of outputs. In this regard, the accuracy and repeatability of the robotic arm were evaluated in 10 pints and 10 repetitions. It was tried to put each point in one segments to evaluate the differences as shown in Figure 108 and Figure 109. The results of experimentations were shown in Table 36.

As the Figure 110 shows, the average accuracy in x and Y directions were 10.91, and 9.52 mm, respectively. The average repeatability of the mentioned 11 points was 12.74 mm. The best accuracy in x and y directions were belonging to point-2 by 2.55 mm, and point-9 by 0.83 mm, respectively. The best repeatability was belonging to point-4 by 8.1 mm. The accuracy-x of points 4, 6, 7, and 9 were more than the average-x value and the accuracy-y of points 1, 2, 4, and 7 were more than the average-y value. The repeatability of the points was not significantly different in comparing by the average value of repeatability. There was not found any relationship between the distance of pint and its accuracy and repeatability, then the average values of each parameter were presented as the final accuracy in x and y directions, and repeatability as 10.91, 9.52, and 12.74 mm, respectively. As a conclusion, HRHC system has enough accuracy and repeatability to do the harvesting procedure for pumpkin. In this application, a 15mm accuracy and repeatability were the required values which the designed system is more accurate than the requirements. Then the HRHC system can do the harvesting process with high accuracy.

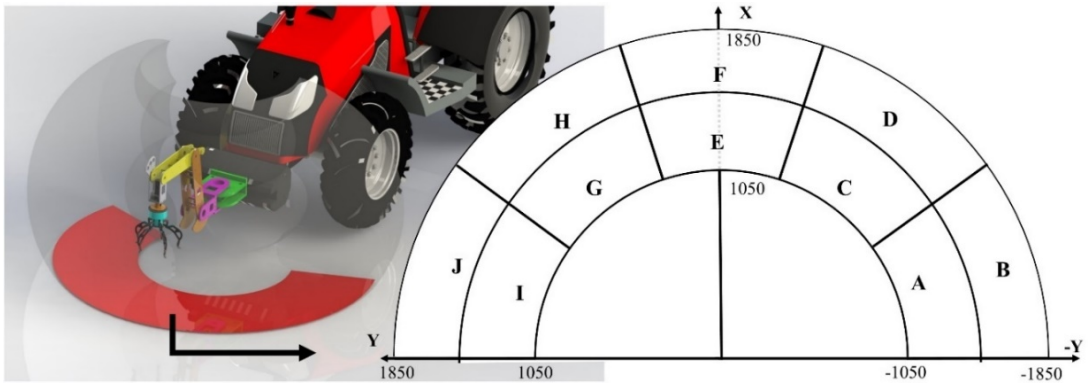

Figure 107. Harvesting area of the workspace.

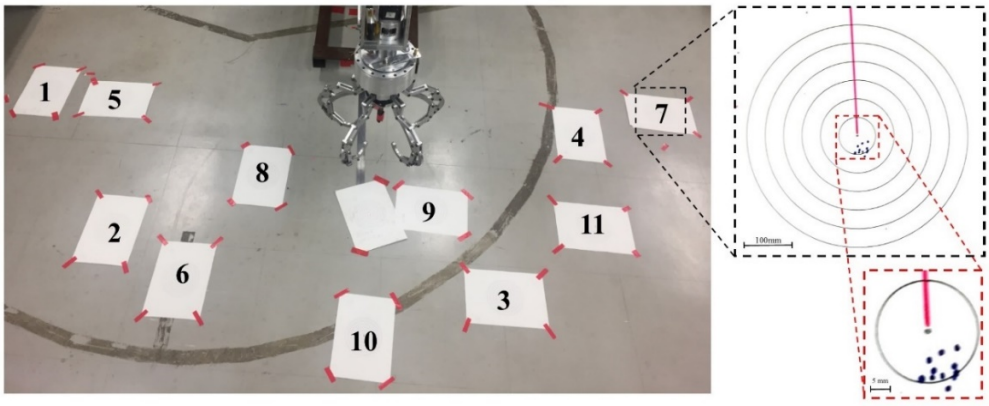

Figure 108. Accuracy and repeatability experimentation illustration, on temporary stage.

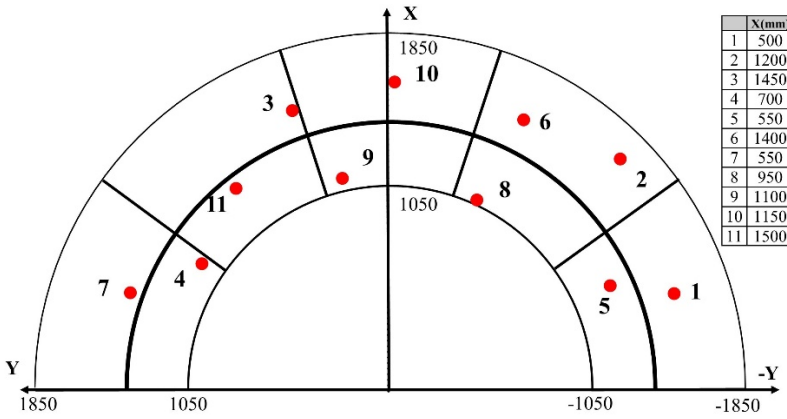

	X(mm)	Y (mm)	Z (mm)
1	500	-1470	-110
2	1200	-1200	-110
3	1450	500	-110
4	700	950	-110
5	550	-1150	-110
6	1400	-700	-110
7	550	1350	-110
8	950	-450	-110
9	1100	250	-110
10	1150	20	-110
11	1500	900	-110

Figure 109. The location of experimented positions.

Table 36. The polar plots of accuracy and repeatability experimentation.

Position-1

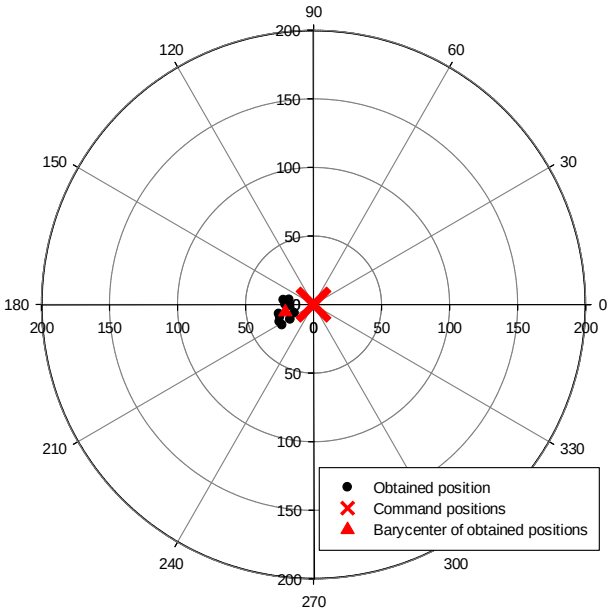

Position-2

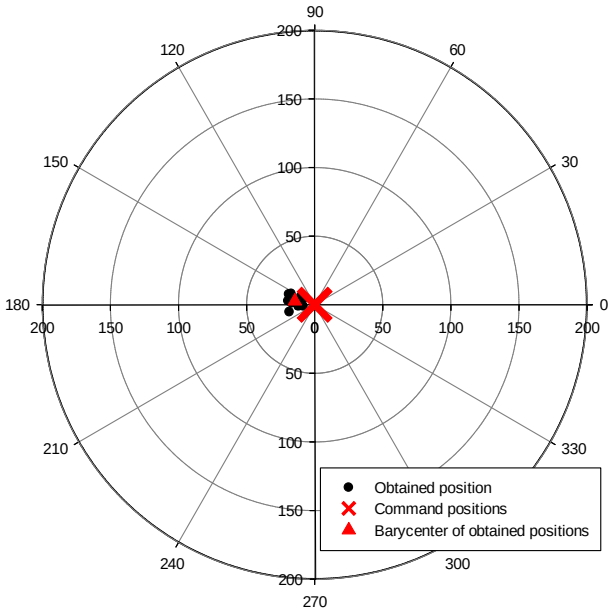

Position-3

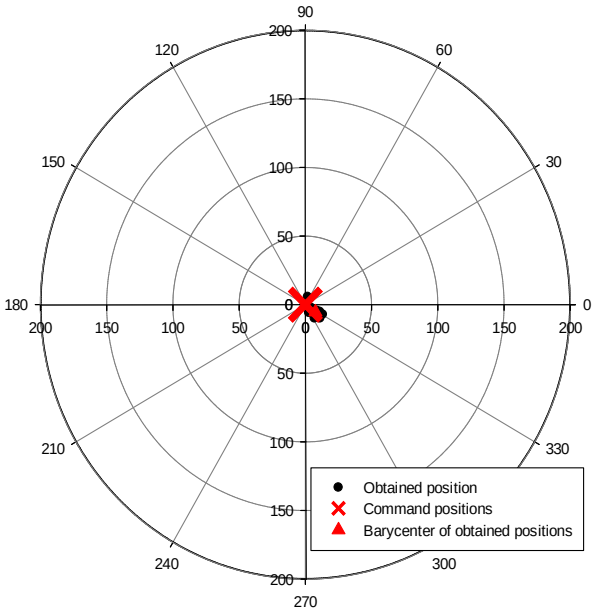

Position-4

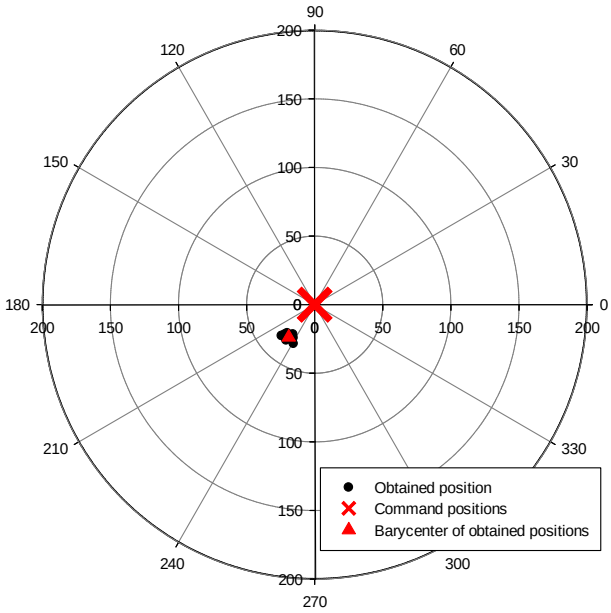

Position-5

Position-6

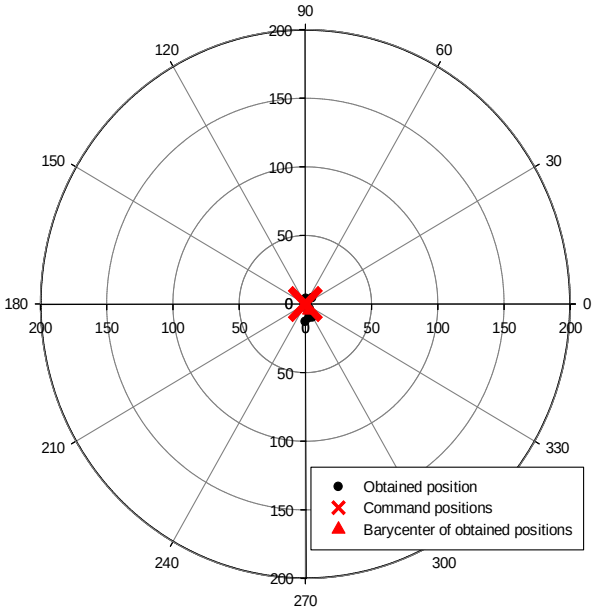

Position-7

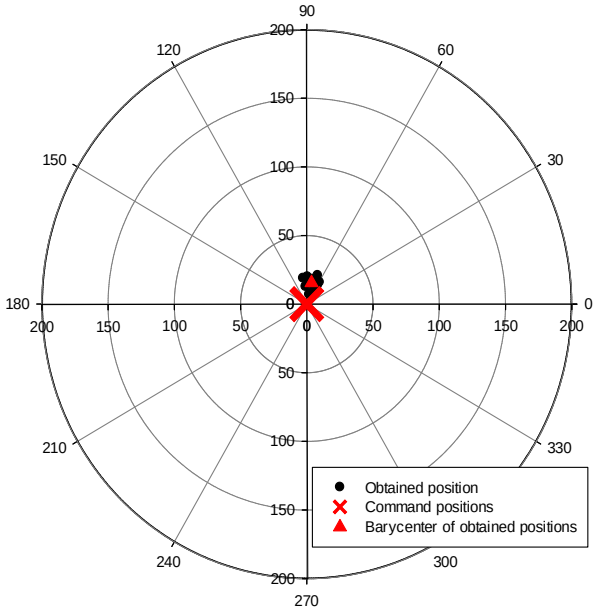

Position-8

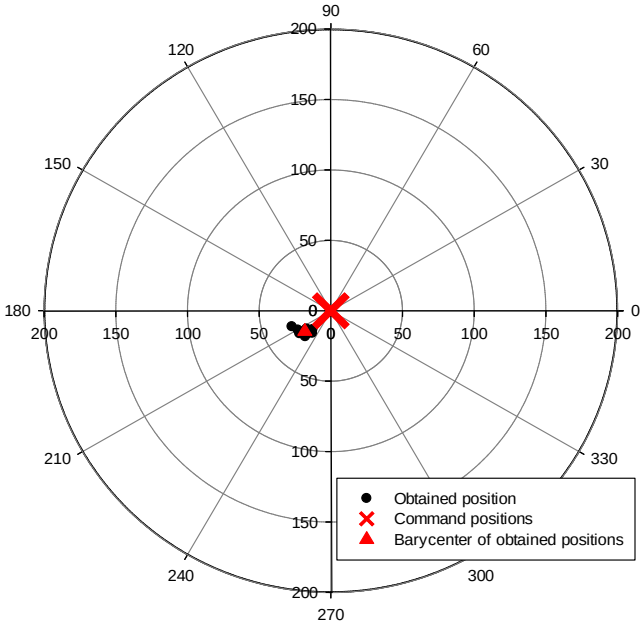

Position-9

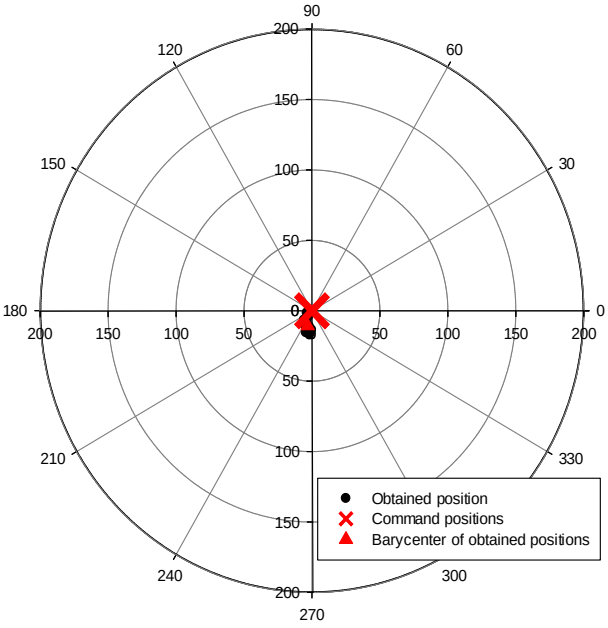

Position-10

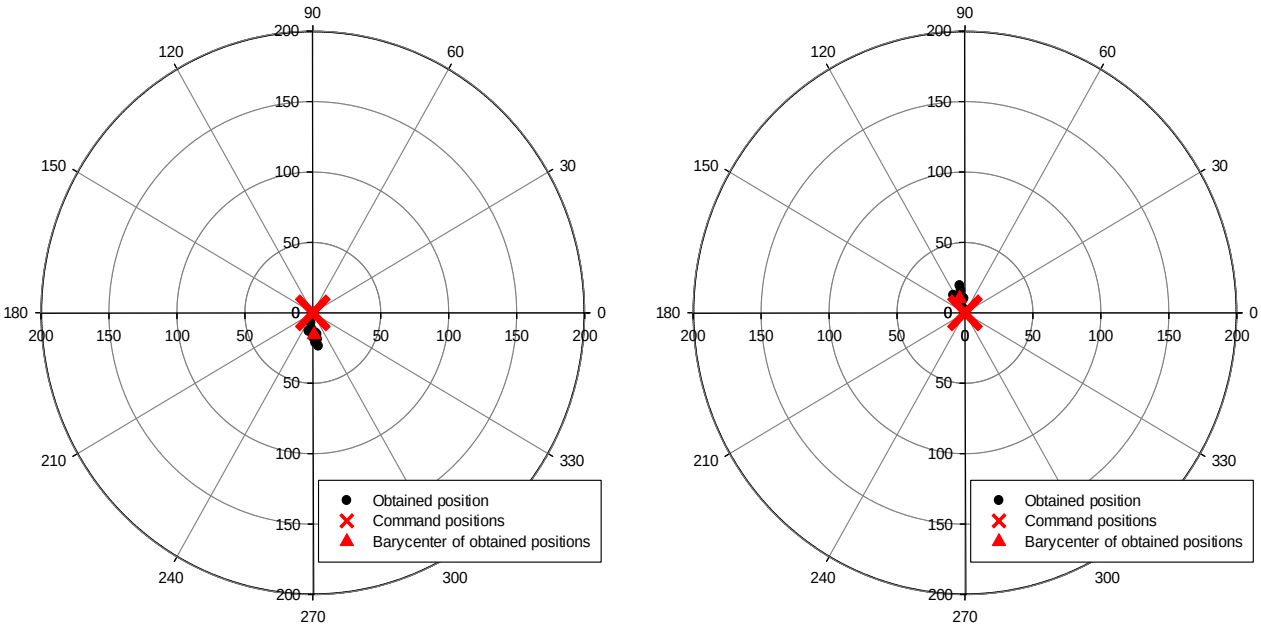
Obtained position
Command positions
Barycenter of obtained positions
Obtained position
Command positions
Barycenter of obtained positions

Position-11

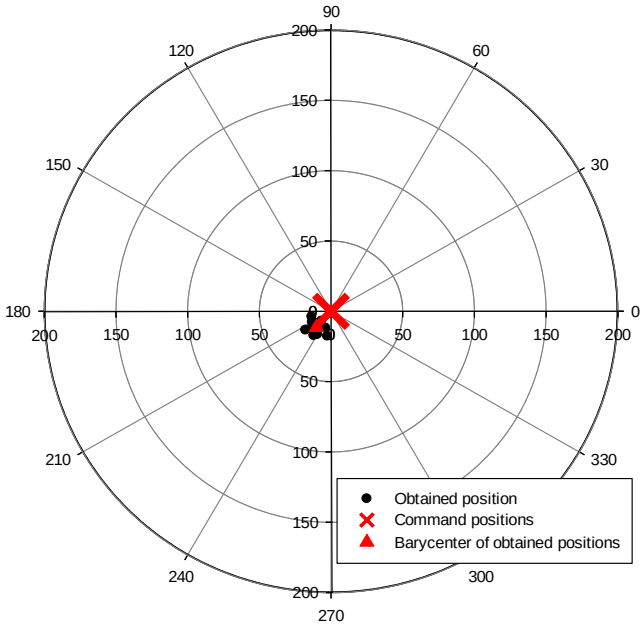
Obtained position
Command positions
Barycenter of obtained positions

Table 37. The scatter plots of accuracy and repeatability experimentation.

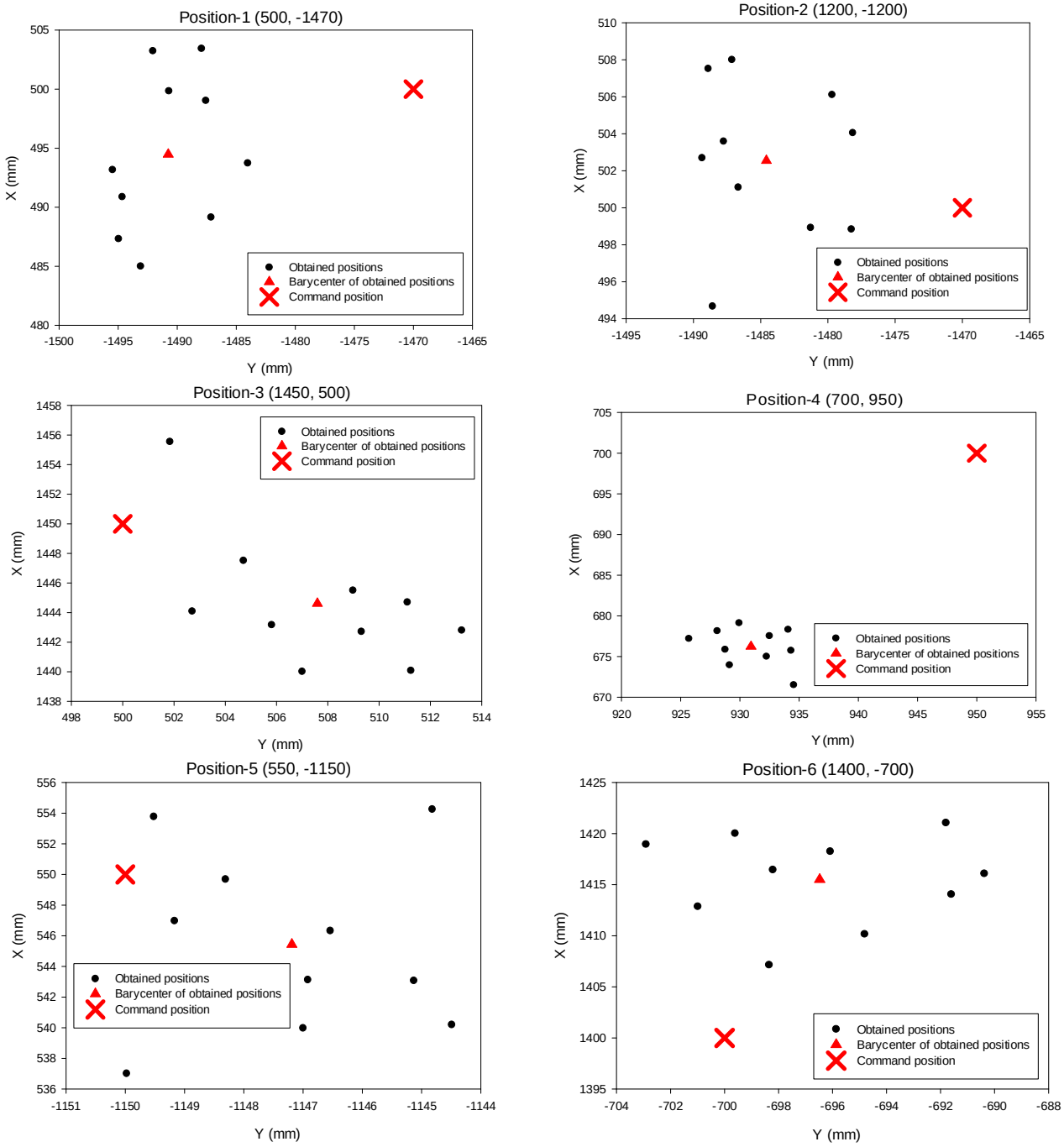

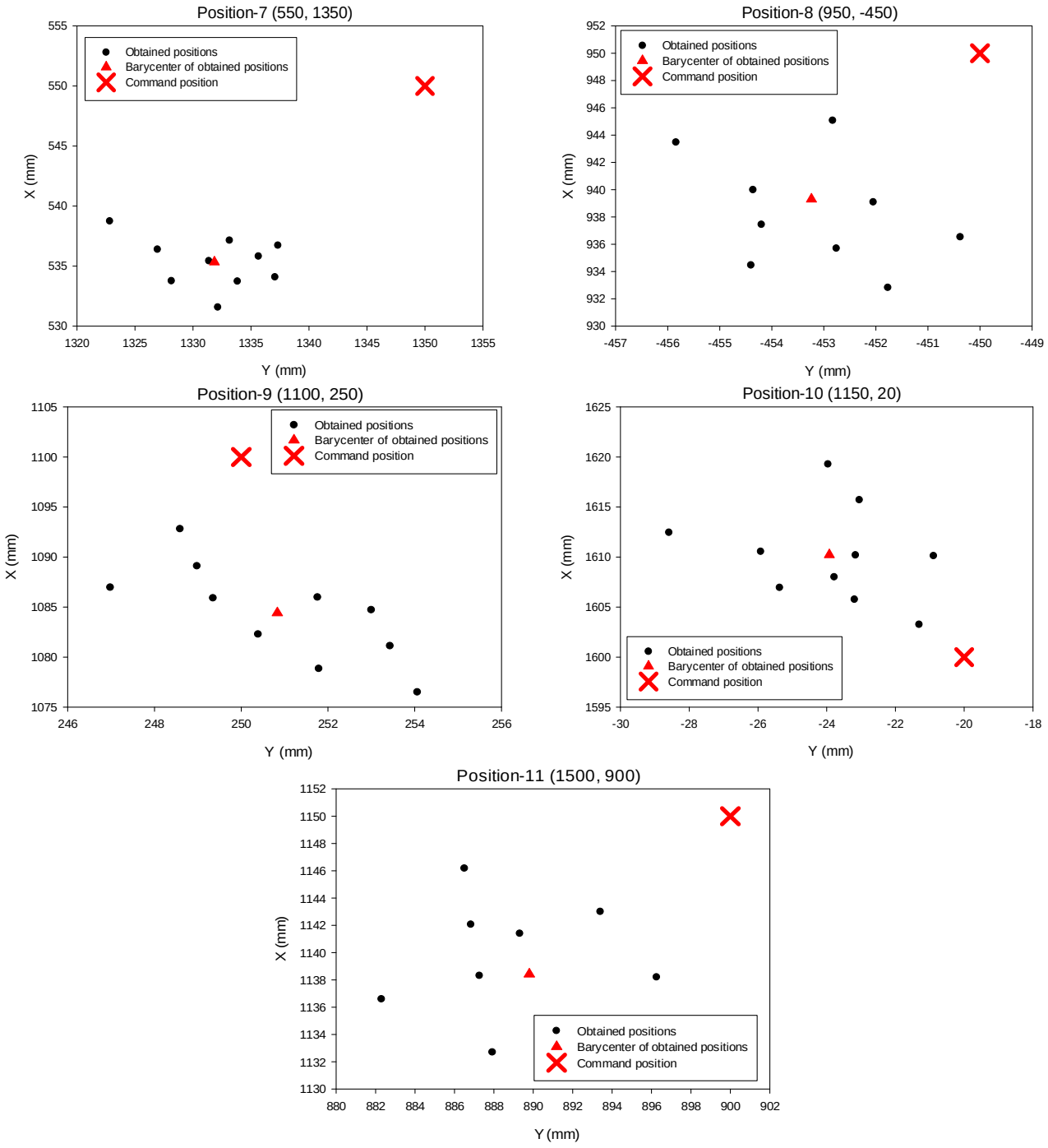

Table 38. Accuracy and repeatability results, on temporary stage.

Parameters		Experiment positions											Average (mm)
		1	2	3	4	5	6	7	8	9	10	11	
Accuracy	x	5.52	2.55	5.39	23.77	4.56	15.5	14.66	10.7	15.56	10.23	11.57	**10.91**
	y	20.77	14.58	7.6	19.1	2.81	3.53	18.16	3.24	0.83	3.92	10.2	**9.52**
Repeatability		13.9	12.27	14.56	8.1	14.7	12.47	12.26	12.53	12.87	12.65	13.83	**12.74**

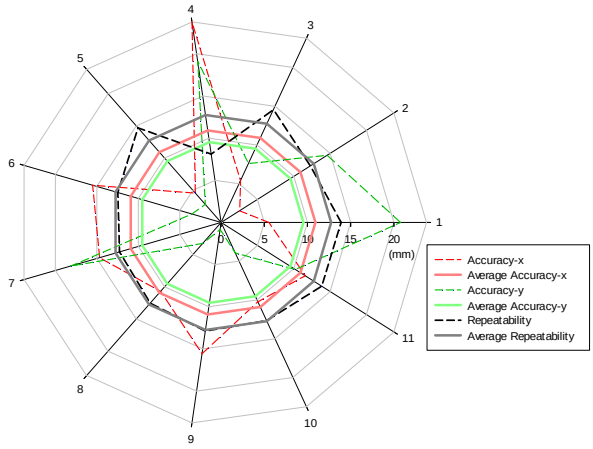

Figure 110. The comparison of accuracy in x and y directions, and repeatability.

When the robotic arm was installed on robot tractor, the accuracy and repeatability experimentation retested (Figure 111). All the indicators values including accuracy in X and Y directions, and repeatability decrease so that the accuracy in X and Y directions and repeatability reduced to 4.85, 4.15, and 5.23 mm, respectively. This results indicated that the 56% of the accuracy and 59% of repeatabilty values was because of the stage vibration. Finally, the accuracy of final system was as reported in Table 39.

Figure 111. Accuracy and repeatability experimentation illustration, installed on robot tractor.

Table 39. Accuracy and repeatability results, installed on robot tractor.

Parameters		Experiment positions											Average (mm)
		1	2	3	4	5	6	7	8	9	10	11	
Accuracy	x	4.26	7.29	6.59	2.73	4.66	5.24	4.85	1.51	11.67	1.43	7.20	**4.85**
	y	0.64	0.33	8.49	9.59	2.00	3.83	4.15	3.37	8.80	0.50	1.98	**4.15**
Repeatability		4.62	4.87	4.84	5.74	5.77	6.01	5.23	6.09	3.56	6.15	4.63	**5.23**

7.7. Control resolution

System resolution, control resolution, or movement resolution (abbreviated as SR) is the minimum movability of a robotic system in the linear axis. The resolution of a robot system is a parameter figured out by the design of the control unit and it is strongly depending on the designed structure of robotic arm, actuators, and controlling system. It is important to distinguish the programming resolution from the control resolution. The programming resolution is the smallest allowable position increment in robot programs and is referred to as the basic resolution unit. The control resolution is the smallest change in position that the feedback device can sense. For example, best performance is obtained when programming resolution is equal to control resolution. In this case, both resolutions can be replaced with one term: the system resolution. In this study, the system resolution is the smallest allowable position which the designed robotic arm can move. In this regard, several experimentations were done to reach the maximum control resolution. The controlling program was set to move on 20 squares which have offset entities of 1 mm. The manipulator had to move linear to complete 20 squares with the sides of 40, 38, 36, …,4, and 2 mm. The SR and its tolerance were calculated in X, and Z axis by using equations as follow:

$$SR_n\ (mm) = \frac{L_f}{2N \times offset} \tag{69}$$

$$System\ resolution\ tolorance\ (mm) = Expected\ offset - SR_n \tag{70}$$

Which SR_n, L_f, and N was system resolution, length of biggest square, and number of squares. The experiments were done and the results was shown in Figure 112. The results show that the sides lengths of biggest square were 39 and 43 mm in x and Z axis except of 40 mm which means the system resolution has a tolerance. According to the calculations, the SR_x, and SR_Z were 1 ± 0.075, and $1 \pm 0.025\ mm$, respectively (Figure 112). The system can have a tolerance of 75, and 25 μm in X and Z axis, respectively. Based on the archived results, these values of resolution met the requirements and defined objectives for agricultural application. In the field application, the resolution of 5 mm was acceptable, which the designed system is more accurate than required indicator (Figure 113).

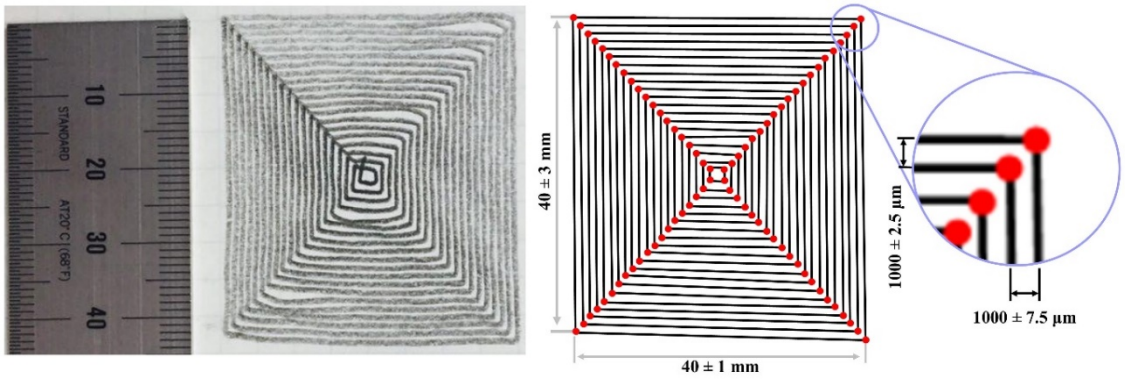

Figure 112. The results of movement experimentation.

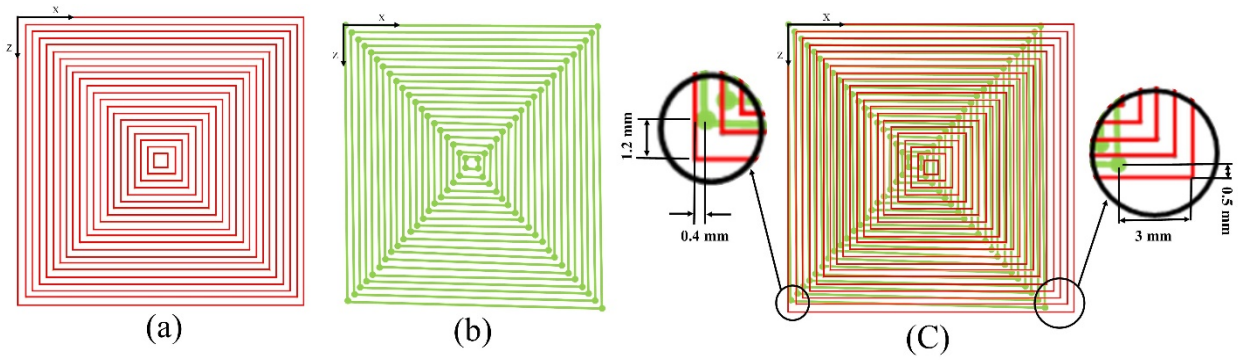

Figure 113. (a) Desired path, (b) experimentation result, and (c) comparison.

7.8. Discussion and conclusion

After finishing the performance evaluation of the HRHC system, it was needed to compare the result with the previous studies and developments. As reported by Bac et al. (2014), almost 50 projects in the field of harvesting robots in agriculture were presented from 1984 to 2012. Between these 50 projects, one or several quantitative performance indicators were reported for 76% (38/50) of the projects. However, few instances were reported for several of the individual indicators: 19 for localization success, 7 for false-positive fruit detection, 20 for detachment success, 11 for harvest success, 10 for fruit damage, 3 for peduncle damage, and 28 for cycle time. In this section, the harvest success, cycle time, and damage rate were compared by previous studies. Some other parameters including workspace, accuracy, repeatability, and controlling resolution were not discussed in those a bow mentioned projects. Most of the projects concerned autonomous robots 74% (37/50). Only a few authors 12% (6/50) reported the number of attempts the robot made to harvest a fruit. The average number of attempts was 1.7 (0.8) per successfully detached ripe fruit. Most performance tests were done in the field 68% (34/50), a few in the lab 16% (8/50), or the location of tests were not reported 16% (8/50).

In the case of HRHC system, the performance tests were done mostly in the lab and some in the field conditions. The average values and range of localization success, detachment success, harvest success, fruit damage, and peduncle damage of the previous studies are shown in Figure 114. Localization success (85%; 59–100%) was, on average, slightly higher than detachment success (75%; 42–93%). Overall harvest success was 66% (40–86%). The harvesting success of HRHC system (100%) was quite higher than the average of previous robots. Fruit damage was 5% (25–80%) of the localized ripe fruit, which in the case of HRHC system no damage on the pumpkin was detected. Cycle time showed an extensive range of 1–227 s with an average of 33 s (N = 28) as shown in Figure 115. The cycle time of HRHC system (46.9 s) was longer than the average value of previous projects. There were no classified reports for the cycle time of similar heavyweight crops like pumpkin, then the comparison was not possible in this case. The only reports were presented about “Robotic melon harvesting “by Yael et al. (2000) by cycle time of 15s; “Design and control of a heavy material handling manipulator for agricultural robots” by Sakai et al. (2008) to harvest watermelon by cycle time of 14s; and “Development of multi-functional tele-operative modular robotic system for greenhouse watermelon” by Heon and Si-Chan (2003) to harvest watermelon in artificial environment by cycle time of 15s. For cucumber harvesting, a cycle time of 10 s was proven (E.J. van Henten et al., 2002). The cycle time achieved was a factor of 12 too long (124 s) and clearly shows that a gap must be bridged. For orange harvesting, comparing cycle time was possible for only one project: 3 s required vs 3–7 s achieved (R. C. Harrell, Adsit, Munilla, & Slaughter, 2009), i.e., a factor of about 2 too long. Although this gap is smaller, all performance indicators are required for a more conclusive analysis.

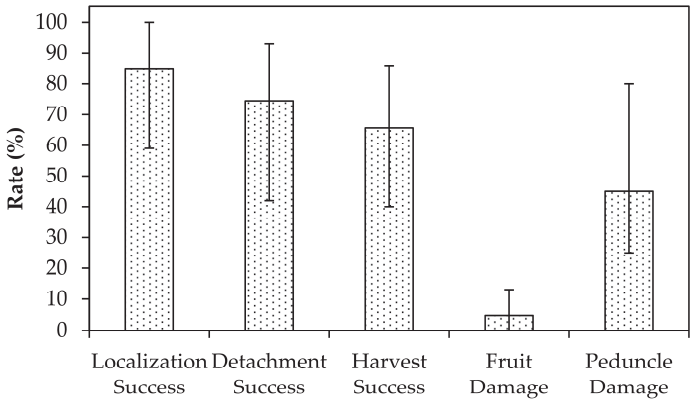

Figure 114. Averages and range of reported quantitative performance indicators: localization success, detachment success, harvest success, fruit damage, and peduncle damage. N represents the number of distinct projects.

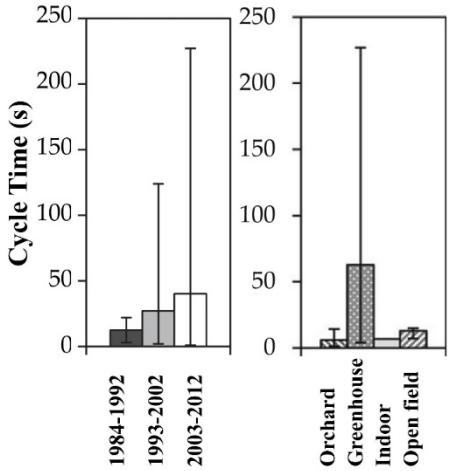

Figure 115. Performance indicators for three decades (left), and four production environments (right).

As Bac et al. (2014) was reported, on average, localization success of harvesting robots was 85%, detachment success was 75%, harvest success was 66%, fruit damage was 5%, peduncle damage was 45%, and cycle time was 33 s which a kiwi harvesting robot has a cycle time of 1 s. Moreover, the performance of harvesting robots did not improve in the past three decades, and none of these 50 robots was commercialized. They recommended to simplifying the task, enhancing the robot, defining requirements and measuring performance, and considering additional requirements for successful implementation. As the results of performance evaluation of HRHC system, the workspace, harvesting surface, and harvesting length were $5.662\times10^{9}\ mm^{3}$, $2.86\times10^{6}\ mm^{2}$, and $800\ mm$, respectively. The average values of accuracy in x and y directions, and repeatability were 10.91, 9.52, and 12.74 mm, respectively, and it had a tolerance of 75, and $25\ \mu m$ for a control resolution of 1mm in X and Z axis, respectively. As a conclusion, the performance indicators were found acceptable the harvest pumpkin, however this performance can improve by some mechanical and controlling modifications in the future designs. Generally, the experiments output meets the determined requirements and the HRHC system found applicable to harvest pumpkin in the field.

Chapter 8. Conclusion

8.1. Introduction

The agriculture industry has met different challenges including self-sufficiency in food, rural to urban migration, the age distribution of farmers, declining farming population, new agricultural technology necessity; and time-consume operate training. Some heavyweight crops such as pumpkin, watermelon, melon, and cabbage support the food supplies in Japan while the number of farmers keeps decreasing is such fields because of physical effort and inadequate income. Even though the mentioned crops are expensively priced in Japanese markets. The harvesting of this crops not only needed powerful farmers but also current equipment is not proper for the precision harvesting of such crops which increase the damage possibility, financial loss, labor cost, chance of injury, and decrease the harvesting efficiency. Most of the developed agricultural robot was focused on the small sized and light weighted crops

Based on the mentioned, this study was presented the development procedure and performance evaluation of a specially designed robotic system for heavy-weight crops harvesting (abbreviated as HRHC system). The objectives and originalities of this study were (1) development of an applicable low-cost robotic arm for farm use with optimized degree of freedom (DOF), (2) development of an optimized controlling algorithm for harvesting, (3) economic evaluation and optimization of design robotic arm, (4) DOF optimization (5) development of a PLC controlling system, (6) accuracy, resolution and reputability evaluation, (7) rapid harvesting technique to improve harvesting cycle-time and efficiency of the system, (8) parametrization of physical and mechanical properties of pumpkin, (9) characterization of pumpkin, (10) development of a specifically designed end effector (EE) to harvest pumpkin, (11) development of rapid harvesting methodology, and (12) develop the infrastructure for communication system: EE vs Robotic arm, and Robotic arm vs Robot tractor, and recognition system.

In this research (1) the heavy crops robotic harvesting system including robot tractor, robotic arm, end-effector and controlling unit and their components were introduced, (2) development procedure of robotic arm including designing procedure, standards, torque and inertia calculation, computer simulation, manufacturing methodology, and calibration was presented, (3) pumpkins as target crop have taken under different evaluation, (4) end-effector development was explained, (5) harvesting methodology, design procedure, structure design, component simulations, different calculation, modification stages, and manufacturing, was explained, (6) the controlling system including robot tractor TECU, PLC system, amplifiers, servo system, wires, power source, algorithm, and data communication were presented, and finally (7) the application of system was evaluated by different field and laboratory experimentation including: harvesting success rate, cycle time, damage rate, working space, accuracy, repeatability, and control resolution.

8.2. Material and methods of harvesting robot for heavy-weight crops (HRHC)

In this chapter, the general illustrations of the heavy crops robotic harvesting system (abbreviated as HRHC) were discussed. Agricultural robots usually consist of three units: a mobile platform, actuating system, and recognizing system. The HRHC system also includes a robot tractor as a mobile platform, a controlling system, a robotic arm and end-effector as an actuating system. The vision system and image processing algorithm was not mentioned because it was a separate study. The robot tractor as a mobile platform was a robot tractor which was developed in the laboratory of vehicle robotics in the Hokkaido University. The robotic arm as a part of the actuating system was a newly designed articulated robotic arm for outdoor applications, specifically agricultural applications, in terms of material, flexibility, actuator type, power source, rapid reparability, and cost-effectiveness. The end-effector as a complementary part of the actuating system was developed for harvesting the heavy crops (like pumpkin) which consists of two main unit including (1) frame structure, and (2) fingers and also some sub-units as the main connector, linear screw, and joint-4 structure. The controlling system as the brain of the actuating system was based on a

programmable logic controller (PLC) system. This unit consists of a position board installed on a PC, a controlling program, servo motors, servo amplifiers, and optical cables for data transfer as compact circuits.

As a general point of HRHC system, an auto-guidance system will guide the robot tractor in the field by using GPS and IMU; the vision system will recognize the targets and send commands to the main PC; the PC will calculate the location of target and convert it by using developed algorithm; after receiving the location command, the manipulator will move to the location of pumpkin by using a kinematic algorithm; the end-effector will grasp the target crop and the manipulator will lift that; finally, the whole system will harvest the crop by using designed harvesting methodology. This loop will complete by carrying the crop to a mobile truck.

8.3. Robotic Arm

In this chapter, the development procedure of a robotic arm for farm use was presented. The limitations of current robotics systems including their sensitivity in facing by agricultural complex conditions such as vibration, oscillation, and light reflection, and dusty environment and limitation of workspace and payload, were discussed. The aims to develop the robotic arm were (1) Development of an applicable low-cost robotic arm for farm use by optimized degrees of freedom (DOF), (2) economic evaluation and optimization of design robotic arm, (3) DOF optimization, and (4) accuracy, resolution and reputability evaluation.

The components designed in Solidworks software. In this case, material selection, boundary conditions, meshing method, and a factor of safety (FOS) was included. A standard design process for robotic structures was used consists of nine main stages: (1) defining the problem, (2) synthesis, (3) creating a prototype model, (4) simulation/calculation/modification, (5) manufacture of the robot, (6) programming, (7) testing/calibration, (8) final evaluation, and (9) definition of optimal conditions. A 4-DOF with serial links due to its simplicity in structure and cost efficiency was selected. All dynamic and static simulations and motion studies were analyzed by using Solidworks software. After many modifications in joint location and links length, the aluminum (AL5052) and steel (ASTM A36) materials were chosen for the structure because of their specification adoption with the application of robotic arm. Several ISO and JIS standards were used for technical drawings, material, and other aspects of design. The DOF selection was done by comparison of the workspace and harvesting area of 1-DOF to 5-DOF. The servo motor selections were done by joint's torque calculations and moment of inertia. The Payload Per Weight (PPW) and repeatability of robots was discussed. The static and dynamic simulation was down by using Solidworks software. After reviewing the various methods, the GCLT method as an efficient way to harvest heavy crops were selected which includes (1) grasping/picking the crop; (2) cutting the stem; (3) lifting; and (4) transportation stages.

The results show that a 4-DOF could be an adequate structure which can support a maximum workspace volume (V_n) and covered land surface for harvesting (S_n), and also a minimum cost. Based on these evaluations, a 4-DOF structure was selected to develop a harvesting robotic system. The average PPW of RAVeBots-1 and some industrial robotic arms which meet some of the requirements was 0.2 and 0.084, respectively. The analysis shows that designed workspace volume (V_d), front access (FA) and harvesting area (HA) of RAVEbots-1 were $8.024\times10^9\ mm^3$, $3.518\times10^6\ mm^2$, and $808\ mm$, respectively.

8.4. Pumpkin characterization

In this chapter, the physical properties of pumpkin as an object crop under test different experimentation was presented. First, the anatomy of pumpkin was discussed generally. Then the popular verities of pumpkin (Kabocha) in Japan were explained and the tested verities including JEJEJ, TC2A, Hokutokou, Sukuna, Kikusui, and Ebisu were presented. As the pumpkins anatomy in Japan (the varieties of pumpkin in Japan) is slightly different than other pumpkins in Europe and USA; and the pumpkin robotic harvesting system was needed to some physical tests on pumpkins to extract the physical properties parameters, three different experimentations were designed. These three experimentations were including (1) pumpkin orientation in field and general physical properties, (2) Compression strength test, and (3) Bending-shear test.

The experimentations of pumpkin orientation in the field and general physical properties were important because the location and orientation of each pumpkin are unique and unpredictable in the field and depend on the soil density and solar irradiation. In this regard, several experimentations were done in the Hokkaido agricultural research center (NARO). The aims of these experimentations were investigation of pumpkin orientation, pure weight, lift weight, and possible harvesting methodologies consideration. The orientation angle of stem in pure situation (θ_{PSO}) and lift situation (θ_{LSO}) was measured. The compression test was done by using compression testing device (INSTRON 5584) when the pumpkins were fixed on a plate and the compression force was applied to a parallel plate when the stem orientation was approximately orthogonal with plates. The force applied with speed of 30 mm/s in room temperature until the pumpkin structure collapsed and the rupture force was measured. By using that force, the strain and the elastic/deformability module of pumpkins as a convex body were determined.

The bending-shear test was designed to measure needed force to cut the stem of pumpkins. The objective of this experimentation was a characterization of pumpkin stem under the bending-shear test to modify an optimized cutting system by using specially designed loading bars which applies the force with blades. Four different loading tools (blades) was designed for this experimentation including flat, single angles (with $30^{\circ}, 45^{\circ}$, and 60°), and double angles ($with\ 30^{\circ}, 45^{\circ}$, and 60°), respectively. The force was applied on each stem until flexural level and the cutting force was measured. By using related equations, elasticity modulus in bending (E_{bend}), flexural stress (σ_f) and strain (ε_f) was calculated.

The field experimentations were indicated that the average pumpkin's lift weight was 26% more than pumpkin's pure weight. This means in during of harvesting, the pumpkin's lift weight has a significant difference in pure weight. The experiments show that the SO could not be -90° because of grows procedure and anatomy of pumpkin. Most of the pumpkins has θ_{PSO} between -90° and $+90^{\circ}$, and less than 1% could have SO of $+90^{\circ}$ which was ignorable. After lifting, the θ_{LSO} of all of specimens was changed to the range of $-90^{\circ} < \theta_{LSO} < +90^{\circ}$ due to the applied force from stem connections. The lifting technique combination with pumpkin parametrization were simplified the harvesting algorithm in during of robotic harvesting, specifically in the stem cutting stage. The physical properties experimentations show that the average weight of JEJEJ, TC2A, Hokutokou, Sukuna, Kikusui, and Ebisu were 3.13, 2.58, 3.12, 2.8, 1.16, and 2.37 Kg, respectively. The maximum ($F_{ct,max}$), minimum ($F_{ct,min}$) and average ($F_{ct,avg}$) of F_{ct} in JEJEJ, TC2A, Hokutokou, Sukuna, Kikusui, and Ebisu was 4.66, 4.58, 4.61, 1.94, 2.21, and 2.5 KN; 2.81, 2.06, 2.24, 1.83, 1.53, 1.74 KN; and 3.37, 3.1, 3.23, 1.88, 1.92, 2.22 KN, respectively. The results of bending-shear test were shown that the cutting period of TC2A (2.03 s) and Hokutokou (1.39 s) was minimum value when the single angles blade with 60° (S-60) was used, and also the minimum stress value to cut the stems was 2.84, 3.3, and 2.01 $^{N}/_{mm^2}$ for JEJEJ, TC2A, and Hokutokou, respectively. These results indicate that the single angles blade with 60° angle is the appropriated blade to harvest the mentioned varieties of pumpkin with minimum time-consumption and stress.

8.5. End-effector

In this chapter, the development procedure of a specifically designed end-effector (abbreviated as EE) for pumpkin harvesting was presented. The objectives of this chapter were the development of an EE a and a unique harvesting methodology based on the properties of target crop (Pumpkin). In this regard, after physical behavior evaluation of pumpkin, designing the special EE, kinematic calculation, and computer simulations, the pumpkin robotic harvesting methodology was designed which consists of six steps (1) reorganization, (2) adjustment of EE's orientation (O_{ee}) along pumpkin location, (3) grasping, (4) lifting, (5) cutting stem by rotation, (6) and transportation to a trunk. The components of EE were designed in Solidworks software and after several modifications in structure, the final components were assembled. The EE consist of two main unit including (1) frame, and (2) fingers and also some sub-units including the main connector, linear screw, and joint-4 structure. The EE contains 5 fingers which designed and optimized to grasp and harvest heavy-weight crops like pumpkin, watermelon, and cabbage. The fingers were specially designed mechanism including 7 links, 8 joints which had the mobility of 1 ($M = 1$). It was designed based

on the extracted physical properties of pumpkin in during of experiments in chapter 4. The structure statically simulated by using Solidworks software, and dynamically optimized in SAM software. One of the initiated technique to design this system was inventing the administrate power transmission system which manages the power, increases the harvesting speed and efficiency, and decreased the size and weight of EE. The fingers have combined mechanism to support 170 to 500 mm in diameter.

The EE has included 92 components (21-components in the frame and 71-components in the fingers. The inner structure of frame includes a main screw, power transportation, rotary connector, and ball bearings. The material of structure was mainly AL5052, however, some components were made of stainless steel. The mechanism of fingers was selected, optimized and adapted based on the physical properties of pumpkins; was optimized in SAM software by using determined mechanism; was assembled by using Solidworks; and after several modifications, it was simulated as static and dynamic aspects again. The kinematic and inertia calculations, and CAD and kinematic simulation of the fingers mechanism were done. The results show that the maximum stress of finger in the main linkage is 9.8×10^{7} and $1.2\times10^{8}\ N.m^{2}$ in the opened and closed mode respectively. However, these stresses value are samller than yield strength of AL5202. However, the finger damage was possible under impact force because of unpredictable farm environment that increase the rupture possibility. The improved design was modified by adding some filets on the edges which reduced the stress concentration and the stress values were decreased to 6.2×10^{7} and $7.8\times10^{7}\ N.m^{2}$ in the opened and closed mode, respectively. The final simulation data proved that the fingers components have enough capability under the maximum capacity of the system. These results show that the designed EE can harvest the mentioned varieties of pumpkin because the range of radius, volume and mass can cover the extracted physical parameter of pumpkins. The second order motion with included acceleration and deceleration, can reduce backlash of the used servo motor, control the motion velocity, provide minimum hodograph, decrease the crop damage possibility, and protect the finger structure from impact forces.

8.6. Controlling unit

In this chapter, the Control Unit of HRHC system was discussed. The controlling unit of HRHC system consists of a PC, a position board, Amplifiers, servo motors, switching unit, emergency switches, RTK-GPS, TECU, and IMU. The robot tractor has a TECU (Tractor Engine Control Unit) which was connected to a PC. The position data received from RTK-GPS and camera. The positioning system which installed on PCI express port of PC, transfer the signals to the PC. The switch unit controls the servo motor rotation by using different components such as amplifiers, and magnetic switches. As another perspective, the position signals which come from RTK-GPS and camera, the analysis in the PC and the PC sends the commands to servo motor via position board and switch unit, and TECU directly. This circulation repeats for several times until finishing a mission. The controlling unit of robotic arm was based on a programmable logic controller (PLC) system which consists of a position board installed on a PC, a controlling program, servo motors, servo amplifiers, and optical cables for data transfer as compact circuits. The controlling algorithm was developed by using Denavit and Hartenberg method in forwarding kinematics and inverse kinematics calculations.

8.7. Field experimentations of HRHC system

The last chapter was discussed the performance evaluations of the designed HRHC system. The evaluations were focused on seven parameters including harvesting success rate, cycle time, damage rate, working space, accuracy, repeatability, and control resolution. The harvesting success rate, cycle time, damage rate was done in 5 points and 5 repetitions. As the accuracy and repeatability needed more detailed evaluations, the related experimentations were done in 11 points and 10 repetitions. The evaluations show that the HRHC system has harvesting success rate and damage rate of 92% and 0%, respectively. The average cycle time and full cycle time of system were 42.4 and 53s, respectively. The final workspace parameters of modified system including the workspace volume, harvesting surface, and harvesting length of the were $5.662\times10^{9}\ mm^{3}$, $2.86\times10^{6}\ mm^{2}$, and $800\ mm$, respectively, which was 70.6, 81.3, and 99%, of required parameters in designed system, respectively. The accuracy and repeatability experiment results

show that average accuracy in x and y directions, and repeatability were 10.91, 9.52, and 12.74 mm, respectively. According to the controlling resolution results, the SR_x, and SR_Z were 1 ± 0.075, and $1 \pm 0.025\ mm$, respectively, which means that the system had a tolerance of 75, and $25\ \mu m$ in X and Z axis, respectively. At the end of this chapter, the performance indicators were compared by previous harvesting robots in agriculture projects between 1984 and 2012. The HRHC system harvest success (100%) was higher than overall average harvest success of previous studies 66% (40–86%). Overall average fruit damage and cycle time of previous projects were 5% (25–80%) and 33 s (N = 28), respectively. These values were 0% and 46.9 s in the case of HRHC system. As a conclusion, the experiments output meets the determined requirements and the HRHC system found applicable to harvest pumpkin in the field. However, we believe that some modifications and more experimentations are needed for the future studies.

References

ABB. (Swedish-Swiss). ABB official website, from http://new.abb.com/

Akashi. (1990). "50 History" Kawasaki Heavy Industries.

Akinori, I. (2006). *Operating System of a Double-Front Work Machine for Simultaneous Operation*. Paper presented at the The 23rd International Symposium on Automation and Robotics in Construction-ISARC.

Akio, N., Imai, Y., Ishikawa, M., & Kaneko, M. (2003). *Development of a High-speed Multifingered Hand System and Its Application to Catching*. Paper presented at the Proc. of IEEE/RSJ Int. Conf. on Intelligent Robots and Systems.

Akio, N., & Masatoshi, I. (2000). Optimal grasping using visual and tactile feedback. *Journal of the RSJ, 18*(2), 261-269 (in Japanese).

Akio, N., Yoshihiro, N., Idaku, I., & Masatoshi, I. (1999). *1ms grasping system using visual and force feedback*. Paper presented at the Video Proceedings of IEEE Int. Conf. Robotics and Automation.

Akio, N., Yoshihiro, N., Idaku, I., & Masatoshi, I. (1999). *Sensory-motor fusion grasping system using high speed sensory feedback*. Paper presented at the Proc. of 4th Robotics Symposia.

Akio, N., Yoshihiro, N., Idaku, I., & Masatoshi, I. (2000). 1ms sensory-motor fusion system. *IEEE/ASME Trans. on Mechatronics, 5*(3), 244-252.

Ando, T., Takeda, M., Maruyama, T., Susuki, Y., Hirose, T., Fujioka, S., & Mizuno, O. (2013). Biosignal-based Relaxation Evaluation of Head-care Robot. *35th Annual International Conference of the IEEE Engineering in Medicine and Biology Society*.

Andújar, D., Escolà, A., Rosell-Polo, J. R., Fernández-Quintanilla, C., & Dorado, J. (2013). Potential of a terrestrial LiDAR-based system to characterise weed vegetation in maize crops. *Computers and Electronics in Agriculture, 92*, 11-15. doi: http://dx.doi.org/10.1016/j.compag.2012.12.012

Angeles, J. (1997). Fundamentals of robotic mechanical systems (Theory, methods and algorithms). *Springer, New York*.

Anzawa, K., Sasaki, H., Jeong, S., & Takahashi, T. (2010). Development of a Robot Hand with Low Backlash 3D Cam Mechanisms , Prototype of a Light-weight Robot Hand and Evaluation of the Mechanisms. *Journal of the RSJ, 28*(7), 889-896.

Arai, F., Ogawa, M., & Fukuda, T. (1999). Selective manipulation of a microbe in a microchannel using a teleoperated laser scanning manipulator and dielectrophoresis. *Advanced Robotics, 13*(3), 343-345.

Arai, H., & Tachi, S. (1991). Position control of a manipulator with passive joints using dynamic coupling. *IEEE Trans. on Robotics and Automation, 7*(4), 528-534.

Arai, T., & Nakano, E. (1956). Birateral Master-Slave Control for Manipulators with Different Configurations. *Journal of the Robotics Society of Japan, 4*(5), 469-479.

Arata, J., Saito, Y., & Fujimoto, H. (2011). Development of an outer shell type 2 DOF bending manipulator using a spring-link mechanism. *Journal of the robotics society of Japan, 29*(6), 523-531.

Arikawa, K. (2009). Mobility analysis of robotic mechanisms using computer algebra –basic algorithm and application examples. *Journal of the RSJ, 27*(8), 900-909.

Arimoto, S., Sekimoto, M., Hashiguchi, H., & Ozawa, R. (2005). Natural resolution of ill-posedness of inverse kinematics for redundant robots: A challenge to bernstein's degrees-of-freedom problem. *Advanced robotics, 19*(4), 401-434.

Arndt, G., Rudziejewski, R., & Stewart, V. A. (1997). On the future of automated selective asparagus harvesting technology. *Computers and Electronics in Agriculture, 16*(2), 137-145. doi: http://dx.doi.org/10.1016/S0168-1699(96)00033-6

Asadollahpour, A., Omidinajafabadi, M., & Jamalhosseini, S. (2014). Factors affecting the conversion to organic farming in Iran: A case study of mazandaran rice producers. *J Sci Int (Lahore), 26*(4), 1844-1860.

Asama, H., Ozaki, K., Matsumoto, A., Ishida, Y., & Endo, I. (1992). A method of cooperative task assignment by multiple autonomous robots based on decentralized management using communication. *Journal of the Robotics Society of Japan, 10*(7), 955-963.

Åstrand, B., & Baerveldt, A.-J. (2005). A vision based row-following system for agricultural field machinery. *Mechatronics, 15*(2), 251-269. doi: http://dx.doi.org/10.1016/j.mechatronics.2004.05.005

Atsushi, T., Ryo, M., Daisuke, K., & Ryohei, K. (2010). Construction of a brain-machine hybrid system to investigate adaptive functionality of a micro brain. *Journal of the Robotics Society of Japan, 28*(4), 77-86.

B. S., L., & U. A., R. (2006). Development of a Canopy Volume Reduction Technique for Easy Assessment and Harvesting of Valencia Citrus Fruits. *49*(6). doi: 10.13031/2013.22286

Bac, C. W., van Henten, E. J., Hemming, J., & Edan, Y. (2014). Harvesting Robots for High-value Crops: State-of-the-art Review and Challenges Ahead. *Journal of Field Robotics, 31*(6), 888-911. doi: http://dx.doi.org/10.1002/rob.21525/10.1002/rob.21525

Baeten, J., Donné, K., Boedrij, S., Beckers, W., & Claesen, E. (2008). Autonomous Fruit Picking Machine: A Robotic Apple Harvester. In C. Laugier & R. Siegwart (Eds.), *Field and Service Robotics: Results of the 6th International Conference* (pp. 531-539). Berlin, Heidelberg: Springer Berlin Heidelberg.

Bakker, T., van Asselt, K., Bontsema, J., Müller, J., & van Straten, G. (2011). Autonomous navigation using a robot platform in a sugar beet field. *Biosystems Engineering, 109*(4), 357-368. doi: http://dx.doi.org/10.1016/j.biosystemseng.2011.05.001

Balafoutis, C. A., & Patel, R. V. (1991). *Dynamic analysis of robot manipulators*. Concordia University, Montreal, Canada: Springer Science and Business Media, LLC.

Bales, C., & Vlamakis, M. (2010). *Engineering drawing & CAD standards*. Moraine valley community college.

Balkan, T., Özgören, M. K., Sahir Arıkan, M. A., & Baykurt, H. M. (2000). A method of inverse kinematics solution including singular and multiple configurations for a class of robotic manipulators. *Mechanism and machine theory, 35*(9), 1221-1237. doi: http://dx.doi.org/10.1016/S0094-114X(99)00079-8

Barati, M., Khoogar, A. R., & Nasirian, M. (2011). Estimation and calibration of robot link parameters with intelligent techniques *Iranian journal of electrical & electronic engineering, 7*(4).

Barawid, J., Oscar, C., Mizushima, A., Ishii, K., & Noguchi, N. (2007). Development of an autonomous navigation system using a two-dimensional laser scanner in an orchard application. *Biosystems Engineering, 96*(2), 139-149. doi: http://dx.doi.org/10.1016/j.biosystemseng.2006.10.012

Barawid Jr, O. C., Mizushima, A., Ishii, K., & Noguchi, N. (2007). Development of an Autonomous Navigation System using a Two-dimensional Laser Scanner in an Orchard Application. *Biosystems Engineering, 96*(2), 139-149. doi: http://dx.doi.org/10.1016/j.biosystemseng.2006.10.012

Belforte, G., Deboli, R., Gay, P., Piccarolo, P., & Ricauda Aimonino, D. (2006). Robot design and testing for greenhouse applications. *Biosystems engineering, 95*(3), 309-321. doi: http://dx.doi.org/10.1016/j.biosystemseng.2006.07.004

Bell, T. (2000). Automatic tractor guidance using carrier-phase differential GPS. *Computers and electronics in agriculture, 25*(1–2), 53-66. doi: http://dx.doi.org/10.1016/S0168-1699(99)00055-1

Benson, E. R., Reid, J. F., & Zhang, Q. (2003). Machine vision-based guidance system for agricultural grain harvesters using cut-edge detection. *Biosystems engineering, 86*(4), 389-398. doi: http://dx.doi.org/10.1016/j.biosystemseng.2003.07.002

Blahovec, J. (1994). Elastic and strength properties of round agricultural products *Internation Agrophysics, 8*, 534-546.

Blanes, C., Mellado, M., & Beltrán, P. (2016). Tactile sensing with accelerometers in prehensile grippers for robots. *Mechatronics, 33*, 1-12. doi: http://dx.doi.org/10.1016/j.mechatronics.2015.11.007

Blanes, C., Ortiz, C., Mellado, M., & Beltrán, P. (2015). Assessment of eggplant firmness with accelerometers on a pneumatic robot gripper. *Computers and electronics in agriculture, 113*, 44-50. doi: http://dx.doi.org/10.1016/j.compag.2015.01.013

Blas, M. R., & Blanke, M. (2011). Stereo vision with texture learning for fault-tolerant automatic baling. *Computers and electronics in agriculture, 75*(1), 159-168. doi: http://dx.doi.org/10.1016/j.compag.2010.10.012

Bochtis, D. D., Sørensen, C. G., & Vougioukas, S. G. (2010). Path planning for in-field navigation-aiding of service units. *Computers and electronics in agriculture, 74*(1), 80-90. doi: http://dx.doi.org/10.1016/j.compag.2010.06.008

Brosnan, T., & Sun, D.-W. (2002). Inspection and grading of agricultural and food products by computer vision systems—a review. *Computers and electronics in agriculture, 36*(2–3), 193-213. doi: http://dx.doi.org/10.1016/S0168-1699(02)00101-1

Carter, C., Ball, T., Ward, E., Fuchs, S., Durfey, J. E., Cavalieri, R. P., & Folwell, R. J. (2007). Performance and Economic Analysis of a Selective Asparagus Harvester. *23*(5). doi: https://doi.org/10.13031/2013.23665/10.13031/2013.23665

Cassinis, R., & Tampalini, F. (2007). AMIRoLoS an active marker internet-based robot localization system. *Robotics and autonomous systems, 55*(4), 306-315. doi: http://dx.doi.org/10.1016/j.robot.2006.11.001

Chateau, T., Debain, C., Collange, F., Trassoudaine, L., & Alizon, J. (2000). Automatic guidance of agricultural vehicles using a laser sensor. *Computers and electronics in agriculture, 28*(3), 243-257. doi: http://dx.doi.org/10.1016/S0168-1699(00)00130-7

Chayooth, T., Takubo, T., Ohara, K., Mae, Y., & Arai, T. (2011). Dynamic Rolling-Walk Motion by the Limb Mechanism Robot ASTERISK. *Advanced robotics, 25*(1-2), 75-91.

Chen, Y.-R., Chao, K., & Kim, M. S. (2002). Machine vision technology for agricultural applications. *Computers and electronics in agriculture, 36*(2–3), 173-191. doi: http://dx.doi.org/10.1016/S0168-1699(02)00100-X

Cho, S. I., Ki, N. H., Lee, J. H., & Choi, C. H. (1996). *Autonomous speed sprayer using fuzzy control*. Paper presented at the International Conference on Agricultural Machinery Engineering, , Seoul,.

Cho, S. I., & N.H. Ki. (1996). Unmanned combine operation using fuzzy logic control. *Appl. Eng. Agric., 12*(2), 247-251.

Choi, H., & Koç, M. (2006). Design and feasibility tests of a flexible gripper based on inflatable rubber pockets. *International journal of machine tools and manufacture, 46*(12–13), 1350-1361. doi: http://dx.doi.org/10.1016/j.ijmachtools.2005.10.009

Chuang, C.-L., Ouyang, C.-S., Lin, T.-T., Yang, M.-M., Yang, E.-C., Huang, T.-W., . . . Jiang, J.-A. (2011). Automatic X-ray quarantine scanner and pest infestation detector for agricultural products. *Computers and electronics in agriculture, 77*(1), 41-59. doi: http://dx.doi.org/10.1016/j.compag.2011.03.007

Coen, T., Vanrenterghem, A., Saeys, W., & De Baerdemaeker, J. (2008). Autopilot for a combine harvester. *Computers and electronics in agriculture, 63*(1), 57-64. doi: http://dx.doi.org/10.1016/j.compag.2008.01.014

Cox, S. (2002). Information technology: the global key to precision agriculture and sustainability. *Computers and electronics in agriculture, 36*(2–3), 93-111. doi: http://dx.doi.org/10.1016/S0168-1699(02)00095-9

Craessaerts, G., Maertens, K., & De Baerdemaeker, J. (2005). A Windows-based design environment for combine automation via CANbus. *Computers and electronics in agriculture, 49*(2), 233-245. doi: http://dx.doi.org/10.1016/j.compag.2005.04.007

De-An, Z., Jidong, L., Wei, J., Ying, Z., & Yu, C. (2011). Design and control of an apple harvesting robot. *Biosystems engineering, 110*(2), 112-122. doi: https://doi.org/10.1016/j.biosystemseng.2011.07.005

Denavit, J., & Hartenberg, R. S. (1955a). A kinematic notation for lower-pair mechanisms based on matrices. *Trans. of the ASME. Journal of Applied Mechanics, 22*, 215-221.

Denavit, J., & Hartenberg, R. S. (1955b). A kinematic notation for lower-pair mechanisms based on matrices. *Journal of applied mechanics, 1*, 215-221.

DENSO Co. (Japan). DENSO official website Retrieved https://www.denso.com/global/en/

Dong, F., Heinemann, W., & Kasper, R. (2011). Development of a row guidance system for an autonomous robot for white asparagus harvesting. *Computers and Electronics in Agriculture, 79*(2), 216-225. doi: http://dx.doi.org/10.1016/j.compag.2011.10.002

Drake, P. (1999). *Dimensioning and tolerancing handbook*.

Edan, Y. (1995). Design of an autonomous agricultural robot. *Applied Intelligence, 5*(1), 41-50. doi: 10.1007/bf00872782

Egawa, S., Niino, T., & Higuchi, T. (1997). Pulse-driven induction-type electrostatic film actuator. *Journal of the Robotics Society of Japan, 15*(3), 61-68.

Eizicovits, D., van Tuijl, B., Berman, S., & Edan, Y. (2016). Integration of perception capabilities in gripper design using graspability maps. *Biosystems Engineering, 146*, 98-113. doi: http://dx.doi.org/10.1016/j.biosystemseng.2015.12.016

Ejiri, M., Uno, T., Yoda, H., Goto, T., & Takeyasu, K. (1972). A prototype intelligent robot that assembles objects from plan drawings. *IEEE Trans. Computers, C-21*(2), 161-170.

Emmanuel, B., Vander, P., & Yasuyoshi, Y. (2007). Feeling a rigid virtual world through an impulsive haptic display. *Advanced robotics, 21*(12), 1411-1440.

Faizollahzadeh Ardabili, S., Mahmoudi, A., Mesri Gundoshmian, T., & Roshanianfard, A. (2016). Modeling and comparison of fuzzy and on/off controller in a mushroom growing hall. *Measurement, 90*, 127-134. doi: http://dx.doi.org/10.1016/j.measurement.2016.04.050

FANUC CO. (Japan). FANUC corporation official website. http://fanuc.co.jp/eindex.html

FCA Group. (Italy). Comau official website Retrieved http://www.comau.com/en/

Feng, C., Xiao, Y., Willette, A., McGee, W., & Kamat, V. R. (2015). Vision guided autonomous robotic assembly and as-built scanning on unstructured construction sites. *Automation in Construction*. doi: http://dx.doi.org/10.1016/j.autcon.2015.06.002

Foster, C. A., Strosser, R. P., Peters, J., & Sun, J.-Q. (2005). Automatic velocity control of a self-propelled windrower. *Computers and electronics in agriculture, 47*(1), 41-58. doi: http://dx.doi.org/10.1016/j.compag.2004.10.001

Fountas, S., Carli, G., Sørensen, C. G., Tsiropoulos, Z., Cavalaris, C., Vatsanidou, A., . . . Tisserye, B. (2015). Farm management information systems: Current situation and future perspectives. *Computers and Electronics in Agriculture, 115*, 40-50. doi: http://dx.doi.org/10.1016/j.compag.2015.05.011

Fountas, S., Sorensen, C. G., Tsiropoulos, Z., Cavalaris, C., Liakos, V., & Gemtos, T. (2015). Farm machinery management information system. *Computers and Electronics in Agriculture, 110*, 131-138. doi: http://dx.doi.org/10.1016/j.compag.2014.11.011

Fricke, T., Richter, F., & Wachendorf, M. (2011). Assessment of forage mass from grassland swards by height measurement using an ultrasonic sensor. *Computers and Electronics in Agriculture, 79*(2), 142-152. doi: http://dx.doi.org/10.1016/j.compag.2011.09.005

Fujie, M. (1993). Quadrupwdal walking robot for hazardouts environment. *Journal of the Robotics Society of Japan, 11*(3), 366-371.

Fujisawa, E., Seki, T., & Narita, S. (1985). Supervisory system and singing voice tracking subsystem of WABOT -2. *Journal of the RSJ, 3*(4), 373-380.

Fujiwara, S., Kanehara, R., Okada, T., & Sanemori, T. (1994). Development of an articulated multi-vehicle robot for monitoring and testing in pipe. *Journal of the Robotics Society of Japan, 12*(2), 318-327.

Fukuda, S., & Arimoto, S. (1989). Fast interference check method using octree representation. *Advanced Robotics, 3*(3), 193-212.

Fukuda, T., Hosokai, H., & Kondo, Y. (1990). A study of the brachiation type of mobile robot (1st report, analysis of dynamics and simulation). *Transactions of the JSME (C), 56*(527), 1839-1846.

Fumihito, A., Masanobu, O., & Toshio, F. (2002). Non-contact micromanipulation by bilateral control - control of micro tool using laser micromanipulator *Journal of the RSJ, 20*(4), 417-424.

Funda, J., Taylor, R. H., & Paul, R. P. (1990). On homogeneous transforms, quaternions, and computational efficiency. *IEEE Trans.Robot. Automat, 6*, 382-388.

Furukawa, N., Namiki, A., Senoo, T., & Ishikawa, M. (2006). *Dynamic regrasping using a high-speed multifingered hand and a high-speed vision system*. Paper presented at the Proc. of IEEE Int. Conf. on Robotics and Automation.

Furusho, J. (1983). A control study of dynamical locomotion robot - a low order model and a hierarchical control strategy -. *Journal of the Robotics Society of Japan, 1*(3), 182-190.

Furusho, J., Sano, A., & Goto, A. (1989). Dynamic control of a quaduped robot based on free movement in a gravity field. *Transactions of the JSME (c), 55*(518), 2575-2582.

G, T., H, I., & T, I. (1997). *Mobile robot navigation by distributed vision agents*. Paper presented at the International Conference on Computational Intelligence and Multimedia Applications (ICCIMA'97).

García-Pérez, L., García-Alegre, M. C., Ribeiro, A., & Guinea, D. (2008). An agent of behaviour architecture for unmanned control of a farming vehicle. *Computers and Electronics in Agriculture, 60*(1), 39-48. doi: http://dx.doi.org/10.1016/j.compag.2007.06.004

Gen-ichiro, K., Kunikatsu, T., & Masahiro, M. (1971). Pattern Recognition by the Artificial -Tactile Sense. *Transactions of the Society of Instrument and Control Engineers, 7*(1), 25-30.

Gen, E., & Shigeo, H. (1998). *Study on roller-walker : Straightfoward roller-walk using 4 legs*. Paper presented at the Proc. of 16th Annual Conference of the RSJ.

Gen, E., & Shigeo, H. (2000). Study on roller-walker-system integration and basic experiments. *Journal of the RSJ, 18*(2), 270-277.

Gen, E., & Shigeo, H. (2012). Study on roller-walker-improvement of locomotive efficiency of quadruped robots by passive wheels. *Advanced robotics, 26*(8-9), 969-988.

Ghazvini, M. (1993). Reducing the inverse kinematics of manipulators to the solution of a generalized eigenproblem. In G. Angeles & K. Hommel (Eds.), *Computational Kinematics, Solid Mechanics and its Applications* (pp. 15-26).

Ghorani, F. (2017). Engineering drawing standards, from http://tolerancing.net/engineering-drawing/engineering-drawing-standards.html

Giulio, F. M. R. (2006). Agricultural Robot for Radicchio Harvesting. *Journal of Field Robotics, 23*(6/7), 363-377.

Global Harvest Initiative. (2013). Global Agricultural Productivity report. In L. Ellen, C. William, S. Erica & F. Keith (Eds.).

Global Harvest Initiative. (2014). Global Agricultural Productivity report. In L. Ellen, C. William, S. Erica & F. Keith (Eds.).

Global Harvest Initiative. (2015). Global Agricultural Productivity report. In M. Zeigler & A. Steensland (Eds.).

Global Harvest Initiative. (2016). Global Agricultural Productivity report. In M. Zeigler & A. Steensland (Eds.).

Gonzalez de Santos, P., Cobano, J. A., Garcia, E., Estremera, J., & Armada, M. A. (2007). A six-legged robot-based system for humanitarian demining missions. *Mechatronics, 17*(8), 417-430. doi: http://dx.doi.org/10.1016/j.mechatronics.2007.04.014

Goto, T., T., I., & Takeyasu, K. (1974). *Precise insert operation by tactile controlled robot HI-T-HAND Expert 2*. Paper presented at the Proc. 4th Int. Symp. Industrial Robots.

Goto, T., Takeyasu, K., & Inoyama, T. (1980). Control Algorithm for Precision Insert Operation Robots. *IEEE Transaction on System, Man and Cybernetics, SMC-10*(1), 19-25.

Guijarro, M., Pajares, G., Riomoros, I., Herrera, P. J., Burgos-Artizzu, X. P., & Ribeiro, A. (2011). Automatic segmentation of relevant textures in agricultural images. *Computers and electronics in agriculture, 75*(1), 75-83. doi: http://dx.doi.org/10.1016/j.compag.2010.09.013

Gunston, B. (1989). *World encyclopedia of aero engines*. Patrick Stephens: Cambridge, England.

Hameed, I. A., Bochtis, D. D., Sørensen, C. G., & Nøremark, M. (2010). Automated generation of guidance lines for operational field planning. *Biosystems Engineering, 107*(4), 294-306. doi: http://dx.doi.org/10.1016/j.biosystemseng.2010.09.001

Hamilton, W. R. (2000). *The hodograph, or a new method of expressing in symbolical language the newtonian law of attraction*: Proceedings of the Royal Irish Academy.

Harrell, R. C., Adsit, P. D., Munilla, R. D., & Slaughter, D. C. (2009). Robotic picking of citrus. *Robotica, 8*(4), 269-278. doi: 10.1017/S0263574700000308

Harrell, R. C., Adsit, P. D., Pool, T. A., & Hoffman, R. (1990). The Florida robotic grove lab. *ASABE, 33*(2), 391-399.

Haruhisa, K., & Kunitoshi, N. (1986). Parameter identification of mevhanical manipulators. *Transactions of the SICE, 22*(1), 76-83.

Hasegawa, T., & kameyama, S. (1989). Geometric modeling of manipulation environment by interactive teaching and automated accuracy improvement. *Transactions of the Society of Instrument and Control Engineers, 25*(12), 1371-1378.

Hasegawa, T., Suehiro, T., Ogasawara, T., Matsui, T., Kitagaki, K., & Takase, K. (1990). *An Integrated Tele-Robotics System with a Geometric Environment Model and Manipulation Skills*. Paper presented at the IEEE International Workshop on Intelligent Robots and Systems.

Hasegawa, T., Suehiro, T., & Takase, K. (1991). An Integrated Robot System with a Geometric Environment Model and Manipulation Skills. *Journal of the RSJ, 9*(6), 66-78 (in Japanese).

Hasegawa, T., & Terasaki, H. (1987). Collision avoidance for multi-joint manipulators, divide and conquer approach by determining intermediate goals. *Transactions of the Society of Instrument and Control Engineers, 23*(8), 842-848.

Hasegawa, T., & Terasaki, H. (1988). Collision avoidance: Divide and conquer approach by space characterization and intermediate goals. *IEEE Trans. on Systems, Man, and Cybernetics, SMC18*(3), 337-347.

Hayashi, S., Saito, S., Iwasaki, Y., Yamamoto, S., Nagoya, T., & Kano, K. (2011). Development of Circulating-Type Movable Bench System for Strawberry Cultivation. *Japan Agricultural Research Quarterly: JARQ, 45*(3), 285-293. doi: 10.6090/jarq.45.285

Hayashi, S., Shigematsu, K., Yamamoto, S., Kobayashi, K., Kohno, Y., Kamata, J., & Kurita, M. (2010). Evaluation of a strawberry-harvesting robot in a field test. *Biosystems Engineering, 105*(2), 160-171. doi: http://dx.doi.org/10.1016/j.biosystemseng.2009.09.011

Heon, H., & Si-Chan, K. (2003, 20-24 July 2003). *Development of multi-functional tele-operative modular robotic system for greenhouse watermelon.* Paper presented at the Proceedings 2003 IEEE/ASME International Conference on Advanced Intelligent Mechatronics (AIM 2003).

Hideo, H., & Haruhiko, A. (1976). Mechanics of gripping form by artificial fingers. *Transactions of the SICE, 12*(5), 536-542.

Hideo, H., Tsuneo, Y., & Yoshihiko, N. (1983). Redundancy analysis of articulated robot arms and its utilization for tasks with priority. *Transactions of the SICE, 19*(5), 421-426.

Hideo, M., Shinji, K., Hiroshi, I., Satoshi, Y., & Yukiko, C. (1987). Self-contained mobile robot in campus road (a mobile robot strategy and its application to harunobu-4). *Journal of the RSJ, 5*(5), (in Japanese).

Hidetoshi, I., Norifumi, Y., Takuro, K., Shiro, N., Hiroaki, D., Shogo, H., . . . Eiji, N. (2010). Step climbing of a wheelchair using a wheeled robot with passive joint manipulators. *Journal of the Robotics Society of Japan, 28*(7), 802-810.

Hideyuki, M., Naoyuki, T., Kuniyasu, M., Hitoshi, K., & Hideo, F. (2010). Development of a Car Window Installation Assist Robot. *Journal of the Robotics Society of Japan, 28*(5), 624-630.

Hirai, S., & Sato, T. (1984). Language-mediated master-slave manipulator. *Transactions of the Society of Instrument and Control Engineers, 20*(1).

Hirata, Y., Kosuge, K., Asama, H., Kaetsu, H., & Kawabata, K. (2003). Transportation of a single object by multiple distributed robot helpers with caster-like dynamics (DR helpers) in cooperation with a human. *Journal of the RSJ, 21*(7), 80-88.

Hiroaki, H., Taiki, I., Keita, I., & Fumio, M. (2012). Identifying the building blocks of a human walking based on the emg ratio of agonist-antagonist muscle pairs. *Journal of Robotics Society of Japan, 30*(5), 524-533.

Hirochika, I. (1971). Computer controlled bilateral manipulator. *Bulletin of the JSME, 14*(69), 199-207.

Hirochika, I., Hiroshi, M., Masayuki, I., Shigeki, I., & Fumihiko, I. (1989). Development of Window Control LSI Chip for Multi Window Robot Vision System. *Transactions of SICE, 23*(12), 1289-1295.

Hirofumi, M., & Isao, S. (1984). Dynamic walk of a biped. *The International Journal of Robotics Research, 3*(2), 60-74.

Hirohiko, A. (2002). Human interface for maneuvering nonholonomic systems. *Journal of the Robotics Society of Japan, 25*(5), 554-561.

Hirohiko, A. (2003). Human Interface for Maneuvering Nonholonomic Systems. *Journal of the Robotics Society of Japan, 25*(5), 554-561.

Hirohiko, A. (2010). Force-controlled metal spinning machine for forming non-axisymmetric shapes. *Journal of the Robotics Society of Japan, 28*(1), 49-50.

Hirohiko, A., & Susumu, T. (1989). Position control of a manipulator with passive joints using coupled dynamics. *Transactions of the SICE, 25*(9), 1012-1017.

Hirohisa, H., Toshihiro, M., & Kunikatsu, T. (1991a). A fast algorithm for the analysis of the constraint for motion of polyhedra in contact and its application to departure motion planning. *Journal of the RSJ, 9*(7), 841-848.

Hirohisa, H., Toshihiro, M., & Kunikatsu, T. (1991b). A general algorithm for deriving constraint of contact between polyhedra from geometric model. *Journal of the RSJ, 9*(4), 415-426 (in Japanese).

Hiromasa, O., Takahiko, I., & Masatoshi, I. (2009). High-Speed Focusing Vision: Coupling of Image Processing System with Tunable Optics without Speed Bottleneck. *Journal of the Robotics Society of Japan, 27*(7), 739-748.

Hirose, S., Fukuda, Y., & Kikuchi, H. (1985). Control system of quadruped walking vehicle *Journal of the Robotics Society of Japan, 3*(2), 304-324.

Hirose, S., Morishima, A., Tsukagoshi, S., Tsumaki, T., & Monobe, H. (1991). Design of snake like vehicle: Articulated body mobile robot KR II. *Journal of the Robotics Society of Japan, 9*(5), 551-559.

Hirukawa, H., Matsui, T., & Takase, K. (1994). Automatic determination of possible velocity and applicable force of frictionless objects in contact from a geometric model. *IEEE Trans. on Robotics and Automation, 10*(3), 309-322.

Hisashi, T., Akihiro, N., Shinichi, H., Junichi, Hayakawa, & Shinichi, O. (2008). Miuro, the robot that play your favorite music at your favorite place. *Journal of the RSJ, 26*(1), 34-35.

Hitoshi, M., Kazuo, T., & Kiyoshi, K. (1995). Manipulation of an unknown object by multifingered hand with rolling contact using tactile feedback. *Transactions of the Society of Instrument and Control Engineers, 31*(9), 1462-1470.

Hokkaido Food library. (2017). A vegetable closely connected to traditional Japanese events, from http://hokkaidofoodlibrary.com/3718/

Horoshi, I., Masashi, Y., & Saburo, T. (1991). Reconstructing Structure of an Indoor Environment Using Active Omni-Directional Vision. *Journal of the Robotics Society of Japan, 9*(5), 541-550.

Hu, J., Yan, X., Ma, J., Qi, C., Francis, K., & Mao, H. (2014). Dimensional synthesis and kinematics simulation of a high-speed plug seedling transplanting robot. *Computers and Electronics in Agriculture, 107*, 64-72. doi: http://dx.doi.org/10.1016/j.compag.2014.06.004

Hyon, S. (2009). Compliant terrain adaptation for biped humanoids without measuring ground surface and contact forces. *IEEE Transactions on Robotics & Automation, 25*(1), 171-178.

Hyon, S., & Cheng, G. (2006). *Gravity compensation and full-body balancing for humanoid robots*. Paper presented at the Proceedings of IEEE-RAS International Conference on Humanoid Robots.

Hyon, S., Morimoto, J., Matsubara, T., Noda, T., Kawato, M., & Xo, R. (2011). *Hybrid drive exoskeleton robot that can balance*. Paper presented at the in Proc. IEEE/RSJ International Conference on Intelligent Robots and Systems, 2011.9, San Francisco, US.

I. Godler, A. Akahane, T. Maruyama, & T. Yamashita. (1995). Angular Acceleration Sensor Composed of two Discs and Optical Pick-Up - Analysis of Basic Performances. *Transactions of SICE, 31*(8), 982-990.

Ichiro, W., Takahiro, O., & Yoshihiko, K. (2007). Robot-assisted activities for elderly people using a life-like teddy bear robot. *Proc. of RSJ2007, 2B26*.

Ikeuchi, K., Nagata, S., Horn, B., & Nishihar, K. (1985). Determining Gripper Configuration in Bin Picking Tasks Using Photometric Stereo System and PRISM Stereo Syste. *Transaction of IECE, J68-D*(4), 546-553.

Ikuta, M, N., & H, I. (2000). *General evaluation method for safety control of human-care robots*. Paper presented at the Proc. of ASME the 2000 International Mechanical Engineering Congress & Exposition.

Ikuta, K., & Nokata, M. (2001). Safety evaluation method of human-care robot design. *Integration of Assistive Technology in the Information Age, IOS Press*, 307-316.

Ikuta, K., Nokata , M., & Ishii, H. (2001). *General danger-evaluation method of human-care robot control and development of special simulator*. Paper presented at the Proc. of the 2001 IEEE Robotics and Automation Conference (ICRA'01).

Ikuta, K., Nokata, M., & Ishii, H. (2001). Safety evaluation method of human-care robot control and special robot simulator. *Integration of Assistive Technology in the Information Age, IOS Press*, 317-326.

Iñigo-Blasco, P., Diaz-del-Rio, F., Romero-Ternero, M. C., Cagigas-Muñiz, D., & Vicente-Diaz, S. (2012). Robotics software frameworks for multi-agent robotic systems development. *Robotics and Autonomous Systems, 60*(6), 803-821. doi: http://dx.doi.org/10.1016/j.robot.2012.02.004

Inoue, H., Ogasawara, T., Shiroshita, O., & Naito, O. (1981). *Design and implementation of high level robot language*. Paper presented at the Proc. of 11th International Symposium on Industrial Robots.

Ishiguro, H. (1997). *Distributed vision system: A perceptual information infrastructure for robot navigation*. Paper presented at the International Joint Conference on Artificiall Intelligence (IJCAI'97).

Ishiguro, H., Tanaka, G., & Ishida, T. (1996). *Distributed vision system for real world agents*. Paper presented at the Proc. ICMAS'96 Workshop on Learning, Interaction and Organizations in Multiagent Environments.

ISO: International Organization for Standardization. (1998). Manipulating industrial robots - Performance criteria and related test methods, ISO 9283.

Itsuro Matsumoto, N., Kyura, Satoru Nio, Hajime Fujii, Takeo Suzuki,. (1978). Industrial Robots Motoman-L. *Yaskawa Technical Review, 42*(3), 184-193.

Iwamoto, T., Yamamoto, H., Fujie, M., & Nakano, Y. (1984). Mechanism and Control of Transformable Crawler Vehicle with Active Adaptability to Terrain Variations. *Journal of the RSJ, 2*(3), 200-208.

Jan Gliński, Józef Horabik, & Lipiec, J. (2011). Encyclopedia of agrophysics *Encyclopedia of earth sciences series*. Polish Academy of Sciences, Lublin, Poland.

Jansson, G. (1990). Non-visual guidance of walking. *Ed. R.Warren, Perception and Control of Self-Motion, Lawrence Erbaum Associates Pub.*

Jeon, H. Y., & Tian, L. F. (2009). Direct application end effector for a precise weed control robot. *Biosystems Engineering, 104*(4), 458-464. doi: http://dx.doi.org/10.1016/j.biosystemseng.2009.09.005

Jeong Yongjin, R. K., Yumi Iwashita, Tsutomu Hasegawa,. (2012). Study on CPS-SLAM -Improvement of Measurement Precision and Application for Tunnel Shape Measurement System. *Journal of the Robotics Society of Japan, 30*(2), 180-187.

Jeong Yongjin, R. K., Yumi Iwashita, Tsutomu Hasegawa,. (2013). Global localization for mobile robot using large-scale 3D environmental map and RGB-D camera. *Journal of the Robotics Society of Japan, 31*(9), 896-906.

Jiang, S., & Fumio, N. (2001). *Biologically Inspired Spinal locomotion Controller for Humanoid Robot*. Paper presented at the Proceedings of The 19th Annual Conference of the Robotic Society of Japan.

Jumpei Arata, Y. S. H. F. (2011). Development of an Outer Shell Type 2 DOF Bending Manipulator using a Spring-link Mechanism. *Journal of the Robotics Society of Japan, 29*(6), 523-531.

Jun, M., & Katsushi, I. (1996). Task-oriented generation of visual sensing strategies. *Journal of the Robotics Society of Japan, 14*(4), 574-585.

Jun, M., & Katsushi, I. (1998). Task-Oriented Generation of Visual Sensing Strategies in Assmebly Tasks. *IEEE Trans. on Pattern Analysis and Machine Intelligence, 20*(2), 126-137.

K.Takase. (1977). Task-Oriented Variable Control of Manipulator and Its Software Servoing System. *Proc.of IFAC Sympo.on Information -Control in Manufacturing, 139-145*.

Kahori, K., Ryu, K., & Hiroshi, Y. (2010). EMG-to-motion classification for prosthetic applications - a self-organizing approach with level of proficiency. *Journal of the Robotics Society of Japan, 28*(7), 783-791.

Kahori, K., Ryu, K., & Hiroshi, Y. (2010). Evaluation method of proficiency level of operating myoelectric hand using emg signal. *In Proceedings of 32nd Annual Int Conf of IEEE Eng Med Biol Soc*, 3373-3376.

Kajita, S., Kanehiro, F., Kaneko, K., Fujiwara, K., Harada, K., Yokoi, K., & Hirukawa, H. (2004). Resolved momentum control: Motion generation of humanoid robot based on the linear and angular momenta2004. *Journal of the RSJ, 22*(6), 772-779.

Kajita, S., & Tani, K. (1995). Dynamic biped walk on an uneven terrain based on linear inverted pendulum mode. *Transactions of the SICE, 31*(10), 1705-1714.

Kameyama, M., Egami, H., & Higuchi, T. (1988). Design of an ultra-high-speed inverse-kinematic processor for robot control. *Journal of the Robotics Society of Japan, 6*(1), 3-13.

Kameyama, M., Matsumoto, T., Egami, H., & Higuchi, T. (1989). Implementation of a high performance LSI for inverse kinematics computation. *Proceedings of the 1989 IEEE International Conference on Robotics and Automation*, 757-762.

Kameyama, M., Matsumoto, T., Egami, H., & Higuchi, T. (1991). A special-purpose LSI for inverse kinematics computation. *IEICE, 74*(11), 3829-3837.

Kanade, T., Kano, H., Kimura, S., Kawamura, E., Yoshida, A., & Oda, K. (1997). Development of a Video-Rate Stereo Machine. *Journal of the Robotics Society of Japan, 15*(2), 261-267.

Karlik, B., & Aydin, S. (2000). An improved approach to the solution of inverse kinematics problems for robot manipulators. *Engineering Applications of Artificial Intelligence, 13*(2), 159-164. doi: http://dx.doi.org/10.1016/S0952-1976(99)00050-0

Kashioka, S., Ejiri, M., & Sakamoto, Y. (1976). A Transistor Assembly System Utilizing Time-shared Visual Image Processing. *Transaction of the IEEJ, C-96*(1), 9-16.

Kato, I., Fujie, M., Yoshida, T., Ichiryu, K., & Nakano, Y. (1986). Development of Legged Walking Robots. *Hitachi review, 68*(10), 787-792.

Kato, I., Ohteru, S., Kobayashi, H., Shirai, K., & Uchiyama, A. (1973). *Power macine with senses and limbs.*

Kato, I., Ohteru, S., Shirai, K., Narita, S., Sugano, S., Matsushima, T., . . . Fujisawa, E. (1987). The Robot Musician 'WABOT-2, Sensing in Robotics Control. *Elsevier Science Publishers B.V. (North-Holland) Robotics 3*, 143-155.

Kato, S. O., H, K., K, s., & A, U. (1973). Information-power machine with senses and limbs. *On theory and practice of rpbpts and manipulators, 1*, 12-24.

Katsushi, I., & Takashi, S. (1993). Task model for assembly plan from observation system. *Journal of the Robotics Society of Japan, 11*(2), 281-290.

Kawamura, S., Choe, W., Tanaka, S., & Kino, H. (1997). Development of an Ultrahigh Speed Robot FALCON Using Parallel Wire Drive Systems. *Journal of the Robotics Society of Japan, 15*(1), 82-89.

Kawamura, S., Miyazaki, F., & Arimoto, S. (1986). Learning control of motion for robot manipulator. *Transactions of the Society of Instrument and Control Engineers, 22*(4), 443-450 (in Japanese).

Kawamura, S., Miyazaki, F., & Arimoto, S. (1986). Proposal of betterment process: A learning control method for dynamical systems. *Transactions of the Society of Instrument and Control Engineers, 22*(1), 56-62 (in Japanese).

Kawasaki, H., Uchiyama, K., & komatu, T. (2000). Anthropomorphic Robot Hand with Distributed Tactile Sensor Aiming at Platform of Robotics Researchs. *Trans. of JRM, 6*(651-c).

Kawasaki Heavy Industries Ltd. (USA). Kawasaki official website Retrieved https://robotics.kawasaki.com/en1/

Kazuhiro Kosuge, K. F., Tatsuaki Yokoyama,. (1988). Virtual Internal Model Following Control System - Application to Mechanical Impedance Control *Transactions of the SICE, 24*(1), 55-62.

Kazuo, M., Yoshitsugu, T., Tatsuo, M., & Satoru, K. (2000). Precise task execution and tele-sensing in space by sensor-fused telerobotics. *Journal of the Robotics Society of Japan, 18*(8), 1184-1198 (in Japanese).

Kazuo, M., Yoshitsugu, T., Toshiaki, I., Shoichi, I., & Tadashi, K. (1994). New 3-DOF Parallel mechanism and application to space-born smart end-effector. *Journal of the Robotics Society of Japan, 12*(1), 105-111.

Kazuya Yoshida, R. K., Yoji Umetani,. (1991). Coordinated Control of Multiple Manipulators in Space Robots (Optimization of Control Torque using a Stabilizing Arm). *Journal of the Robotics Society of Japan, 9*(6), 718-726.

Keicher, R., & Seufert, H. (2000). Automatic guidance for agricultural vehicles in Europe. *Computers and Electronics in Agriculture, 25*(1–2), 169-194. doi: http://dx.doi.org/10.1016/S0168-1699(99)00062-9

Keisuke Arikawa. (2009). Mobility Analysis of Robotic Mechanisms Using Computer Algebra –Basic Algorithm and Application Examples. *Journal of the RSJ, 27*(8), 900-909.

Kenta Tanaka, Y. K., Yasuyoshi Yokokohji,. (2009). Desired Trajectory and Sensory Feedback Control Law Synthesis for an Origami-Folding Robot based on the Statistical Feature of Direct Teaching by a Human. *Journal of the Robotics Society of Japan, 27*(6), 585-695.

Khodabakhshian, R., & Emadi, B. (2011). Determination of the modulus of elasticity in agricultural seeds on the basis of elasticity theory. *Middle-East Journal of Scientific Research, 7*(3), 367-373.

Kim, Y. Y., Hwang, H., & Cho, S. I. (2008). A hybrid robotic system for harvesting heavy produce. *Engineering in Agriculture, Environment and Food, 1*(1), 18-23. doi: http://dx.doi.org/10.1016/S1881-8366(08)80009-2

Kimura, H., Fukuoka , Y., & Konaga, K. (2001). Adaptive dynamic walking of a quadruped robot by using neural system model. *Advanced Robotics, 15*(8), 859-876.

Kimura, H., Shimoyama, I., & Miura, H. (1988). Mechanical Analysis of Quadrupedal Walking Robot. *Journal of the Robotics Society of Japan, 6*(5), 367-379.

Kishi, K., Fujie, M., Hashizume, M., Sakuma, I., & Dohi, T. (2009). MR-compatible Surgical Support Manipulator System with Rod-driven Instruments. *Journal of the RSJ, 27*(6), 652-660.

Kishi, K., Nakamoto, H., Hashizume, M., Fujie, M., Sakuma, I., & Dohi, T. (2007). Compact manipulator system for guiding needle with real-time navigation based on MR images. *Journal of the Society of Computer Aided Surgery, 9*(2), 103-111.

Kita, N., Rougeaux, S., Kuniyoshi, Y., & Sakane, S. (1995). Real-time Binocular Tracking Based on Virtual Horopter. *Journal of the Robotics Society of Japan, 13*(5), 101-108.

Kitagaki, K., Suehiro, T., Ogasawara, T., & Liu, Y.-H. (1997). Sensor Based Parallel Processing Manipulation System: TAKUMI. *Journal of the RSJ, 15*(3), 363-372.

Kobayashi, H., Hara, F., Uchida, G., & Ohno, M. (1994). Study on face robot for active human interface -mechanisms of face robot and facial expressions of 6 basic emotions. *Journal of the Robotics Society of Japan, 12*(1), 155-163.

Kobayashi, M., Urabe, H., Ogawa, S., Haruta, Y., Akamatsu, M., & Koike, M. (2000). Off-line Teaching System of a Robot Cell for Steel Pipes. *Proceedings of 18th Annual Conference of the RSJ, 2*, 707-708.

Kohei Okumura, H. O., Masatoshi Ishikawa,. (2011). Optical Gaze Control System to Realize More High-speed Active Vision. *Journal of the Robotics Society of Japan, 29*(2), 201-211.

Kohno, Y., Kondo, N., Iida, M., Kurita, M., Shiigi, T., Ogawa, Y., . . . Okamoto, S. (2011). Development of a Mobile Grading Machine for Citrus Fruit. *Engineering in Agriculture, Environment and Food, 4*(1), 7-11. doi: http://dx.doi.org/10.1016/S1881-8366(11)80002-9

Koichi Suzumori. (1989). Flexible Microactuator (1 st report, Static characteristics of 3-DOF actuator). *Transactions of the JSME Series C, 55*(518), 2547-2552.

Koichi Suzumori, S. I., Hirohisa Tanaka,. (1986-7). *Development of Micromanipulator (1)*. Paper presented at the Proc. of 6th Annual Conf. of the RSJ.

Koji Ikuta, M. N. (1998). General Safety Evaluation Method of Control Stratagy for Welfare Robot. *Proc. of 3th Robotics Symposia*, 119-126.

Koji IKUTA, M. N. (1999a). *General Evaluation Method of Safety for Human-Care Robots*. Paper presented at the Proc. of the 1999 IEEE Robotics and Automation Conference (ICRA'99).

Koji Ikuta, M. N. (1999b). General Evaluation Method of Safety Strategies for Welfare Robot - Evaluation of Safety Design by Quantifying Dangerousness. *Journal of the Robotics Society of Japan, 17*(3), 363-370 (in japanese).

Koji Ikuta, M. N., Hideki Ishii,. (2001). General Danger Evaluation Method for Control Strategy of Human-care Robot. *Journal of the Robotics Society of Japan, 19*(1), 81-90 (in Japanese).

Kondo, N. (2010). Automation on fruit and vegetable grading system and food traceability. *Trends in Food Science & Technology, 21*(3), 145-152. doi: http://dx.doi.org/10.1016/j.tifs.2009.09.002

Kondo, N., Monta, M., & Fujiura, T. (1996). Fruit harvesting robots in Japan. *Advances in Space Research, 18*(1–2), 181-184. doi: http://dx.doi.org/10.1016/0273-1177(95)00806-P

Kondo, N., Nishitsuji, Y., Ling, P. P., & Ting, K. C. (1996). Visual Feedback Guided Robotic Cherry Tomato Harvesting. *39*(6). doi: https://doi.org/10.13031/2013.27744

Kondo, N., Yamamoto, K., Shimizu, H., Yata, K., Kurita, M., Shiigi, T., . . . Nishizu, T. (2009). A Machine Vision System for Tomato Cluster Harvesting Robot. *Engineering in Agriculture, Environment and Food, 2*(2), 60-65. doi: http://dx.doi.org/10.1016/S1881-8366(09)80017-7

Korayem, M. H., Shafei, A. M., & Seidi, E. (2014). Symbolic derivation of governing equations for dual-arm mobile manipulators used in fruit-picking and the pruning of tall trees. *Computers and Electronics in Agriculture, 105*, 95-102. doi: http://dx.doi.org/10.1016/j.compag.2014.04.013

Kosei Kitagaki, T. S., Tsukasa Ogasawara, Yun-Hui Liu,. (1997). Sensor Based Parallel Processing Manipulation System: TAKUMI. *Journal of the RSJ, 15*(3), 363-372.

Kosuge, K., Furuta, K., & Yokoyama, T. (1988). Virtual internal model following control system - application to mechanical impedance control *Transactions of the SICE, 24*(1), 55-62.

Kosuke Kishi, Hidekazu Nakamoto, M. H. M. G. F. I. S. T. D. (2007). Compact Manipulator System for Guiding Needle with Real-time Navigation Based on MR Images. *Journal of the Society of Computer Aided Surgery, 9*(2), 103-111.

Kosuke Kishi, Masakatsu G Fujie, Makoto Hashizume, Ichiro Sakuma, Takeyoshi Dohi. (2009). MR-compatible Surgical Support Manipulator System with Rod-driven Instruments. *Journal of the RSJ, 27*(6), 652-660.

kotani, S., Mori, H., & Charkari, N. M. (1996). anger estimation of the Robotic Travel Aid(RoTA) at Intersection. *Robotics and Automation systems 18*, 232-235.

Kouji Murakami, T. H., Yoshihiko Kimuro, Yosuke Senta, Takafumi Ienaga, Daisaku Arita, Ryo Kurazume,. (2008). A Method to Manage Data Flow between Intelligent Robots and an Intelligent Environment. *Journal of the Robotics Society of Japan, 26*(2), 192-199.

Kousuke. Sato, S. I. (1988). Liquid Crystal Range Finder - High Speed Range Imaging System Using Liquid Crystal Shutter *Transaction of IECE, J71-D*(7), 1249-1257.

Kunikatsu Takase. (1976). Generalized Decomposition and Control of a Motion of a Manipulator. *Transactions of the SICE, 12*(3), 300-306.

Kuniyoshi, H, I., & M, I. (1991). Teaching by Showing : Generating Robot Command Sequences Based on Real Time Visual Recognition of Human Pick and Place Actions. *Journal of the Robotics Society of Japan, 9*(3), 295-303 (in Japanese).

Kurashiki, K., Fukao, T., Ishiyama, K., Kamiya, T., & Murakami, N. (2010, 21-22 Dec. 2010). *Orchard traveling UGV using particle filter based localization and inverse optimal control*. Paper presented at the 2010 IEEE/SICE International Symposium on System Integration.

Kurashiki, K., Fukao, T., Nagata, J., Ishiyama, K., Kamiya, T., & Murakami, N. (2010). Laser-based Vehicle Control in Orchard. *IFAC Proceedings Volumes, 43*(26), 127-132. doi: http://dx.doi.org/10.3182/20101206-3-JP-3009.00022

Kurita, H., Iida, M., Suguri, M., & Masuda, R. (2012). Application of Image Processing Technology for Unloading Automation of Robotic Head-Feeding Combine Harvester. *Engineering in Agriculture, Environment and Food, 5*(4), 146-151. doi: http://dx.doi.org/10.1016/S1881-8366(12)80011-5

Kyoichi, T. (2000). A Beach Ball Volley Playing Robot with a Human. *Journal of the RSJ, 18*(5), 721-727.

Lee, H.-Y., & Liang, C.-G. (1988). Displacement analysis of the general spatial 7-link 7R mechanism. *Mechanism and Machine Theory, 23*(3), 219-226. doi: http://dx.doi.org/10.1016/0094-114X(88)90107-3

Lee, J.-E., Kim, J.-H., Kim, S.-J., Kim, Y.-G., Lee, J.-H., & Park, G.-T. (2012). Human and robot localization using histogram of oriented gradients(HOG) feature for an active information display in intelligent space. *Advanced Science Letters (ASL), 9*, 99-106.

Lee, J. H., Cho, S. I., & Lee, J. Y. (1998). Autonomous speed sprayer using DGPS and fuzzy control (1). J. Korean Soc. *Agric. Mach, 23*(1), 21-24 (in Korean with English abstract).

Lee, K.-H., & Ehsani, R. (2008). Comparison of two 2D laser scanners for sensing object distances, shapes, and surface patterns. *Computers and Electronics in Agriculture, 60*(2), 250-262. doi: http://dx.doi.org/10.1016/j.compag.2007.08.007

Libin, Z., Qinghua, Y., Guanjun, B., Yan, W., Liyong, Q., Feng, G., & Fang, X. (2008). Overview of research on agricultural robots in China. *International Journal of Agricultural and Biological Engineering, 1*(1), 12-21.

Luciano, C. A., Pimenta, G. A. S., Pereira, M., Goncalves, M., Michael, N., Turpin, M., & Kumar, V. (2013). Decentralized Controllers for Perimeter Surveillance with Teams of Aerial Robots. *Advanced Robotics, 27*(9), 697-709.

Ludger O. Figura, & Teixeira, A. A. (2007). *Food Physics, Physical Properties — Measurement and Applications*.

M, M., & T, Y. (1964). Mechanical Fingers as Control Organ and Its Fundamental Analyses. *Preprints of Joint Automatic Control Conference, USA*, 106-113.

M, N., & N, S. (2009). Development of Image Recognition Device and Image Rcecognition Module. *Journal of the Robotics Society of Japan, 27*(2), 8-12.

M, T. (2001). Development of mini assembly plant CAC -Circular Assembly Cell. *Journal of the RSJ, 19*(1), 37-38.

M. Mitsuishi, S. W., Y.Hatamura, and T. Nagao, B.Kramer,. (1992). A User-Friendly Manufacturing System for "Hyper-Environments". *Proceedings of the 1992 IEEE International Conference on Robotics and Automation*, 25-31.

M. Oda. (2000). Attitude Control experiments of a Robot Satellite. *Journal of Spacecraft and Rockets, 37*(6), 788-793, American Institute of Aeronautics and Astronautics, 2000.

Machida, K., Toda, Y., Iwata, T., & Komatsu, T. (1992). Smart end effector for dexterous manipulation in space. *J. of Guidance, Control, and Dynamics, 15*(1), 10-16.

Mae, Y., Takahashi, Y., Arai, T., Inoue, K., & Koyachi, N. (2004). Omni-directional Locomotion of Robots with Limb Mechanism. *Journal of Robotics Society of Japan, 22*(3), 329-335.

Maeda, H., Fujiwara, S., Kitano, H., & Yamashita, H. (2002). Development of the Omni directional Power-assisted Cart. *Advanced Robotics, 15*(3), 351-356.

Maeno, T., Hiromitsu, S., & Kawa, T. (2001). Control of Grasping Force by Estimating Stick/Slip Distribution at the Contact Interface of an Elastic Finger Having Curved Surface. *Journal of the Robotics Society of Japan, 19*(1), 91-99.

Makino, H., Murata, M., & Furuya, N. (1982). Development of the SCARA Robot. *Seimitsu-Kikai (J. of JSPE), 48*(3), 378-383.

Makoto, J., Fumio, O., Takashi, Y., Tyoichi, T., Mikio, T., Masakazu, K., . . . Shintaro, N. (199). Development of a Force-Controlled Finishing Robot System with a Task-Directed Robot Language. *Journal of the RSJ, 14*(8), 1178-1185.

Makoto, K., & Toshiharu, N. (1993). Basic Study of Six-Axis Force Sensor Design Based on Combination Theory. *Journal of the Robotics Society of Japan, 11*(8), 157-167.

Makoto Kaneko, T. K., Satoshi Matsunaga, Toshio Tsuji, Shinji Tanaka,. (2003). *Touching Stomach by Air*. Paper presented at the IEEE International Conference on Robotics and Automation.

Manabu, H., Kazuhiko, S., Tetsuji, H., Shin'ichi, K., & Shotaro, I. (1999). Development of Vision System for Logistics Robot using Stereo Vision with Random-dot Pattern Projection. *Journal of the RSJ, 17*(1), 48-49.

Masahiko, N., Yoshihiko, M., Miwa, U., Keiju, O., Hiroyuki, N., Ryota, H., . . . Yuka, K. (2009). Developement of RSNP (Robot Service Network Protocol) 2.0 Targeting a Robot Service Platform in Diffusion Period. *Journal of the RSJ, 27*(8), 857-867.

Masahiko NARITA, Y. M., Miwa UEKI, Keiju OKABAYASHIi, Chuzo AKIGUCHI, Ryota HIRUTA, Hideyuki KURATA, Yuka KATO,. (2010). RSi Activity to Realize and Support Actual Robot Service Developments on the Internet. *Journal of the RSJ, 28*(7), 829-840.

Masahiko NARITA, Yoshihiko MURAKAWA. (2011). Standardization on Robot Service and RSi (Robot Service Initiative) Activities. *Journal of the RSJ, 29*(4), 353-356.

MasakiOshima, Y. S. (1982). Object Recognition Using Tree-Dimentional Information. *Transaction of IECE, j65-D*(5), 30-35.

Masaru Ishii, Tadashi Nadata,. (1974). Feature Extraction of 3-Dimensional Objects with a Laser Tracker. *Transactions of SICE, 10*(5), 599-605.

Masaru Uchiyama. (1979a). Study of the Computer Control of the Motion of a Mechanical Arm (1st Report, Calculation of the Coordinative Motion Considering Singular Points). *Transactions of the JSME, Series C, 45*(391), 314-322.

Masaru Uchiyama. (1979b). Study of the Computer Control of the Motion of a Mechanical Arm (2nd Report, Control of the Coordinative Motion Utilizing a Mathematical Model). *Transactions of the JSME, Series C, 45*(391), 323-335.

Masaru Uchiyama. (1979c). Study of the Computer Control of the Motion of a Mechanical Arm (3rd Report, Dynamic Vision and Visual Feedback). *Transactions of the JSME, Series C, 45*(391), 336-345.

Masaru Uchiyama and Ken-ichi Iimura, F. P. a. P. D., Kunihiko Unno, Osamu Toyama,. (1992). *A New Design of a Very Fast 6-DOF Parallel Robot*. Paper presented at the PROCEEDINGS 23rd International Symposium on Industrial Robots, Barcelona.

Masaru Uchiyama, T. S., Kazuyuki Masukawa,. (1996). Dynamic Control Experiment on a Parallel Robot HEXA. *Journal of the Robotics Society of Japan, 14*(2), 297-304.

Masaru. Uchiyama, Y. N., Kyojiro. Hakomori,. (1987). Evaluation of Robot Force Sensor Structure Using Singural Value Decompsition. *Journal of the RSJ, 5*(1), 4-10.

Masaru. Uchiyama, Y. N., Kyojiro. Hakomori,. (1991). Evaluation of the RobotForce Sensor Structure Using Singular Value Decomposition. *Advanced Robotics, 5*(1), 39-52.

Masatoshi Ishikawa, M. S. (1981). A Method for Measuring the Center Position of a Two Dimensional Distributed Load Using Pressure-Conductive Rubber. *Transactions of SICE, 17*(9), 945-950.

Masayoshi, K., Taketoshi, M., & Tadashi, N. (1973). A Study of a Memory Structure and Its Application to a Route- Finding Problem for an Intelligent Robot. *Transactions of the Society of Instrument and Control Engineers, 9*(1), 45-50 (in Japanese).

Masayuki, I., & Hirochika, I. (1983). *Hand Eye Coordination in Rope Handling*. Paper presented at the The First International Symposium, The MIT Press, Michael Brady and Richard Paul.
Masayuki, I., & Hirochika, I. (1985). Hand Eye Coordination in Rope Handling. *Journal of the RSJ, 3*(6), 32-41.
Masayuki, I., & Hirochika, I. (1987). Rope Handling by a Robot with Visual Feedback. *Advanced Robotics, 2*(1), 39-54.
Masayuki Inaba, Y. H., Hirochika Inoue,. (1998). A full-Body Tactile Sensor Suit Using Electrically Conductive Fabric. *Journal of the Robotics Society of Japan, 16*(1), 80-86.
Matsuoka, K. (1977). *A model of repetitive hopping movements in man*. Paper presented at the Proceedings of 5th World Congress of Theory of Machines and Mechanisms.
Matsushima, T., Kanamori, K., & Ohteru, S. (1985). Automated Recognition System of Musical Score (Vision System of the WABOT-2). *Journal of the RSJ, 3*(4), 354-360.
Matsuyama, J. (2001). Small-size and high-precision robot with closed-loop mechanism. *Journal of the RSJ, 19*(1), 41-42.
Mayumi, U. (1994). Compliant Motion Control of Arm-Hand System. *Yaskawa Technical Review, 224th issue, 58*(3), 183-188.
McFarlane, N. J. B. (1991). A computer-vision algorithm for automatic guidance of microplant harvesting. *Computers and Electronics in Agriculture, 6*(2), 95-106. doi: http://dx.doi.org/10.1016/0168-1699(91)90026-6
Minegishi, R., Takashima, A., Kurabayashi, D., & Kanzaki, R. (2012). Construction of a brain-machine hybrid system to evaluate adaptability of an insect. *Robotics and Autonomous Systems, 60*(692-699).
Miomir, V. (1989). *Applied dynamics of manipulation robots (Modelling, Analysis and Examples)*: Springer.
Mitrovic, D. (2006). *Learning motor control for simulated robot arms*. Master of Science, University Of Edinburgh.
Mitsubishi Electronic. (2014). Servo Amplifiers and Motors, Biginners manual, MR-J4-A(-RJ)/A4(-RJ), MR-J4-B(-RJ)/B4(-RJ), Mr-J4W-B.
Mitsubishi Electronic. (2015). C Controller/Personal Computer Embedded Type Servo System Controllers.
Mitsushige, O. (1997). Coordinated Control of the Satellite's Attitude and Its Manipulator Stability of the Satellite Attitude Against the Robot Arm Motion. *Journal of the Robotics Society of Japan, 15*(4), 590-600 (in Japanese).
Miura, J., & Ikeuchi, K. (1999). Task planning of assembly of flexible objects and vision-based verification. *Robotica, 16*(3), 297-307.
Miyagawa, T., Suzumori, K., Kimura, M., & Hasegawa, Y. (1999). Development of Micro Inspection Robot for Small Piping. *Journal of the Robotics Society of Japan, 17*(3), 389-395.
Miyazaki, F., & Arimoto, S. (1980). A Control Theoretic Study on Dynamical Biped Locomotion. *ASME Journal of Dynamic Systems, Measurement, and Control, 102*(233-239).
Montalvo, M., Pajares, G., Guerrero, J. M., Romeo, J., Guijarro, M., Ribeiro, A., . . . Cruz, J. M. (2012). Automatic detection of crop rows in maize fields with high weeds pressure. *Expert Systems with Applications, 39*(15), 11889-11897. doi: http://dx.doi.org/10.1016/j.eswa.2012.02.117
Mori, H., Charkari, N. M., & Matsushita, T. (1994). On-Line Vehicle and Pedestrian Detection Based on Sign Pattern. *IEEE Trans. On Industrial Electronics, 41*(4).
Mori, M. (1970). Uncanny Valley. *Energy, Esso Standard Japan, 7*, 33-35 (In Japanese).
Mori, M. (2012, June 2012). The Uncanny Valley. *IEEE ROBOTICS & AUTOMATION magazine, 7*, 98-100.
Morita, T. (1999). Tracking vision system for real-time motion analysis. *Advanced Robotics, 12*(6), 609-617.
Murakami, N., Ito, A., Will, J. D., Steffen, M., Inoue, K., Kita, K., & Miyaura, S. (2008). Development of a teleoperation system for agricultural vehicles. *Computers and Electronics in Agriculture, 63*(1), 81-88. doi: http://dx.doi.org/10.1016/j.compag.2008.01.015
Nagasaka, Y., Umeda, N., Kanetai, Y., Taniwaki, K., & Sasaki, Y. (2004). Autonomous guidance for rice transplanting using global positioning and gyroscopes. *Computers and Electronics in Agriculture, 43*(3), 223-234. doi: http://dx.doi.org/10.1016/j.compag.2004.01.005
Nakabo, Y., Ishii, I., & Ishikawa, M. (1997). 1 ms Target Tracking System Using Massively Parallel Processing Vision. *Journal of the Robotics Society of Japan, 15*(3), 417-421.
Nakamura, Y., Yamane, K., & Nagashima, F. (1998). Dynamics Computation of Structure-Varying Kinematic Chains and Its Application to Human Figures. *Journal of the Robotics Society of Japan, 16*(8), 124-131.
Nakano, E., Ozaki, S., Ishida, T., & Kato, I. (1974). *Cooperational Control of the Anthropomorphous Manipulator "MELARM"*. Paper presented at the Proc. 4th International Symposium on Industrial Robots.
Nakashima, K., Hasunuma, H., Habata, O., & Kanazawa, H. (2012). Development of the automatic cell processing machine in the Kawasaki Heavy Industries, LTD. *Regenerative Medicine, 11*(3), 58-62.
Nakayama, A., Machino, T., Kitagishi, I., Iwaki, S., & Okudaira, M. (2005). A Proposal of MotionMedia Contents Sharing via Audio and its Application to Network Communication Services. *Journal of the RSJ, 23*(5), 96-105.
NASA. (1994). *Engineering drawing standards manual*: Mechanical Engineering Branch Goddard Space Flight Center Greenbelt, Maryland.
Nishiwaki, K., & Kagami, S. (2011). Robust Walking Control of Humanoids on Unknown Rough Terrain via Short Cycle Motion Generation Using Absolute Position Estimates. *Journal of the Robotics Society of Japan, 29*(1), 111-121.
Noborio, H., & Arimoto, S. (1989). Proximity two point determination algorithm of robot and obstacle using octree. *Journal of the Robotics Society of Japan, 7*(3), 151-160 (in japanese).
Noborio, H., Fukuda, S., & Arimoto, S. (1987a). BRepからオクトツリーへの変換アルゴリズムとその評価. *Transactions of Information Processing Society of Japan, 28*(10), 1003-1012 (in Japanese).

Noborio, H., Fukuda, S., & Arimoto, S. (1987b). A New Interference Check Algorithm Using Octree. *Proceedings of the 1987 IEEE International Conference on Robotics and Automation*, 1480.

Noborio, H., Fukuda, S., & Arimoto, S. (1987). A new interference check algorithm using octree representation. *Journal of the RSJ, 5*(3), 189-198 (in Japanese).

Noborio, H., Fukuda, S., & Arimoto, S. (1988a). Construction ofthe Octree Approximating Three-Dimensional Objects by Using Multiple Views. *IEEE Trans. on Pattern Analysis and Machine Intelligence, PAMI-10*(6), 769-782.

Noborio, H., Fukuda, S., & Arimoto, S. (1988b). 複数枚の画像を用いて３次元物体を近似したオクトツリーを生成する一手法. *Transactions of Information Processing Society of Japan, 29*(2), 178-189 (in japanese).

Noboru Tsunashima, S. K. (2009). Reproduction of Human Motion Using Different Structural Haptic System. *Proc. of RSJ 2006, AC3H3-06*.

Noguchi, N., & Barawid Jr, O. C. (2011). Robot Farming System Using Multiple Robot Tractors in Japan Agriculture. *IFAC Proceedings Volumes, 44*(1), 633-637. doi: http://dx.doi.org/10.3182/20110828-6-IT-1002.03838

Ogasawara, T., & Inoue, H. (1984). COSMOS: A Total Programming System for Integrated Intelligent Robot. *Journal of the RSJ, 2*(6), 507-525 (in Japanesee).

Ohmichi, T., & Ibe, T. (1984). Development of Vehicle with Legs and Wheels. *Journal of the Robotics Society of Japan, 2*(3), 244-251.

Ohteru, S., Shirai, K., & Narita, S. (1985). The Robot Musician 'WABOT-2' (WAseda roBOT-2). *Journal of the RSJ, 3*(4), 337-338.

Okada, T., & Sanemori, T. (1987). MOGRER: A Vehicle Study and Realization for In-Pipe Inspection Tasks. *IEEE J. of Robotics and Automation, 3*(6), 573-582.

Okada, T., Tanaka, W., Botelho, A., & Shimizu, T. (2011). Driving Mechanism of a Legged and Wheeled Mobile Robot with Minimal DOFs and Control for Reversible Switching between Walking and Rolling. *Journal of the Robotics Society of Japan, 29*(3), 306-316.

Okada, T., Tezuka, S., & Sasaki, Y. (2011). *Sensor-Based Control of a Skid-Steering Mobile Robot Combined with Feet for Moving on All Terrain*. Paper presented at the Proc. of the 14th Conf. on CLAWAR, UPMC(Paris), pp.666-675, September 6th.

ONISH, K. (1998). The Open Controller of the MHI PA-10 Robot. *Journal of Japan Robot Association "Robot", 121*, 34-38.

OTC Daihen Inc. (Japan). OTC Daihen official website Retrieved http://www.daihen-usa.com/

Panasonic, C. (2011). Tele-communication assist robot HOSPI-Rimo, from http://panasonic.co.jp/corp/news/official.data/data.dir/jn110926-1/jn110926-1.html

Patterson, D., & Hennessy, J. (2012). *Computer Organization and Design: The Hardware/Software Interface*.

Pérez-Ruiz, M., Gonzalez-de-Santos, P., Ribeiro, A., Fernandez-Quintanilla, C., Peruzzi, A., Vieri, M., . . . Agüera, J. (2015). Highlights and preliminary results for autonomous crop protection. *Computers and Electronics in Agriculture, 110*, 150-161. doi: http://dx.doi.org/10.1016/j.compag.2014.11.010

Peter, W. S., & Michael, J. D. (1988). Computer Vision to Locate Fruit on a Tree. *31*(1). doi: 10.13031/2013.30697

Pettersson, A., Davis, S., Gray, J. O., Dodd, T. J., & Ohlsson, T. (2010). Design of a magnetorheological robot gripper for handling of delicate food products with varying shapes. *Journal of Food Engineering, 98*(3), 332-338. doi: http://dx.doi.org/10.1016/j.jfoodeng.2009.11.020

Pettersson, A., Ohlsson, T., Davis, S., Gray, J. O., & Dodd, T. J. (2011). A hygienically designed force gripper for flexible handling of variable and easily damaged natural food products. *Innovative Food Science & Emerging Technologies, 12*(3), 344-351. doi: http://dx.doi.org/10.1016/j.ifset.2011.03.002

Plá, F., Juste, F., & Ferri, F. (1993). Feature extraction of spherical objects in image analysis: an application to robotic citrus harvesting. *Computers and Electronics in Agriculture, 8*(1), 57-72. doi: http://dx.doi.org/10.1016/0168-1699(93)90058-9

Qiao, J., Sasao, A., Shibusawa, S., Kondo, N., & Morimoto, E. (2005). Mapping Yield and Quality using the Mobile Fruit Grading Robot. *Biosystems Engineering, 90*(2), 135-142. doi: http://dx.doi.org/10.1016/j.biosystemseng.2004.10.002

R, M., T, S., H, U., H, N., K, M., & H, K. (2010). Practical Design and Use of Transfer System by Autonomous Mobile Robot Group. *Journal of the RSJ, 28*(3), 71-78.

R.L. Schafer, & Young, R. E. (1979). An automatic guidance system for tractors. *Trans. ASAE,, 22*(1), 46-49,56.

Raghavan, M., & Roth, B. (1990). Inverse kinematics of the general 6R manipulator and related linkages. *Transactions of the ASME, Journal of Mechanical Design, 115*, 228-235.

Rajendra, P., Kondo, N., Ninomiya, K., Kamata, J., Kurita, M., Shiigi, T., . . . Kohno, Y. (2009). Machine Vision Algorithm for Robots to Harvest Strawberries in Tabletop Culture Greenhouses. *Engineering in Agriculture, Environment and Food, 2*(1), 24-30. doi: http://dx.doi.org/10.1016/S1881-8366(09)80023-2

Raparelli, T. (2011). Development of a new harvesting module for saffron flower detachment. *Romanian review of precision mechanics, optics & mechatronics, 39*, 163-168.

Rath, T., & Kawollek, M. (2009). Robotic harvesting of Gerbera Jamesonii based on detection and three-dimensional modeling of cut flower pedicels. *Computers and Electronics in Agriculture, 66*(1), 85-92. doi: http://dx.doi.org/10.1016/j.compag.2008.12.006

Reid, J. F., Zhang, Q., Noguchi, N., & Dickson, M. (2000). Agricultural automatic guidance research in North America. *Computers and Electronics in Agriculture, 25*(1–2), 155-167. doi: http://dx.doi.org/10.1016/S0168-1699(99)00061-7

Roshanianfard, A., & Noguchi, N. (2016). Development of a 5DOF robotic arm (RAVebots-1) applied to heavy products harvesting. *IFAC-PapersOnLine, 49*(16), 155-160. doi: http://dx.doi.org/10.1016/j.ifacol.2016.10.029

Roshanianfard, A., & Noguchi, N. (2017). *Development of a heavyweight crop robotic harvesting system (HRHC)*. Paper presented at the The 3rd International Conference on Control, Automation and Robotics (ICCAR 2017), Nagoya, Japan.

Roshanianfard, A., & Noguchi, N. (2018). Kinematics analysis and simulation of a 5DOF articulated robotic arm applied to heavy products harvesting. *Tarim Bilimleri Dergisi-Journal of Agricultural Sciences, 24*(1).

Roshanianfard, A., & Shahgholi, G. (2017). Performance Characterization of Automatic Creep Testing Device for Agricultural Product. *33*(3). doi: 10.13031/aea.12122

Roy, H. (1987). Economic Analysis of Robotic Citrus Harvesting in Florida. *30*(2), 298. doi: 10.13031/2013.31943

RSJ. (2015). RSJ, The robotics society of Japan, from http://www.rsj.or.jp/en

Ryo, K., Yukihiro, T., Kouji, M., & Tsutomu, H. (2007). Study on CPS SLAM - 3D Laser Measurement System for Large Scale Architectures. *Journal of the Robotics Society of Japan, 25*(8), 1234-1242.

Ryosuke Masuda, S. S., Kensuke Hasegawa,. (1981). Optical Proximity Sensor by Using Phase Information. *Transactions of SICE, 17*(9), 945-950.

S. Hirose, S. O., Y. Umetani,. (1981). Active Cord Mechanism with Oblique Swivel Joints and Its Control. *Transactions of the SICE, 17*(6), 686-692.

S.Fujii, & S.Kurono. (1975). Co-ordinated Computer Control of a pair of Manipulators. *Proceedings of 4th World Congress of the Theory of Machines and Mechanisms*, 411-417.

S.Sakakibara, A.Terada, & K.Ban. (1996). *An Innovative Automatic Assembly System Where a Two-armed Intelligent Robot Builds Mini Robots*. Paper presented at the 27th International Symposium on Industrial Robots (ISIR).

Saito, M., Tamaki, K., Nishiwaki, K., Nagasaka, Y., & Motobayashi, K. (2013). Development of Robot Combine Harvester for Beans using CAN Bus Network. *IFAC Proceedings Volumes, 46*(18), 148-153. doi: http://dx.doi.org/10.3182/20130828-2-SF-3019.00058

Sakai, S., Iida, M., Osuka, K., & Umeda, M. (2008). Design and control of a heavy material handling manipulator for agricultural robots. [journal article]. *Autonomous Robots, 25*(3), 189-204. doi: 10.1007/s10514-008-9090-y

Sakakibara, o., Kan, K., Hosoda, Y., Hattori, M., & Fujie, M. (1990). Low Impact Foot Trajectory for a Quadruped Walking Machine. *Journal of the Robotics Society of Japan, 8*(6), 662-671.

Saku Egawa, T. N., Toshiro Higuchi,. (1997). Pulse-driven Induction-type Electrostatic Film Actuator. *Journal of the Robotics Society of Japan, 15*(3), 61-68.

Sarig, Y. (1993). Robotics of Fruit Harvesting: A State-of-the-art Review. *Journal of Agricultural Engineering Research, 54*(4), 265-280. doi: http://dx.doi.org/10.1006/jaer.1993.1020

Sato, T., & Hirai, S. (1987). Language-Aided Teleoperation System (LARTS) for Advanced Teleoperation System. *IEEE J. Robotics and Automation, AR-3*(5).

Satoru, G. (2011). *ROBOT ARMS*. InTech.

Satoshi, K., Masayuki, I., & Hirochika, I. (1997). Construction and Implementation of Software Platform in Remote-Brained Robot Approach. *Journal of the Robotics Society of Japan, 15*(4), 548-553 (in Japanese).

Sawada, T., & Kanohara, N. (1982). マイクロロボット≪ムーブマスター≫とそのコントローラにおけるマイクロコンピュータ技術 *Mitsubishi Electric Technical Report* (Vol. 56).

SBJ. (2015). *Statistical handbook of Japan,* : Statistics Bureau Ministry of Internal Affairs and Communications Japan.

SBJ. (2016). *Statistical handbook of Japan,* : Statistics bureau ministry of internal affairs and communications Japan.

Seiichi, M. (1995). Factors Associated with and Fitness Effects of Nest-Raiding in the Three-Spined Sticleback, Gasterosteus Aculeatus, in a natural Situation. *Behaviour 132*, 1012-1023.

Seiichiro, K., Yuki, Y., & Kiyoshi, O. (2009). Stability Analysis and Experimental Validation of a Motion-Copying System. *IEEE Transactions on Industrial Electronics, 56*(10), 3096-3913.

Senoo, T., Namiki, A., & Ishikaw, M. (2008). *High-speed Throwing Motion Based on Kinetic Chain Approach*. Paper presented at the Proc. of IEEE/RSJ Int. Conf. on Intelligent Robots and Systems.

Senoo, T., Namiki, A., & Ishikawa, M. (2004). *High-Speed Batting Using a Multi-Jointed Manipulator*. Paper presented at the Proc. of IEEE Int. Conf. on Robotics and Automation.

Senoo, T., Namiki, A., & Ishikawa, M. (2006). *Ball Control in High-Speed Batting Motion using Hybrid Trajectory Generator*. Paper presented at the Proc. of IEEE Int. Conf. on Robotics and Automation.

Serdar, K., & Zafer, B. (2006). Industrial robotics theory modeling and control. In C. Sam (Ed.), (pp. 964).

Shamshiri, R., Ismail, W., & Ishak, W. (2012). Nonlinear tracking control of a two link oil palm harvesting robot manipulator. *International Journal of Agricultural and Biological Engineering, 5*(2), 9-19.

Shanhai Jin, R. K., Motoji Yamamoto,. (2012). Realtime Quadratic Sliding Mode Filter for Removing Noise. *Advanced Robotics, 26*(8-9), 877-896.

Shanhai Jin, R. K., Motoji Yamamoto,. (2014). Improving Velocity Feedback for Position Control by Using a Discrete-Time Sliding Mode Filtering with Adaptive Windowing. *Advanced Robotics, 28*(14), 943-953.

Sheng, C. T., Chen, C. H., & Hwang, Y. S. (1997). *Development of an ultrasonic autonomous vehicle I agriculture*. Paper presented at the Proc. ARBIP95, vol. 1, 3–6 November 1996, Kobe University, Kobe,.

Shigeo Hirose, Y. U. (1981). *An Active Cord Mechanism with Oblique Swivel Joints and Its Control*. Paper presented at the Proc. 4th RoManSy Symp., Zaborow, Poland, PWN-Polish Scientific Publishers.

Shigeoki, H., & Tomomasa, S. (1984). Language Directed Master-Slave Manipulation Method Using LARTS/T. *Journal of the Robotics Society of Japan, 2*(6), 526-535.

Shigeoki Hirai, T. S. (1984). A Language Based Master-Slave Manipulator System. *Transactions of the Society of Instrument and Control Engineers, 20*(1), (in Japanese).

Shigeyuki Hirai, T. S., Toshihiro Matsui,. (1990). *Integration of a Task Knowledge Base and a Cooperative Maneuvering System for a Telerobot: MEISTER*. Paper presented at the IEEE Int.Workshop on Intelligent Robots and Systems.

Shimon, Y. N. (1999). *Handbook of Industrial Robotic, 2nd Edition*.

Shimonabe, N., Onishi, K., Ohira, M., Hinami, K., & Sugiura, A. (2012). Advanced INLAY System for Reactor Vessel. *Journal of Japan Robotics Society, 30*(1), 47-78.

Shin'ichiro Nakaoka, A. N., Fumio Kanehiro, Kenji Kaneko, Mitsuharu Morisawa, Hirohisa Hirukawa, Katsushi Ikeuchi,. (2007). Learning from Observation Paradigm: Leg Task Models for Enabling a Biped Humanoid Robot to Imitate Human Dances. *International Journal of Robotics Research, 26*(8), 829-844.

Shinichi Hirai, H. A., Hidekatsu Tokumaru. (1988). Kinematics of Manipulation Using the Theory of Polyhedral Convex Cones and Its Applications to Grasping and Assembly Operations. *Transactions of the SICE, 24*(12), 1284-1291.

Shinichiro, N., Atushi, N., Fumio, K., Kenji, K., Mitsuharu, M., & Katsushi, I. (2005). *Task Model of Lower Body Motion for a Biped Humanoid Robot to Imitate Human Dances*. Paper presented at the Proceedings of the 2005 IEEE/RSJ International Conference on Intelligent Robots and Systems.

Shinichiro Nakaoka, A. N., Fumio Kanehiro, Kenji Kaneko, Mitsuharu Morisawa, Hirohisa Hirukawa, Katsushi Ikeuchi,. (2006). Leg Task Models for Reproducing Human Dance Motions on Biped Humanoid Robots *Journal of the RSJ, 24*(3), 388-399.

Shinji, K., Murase, Y., Okabayashi, K., Ueki, M., Yusuke, Y., Sawazaki, N., . . . Tsuno, A. (2005). Development of Service Robot "enon". *robotics, 167*, 13-18.

Shirai, K., & Fujisawa, H. (1974). An algorithm for spoken sentence recognition and its application to the speech input-output system. *IEEE Trans. Systems, Man and Cybernetics, 4*(5), 475-479.

Shirai, K., Kobayashi, T., Iwata, K., & Fukasawa, Y. (1985). Speech I/O System Realizing Flexible Conversation for Robot - The Conversational System of WABOT-2. *Journal of the RSJ, 3*(4), 362-371.

Shirai, Y. (1976). A Method for Recognition of Complex Objects from Light Intensity Data. *Journal of the IPS, 17*(7), 611-617.

Shusaku, N. (2000). Development of Steam Generator Tube Sheet Walking Robot "MR-III" and the Present State of the Automatic Eddy Current Test System.

Şirinterlikçi, A., Tiryakioğlu, M., Bird, A., Harris, A., & Kweder, K. (2009). Repeatability and accuracy of an industrial robot: Laboratory experience for a design of experiments course. *The technology interface journal*.

Sissons, R. (1939). Plowing in circles saves time. *Prairie Farmer, 111*(20), 7.

Sogo, T., Ishiguro, H., & Ishida, T. (1999). Mobile Robot Navigation by Distributed Vision Agents. *Approaches to Intelligent Agents (H. Nakashima and C. Zhang Eds.), Lecture Notes in Artificial Intelligence, 1733, Springer-Verlag, Berlin, pp. 96-110, 1999. (Second Pacific Rim International Workshop on Multi Agents (PRIMA'99))*.

Starcevic, N., Thullner, C., Bux, M., & Müller, J. (2010). 3D path planning for a biomass processing robot via motion simulation. *Robotics and Computer-Integrated Manufacturing, 26*(1), 109-118. doi: http://dx.doi.org/10.1016/j.rcim.2009.05.001

Suehiro, T., & Takase, K. (1988). 接触運動の表現と制御およびその組み立て作業への応用. *Journal of the RSJ, 6*(6), 31-38.

Suehiro, T., & Takase, K. (1990). Skill Based Manipulation System. *Journal of the RSJ, 8*(5), 551-562.

Sueo Matsubara. (1975). 機械動物メカニマル. *日本の科学と技術 沖縄海洋博記念特集 海洋, 日本科学技術振興財団, 16*(175), 75-79.

Sugano, S., Tanaka, Y., Ohoka, T., & Kato, I. (1985). Autonomic Limb Control of the Information Processing Robot - Movement control system of robot musician 'WABOT-2. *Journal of the RSJ, 3*(4), 339-352.

Susumu, T., Naoki, K., Hideaki, N., Kouichi, W., & Kouta, M. (2008). TELEsarPHONE: Mutual Telexistence Master Slave Communication System based on Retroreflective Projection Technology. *SICE Journal of Control , Measurement, and System Integration, 1*(5), 335-344.

Susumu Tachi. (2006). 相互テレイグジスタンス用人型ロボット「テレサ 2」. *Journal of the Japan Society of Mechanical Engineers, 1091051452-453*.

Suzumori, K. (1989). Flexible microactuator (1 st report, static characteristics of 3-dof actuator). *Transactions of the JSME Series C, 55*(518), 2547-2552.

Suzumori, K., Iikura, S., & Tanaka, H. (1986-7). *Development of micromanipulator (1)*. Paper presented at the Proc. of 6th Annual Conf. of the RSJ.

Tachi, S., Tanie, K., Komoriya, K., Hosoda, Y., & Abe, M. (1981). Guide dog robot (Its basic plan and some experiments with MELDOG MARK I). *Machine Theory, 16*(1), 21-29.

Tadashi Yanmashita. (1964). Mechanical Fingers Controlled by Machine and Their Applications to Materials Handling. *Journal of the Society of Instrument and Control Engineering, 3*(6), 429-439.

Takai, R., Barawid Jr, O., Ishii, K., & Noguchi, N. (2010). Development of Crawler-Type Robot Tractor based on GPS and IMU. *IFAC Proceedings Volumes, 43*(26), 151-156. doi: http://dx.doi.org/10.3182/20101206-3-JP-3009.00026

Takase, K. (1977). Task-oriented variable control of manipulator and its software servoing system. *Proc.of IFAC Sympo.on Information -Control in Manufacturing, 139-145*.

Takashi Suehiro, & Kunikatsu Takase. (1990). Skill Based Manipyulation System. *Journal of the Robotics Society of Japan, 8*(5), 551-562.

Takashi SUEHIRO, K. I. (1993). Fine Localization Based on Face Contact Constraints. *Journal of the Robotics Society of Japan, 11*(4), 541-549.

Takaya, A., Tomoaki, N., Takayuki, N., Kotaro, F., Mikio, N., & Naoto, I. (2012). Online Object Categorization Using Multimodal Information Autonomously Acquired by a Mobile Robot. *Advanced Robotics, 26*(17), 1995-2020.

Takaya Araki, T. N., Takayuki Nagai, Shogo Nagasaka, Tadahiro Taniguchi, Naoto Iwahashi,. (2012). *Online Learning of Concepts and Words Using Multimodal LDA and Hierarchical Pitman-Yor Language Model*. Paper presented at the IEEE/RSJ International Conference on Intelligent Robots and Systems.

Takayama, T., & Hirose, S. (2004). Study on 3D Active Cord Mechanism with Helical Rotational Motion. *Journal of the Robotics Society of Japan, 22*(5), 625-635.

Takenaka, T., Matsumoto, T., Yoshiike, T., & Shirokura, S. (2011). Running Gait Generation for Biped Robot with Horizontal Force Limit. *Journal of the RSJ, 29*(9), 849-856.

Takeshi Takaki, T. O. (2005). Load-Sensitive Continuously Variable Transmission for Robot Hands. *Journal of the Robotics Society of Japan, 23*(2), 238-244.

Takeshi Takaki, T. O. (2006). 100 [g]-100 [N] Robot Finger with Load-Sensitive Continuously Variable Transmission. *Journal of the Robotics Society of Japan, 24*(2), 263-269.

Takeshi, U., Masakazu, E., & Takeshi, T. (1976). A Method of Real-time Recognition of Moving Objects and Its Application. *Transaction of the IEEJ, 96*(3), 49-55 (in Japanese).

Taku Senoo, A. N., Masatoshi Ishikawa,. (2006). Hybrid Trajectory Generation of an Articulated Manipulator for High-speed Batting. *Journal of the Robotics Society of Japan, 24*(4), 515-522.

Takushi, S., Katsumi, K., Hiroshi, I., & Toru, I. (1999). Mobile Robot Navigation by a Distributed Vision System. *Journal of the RSJ, 17*(7), 0-7.

Tamaki, K., Nagasaka, Y., Nishiwaki, K., Saito, M., Kikuchi, Y., & Motobayashi, K. (2013). A Robot System for Paddy Field Farming in Japan. *IFAC Proceedings Volumes, 46*(18), 143-147. doi: http://dx.doi.org/10.3182/20130828-2-SF-3019.00013

Tamio Yanikawa, T. A. (2002). Micro Finger Module with 3 DOF Translattional Motion. *Journal of the Robotics Society of Japan, 20*(2196-205).

Tanaka, K., Kihara, Y., & Yokokohji, Y. (2009). Desired Trajectory and Sensory Feedback Control Law Synthesis for an Origami-Folding Robot based on the Statistical Feature of Direct Teaching by a Human. *Journal of the Robotics Society of Japan, 27*(6), 585-695.

Tanigaki, K., Fujiura, T., Akase, A., & Imagawa, J. (2008). Cherry-harvesting robot. *Computers and Electronics in Agriculture, 63*(1), 65-72. doi: http://dx.doi.org/10.1016/j.compag.2008.01.018

Tanikawa, T., & Arai, T. (1999). Development of a Micro-Manipulation System Having a Two-Fingered Micro-Hand. *IEEE Transactions on Robotics & Automation, 15*(1), 152-162.

Tanner, H. G., Kyriakopoulos, K. J., & Krikelis, N. I. (2001). Advanced agricultural robots: kinematics and dynamics of multiple mobile manipulators handling non-rigid material. *Computers and Electronics in Agriculture, 31*(1), 91-105. doi: http://dx.doi.org/10.1016/S0168-1699(00)00176-9

Tarou, K., Ichirou, R., & Jirou, K. (2011). Self-Regulation Mechanism: A Principle for Continual Autonomous Learning in Open-Ended Environments. *Journal of the Robotics Society of Japan, 29*(1), 77-88.

Tellaeche, A., Pajares, G., Burgos-Artizzu, X. P., & Ribeiro, A. (2011). A computer vision approach for weeds identification through Support Vector Machines. *Applied Soft Computing, 11*(1), 908-915. doi: http://dx.doi.org/10.1016/j.asoc.2010.01.011

Terada, N., Shinoda, H., & Ando, S. (1997). Tensor Cell Tactile Sensor Utilizing Multimode Acoustic Resonance. *Transactions of SICE, 33*(4), 234-240.

Tetsuo Kotoku, K. T., Kazuhito Yokoi, Akio Fujikawa,. (1992). Fundamental Experiments on Bilateral Master-Slave Teleoperation Using Virtual Environments. *Transactions of the SICE, 28*(6), 750-759.

Tetsuya Morizono, M. I., Takahiro Wada, Jing-Long Wu, Sadao Kawamura,. (1997). A Trial of Virtual Tennis using a Parallel Wire Drive System. *Journal of the Robotics Society of Japan, 15*(1), 153-161.

Tillett, N. D. (1991). Automatic guidance sensors for agricultural field machines:A review. *Journal of Agricultural Engineering Research, 50*, 167-187. doi: http://dx.doi.org/10.1016/S0021-8634(05)80012-5

Tinbergen, N. (1951). The Study of Instinct. *The Clarendon Press Oxford, （永野訳, “本能の研究”, 三共出版, 1975）. (in Japanese).*

Tokuji Okada. (1979). Object-Handling System for Manual Industry. *IEEE Trans. on SMC, 9*(2), 78-89.

Tokuji Okada, K. K. (2005). Measurement of Resultant Acceleration in 3D Space Based on Sensing a Metallic Ball Position on Elastic Layer Located at Inside of a Spherical Shell. *Transactions of SICE, 41*(10), 787-796.

Tomohiro Kawahara, M. K. (2005). *Non-Contact Stiffness Imager for Medical Application*. Paper presented at the IEEE International Conference on Information Acquisition.

Tomohiro Kawahara, S. M., Shinji Tanaka, Makoto Kaneko,. (2006). Non-contact Stiffness Imager. *Journal of the RSJ, 24*(3), 363-369.

Tomokazu, H., Hiroshi, M., & Noriaki, K. (1998). The Developing of the Method of Initializing Angle of the Robot Arm Which Has a Reduction Gear Using a Incremental Encoder. *Journal of the Robotics Society of Japan, 16*(1), 48-49.

Tomomasa, S., Hideyuki, K., Tatsuya, H., & Taketoshi, M. (2007). Modeling, Recognition and Supporting Trajectory Generation of Daily Object-handling based on Acquired Motion Models. *Journal of the Robotics Society of Japan, 25*(1).

Tomomasa, S., Toshihiro, M., & Shigeoki, H. (1991). A Telerobot System Featuring Man-robot Cooperative Task Execution. *Journal of the RSJ, 9*(5), 602-613 (in Japanese).

Tomomasa, S., Yoshifumi, N., Junri, I., Yotaro, H., & Hiroshi, M. (1995). Active Understanding of Human Intention by a Robot through Monitoring of Human Behavior. *Journal of the RSJ, 13*(4), 545-552.

Tomomasa Sato, S. H. (1986). ワールドモデルを利用したテレオペレータシステムの構成法　--物体の操作知識を核としたモデルの構成--. *ournal of the Robotics Society of Japan, 4*(4), 353-363 (in Japanese).

Tomomasa Sato, S. H. (1987). MEISTER: A Model Enhanced Intelligent and Skillful Teleoperational Robot System. *4th Int. Sym. on Robotics Research*, *MIT Press.*

Tomomasa Sato, S. H., Toshihiro Matsui,. (1991). *A Telerobot System MEISTER: An Integration of Task Knowledge Base and Cooperative Maneuvaring System*. Paper presented at the 11th Int. Conf. on Structural Mechanics in Reactor Technology.

Tomoyuki, T., Atsushi, K., Akihiko, s., & Shizuko, H. (1996). Control Methods of Walk Training System. *Transactions of the JSME (C), 62*(597), 1928-1934.

Torii, T. (2000). Research in autonomous agriculture vehicles in Japan. *Computers and Electronics in Agriculture, 25*(1–2), 133-153. doi: http://dx.doi.org/10.1016/S0168-1699(99)00060-5

Toru Omata, K. N. (1995). Statics of Power Grasps with a Multifingered Hand. *Journal of the Robotics Society of Japan, 13*(4), 525-531.

Toshio. Matsushita. (1984). A Robot Vision Language for Detection and Measurement of Tree-Dimensional Objects. *Journal of the Robotics Society of Japan, 2*(6), 536-544.

Toyama, S., & Yamamoto, G. (2009a, 10-15 Oct. 2009). *Development of Wearable-Agri-Robot ∼mechanism for agricultural work&#x223C.* Paper presented at the 2009 IEEE/RSJ International Conference on Intelligent Robots and Systems.

Toyama, S., & Yamamoto, G. (2009b, 10-15 Oct. 2009). *Development of Wearable-Agri-Robot mechanism for agricultural work.* Paper presented at the 2009 IEEE/RSJ International Conference on Intelligent Robots and Systems.

Tsuneo. Yoshikawa. (1984). Measure of Manipulability for Robot Manipulators. *Journal of the Robotics Society of Japan, 2*(1), 63-67.

Tsutomu, & Hasegawa. (1981). Modelling and Monitoring a Manipulation Environment. *Transactions of the SICE, 17*(5), 589-595 (in Japanese). doi: https://www.jstage.jst.go.jp/article/sicetr1965/17/5/17_5_589/_pdf

Tsutomu, h. (1986). Collision Avoidance Using Characterized Description of Free Space. *Transactions of the Society of Instrument and Control Engineers, 22*(6), 616-622.

Tsutomu Hasegawa. (2008). Robot Town:A Robotics Structured Environment Platform. *Journal of the Robotics Society of Japan, 26*(5), 411-414.

Ueki, M., Yusuke, Y., Murase, Y., Sawasaki, N., Shiraishi, A., Kanda, S., . . . Miyamura, K. (2004). *Development of the Home Robot MARON-1*. Paper presented at the Proc. of the Mechatronics & Robotics conference 2004, Aachen, Germany.

Uno, T., Ejiri, M., & Tokunaga, T. (1976). A Method of Real-time Recognition of Moving Objects and its Application. *Pattern Recognition, 8*, 201-208.

USDA. (2015). Farm Demographics - U.S. Farmers by Gender, Age, Race, Ethnicity, and More.

van Henten, E. J., Hemming, J., van Tuijl, B. A. J., Kornet, J. G., Meuleman, J., Bontsema, J., & van Os, E. A. (2002). An Autonomous Robot for Harvesting Cucumbers in Greenhouses. [journal article]. *Autonomous Robots, 13*(3), 241-258. doi: 10.1023/a:1020568125418

Van Henten, E. J., Van't Slot, D. A., Hol, C. W. J., & Van Willigenburg, L. G. (2009). Optimal manipulator design for a cucumber harvesting robot. *Computers and Electronics in Agriculture, 65*(2), 247-257. doi: http://dx.doi.org/10.1016/j.compag.2008.11.004

Vibhute, A., & Bodhe, S. K. (2012). Applications of image processing in agriculture. *International journal of computer applications, 52*.

Vinogradov, O. (2000). *Fundamentals of kinematics and dynamic of machines and mechanisms*. CRC Press LLC.

Wang, S.-C., Hikita, H., Kubo, H., Zhao, Y.-S., Huang, Z., & Ifukube, T. (2003). Kinematics and dynamics of a 6 degree-of-freedom fully parallel manipulator with elastic joints. *Mechanism and Machine Theory, 38*(5), 439-461. doi: http://dx.doi.org/10.1016/S0094-114X(02)00132-5

Watanabe, I. (2015). Smart Architecture and Integration Lead Intelligence to the Next Generation

Watanabe, I., & Uchiyama, T. (1989). A Teleoperation System for Space Experiments. *Journal of the Robotics Society of Japan, 7*(6), 115-120.

Weiss, U., & Biber, P. (2011). Plant detection and mapping for agricultural robots using a 3D LIDAR sensor. *Robotics and Autonomous Systems, 59*(5), 265-273. doi: http://dx.doi.org/10.1016/j.robot.2011.02.011

Widden, M. B., & Blair, J. R. (1972). A new automatic tractor guidance system. *Journal of Agricultural Engineering Research, 17*(1), 10-21. doi: http://dx.doi.org/10.1016/S0021-8634(72)80012-X

Wikipedia. (2016). Pumpkin, from https://en.wikipedia.org/wiki/Pumpkin

Wikipedia. (2017a). CAN bus, from https://en.wikipedia.org/wiki/CAN_bus
Wikipedia. (2017b). Kabocha, from https://en.wikipedia.org/wiki/Kabocha
Wilhelm, Luther, R., Dwayne, A. S., & and Gerald, H. B. (2004). Chapter 3: in Food & Process Engineering Technology *Texture of Food Materials* (pp. 53-64). St. Joseph, Mich.: ASABE.
Wilhelm, L. R., Suter, D. A., & Brusewitz, G. H. (2005). *Texture of Food Materials*. St. Joseph, Mich.: ASABE.
Willrodt, F. L. (1924). US Patent No. 1506706.
Wilson, J. N. (2000). Guidance of agricultural vehicles — a historical perspective. *Computers and Electronics in Agriculture, 25*(1–2), 3-9. doi: http://dx.doi.org/10.1016/S0168-1699(99)00052-6
WordPress. (2017). Pumpkin Anatomy Retrieved http://www.pumpkin.com.au/history/pumpkin-anatomy/
Y, M., Y, Y., S, K., N, S., K, O., & T, A. (2005). *Development of Production-Type Service Robot*. Paper presented at the The 36th International Symposium on Robotics, TU313, Tokyo, Japan.
Y. H. Liu, S. A. (1990). *Sensor-based coordination planning of two mobile robots in unknown environments*. Paper presented at the Proceedings of Japan-USA Symposium on Flexible Automation.
Y. H. Liu, S. K., T. Naniwa, H. Noborio, S. Arimoto,. (1989). *A practical algorithm for planning a collision-free coordination of multiple mobile robots*. Paper presented at the Proceedings of IEEE Int. Conf. on Robotics and Automation.
Y. Kuniyoshi. (1995). *Behavior Matching by Observation for Multi-Robot Cooperation*. Paper presented at the Proceedings of. 7th International Symposium on Robotics Research (ISRR), (In G. Giralt and G. Hirzinger (eds.), Robotics Research -- The Seventh International Symposium, Springer, ISBN 3-540-76043-1.
Y. Kuniyoshi, H. I. (1993). *Qualitative Recognition of Ongoing Human Action Sequences*. Paper presented at the Proceedings of International Joint Conference on Artificial Intelligence.
Y. Kuniyoshi, M. I., H. Inoue,. (1994). Learning by Watching: Extracting Reusable Task Knowledge from Visual Observation of Human Performance. *IEEE Transactions on Robotics and Automation, 10*(6), 799-822.
Y. Sakawa, F. M., S. Fukushima,. (1986). Modeling and Feedback Control of a Flexible Arm. *J. Robotic Systems, 2*(4), 35-54.
Y.Yokokohji, & T.Yoshikawa. (1994). Bilateral Control of Master-Slave Manipulators for Ideal Kinesthetic Coupling - Formulation and Experiment. *IEEE Transaction on Robotics and Automation, 10*(5), 605-620.
Yael, E., Dima, R., Tamar, F., & Gaines, E. M. (2000). Robotic melon harvesting. *IEEE Transactions on Robotics and Automation, 16*(6), 831-835. doi: 10.1109/70.897793
Yagi, Y. (1995). Real-time Omnidirectional Image Sensors. *Journal of the RSJ, 13*(3), 347-350.
Yahya, S., Moghavvemi, M., & Mohamed, H. A. F. (2011). Geometrical approach of planar hyper-redundant manipulators: Inverse kinematics, path planning and workspace. *Simulation Modelling Practice and Theory, 19*(1), 406-422. doi: http://dx.doi.org/10.1016/j.simpat.2010.08.001
Yakabe, H., Maruyama, Y., Yano, K., Nakashima, M., Inokuchi, H., & Kawai, F. (1995). Development of the Semi-Automatic Hot-Line Work Robot System "Phase II". *Yaskawa Technical Review, 59*(227), 154-161.
Yamafuji, K., Kobayashi, T., Kawanura, T., & Kondo, Y. (1992). A Study of the Brachiation Type of Mobile Robot (1st Report, Analysis of Dynamics and Simulation). *Journal of the RSJ, 10*(5), 648-655.
Yamaguchi, J., Kinoshita, N., Takanishi, A., & Kato, I. (1996). Development of a Biped Walking Robot Adapting to an Unknown Uneven Surface. *Journal of the Robotics Society of Japan, 14*(4), 546-559.
Yamakawa, Y., Namiki, A., Ishikawa, M., & Shimojo, M. (2009). Knotting Manipulation of a Flexible Rope Using a High-speed Multifingered Hand and High-speed Visual and Tactile Sensory Feedback. *Journal of the Robotics Society of Japan, 27*(9), 1016-1024 (in Japanese).
Yang, L., & Noguchi, N. (2014). Development of a Wheel-Type Robot Tractor and its Utilization. *IFAC Proceedings Volumes, 47*(3), 11571-11576. doi: http://dx.doi.org/10.3182/20140824-6-ZA-1003.00952
Yanikawa, T., & Arai, T. (1997). Micro Finger Module with 3 DOF Translattional Motion. *Journal of the Robotics Society of Japan, 20*(2196-205).
Yaskawa Inc. (America). Yaskawa Motoman offical website Retrieved https://www.motoman.com/
Yasuhisa Hirata, K. K., Hajime Asama, Hayato Kaetsu, Kuniaki Kawabata,. (2003). Transportation of a Single Object by Multiple Distributed Robot Helpers with Caster-like Dynamics (DR Helpers) in Cooperation with a Human. *Journal of the RSJ, 21*(7), 80-88.
yon, S., Hale, J. G., & Cheng, G. (2007). Full-body Compliant Human-Humanoid Interaction: Balancing in the Presence of Unknown External Forces. *IEEE Transactions on Robotics & Automation*.
Yoshiaki, S., & Hirochika, I. (1973). Guiding a Robot by Visual Feedback in Assembling Tasks. *Pattern Recognition, 5*, 99-108.
Yoshiaki Shirai, H. I. (1971). ビジュアル・フィードバックを利用したロボットの組み合わせ作業. *電子技術総合研究所彙報, 35*(3), 327-333 (in Japanese).
Yoshihiko Nakamura, K. Y., Fumio Nagashima,. (1998). Dynamics Computation of Structure-Varying Kinematic Chains and Its Application to Human Figures. *Journal of the Robotics Society of Japan, 16*(8), 124-131.
Yoshihiko Nakmura, O. J. S., Woojin Chung,. (1995). Theoretical Design and Nonlinear Control of a Nonholonomic Manipulator. *Journal of the Robotics Society of Japan, 13*(5), 74-682.

Yoshihiro Watanabe, T. K., Masatoshi Ishikawa,. (2007). Real-time Three-dimensional Sensing for a Moving/Deforming Object using High-speed Vision for Numerous-point Analysis. *Journal of the Robotics Society of Japan, 25*(6), 1005-1013.

Yoshino, R. (2000). Stabilizing Control of High-Speed Walking Robot by Walking Pattern Regulator. *Journal of the RSJ, 18*(8), 1122-1132.

Yoshitaka, S., Mitsuo, F., Yasunori, T., & Kazumi, F. (2007). Development and practical use of FSJ robot system. *Journal of the Robotics Society of Japan, 25*(1), 78-79.

Yuji, H., Masashi, K., & Kenjiro, Y. (2010). Autonomous Moving Technology for Future Urban Mobility Element. *Hitachi Review, 92*(11), 854-858.

Yuji Ichimaru, H. I., Toshiki Ito, Toshiyuki Kono,. (2011). Environment Recognition for Robots. *Yaskawa technical review, 75*(2), 101-104.

Yuji Tsusaka, Y. F., Hirochika Inoue,. (1987). Parallel Manipulator: Its Design and Mechanical Characteristics. *Journal of the Robotics Society of Japan, 5*(3), 180-188.

Yuji Yamakawa, A. N., Masatoshi Ishikawa,. (2012). Dynamic Folding of a Cloth using a High-speed Multifingered Hnad System. *Journal of the Robotics Society of Japan, 30*(2), 225-232.

Yuji Yamakawa, A. N., Masatoshi Ishikawa, Makoto Shimojo,. (2009). Knotting Manipulation of a Flexible Rope Using a High-speed Multifingered Hand and High-speed Visual and Tactile Sensory Feedback. *Journal of the Robotics Society of Japan, 27*(9), 1016-1024.

Yuka KATO. 日本ロボット学会第30回記念一般公開事業　ロボットコンテスト「RSNPを利用したロボットサービスコンテスト」. *Journal of the RSJ (in Japanese)*.

Yun-Hui, L., & Suguru, A. (1990). Motion Planning Based on Local Sensor Information For Two Mobile Robots Amidst Unknown Environments. *Journal of the Robotics Society of Japan, 10*(2), 216-225 (in Japanese).

Yutaka Yakano, e. a. (1975). Robot for Arc Welding "Mr. AROS". *Hitachi Review, 7*(10), 17-22.

Zhang, C. (2017). *Development of a multi-robot tractor system for farm work.* Ph.D., Hokkaido university, Graduate school of agriculture.

Zhang, C., Yang, L., & Noguchi, N. (2014). Development of a Human-driven tractor following a Robot System. *IFAC Proceedings Volumes, 47*(3), 11559-11564. doi: http://dx.doi.org/10.3182/20140824-6-ZA-1003.00751

Zhang, C., Yang, L., & Noguchi, N. (2015). Development of a robot tractor controlled by a human-driven tractor system. *Engineering in Agriculture, Environment and Food, 8*(1), 7-12. doi: http://dx.doi.org/10.1016/j.eaef.2015.01.003

Zhang, C., Yang, L., Zhang, Z., & Noguchi, N. (2013). Development of Robot Tractor Associating with Human-drive Tractor for Farm Work. *IFAC Proceedings Volumes, 46*(4), 83-88. doi: http://dx.doi.org/10.3182/20130327-3-JP-3017.00022

Zhang, Z., Noguchi, N., Ishii, K., Yang, L., & Zhang, C. (2013). Development of a Robot Combine Harvester for Wheat and Paddy Harvesting. *IFAC Proceedings Volumes, 46*(4), 45-48. doi: http://dx.doi.org/10.3182/20130327-3-JP-3017.00013

Zion, B., Mann, M., Levin, D., Shilo, A., Rubinstein, D., & Shmulevich, I. (2014). Harvest-order planning for a multiarm robotic harvester. *Computers and Electronics in Agriculture, 103*, 75-81. doi: http://dx.doi.org/10.1016/j.compag.2014.02.008

Zweig, S. (2007). *Mobile robot with wireless location sensing apparatus.* Retrieved from https://www.google.com/patents/US20070061041

Appendices

Appendix 1. The drawings of the designed robotic arm (RAVeBots-1).

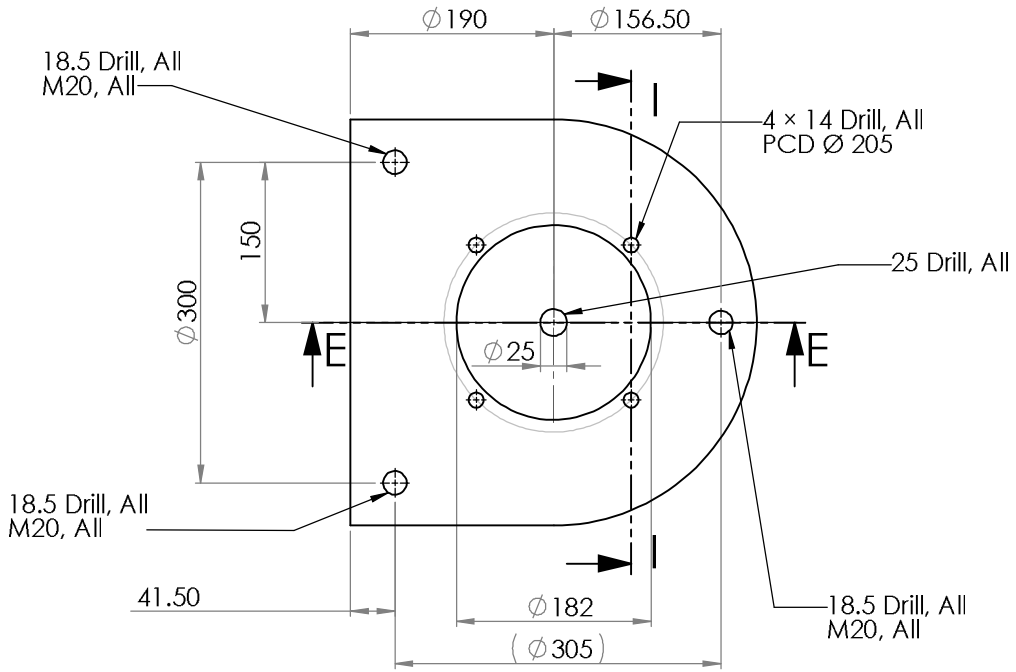

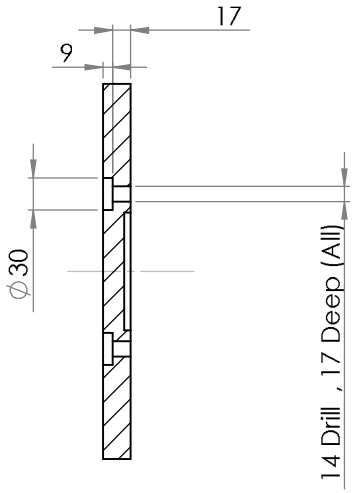

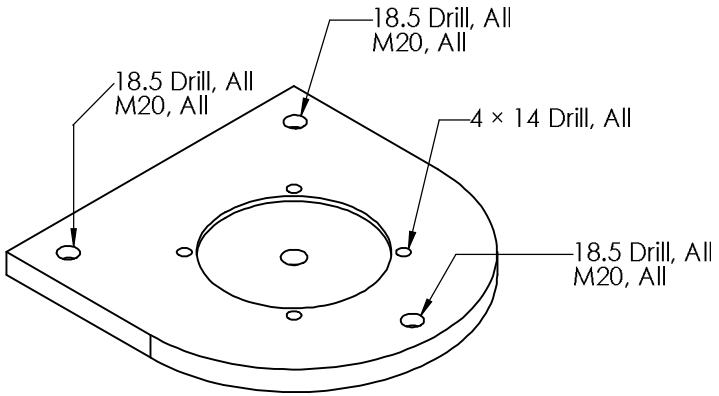

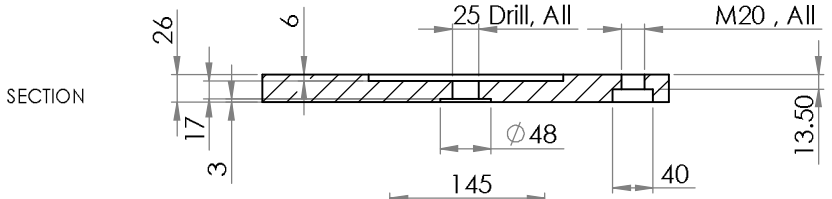

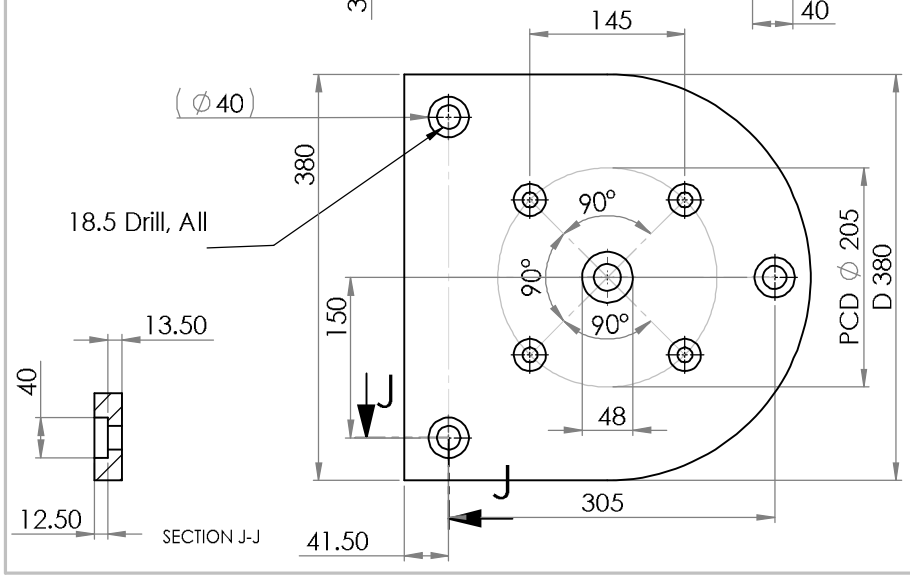

UNLESS OTHERWISE SPECIFIED: DIMENSIONS ARE IN MILLIMETERS SURFACE FINISH: TOLERANCES: LINEAR: ANGULAR:		FINISH:		DEBUR AND BREAK SHARP EDGES		DO NOT SCALE DRAWING	REVISION
	NAME	SIGNATURE	DATE			TITLE:	
DRAWN							
CHK'D							
APPV'D							
MFG							
Q.A				MATERIAL: Iron		DWG NO. a1_1	A3
				WEIGHT:		SCALE:1:5	SHEET 1 OF 1

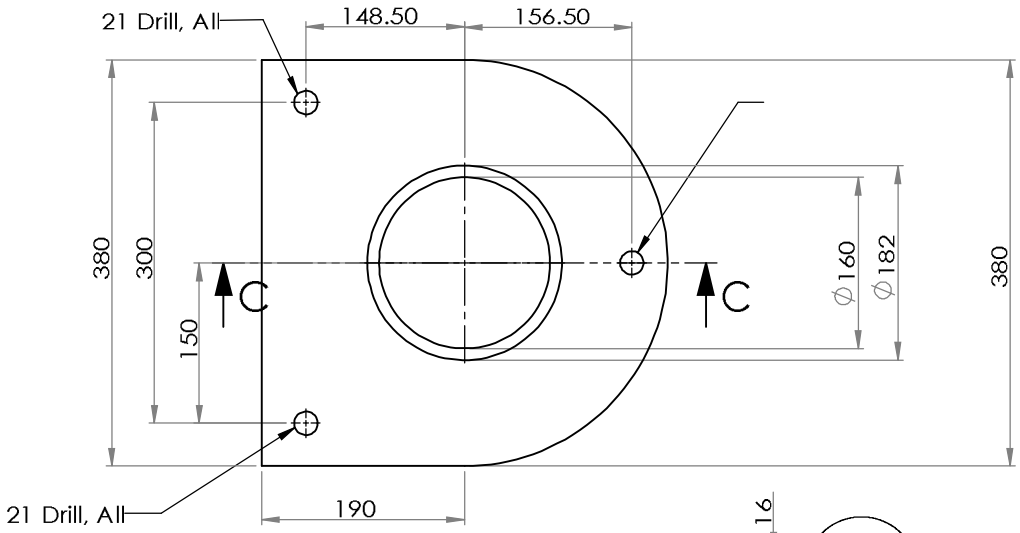

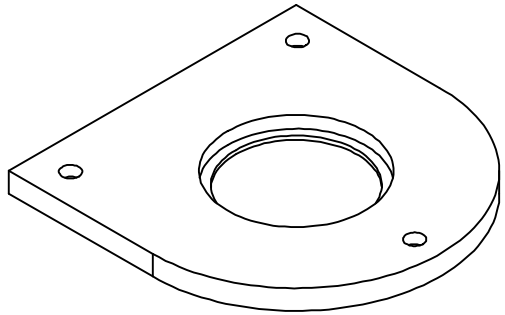

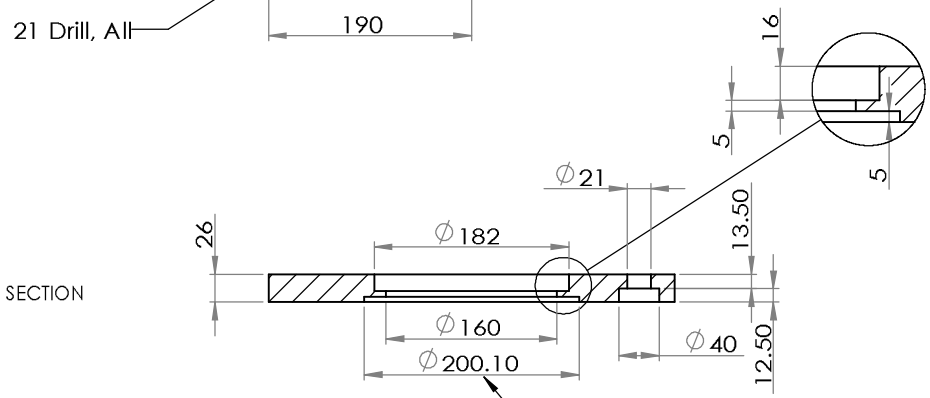

SECTION

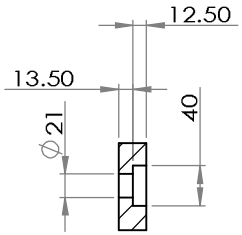

SECTION

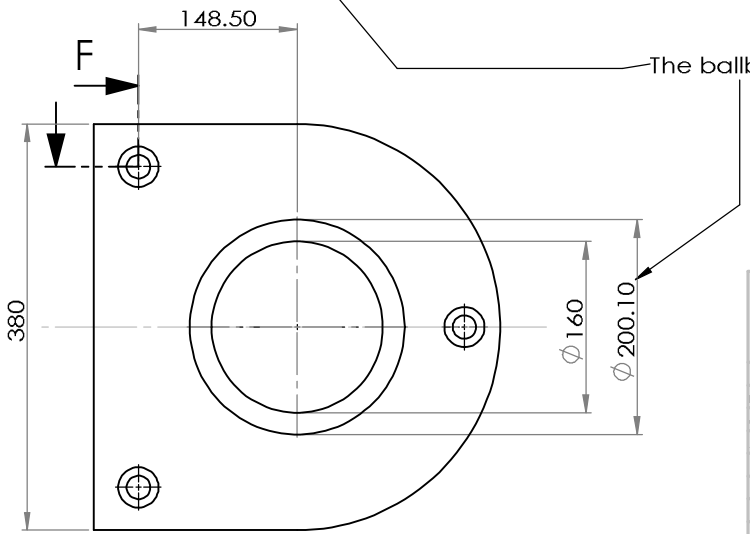

The ballbearing outside diameter is 200mm

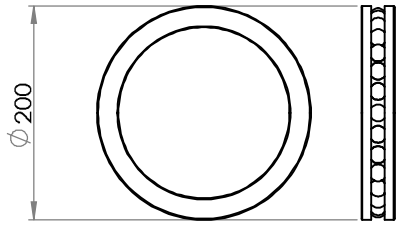

UNLESS OTHERWISE SPECIFIED: DIMENSIONS ARE IN MILLIMETERS SURFACE FINISH: TOLERANCES: LINEAR: ANGULAR:		FINISH:		DEBUR AND BREAK SHARP EDGES		DO NOT SCALE DRAWING	REVISION
	NAME	SIGNATURE	DATE			TITLE:	
DRAWN							
CHK'D							
APPV'D							
MFG							
Q.A				MATERIAL: Iron		DWG NO. a2_1	A3
				WEIGHT:		SCALE:1:5	SHEET 1 OF 1

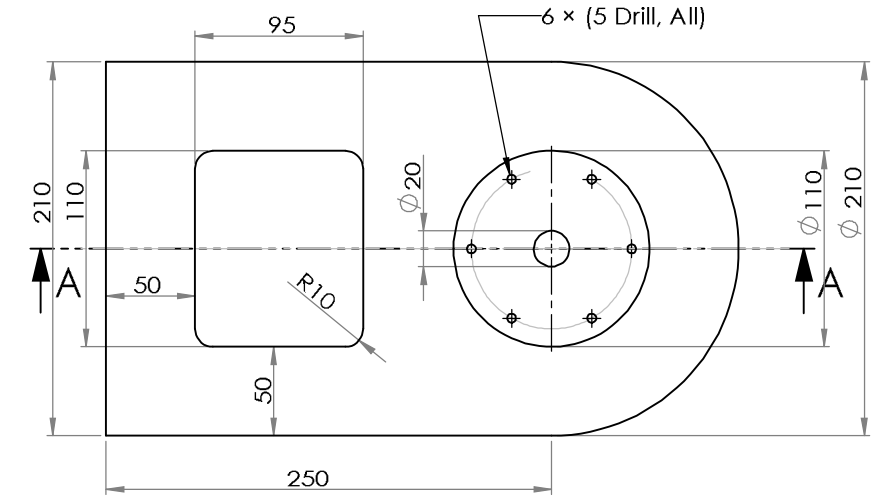

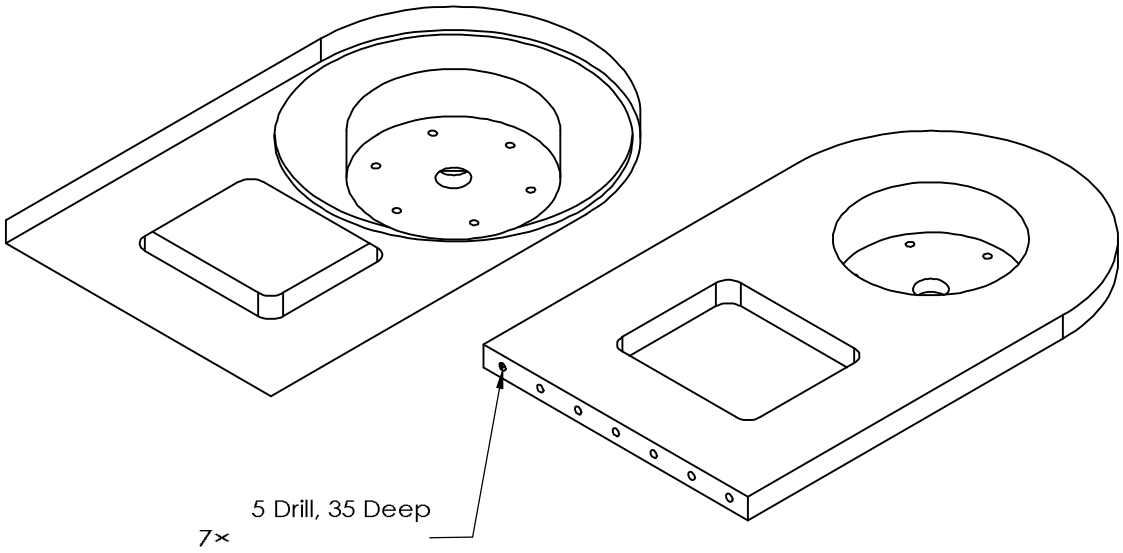

SECTION A-A

SCALE 1 : 3

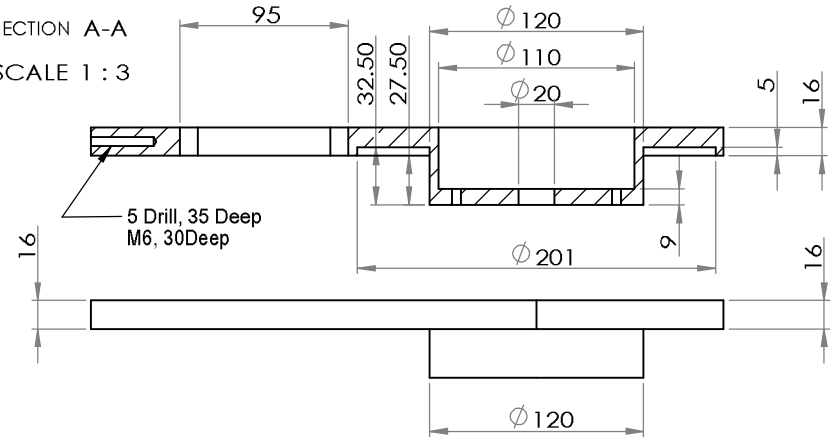

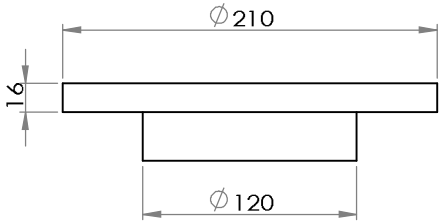

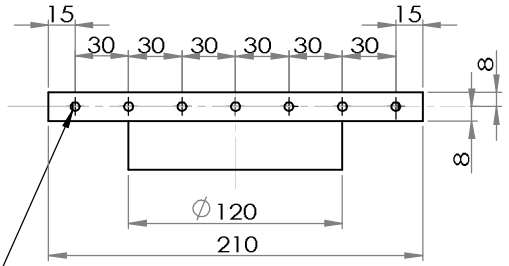

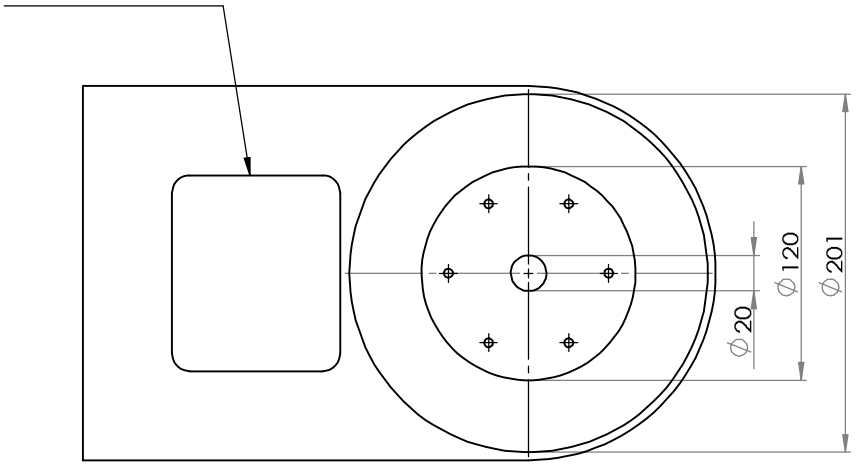

5 Drill, 35 Deep
7×

UNLESS OTHERWISE SPECIFIED: DIMENSIONS ARE IN MILLIMETERS SURFACE FINISH: TOLERANCES: LINEAR: ANGULAR:		FINISH:		DEBUR AND BREAK SHARP EDGES		DO NOT SCALE DRAWING	REVISION
	NAME	SIGNATURE	DATE			TITLE:	
DRAWN							
CHK'D							
APPV'D							
MFG							
Q.A				MATERIAL: Iron		DWG NO. a4_1	A3
				WEIGHT:		SCALE:1:3	SHEET 1 OF 1

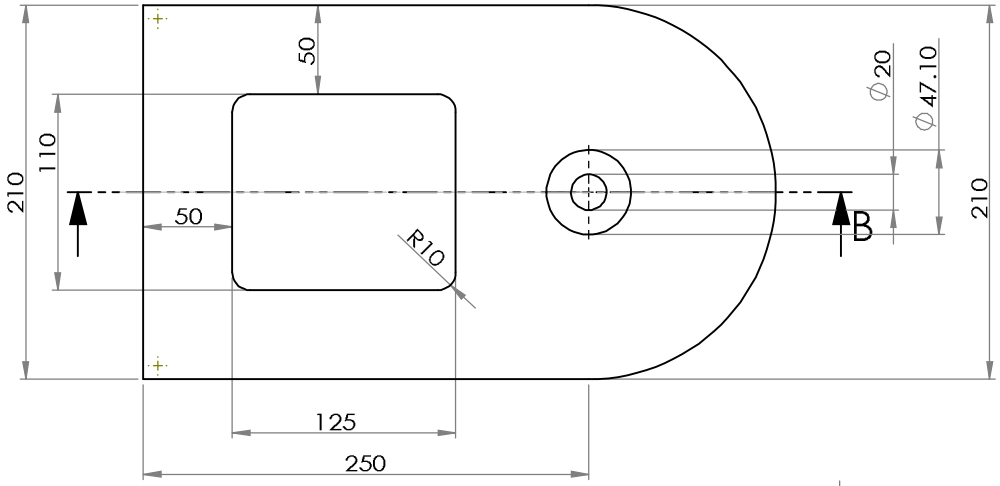

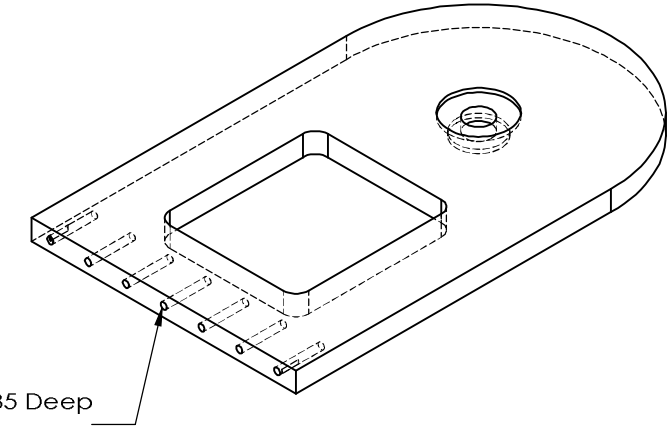

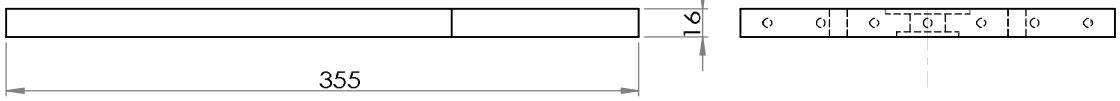

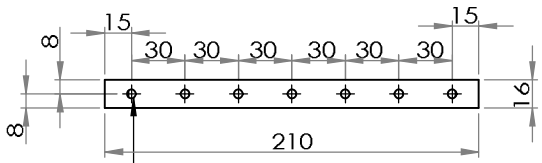

7× 5 Drill, 35 Deep
M6, 30 Deep

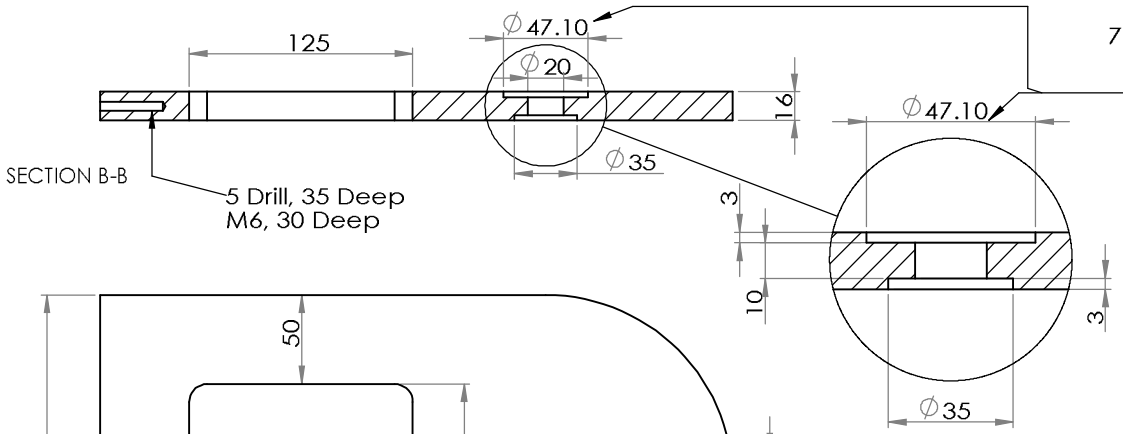

The outer diameter
of ballbearing is
47 mm

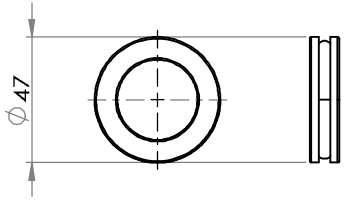

SCALE 1 : 2 SCALE 1 : 2

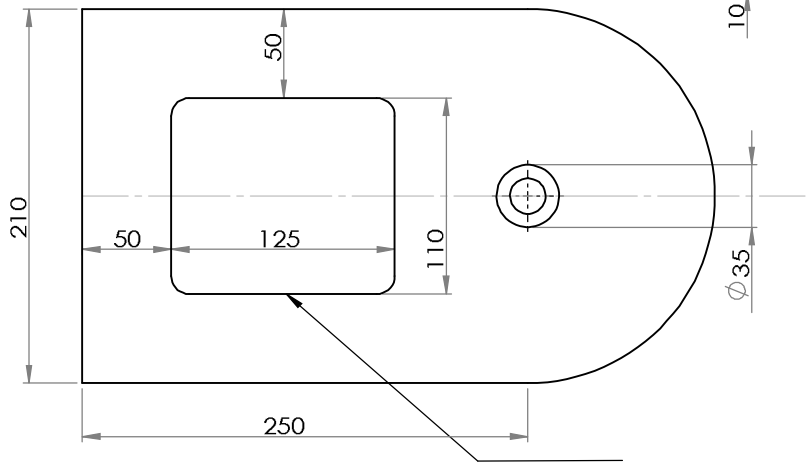

UNLESS OTHERWISE SPECIFIED: DIMENSIONS ARE IN MILLIMETERS SURFACE FINISH: TOLERANCES: LINEAR: ANGULAR:		FINISH:		DEBUR AND BREAK SHARP EDGES		DO NOT SCALE DRAWING	REVISION
	NAME	SIGNATURE	DATE			TITLE:	
DRAWN							
CHK'D							
APPV'D							
MFG							
Q.A				MATERIAL: Iron		DWG NO. a5_1	A3
				WEIGHT:		SCALE:1:1	SHEET 1 OF 1

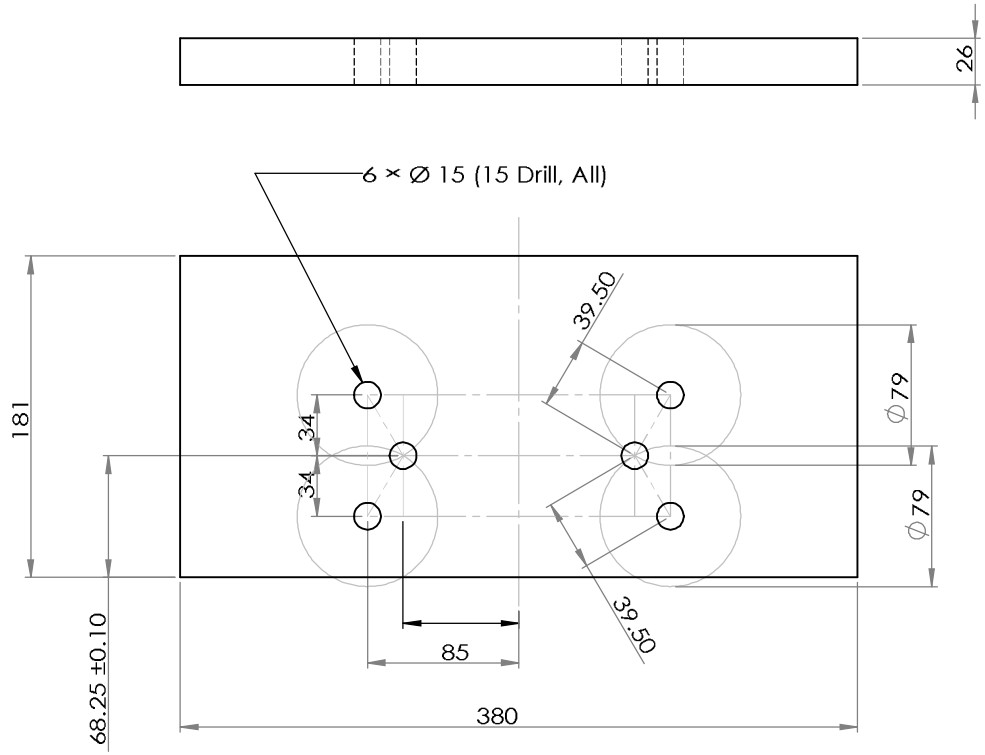

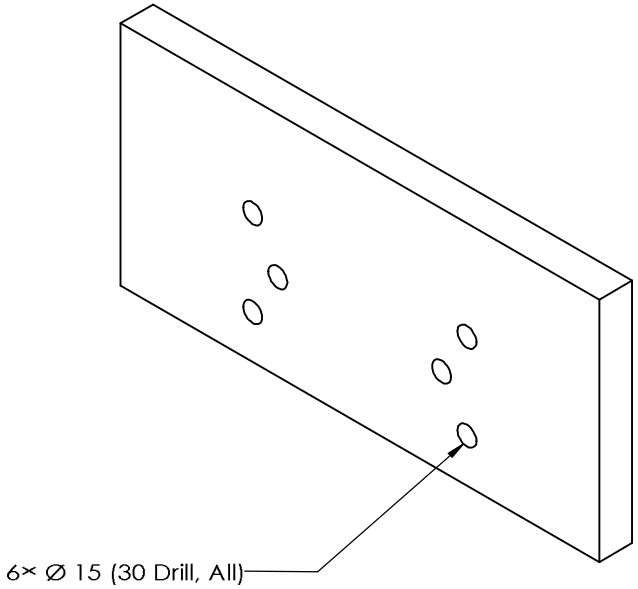

UNLESS OTHERWISE SPECIFIED: DIMENSIONS ARE IN MILLIMETERS SURFACE FINISH: TOLERANCES: LINEAR: ANGULAR:		FINISH:			DEBUR AND BREAK SHARP EDGES	DO NOT SCALE DRAWING	REVISION
	NAME	SIGNATURE	DATE			TITLE:	
DRAWN							
CHK'D							
APPV'D							
MFG							
Q.A				MATERIAL: Iron		DWG NO. a6_1	A3
				WEIGHT:		SCALE:1:1	SHEET 1 OF 1

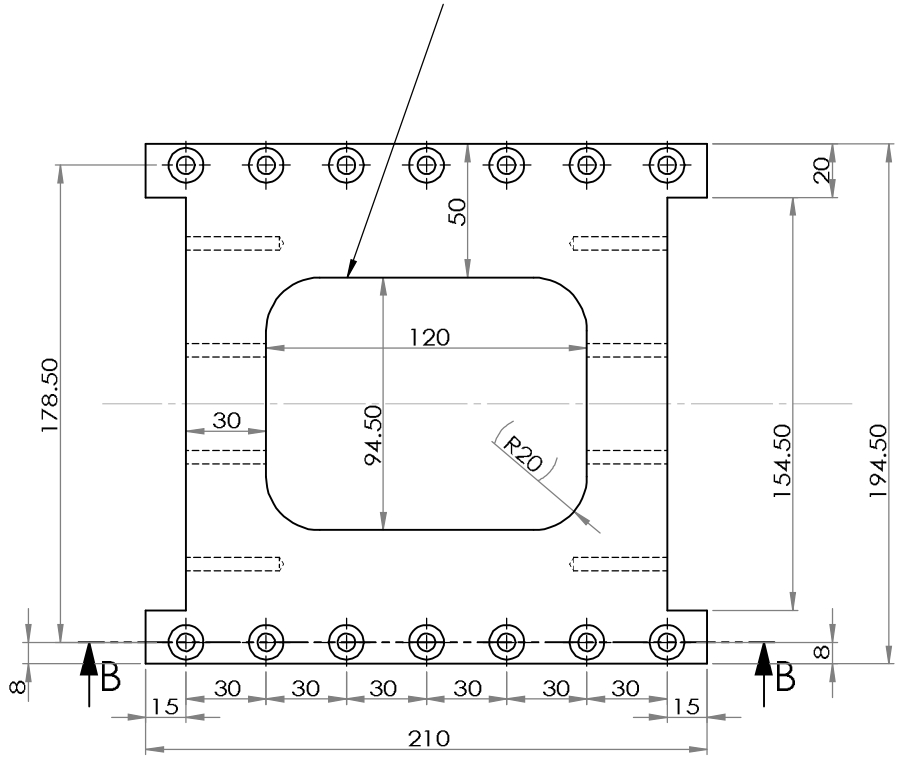

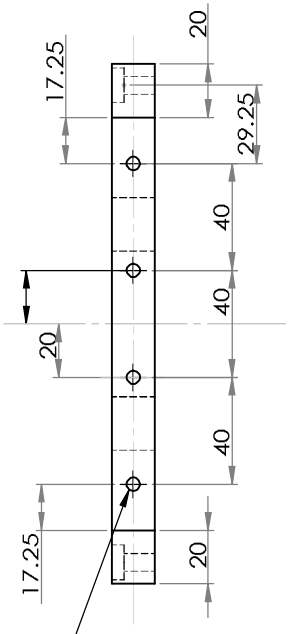

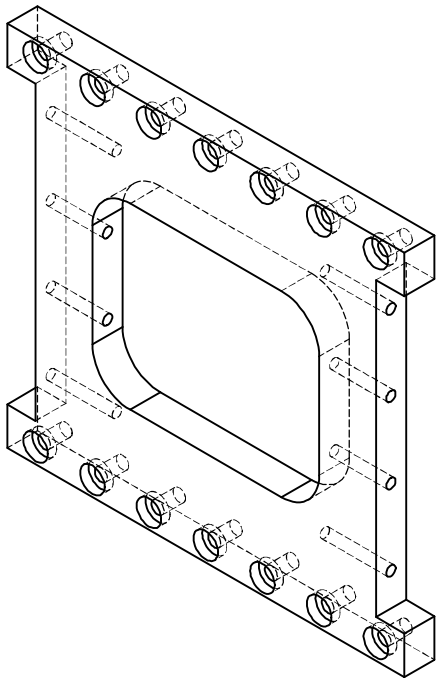

4 × 4.2 Drill, 35 Deep
M5 ×

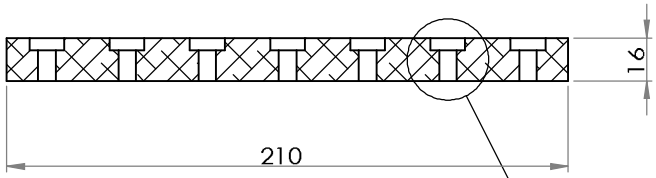

SECTION

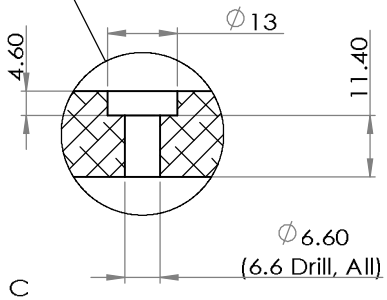

DETAIL C

SCALE 1 : 1

UNLESS OTHERWISE SPECIFIED: DIMENSIONS ARE IN MILLIMETERS SURFACE FINISH: TOLERANCES: LINEAR: ANGULAR:	FINISH:		DEBUR AND BREAK SHARP EDGES	DO NOT SCALE DRAWING	REVISION	
	NAME	SIGNATURE	DATE	TITLE:		
DRAWN						
CHK'D						
APPV'D						
MFG						
Q.A				MATERIAL: Iron	DWG NO. vert10	A3
				WEIGHT:	SCALE:1:2	SHEET 1 OF 1

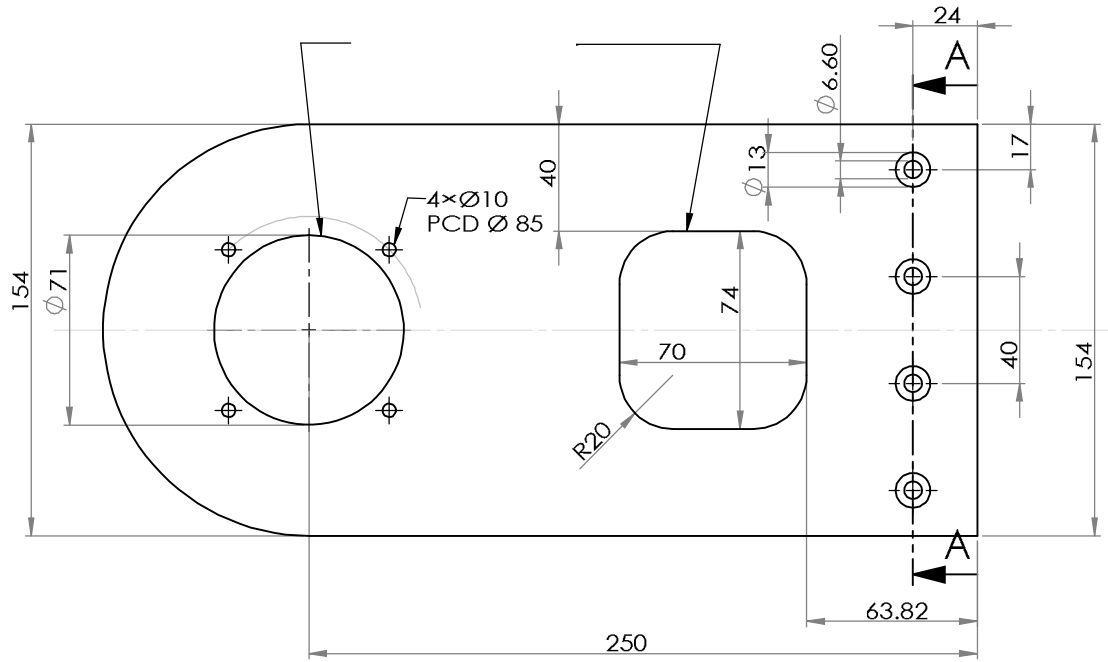

SECTION

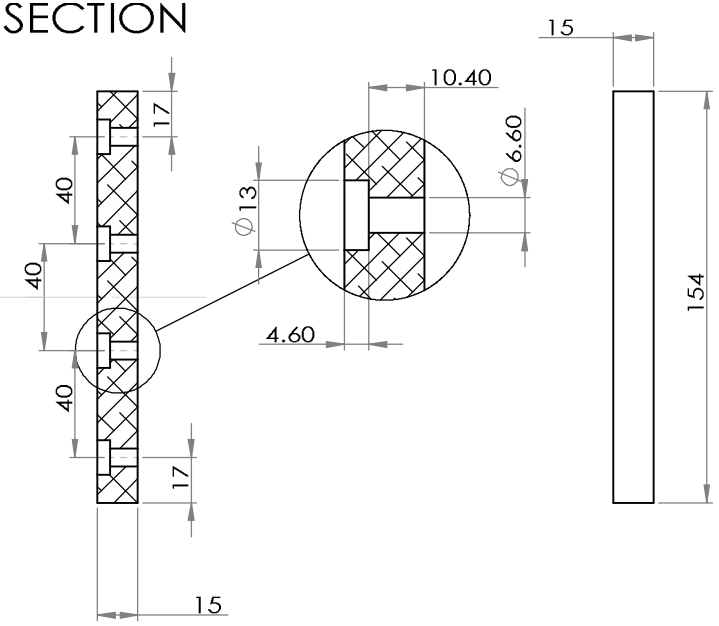

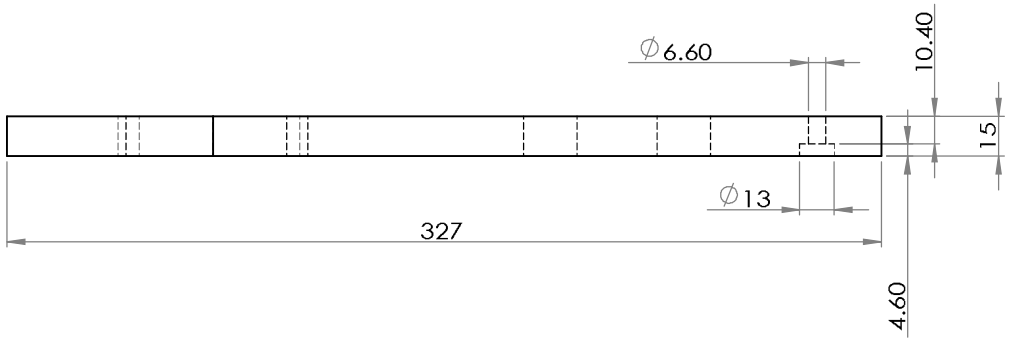

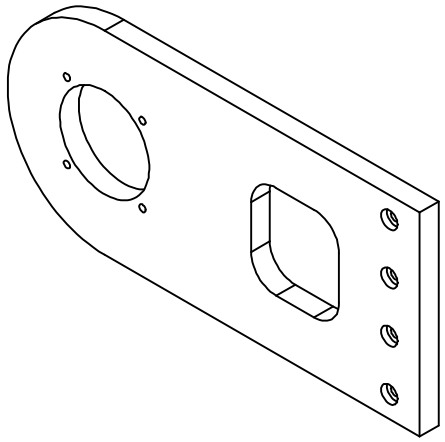

UNLESS OTHERWISE SPECIFIED: DIMENSIONS ARE IN MILLIMETERS SURFACE FINISH: TOLERANCES: LINEAR: ANGULAR:		FINISH:		DEBUR AND BREAK SHARP EDGES		DO NOT SCALE DRAWING	REVISION
	NAME	SIGNATURE	DATE			TITLE:	
DRAWN							
CHK'D							
APPV'D							
MFG							
Q.A				MATERIAL: Iron		DWG NO. vert33	A3
				WEIGHT:		SCALE:1:2	SHEET 1 OF 1

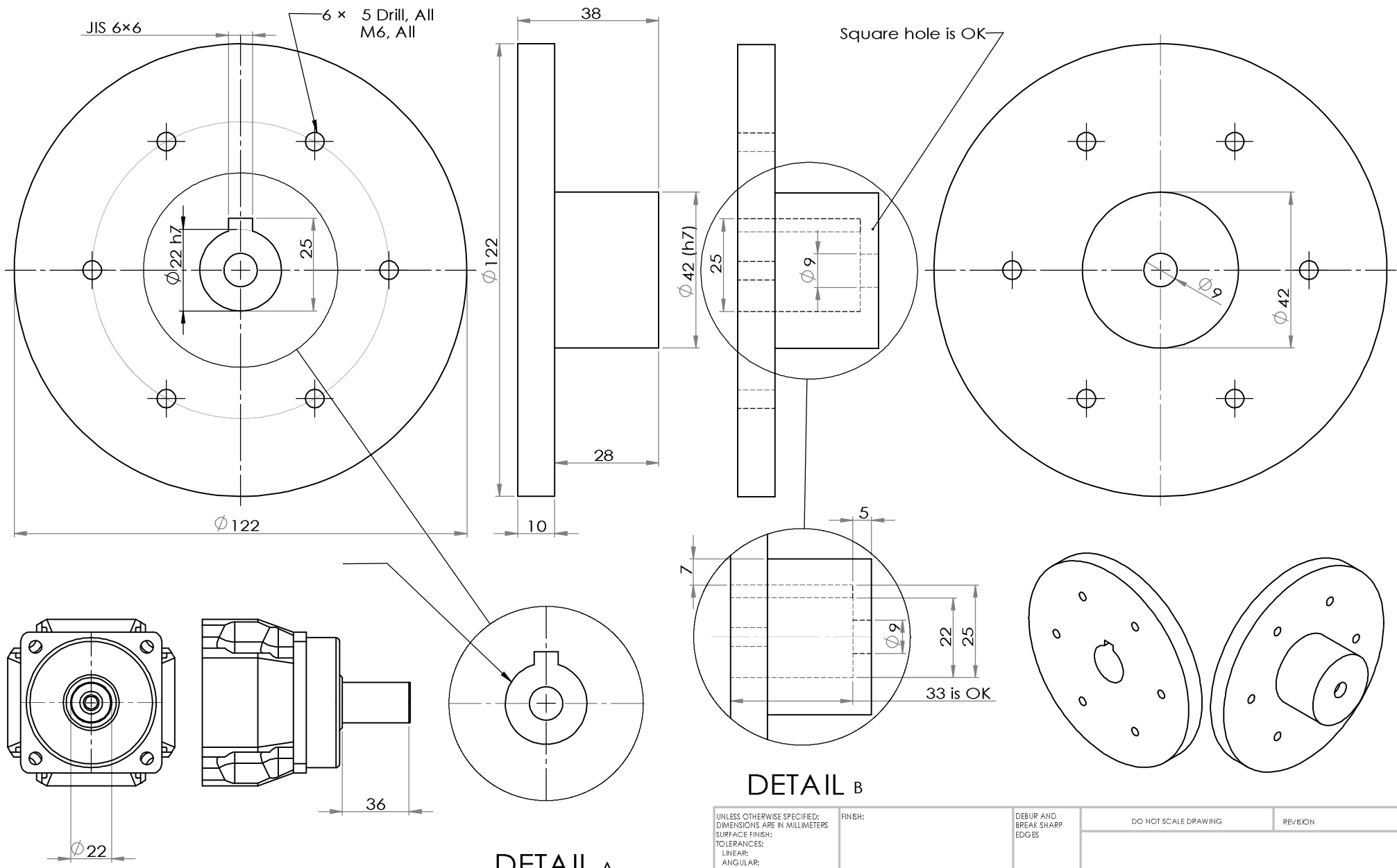

The servo motor by mentioned diameters wil attache to this hole with key

UNLESS OTHERWISE SPECIFIED: DIMENSIONS ARE IN MILLIMETERS SURFACE FINISH: TOLERANCES: LINEAR: ANGULAR:		FINISH:		DEBUR AND BREAK SHARP EDGES	DO NOT SCALE DRAWING	REVISION
	NAME	SIGNATURE	DATE		TITLE:	
DRAWN						
CHK'D						
APPV'D						
MFG						
Q.A				MATERIAL: Iron	DWG NO. a7_1	A3
				WEIGHT:	SCALE:1:2	SHEET 1 OF 1

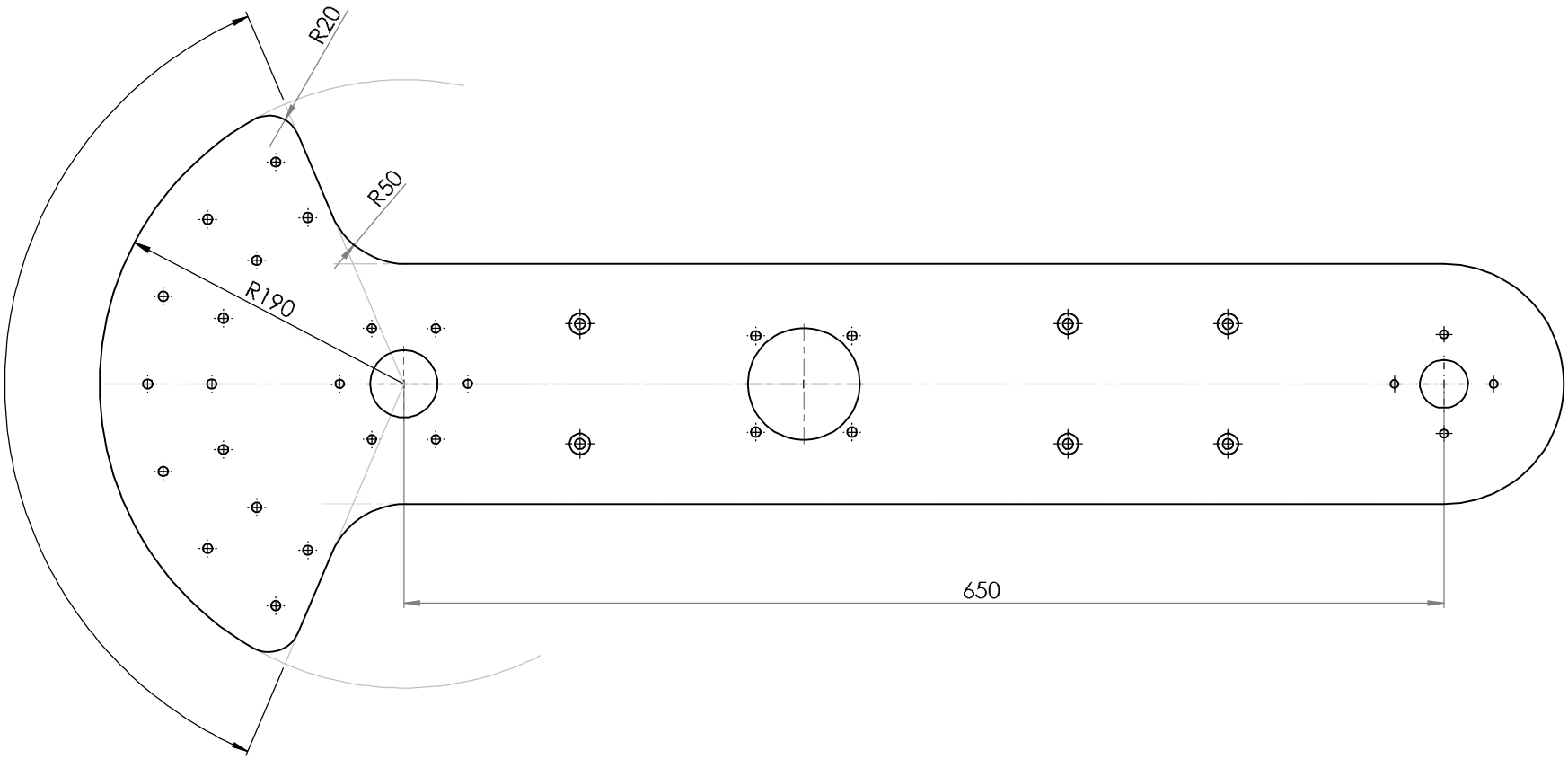

SCALE 1 : 3

UNLESS OTHERWISE SPECIFIED: DIMENSIONS ARE IN MILLIMETERS SURFACE FINISH: TOLERANCES: LINEAR: ANGULAR:		FINISH:			DEBUR AND BREAK SHARP EDGES	DO NOT SCALE DRAWING	REVISION
	NAME	SIGNATURE	DATE			TITLE:	
DRAWN							
CHK'D							
APPV'D							
MFG							
Q.A				MATERIAL:		DWG NO. a8_1(2)	A3
				WEIGHT:		SCALE:1:5	SHEET 1 OF 1

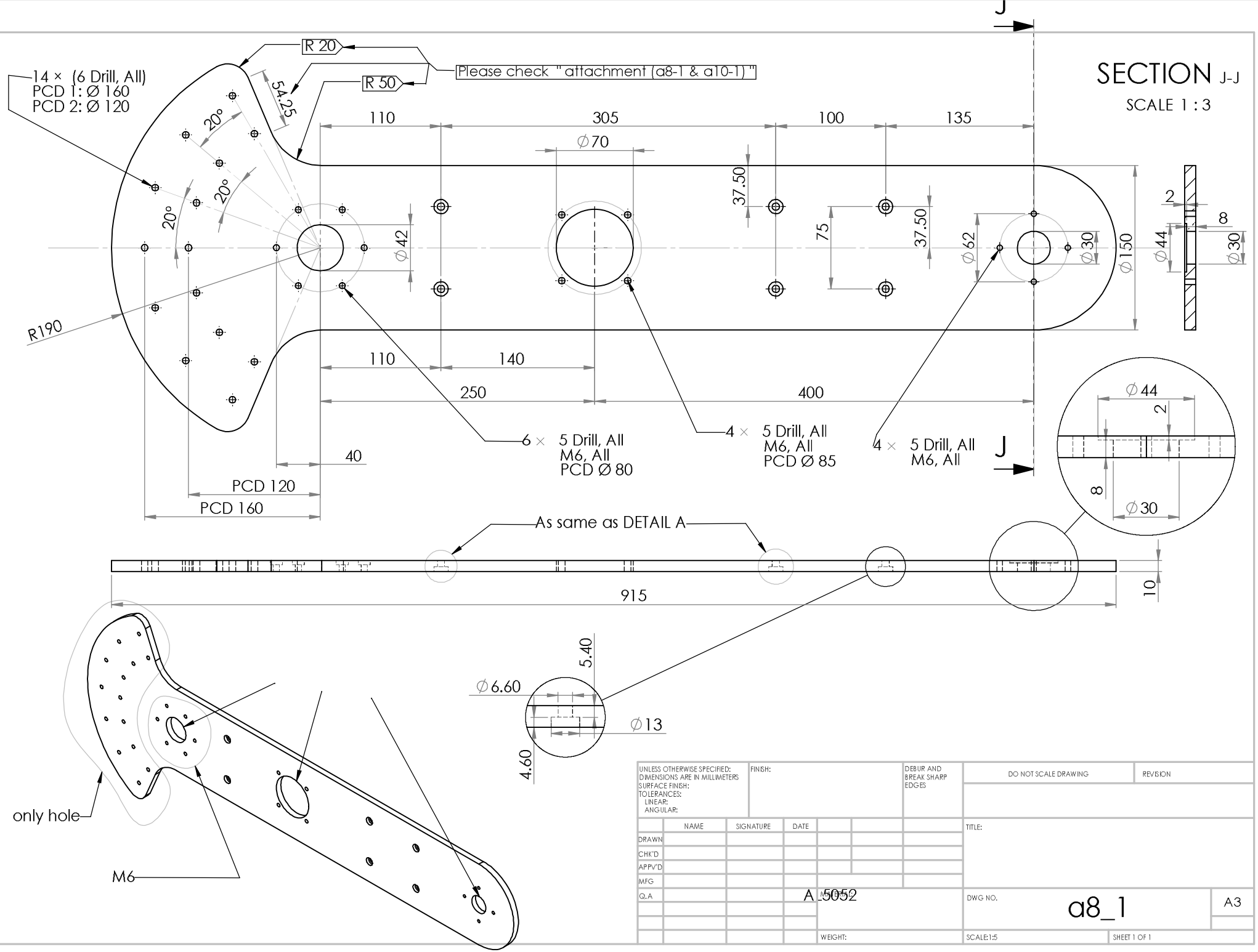
SECTION J-J
SCALE 1 : 3
14 × (6 Drill, All)
PCD 1: Ø 160
PCD 2: Ø 120
R 20
R 50
Please check " attachment (a8-1 & a10-1) "
54.25
20°
20°
20°
20°
110
305
100
135
Ø70
37.50
37.50
75
Ø42
Ø62
Ø30
Ø150
2
8
Ø44
Ø30
R190
110
140
250
400
40
PCD 120
PCD 160
6 × 5 Drill, All
M6, All
PCD Ø 80
4 × 5 Drill, All
M6, All
PCD Ø 85
4 × 5 Drill, All
M6, All
J
J
Ø44
2
8
Ø30
As same as DETAIL A
915
10
Ø6.60
5.40
Ø13
4.60
only hole
M6
UNLESS OTHERWISE SPECIFIED:
DIMENSIONS ARE IN MILLIMETERS
SURFACE FINISH:
TOLERANCES:
LINEAR:
ANGULAR:
FINISH:
DEBUR AND
BREAK SHARP
EDGES
DO NOT SCALE DRAWING
REVISION
NAME
SIGNATURE
DATE
DRAWN
CHK'D
APPV'D
MFG
Q.A
TITLE:
A_5052
DWG NO.
a8_1
A3
WEIGHT:
SCALE:1:5
SHEET 1 OF 1

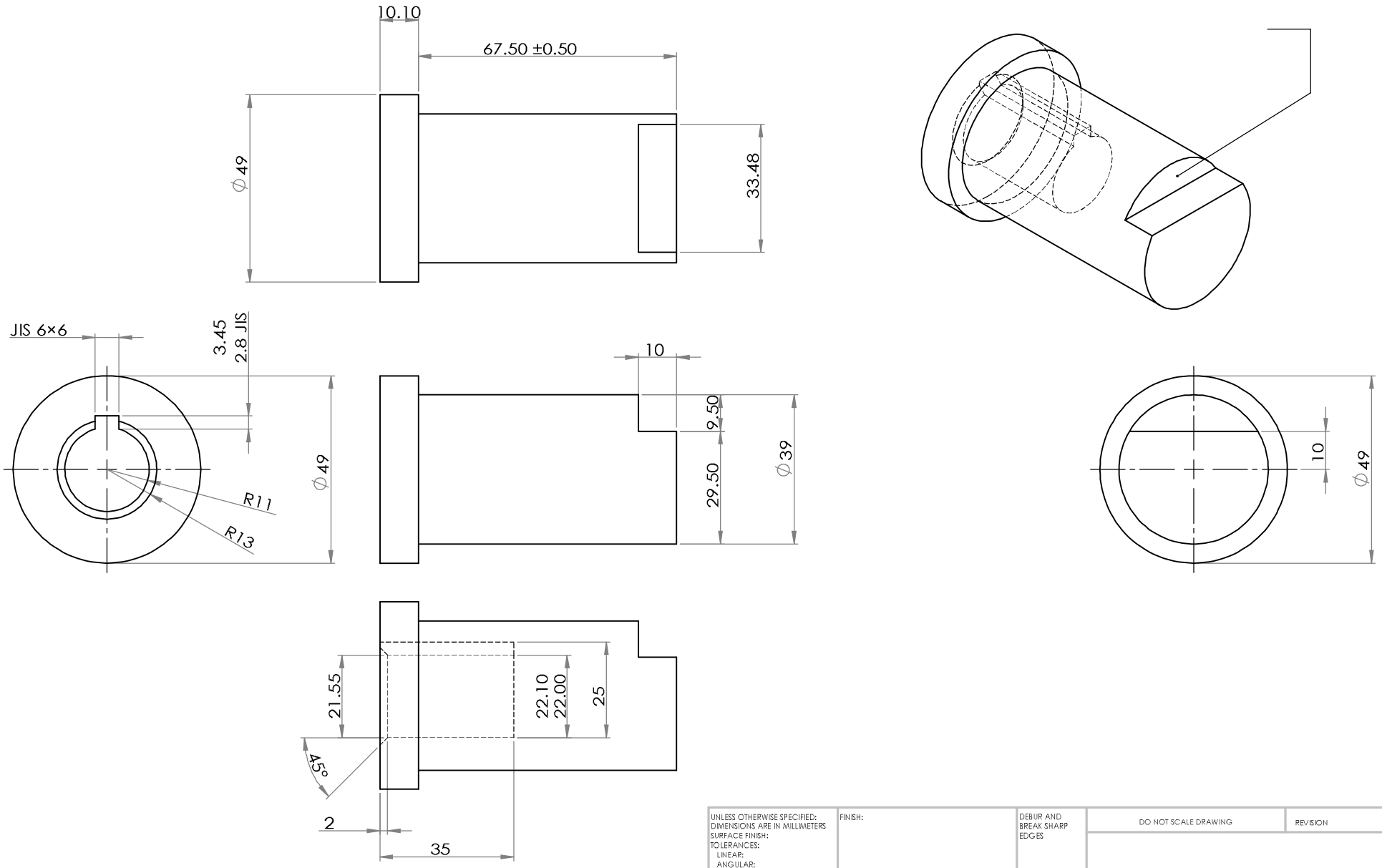

UNLESS OTHERWISE SPECIFIED: DIMENSIONS ARE IN MILLIMETERS SURFACE FINISH: TOLERANCES: LINEAR: ANGULAR:		FINISH:		DEBUR AND BREAK SHARP EDGES		DO NOT SCALE DRAWING	REVISION
	NAME	SIGNATURE	DATE			TITLE:	
DRAWN							
CHK'D							
APPV'D							
MFG							
Q.A				MATERIAL: Iron		DWG NO. a9_1	A3
				WEIGHT:		SCALE:1:1	SHEET 1 OF 1

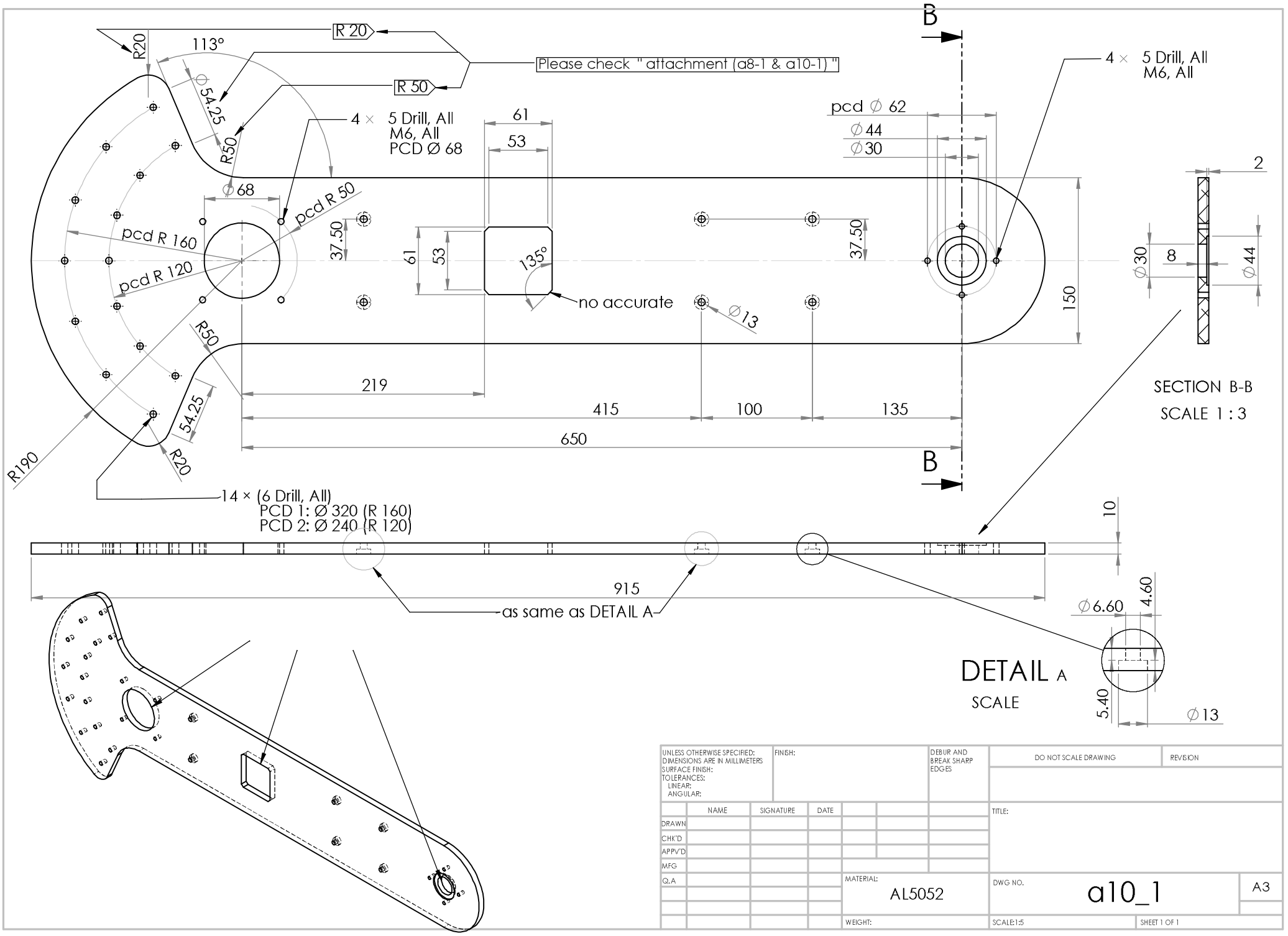

UNLESS OTHERWISE SPECIFIED: DIMENSIONS ARE IN MILLIMETERS SURFACE FINISH: TOLERANCES: LINEAR: ANGULAR:	FINISH:		DEBUR AND BREAK SHARP EDGES	DO NOT SCALE DRAWING	REVISION	
	NAME	SIGNATURE	DATE	TITLE:		
DRAWN						
CHK'D						
APPV'D						
MFG						
Q.A						
				MATERIAL: AL5052	DWG NO. a10_1	A3
				WEIGHT:	SCALE:1:5	SHEET 1 OF 1

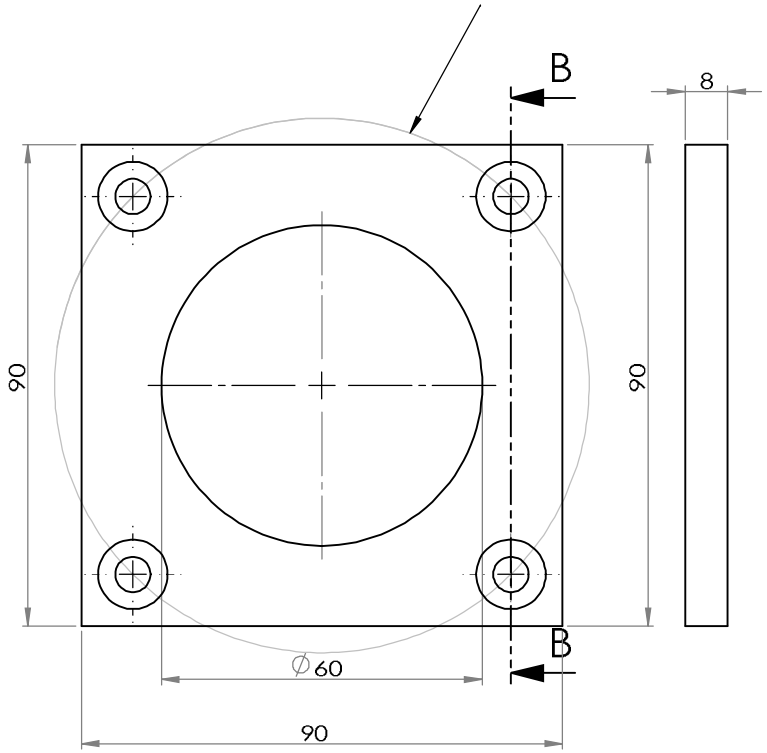

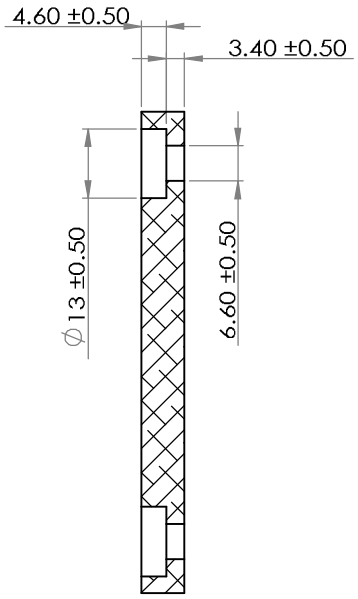

SECTION B-B
SCALE

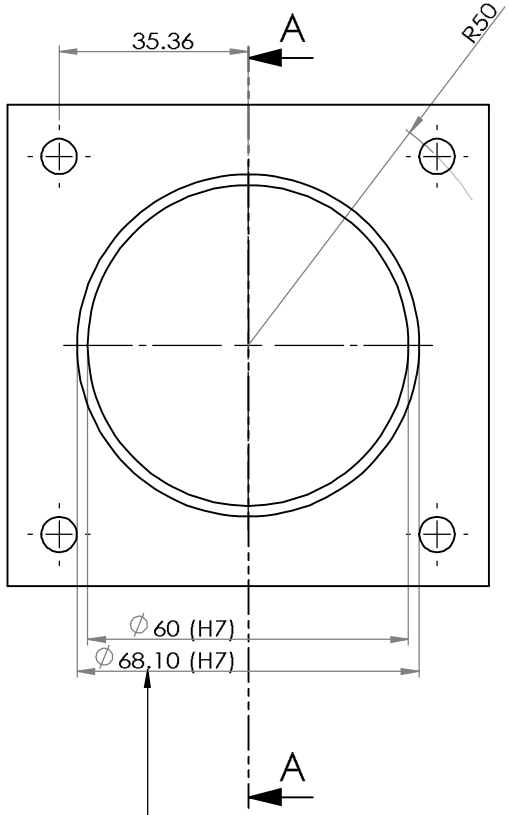

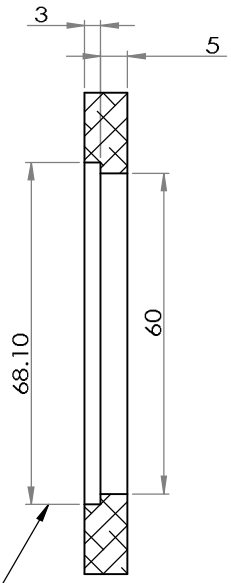

SECTION A-A
SCALE

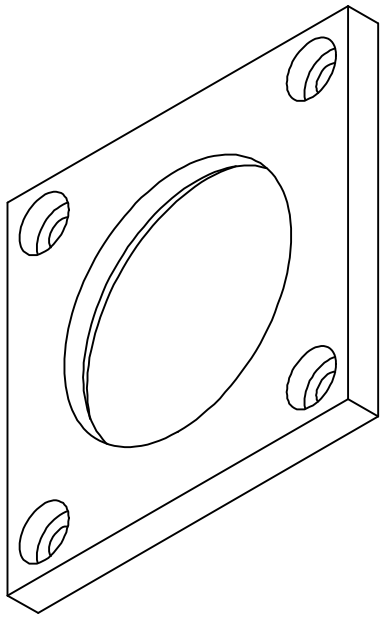

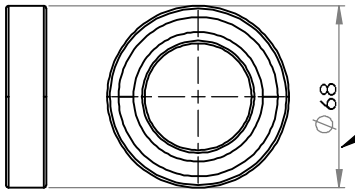

The outside diameter of ball bearing is 68 mm

1:2

1:2

UNLESS OTHERWISE SPECIFIED: DIMENSIONS ARE IN MILLIMETERS SURFACE FINISH: TOLERANCES: LINEAR: ANGULAR:		FINISH:		DEBUR AND BREAK SHARP EDGES	DO NOT SCALE DRAWING	REVISION
	NAME	SIGNATURE	DATE		TITLE:	
DRAWN						
CHK'D						
APPV'D						
MFG						
Q.A				MATERIAL: AL5052	DWG NO. a11_1	A3
				WEIGHT:	SCALE:1:2	SHEET 1 OF 1

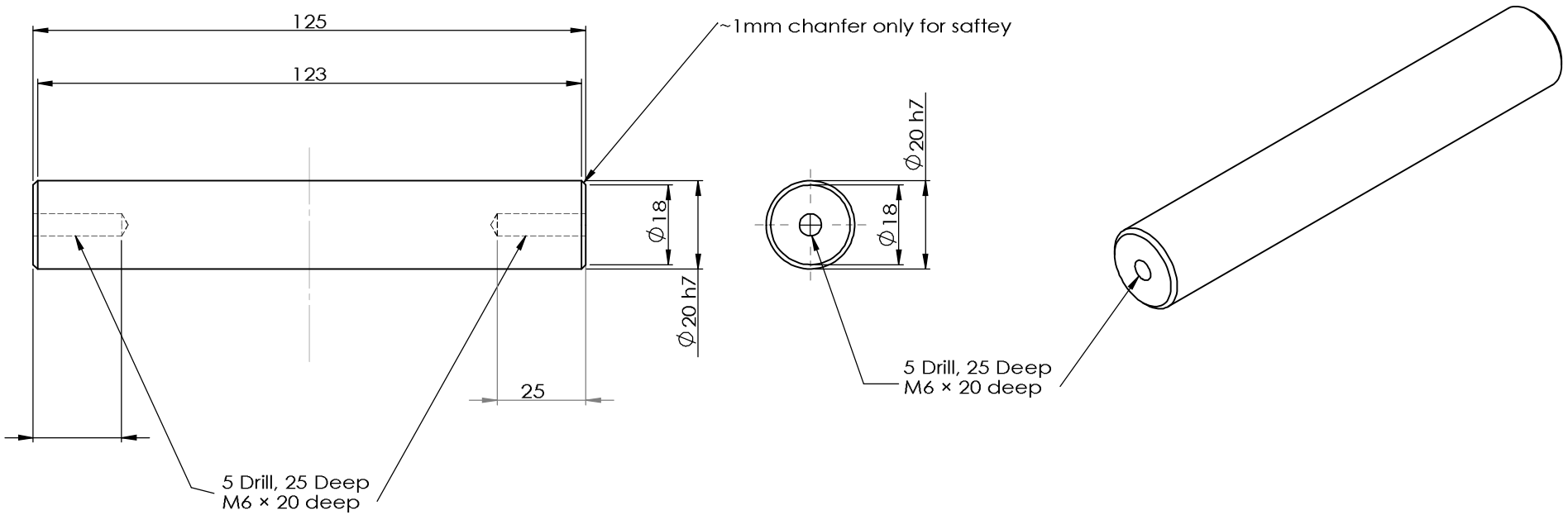

UNLESS OTHERWISE SPECIFIED: DIMENSIONS ARE IN MILLIMETERS SURFACE FINISH: TOLERANCES: LINEAR: ANGULAR:	FINISH:		DEBUR AND BREAK SHARP EDGES	DO NOT SCALE DRAWING	REVISION	
	NAME	SIGNATURE	DATE	TITLE:		
DRAWN						
CHK'D						
APPV'D						
MFG						
Q.A				MATERIAL: PVC	DWG NO. a12_1	A3
				WEIGHT:	SCALE:1:1	SHEET 1 OF 1

Left

In this drawing we can send special file to feed your laser cutting system directly.

Right

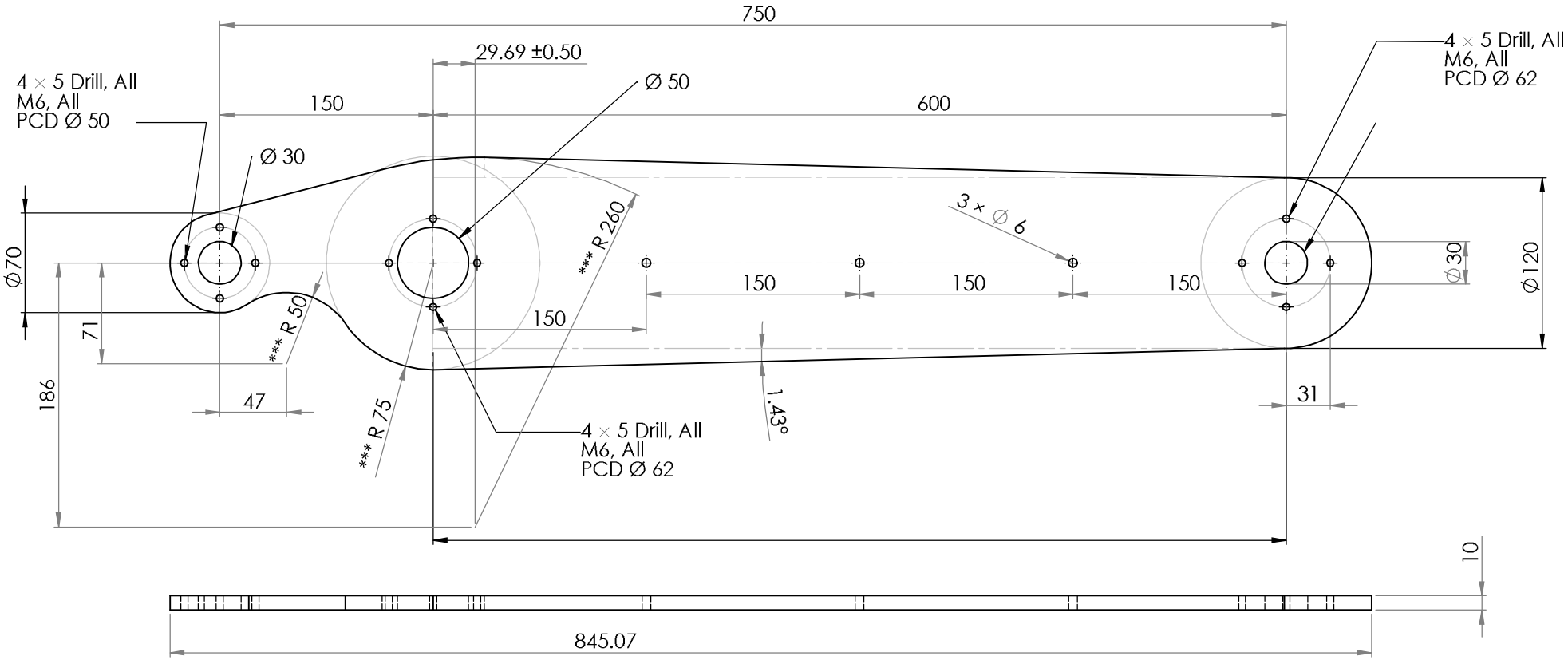

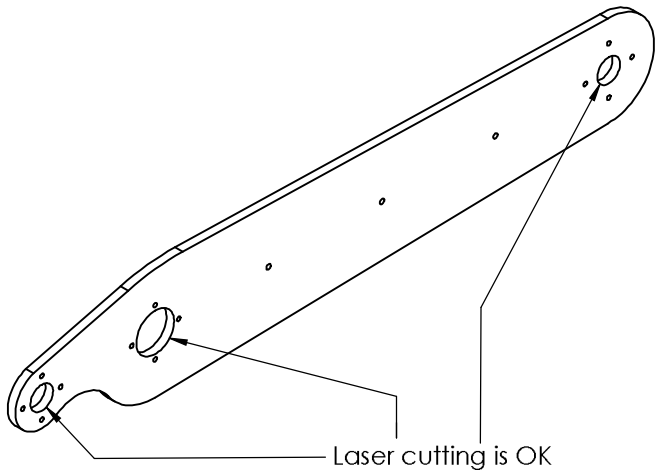

*** not need so accuracy

UNLESS OTHERWISE SPECIFIED: DIMENSIONS ARE IN MILLIMETERS SURFACE FINISH: TOLERANCES: LINEAR: ANGULAR:	FINISH:		DEBUR AND BREAK SHARP EDGES	DO NOT SCALE DRAWING	REVISION	
	NAME	SIGNATURE	DATE	TITLE:		
DRAWN						
CHK'D						
APPV'D						
MFG						
Q.A				MATERIAL: AL5052	DWG NO. a13_1	A3
				WEIGHT:	SCALE:1:5	SHEET 1 OF 1

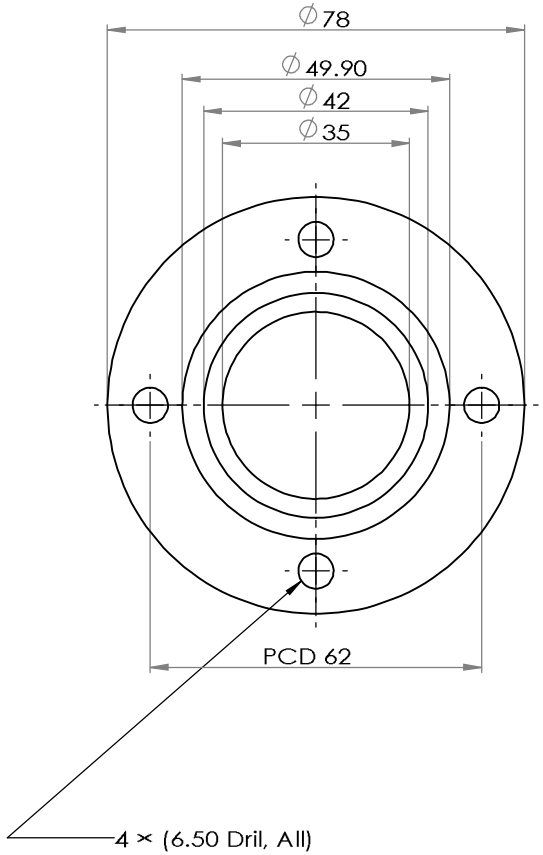

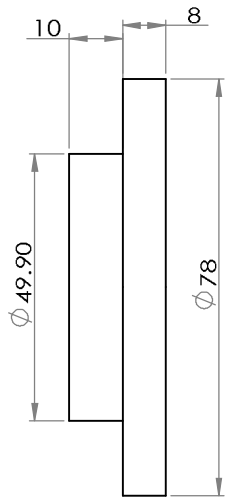

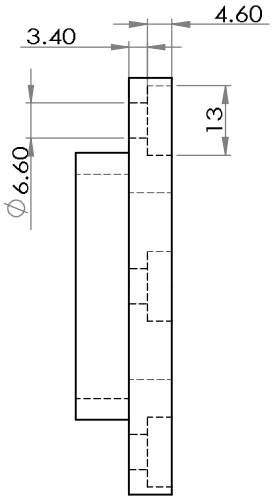

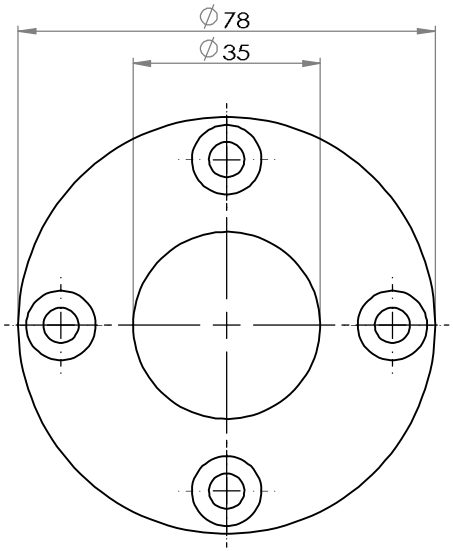

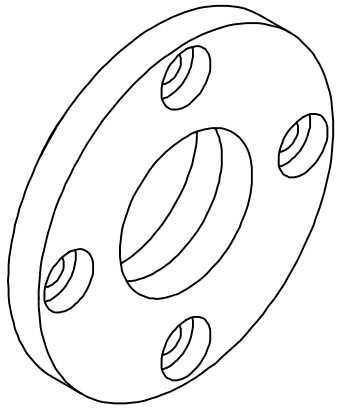

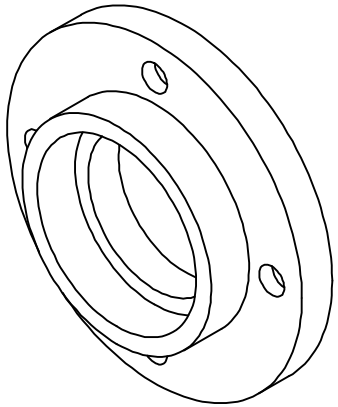

UNLESS OTHERWISE SPECIFIED: DIMENSIONS ARE IN MILLIMETERS SURFACE FINISH: TOLERANCES: LINEAR: ANGULAR:		FINISH:		DEBUR AND BREAK SHARP EDGES		DO NOT SCALE DRAWING	REVISION
	NAME	SIGNATURE	DATE			TITLE:	
DRAWN							
CHK'D							
APPV'D							
MFG							
Q.A				MATERIAL: AL5052		DWG NO. a14_1	A3
				WEIGHT:		SCALE:1:1	SHEET 1 OF 1

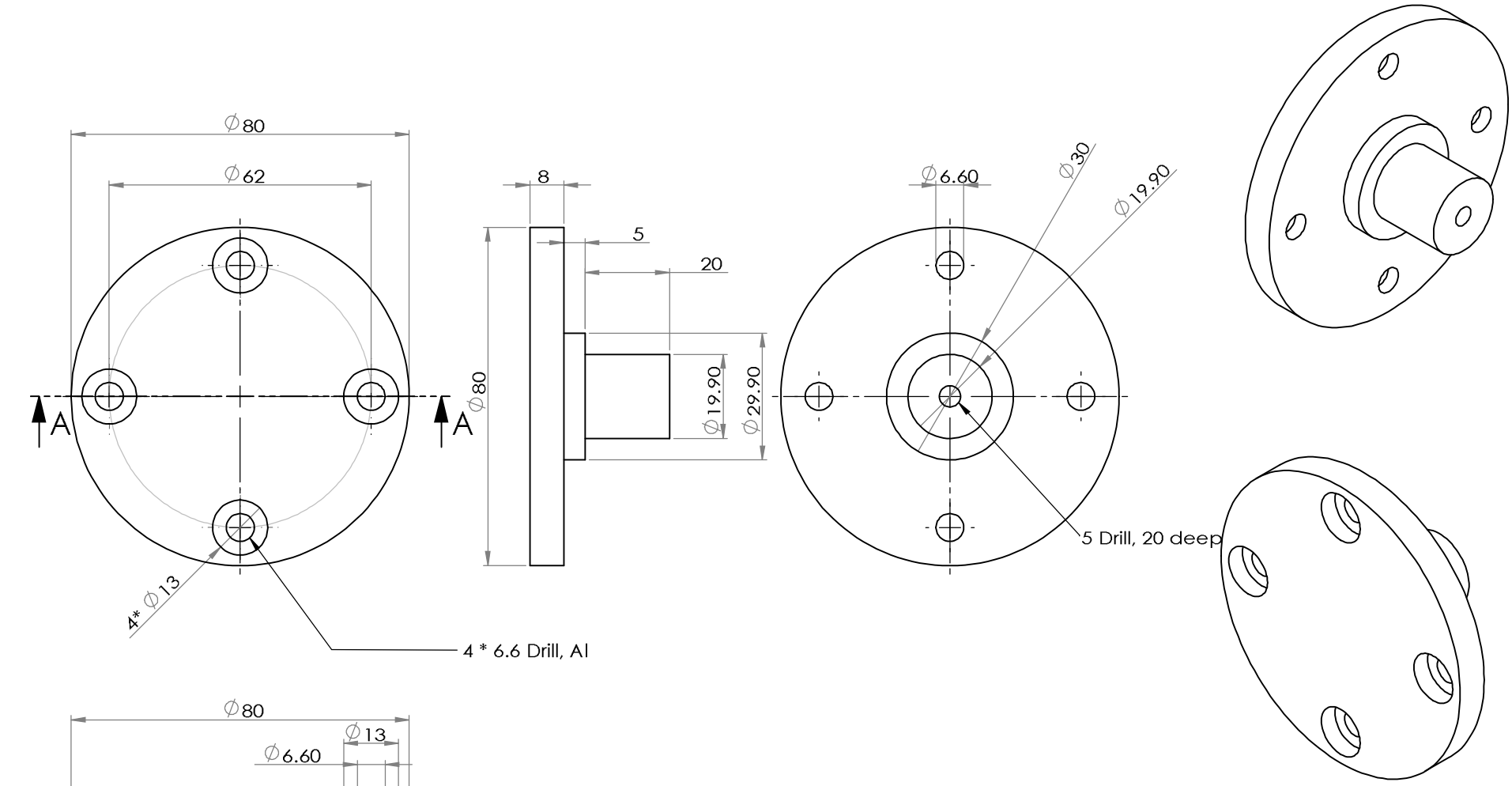

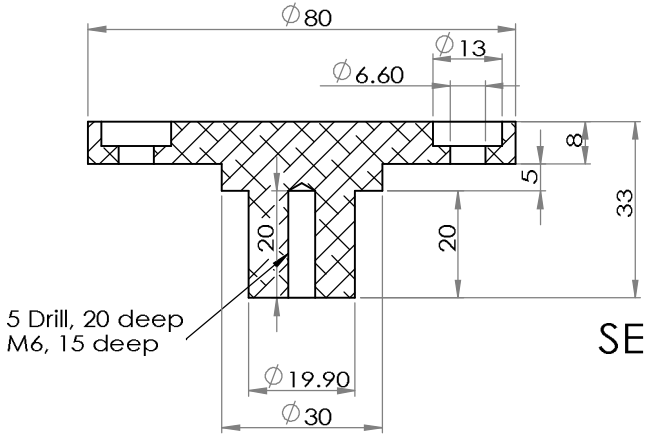

SECTION A-A

UNLESS OTHERWISE SPECIFIED: DIMENSIONS ARE IN MILLIMETERS SURFACE FINISH: TOLERANCES: LINEAR: ANGULAR:		FINISH:		DEBUR AND BREAK SHARP EDGES		DO NOT SCALE DRAWING	REVISION
	NAME	SIGNATURE	DATE			TITLE:	
DRAWN							
CHK'D							
APPV'D							
MFG							
Q.A				MATERIAL: AL5052		DWG NO. a26_1	A3
				WEIGHT:		SCALE:1:1	SHEET 1 OF 1

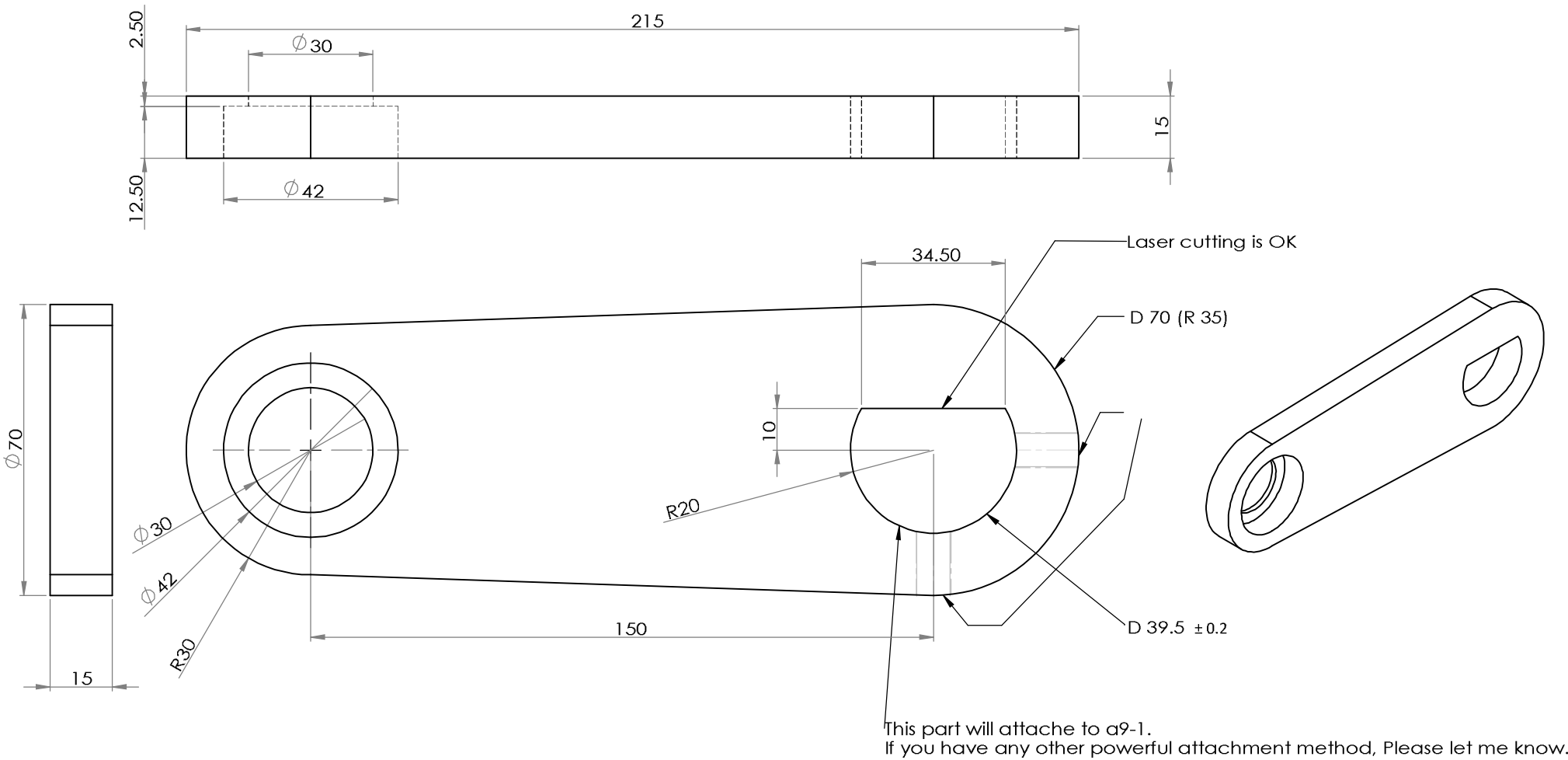

UNLESS OTHERWISE SPECIFIED: DIMENSIONS ARE IN MILLIMETERS SURFACE FINISH: TOLERANCES: LINEAR: ANGULAR:	FINISH:		DEBUR AND BREAK SHARP EDGES	DO NOT SCALE DRAWING	REVISION	
	NAME	SIGNATURE	DATE	TITLE:		
DRAWN						
CHK'D						
APPV'D						
MFG						
Q.A				MATERIAL: AL5052	DWG NO. a15_1	A3
				WEIGHT:	SCALE:1:1	SHEET 1 OF 1

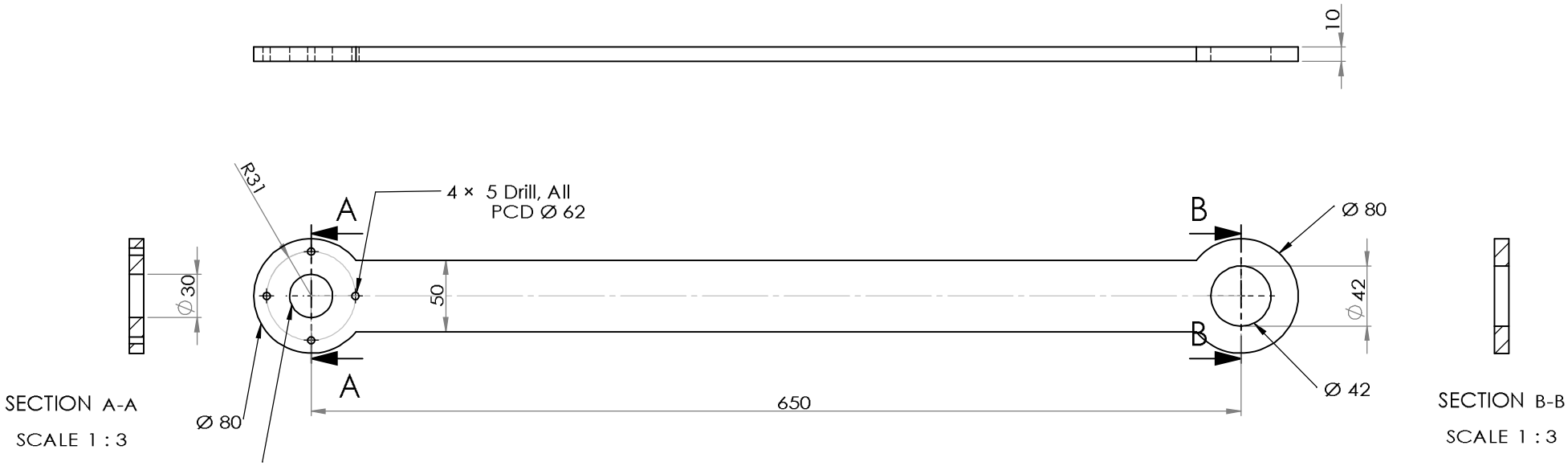

SECTION A-A

SCALE 1 : 3

SECTION B-B

SCALE 1 : 3

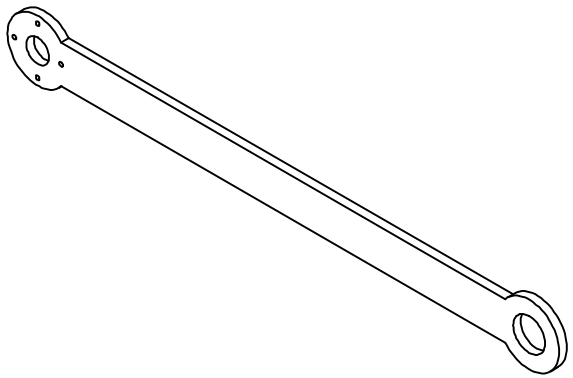

UNLESS OTHERWISE SPECIFIED: DIMENSIONS ARE IN MILLIMETERS SURFACE FINISH: TOLERANCES: LINEAR: ANGULAR:		FINISH:			DEBUR AND BREAK SHARP EDGES	DO NOT SCALE DRAWING	REVISION
	NAME	SIGNATURE	DATE			TITLE:	
DRAWN							
CHK'D							
APPV'D							
MFG							
Q.A				MATERIAL: AL5052		DWG NO. a16_1	A3
				WEIGHT:		SCALE:1:5	SHEET 1 OF 1

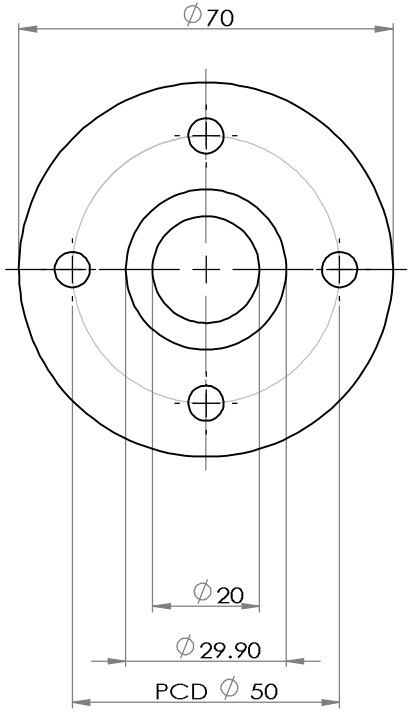

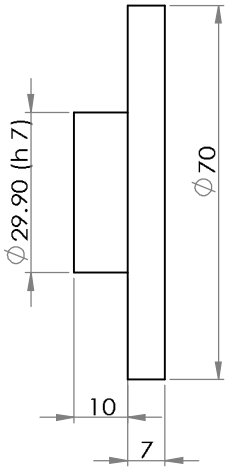

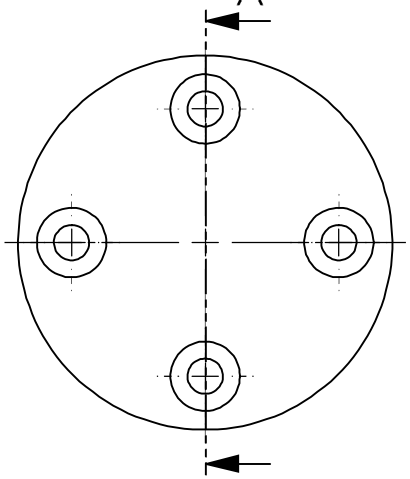

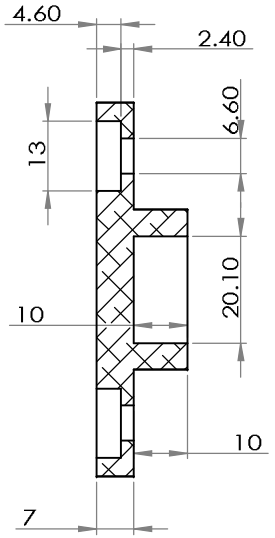

SECTION A-A

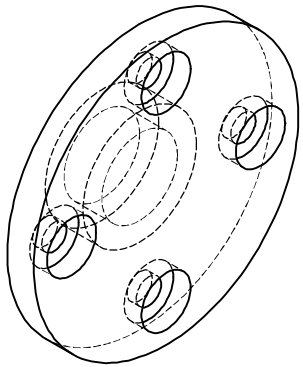

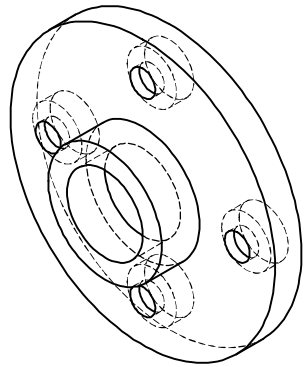

UNLESS OTHERWISE SPECIFIED: DIMENSIONS ARE IN MILLIMETERS SURFACE FINISH: TOLERANCES: LINEAR: ANGULAR:		FINISH:		DEBUR AND BREAK SHARP EDGES		DO NOT SCALE DRAWING	REVISION
	NAME	SIGNATURE	DATE			TITLE:	
DRAWN							
CHK'D							
APPV'D							
MFG							
Q.A				MATERIAL: AL5052		DWG NO. a17_1	A3
				WEIGHT:		SCALE:1:1	SHEET 1 OF 1

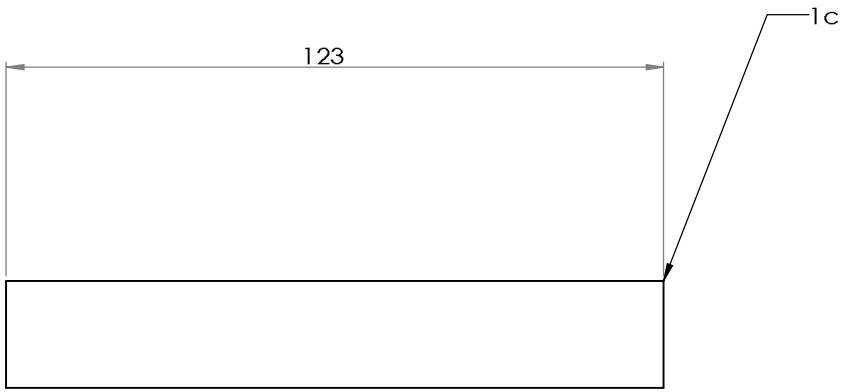

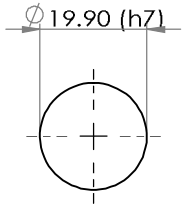

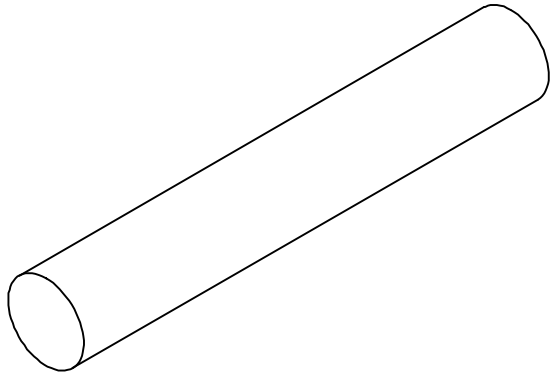

UNLESS OTHERWISE SPECIFIED: DIMENSIONS ARE IN MILLIMETERS SURFACE FINISH: TOLERANCES: LINEAR: ANGULAR:		FINISH:			DEBUR AND BREAK SHARP EDGES	DO NOT SCALE DRAWING	REVISION
	NAME	SIGNATURE	DATE			TITLE:	
DRAWN							
CHK'D							
APPV'D							
MFG							
Q.A				MATERIAL: Iron		DWG NO. a18_1	A3
				WEIGHT:		SCALE:1:1	SHEET 1 OF 1

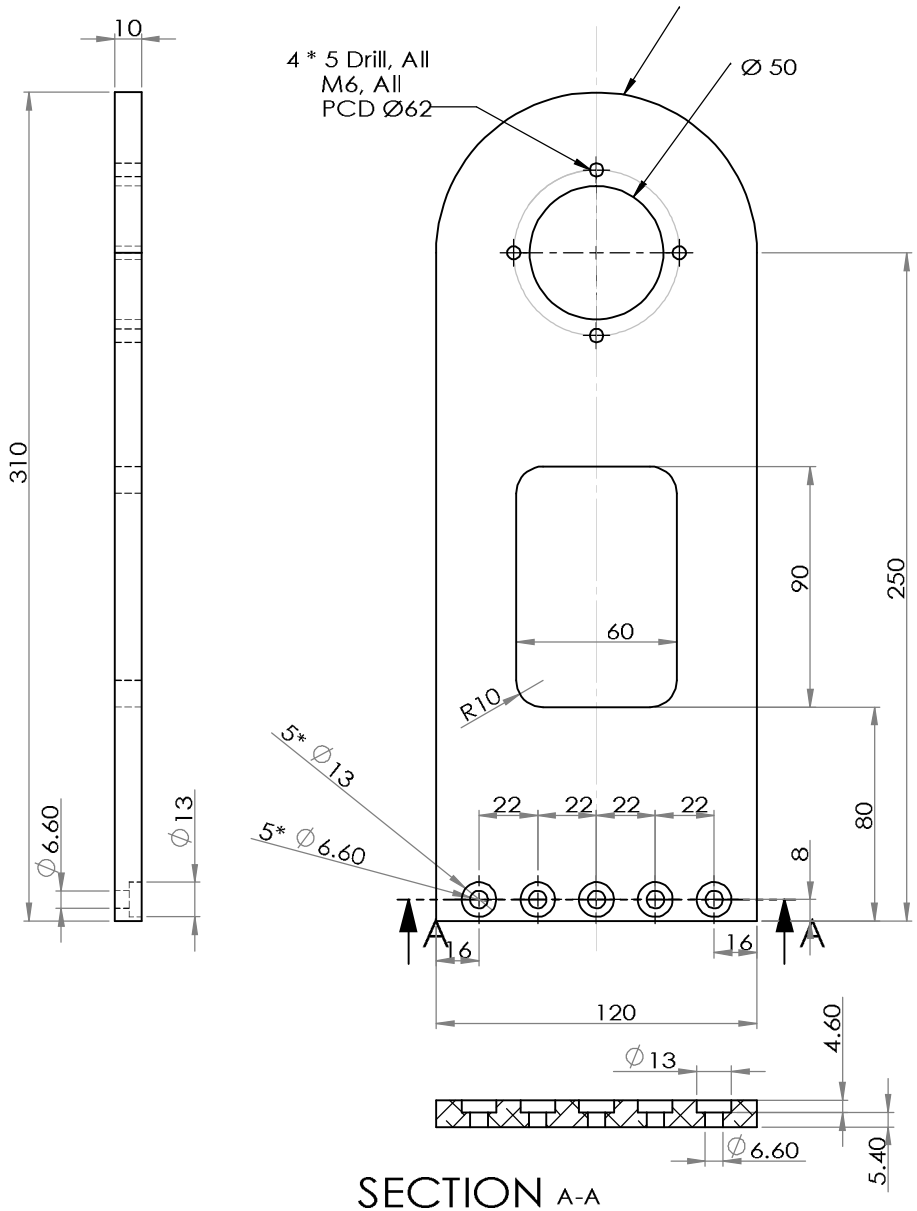

SECTION A-A

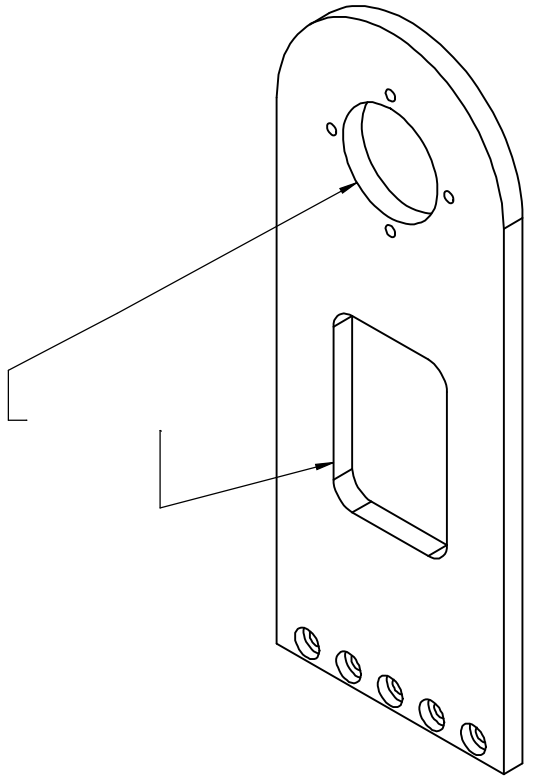

UNLESS OTHERWISE SPECIFIED: DIMENSIONS ARE IN MILLIMETERS SURFACE FINISH: TOLERANCES: LINEAR: ANGULAR:		FINISH:		DEBUR AND BREAK SHARP EDGES			DO NOT SCALE DRAWING	REVISION
	NAME	SIGNATURE	DATE				TITLE:	
DRAWN								
CHK'D								
APPV'D								
MFG								
Q.A				MATERIAL: AL5052			DWG NO. a20_1	A3
				WEIGHT:			SCALE:1:2	SHEET 1 OF 1

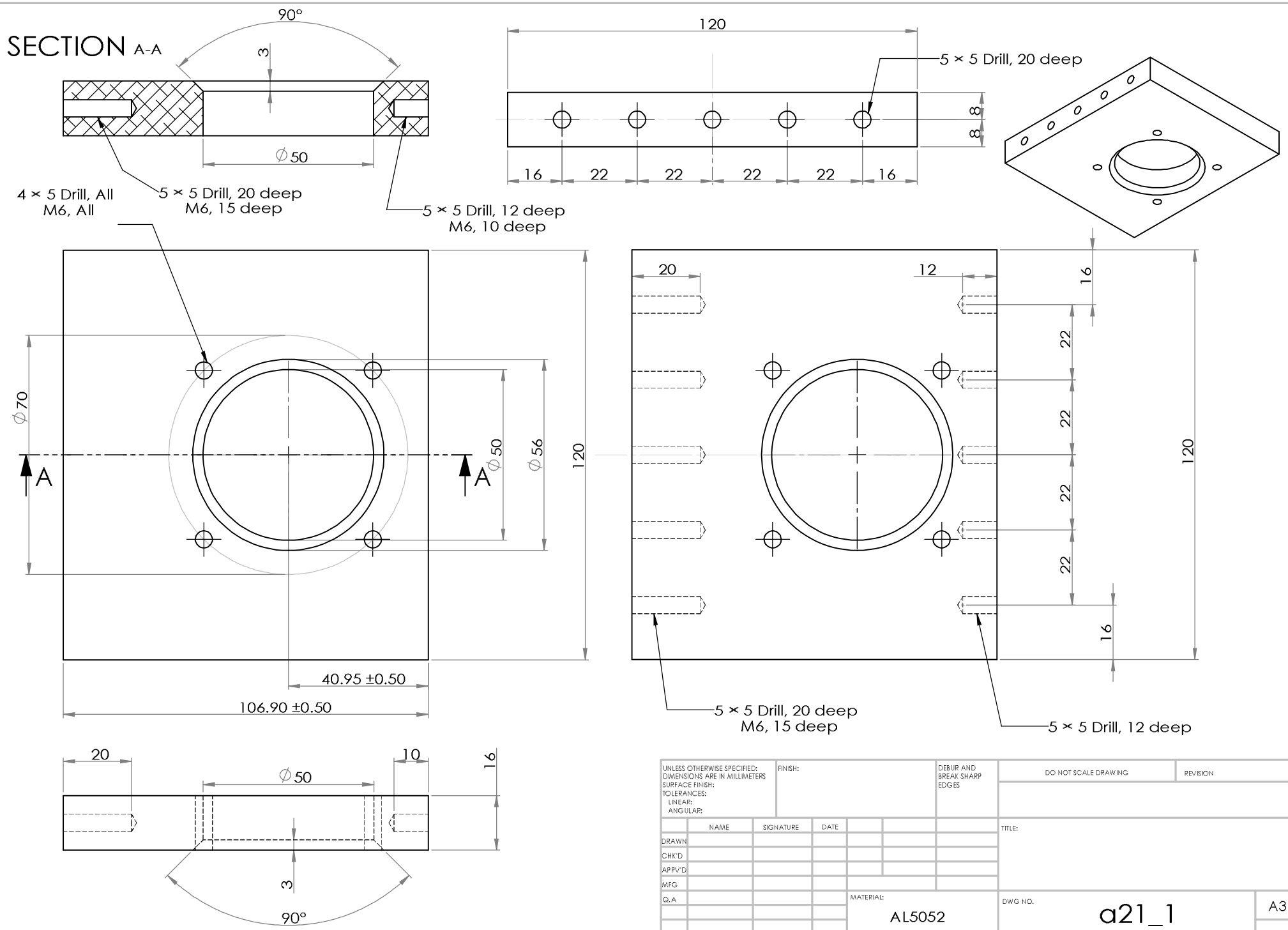

UNLESS OTHERWISE SPECIFIED: DIMENSIONS ARE IN MILLIMETERS SURFACE FINISH: TOLERANCES: LINEAR: ANGULAR:	FINISH:		DEBUR AND BREAK SHARP EDGES	DO NOT SCALE DRAWING	REVISION	
	NAME	SIGNATURE	DATE	TITLE:		
DRAWN						
CHK'D						
APPV'D						
MFG						
Q.A						
				MATERIAL: AL5052	DWG NO. a21_1	A3
				WEIGHT:	SCALE:1:1	SHEET 1 OF 1

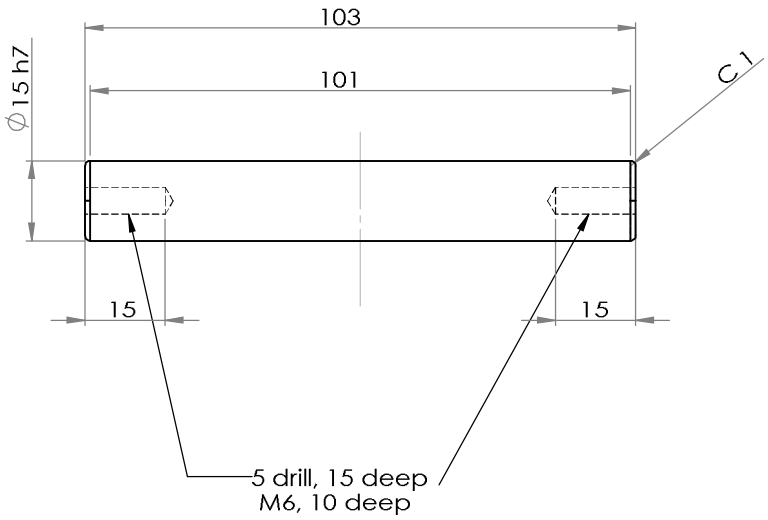

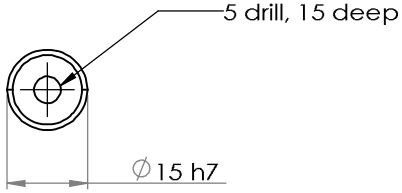

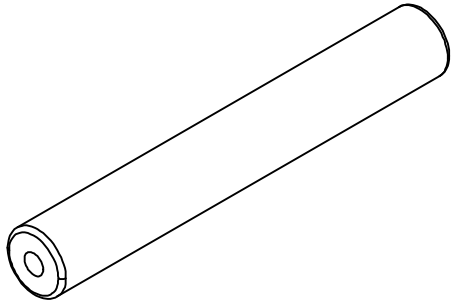

UNLESS OTHERWISE SPECIFIED: DIMENSIONS ARE IN MILLIMETERS SURFACE FINISH: TOLERANCES: LINEAR: ANGULAR:		FINISH:		DEBUR AND BREAK SHARP EDGES		DO NOT SCALE DRAWING	REVISION
	NAME	SIGNATURE	DATE			TITLE:	
DRAWN							
CHK'D							
APPV'D							
MFG							
Q.A				MATERIAL: PVC		DWG NO. a23_1	A3
				WEIGHT:		SCALE:1:1	SHEET 1 OF 1

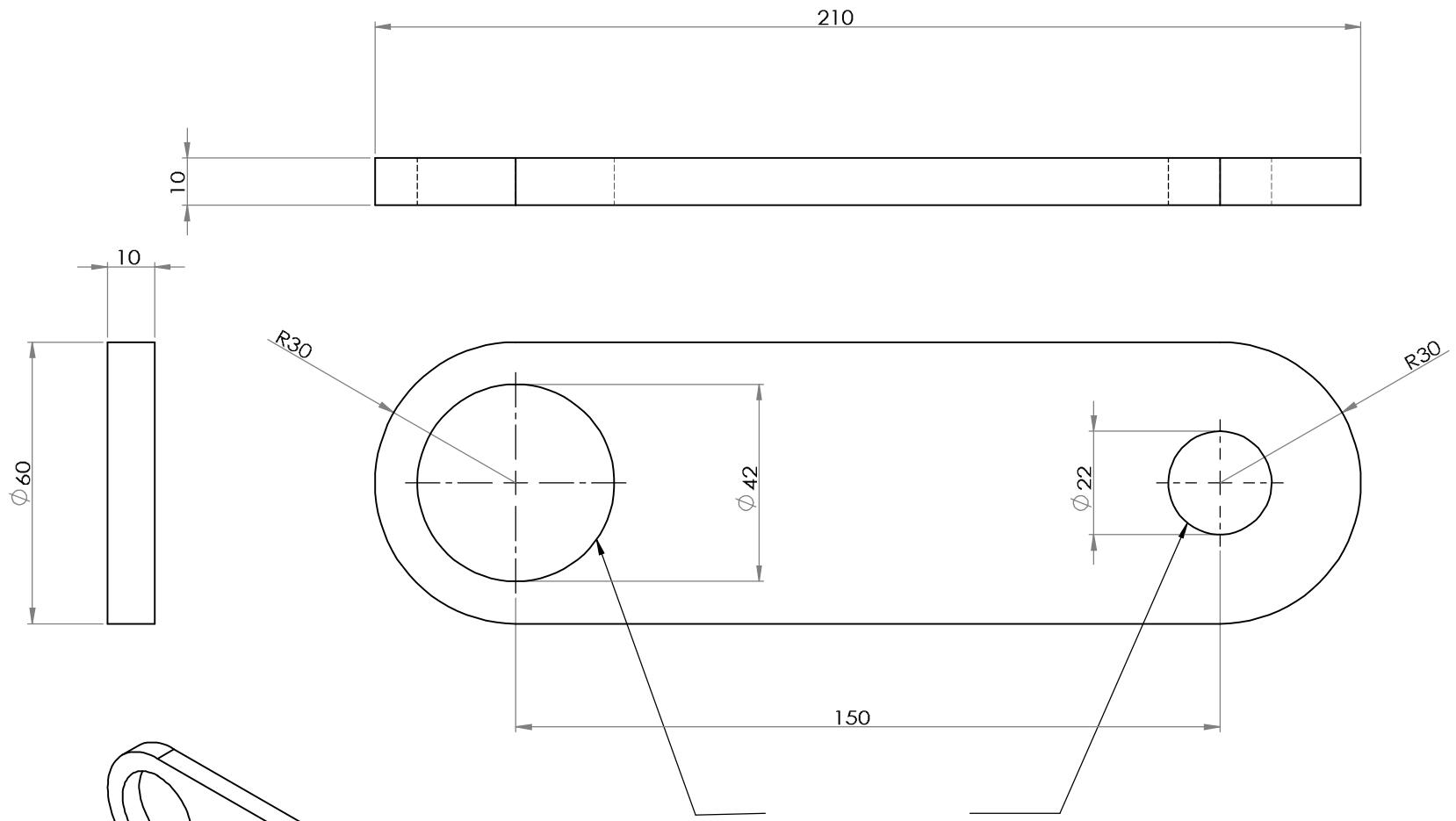

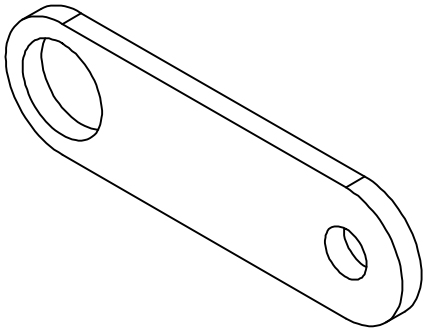

SCALE 1 : 2

UNLESS OTHERWISE SPECIFIED: DIMENSIONS ARE IN MILLIMETERS SURFACE FINISH: TOLERANCES: LINEAR: ANGULAR:		FINISH:		DEBUR AND BREAK SHARP EDGES		DO NOT SCALE DRAWING	REVISION
	NAME	SIGNATURE	DATE			TITLE:	
DRAWN							
CHK'D							
APPV'D							
MFG							
Q.A				MATERIAL: AL5052		DWG NO. a24_1	A3
				WEIGHT:		SCALE:1:1	SHEET 1 OF 1

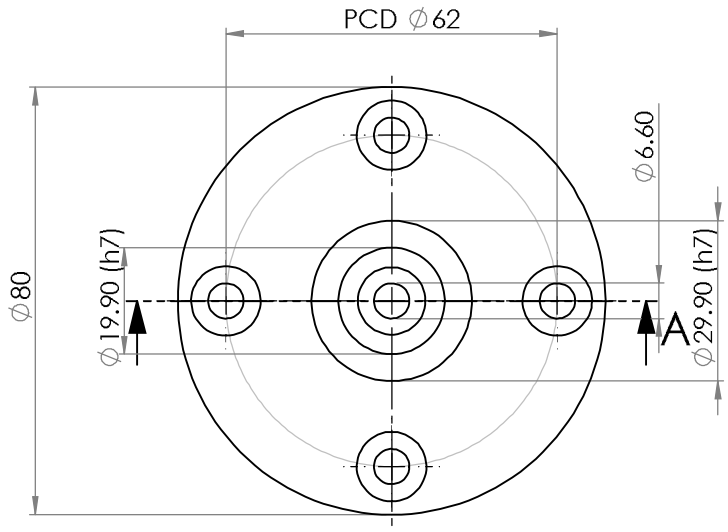

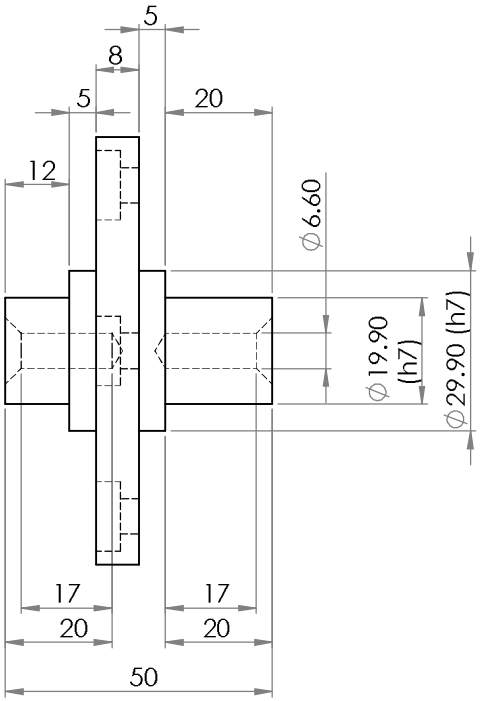

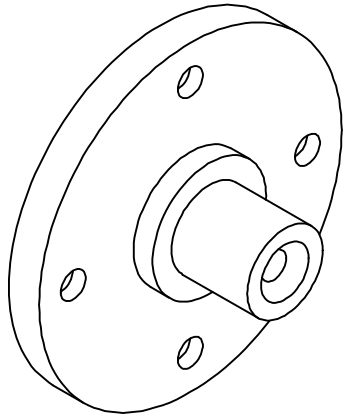

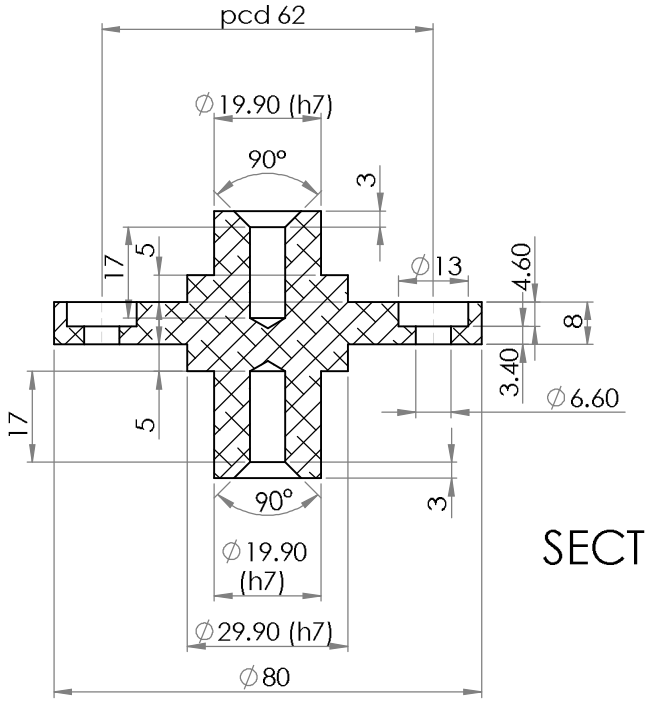

SECTION A-A

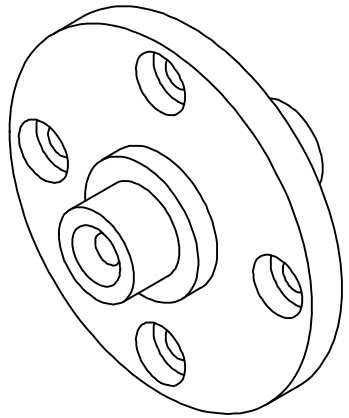

UNLESS OTHERWISE SPECIFIED: DIMENSIONS ARE IN MILLIMETERS SURFACE FINISH: TOLERANCES: LINEAR: ANGULAR:		FINISH:		DEBUR AND BREAK SHARP EDGES	DO NOT SCALE DRAWING	REVISION
	NAME	SIGNATURE	DATE		TITLE:	
DRAWN						
CHK'D						
APPV'D						
MFG						
Q.A				MATERIAL: AL5052	DWG NO. a26 - Copy_1	A3
				WEIGHT:	SCALE:1:1	SHEET 1 OF 1

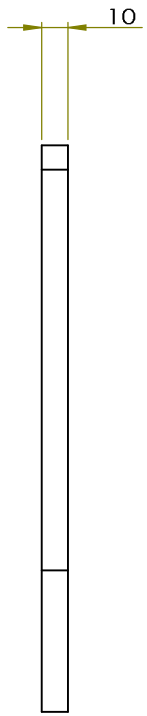

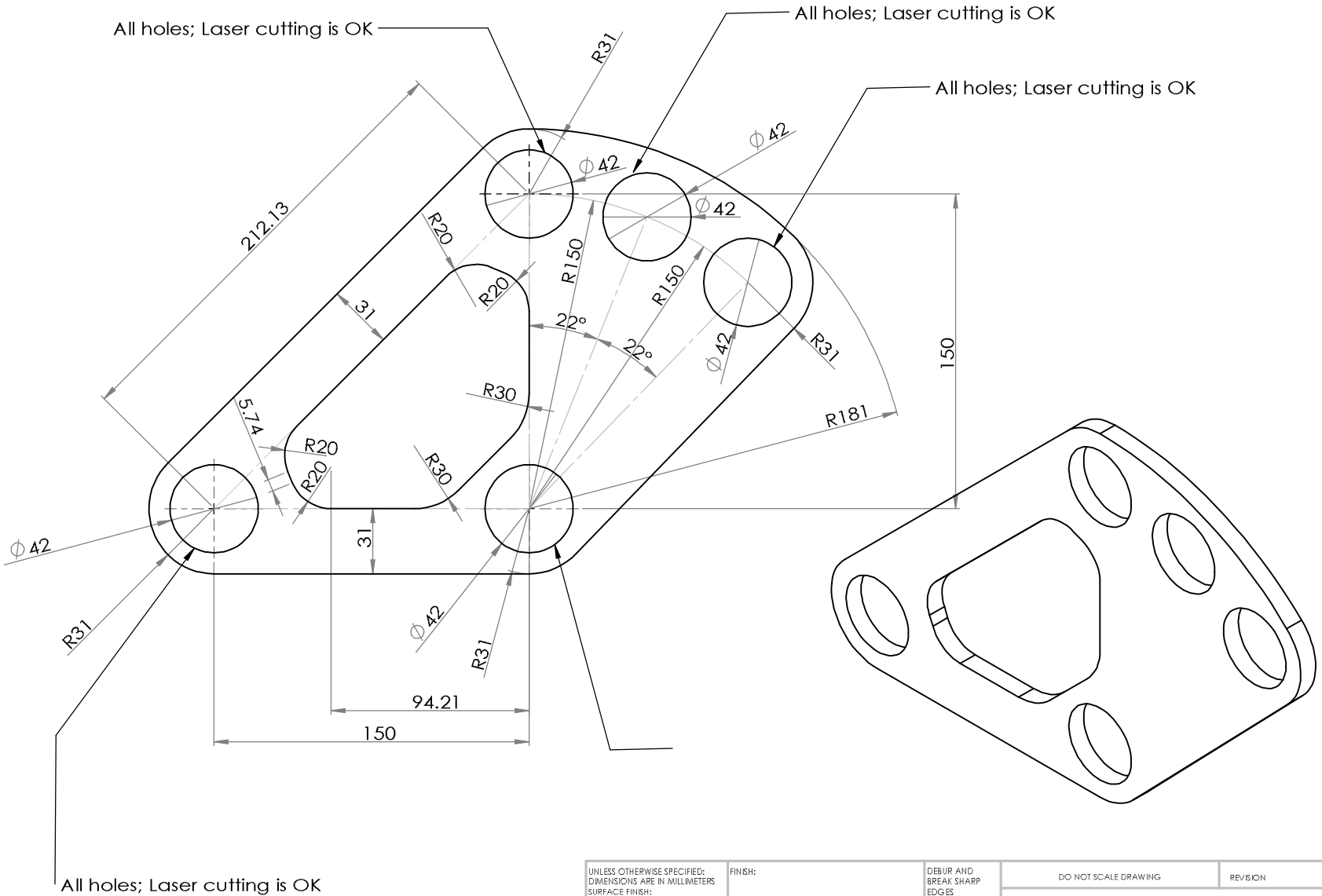

UNLESS OTHERWISE SPECIFIED: DIMENSIONS ARE IN MILLIMETERS SURFACE FINISH: TOLERANCES: LINEAR: ANGULAR:		FINISH:		DEBUR AND BREAK SHARP EDGES		DO NOT SCALE DRAWING	REVISION
	NAME	SIGNATURE	DATE			TITLE:	
DRAWN							
CHK'D							
APPV'D							
MFG							
Q.A				MATERIAL: AL5052		DWG NO. a25_1	A3
				WEIGHT:		SCALE:1:2	SHEET 1 OF 1

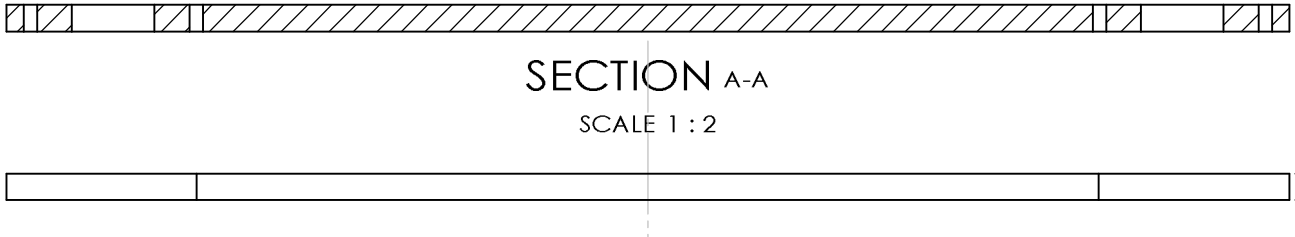

SECTION A-A

SCALE 1 : 2

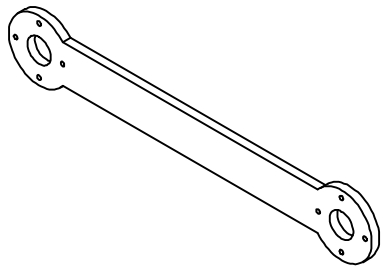

SCALE 1 : 2

UNLESS OTHERWISE SPECIFIED: DIMENSIONS ARE IN MILLIMETERS SURFACE FINISH: TOLERANCES: LINEAR: ANGULAR:		FINISH:		DEBUR AND BREAK SHARP EDGES		DO NOT SCALE DRAWING	REVISION
	NAME	SIGNATURE	DATE			TITLE:	
DRAWN							
CHK'D							
APPV'D							
MFG							
Q.A				MATERIAL: AL5052		DWG NO. a27_1	A3
				WEIGHT:		SCALE:1:5	SHEET 1 OF 1

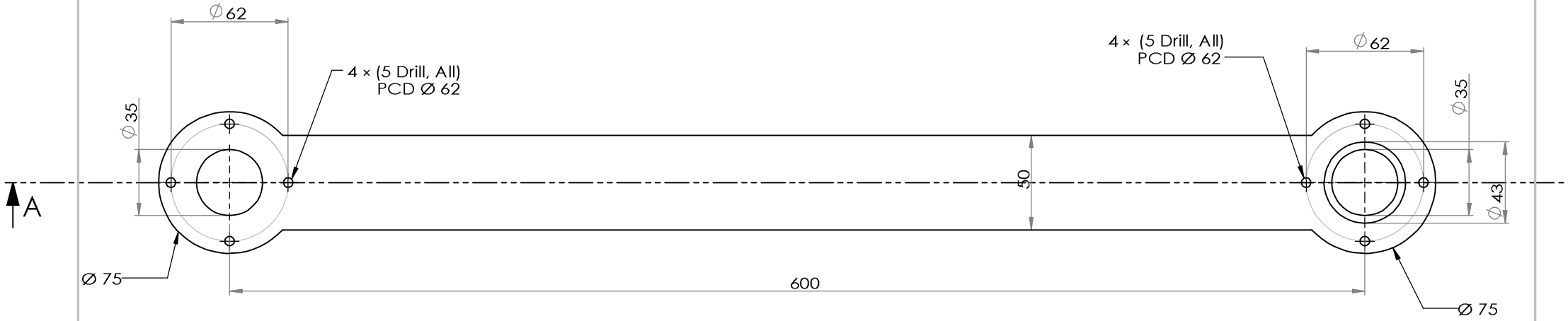

SECTION A-A

SCALE 1 : 2

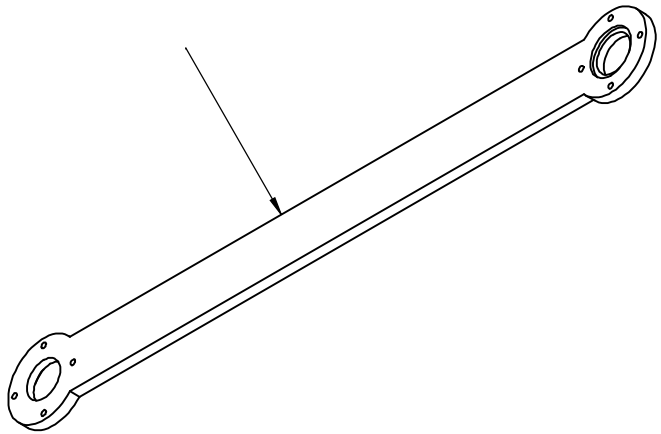

SCALE 1 : 2

UNLESS OTHERWISE SPECIFIED: DIMENSIONS ARE IN MILLIMETERS SURFACE FINISH: TOLERANCES: LINEAR: ANGULAR:		FINISH:		DEBUR AND BREAK SHARP EDGES		DO NOT SCALE DRAWING	REVISION
	NAME	SIGNATURE	DATE			TITLE:	
DRAWN							
CHK'D							
APPV'D							
MFG							
Q.A				MATERIAL: AL5052		DWG NO. a28_1	A3
				WEIGHT:		SCALE:1:5	SHEET 1 OF 1

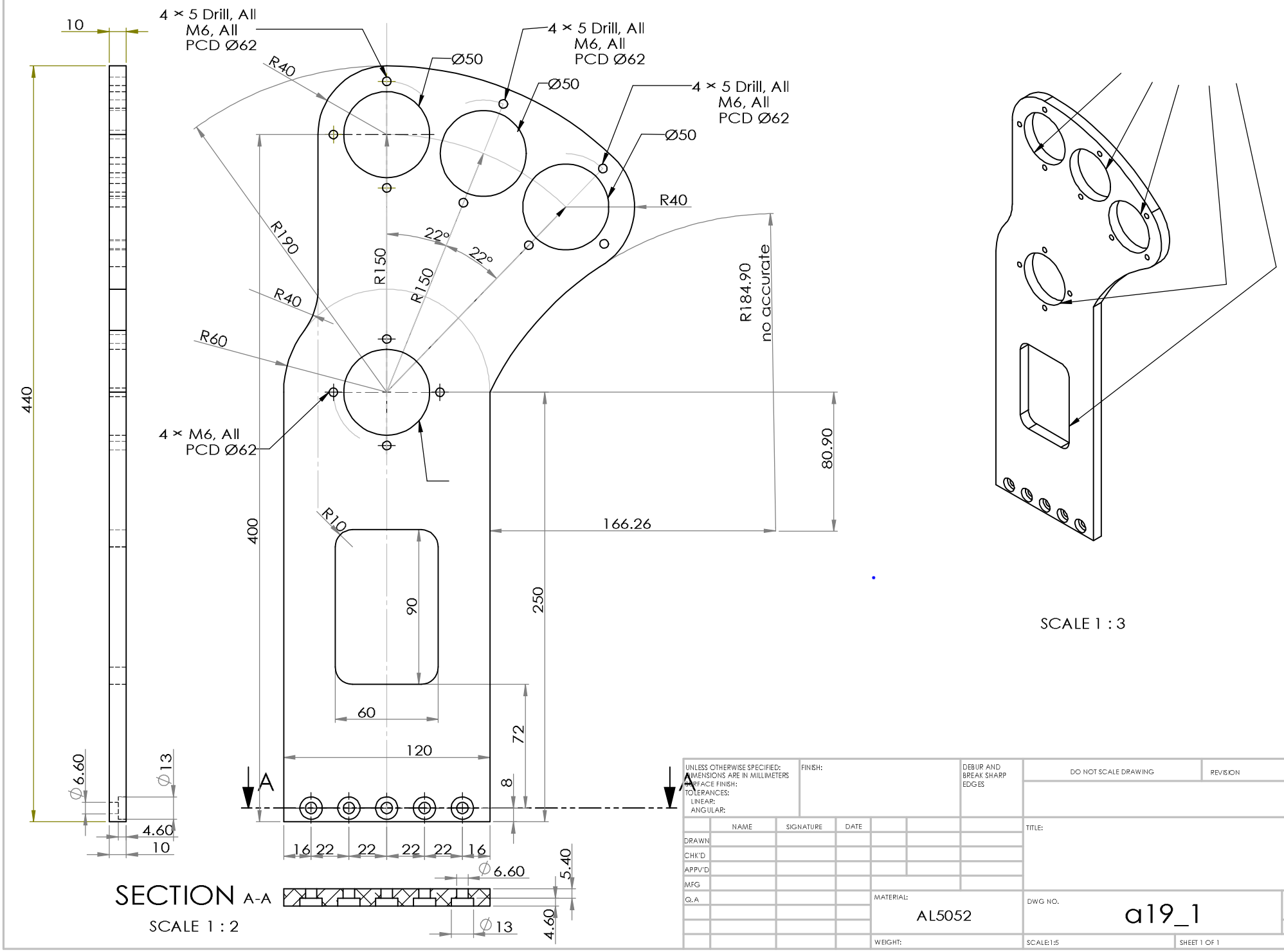
10
4 × 5 Drill, All
M6, All
PCD Ø62
R40
Ø50
4 × 5 Drill, All
M6, All
PCD Ø62
Ø50
4 × 5 Drill, All
M6, All
PCD Ø62
Ø50
R40
R190
22°
22°
R150
R150
R184.90
no accurate
R40
R60
4 × M6, All
PCD Ø62
80.90
440
400
R10
166.26
250
90
60
120
72
8
A
A
Ø6.60
Ø13
4.60
10
16 22 22 22 22 16
Ø6.60
5.40
Ø13
4.60
SECTION A-A
SCALE 1 : 2
SCALE 1 : 3
UNLESS OTHERWISE SPECIFIED:
DIMENSIONS ARE IN MILLIMETERS
SURFACE FINISH:
TOLERANCES:
LINEAR:
ANGULAR:
FINISH:
DEBUR AND
BREAK SHARP
EDGES
DO NOT SCALE DRAWING
REVISION
NAME
SIGNATURE
DATE
DRAWN
CHK'D
APPV'D
MFG
Q.A
TITLE:
MATERIAL:
AL5052
DWG NO.
a19_1
A3
WEIGHT:
SCALE:1:5
SHEET 1 OF 1

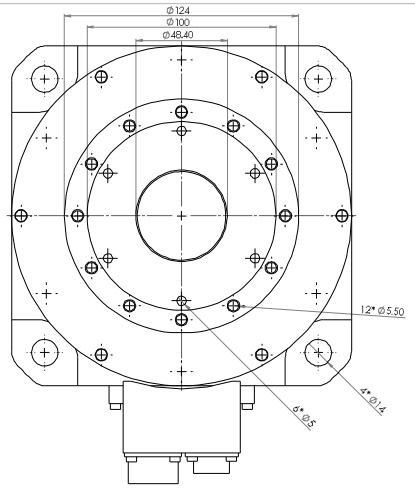

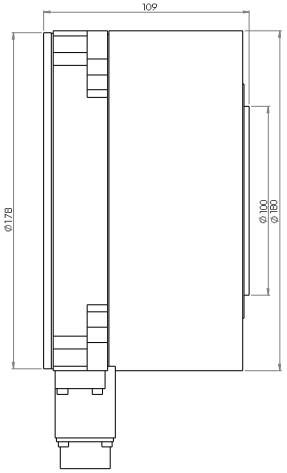

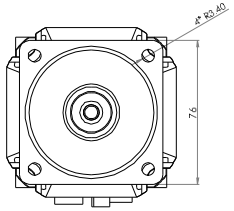

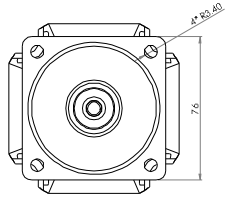

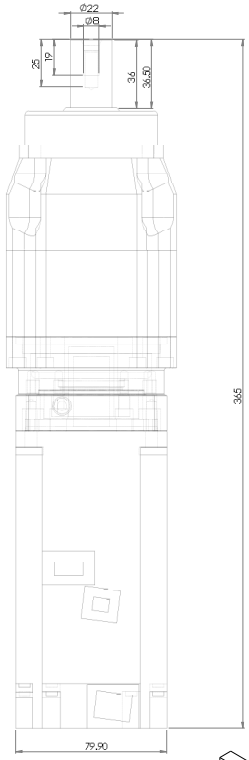

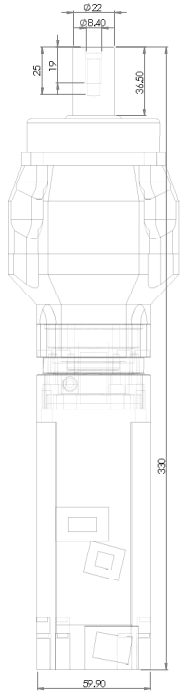

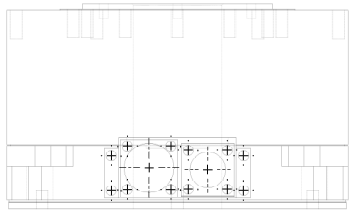

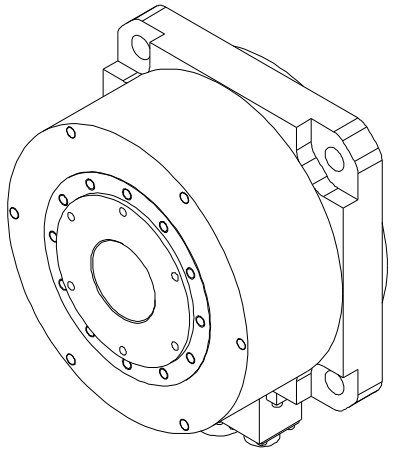

ITEM NO.	PART NUMBER	DESCRIPTION	QTY.
2	hm-rfm018e20_a		1

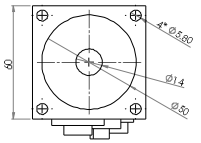

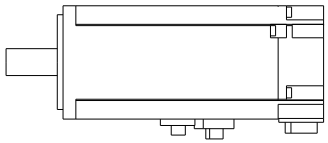

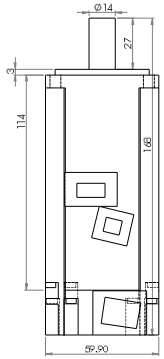

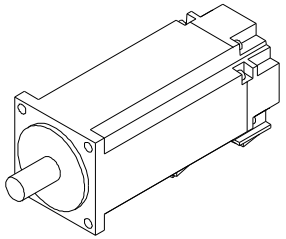

ITEM NO.	PART NUMBER	DESCRIPTION	QTY.
33, 56	hf-mp43b_b		1

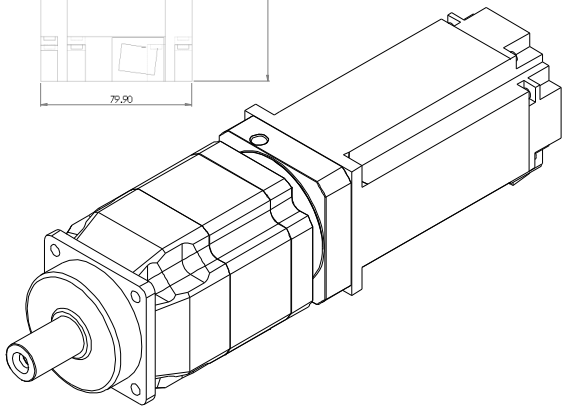

ITEM NO.	PART NUMBER	DESCRIPTION	QTY.
18	hf-mp73b_b		2
19, 20, 21, 22	PAT-B22A3015-100_P_-G5__20101027		2

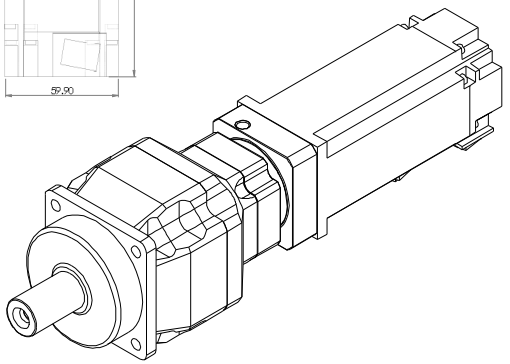

ITEM NO.	PART NUMBER	DESCRIPTION	QTY.
33	hf-mp43b_b		1
34, 35, 36, 37	PAT-B22G5015-100_P_-E4__20101022		1

servo motors

A1

ITEM NO.	PART NUMBER	DESCRIPTION	QTY.
3	continuous thread hexagon head bolt_d_jis_JIS B 1180 Continuous thread hexagon head bolt A M12 X 45 --N		4

ITEM NO.	PART NUMBER	DESCRIPTION	QTY.
8	hexagon socket head cap screw_jis_JIS B 1176 M4 x 16 (16) --S		6

ITEM NO.	PART NUMBER	DESCRIPTION	QTY.
13	hexagon socket head cap screw_jis_JIS B 1176 M6 x 45 (45) --S		14

ITEM NO.	PART NUMBER	DESCRIPTION	QTY.
17	hexagon socket head cap screw_jis_JIS B 1176 M5 x 35 (22) --N		4

ITEM NO.	PART NUMBER	DESCRIPTION	QTY.
23	hexagon socket head cap screw_jis_JIS B 1176 M6 x 20 (20) --N		29

ITEM NO.	PART NUMBER	DESCRIPTION	QTY.
24	hexagon socket head cap screw_jis_JIS B 1176 M6 x 25 (25) --N		4

ITEM NO.	PART NUMBER	DESCRIPTION	QTY.
27	hexagon socket head cap screw_jis_JIS B 1176 M5 x 16 (16) --N		6

ITEM NO.	PART NUMBER	DESCRIPTION	QTY.
28	hexagon socket button head screw_JIS_JIS B 1174 M8 x 20 (20) --N		1

ITEM NO.	PART NUMBER	DESCRIPTION	QTY.
38	hexagon socket head cap screw_jis_JIS B 1176 M6 x 16 (16) --N		9

ITEM NO.	PART NUMBER	DESCRIPTION	QTY.
39	hexagon socket head cap screw_jis_JIS B 1176 M5 x 20 (20) --N		8

ITEM NO.	PART NUMBER	DESCRIPTION	QTY.
14	hex screw gradeab_iso_ISO 4017 - M20 x 120-S		3

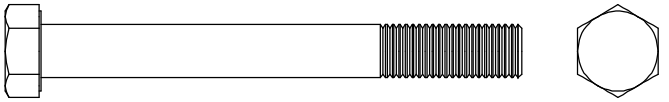

ITEM NO.	PART NUMBER	DESCRIPTION	QTY.
48	nominal diameter hexagon head bolt_c_jis_JIS B 1180 Nominal diameter hexagon head bolt C M20 X 180 --52WS		1

ITEM NO.	PART NUMBER	DESCRIPTION	QTY.
44	hexagon socket head cap screw_jis_JIS B 1176 M6 x 12 (12) --N		64

ITEM NO.	PART NUMBER	DESCRIPTION	QTY.
47	hexagon socket head cap screw_jis_JIS B 1176 M6 x 40 (24) --N		8

ITEM NO.	PART NUMBER	DESCRIPTION	QTY.
1	hexagon socket button head screw_JIS_JIS B 1174 M6 x 25 (25) --N		1

SCALE 1 : 1

UNLESS OTHERWISE SPECIFIED: DIMENSIONS ARE IN MILLIMETERS SURFACE FINISH: TOLERANCES: LINEAR: ANGULAR:			FINISH:			DRILL AND DEBURR SHARP EDGES	DO NOT SCALE DRAWING	REVISION
	NAME	SIGNATURE	DATE				TITLE:	
DRAWN								
CHKD								
APPVD								
MFG								
Q.A.								
			MATERIAL:				DWG NO. bolts	A1
			WEIGHT:				SCALE:1:1	SHEET 1 OF 1

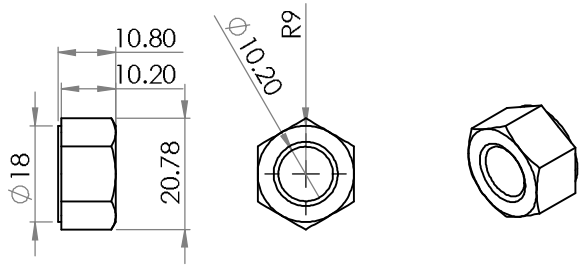

ITEM NO.	PART NUMBER	DESCRIPTION	QTY.
4	hexagon nut style 1_ab_jis_JIS B 1181 Hexagon nut - style 1 A M12 - W --N		4

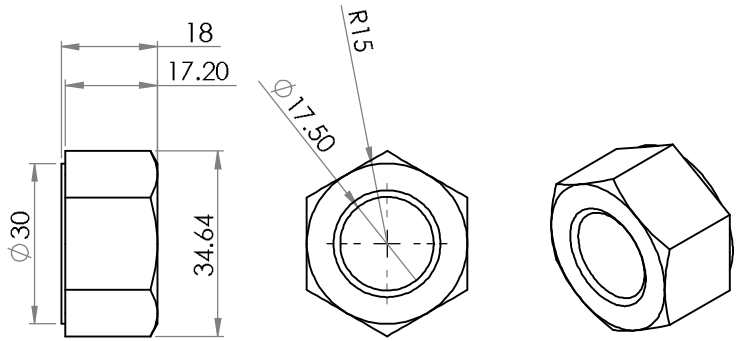

ITEM NO.	PART NUMBER	DESCRIPTION	QTY.
15	hex nut style 1 gradeab_iso_Hexagon Nut ISO - 4032 - M20 - W - N		3

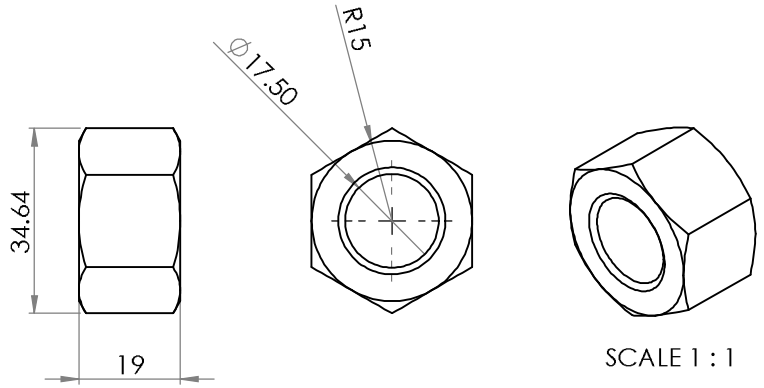

SCALE 1 : 1

ITEM NO.	PART NUMBER	DESCRIPTION	QTY.
49	hexagon nut_c_jis_JIS B 1181 Hexagon nut C M20 –N		2

UNLESS OTHERWISE SPECIFIED: DIMENSIONS ARE IN MILLIMETERS SURFACE FINISH: TOLERANCES: LINEAR: ANGULAR:		FINISH:			DEBUR AND BREAK SHARP EDGES	DO NOT SCALE DRAWING	REVISION
	NAME	SIGNATURE	DATE			TITLE:	
DRAWN							
CHK'D							
APPV'D							
MFG							
Q.A				MATERIAL:		DWG NO. nuts	A3
				WEIGHT:		SCALE:5:1	SHEET 1 OF 1

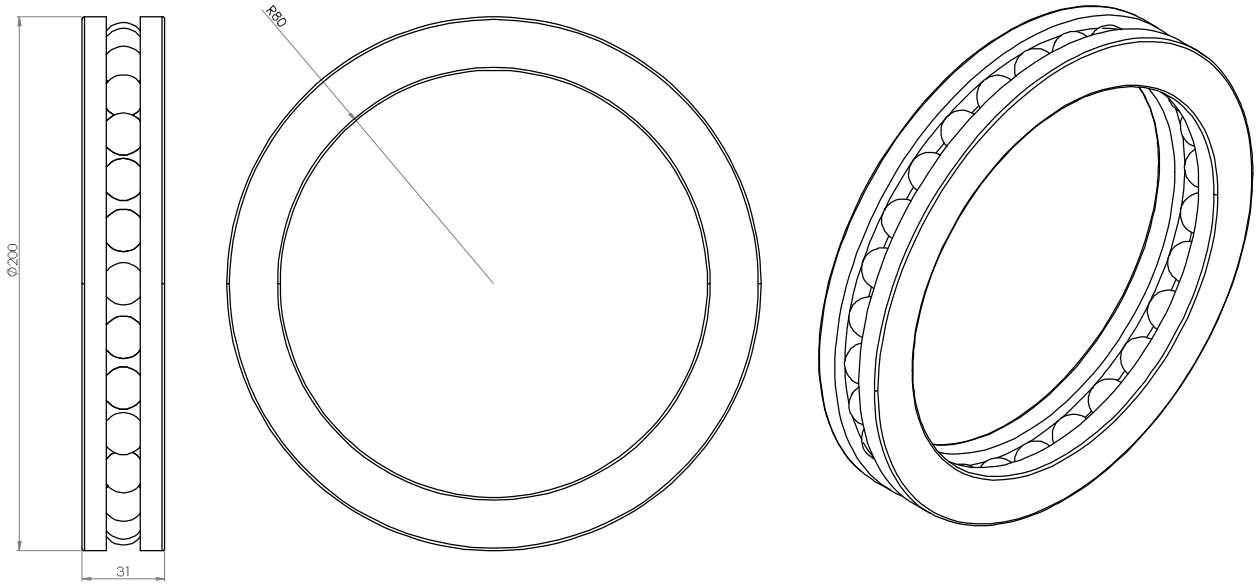

ITEM NO.	PART NUMBER	DESCRIPTION	QTY.
6	thrust ball bearing_68_jis_JIS B 1512-4 - 11160200 - 28,DE,NC,28_68	NSK 31132x	1

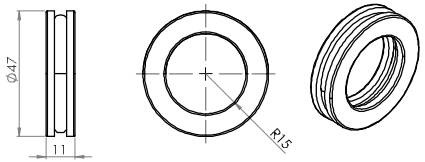

ITEM NO.	PART NUMBER	DESCRIPTION	QTY.
9	thrust ball bearing_68_jis_JIS B 1512-4 - 113047 - 16,SI,NC,T6_68	NSK 51106	1

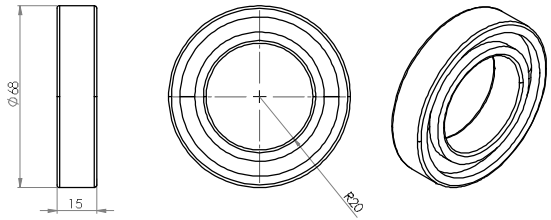

ITEM NO.	PART NUMBER	DESCRIPTION	QTY.
30	radial ball bearing_68_jis_JIS B 1512-1 - 1040 - B,16,SI,NC,T6_68	NSK 6008	1

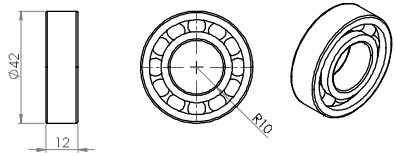

ITEM NO.	PART NUMBER	DESCRIPTION	QTY.
43	radial ball bearing_68_jis_JIS B 1512-1 - 1020 - B,12,DE,NC,12_68	NSK 6003	11

UNLESS OTHERWISE SPECIFIED: DIMENSIONS ARE IN MILLIMETERS SURFACE FINISH: TOLERANCES: LINEAR: ANGULAR:				FINISH:			DEBUR AND BREAK SHARP EDGES	DO NOT SCALE DRAWING	REVISION
	NAME	SIGNATURE	DATE					TITLE: NSK 31132x
DRAWN	AS Rahmanifard							
CHKD								
APPVD								
MFG								
Q.A.				MATERIAL:			DWG NO. Bearings	A1
				WEIGHT:			SCALE:1:1	SHEET 1 OF 1

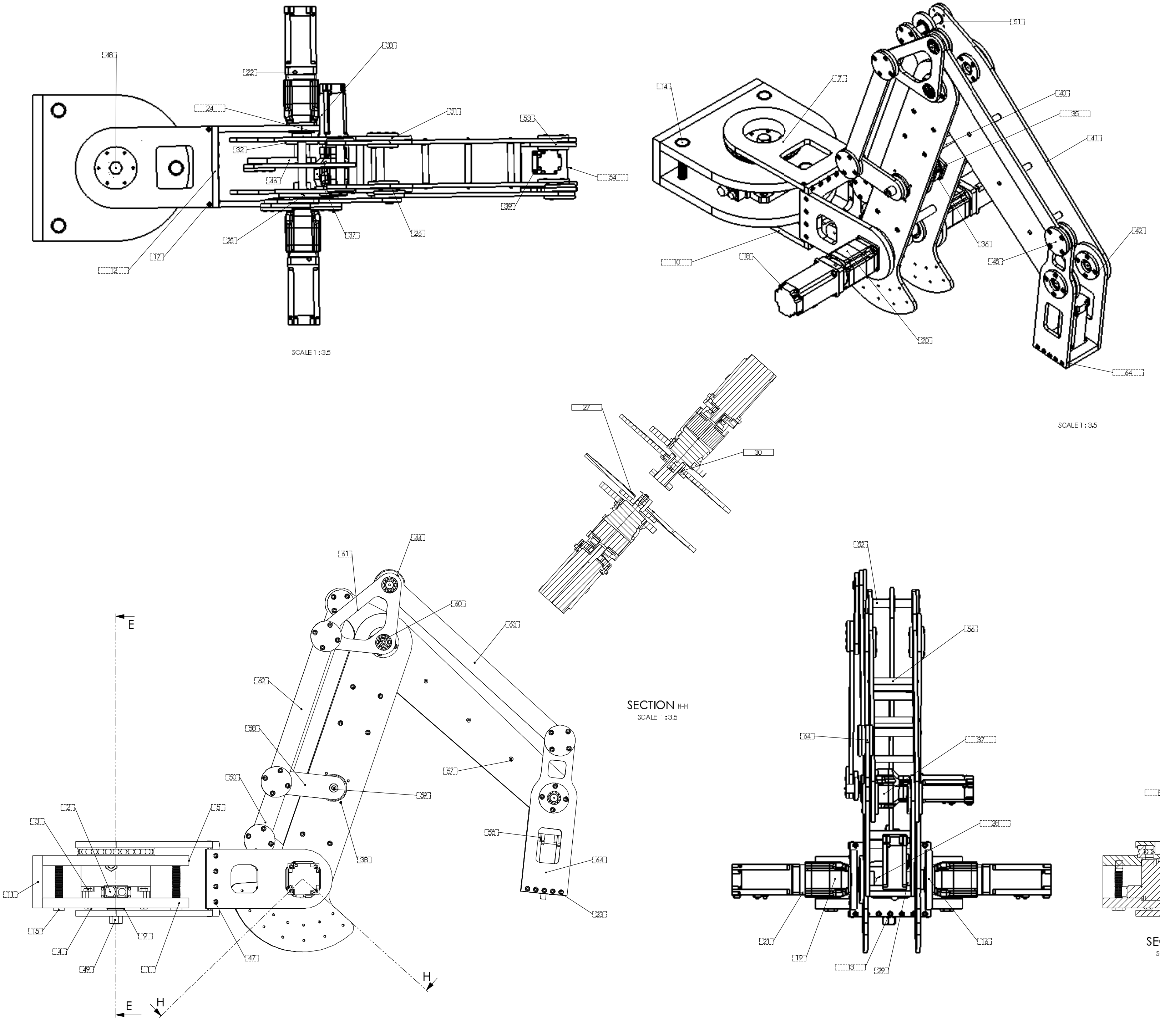

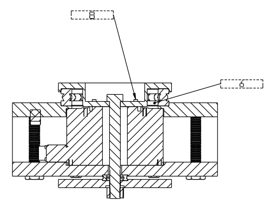

ITEM NO.	PART NUMBER	DESCRIPTION	Default/ QTY.
1	a1_1		1
2	tm-rfm018e20_a		1
3	continuous thread hexagon head bolt_a_jis_JIS B 1180 Continuous thread hexagon head bolt A M12 x 45 --N		4
4	hexagon nut style 1_ab_jis_JIS B 1181 Hexagon nut - style 1 A M12 - W--N		4
5	a2_1		1
6	thrust ball bearing_68_jis_JIS B 1512-4 - 11160200 - 28,DE,NC,28_68		1
7	a4_1		1
8	hexagon socket head cap screw_jis_JIS B 1176 M4 x 16 (16) --S		6
9	thrust ball bearing_68_jis_JIS B 1512-4 - 113047 - 16,SI,NC,16_68		1
10	a5_1		1
11	a6_1		1
12	vert10		1
13	hexagon socket head cap screw_jis_JIS B 1176 M6 x 45 (45) --S		14
14	hexscrew gradeab_iso_ISO 4017 - M20 x 120-S		3
15	hexnut style 1 gradeab_iso_Hexagon Nut ISO - 4032 - M20 - W - N		3
16	vert33		2
17	hexagon socket head cap screw_jis_JIS B 1176 M5 x 35 (22) --N		4
18	hf-mp73b_b		2
19	AFX075A2		2
20	AFX075A2-1		2
21	P1301300001		2
22	P0403300202		2
23	hexagon socket head cap screw_jis_JIS B 1176 M6 x 20 (20) --N		29
24	hexagon socket head cap screw_jis_JIS B 1176 M6 x 25 (25) --N		4
25	a7_1		1
26	a8_1		1
27	hexagon socket head cap screw_jis_JIS B 1176 M5 x 16 (16) --N		6
28	hexagon socket button head screw_jis_JIS B 1174 M8 x 20 (20) --N		1
29	a9_1		1
30	radial ball bearing_68_jis_JIS B 1512-1 - 1040 - B.16,SI,NC,16_68		1
31	a10_1		1
32	a11_1		1
33	hf-mp43b_b		1
34	AB0902-1		1
35	P1301200001		1
36	P0403200503		1
37	AFX0752		1
38	hexagon socket head cap screw_jis_JIS B 1176 M6 x 16 (16) --N		9
39	hexagon socket head cap screw_jis_JIS B 1176 M5 x 20 (20) --N		8
40	a12_1		6
41	a13_1		2
42	a14_1		5
43	radial ball bearing_68_jis_JIS B 1512-1 - 1020 - B.12,DE,NC,12_68		11
44	hexagon socket head cap screw_jis_JIS B 1176 M6 x 12 (12) --N		64
45	a26_1		8
46	a15_1		1
47	hexagon socket head cap screw_jis_JIS B 1176 M6 x 40 (24) --N		8
48	nominal diameter hexagon head bolt_c_jis_JIS B 1180 Nominal diameter hexagon head bolt C M20 x 180 --52WS		1
49	hexagon nut_c_jis_JIS B 1181 Hexagon nut C M20 --N		2
50	a16_1		1
51	a17_1		2
52	a18_1		1
53	a20_1		1
54	a21_1		1
55	a22-s43_1		1
56	a23_1		3
57	hexagon socket button head screw_jis_JIS B 1174 M6 x 20 (20) --N		6
58	a24_1		1
59	hexagon socket button head screw_jis_JIS B 1174 M6 x 25 (25) --N		1
60	a26 - Copy_1		1
61	a25_1		1
62	a27_1		1
63	a28_1		1
64	a19_1		1

SCALE 1 : 3.5

Assem3 - Copy

A1

Appendix 2. The drawings of joint-1 modifications.

ITEM NO.	PART NUMBER	DESCRIPTION	QTY.
1	Modify-a2-1 - Copy	Manufacturing	1
2	Modify-a1-1	Manufacturing	1
3	Z8009	NSK 6008	2
4	thrust ball bearing_68_jis_JIS B 1512-4 - 11160200 - 28,DE,NC,28_68	NSK 31132x	1
5	Spacer	Manufacturing	5
6	a4_1		1
7	Fixer	Manufacturing	1
8	Fixer - Up	Manufacturing	1
9	3	Manufacturing	1
10	J1-Assembly	Servo motor	1
11	vert10		1
12	a5_1	**Modification only	1
13	thrust ball bearing_68_jis_JIS B 1512-4 - 113047 - 16,SI,NC,16_68	NSK 51106	1
14	hanger-main-1	Manufacturing	1
15	hanger-sub-1	Manufacturing	2

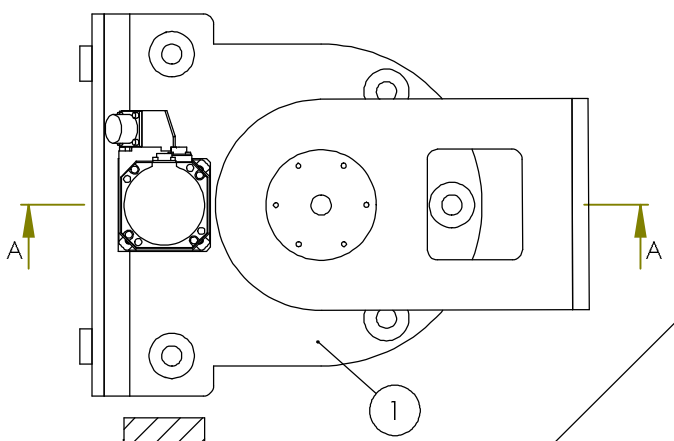

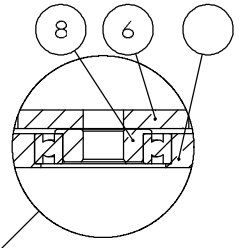

DETAIL C
SCALE 2 : 5

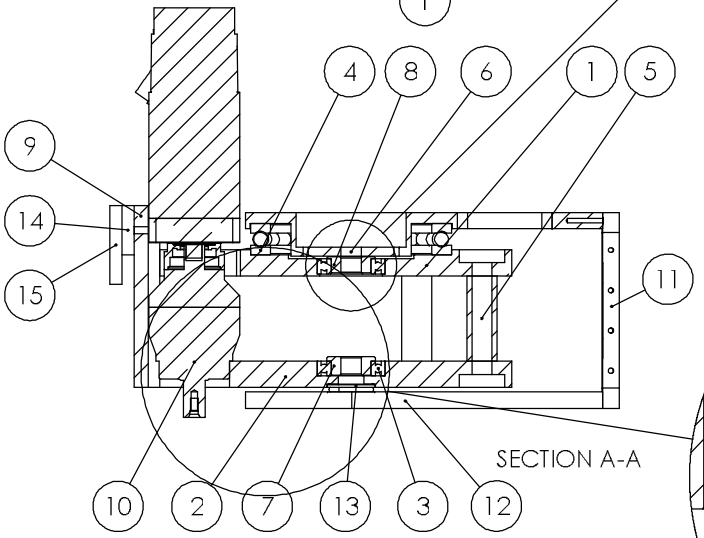

SECTION A-A

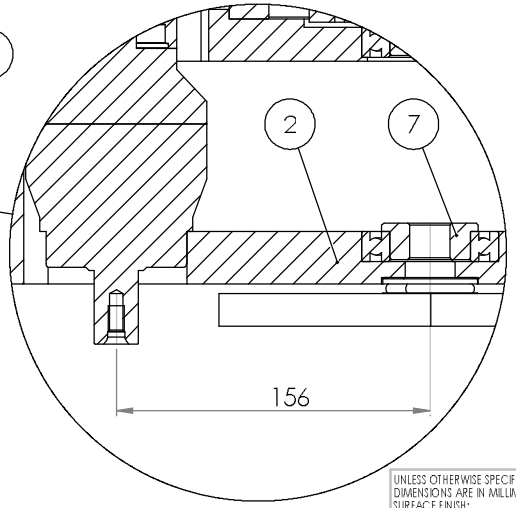

DETAIL D
SCALE 2 : 5

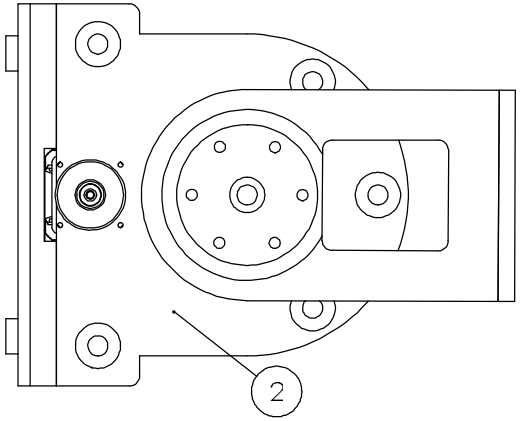

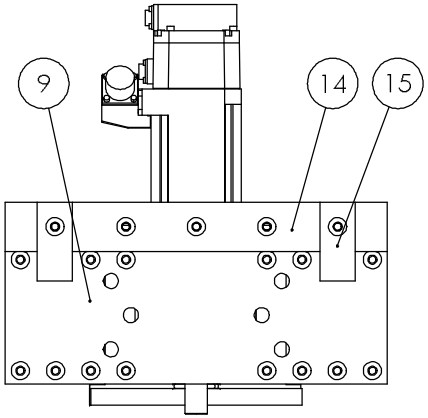

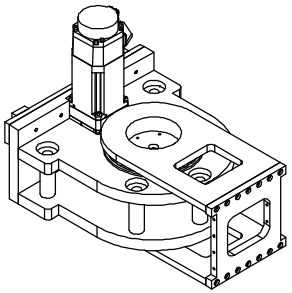

UNLESS OTHERWISE SPECIFIED: DIMENSIONS ARE IN MILLIMETERS SURFACE FINISH: TOLERANCES: LINEAR: ANGULAR:		FINISH:		DEBURR AND BREAK SHARP EDGES	DO NOT SCALE DRAWING	REVISION	
	NAME	SIGNATURE	DATE		TITLE:		
DRAWN							
CHK'D							
APP'VD							
MFG							
Q.A				MATERIAL:	DWG NO. Third assembly		A3
				WEIGHT:	SCALE:1:5	SHEET 1 OF 1	

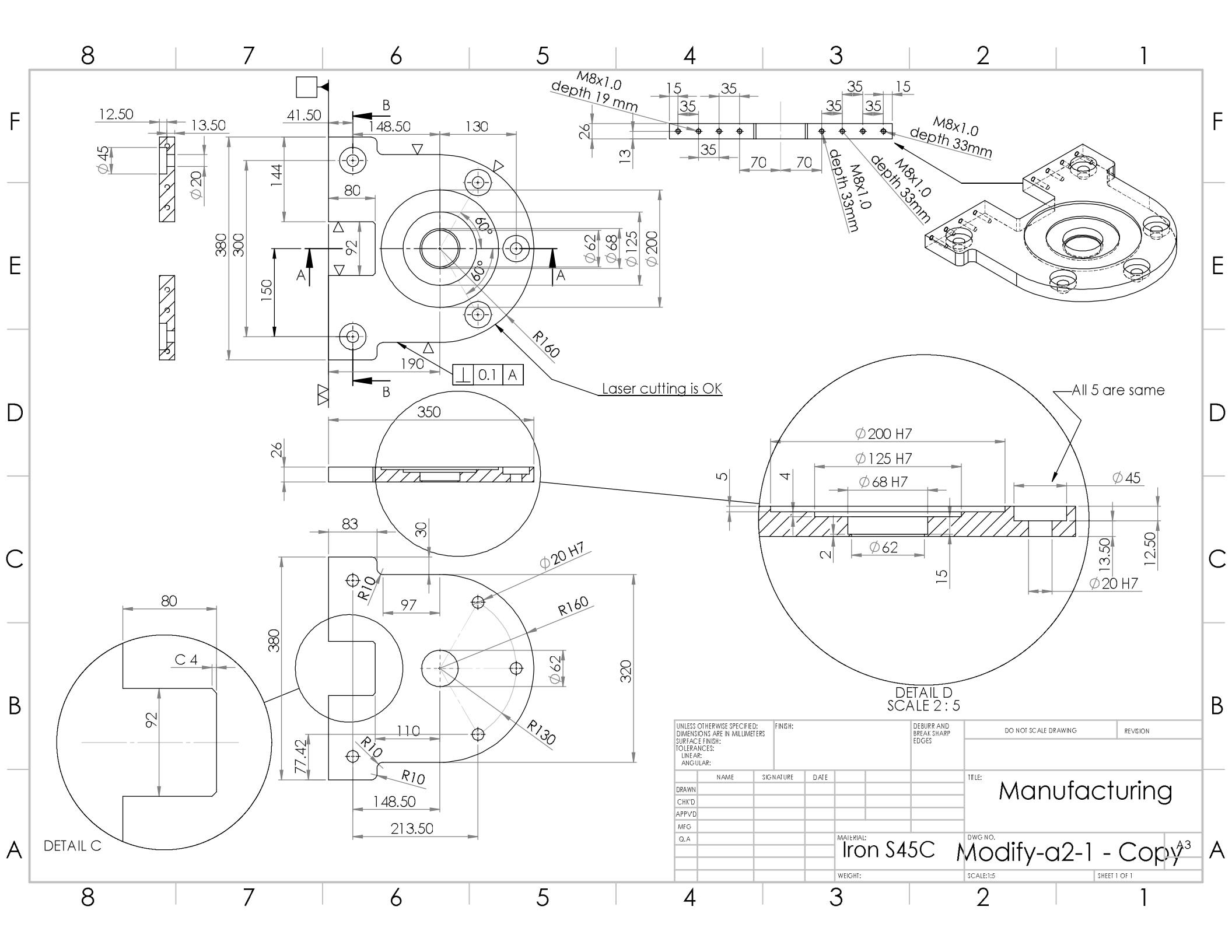
M8x1.0
depth 19 mm
M8x1.0
depth 33mm
M8x1.0
depth 33mm
M8x1.0
depth 33mm
12.50
13.50
41.50
148.50
130
144
80
92
380
300
150
190
60°
60°
R160
0.1 A
Laser cutting is OK
All 5 are same
350
26
83
30
80
C 4
92
380
R10
97
20 H7
R160
62
320
110
77.42
R10
R10
R130
148.50
213.50
DETAIL C
200 H7
125 H7
68 H7
45
62
20 H7
DETAIL D
SCALE 2 : 5
UNLESS OTHERWISE SPECIFIED:
DIMENSIONS ARE IN MILLIMETERS
SURFACE FINISH:
TOLERANCES:
LINEAR:
ANGULAR:
FINISH:
DEBURR AND BREAK SHARP EDGES
DO NOT SCALE DRAWING
REVISION
NAME
SIGNATURE
DATE
DRAWN
CHK'D
APP'VD
MFG
Q.A
TITLE:
Manufacturing
MATERIAL:
Iron S45C
DWG NO.
Modify-a2-1 - Copy
A3
WEIGHT:
SCALE:1:5
SHEET 1 OF 1

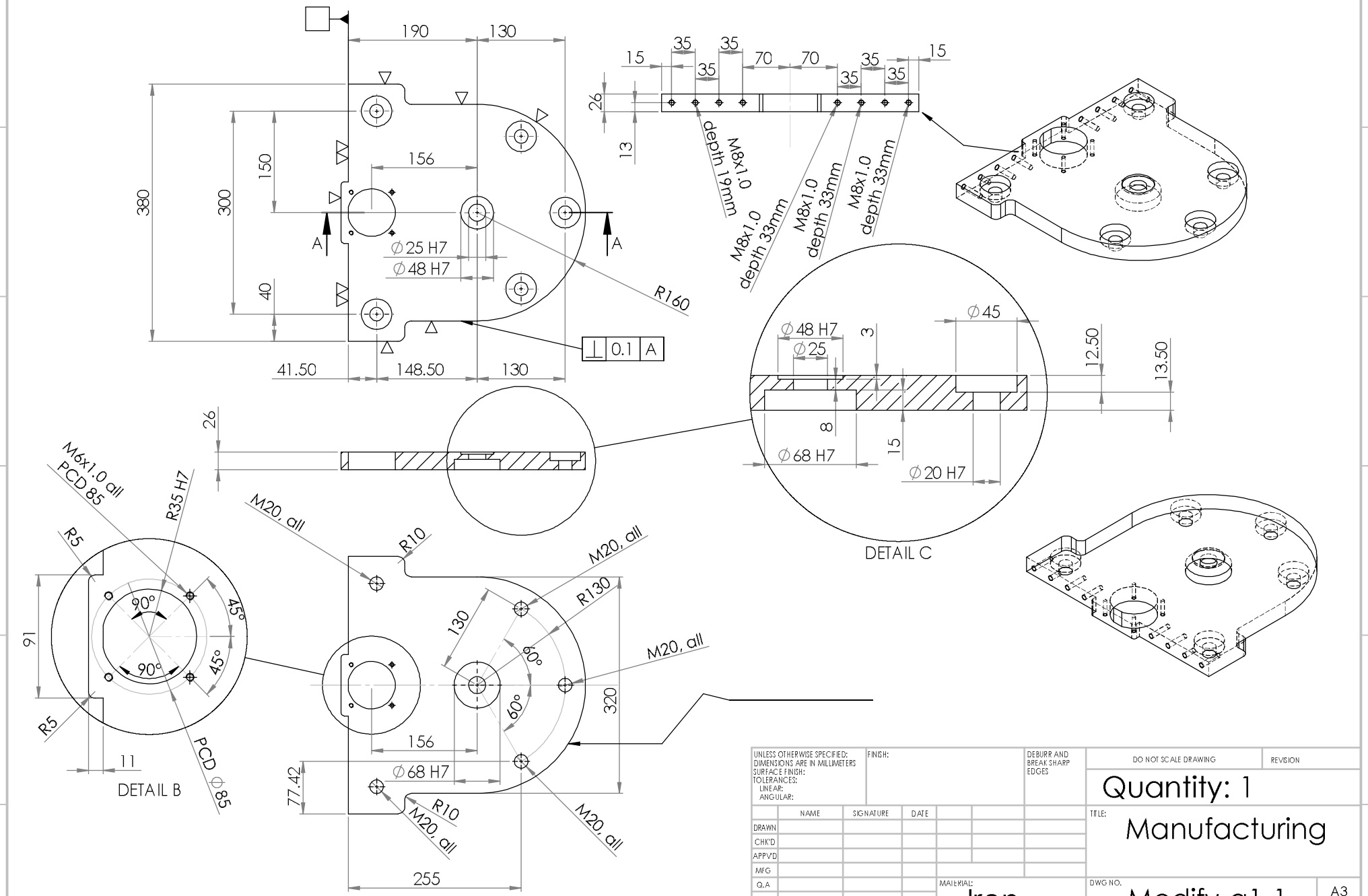
190
130
380
300
150
40
156
A
A
Ø25 H7
Ø48 H7
R160
0.1 A
41.50
148.50
130
15
35
35
70
70
35
15
35
35
26
13
M8x1.0 depth 19mm
M8x1.0 depth 33mm
M8x1.0 depth 33mm
M8x1.0 depth 33mm
Ø48 H7
Ø25
3
Ø45
12.50
13.50
8
15
Ø68 H7
Ø20 H7
DETAIL C
26
M6x1.0 all PCD 85
R35 H7
R5
90°
90°
45°
45°
91
R5
11
PCD Ø85
DETAIL B
M20, all
R10
M20, all
R130
130
60°
60°
M20, all
320
156
77.42
Ø68 H7
R10
M20, all
M20, all
255
UNLESS OTHERWISE SPECIFIED:
DIMENSIONS ARE IN MILLIMETERS
SURFACE FINISH:
TOLERANCES:
LINEAR:
ANGULAR:
FINISH:
DEBURR AND BREAK SHARP EDGES
DO NOT SCALE DRAWING
REVISION
Quantity: 1
NAME
SIGNATURE
DATE
DRAWN
CHK'D
APP'VD
MFG
Q.A
TITLE:
Manufacturing
MATERIAL:
Iron
DWG NO.
Modify-a1-1
A3
WEIGHT:
SCALE:1:5
SHEET 1 OF 1

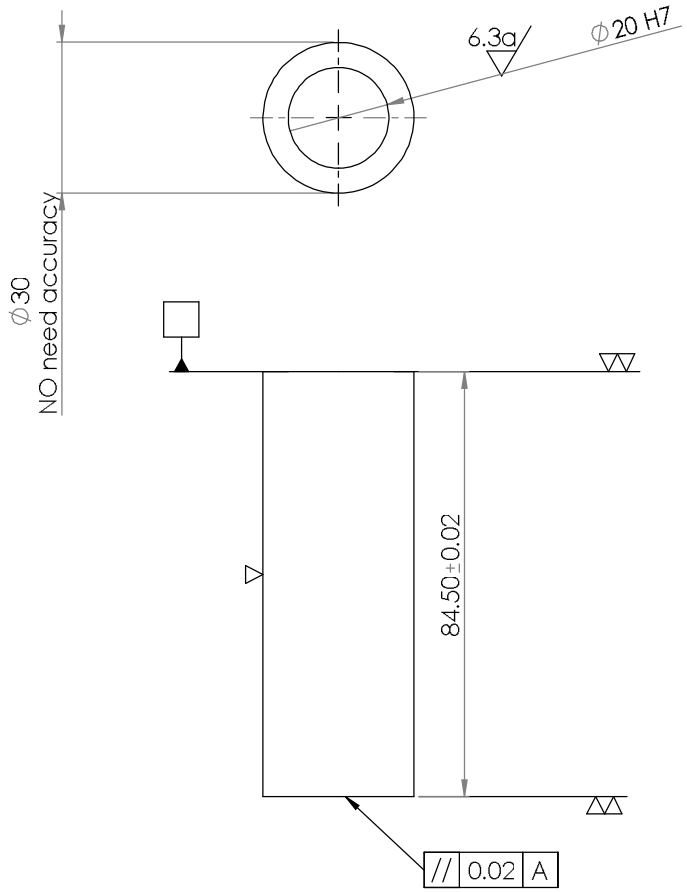

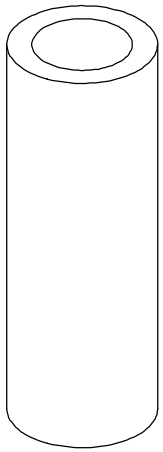

UNLESS OTHERWISE SPECIFIED: DIMENSIONS ARE IN MILLIMETERS SURFACE FINISH: TOLERANCES: LINEAR: ANGULAR:		FINISH:			DEBURR AND BREAK SHARP EDGES	DO NOT SCALE DRAWING	REVISION
						QTY (Quantity): 5	
	NAME	SIGNATURE	DATE			TITLE: Spacer	
DRAWN							
CHK'D							
APP'VD							
MFG							
Q.A				MATERIAL: Iron		DWG NO. Spacer	A3
				WEIGHT:		SCALE:1:1	SHEET 1 OF 1

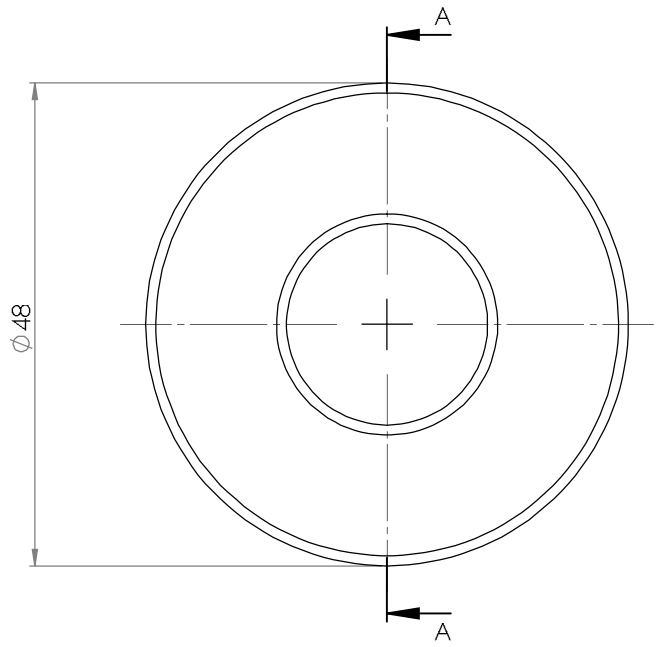

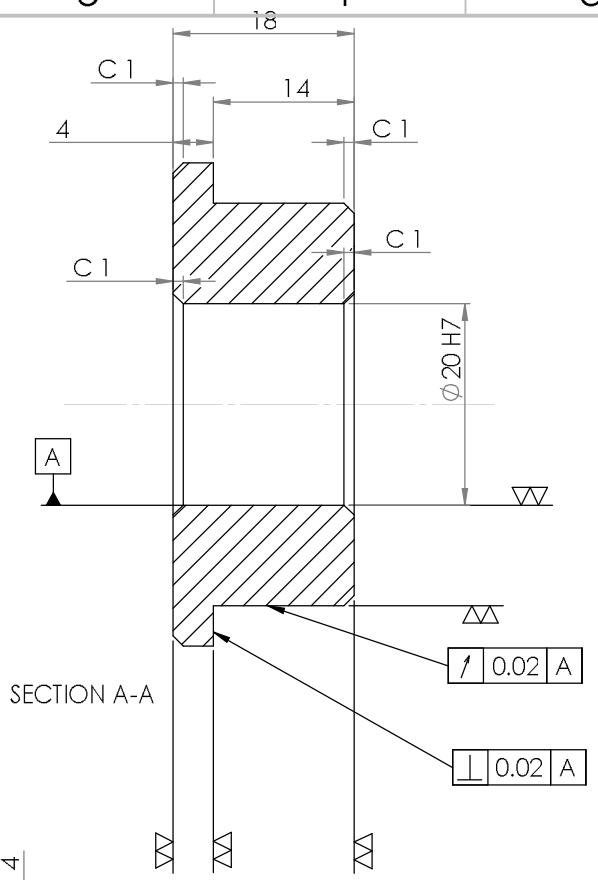

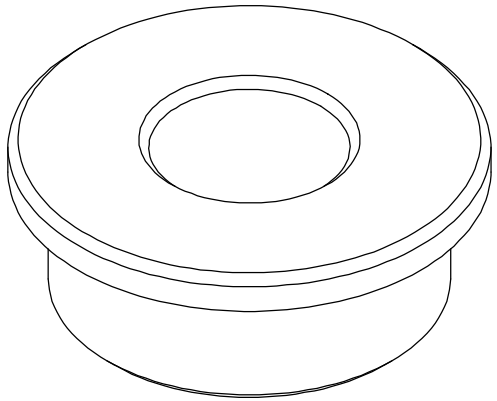

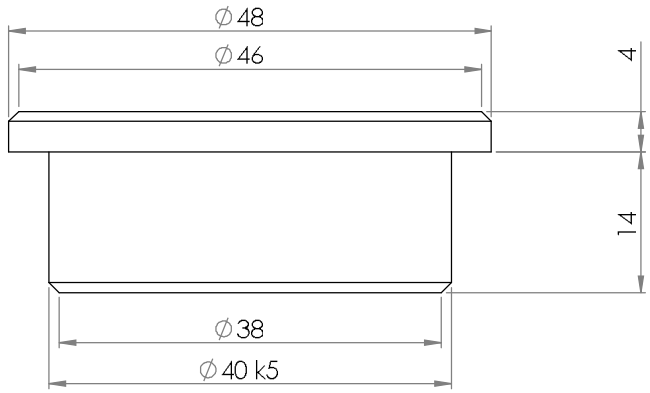

UNLESS OTHERWISE SPECIFIED: DIMENSIONS ARE IN MILLIMETERS SURFACE FINISH: TOLERANCES: LINEAR: ANGULAR:	FINISH:		DEBURR AND BREAK SHARP EDGES	DO NOT SCALE DRAWING	REVISION	
	NAME	SIGNATURE	DATE	TITLE: Manufacturing		
DRAWN						
CHK'D						
APP'VD						
MFG						
Q.A				MATERIAL: Iron	DWG NO. Fixer	A3
				WEIGHT:	SCALE:2:1	SHEET 1 OF 1

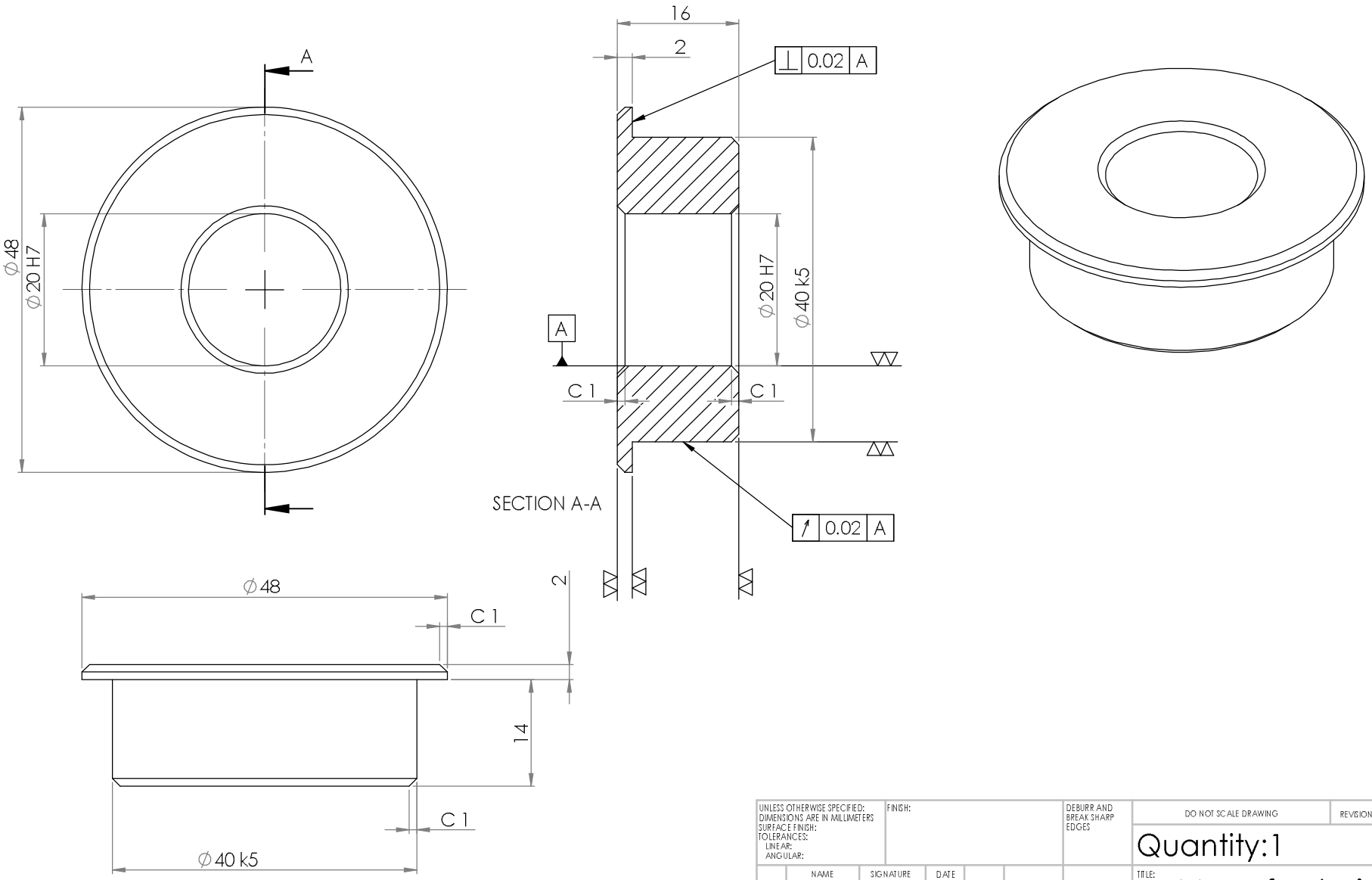

UNLESS OTHERWISE SPECIFIED: DIMENSIONS ARE IN MILLIMETERS SURFACE FINISH: TOLERANCES: LINEAR: ANGULAR:	FINISH:		DEBURR AND BREAK SHARP EDGES	DO NOT SCALE DRAWING	REVISION	
				Quantity:1		
	NAME	SIGNATURE	DATE	TITLE: Manufacturing		
DRAWN						
CHK'D						
APP'VD						
MFG						
Q.A				MATERIAL: Iron	DWG NO. Fixer - Up	A3
				WEIGHT:	SCALE:2:1	SHEET 1 OF 1

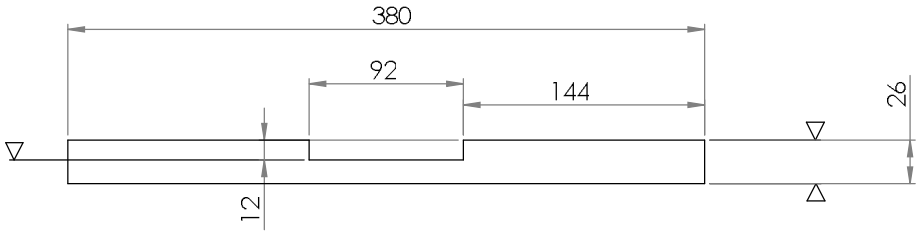

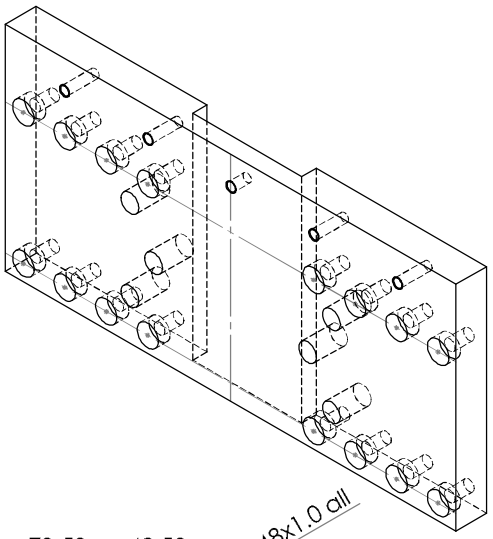

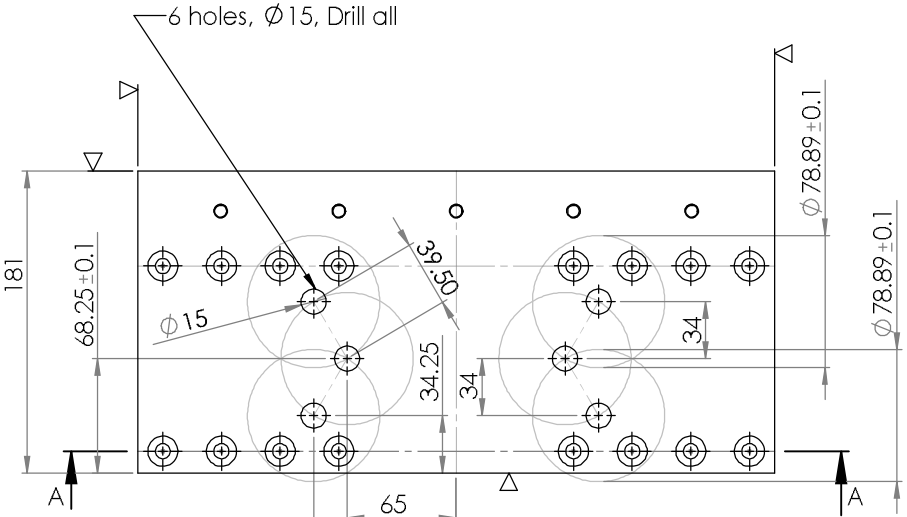

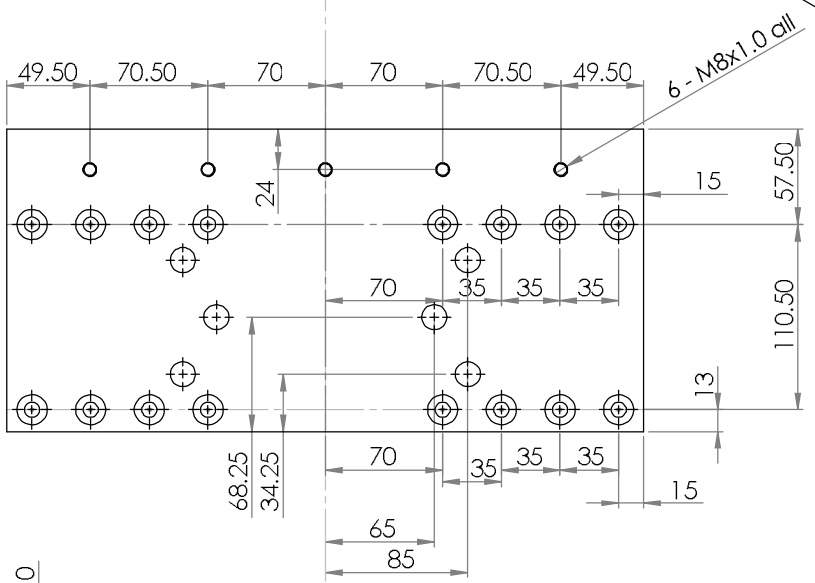

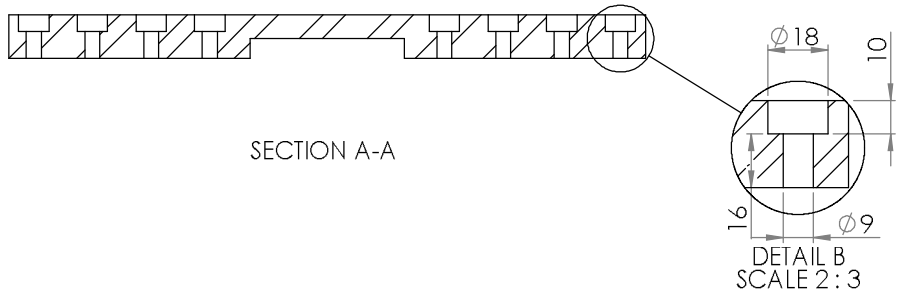

SECTION A-A

DETAIL B
SCALE 2 : 3

UNLESS OTHERWISE SPECIFIED: DIMENSIONS ARE IN MILLIMETERS SURFACE FINISH: TOLERANCES: LINEAR: ANGULAR:		FINISH:		DEBURR AND BREAK SHARP EDGES		DO NOT SCALE DRAWING	REVISION
	NAME	SIGNATURE	DATE			TITLE:	
DRAWN						Manufacturing	
CHK'D							
APP'VD							
MFG							
Q.A				MATERIAL:		DWG NO.	A3
				Iron		3	
				WEIGHT:		SCALE:1:2	SHEET 1 OF 1

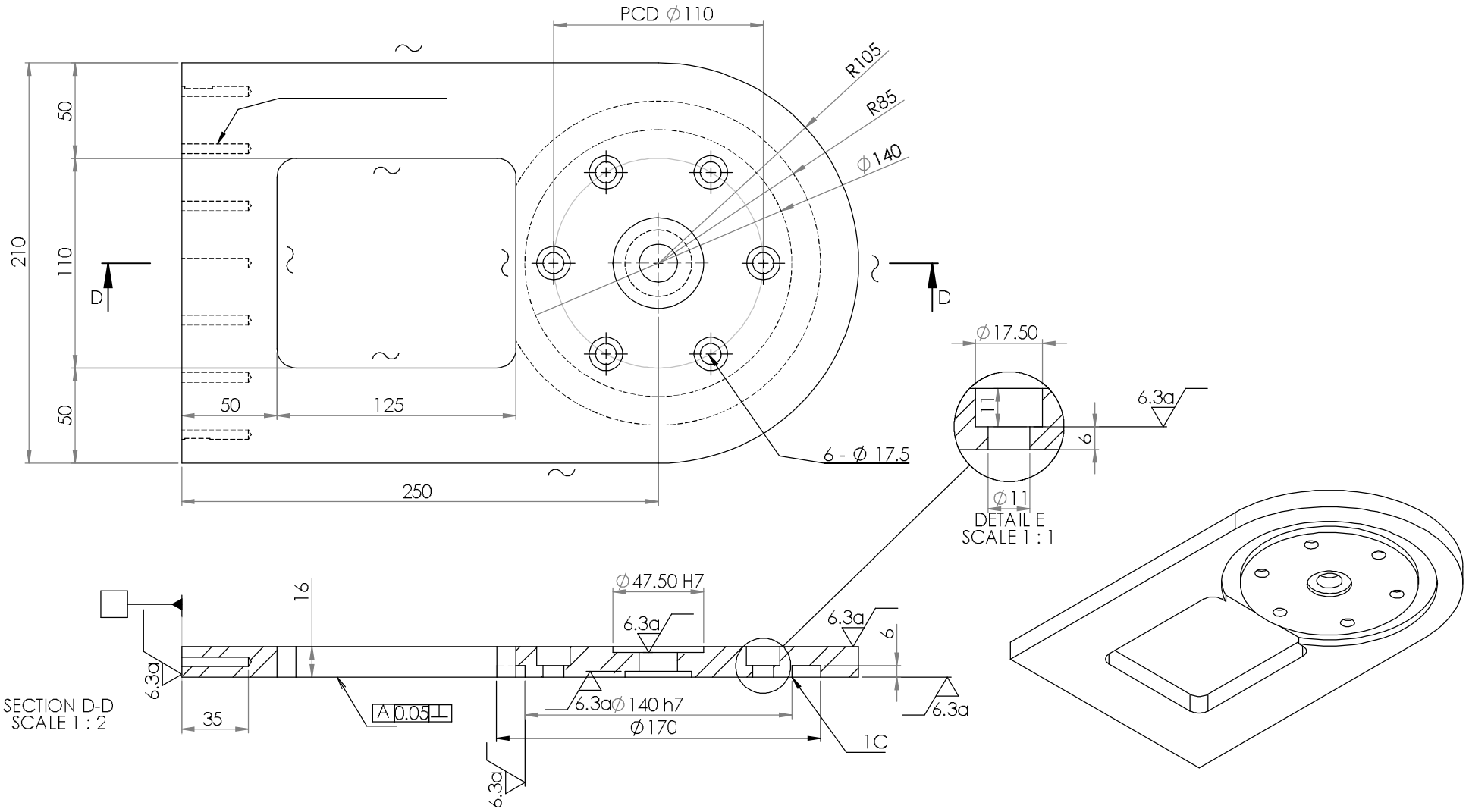

UNLESS OTHERWISE SPECIFIED: DIMENSIONS ARE IN MILLIMETERS SURFACE FINISH: TOLERANCES: LINEAR: ANGULAR:		FINISH:		DEBURR AND BREAK SHARP EDGES	DO NOT SCALE DRAWING	REVISION
	NAME	SIGNATURE	DATE		TITLE:	
DRAWN					**Modification only	
CHK'D						
APP'VD						
MFG						
Q.A				MATERIAL:	DWG NO. a5_1	A3
				WEIGHT:	SCALE:1:5	SHEET 1 OF 1

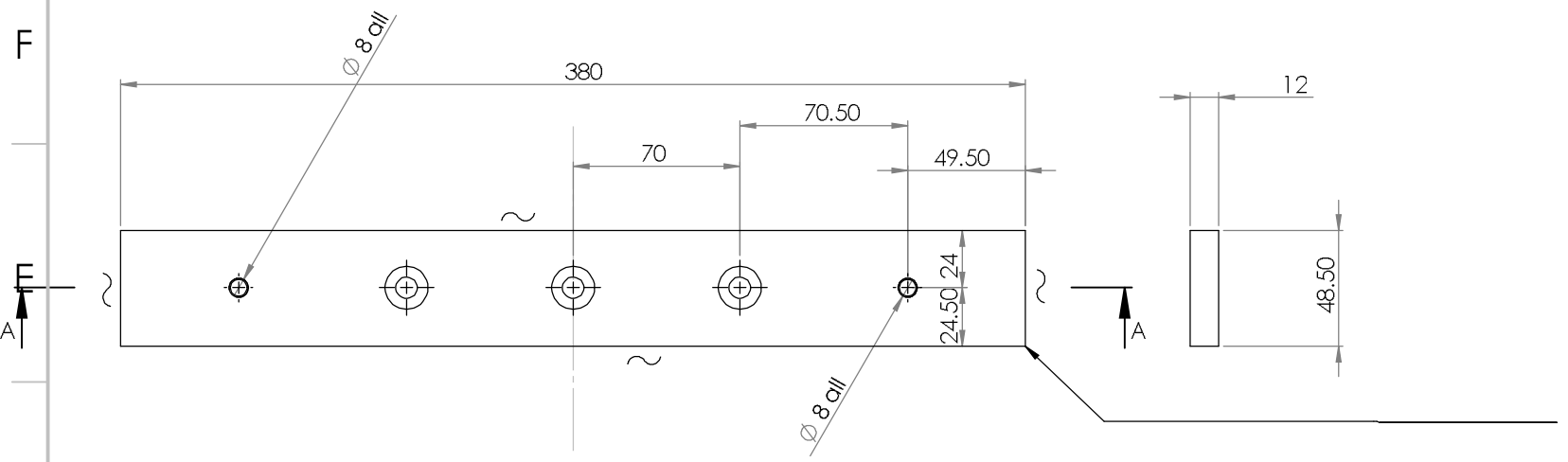

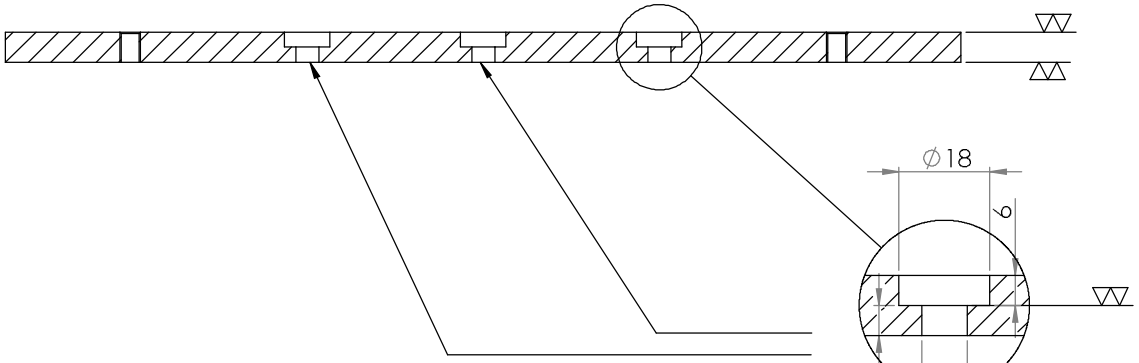

DETAIL B
SCALE 1 : 1

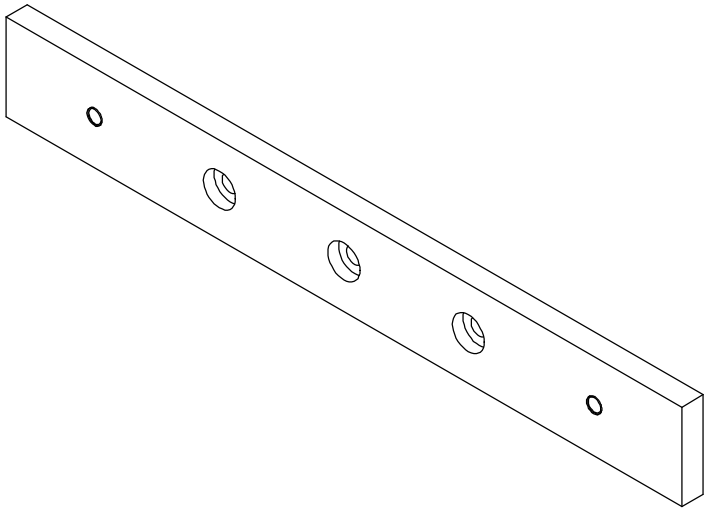

UNLESS OTHERWISE SPECIFIED: DIMENSIONS ARE IN MILLIMETERS SURFACE FINISH: TOLERANCES: LINEAR: ANGULAR:		FINISH:		DEBURR AND BREAK SHARP EDGES	DO NOT SCALE DRAWING	REVISION
	NAME	SIGNATURE	DATE		Quantity	
DRAWN					TITLE: Manufacturing	
CHK'D						
APP'VD						
MFG						
Q.A				MATERIAL: Iron	DWG NO. hanger-main-1	A3
				WEIGHT:	SCALE:1:2	SHEET 1 OF 1

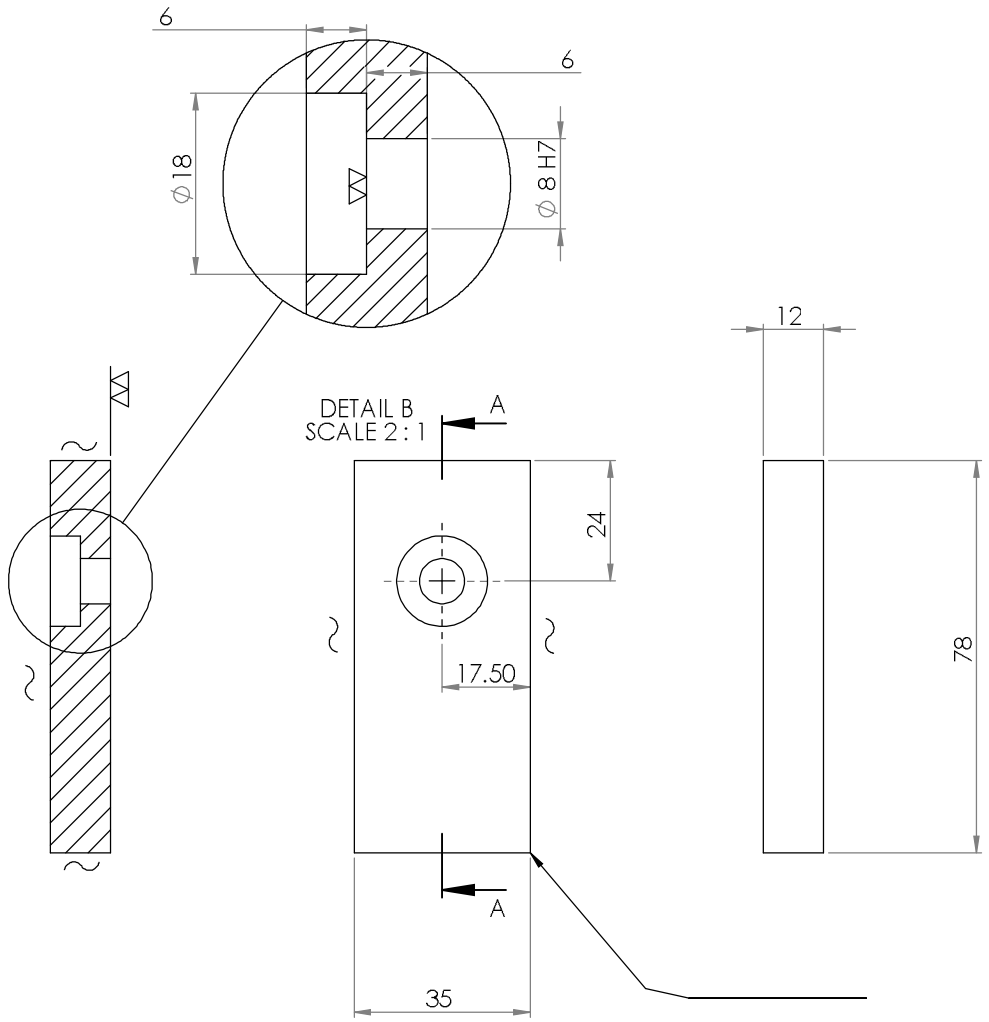

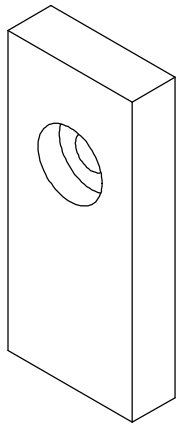

UNLESS OTHERWISE SPECIFIED: DIMENSIONS ARE IN MILLIMETERS SURFACE FINISH: TOLERANCES: LINEAR: ANGULAR:		FINISH:			DEBURR AND BREAK SHARP EDGES	DO NOT SCALE DRAWING	REVISION
						Quantity: 2	
	NAME	SIGNATURE	DATE			TITLE: Manufacturing	
DRAWN							
CHK'D							
APP'VD							
MFG							
Q.A				MATERIAL: Iron		DWG NO. hanger-sub-1	A3
				WEIGHT:		SCALE:1:1	SHEET 1 OF 1

Appendix 3. The drawings of designed end-effector (EE).

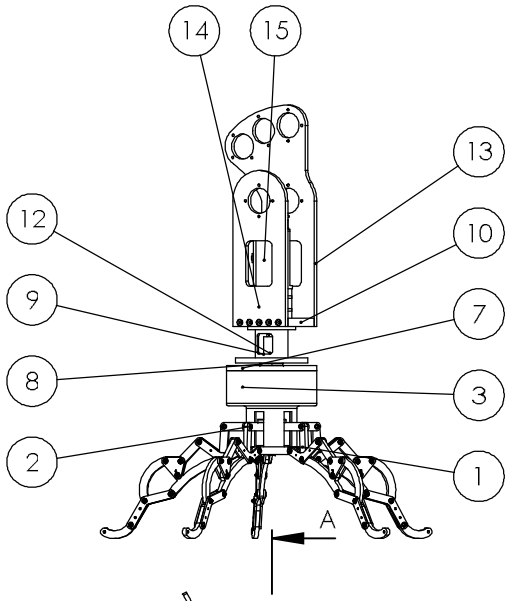

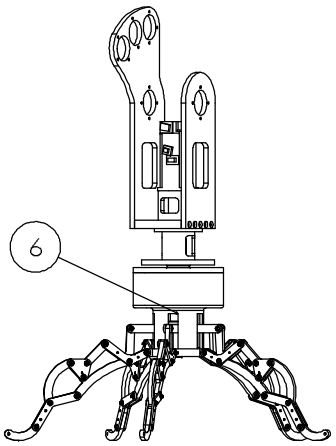

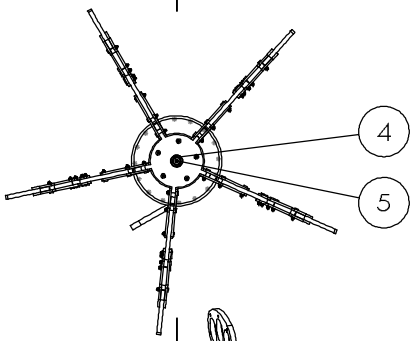

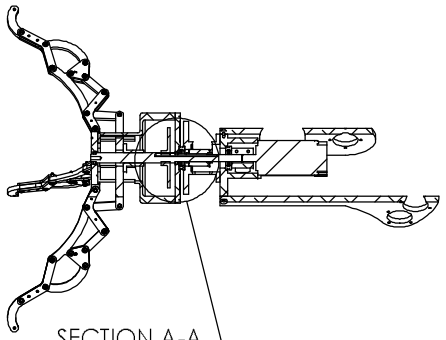

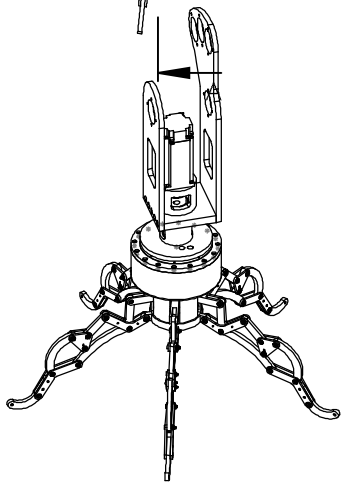

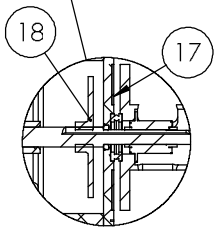

DETAIL B
SCALE 1 : 5

ITEM NO.	PART NUMBER	DESCRIPTION	QTY.
1	15-2	Manufacturing	1
2	13-2	Manufacturing	1
3	7-2	Manufacturing	1
4	14	Ball bearing	2
5	10-2	Main screw	1
6	12-3-brass	Main nut	1
7	6	Manufacturing	1
8	3	NSK 51106	2
9	4	Manufacturing	1
10	1	Manufacturing	1
11	2	Connector	1
12	5	Rotary connector	1
13	a19_1	L4	1
14	a20	L4	1
15	a22-s43	Servo motor	1
16	Finger with bearings		5
17	a21	Manufacturing	1
18	a23	Manufacturing	1

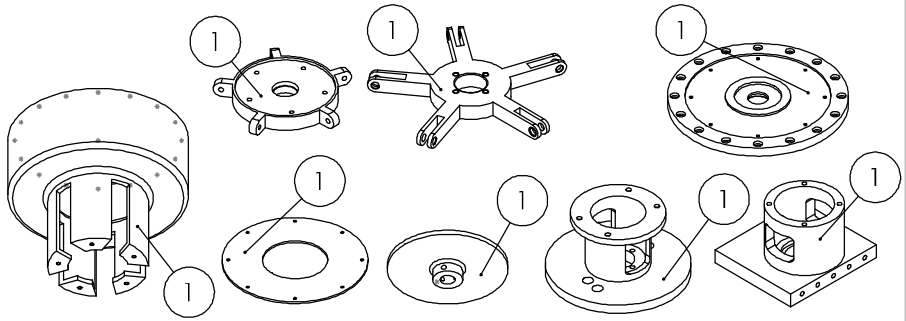

UNLESS OTHERWISE SPECIFIED: DIMENSIONS ARE IN MILLIMETERS SURFACE FINISH: TOLERANCES: LINEAR: ANGULAR:		FINISH:		DEBURR AND BREAK SHARP EDGES	DO NOT SCALE DRAWING	REVISION
	NAME	SIGNATURE	DATE		TITLE:	
DRAWN						
CHK'D						
APP'VD						
MFG						
Q.A				MATERIAL:	DWG NO.	A3
					Assem3 - Copy - Copy	
				WEIGHT:	SCALE:1:10	SHEET 1 OF 1

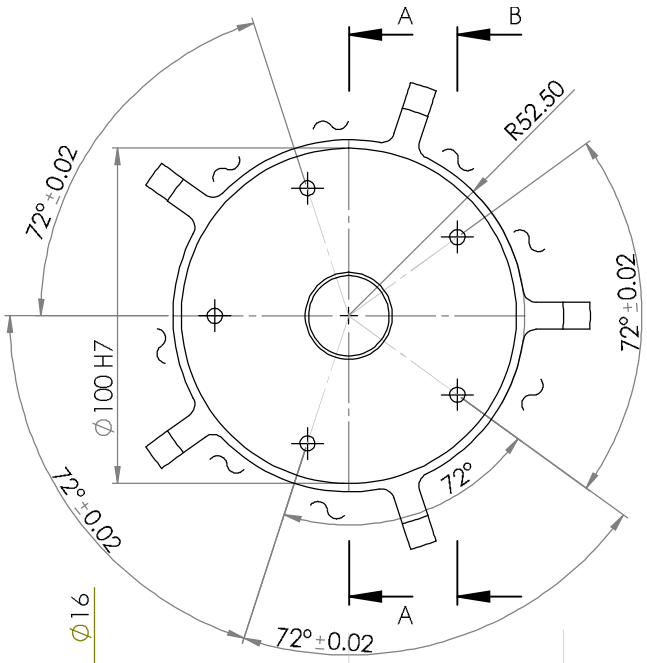

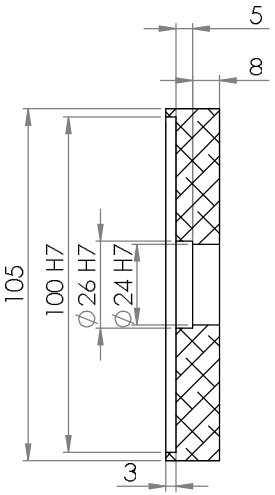

SECTION A-A

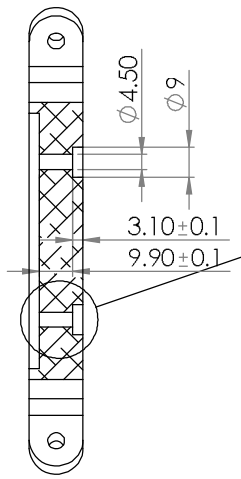

SECTION B-B

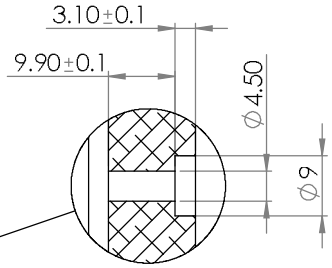

DETAIL C
SCALE 2 : 1

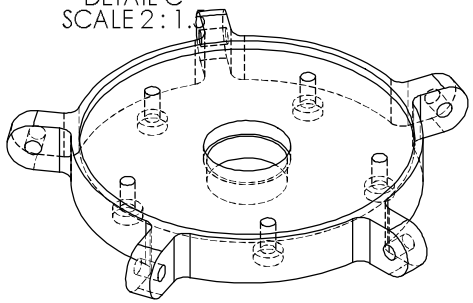

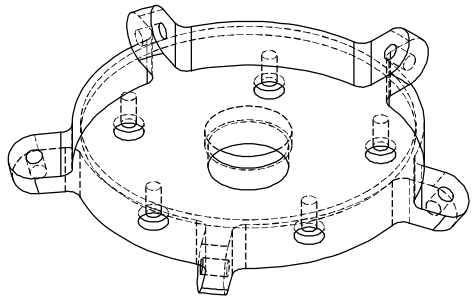

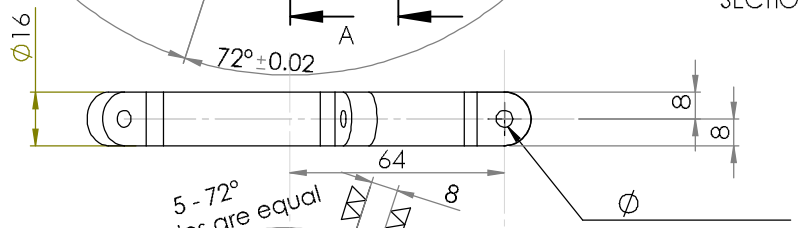

~ = laser cutting is ok

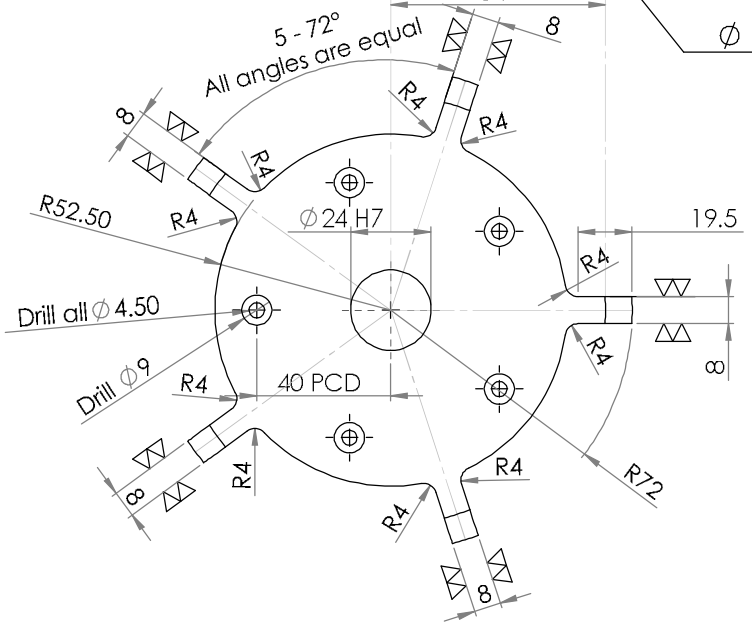

UNLESS OTHERWISE SPECIFIED: DIMENSIONS ARE IN MILLIMETERS SURFACE FINISH: TOLERANCES: LINEAR: ANGULAR:		FINISH:		DEBURR AND BREAK SHARP EDGES	DO NOT SCALE DRAWING	REVISION
					Quantity =1	
	NAME	SIGNATURE	DATE		TITLE: Manufacturing	
DRAWN						
CHK'D						
APP'VD						
MFG						
Q.A				MATERIAL: AL5052P-H112-JISH4000	DWG NO. 15-2	A3
				WEIGHT:	SCALE:1:2	SHEET 1 OF 1

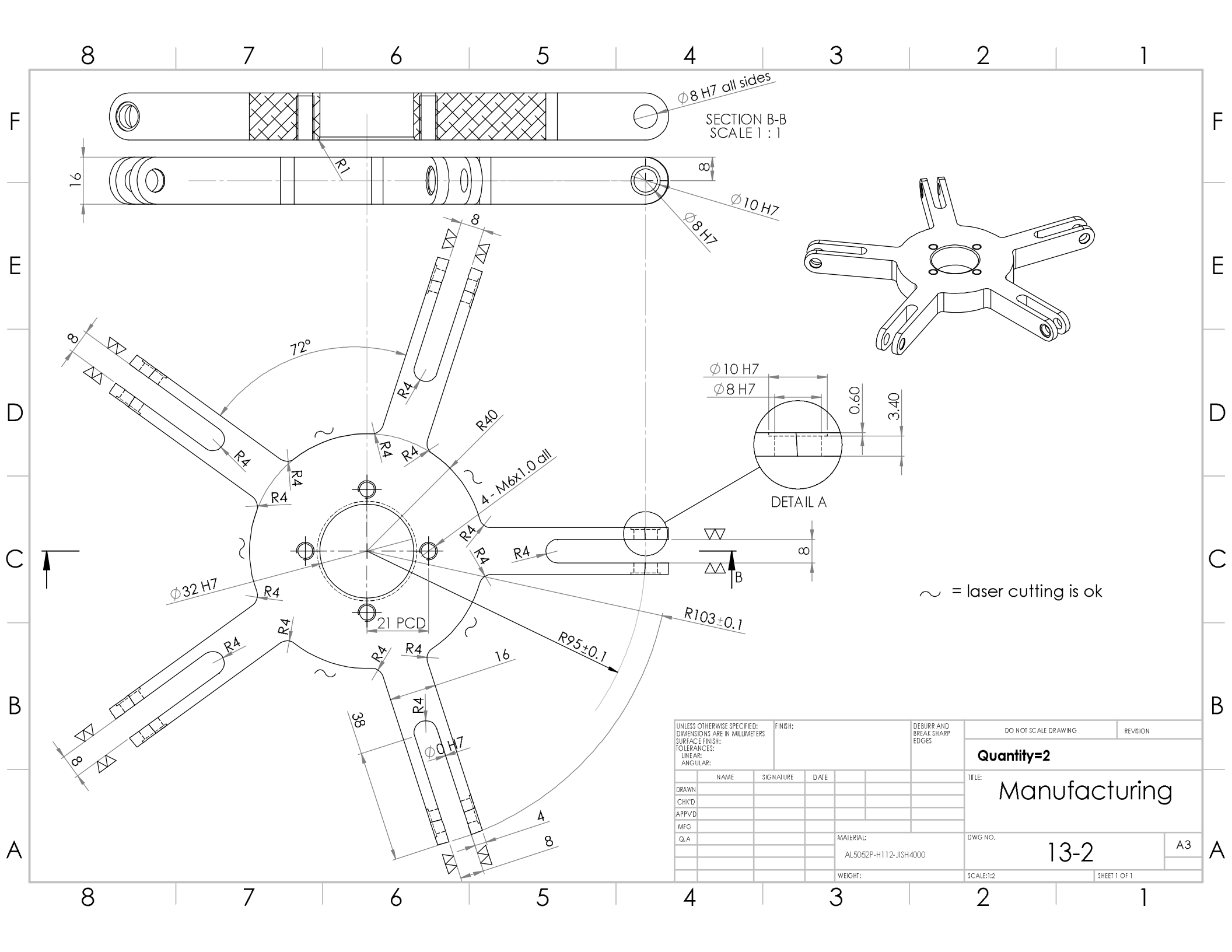

UNLESS OTHERWISE SPECIFIED: DIMENSIONS ARE IN MILLIMETERS SURFACE FINISH: TOLERANCES: LINEAR: ANGULAR:	FINISH:		DEBURR AND BREAK SHARP EDGES	DO NOT SCALE DRAWING		REVISION
				Quantity=2		
	NAME	SIGNATURE	DATE	TITLE:		
DRAWN				Manufacturing		
CHK'D						
APP'VD						
MFG						
Q.A				MATERIAL:	DWG NO.	A3
				AL5052P-H112-JISH4000	13-2	
				WEIGHT:	SCALE:1:2	SHEET 1 OF 1

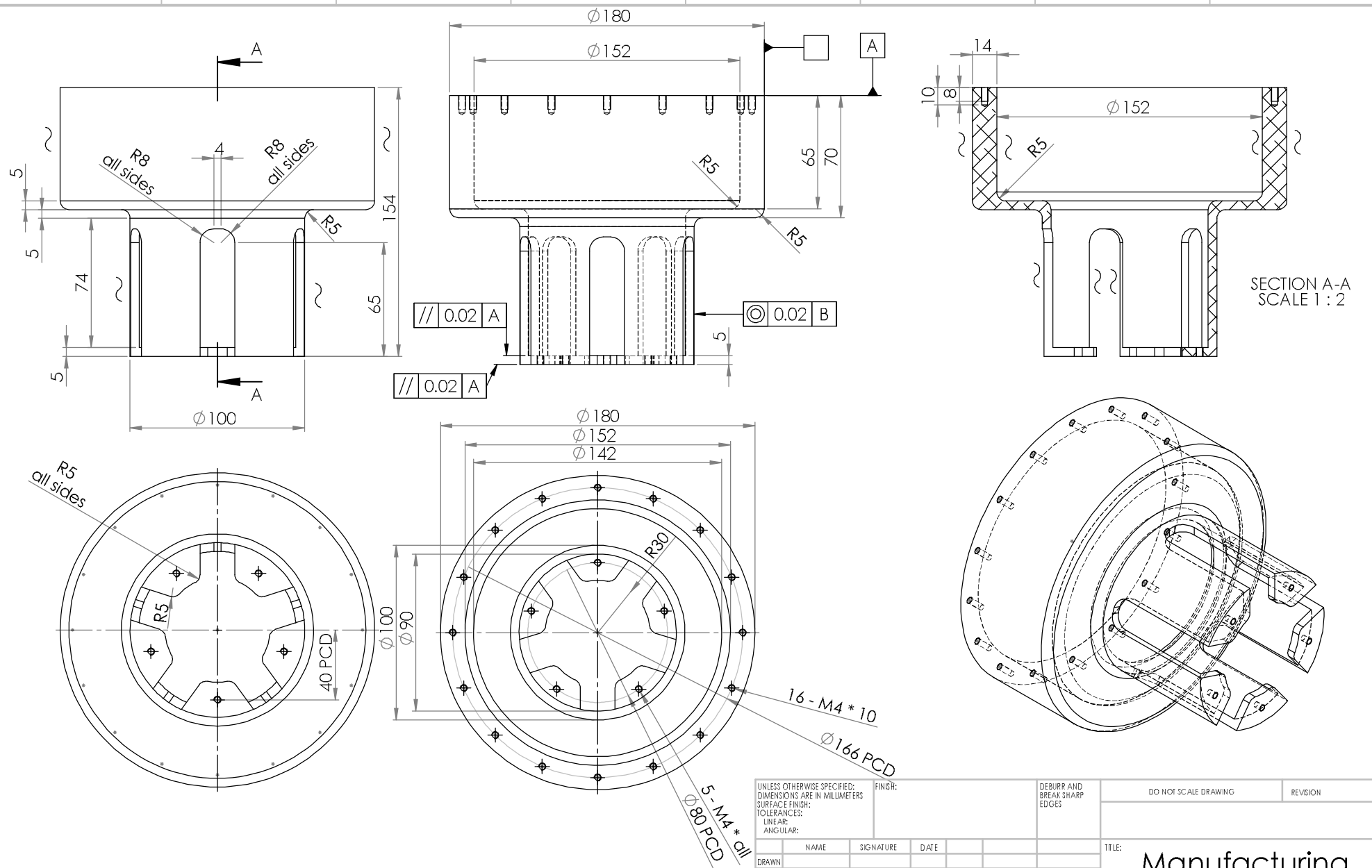

UNLESS OTHERWISE SPECIFIED: DIMENSIONS ARE IN MILLIMETERS SURFACE FINISH: TOLERANCES: LINEAR: ANGULAR:		FINISH:		DEBURR AND BREAK SHARP EDGES	DO NOT SCALE DRAWING	REVISION
	NAME	SIGNATURE	DATE		TITLE: Manufacturing	
DRAWN						
CHK'D						
APP'VD						
MFG						
Q.A						
				MATERIAL: AL5052P-H112-JISH4000	DWG NO. 7-2	A3
				WEIGHT:	SCALE:1:5	SHEET 1 OF 1

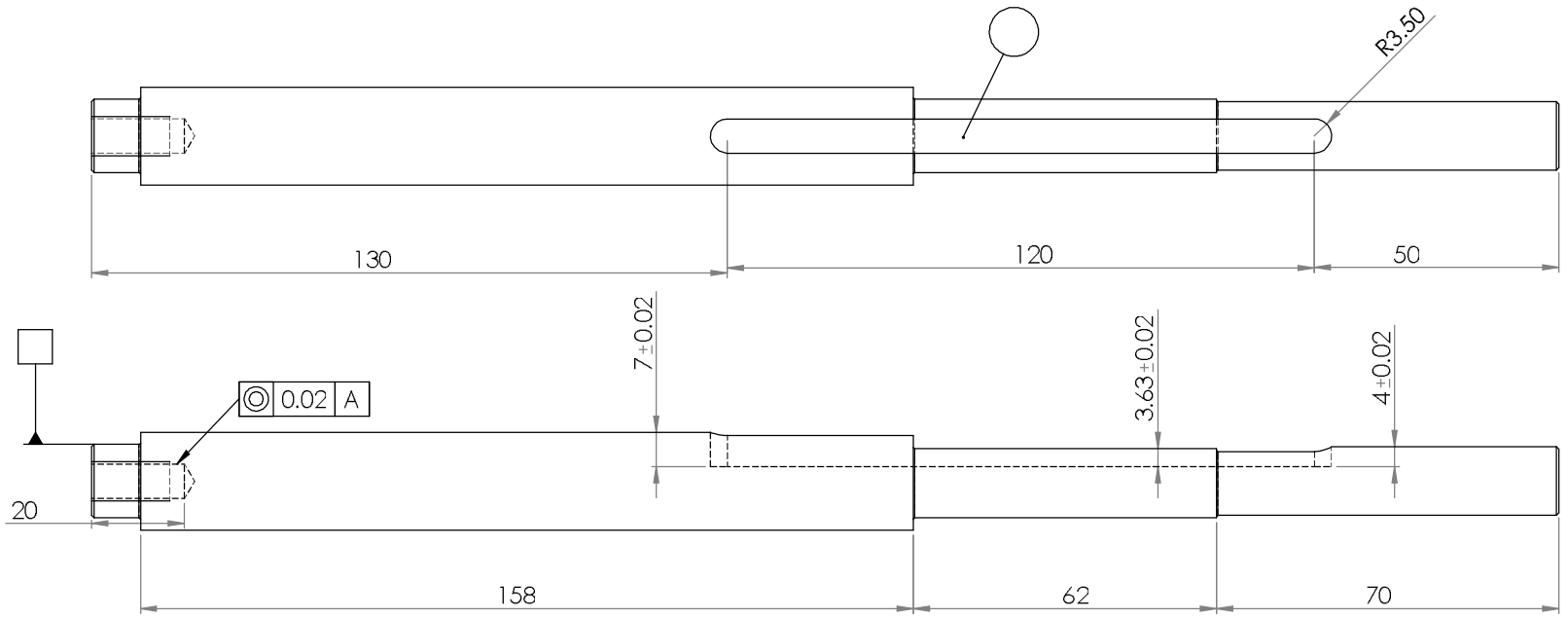

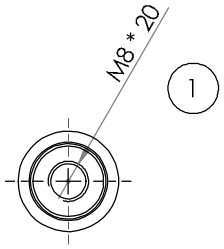

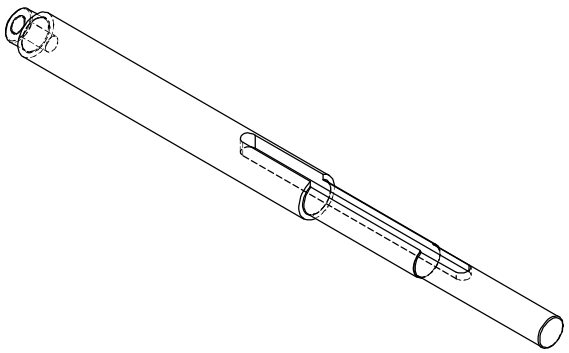

This components is only for modification.
It is a screw which already bought and only modifications are:
1- M8*20 at one end
2 groove

UNLESS OTHERWISE SPECIFIED: DIMENSIONS ARE IN MILLIMETERS SURFACE FINISH: TOLERANCES: LINEAR: ANGULAR:	FINISH:				DEBURR AND BREAK SHARP EDGES	DO NOT SCALE DRAWING / REVISION
						Quantity =2
	NAME	SIGNATURE	DATE			TITLE: Main screw **Only modification**
DRAWN						
CHK'D						
APP'VD						
MFG						
Q.A				MATERIAL:		DWG NO. 10-2 / A3
				WEIGHT:		SCALE:1:2 / SHEET 1 OF 1

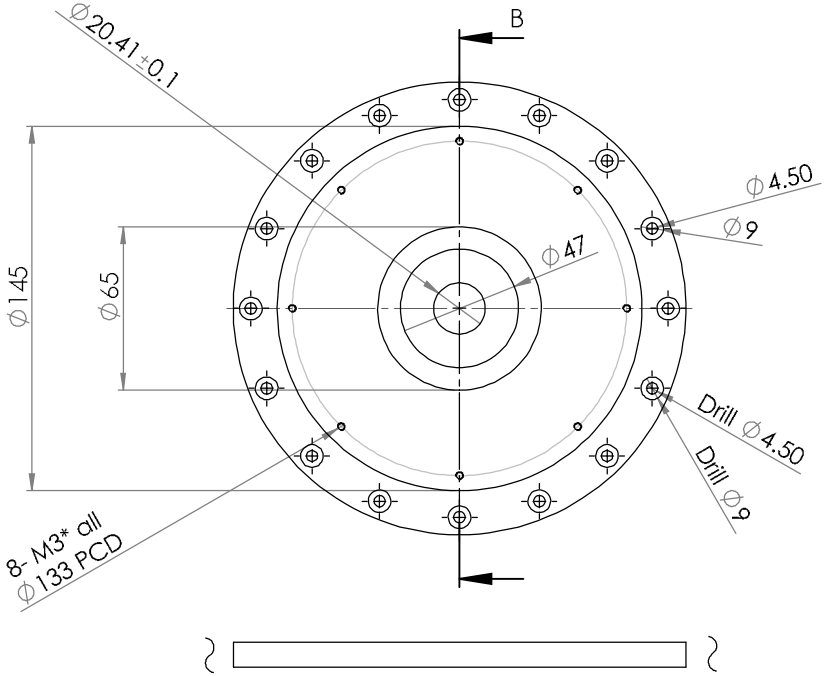

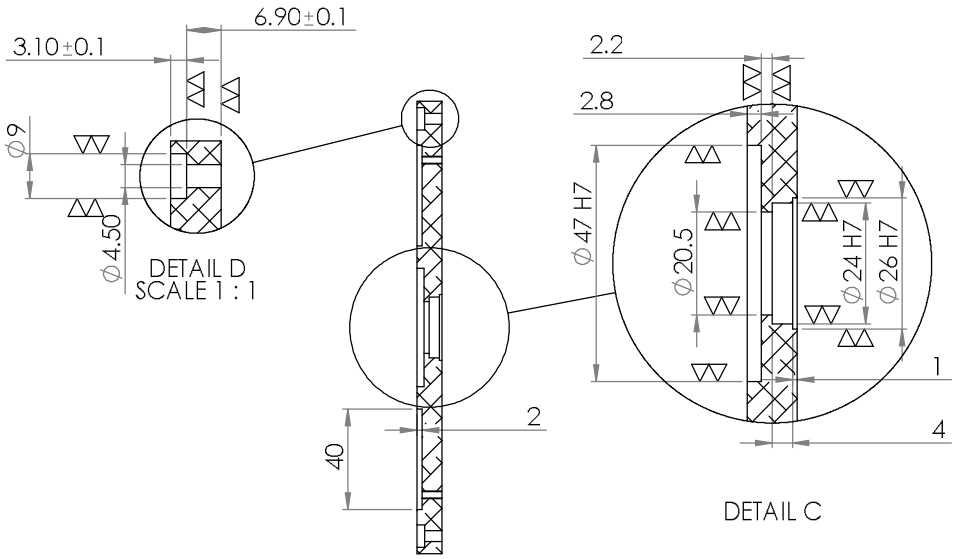

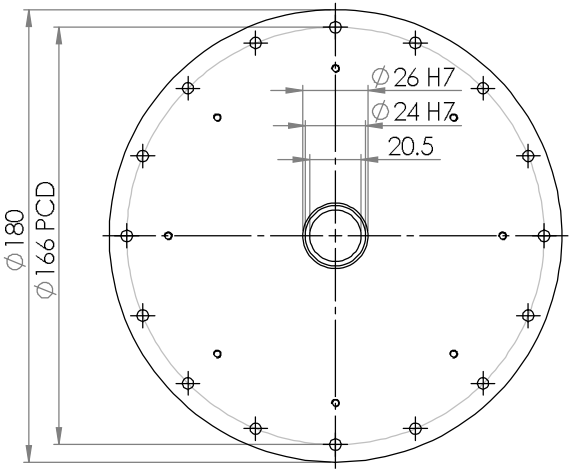

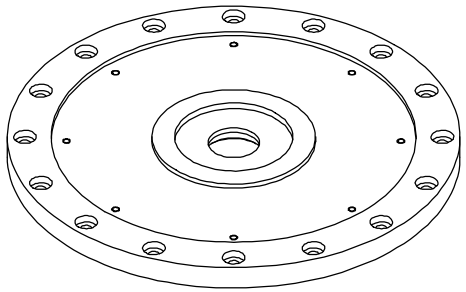

UNLESS OTHERWISE SPECIFIED: DIMENSIONS ARE IN MILLIMETERS SURFACE FINISH: TOLERANCES: LINEAR: ANGULAR:		FINISH:		DEBURR AND BREAK SHARP EDGES	DO NOT SCALE DRAWING	REVISION
					Quantity =1	
	NAME	SIGNATURE	DATE		TITLE: Manufacturing	
DRAWN						
CHK'D						
APP'VD						
MFG						
Q.A						
				MATERIAL: AL5052P-H112-JISH4000	DWG NO. 6	A3
				WEIGHT:	SCALE:1:2	SHEET 1 OF 1

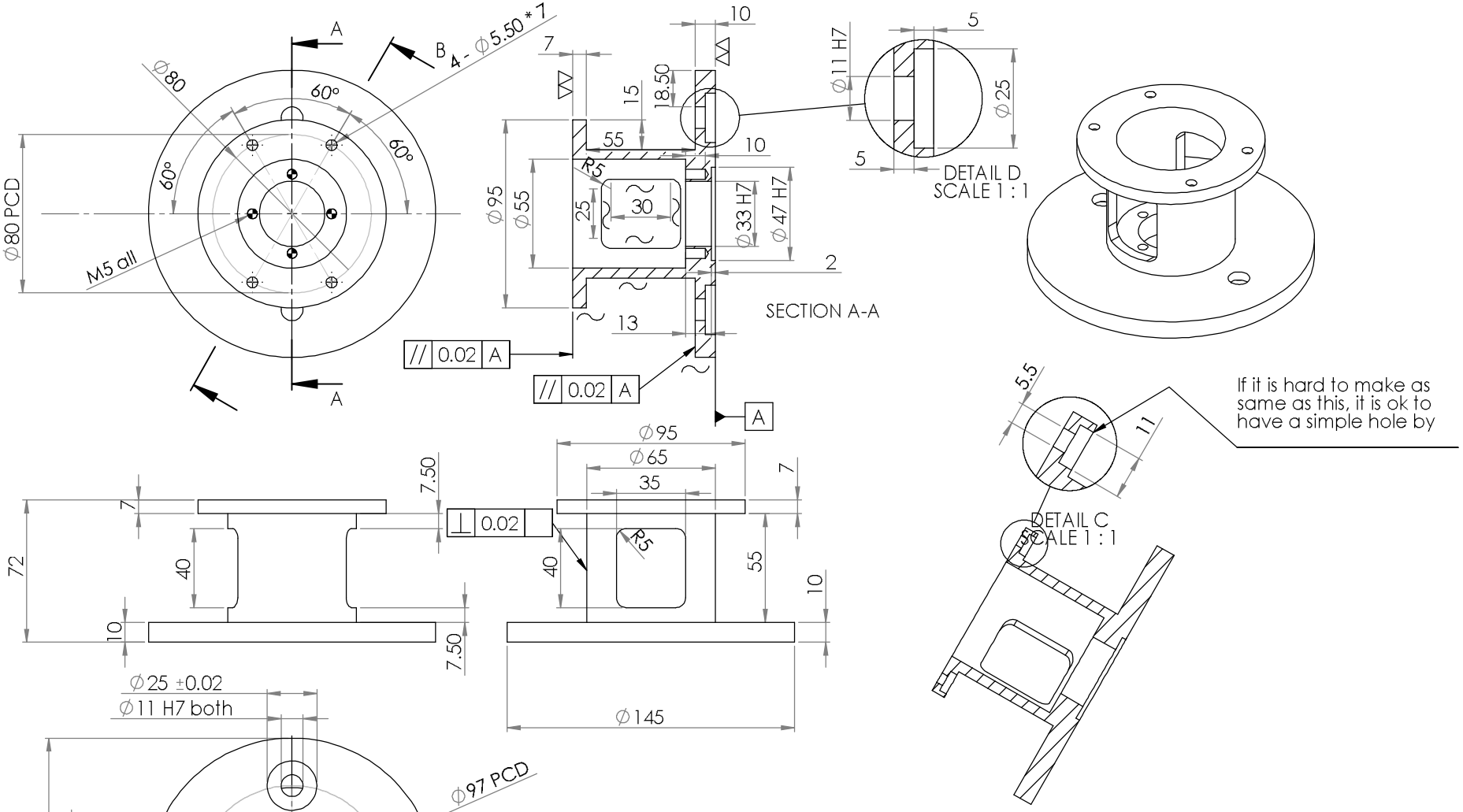

UNLESS OTHERWISE SPECIFIED: DIMENSIONS ARE IN MILLIMETERS SURFACE FINISH: TOLERANCES: LINEAR: ANGULAR:		FINISH:		DEBURR AND BREAK SHARP EDGES	DO NOT SCALE DRAWING	REVISION
					Quantity =1	
	NAME	SIGNATURE	DATE		TITLE: Manufacturing	
DRAWN						
CHK'D						
APP'VD						
MFG						
Q.A						
				MATERIAL: AL5052P-H112-JISH4000	DWG NO. 4	A3
				WEIGHT:	SCALE:1:2	SHEET 1 OF 1

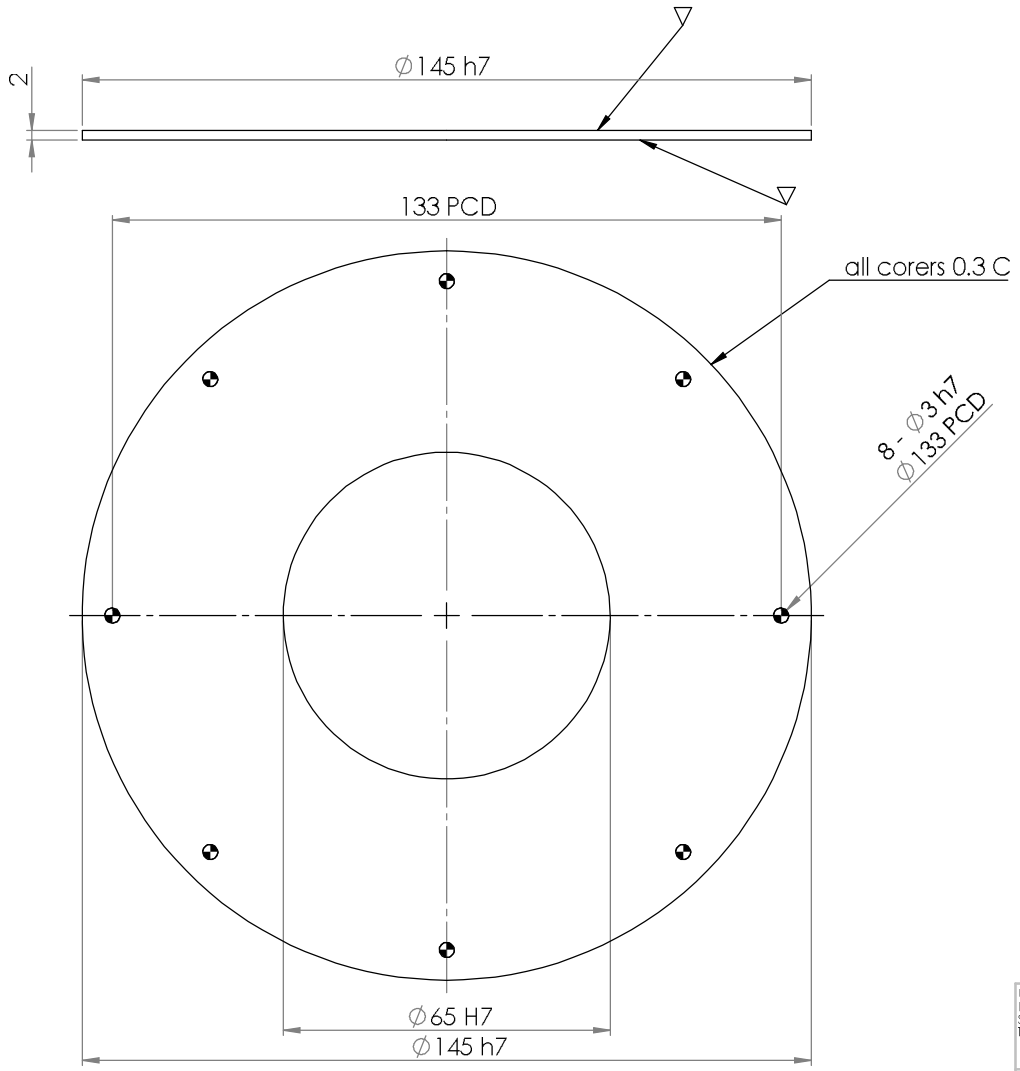

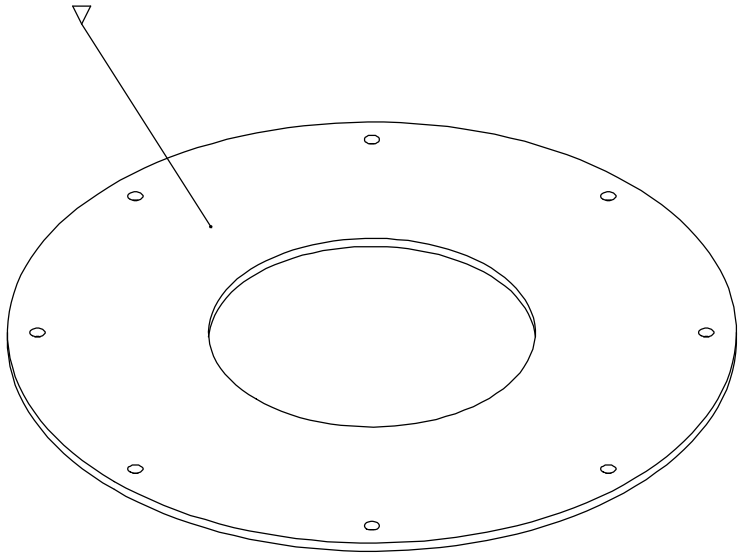

UNLESS OTHERWISE SPECIFIED: DIMENSIONS ARE IN MILLIMETERS SURFACE FINISH: TOLERANCES: LINEAR: ANGULAR:		FINISH:		DEBURR AND BREAK SHARP EDGES		DO NOT SCALE DRAWING	REVISION
						Quantity =2	
	NAME	SIGNATURE	DATE			TITLE: Manufacturing	
DRAWN							
CHK'D							
APP'VD							
MFG							
Q.A				MATERIAL: Stainless steel		DWG NO. a21	A3
				WEIGHT:		SCALE:1:2	SHEET 1 OF 1

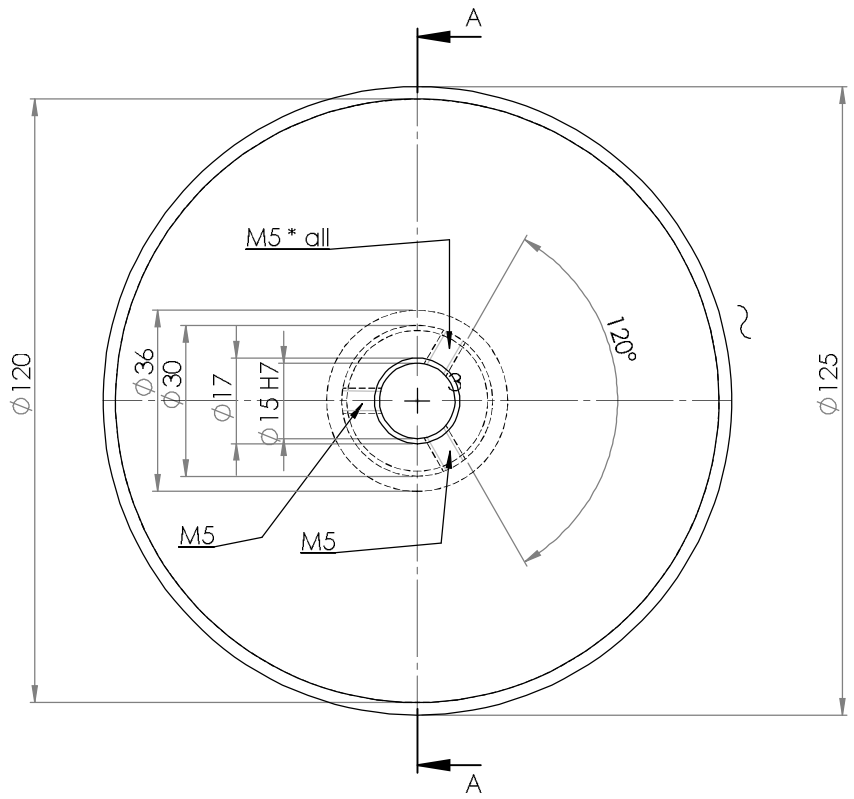

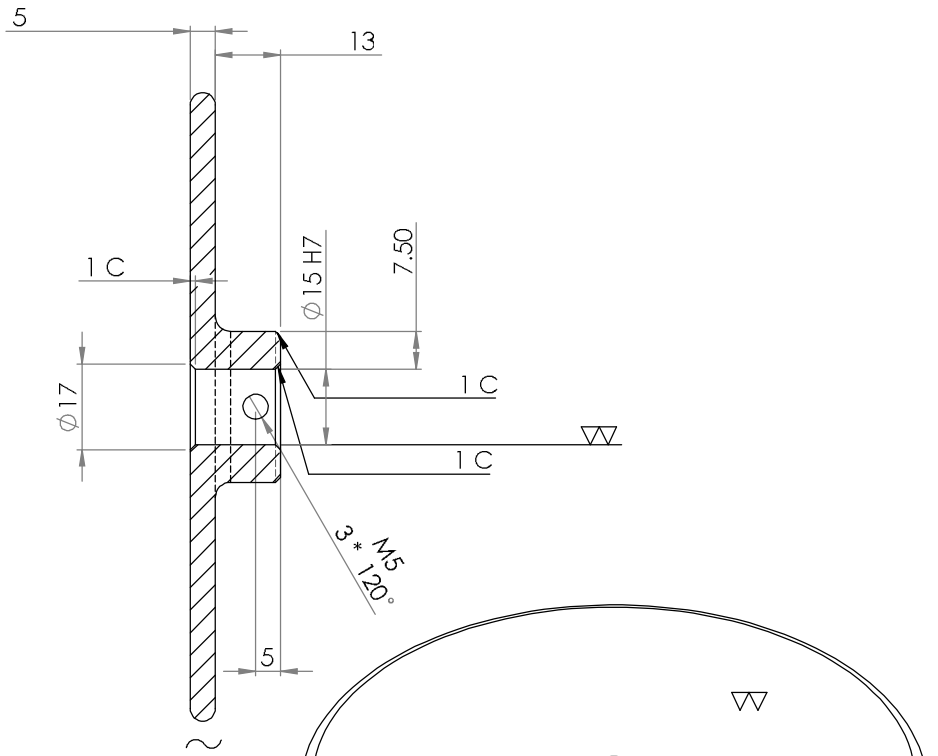

SECTION A-A
SCALE 1 : 1

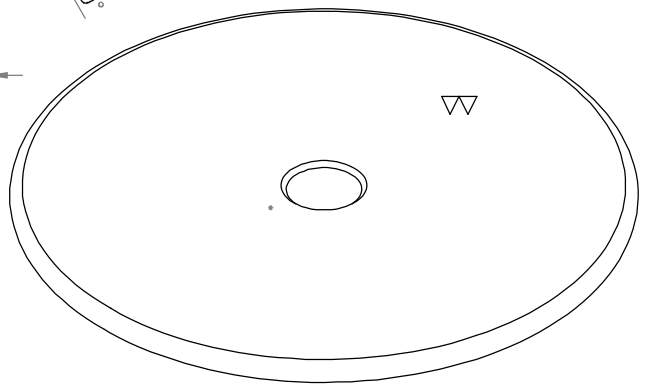

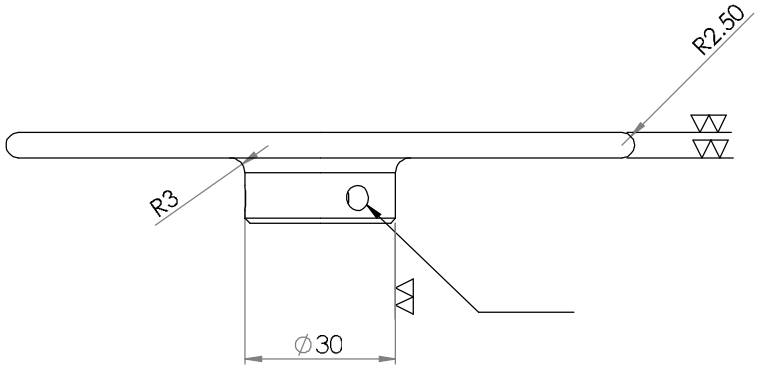

UNLESS OTHERWISE SPECIFIED: DIMENSIONS ARE IN MILLIMETERS SURFACE FINISH: TOLERANCES: LINEAR: ANGULAR:		FINISH:		DEBURR AND BREAK SHARP EDGES		DO NOT SCALE DRAWING	REVISION
	NAME	SIGNATURE	DATE			TITLE: Manufacturing	
DRAWN							
CHK'D							
APP'VD							
MFG							
Q.A				MATERIAL: Stainless steel		DWG NO. a23	A3
				WEIGHT:		SCALE:1:2	SHEET 1 OF 1

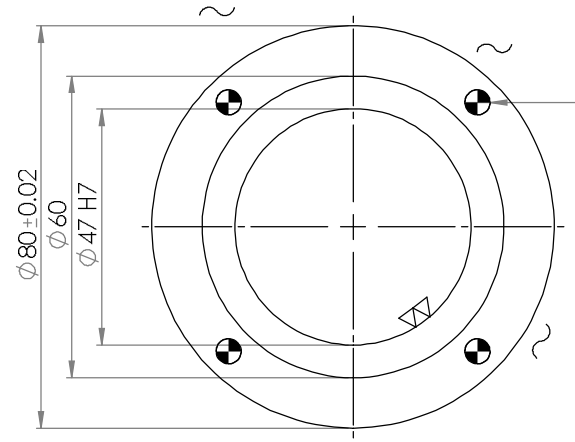

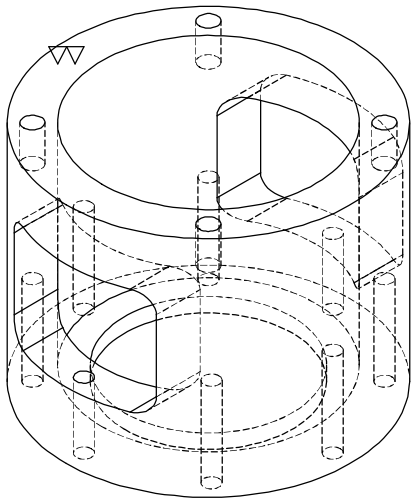

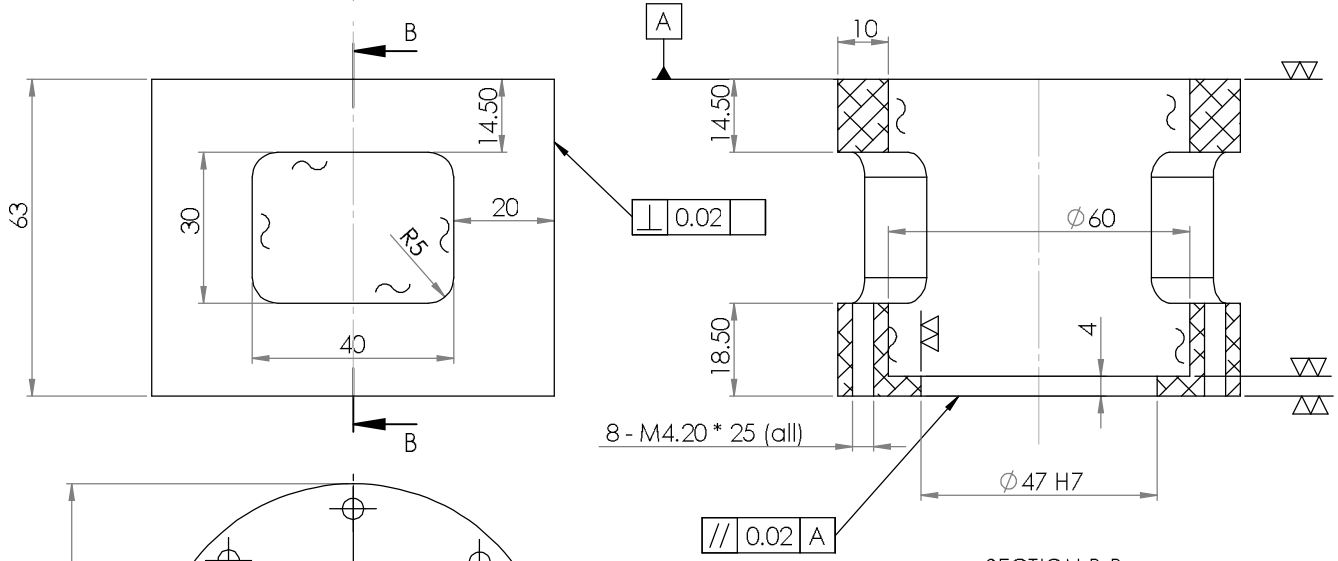

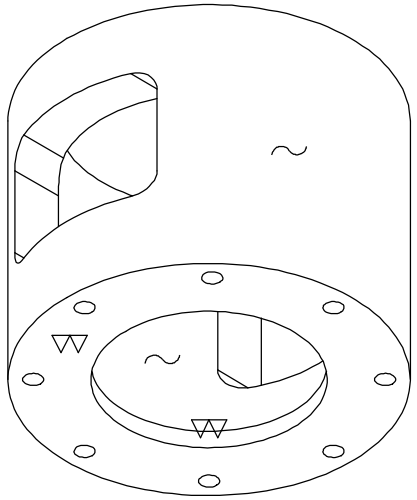

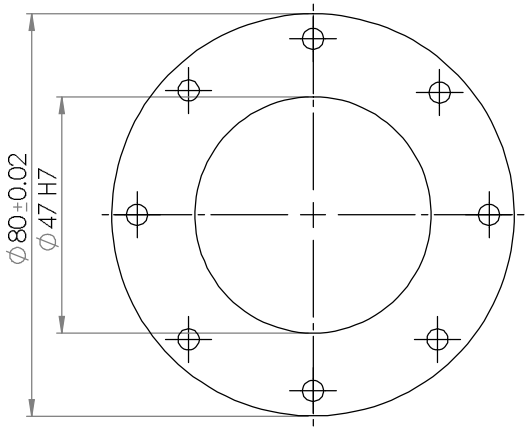

UNLESS OTHERWISE SPECIFIED: DIMENSIONS ARE IN MILLIMETERS SURFACE FINISH: TOLERANCES: LINEAR: ANGULAR:	FINISH:		DEBURR AND BREAK SHARP EDGES	DO NOT SCALE DRAWING	REVISION	
	NAME	SIGNATURE	DATE	TITLE: Manufacturing		
DRAWN						
CHK'D						
APP'VD						
MFG						
Q.A			MATERIAL:	DWG NO. 1 - 1	A3	
			WEIGHT:	SCALE:1:1	SHEET 1 OF 1	

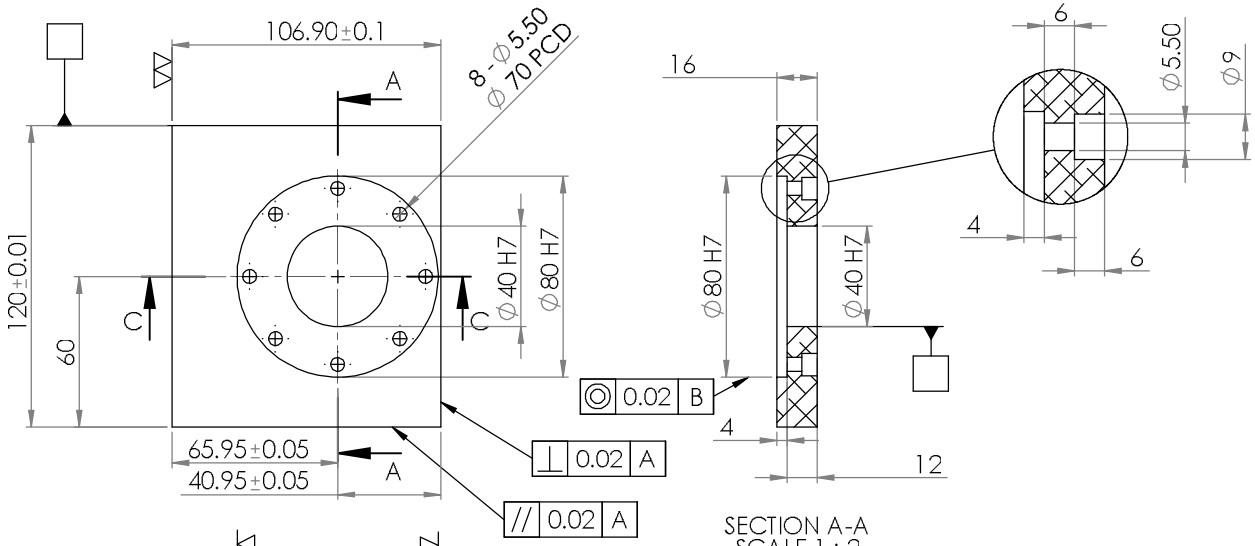

SECTION A-A
SCALE 1 : 2

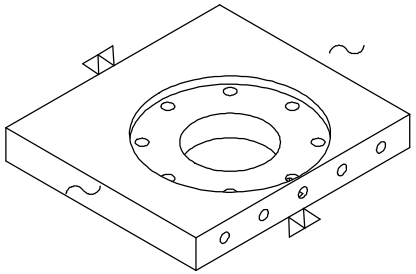

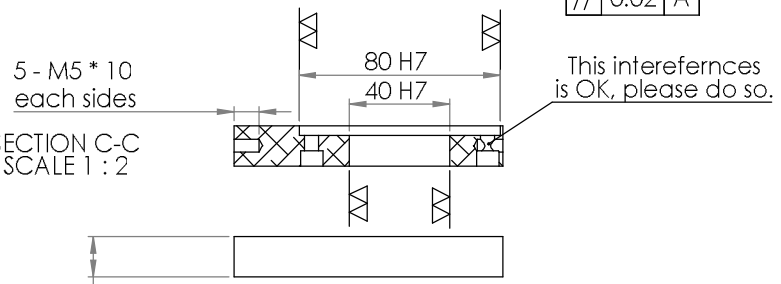

SECTION C-C
SCALE 1 : 2

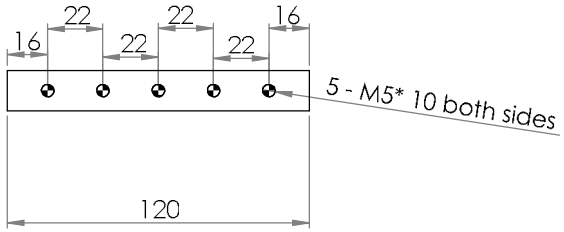

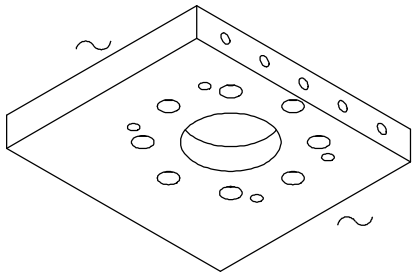

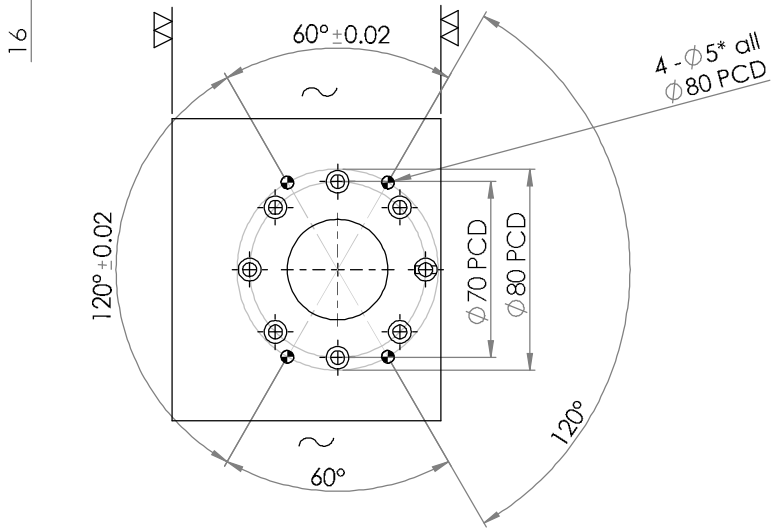

UNLESS OTHERWISE SPECIFIED: DIMENSIONS ARE IN MILLIMETERS SURFACE FINISH: TOLERANCES: LINEAR: ANGULAR:		FINISH:		DEBURR AND BREAK SHARP EDGES	DO NOT SCALE DRAWING	REVISION	
	NAME	SIGNATURE	DATE		TITLE: Manufacturing		
DRAWN							
CHK'D							
APP'VD							
MFG							
Q.A				MATERIAL:	DWG NO. 1-2		A3
				WEIGHT:	SCALE:1:1	SHEET 1 OF 1	

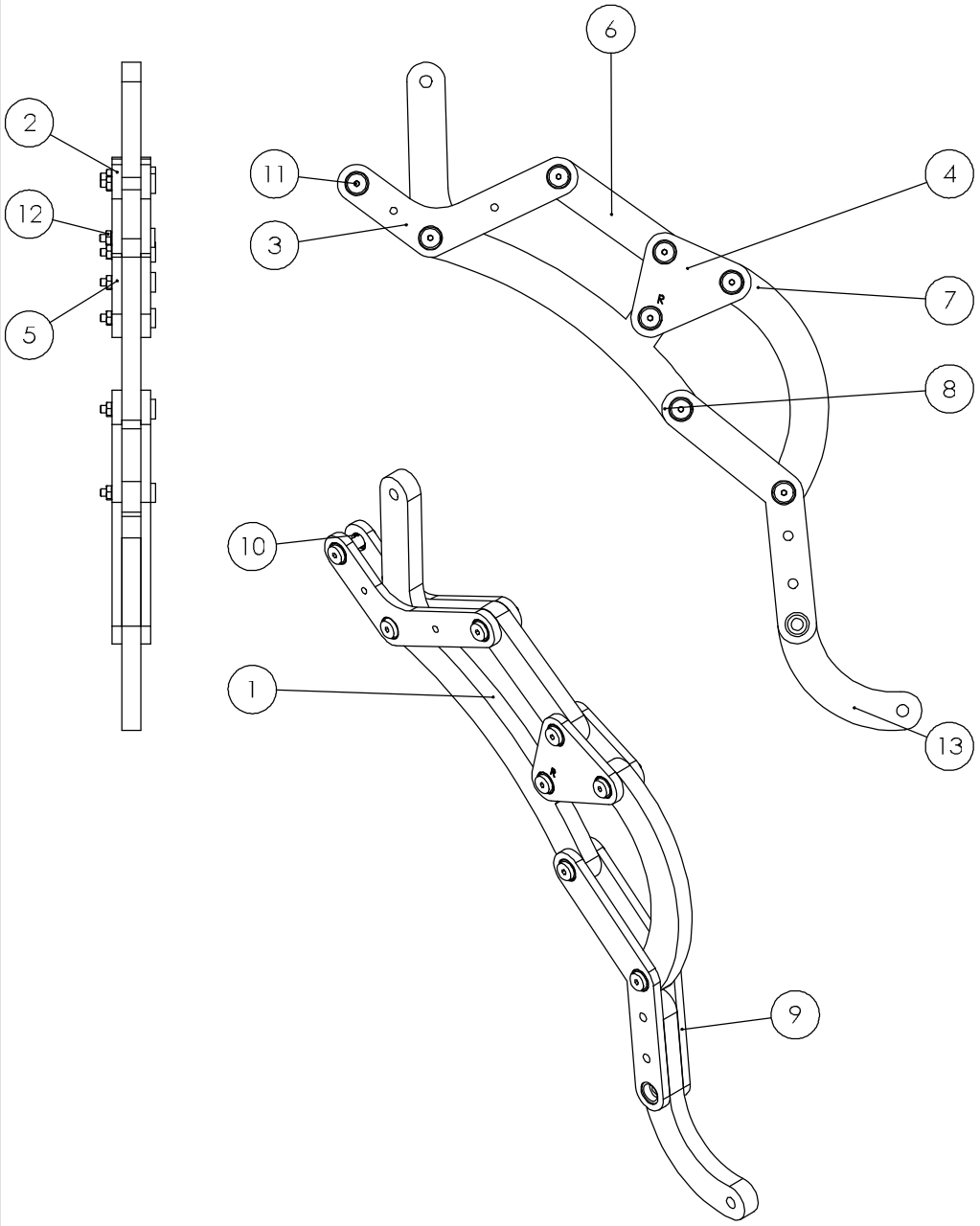

ITEM NO.	PART NUMBER	DESCRIPTION	QTY.
1	F-2 - Improved		1
2	F-3-Left - Improved		1
3	F-3-Right - Improved		1
4	F-5-Right	3DP	1
5	F-5-Left	3DP	1
6	F-4	3DP	1
7	F-6	3DP	1
8	F-7-Right	3DP	1
9	F-7-Left- Copy	3DP	1
10	FL675ZZ_2_03	Ball bearing	16
11	DBTB3-16-5_2_03	Screw	8
12	JIS B 1181 Hexagon nut - style 1 A M3 - W - -N		8
13	17	3DP	1

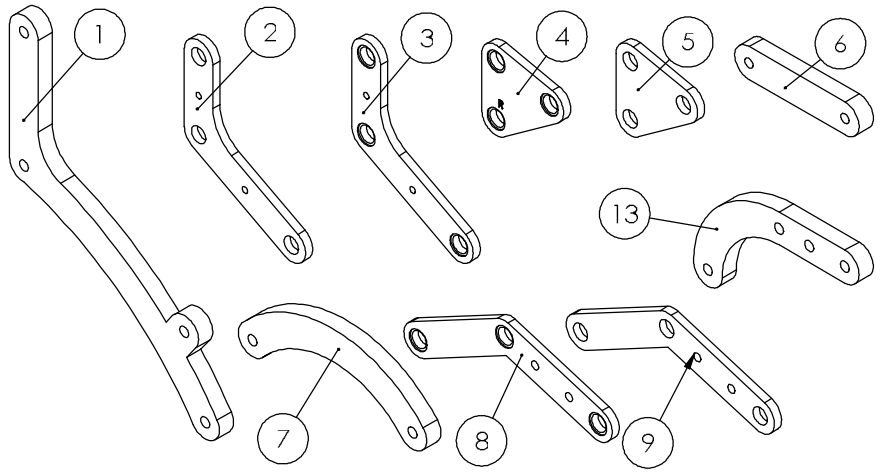

UNLESS OTHERWISE SPECIFIED: DIMENSIONS ARE IN MILLIMETERS SURFACE FINISH: TOLERANCES: LINEAR: ANGULAR:			FINISH:			DEBURR AND BREAK SHARP EDGES	DO NOT SCALE DRAWING
	NAME	SIGNATURE	DATE				TITLE:
DRAWN							
CHK'D							
APP'VD							
MFG							
Q.A				MATERIAL:			DWG NO.
							A3
				WEIGHT:		SCALE:1:2	SHEET 1 OF 1

Finger with bearings

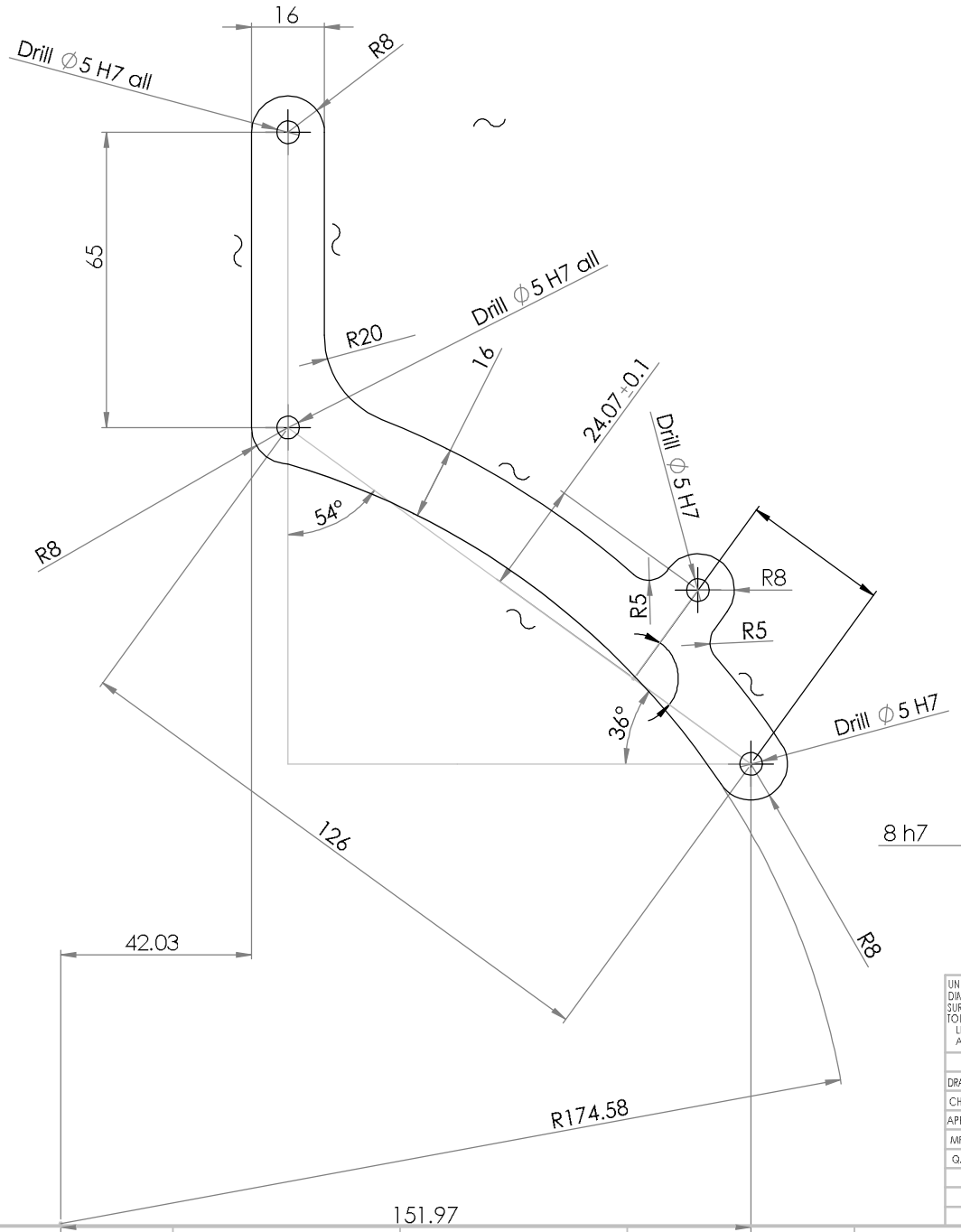

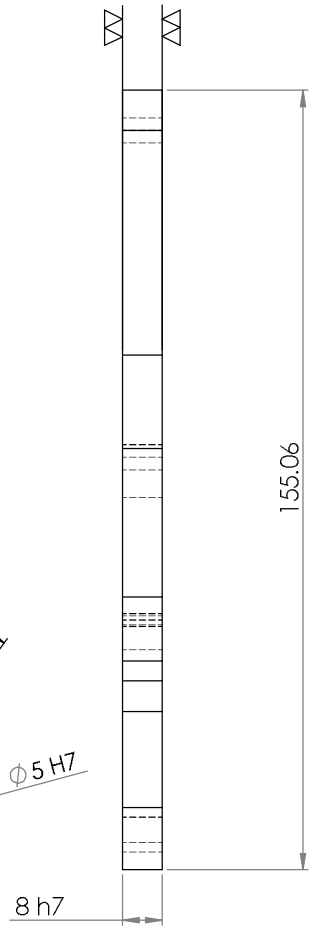

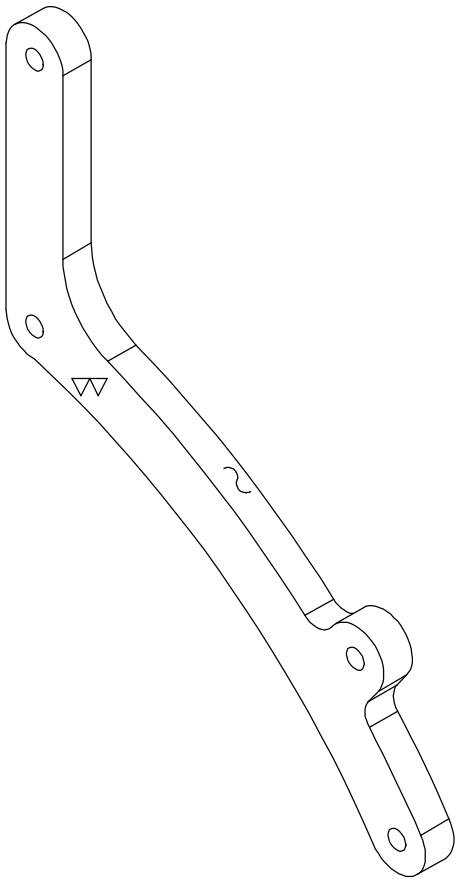

UNLESS OTHERWISE SPECIFIED: DIMENSIONS ARE IN MILLIMETERS SURFACE FINISH: TOLERANCES: LINEAR: ANGULAR:		FINISH:		DEBURR AND BREAK SHARP EDGES	DO NOT SCALE DRAWING	REVISION
					Quantity =10	
	NAME	SIGNATURE	DATE		TITLE: 3DP	
DRAWN						
CHK'D						
APP'VD						
MFG						
Q.A						
				MATERIAL: AL5052P-H112-JIS H4000	DWG NO. F-2	A3
				WEIGHT:	SCALE:1:1	SHEET 1 OF 1

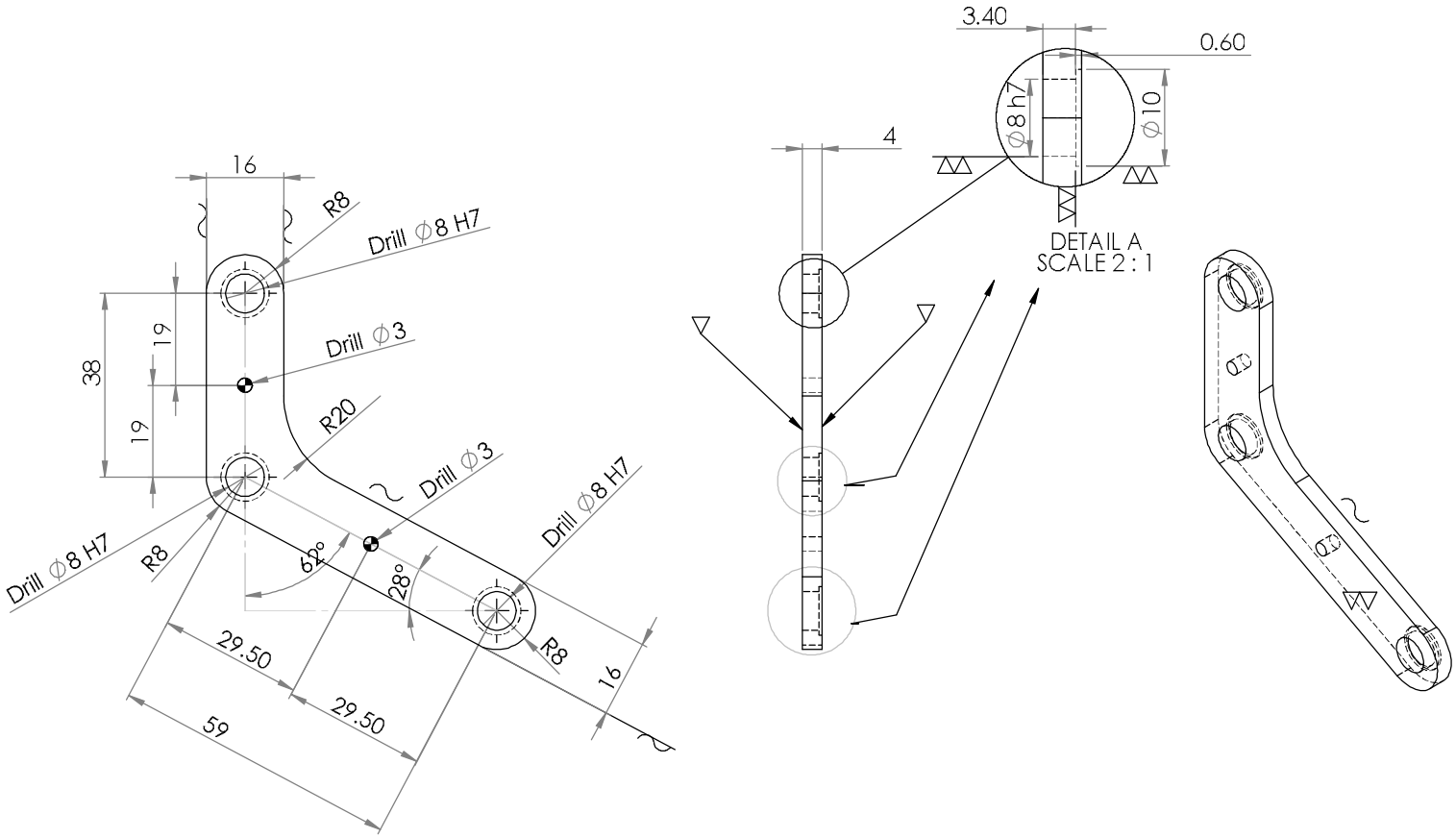

~ =laser cutting is OK.

UNLESS OTHERWISE SPECIFIED: DIMENSIONS ARE IN MILLIMETERS SURFACE FINISH: TOLERANCES: LINEAR: ANGULAR:		FINISH:		DEBURR AND BREAK SHARP EDGES	DO NOT SCALE DRAWING	REVISION
					Quantity =10	
	NAME	SIGNATURE	DATE		TITLE:	
DRAWN						
CHK'D						
APP'VD						
MFG						
Q.A					DWG NO.	A3
			MATERIAL: AL5052P-H112-JISH4000		F-3-Left - Improved	
			WEIGHT:		SCALE:1:1	SHEET 1 OF 1

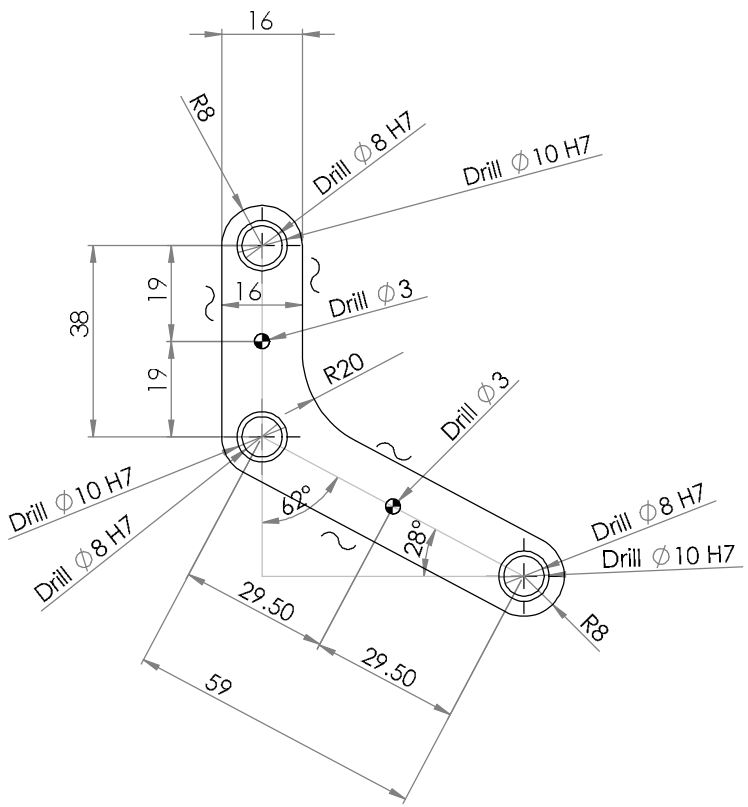

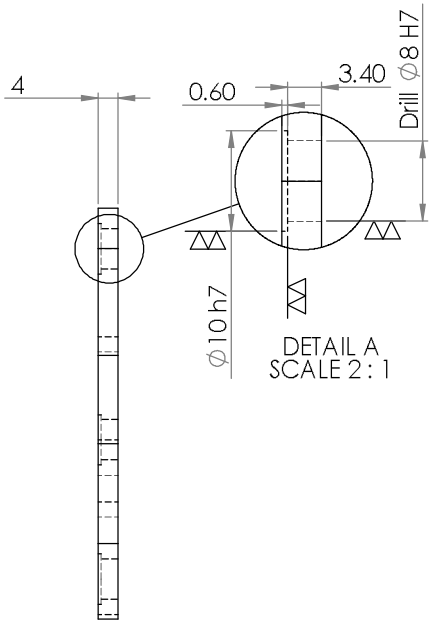

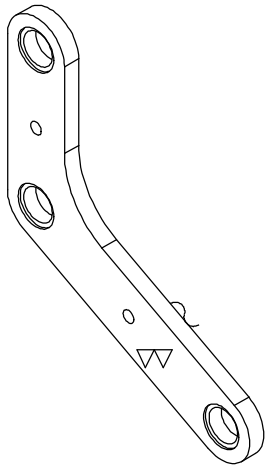

~ = laser cutting is ok.

UNLESS OTHERWISE SPECIFIED: DIMENSIONS ARE IN MILLIMETERS SURFACE FINISH: TOLERANCES: LINEAR: ANGULAR:		FINISH:			DEBURR AND BREAK SHARP EDGES	DO NOT SCALE DRAWING	REVISION
						Quantity =10	
	NAME	SIGNATURE	DATE			TITLE:	
DRAWN							
CHK'D							
APP'VD							
MFG							
Q.A						DWG NO.	A3
				MATERIAL: AL5052P-H112 -JISH4000		F-3-Right - Improved	
				WEIGHT:		SCALE:1:1	SHEET 1 OF 1

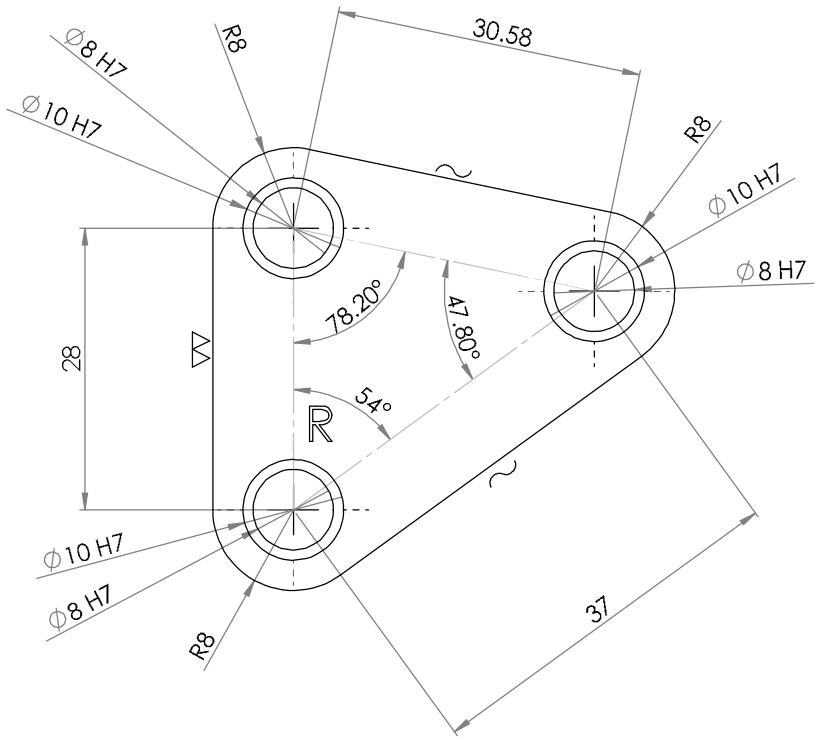

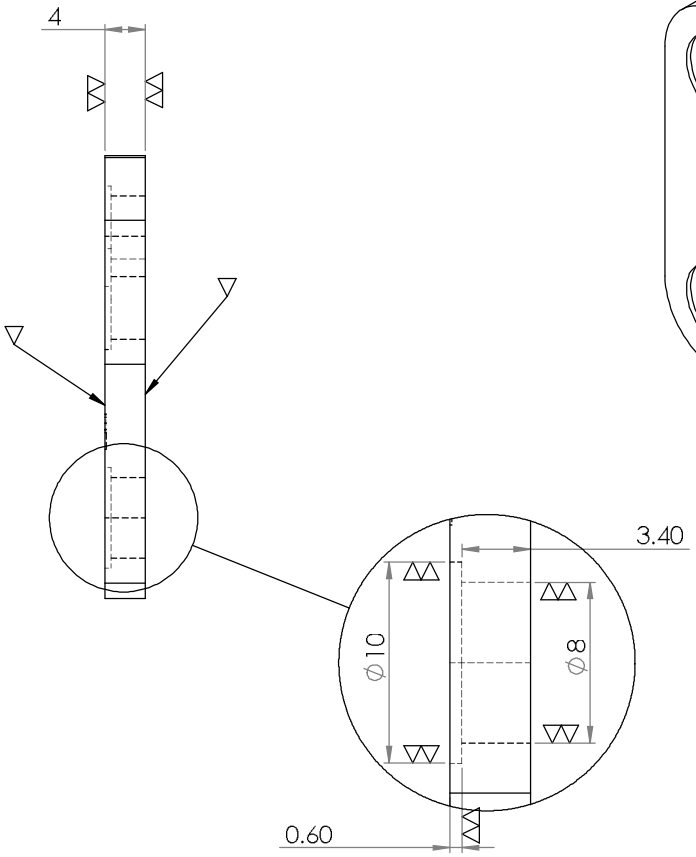

DETAIL A
SCALE 4 : 1

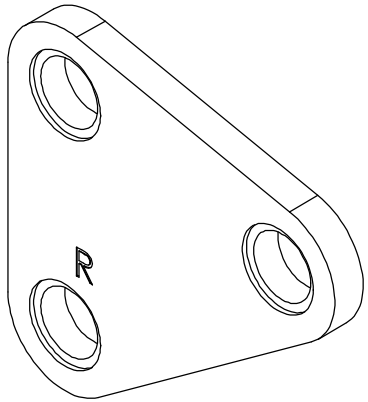

UNLESS OTHERWISE SPECIFIED: DIMENSIONS ARE IN MILLIMETERS SURFACE FINISH: TOLERANCES: LINEAR: ANGULAR:		FINISH:			DEBURR AND BREAK SHARP EDGES	DO NOT SCALE DRAWING	REVISION
						Quantity =10	
	NAME	SIGNATURE	DATE			TITLE: 3DP	
DRAWN							
CHK'D							
APP'VD							
MFG							
Q.A				MATERIAL: AL5052P-H112-JISH4000		DWG NO. F-5-Right	A3
				WEIGHT:		SCALE:2:1	SHEET 1 OF 1

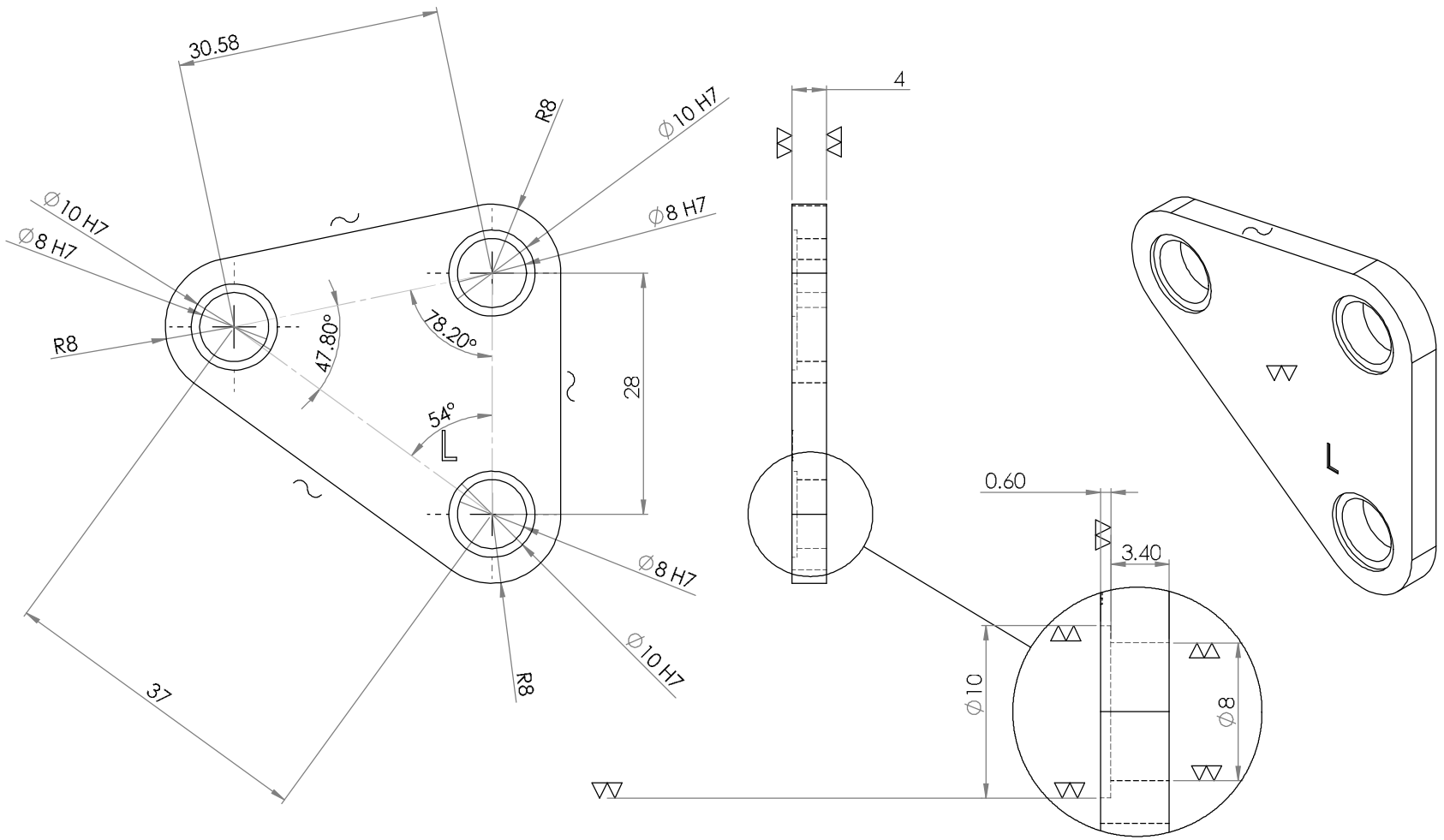

DETAIL A
SCALE 4 : 1

UNLESS OTHERWISE SPECIFIED:
DIMENSIONS ARE IN MILLIMETERS
SURFACE FINISH:
TOLERANCES:
LINEAR:
ANGULAR:

FINISH:

DEBURR AND BREAK SHARP EDGES

DO NOT SCALE DRAWING

REVISION

Quantity =10

	NAME	SIGNATURE	DATE
DRAWN			
CHK'D			
APP'VD			
MFG			
Q.A			

TITLE:

3DP

MATERIAL:
AL5052P-H112-JISH4000

DWG NO.
F-5-Left

A3

WEIGHT:

SCALE:2:1

SHEET 1 OF 1

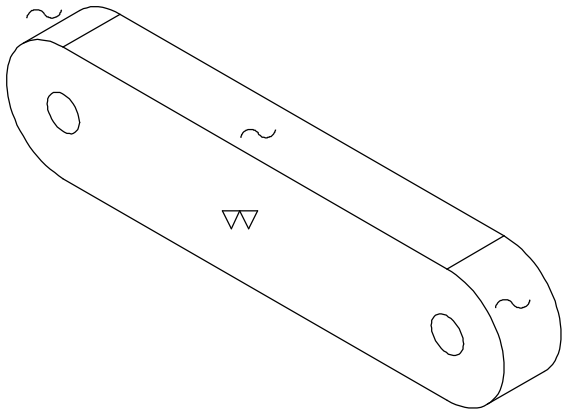

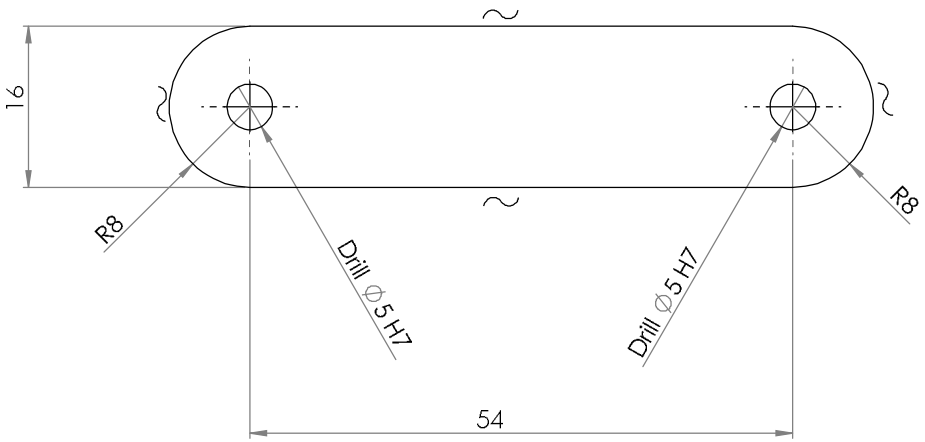

UNLESS OTHERWISE SPECIFIED: DIMENSIONS ARE IN MILLIMETERS SURFACE FINISH: TOLERANCES: LINEAR: ANGULAR:		FINISH:			DEBURR AND BREAK SHARP EDGES	DO NOT SCALE DRAWING	REVISION
						Quantity =10	
	NAME	SIGNATURE	DATE			TITLE:	
DRAWN						3DP	
CHK'D							
APP'VD							
MFG							
Q.A				MATERIAL:		DWG NO.	A3
				AL5052P-H112-JISH4000		F-4	
				WEIGHT:		SCALE:2:1	SHEET 1 OF 1

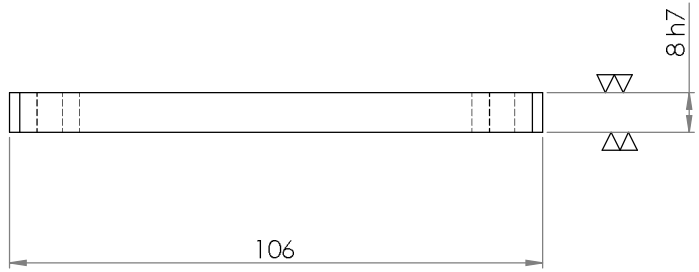

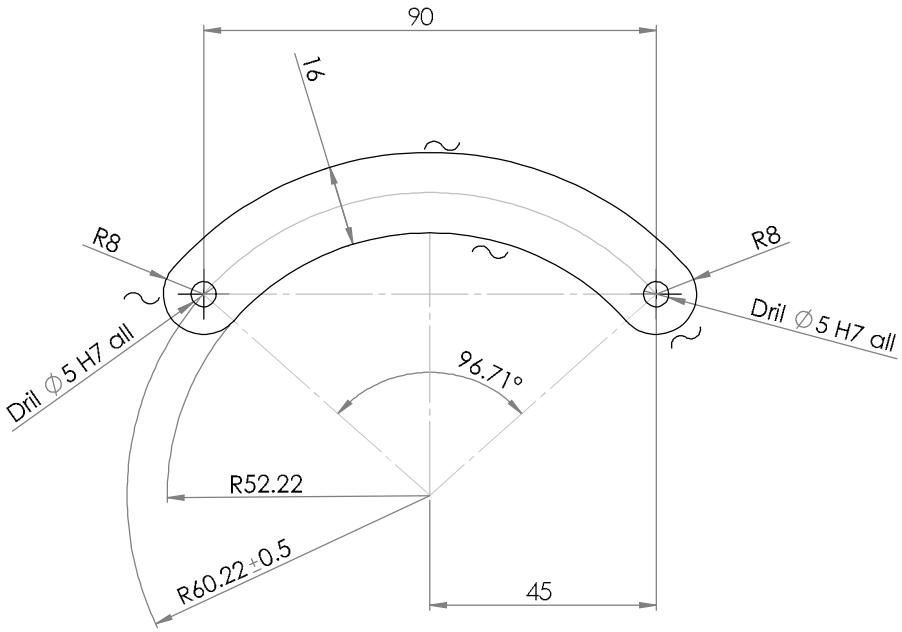

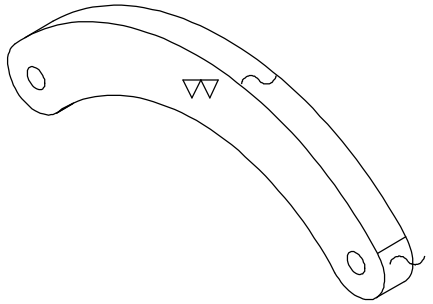

UNLESS OTHERWISE SPECIFIED: DIMENSIONS ARE IN MILLIMETERS SURFACE FINISH: TOLERANCES: LINEAR: ANGULAR:		FINISH:		DEBURR AND BREAK SHARP EDGES		DO NOT SCALE DRAWING	REVISION
						Quantity =10	
	NAME	SIGNATURE	DATE			TITLE:	
DRAWN						3DP	
CHK'D							
APP'VD							
MFG							
Q.A				MATERIAL:		DWG NO.	A3
				AL5052P-H112-JISH4000		F-6	
				WEIGHT:		SCALE:2:1	SHEET 1 OF 1

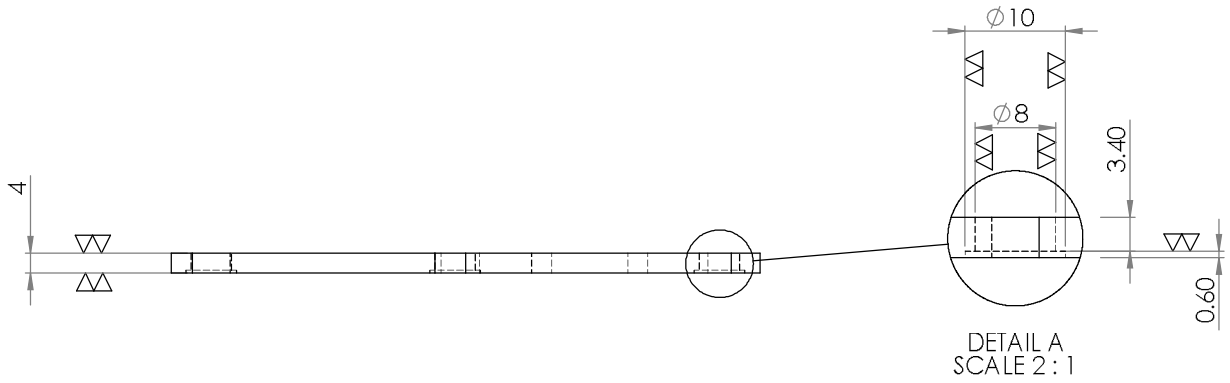

DETAIL A
SCALE 2 : 1

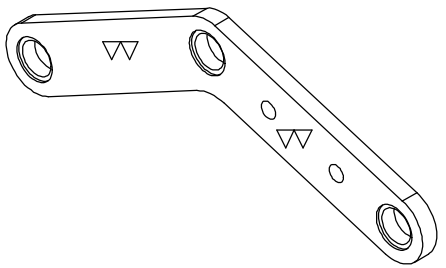

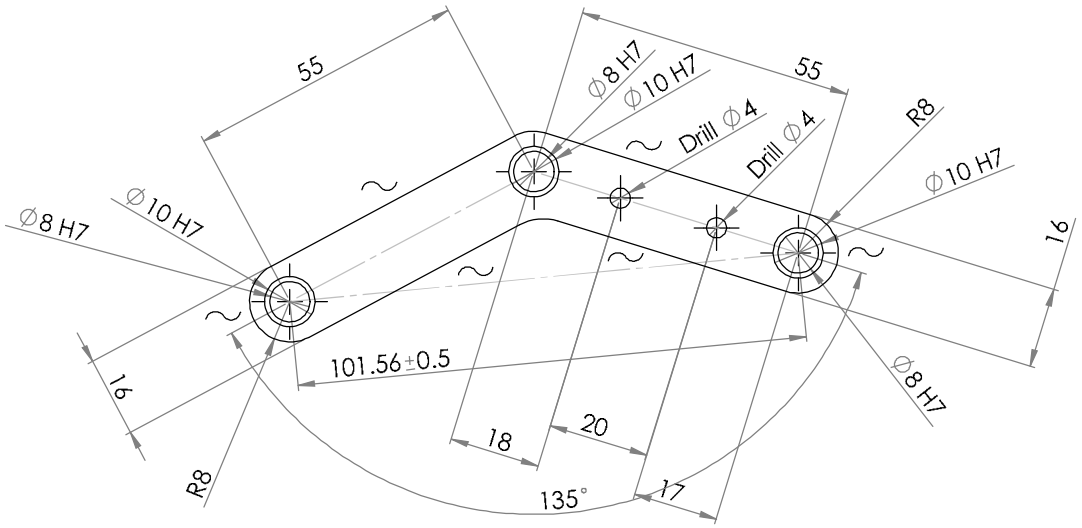

UNLESS OTHERWISE SPECIFIED: DIMENSIONS ARE IN MILLIMETERS SURFACE FINISH: TOLERANCES: LINEAR: ANGULAR:		FINISH:		DEBURR AND BREAK SHARP EDGES	DO NOT SCALE DRAWING		REVISION
					Quantity =10		
	NAME	SIGNATURE	DATE		TITLE:		
DRAWN					3DP		
CHK'D							
APP'VD							
MFG							
Q.A					MATERIAL:	DWG NO.	A3
					AL5052P-H112-JISH4000	F-7-Right	
					WEIGHT:	SCALE:1:1	SHEET 1 OF 1

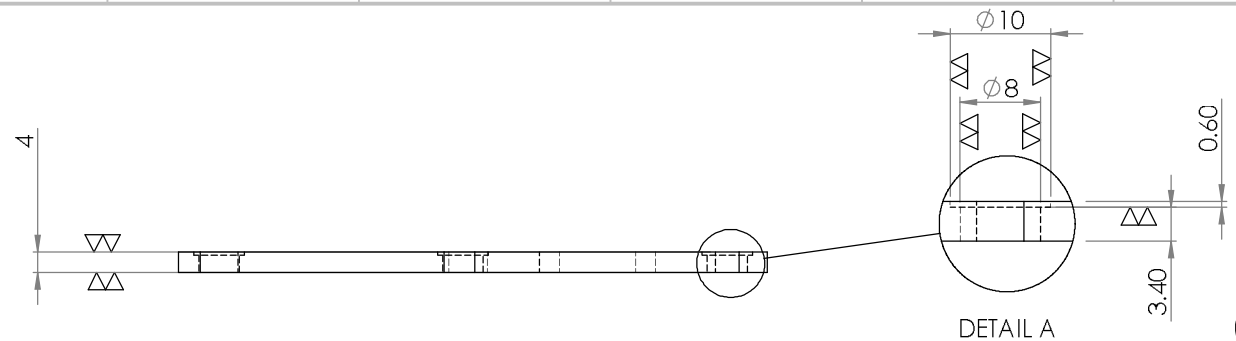

DETAIL A
SCALE 2 : 1

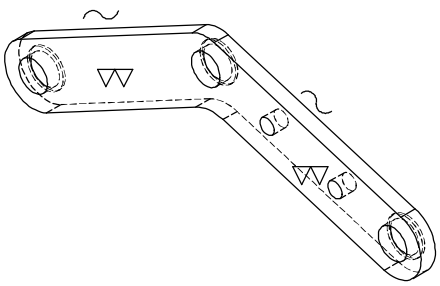

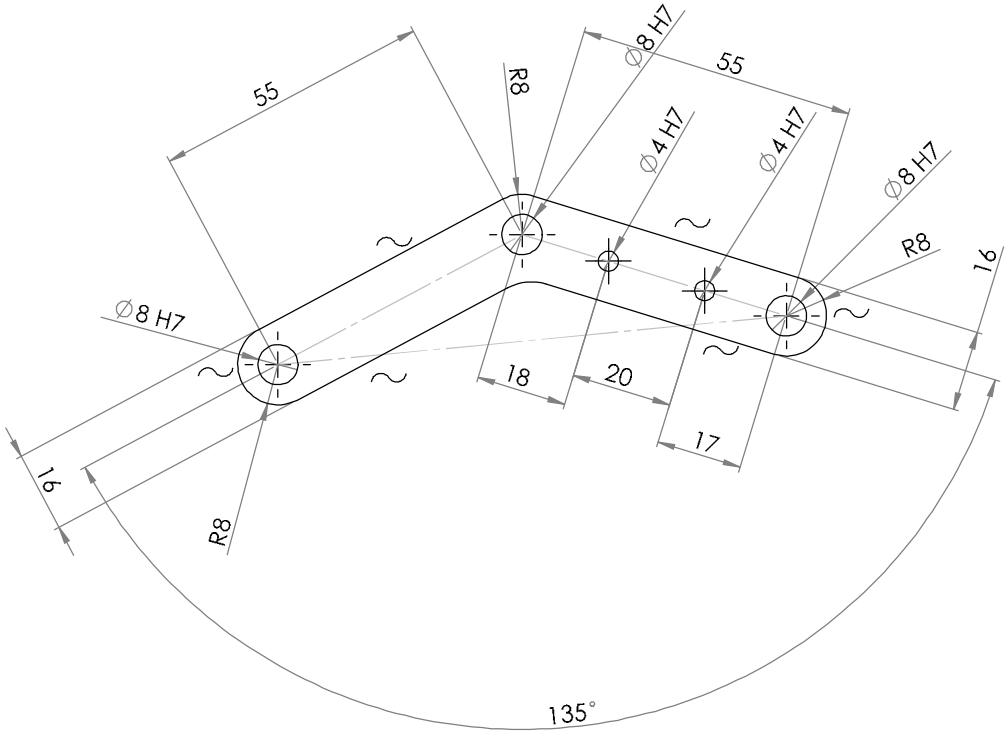

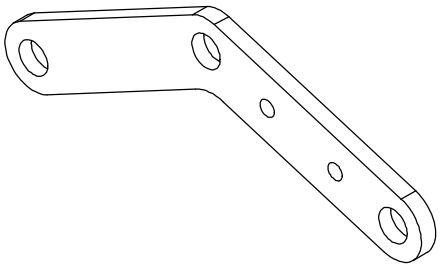

UNLESS OTHERWISE SPECIFIED: DIMENSIONS ARE IN MILLIMETERS SURFACE FINISH: TOLERANCES: LINEAR: ANGULAR:		FINISH:		DEBURR AND BREAK SHARP EDGES		DO NOT SCALE DRAWING	REVISION
						Quantity =10	
	NAME	SIGNATURE	DATE			TITLE:	
DRAWN						3DP	
CHK'D							
APP'VD							
MFG							
Q.A				MATERIAL:		DWG NO.	A3
				AL5052P-H112-JISH4000		F-7-Left- Copy	
				WEIGHT:		SCALE:1:1	SHEET 1 OF 1

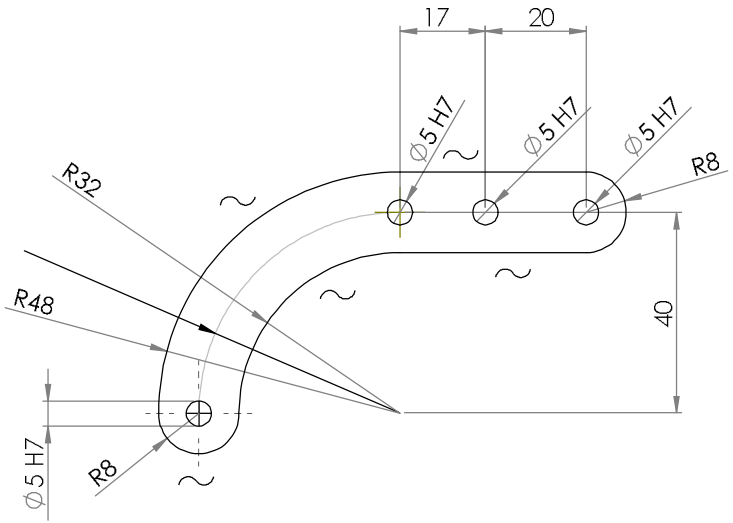

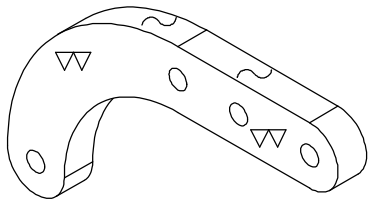

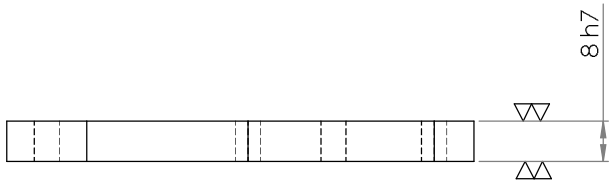

UNLESS OTHERWISE SPECIFIED: DIMENSIONS ARE IN MILLIMETERS SURFACE FINISH: TOLERANCES: LINEAR: ANGULAR:	FINISH:		DEBURR AND BREAK SHARP EDGES	DO NOT SCALE DRAWING	REVISION		
				Quantity =10			
	NAME	SIGNATURE	DATE	TITLE:			
DRAWN				3DP			
CHK'D							
APP'VD							
MFG							
Q.A				MATERIAL:	DWG NO.		A3
				AL5052P-H112-JISH4000	17		
				WEIGHT:	SCALE:2:1	SHEET 1 OF 1	